LEABHARLANN CHOLÁISTE NA TRÍONÓIDE, BAILE ÁTHA CLIATH | TRINITY COLLEGE LIBRARY DUBLIN
Ollscoil Átha Cliath | The University of Dublin

Terms and Conditions of Use of Digitised Theses from Trinity College Library Dublin

Copyright statement

All material supplied by Trinity College Library is protected by copyright (under the Copyright and Related Rights Act, 2000 as amended) and other relevant Intellectual Property Rights. By accessing and using a Digitised Thesis from Trinity College Library you acknowledge that all Intellectual Property Rights in any Works supplied are the sole and exclusive property of the copyright and/or other IPR holder. Specific copyright holders may not be explicitly identified. Use of materials from other sources within a thesis should not be construed as a claim over them.

A non-exclusive, non-transferable licence is hereby granted to those using or reproducing, in whole or in part, the material for valid purposes, providing the copyright owners are acknowledged using the normal conventions. Where specific permission to use material is required, this is identified and such permission must be sought from the copyright holder or agency cited.

Liability statement

By using a Digitised Thesis, I accept that Trinity College Dublin bears no legal responsibility for the accuracy, legality or comprehensiveness of materials contained within the thesis, and that Trinity College Dublin accepts no liability for indirect, consequential, or incidental, damages or losses arising from use of the thesis for whatever reason. Information located in a thesis may be subject to specific use constraints, details of which may not be explicitly described. It is the responsibility of potential and actual users to be aware of such constraints and to abide by them. By making use of material from a digitised thesis, you accept these copyright and disclaimer provisions. Where it is brought to the attention of Trinity College Library that there may be a breach of copyright or other restraint, it is the policy to withdraw or take down access to a thesis while the issue is being resolved.

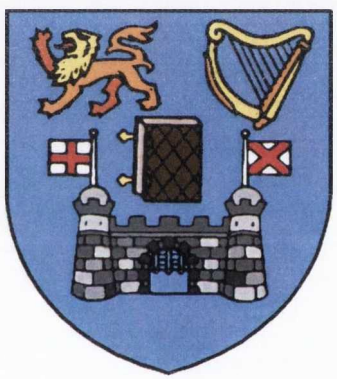
Access Agreement

By using a Digitised Thesis from Trinity College Library you are bound by the following Terms & Conditions. Please read them carefully.

I have read and I understand the following statement: All material supplied via a Digitised Thesis from Trinity College Library is protected by copyright and other intellectual property rights, and duplication or sale of all or part of any of a thesis is not permitted, except that material may be duplicated by you for your research use or for educational purposes in electronic or print form providing the copyright owners are acknowledged using the normal conventions. You must obtain permission for any other use. Electronic or print copies may not be offered, whether for sale or otherwise to anyone. This copy has been supplied on the understanding that it is copyright material and that no quotation from the thesis may be published without proper acknowledgement.

Novel Colorimetric and Fluorescent Sensors for Anions

By Rebecca M. Duke B.A. (Mod.)
October 2010



University of Dublin Trinity College

Based on research carried out under the direction of
Prof. Thorfinnur Gunnlaugsson

A thesis submitted to the Department of Chemistry, University of Dublin, Trinity College for the degree of Doctor of Philosophy.

TRINITY COLLEGE
2 9 MAR 2012
LIBRARY DUBLIN
Thesis 9315

Declaration

This thesis is submitted for the degree of Doctor of Philosophy to the University of Dublin, Trinity College and has not been submitted before for any degree or examination to this or any other university. Other than where acknowledged, all work described herein is original and carried out by the author alone. Permission is granted so that the Library may lend or copy this thesis upon request. This permission covers only single copies made for study purposes, subject to normal conditions of acknowledgment.

For My Mam and Dad

Abstract

This thesis, entitled 'Novel Colorimetric and Fluorescent Sensors for Anions' consists of six Chapters.

Chapter 1 provides an introduction into the field of anion sensing using fluorescent and colorimetric sensors, within the realm of supramolecular chemistry. This chapter details the challenges involved in the development of receptors and sensors capable of detecting anions, as well as the various design principles explored. A brief overview of the recent developments within the field of anion sensing is also given. This is followed by a more focused review on the recently reported naphthalimide-based luminescent and colorimetric sensors for anions, where the anion recognition occurs through hydrogen bonding and/or deprotonation. Particular attention is paid to the work carried out within the Gunnlaugsson group, as well as the recent reports within the literature. The second half of the introduction focuses on the development of colorimetric and fluorescent amidothiourea and amidourea-based sensors for anions. Finally, a summary of the work carried out in this thesis and the aims of the project are outlined.

Chapter 2 deals with the synthesis, characterisation and anion binding capabilities of a new series of 1,8-naphthalimide-based thiourea and urea sensors, which were designed to give rise to enhanced PET upon anion binding causing the fluorescence of the naphthalimide to be quenched. Their anion recognition ability was tested by various spectroscopic methods such as UV-Vis absorption, fluorescence and ^{1}H NMR in DMSO and DMSO-d_6 solutions. The selective colorimetric and fluorescent detection of F^- over AcO^- and $H_2PO_4^-$ was demonstrated by these systems, whereby the former led to a full quenching of the naphthalimide fluorescence emission and a colour change from yellow to purple at high concentrations of F^-. With the view of further extending the series of naphthalimide-based anion sensors, preliminary investigations into the sensing capabilities of a novel bis-naphthalimide sensor are also detailed, as well as the attempted synthesis of a novel 3,4-substituted naphthalimide-based thiourea sensor for anions.

Chapter 3 describes the synthesis and characterisation of several pyridine-based amidothiourea sensors for anions, which were functionalised with electron withdrawing chromophores such as *p*-NO_2 and *p*-CF_3 phenyl groups. The mechanism of the anion interaction with these sensors was elucidated using techniques such as UV-Vis absorption, fluorescence and ^{1}H NMR spectroscopic methods in various solvents, such as in DMSO, in a mixture of 4:1 DMSO-H_2O and in 1% DMSO-MeCN solution. The sensing of various anions, such as biologically important phosphate-based anions, was demonstrated, whereby

both hydrogen bonding and deprotonation interactions were most likely involved in the recognition process.

Chapter 4 discusses the design, synthesis and anion binding capabilities of a family of glycol-based amidothiourea sensors for anions. The structures of these sensors were derived from those discussed in Chapter 3, however, the increased solubility due to the presence of the glycol chain allowed these studies to be carried out in highly competitive media, such as alcohol and mixtures of alcohol water solution. The anion binding capabilities of these sensors were assessed with anions such as AcO^-, $H_2PO_4^-$, F^- and $HP_2O_7^{3-}$, as well as with biological phosphate-based salts. In addition to the anion titrations carried out, spectroscopic pH titrations were also carried out in order to obtain a better understanding of these sensors in solution.

Chapter 5 gives a brief overview of the results reported in Chapters 3-4 of this thesis and then compares and contrasts these results to those reported within the literature. Future work is also discussed.

Chapter 6 outlines the experimental procedures used in Chapters 2-4, and presents the characterisation of the compounds prepared. Finally, literature references and spectroscopic and titration data relevant to Chapters 2-4 are detailed at the end of this thesis. The appendix also provides crystallographic data.

Acknowledgements

I would like to sincerely thank my supervisor, Prof. Thorfinnur Gunnlaugsson for all his advice, encouragement and support throughout my Ph.D experience.

I would also like to take this opportunity to thank the TG Research Group, old and new. Thanks to Celine (Viva La France!), Lisa, Andrew, Debbie, Eoin, Cidalia 'S'. Santos, Emma, Sally, Flo and Lin for all their support in the early years. Thanks to the original second years- Danni, Gary and Niamh and to the original first years- Jen and Christophe. Lots of love to the Frenchies- Celia, Aline, and Julien. Special thanks to Stevo for his attention to detail and the endless supply of chocolate. Thanks to Sam, Brian, Rob, Laura, Elaine, Oxana and Swagata. Thank you to everybody who proof read this thesis.

To Eimear, Therese and Claire Butler, where did the eight years go? Thanks for the good times and for being great friends.

Special thanks to Doireann D. Moore for her friendship, extreme patience, kindness and support. You are a great friend.

A special acknowledgement to Drs. Manuel Ruether and John O Brien, particularly John for his endless enthusiasm for NMR and for all his help over the past four years. Also to Dr. Martin Feeney, Dr. Bernard-Jean Denis and Dr. Tom McCabe for MS and X-Ray crystallography.

Thanks to all the girls; be warned; good times Becks is back!

To my Dad, Emma, Rachel and d 'Aunties'; thanks for all your love, support (emotional and financial!) and constant encouragement throughout my Ph.D. I would also like to thank Mary, Patrick, Sarah and Daniel for their love and support.

Last but not least, David, I really can't find the words to thank you....thanks for everything. I could not have done this without you.

P.S. See you all at The Launch.

Abbreviations

AcO^-	Acetate
ADP	Adenosine diphoshate
AMP	Adenosine monophosphate
Å	Angstrom
A^-	Anion
ATP	Adenosine triphosphate
Br^-	Bromide
CD	Circular Dichroism
$CDCl_3$	Deuterated choroform
CD_3CN	Deuterated acetonitrile
CF_3	Trifluoromethylphenyl group
CH_2Cl_2	Dichloromethane
$CHCl_3$	Chloroform
Cl^-	Chloride ion
CO_2	Carbon dioxide
CT	Charge Transfer
$CSCl_2$	Thiophosgene
D_2O	Deuterated water
DMABA	*p*-(Dimethylamino) benzamido
DMF-d_7	Deuterated dimethyl formamide
DMSO	Dimethyl Sulfoxide
DMSO-d_6	Deuterated DMSO
EET	Electron Energy Transfer
EFA	Evolving Factor Analysis
Eq.	Equivalents
EQ.	Equation
EtOH	Ethanol
ETOAc	Ethyl acetate
ESIPT	Excited State Intramolecular Proton Transfer
ES-MS	Electrospray Mass Spectrometry
F^-	Fluoride
GC	Gas Chromatography
HCl	Hydrochloric acid
$H_2PO_4^-$	Dihydrogen phosphate

$HP_2O_7^{3-}$	Hydrogen pyrophosphate
H_2O	Water
HEPES	*N*-2-Hydroxyethylpiperazine-*N*'-2-ethanesulfonic acid
HF_2^-	Bifluoride
IDA	Indicator Displacement Assay
ICD	Induced Circular Dichroism
ICT	Internal Charge Transfer
INH	Inhibit Logic
ITC	Isothermal titration Calorimetry
K	Binding constant
LE	Locally Excited State
MeCN	Acetonitrile
MeOH	Methanol
NaOH	Sodium hydroxide
NMR	Nuclear Magnetic Resonance
NOE	Nuclear Overhauser Effect
OH^-	Hydroxide ion
PET	Photoinduced Electron Transfer
pK_a	-LogK_a where K_a is the acidity constant
PMPMS	Poly(mercaptopropylmethyl) siloxane
ppm	Parts per million
Psi	Pounds Per Square Inch
PPi	Pyrophosphate
r	Radius
RT	Room Temperature
ROESY	Rotational Nuclear Overhauser Effect Spectroscopy
SO_4^{2-}	Sulfate
StClC	Staphylococcus Typhimurium Chloride Channel
SubPc	Subphthalocyanine
TBA	Tetrabutyl ammonium counterion
TBAF	TBA fluoride
TBAOH	TBA hydroxide
TFA	Trifluoroacetic acid
THF	Tetrahydrofuran
UV	Ultraviolet

ν	Frequency
VT	Variable Temperature
λ	Wavelength
$\Delta\delta H$	Change in the chemical shift of protons

Table of Contents

Chapter 1 - Introduction

1.0 Supramolecular Chemistry 1

1.1 Anion Sensing 2

1.2 The Challenges of Anion Sensing 3

1.3 Colorimetric and Fluorescent Chemosensors 5

1.31 Design Principles 5

1.4 Methods of Measuring Host:Guest Interactions 7

1.5 Anion Receptor Chemistry 7

1.5.1 Neutral H-Bonding Systems: Ureas, Thioureas, Amidoureas and Amidothioureas 9

1.6 Colorimetric Sensing and Photoinduced Electron Transfer (PET) in 4-Amino-1,8-Naphthalimide Sensors 10

1.7 Fluorescent and Colorimetric Naphthalimide Based Sensors for Anions 12

1.7.1 4-Amino-1,8-Naphthalimide Based Urea and Thiourea Sensors for Anions 12

1.7.2 N-Imide Functionalised Naphthalimide Sensors 18

1.7.3 4-Amido-1,8- Naphthalimide Based Sensors For Anions 21

1.7.4 4-Hydrazine Based Urea and Thiourea Naphthalimide Sensors for Anions 23

1.7.5 Alternative Sensing Mechanisms Involving the Naphthalimide Fluorophore: Assemblies, Displacement Assays and Inclusion Complexes 26

1.8 Neutral Amidourea and Amidothiourea Based Sensors for Anions 28

1.8.1 Colorimetric and Fluorescent Amidoureas and Thioureas 28

1.8.2 Heterocyclic Based Amidoureas and Thioureas 31

1.8.3 Fluorescent Amidothiourea Based Sensors for Anions 34

1.8.4 Amidoureas and Thioureas Appended to Scaffolds 36

1.9 Work Described Within This Thesis 39

Chapter 2 – Naphthalimide Based Thiourea and Urea Sensors for Anions

2.0 Introduction and Objectives of Current Studies 41

2.1 Synthesis and Characterisation of 4-Amino-1,8- Naphthalimide Based Thiourea and Urea Sensors 4a-4c 42

2.2 Photophysical Evaluation of Sensors 4a-4c 45
2.2.1 Absorption and Fluorescence Titration of **4a** with AcO^- 46
2.2.2 Absorption and Fluorescence Titration of **4a** with $H_2PO_4^-$ 48
2.2.3 Titration of **4a** with F^- 50
2.3 Absorption and Fluorescence Titration of Sensor 4b with Anions 53
2.4 Absorption and Fluorescence Titration of Sensor 4c with Anions 55
2.5 Absorption and Fluorescence Titration of Sensor 4a with TBAOH 56
2.6 Absorption and Fluorescence Titration of Sensor 4a with $TBAF.3H_2O$ 58
2.7 Design, Synthesis and Photophysical Properties of Reference Compounds 2 and 37 60
2.7.1 Absorption and Fluoresence Titration of Reference Compound **2** with F^- and TBAOH 61
2.7.2 Absorption Titration of Reference Compound **37** with AcO^-, F^- and TBAOH 63
2.8 Conclusion of Photophysical Measurements of 4a-c with Anions in DMSO 66
2.9 ^{1}H NMR Titrations of Sensors 4a-c with Anions in DMSO-d_6 68
2.9.1 ^{1}H NMR Titration of Sensor **4a** with AcO^- in DMSO-d_6 68
2.9.2 ^{1}H NMR Titration of Sensor **4a** with $H_2PO_4^-$ in DMSO-d_6 70
2.9.3 ^{1}H NMR Titration of Sensor **4a** with F^- salts in DMSO-d_6 71
2.10 ^{1}H NMR Titration of Sensor 4b with AcO-, $H_2PO_4^-$ and F^- in DMSO-d_6 73
2.11 ^{1}H NMR Titration of Sensor 4c with $TBAF.3H_2O$ in DMSO-d_6 73
2.12 Determination of Binding Constants for 4a-and 4b upon Titration with AcO^- and $H_2PO_4^-$ using ^{1}H NMR Spectroscopy 75
2.13 ^{1}H NMR Titration of Sensor 4a with TBAOH in DMSO-d_6 77
2.14 ^{1}H NMR Titration of Receptor 37 with F^-, TBAOH and AcO^- in DMSO-d_6 78
2.15 Conclusion of ^{1}H NMR Titrations of 4a-c with Anions in DMSO-d_6 80
2.16 Synthesis of the Bis-Naphthalimide Sensor 39 81
2.17 Preliminary Absorption and Fluorescence Titrations of 39 with Anions 83
2.18 Preliminary ^{1}H NMR Titrations of Sensor 39 with $H_2PO_4^-$ in DMSO-d_6 85

2.19	**Development of 3,4-Substituted Naphthalimide-Based Sensors**	**86**
	2.19.1 Synthesis and Characterisation of the Urea Sensor **42**	**87**
2.20	**Photophysical Properties of Sensor 42 in DMSO**	**89**
	2.20.1 Absorption and Fluorescent Anion Titrations of **42** in DMSO	**89**
2.21	**Attempted Synthesis of the 3,4-Substituted Naphthalimide Sensor 47**	**91**
2.22	**Overall Conclusion**	**95**

Chapter 3 – Amidothiourea-Based Sensors for Anions

3.0	**Introduction and Objectives**	**99**
3.1	**Synthesis of *p*-Nitro Phenyl-Based Amidoureas/thioureas 52-54**	**100**
3.2	**Characterisation of Sensors 52-54**	**100**
3.3	**Absorption Titrations of 52-54 with Anions in DMSO**	**107**
3.4	**Absorption Titrations of 54 with Base and the TBA salts of Various Anions in 4:1 DMSO-H_2O Solution**	**111**
3.5	**Absorption Titrations of 54 with Phosphate-Based Biological Anions in 4:1 DMSO-H_2O Solution**	**114**
3.6	**Fitting of the Absorption titrations of 54 with Anions in 4:1 DMSO-H_2O using SPECFIT^{TM}**	**116**
3.7	**^{1}H NMR Titration of 54 in DMSO-d_6**	**118**
3.8	**Conclusion of Absorption and ^{1}H NMR Titrations of 54**	**122**
3.9	**Sensitivity of Sensor 54**	**123**
3.10	**Derivatives of Sensor 54**	**124**
3.11	**Synthesis of Sensors 56, 57 and 27b**	**125**
3.12	**Characterisation of Sensors 56, 57 and 27b**	**126**
3.13	**Absorption and ^{1}H NMR Titrations of 56 with Anions in 4:1 DMSO-H_2O Solution**	**127**
3.14	**Absorption Titrations of 56 and 57 in 1% DMSO in MeCN**	**129**
3.15	**Absorption, Fluorescence and ^{1}H NMR Titrations of 57 with Anions in 1% DMSO in MeCN**	**130**
3.16	**Absorption and ^{1}H NMR Titrations of 27b with Anions in 4:1 DMSO-H_2O Solution**	**132**
3.17	**Structural Isomers of Sensor 54: *m*-Nitro and *o*-Nitro-Phenyl-Based Sensors**	**136**
3.18	**Synthesis and Characterisation of *m*-Nitro and *o*-Nitro Phenyl Based Amidothioureas 61-62**	**136**

3.19 Absorption Spectra of 54, 61, 62 in 4:1 DMSO-H_2O 138

3.20 Absorption and ^1H NMR Titrations of 61 with Anions in 4:1 DMSO-H_2O and DMSO-d_6 Solutions 138

3.21 ^1H NMR Titration of 61 in DMSO-d_6 141

3.22 Absorption Titration of 62 with Anions in 4:1 DMSO-H_2O 142

3.23 ^1H NMR Titrations of 62 with Anions in DMSO-d_6 143

3.24 Overall Conclusion 144

Chapter 4 –Glycol-Based Amidothiourea Sensors

4.0 Introduction and Objectives 147

4.1 Synthesis of the Polyoxyethylene-Based Amidourea Sensors 70, 71, 74 and 75 147

4.1.1 Synthesis of the Iodo-Polyoxyethylene Chains **64** and **66** 147

4.1.2 Synthesis of the Bis-Amidothiourea Sensors **70** and **71** 149

4.1.3 Synthesis of the Tetra-Amidothiourea Sensors **74** and **75** 151

4.2 Absorption Titrations of 70 with Anions in MeOH 154

4.2.1 Absorption Titrations of **71** with Anions in MeOH 157

4.2.2 Absorption Titrations of **70** with Anions in EtOH 159

4.3 Absorption Titrations of 70 and 71 with Anions in Alcohol and Water 160

4.4 Absorption pH Titrations of 70 and 71 in Mixtures of Alcohol and Water Solutions 163

4.5 pH Measurements of 70 and 71 with Anions in Aqueous-Based Solution 167

4.6 Absorption Titrations of Sensors 70 and 71 with Biologically Relevant Phosphate-Based Anions in Alcohol and Water Solutions 168

4.7 Buffer Studies with Sensor 70 172

4.8 Absorption Titrations of the Tetra-Amidothiourea Sensor, 74, with Anions in Alcohol 174

4.8.1 Absorption Titrations of Sensor 75 with Anions in Alcohol 177

4.8.2 Absorption Titrations of 74 and 75 with Anions in Alcohol and Water Solutions 178

4.9 Conclusion 178

Chapter 5 Overview of Thesis and Future Work

5.0	**Overview of Thesis: Introduction**	**181**
5.1	**Amidothioureas Functionalised with Electron Withdrawing Groups**	**181**
5.2	**Amidothioureas Functionalised with Electron Donating Groups**	**182**
5.3	**Amidothioureas in Aqueous-Based Solution**	**182**
5.4	**Future Work**	**183**

Chapter 6 Experimental Procedures

6.0	**General Experimental Details**	**185**
6.1	**NMR Titrations**	**186**
	6.1.1 Preparation of Solutions for NMR Titrations with Anions	**186**
6.2	**UV-Visible Absorption and Fluorescence Titrations**	**186**
	6.2.1 Preparation of Solutions for UV-Visible Absorption and Fluorescence Titrations with Anions	**186**
6.3	**General Synthetic Procedures**	**187**
	6.3.1 Procedure 1: Synthesis of Naphthalimide- Based Ureas and Thioureas	**187**
	6.3.2 Procedure 2: Synthesis of Amidoureas and Amidothioureas	**187**

References **207**

Appendices

Appendix A0	Determination of Binding Constants using SPECFIT™	**215**
Appendix A	Supporting Information for Chapter 2	**217**
Appendix B	Supporting Information for Chapter 3	**233**
Appendix C	Supporting Information for Chapter 4	**249**
Appendix D	Crystallographic Data for **54**	**257**

Publications

Chapter 1

Introduction

1.0 Supramolecular Chemistry

Supramolecular chemistry is concerned with the non covalent interactions between molecules that drive them to assemble in a selective fashion. [1,2] The assembled molecules are often referred to as 'Host-Guest' complexes. The driving forces for their formation are usually electrostatic interactions, including hydrogen bonds, which play a special role due to their directionality (as apposed to charge-charge interactions which are stronger but non-directional), chelation of metal cations and hydrophobic effects. The latter involves the release of water bound (or other polar solvent) molecules. In comparison to classical chemical synthesis, this somewhat younger field of chemistry had its beginning in the late 1960's when Lehn, Pederson and Cram described the cation binding ability of cryptands,[3] crown ethers[4] and cavitands,[5] respectively. This seminal work led to the 1987 Nobel Prize being awarded to this trio.[6] Forty years on, the field has become one of the fastest growing interdisciplinary areas of chemistry, by joining forces with physics, biology and technology.[7]

Supramolecular systems can either be polymeric (which involves solid-state chemistry) or discrete in which case solution studies may lead to a detailed understanding of host-guest interactions. Thus the development of supramolecular chemistry involves gaining more control over molecules, supermolecules and materials. While nanoscale structures in biological systems are often the inspiration for supramolecular research, it remains exceedingly difficult to replicate Nature and bring more than two different neutral molecular species into solution in a predictable manner, without making or breaking covalent bonds.

One of the many themes of supramolecular chemistry is the design of molecular receptors or sensors, which are capable of detecting and signalling the presence of important molecules or analytes. Therefore, molecules have been designed, which may respond to or recognise a physical stimulus (light, heat, electron transfer, *etc.*), by generating a signal that can be measured or used as a control. If selectivity between different analytes is achieved, this is commonly referred to as *'molecular recognition'*. According to Lehn; 'Molecular recognition is defined by the energy and information involved in the binding, by the selection of substrate(s) by a given receptor molecule, and sometimes by a specific function'.[8] Hence, a variety of molecules capable of responding to a wide variety of targets, such as cations,[9] anions[10] and charge neutral species,[11] have been designed and studied to date. In order for a molecule to act as an 'ideal' sensor it should fulfil various criteria, such as sensitivity, selectivity and short response time. Over the past ten years, the development of molecules as 'chemosensors' or chemical sensors for the

detection and transport of anions has become a mature field of research within supramolecular chemistry, which has been driven by an increasing appreciation for the importance of non-covalent anion-receptor interactions.[10,12,13] Anion sensing has also been of great interest within the Gunnlaugsson group[14,15] and therefore, this thesis deals with the design, synthesis and photophysical evaluation of charge neutral organic sensors for the detection of anions. Some of the sensors discussed within this thesis contain the 4-amino-1,8-naphthalimide fluorophore unit as a reporter, which has been previously utilised for sensing purposes within the theses of Dr. Hussey[16] and Dr. Ali.[17] Also detailed within this thesis are the more recently emerged amidourea and amidothiourea anion receptor moieties, of which the former was also shown to bind anions in the thesis of Dr. Quinlan.[18] Although, an introduction to both the field of anion sensing and the photophysical properties of the naphthalimide fluorophore were detailed within the theses above, a brief introduction is also necessary here to aid the reader. This general introduction will be followed by a literature review of naphthalimide and amidourea/thiourea based sensors for anions.

1.1 Anion Sensing

Anions are ubiquitous in the natural world and also play an important role in many biological processes. Indeed, disruption of anion flux across cell membranes is increasingly recognised as a primary determinant of many diseases such as cystic fibrosis,[19] Bartter's syndrome,[20] Dents disease,[21] Pendreds syndrome[22,23] and Osteoperosis.[24] Anion transport systems have recently been identified as being responsible for the trafficking of ADP, ATP, phosphate, citrate, maleate, oxaloacetate, sulfate, glutarate, fumarate and halides. Furthermore, anions are present in approximately 70% of all enzymatic sites, while they also play essential structural roles in many proteins, and are critical for the manipulation and storage of genetic information.[12]

Several X-ray crystal structures have allowed the direct visualisation of enzyme-anionic substrate complexes that are stabilised by multiple hydrogen bonding interactions, such as the histone octamer-phosphate complex, shown in Figure 1.1.[25] Five fully basic phosphate anions interact with the charged lysine and arginine residues at five different sites *via* a combination of hydrogen bonding and electrostatic interactions. Also shown in Figure 1.1 is the 3 Å resolution X-ray crystal structure of the StCLC chloride ion channel.[26] Interestingly, the chloride ion is held within the binding site solely by neutral amino acids. Within the environment, chloride anions are present in the oceans, nitrate and sulfate in acid rain; and carbonates are constituents of bio-mineralized materials.

Anthropogenic anions such as pertechnetate,[27] which is a radioactive product of nuclear fuel reprocessing, and phosphates and nitrates from agriculture also constitute pollution hazards. As well as environmental pollutants, anions can also be harmful to humans and organophosphates and F^- are present in chemical warfare agents, in which the former is a component of nerve gas and the latter is formed upon hydrolysis of sarin gas.[28] Over the past several years, scientific studies have been carried out to determine whether or not fluoride is a beneficial additive in the human diet.[29] These studies have led to the scrutiny of water fluoridation, as dental and skeletal fluorosis have been reported in countries

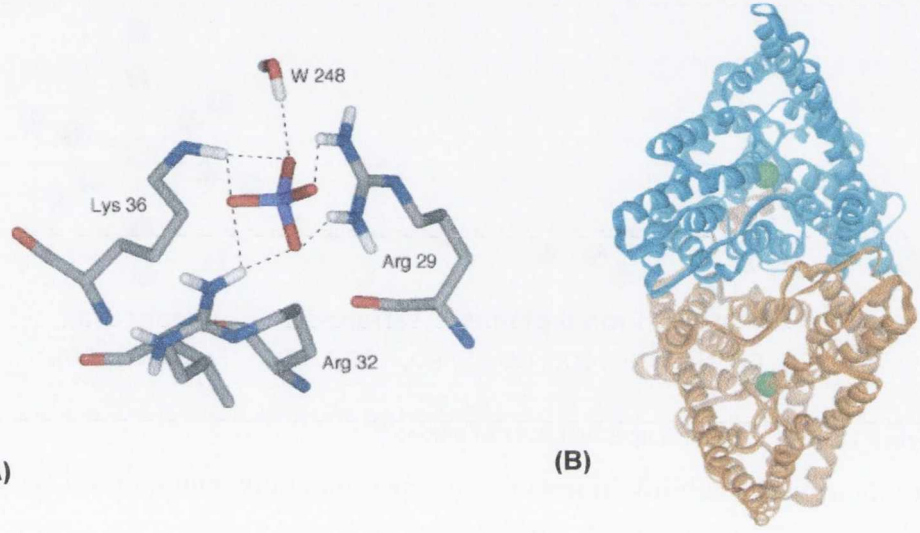


Figure 1.1: (A) The X-ray crystal structure of the amino acid residues that interact with the phosphate anion in the histone-octomer-phosphate complex.[24] Only one of five phosphates is shown. **(B)** Stereo-view of a ribbon representation of the StCIC dimer visualised from the extracellular side. The homo-dimers (brown and cyan) contain a chloride anion (green).[25]

associated with high levels of fluoride in drinking water. Therefore, the development of convenient and inexpensive technological methods to quantitatively determine anions in their respective environments or complex media is an active area of research within industry, diagnostics and therapeutic medicine and also in various kinds of environmental monitoring.

1.2 The Challenges of Anion Sensing

The design and synthesis of anion sensors can be considered more challenging in comparison to those of cation sensors. There are several reasons for this, which is each discussed below.

Anions are often larger than their equivalent isoelectronic cations and hence have a lower charge to radius ratio. *e.g.* K^+ and Cl^-, Δ r = 0.15 Å.[30] They are also more diffuse in nature which makes electrostatic interactions less favourable than their corresponding isoelectronic cations.

Anions can also be pH sensitive. Therefore, receptors must be able to function within the pH window of their target anion in order to be successful. The basic properties of anions must also be taken into account when analysing anion:receptor interactions as they can induce deprotonation of acidic N-H protons of a receptor, an area of research that this thesis also focuses on.[31]

The geometries of anions, shown in Figure 1.2, have a wider range than cationic species. Therefore, a higher degree of design and complementarity is necessary to give rise to selective anion receptors, in comparison to cation sensors.

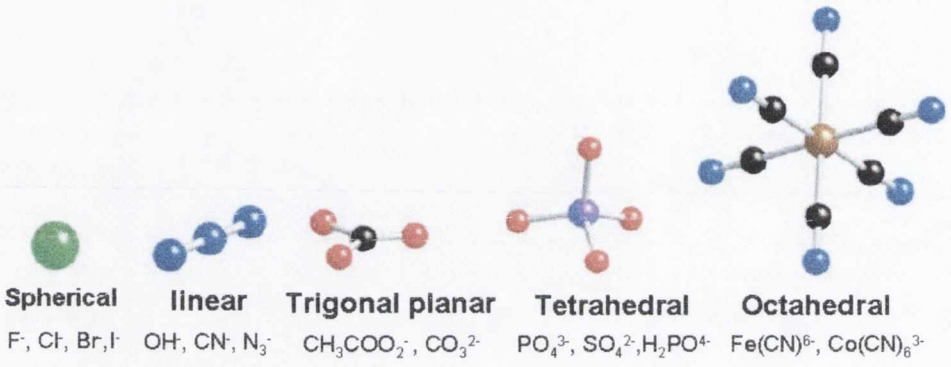


Figure 1.2: The varying shapes and sizes of anions.[12]

Due to their high solubility in organic solvents, tetrabutylammonium (TBA) anion salts are often used in anion binding studies. While the TBA counter-cation is generally regarded as a non-coordinating cation, which does not form ion-pairs in solution, significant ion-pairing in non-polar solvents has been shown to occur.[32] Therefore, depending on the nature of the solvent used for the binding studies, a receptor may have to compete with the counter-cation in order to successfully bind its anion. Consequently, the counter-cations role cannot be overlooked. Additionally, TBA salts are also hygroscopic and can be difficult to keep dry. In the case of TBAF, the attempted removal of all water from the salt results in decomposition.[33]

The binding of anions in solution is greatly affected by the nature (polarity, α, β, *etc*) of the solvent employed.[34-36] Potential anion sensors must, therefore, compete effectively with the solvent environment in which the anion recognition event is to take place. For example, a neutral receptor that binds anions solely through hydrogen bonding interactions is less likely to be capable of competing with the solvation shell surrounding the target anion in competitive media such as alcohol and water and, hence, may only interact with anions in aprotic organic solvents. Therefore, one of the major challenges within the field of anion recognition is the design of receptors that can function in such conditions, which is particularly important in order to achieve sensing in water. Therefore,

the difficulties encountered in achieving sensing in water are due to the unique properties of this solvent, such as its polarity and hydrogen bonding capabilities. For these reasons, the majority of anion sensing achieved by neutral receptors have been reported to date in less competitive solvents, such as DMSO, $CHCl_3$ and MeCN.[37]

Despite the challenges outlined above, a plethora of simple and complex receptors or 'chemosensors' for anions have been developed and their anion sensing capabilities investigated.[10] A vast number of reports within the literature exist detailing the various approaches to the construction of anions sensors, which are described in the following section.

1.3 Colorimetric and Fluorescent Chemosensors

A chemosensor is a molecule of abiotic (synthetic) origin that signals the presence of matter or energy. To date, chemosensors have been designed to detect cationic (*e.g.* K^+, Na^+),[9] anionic (*e.g.* Cl^-, AcO^-)[10] and charge neutral species (*e.g.* saccharides).[11] Both cations and anions have also been simultaneously sensed using ditopic receptors.[38,39] The energetic mechanism by which the interaction of a chemosensor with its analyte occurs is known as signal transduction. Therefore, as mentioned in Section 1.0, chemosensors are usually categorised by their target and their mechanism of signal transduction.

This sensing process is usually achieved by the cooperation of two subunits exhibiting differentiable functions: the binding site and the signalling subunit. The role of the former is to coordination to a certain analyte, whereas the task of the latter consists of conveying this event *via* concomitant changes in usually photophysical or electrochemical properties. These techniques can all be employed to quantify the analytes concentration, or monitor its movement in real-time. This '*binding-site signalling subunit*' approach has been used extensively and thus there are numerous examples in the literature of colorimetric (which upon detection of their analyte there is a colour change, which is often visible to the naked eye),[40] fluorescent[15,41] and electrochemical sensors.[42] As this thesis details the investigation of colorimetric and fluorescent sensors alone, electrochemical sensors will not be discussed herein.

1.3.1 Design Principles

There are two main strategies towards the design of colorimetric and fluorescent sensors for the detection of analytes in solution. Colorimetric and fluorescent sensors may operate whereby the binding site is directly attached, or integrated, into the signalling moiety, such as shown in the schematic of Figure 1.3 (A). Therefore, the mechanism for

signal transduction involves interaction of the analyte with a ligand that is part of the π-system of the signalling moiety. Chromophores which are directly attached to the receptor

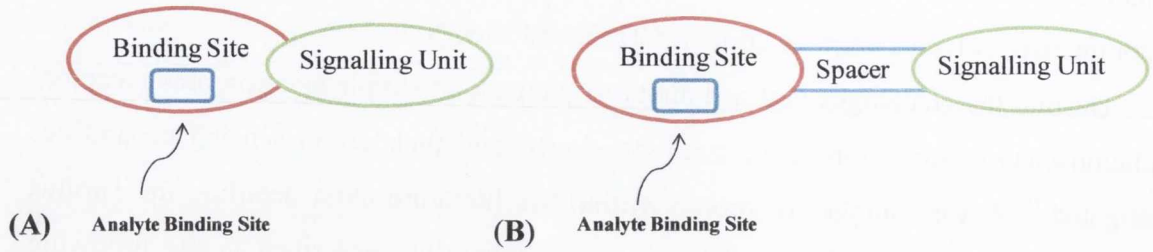


Figure 1.3: Schematic representation of design concepts for the construction of colorimetric and fluorescent sensors.

mainly consist of organic dyes such as azobenzene, nitrobenzene, indoaniline, anthraquinone *etc.*[40] Indeed, as this list shows, many chromophores can also be fluorescent and therefore, give rise to dual responses in both their absorption and fluorescence emission spectra upon analyte interaction.[14]

Alternatively, the receptor moiety and signalling subunit may be intermolecularly or covalently linked by a 'spacer' group, Figure 1.3 (B). When covalently linked, the binding event in colorimetric sensors is communicated from the receptor to the chromophore *via* conjugation with aromatic compounds such as quinoxaline, oxadiazole and porphyrin, to name just a few.[40] However, covalently linked fluorescent probes mainly consist of a receptor and fluorophore, which are electronically independent. This covalent linkage, which separates the receptor and the fluorophore units, is typically a short spacer that minimises any ground state interactions. Photoinduced electron transfer (PET) sensors are an example of such '*fluorophore-spacer-receptor*' probes and 'ideally' only changes in their quantum yield or fluorescence intensity occur upon recognition of analytes. PET sensors were originally developed independently by de Silva[9] and Czarnik,[43] and have been employed in many excellent examples since, such as in the detection of sugars.[11]

In an alternative design strategy, indicator displacement assays (IDA) consist of competitive assays whereby a receptor-chromophore or receptor-fluorophore ensemble is selectively dissociated by the addition of an appropriate competitive analyte. The analyte interacts efficiently with the receptor resulting in a detectable response of the chromophore or fluorophore. Such systems have been, in particular, developed by Anslyn and co-workers and also Fabbrizzi and co-workers.[44,45]

Also, prevalent in the design of chemosensors (particularly for practical purposes), is the need for reversibility in order to provide continuous monitoring of analytes. However, in the case of 'once-off' measurements, such reversibility is not necessary.

Colorimetric sensors that have been developed and involve a specific chemical reaction between the host and guest, are referred to as chromoreactands.[46] It is important to mention the distinction between a sensor and a receptor when discussing the detection of anions by these molecules. For example, a colorimetric or fluorescent response triggered *via* deprotonation does not involve the formation of a stable hydrogen bonded anion-receptor complex and, therefore, does not belong to the class of receptor molecules. However, both these interactions are used to sense anions. Additionally, both interactions can be studied using the same techniques, which are discussed in the following section.

1.4 Methods of Measuring Host:Guest Interactions

As mentioned in Section 1.2, chemosensors often consist of chromogenic or fluorescent signalling moieties. Therefore, a variety of spectroscopic techniques can be employed to study the process of anion binding. These include UV-Vis absorption (where changes in the ground state are probed), fluorescence emission (where changes in the excited state are probed) and ^{1}H nuclear magnetic resonance (NMR), where changes in the chemical structure of the sensor are probed. In addition to these techniques, isothermal titration calorimetry (ITC) may also be used, which provides information on the changes in the energy of the system as a whole (*e.g.* ΔG, H and S). Both absorption and fluorescence spectroscopy reflect changes in the optical properties of the light absorbing/emitting portions of the sensor, whereas ^{1}H NMR (or spectroscopy involving other NMR detectable nuclei) spectroscopy can monitor the changing environment in N-H and C-H protons and thus provide information about the interaction of the receptor and anion. Therefore, each of these techniques allows a different part of the binding process and/or overall equilibrium to be evaluated, which means that a more accurate description of the binding mode, as well as the strength of the interaction can be obtained. Additionally, the techniques described above operate over different sensitivity ranges, typically 10^{-5} M or lower for absorption or fluorescence spectroscopy, 10^{-3} M for NMR spectroscopy and 10^{-4} M for ICT. In this thesis, the use of absorption, fluorescence and NMR spectroscopy will be employed to investigate the anion binding capabilities of various sensors. The next section will give examples of receptors/sensors from the literature.

1.5 Anion Receptor Chemistry

Since the pioneering work of Simmons and Park in 1968,[47] who studied the interaction of protonated tricyclic diamine with Cl^-, the supramolecular chemistry community have devoted significant research effort to the complexation of anionic guests.

A vast literature detailing the sensing of anions by a myriad of simple and complex sensors has since emerged and many reviews dealing with the subject of anion recognition have appeared in the literature over the last ten years.[14,15,37,48-55] Therefore, the following examples are intended only to give a brief overview of the field.

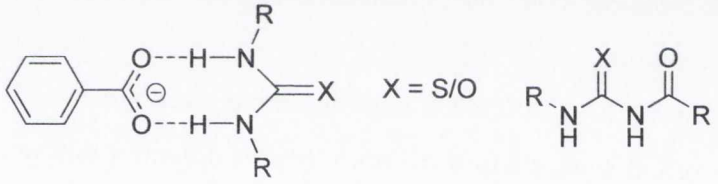
The multitude of anion receptors and sensors functioning *via* the binding site-signalling subunit approach, are often classified by the anion receptor moiety, which may be positively charged or neutral. Classical charged non-metallic moieties, such as quaternary ammonium,[56] guanidinium[57] and imidizolium groups,[58] have been incorporated into anion receptors. Indeed, the incorporation of the naturally occurring amino acid, guanidinium, into synthetic peptides has led to the development of efficient anion receptors, as described in a recent review by Kubik.[59] With regards to neutral non-metallic systems, Bowman-James,[50,60] Sessler,[61-63] Gale,[64-70] Gunnlaugsson,[14,15] Pfeffer,[71,72] Anslyn,[73] and Fabbrizzi[31,74], to name but a few, have collectively illustrated the use of amines, amides, ammoniums, sulfonamides, pyrroles, indoles, hydroxyl groups, ureas and thioureas in the development of neutral organic receptors and sensors for anions. Incorporation of receptor moieties into preorganised scaffolds, such as macrocycles,[75] calixarenes,[76] podands[52] and steroids,[77] has also been explored by various researchers. In addition, the design of complex receptors or 'hybrid' receptors whereby combinations of the aforementioned receptor moieties have been combined, has lead to cooperative and enhanced binding of anions.[78-80] A plethora of metallic based systems have also been developed for the sensing of anions.[81] These mainly include transition metal complexes,[82] lanthanide complexes[83-87] and Lewis acids.[88] In the case of the latter, James *et al.*[89-93] have established the use of boronic acids for the sensing of anions.

Anion recognition in solution has recently been combined with materials chemistry, thus entering the realm of functionalised materials. Most interestingly, these recent examples of functionalised materials show that hydrogen bonding interactions can be effective in polar protic media and in water, despite their intrinsic weakness and the competition of solvent, as their binding site may be in a protective environment. For example, hydro and organo gels can constitute new phases where host-guest interactions can take place protected from the bulk water and, hence, great interest has been focused on low molecular weight gelator compounds,[94] in which the gelator itself may function as an anion receptor or alternatively, may host the anion receptor.[95] Arrays of neutral pyrrole based receptors embedded in hydrogels can detect the presence of anions in water, as reported by Azenbacher and co-workers.[96] Heterogenous conditions have also been applied to metallic systems, and luminescent 1D microporous solids formed by the self assembly

of Tb(III) and benzene-1,3,5-tricarboxylate have been shown to bind fluoride in methanol.[97] The protective environment of a micelle has been used to host Lewis acid-base interactions between UO_2^{2+} complexes and F^-. [98] Additionally, various researchers have recently shown that silica based materials can be functionalised with sensors, giving rise to the detection of F^-,[99] $H_2PO_4^-$,[100] and $P_2O_7^{4-}$ [101] in aqueous solution. As shown above in the selected publications, the field of anion sensing is continuously evolving, giving rise to novel approaches for the selective detection of anions in various environments.

1.5.1 Neutral H-Bonding Systems: Ureas, Thioureas, Amidoureas and Amidothioureas

As mentioned in Section 1.5, anion sensing with neutral organic molecules has been investigated extensively by various researchers. One of the earliest examples of oxo-anion complexation by a neutral receptor was that of a urea containing subunit which was reported by Wilcox *et al.* in 1992.[102] Since then, ureas and thioureas have been utilised in anion binding due to their diprotic receptor site and their ease of synthetic manipulation.



(A) **(B)**

Figure 1.4: (A) Schematic respresentation illustrating why urea and thiourea groups are excellent receptors for oxo-anions. **(B)** Stucture of amidourea/amidothiourea.

Urea and thiourea have particularly high affinities for oxo-anions, as they are capable of forming two linear hydrogen bonds to the anion, as depicted in Figure 1.4. For such reasons, urea and thiourea receptors have been extensively studied within the Gunnlaugsson research group.[14,15]

In many cases the 4-amino-1,8-naphthalimide fluorophore has been utilised as a signalling site in conjunction with urea or thiourea receptor moieties. The 4-amino-1,8-naphthalimide fluorophore offers several advantages over other signalling units and these include: good photo-stability; strong absorption within the visible region (due to an internal charge transfer (ICT) excited state with λ_{max} at *ca.* 450 nm) and high quantum yields of emission in the green part of the electromagnetic spectrum (λ_{max} ~ 540-550 nm).[103] Chapter 2 of this thesis details the design, synthesis and anion binding studies of neutral napthalimide urea and thiourea based sensors, and for this reason an overview of sensors reported recently in the literature, which contain the naphthalimide fluorophore will be

discussed in the following sections. While some of the naphthalimide based sensors discussed contain urea or thiourea binding moieties, other receptor moieties that have been incorporated into this fluorophore for anion sensing will also be presented.

While the sensors in Chapter 2 contain urea and thiourea receptors, hybrid receptors, which were also previously mentioned in Section 1.5, are the subject of Chapters 3 and 4 of this thesis. The hybrid receptors studied are the amidourea and amidothiourea moieties, which as suggested, consist of an amide functionality directly appended to a urea or a thiourea moiety.[79,104] This binding unit is shown above in Figure 1.3. As previously mentioned, the amidourea receptor moiety has been utilised for anion sensing purposes within the Gunnlaugsson group.[105,106] Therefore, these receptors will also be discussed in Section 1.6. However, firstly a more detailed description on the signal transduction methods in colorimetric and fluorescent PET based 4-amino-1,8-naphthalimide derivatives will be given, as it is the sensing mechanism which occurs in many examples within the introduction of this thesis.

1.6 Colorimetric Sensing and Photoinduced Electron Transfer (PET) in 4-Amino-1,8-Naphthalimide Sensors

Figure 1.5 shows a 4-amino-1,8-naphthalimide derivative and the '*push-pull*' nature of the ICT excited state, caused by the electron donating amine and the electron withdrawing imide. Anion interaction in the vicinity of the 4-amino moiety can result in modulation of the ICT character, and hence, this can lead to changes in the absorption and fluorescence emission spectra of the fluorophore.

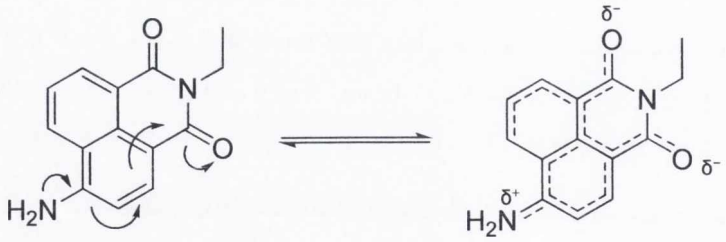


Figure 1.5: Schematic representation of the ICT excited state within the 4-amino-1,8-naphthalimide fluorophore.

The components of a PET sensor were discussed in Section 1.3 and an example of such a sensor is shown in Figure 1.6. Sensor **1a**, which was developed by Gunnlaugsson *et al.*,[107] contains a naphthalimide fluorophore, which functions as the signalling subunit and is the site of both excitation and emission, while the thiourea receptor binds the anion through hydrogen bonding. The function of the methylene spacer is to prevent ground state interactions between the receptor and the fluorophore and so, as in the case of an 'ideal'

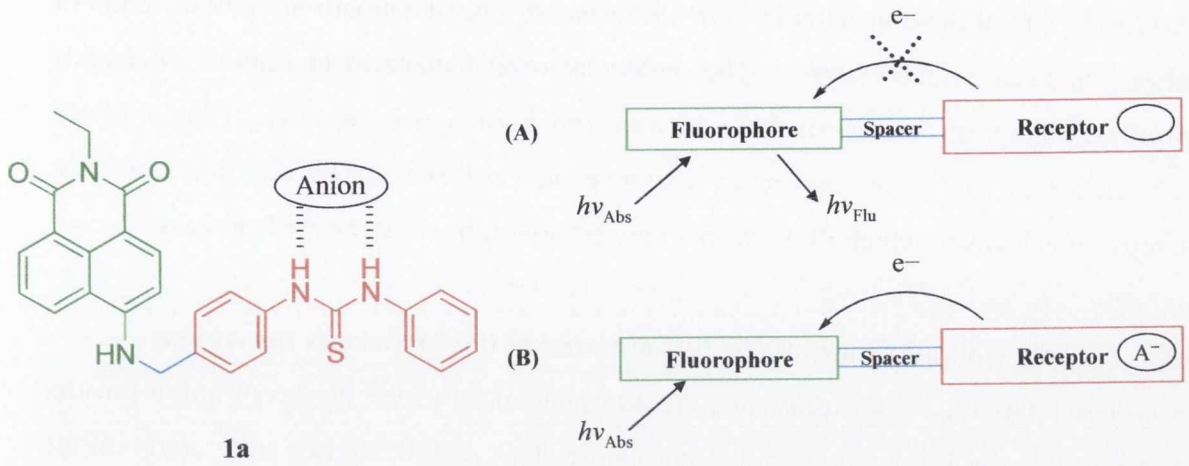


Figure 1.6: Sensor **1a**, which is based on the *fluorophore-spacer-receptor* model, and a schematic representation of the sensor in the **(A)** on and **(B)** off state.

PET sensor, the absorption spectrum of **1a** was not affected by the presence of anions, such as AcO^- or $H_2PO_4^-$, to any great extent. In contrast to this, the emission of **1a** was switched *'off'* upon anion recognition due to enhanced PET from the electron rich thiourea to the naphthalimide, as shown in the schematic representation in Figure 1.6. Hence, the changes in the emission intensity resulted from excited state reduction of the fluorophore by the electron rich anion complexed receptor. This mechanism functions particularly well for 4-amino-1,8-naphthalimide based sensors and target analytes such as cations, anions and neutral molecules have been 'sensed' in this manner.[9] Whether the emission is switched '*off*' or '*on*' for such PET sensors depends on the changes that occur in the oxidation or the reduction potential of the receptor, in comparison to that of the fluorophore, upon analyte recognition. Therefore, PET signalling systems have natural '*all or none*' switchability and in contrast to **1a**, guest-induced '*off-on*' fluorescence is also designable. In comparison to the schematic representation in Figure 1.6, the mechanism of

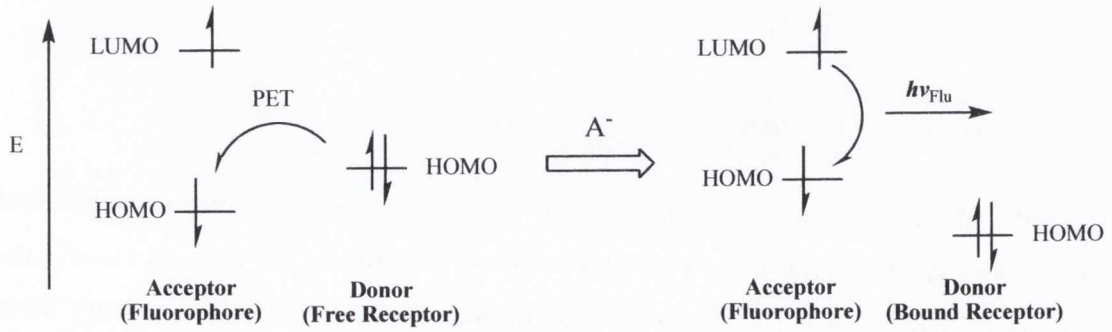


Figure 1.7: *Fluorophore-spacer-receptor* system in the **(A)** '*off*' state and the **(B)** '*on*' state.

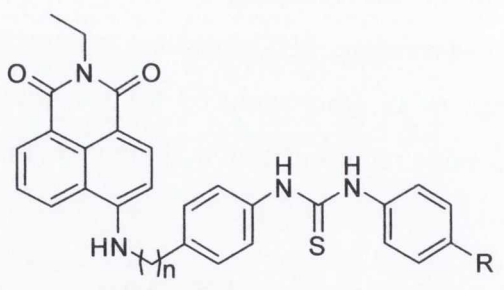
PET sensing can also be visualised from a somewhat more quantitative view in terms of frontier molecular orbital energies. The molecular orbital diagram in Figure 1.7 depicts '*off-on*' switching, in contrast to that which occurred for sensor **1a** above. Diagrams can also be constructed to depict '*on-off*' switching, as well as thermal back electron transfer, a self-repair mechanism, which PET sensors may employ following the PET process.[9]

1.7 Fluorescent and Colorimetric Naphthalimide Based Sensors for Anions

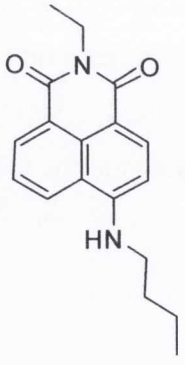
The following review discusses the advances made in the design of anion sensors that incorporate the 1,8-naphthalimide fluorophore. This review focuses particularly on the work carried out within the Gunnlaugsson group[14] over the past five years or so, as well as the recent work reported by various other researchers. The following examples are mainly grouped by the location of the anion receptor moiety on the naphthalimide fluorophore, which is commonly found at the 4-position or the 1,8-imide position, and by the structural similarities of the various anion receptor moieties employed. Finally, alternative sensing mechanisms involving the naphthalimide fluorophore will be discussed.

1.7.1 4-Amino-1,8-Naphthalimide Based Urea and Thiourea Sensors for Anions

As shown previously in Figure 1.5, modification of the 4-amino-1,8-naphthalimide moiety using a thiourea receptor led to the development of the colorimetric and fluorescent anion sensor, **1a**, due to the occurrence of both PET and ICT processes. In order to understand more fully the sensing process, derivatives **1b** and **1c**,[107] as well as **2**,[108] were



1a n = 1, R = H
1b n = 1, R = CF3
1c n = 2, R = CF3



2

synthesised and analysed in the presence of various anions. The absorption spectra of all three sensors in DMSO showed the presence of the ICT transition with λ_{max} at *ca.* 444 nm, which upon excitation gave rise to long wavelength emission at *ca.* 527 nm. Only minor changes were seen in the absorption spectra of **1a-1c** upon titration with AcO^- and $H_2PO_4^-$ and in the case of the latter (Figure 1.8, A) with **1b**, the ICT transition was slightly red-

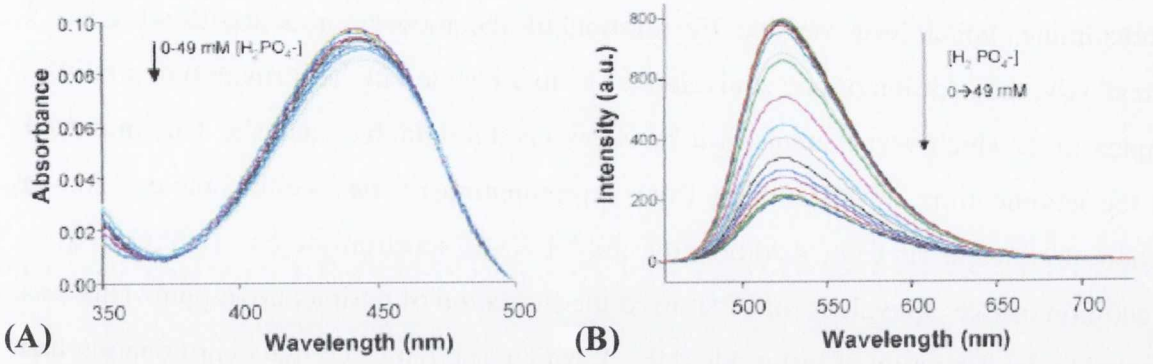


Figure 1.8: (A) The changes in the absorption spectra and emission spectra of **1b** upon titration with $H_2PO_4^-$ in DMSO.[107]

shifted. However, significant changes were seen in the fluorescence emission spectra of **1a-c**, such as shown for **1b** upon titration with $H_2PO_4^-$ in Figure 1.8 (B). The degree of fluorescence quenching observed for **1a-c** upon titration with AcO^- and $H_2PO_4^-$ also differed, depending on the nature of the substituent on the aryl receptors. Hence, the quenching of **1a** and **1c** was somewhat smaller due to the less acidic receptor and the longer spacer, respectively. The changes in the fluorescence emission of **1a** and **1b** upon titration with $H_2PO_4^-$ were fitted to a 1:1 stoichiometry, for which binding constants of $\log K_{1:1}$ = 2.9 (±0.1) and 3.7 (±0.1) were determined, respectively, using the non linear regression analysis program SPECFIT™.[109,110] As for the fluorescence quenching, the higher binding constant of **1b** reflects the increased acidity of the thiourea protons due to the electron withdrawing phenyl-CF_3 group present on the receptor. In contrast to the minor changes observed in the absorption spectra upon the addition of AcO^-, $H_2PO_4^-$, Cl^- or Br^-, sensors **1a-c** showed a response in their absorption spectra, Figure 1.9, when a large excess of F^- was added (*ca.* > 30 mM). Here, new transitions developed at both short and long wavelengths when the ICT transition was red shifted, which occurred with the formation of two clear isobestic points. The changes were accompanied by a striking colour change from yellow-green to purple, which was reversed upon the addition of

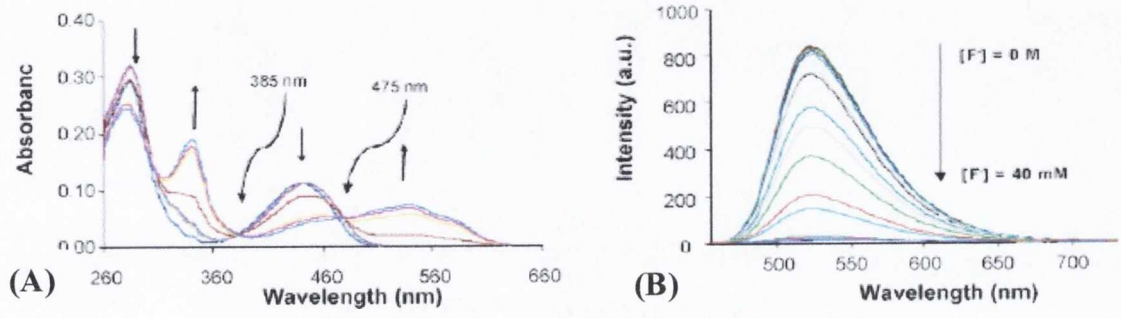
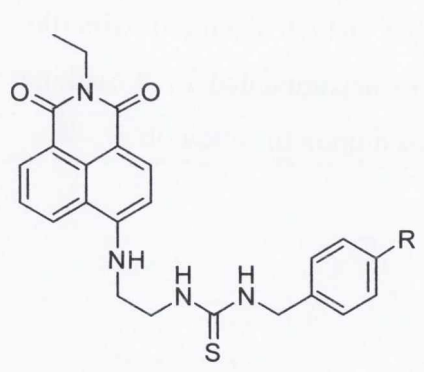


Figure 1.9: (A) The changes in the absorption and emission spectra (B) of **1b** upon titration with $H_2PO_4^-$ in DMSO.[107]

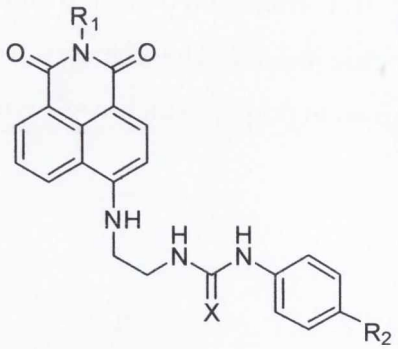
MeOH. These changes were assigned to the deprotonation of the 4-amino moiety of the naphthalimide, which was verified by titration of the model compound **2** with F^-.[108] Interestingly, the addition of one equivalent of F^- to **2** resulted in the formation of a HCO_3^- complex of **2**, which was characterised by X-ray crystallographic analysis. This indicated that the anionic form of **2**, resulting from deprotonation of the 4-amino moiety, led to fixation of atmospheric CO_2. Additionally, the ^1H NMR spectrum of **2** in DMSO-d_6 after the addition of two equivalents of F^- showed the formation of a triplet at 16 ppm. This was assigned to the formation of bifluoride (HF_2^-), which also indicated that deprotonation had occurred. For sensors **1a-c**, the changes in the absorption spectra upon titration with F^- were accompanied by almost complete quenching of the emission in DMSO. Excitation of the new long wavelength absorption at *ca.* 540 nm, which appeared at high concentrations of F^-, as shown in Figure 1.8, resulted in the formation of a new long wavelength emission band, which increased in intensity with the addition of further F^-.

The drastic colour change from yellow to purple observed upon deprotonation with F^- prompted the design of **3** by Pfeffer and Gunnlaugsson *et al.*.[111] It was anticipated that the acidic 4-amino moiety would take part in hydrogen bonding with the N-H protons of the thiourea receptor, hence, resulting in stronger anion-receptor interactions, particularly for $H_2PO_4^-$. Therefore, the design of receptors **1a-c** was modified by the introduction of an ethylamine spacer and also a benzylamine receptor, in order to introduce flexibility into the receptor.

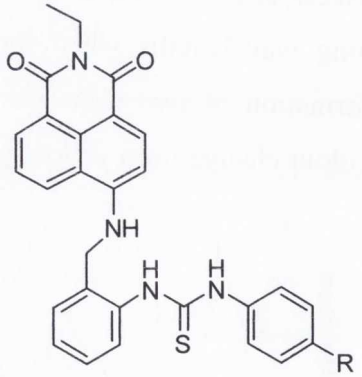
Indeed, ^1H NMR titrations of **3** in DMSO-d_6 clearly demonstrated that the binding of $H_2PO_4^-$ was significantly enhanced due to cooperation between all three of the N-H protons. The 4-amino proton was shifted by *ca.* 1.4 ppm in the presence of $H_2PO_4^-$ where



3 R = H



4a $R_1 = (CH_2)CH_3$ X = S, R_2 = H
4b $R_1 = (CH_2)CH_3$ X = S, $R_2 = CF_3$
4c $R_1 = (CH_2)CH_3$ X = O, $R_2 = CF_3$
4d $R_1 = (CH_2)_3CH_3$ X = S, $R_2 = NO_2$
4e $R_1 = (CH_2)C{=}CH_3$, X = S, R_2 = H



5a R = H
5b R = F

little or no shift was seen upon titration with AcO^-. In the case of F^-, significant broadening of all resonances was observed and, as seen for **2**, the addition of 2.5 equivalents showed the formation of HF_2^- which indicated that deprotonation had occurred. The ^1H NMR titration data for **3** was fitted for the formation of 1:1 complexes, using non linear regression analysis, for which binding constants of $\log K_{1:1}$ = 3.4 (±0.1) and $\log K_{1:1}$ = 3.6 (±0.1) were determined for $H_2PO_4^-$ and AcO^-, respectively. A lower binding constant was reported for the quenching of the emission of **1a** with $H_2PO_4^-$ ($\log K_{1:1}$ = 2.9 (±0.1), therefore, supporting the formation of a complex in which all three N-H's cooperatively bind. In contrast, the changes in the fluorescence emission spectra of **3** upon addition of AcO^- and $H_2PO_4^-$ in DMSO were only minor when compared to those observed for **1a**, showing that the flexible ethyl chain resulted in a reduced rate of PET, caused by the greater distance between the far components of the sensor.

In an attempt to achieve more significant changes in the fluorescence emission spectra of **3** upon addition of anions, sensors **4a-c** were also designed by Gunnlaugsson *et al.*.[112] The design, synthesis and photophysical properties of these receptors are not discussed here, as they are the subject of Chapter 2 of this thesis.

Subsequent to the reports of sensors **4a-c**, Ying-Li *et al.* [113] reported the anion binding capabilities of the nitro derivative, **4d**, in DMSO. Its recognition for various anions was investigated by UV-Vis absorption, fluorescence and ^1H NMR (DMSO-d_6) spectroscopy. These studies showed that receptor **4d** could selectively recognise F^- and AcO^- over Cl^-, Br^-, I^-, HSO_4^- and ClO_4^-, as shown in Figure 1.10. In contrast to that seen for sensor **3**, larger changes were observed in the absorption spectra of **4d** upon addition of only eight equivalents of F^- and AcO^-. This was most likely due to the presence of the electron withdrawing chromogenic *p*-nitro-phenyl group. These changes occurred with a

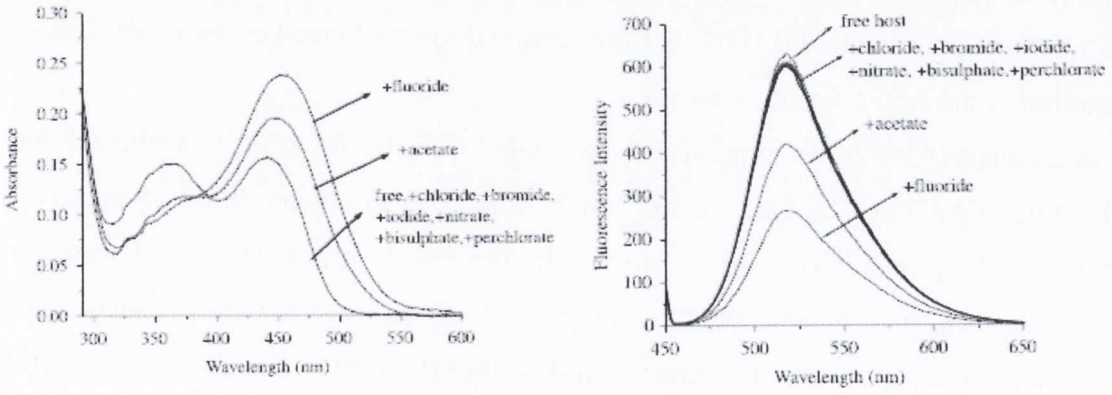


Figure 1.10: (A) The changes in the absorption spectra of compound **4d** (1×10^{-5} M) after addition of eight equivalents of various anions in DMSO. **(B)** The corresponding changes in the emission spectra of **4d** [0.5×10^{-5} M] after the addition of 8 equivalents, λ_{max} = 444 nm.[113]

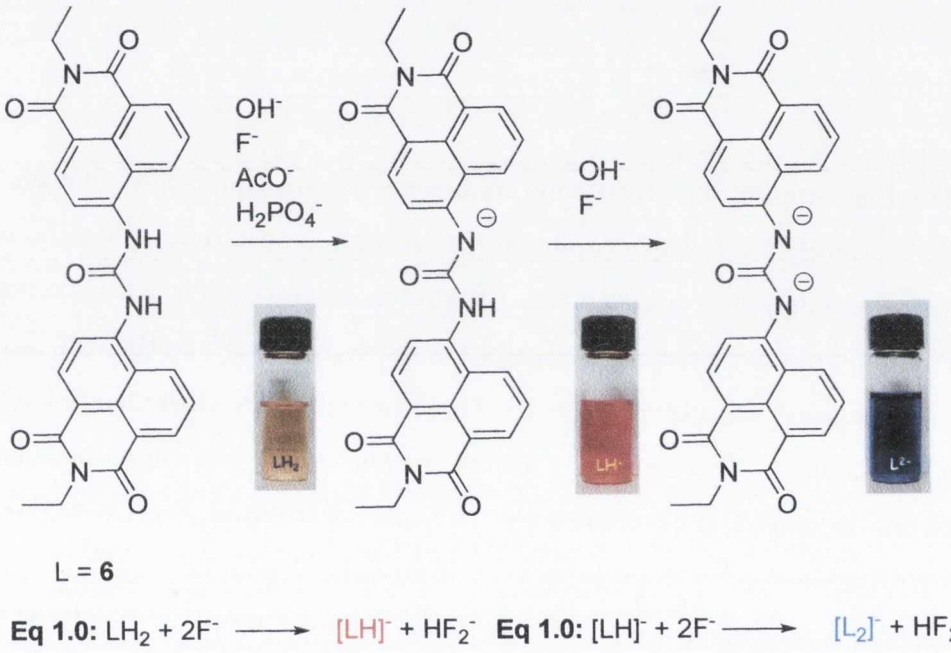
colour change from greenish yellow to bright yellow. These were also followed by a concomitant change in the fluorescence emission, which was quenched by 81% and 55% upon the addition of 0.17 mM F^- and AcO^-, respectively. The changes in the absorption spectra were fitted as above and resulted in high binding constants of $\log K_{1:1} = 4.48$ (±0.1) and $\log K_{1:1} = 4.16$ (±0.1) for F^- and AcO^-, respectively. As for **1a-c**, large changes in the absorption spectra were also observed upon the addition of large concentrations of F^- (*ca.* 70 equivalents) and were assigned to deprotonation of the 4-amino moiety. ^{1}H NMR titrations of **4d** with F^- were also carried out in DMSO-d_6 and, interestingly, it was reported that the formation of the HF_2^- triplet at 16 ppm was not observed, even after the addition of three equivalents of F^-. Therefore, it was concluded that deprotonation did not occur at low concentrations of F^- and that cooperative binding between F^- and **4d** occurred in DMSO-d_6.

As discussed in Section 1.5, various researchers have recently incorporated fluorescent and/or colorimetric organic sensors into materials for sensing. Subsequent to the reports of sensors **4a-c**, Callan *et al.*.[114] reported the incorporation of the structurally similar sensor, **4e**, into poly(mercaptoproplymethyl) siloxane (PMPMS). The polymer bound sensor showed substantial changes in its absorption and fluorescence emission spectra upon titration with F^- in DMSO, with other anions having virtually no effect. An increase in the absorption of the ICT band was observed and it was concluded that these changes were due to a solvent effect with the polymer, as no such absorption increase was observed in MeCN. Concomitant quenching of the fluorescence emission (*ca.* 53% with 70 mM F^-) was also observed. The changes in the fluorescence emission spectra of the polymer upon titration with AcO^-, $H_2PO_4^-$ were also fitted ($\log\beta_{1:1} = 3.10$ and 2.98, respectively) and higher binding constants were determined than for those obtained for the free sensor, **4e** ($\log\beta_{1:1} = 2.55$ and 2.07, respectively). Furthermore, it was concluded by titration of the polymer with TBAOH that the observed spectral changes were not due to deprotonation of the acidic 4-amino moiety.

In an attempt to further improve on the design of **3**, Pfeffer *et al.*[115] evaluated the anion binding capabilities of **5a** and **5b**, which were structurally modified to preserve cooperative binding of $H_2PO_4^-$ whilst restoring the fluorescent properties to that seen for **1a-c**. The electron rich *o*-substituted amino benzyl amine spacer was introduced to facilitate pre-organisation and as for sensors **4a-d**, a phenyl receptor was also employed to increase the acidity of the thiourea N-H protons. Indeed, this design proved somewhat successful with cooperative binding of $H_2PO_4^-$ being observed for both **5a** and **5b**, as determined by ^{1}H NMR titrations in DMSO-d_6. Binding constants of $\log K_{1:1} = 3.7$ and 4.1,

respectively, were estimated from these titrations, as after the addition of three equivalents of $H_2PO_4^-$ the N-H resonances disappeared. As anticipated, the binding constant for **5a** was larger than that reported for the precursor **3**. However, only minor quenching of the fluorescence of **5a** was observed, 6.5% and 31% with $H_2PO_4^-$ and AcO^-, respectively. In contrast, the fluorescence emission of the fluoro-based receptor, **5b**, was quenched by 36% and 60% after the addition of only five equivalents of $H_2PO_4^-$ and AcO^-, respectively.

Fabbrizzi *et al.*[116] have reported the symmetrical bis-naphthalimide based sensor, **6**, which does not contain a spacer, but consists of two naphthalimide fluorophores connected at the 4 position *via* a urea moiety (Figure 1.11).



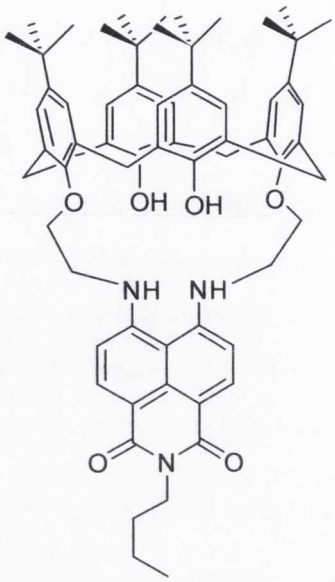
L = **6**

Eq 1.0: $LH_2 + 2F^- \longrightarrow [LH]^- + HF_2^-$ **Eq 1.0:** $[LH]^- + 2F^- \longrightarrow [L_2]^- + HF_2^-$

Figure 1.11: The interaction of sensor **6** with various anions and the corresponding colour changes upon deprotonation.[116]

In the presence of excess F^-, **6** underwent stepwise deprotonation in DMSO of both urea N-H protons, which gave rise to two distinct sets of changes in the visible region of the absorption spectra and therefore, large colour changes, which were clearly visible to the naked eye, as shown in Figure 1.11. These results are not surprising, as the urea protons are located directly at the aryl moiety. The changes in the absorption spectra at the different concentrations ranges of F^- were reversed upon addition of H_2O. Additionally, the formation of $[L]^{2-}$ was supported by titration of sensor **6** with TBAOH and also using ^1H NMR spectroscopy in DMSO-d_6.

The first naphthalimide based calixarene for anion sensing, **7**, was recently reported by Qian and Yoon *et al.* [117]. The naphthalimide fluorophore was connected to the calixarene scaffold *via* the 4-amino and the 5-amino ethyl spacers and therefore, provided



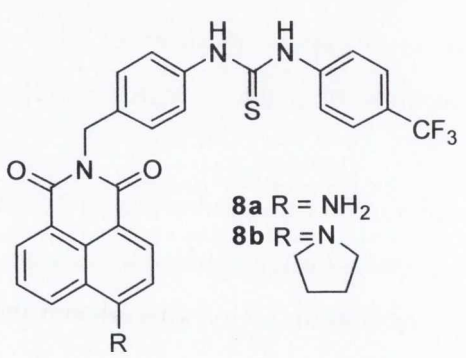
7

a hydrogen bonding pocket, in which four hydrogens were available to interact with anions. Sensor **7** exhibited a typical naphthalimide absorption spectrum in MeCN, which upon excitation at 435 nm, gave rise to a broad fluorescence emission spectrum centred at *ca.* 490 nm. Upon titration with anions such as $H_2PO_4^-$, HSO_4^-, AcO^-, I^-, Br^- and Cl^-, only quenching of the emission was observed for F^-. These changes were attributed to hydrogen bonding and consequent deprotonation, in which the latter was supported by the appearance of the HF_2 triplet at 16 ppm in the ^1H NMR spectrum of **7** in DMSO-d_6 upon titration with F^-.

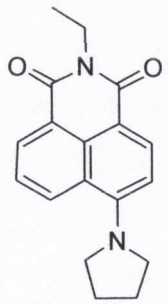
The sensors discussed in this section contain an anion receptor moiety at the 4-position of the naphthalimide fluorophore. However, as previously mentioned, sensors have been designed which contain an anion receptor moiety connected to the naphthalimide *via* the imide moiety. These will be discussed in the following section.

1.7.2 N-Imide Functionalised Naphthalimide Sensors

The structurally similar compounds to **1a-c**, **8a** and **8b**, were also designed and investigated by Gunnlaugsson *et al.* [118,119] and showed that PET quenching occurred upon



8a R = NH_2
8b R = N



9

the addition of anions. As for sensors **1a-c**, no significant changes were observed in the absorption spectra upon titration with the various anions. The reference compound, **9**, which lacks an anion receptor, showed no changes in its absorption or emission spectra upon titration with anions. As in the case of **1a-c**, strong colorimetric detection of F^- by **8a** was also achieved, but at much lower concentrations, *ca.* 0.2 mM. However, no strong colour changes were observed for either **8b** or **9** upon titration with F^-, which both lack the 4-amino proton, indicating that the colour changes were indeed due to deprotonation of this moiety, as previously seen for **1a-c**.[107,119] Similarly to **1a-c**, the fluorescence emission of **8a** was quenched upon titration with AcO^- and a second binding interaction with the 4–amino moiety was observed at high concentrations of anion. Both $H_2PO_4^-$ and F^- also gave rise to quenching of the fluorescence of **8a** and **8b**, where for **8a** the emission was quenched by *ca.* 60% and 95% upon addition of 44 mM $H_2PO_4^-$ and 32 mM F^-, respectively. The changes in the emission of **8a** and **8b** upon titration with anions were analysed using SPECFIT™. Comparison of the binding constants determined to those previously obtained for **1a-c** showed that the location of the anion receptor did not affect the sensitivity of the anion sensing to any great extent.[119] For example, the quenching of the fluorescence of **8a** $\log K_{1:1} = 3.5$ (±0.03) by $H_2PO_4^-$, was of the same magnitude as that observed for **1b** $\log K_{1:1} = 3.7$ (±0.1) under identical conditions. It has been previously shown that the fluorescence emission of such naphthalimide H^+ sensors was only switched on when the receptor moiety was located at the 4-amino moiety,[120] therefore, these compounds are the first examples of naphthalimide based sensors that enable bi-directional PET quenching of their emission by anions.

Pischel *et al.* [121] described the synthesis and photophysical characterisation of the fluorophore-spacer-receptor$_1$-spacer-receptor$_2$ system, **10**, in which PET also occurs through the imide of the naphthalimide moiety in MeCN, upon interaction with cations and anions. The absorption spectrum of sensor **10** in MeCN exhibited transitions at 332 nm and

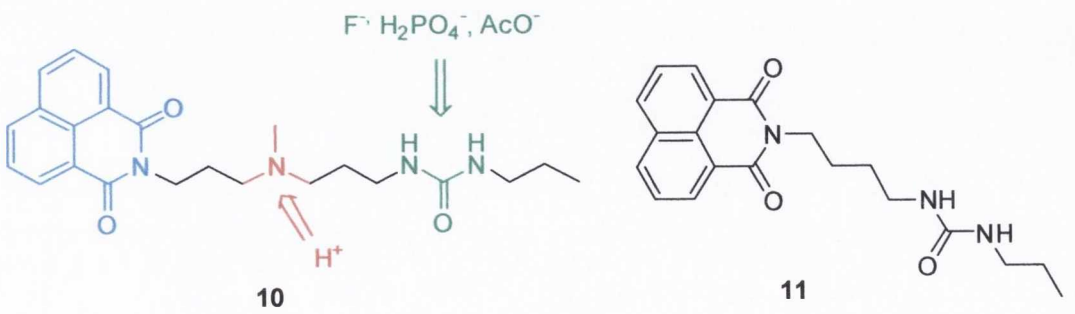
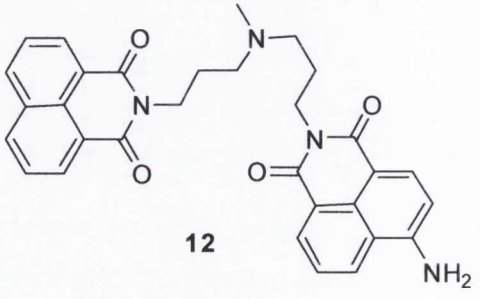


Figure 1.12: The Fluorophore-Spacer-Receptor$_1$-Spacer-Receptor$_2$, **10**, with protons (H^+) and anions (A^-) as inputs and the reference compound, **11**.[121]

345 nm, which upon excitation at 325 nm, gave rise to a fine structured blue emission bands at 364 nm and 380 nm, and a shoulder at 400 nm. Protonation of the amino group of **10** with one equivalent of trifluoroacetic acid (TFA) lead to a 20 times enhancement in the fluorescence of **10**, due to blocking of the PET pathway, however, in contrast to this, anion binding to the urea lead to quenching of the fluorescence emission by PET. Additionally, titrations of mono protonated **10** with F^- lead to quenching of the emission and the simultaneous binding of cations and anions also resulted in quenching of the emission, most likely through electrostatic interactions between the protonated ammonium and the anions. Due to the observed fluorescence quenching of **10** by the amino function, binding constants were obtained by titrating **11** with anions. Significant fluorescent quenching of **11** was observed and, hence, values for the 1:1 complexation of **11** with F^-, AcO^- and $H_2PO_4^-$ were determined, which gave binding constants that were considerably lower than those reported for **8a** and **8b**. ^1H NMR titrations of **10** in DMSO-d_6 were also carried out and the binding constants determined were slightly lower than those obtained from the fluorescence titrations with **11**. The authors speculated that the lower affinity was possibly due to self-aggregation phenomena and competition of the binding site with DMSO. In summary, the blocking or enabling of PET processes resulted in the development of a system, which constitutes an example of functionality integrated two-input inhibit (INH) logic at the molecular level, using protons and anions as chemical input species and the fluorescence of 1,8-naphthalimide fluorophore as output.

Pischel *et al.*[122] extended their design of such logic gates with the bis-naphthalimide sensor **12**, in which different fluorescent responses were triggered by protonation and deprotonation of the sensor with H^+ and F^- ions in MeCN. In contrast to **10**, which contains the urea anion binding receptor moiety, sensor **12** was designed to function solely *via* protonation or deprotonation of the acidic N-H moieties. Additionally, in contrast to the bis-napthalimide **6**, which was reported by Fabbrizzi and co-workers,[116] **12** is un-symmetrical and, therefore, the independent changes for each fluorophore were



12

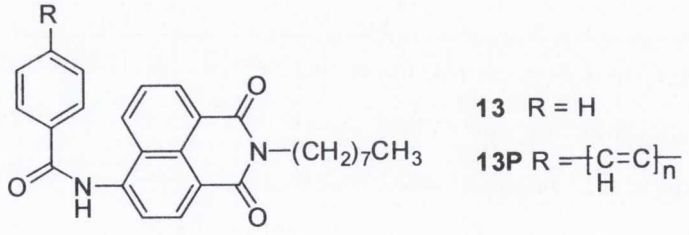
identifiable. Both naphthalimide fluorophores were linked by an aliphatic spacer chain, which consists of a central tertiary amine, the site of protonation and subsequent

deprotonation. Upon protonation, PET quenching of the 1,8-naphthalimide fluorophore was blocked. This resulted in concomitant electronic energy transfer (EET) between both fluorophores. The protonated tertiary amine could then be deprotonated by F^- (< 20 μM), therefore, reactivating PET, which resulted in fluorescence emission quenching of *ca.* 41%. Higher concentrations of F^- (> 1 mM) also resulted in deprotonation of the 4-amino moiety, which lead to further quenching (*ca.* 93%). Therefore, the interplay of PET, EET and ICT gave rise to a one channel fluorescence output with three signal levels (low, medium and high), which the authors classified as a ternary NOR logic gate mimic.

The napthalimide based sensors discussed in this section and also in Section 1.7.1 were functionalised at the 4-amino- or the 1,8-imide site of the naphthalimide structure with alkyl or aromatic amines. Naphthalimide based sensors have also been reported, which are functionalised with an amide moiety at the 4-position, and hence, signal the presence of anions upon deprotonation of this functional group.

1.7.3 4-Amido-1,8-Napthalimide Based Sensors for Anions

The 4-amido based naphthalimide sensor, **13**, was designed and investigated by Tian *et al.*[123] The absorption spectrum of **13** in MeCN exhibited a λ_{max} at 360 nm, which upon excitation gave rise to a broad emission spectrum, as shown in Figure 1.13. It was found that upon titration of **13** with the TBA salts of F^-, Cl^-, Br^- and I^-, large changes were only observed in both the absorption and the emission spectra upon titration with F^-, with



13 R = H

13P R = $-\{C=C\}_n-$
H

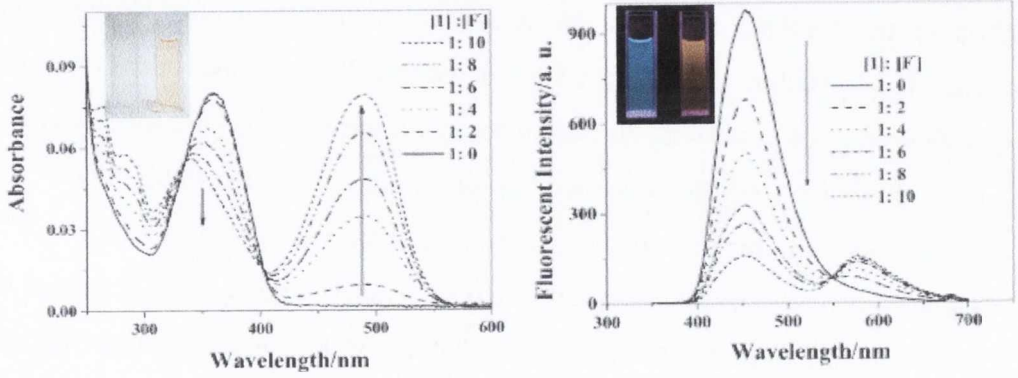
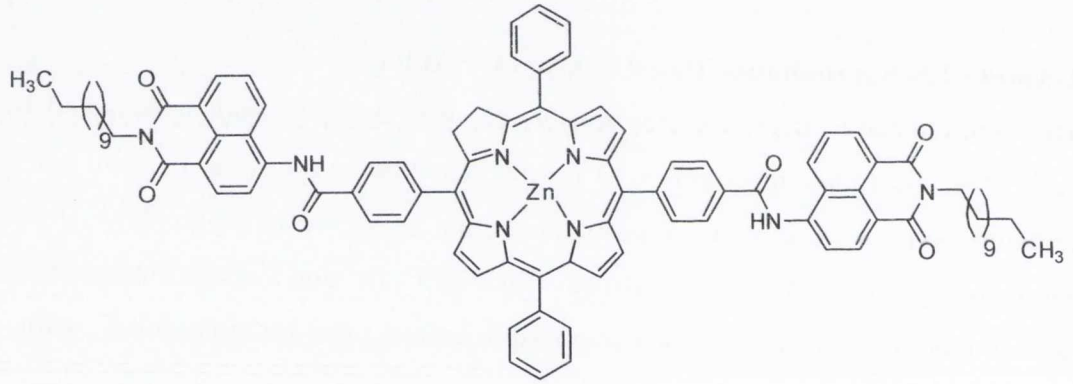


Figure 1.13: The changes in the absorption spectra of **13** [1 × 10^{-5} M] upon addition of F^- in MeCN and the corresponding change in the colour of the solution from colourless to yellow (10 equivalents of F^-). Similarly, the changes in the fluorescence spectra of **13** [1× 10^{-5} M], λ_{ex} = 340 nm.[123]

concomitant colour changes from colourless to yellow, while the fluorescence emission was changed from blue to orange. As seen above for sensor **4a**, Tian *et al.*[124] have also recently employed **13** in the development of fluorescent sensing polymers. Polymer **13P** consists of polyphenylacetylene monomer units which are functionalised with the F^- selective sensor, **13**, in the side chains. The absorption spectrum of **13P** also exhibited a λ_{max} at 360 nm, however, a slight shoulder was present at *ca.* 490 nm due to π-π^* transitions of the polymer backbone. The fluorescence spectrum of **13P** was of lower intensity than that observed for **13**, possibly due to PET from the polymer backbone to the excited state of the naphthalimide fluorophore. Similarly to that seen for **13,** the ability of the polymer, **13P** [1×10^{-5} M] to sense anions in MeCN was investigated and the changes observed were similar to those observed for the free sensor **13**.

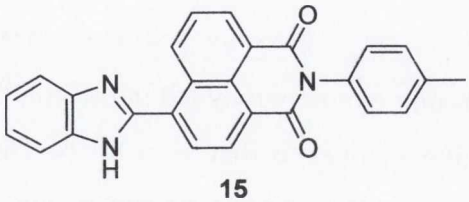
Further utilising this deprotonation mechanism, Tian *et al.*[125] have also covalently attached two 4-amido-1,8-naphthalimide fluorophores to a zinc porphyrin core resulting in



14

a novel F^- ion triggered dual fluorescent molecular switch, **14**. The absorption spectrum of **14** consisted of a naphthalimide absorption at *ca.* 360 nm and the typical Soret and Q bands of the porphyrin at 417 nm, 550 and 590 nm, respectively.[126] However, the addition of F^- resulted in the formation of a new absorption band at 500 nm, significant of deprotonation of the 4-amino moieties and a colour change from pale to dark orange occurred. The deprotonation also resulted in enhanced PET to the porphyrin, which quenched its fluorescence emission. Furthermore, in the presence of F^-, the fluorescence emission of the porphyrin could be regulated '*on-off*' upon excitation at 365 nm or '*off-on*' upon excitation at 504 nm, due to changes in the energy pathways present.

Extending on this work, Tian *et al.*[127] have recently reported the benzoimidizole functionalised naphthalimide, **15**, for the sensing of F^-, a design that also functions *via* deprotonation. The absorption spectrum of **15** showed a λ_{max} at 378 nm for the ICT transition, which was shifted by *ca.* 100 nm and also decreased in absorbance with the formation of a new band at *ca.* 476 nm, upon the addition of F^- in THF. A concomitant



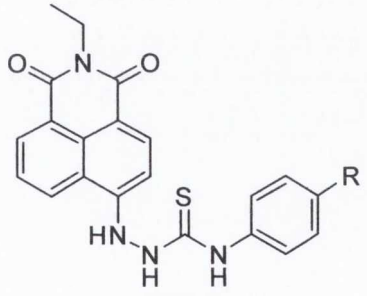
15

colour change from colourless to magenta was also observed. Upon excitation at 378 nm, **15** exhibited a broad fluorescence emission band centred at 478 nm. Upon titration with F^- quenching of the emission and a red shift in the spectrum to 603 nm was observed. The deprotonation was confirmed using ^1H NMR titration in DMSO-d_6, for which the resonance pertaining to the N-H proton of compound **15** disappeared as the concentration of F^- was increased and the resonances for adjacent protons on the benzoimidazole moiety were also shifted upfield.

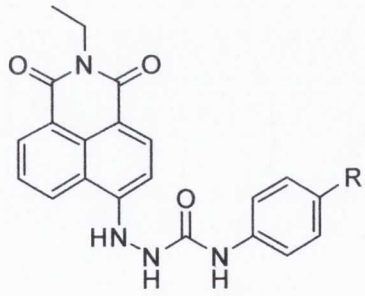
The examples outlined in this section, as well as in the previous sections, detailed the sensing of anions in organic solution such as DMSO, MeCN and THF. However, the following section describes two naphthalimide based anion sensors, which are capable of sensing in more competitive aqueous based solutions.

1.7.4 4-Hydrazine Based Urea and Thiourea Naphthalimide Sensors for Anions

Gunnlaugsson *et al.*[16,128] have reported the novel colorimetric hydrazine based naphthalimide anion sensors, **16a** and **16b**, for use in aqueous solution. In order to gain an understanding of the anion binding ability of the thiourea sensors, **16a** and **16b**, titrations



16a R = CH_3
16b R = CF_3



17a R = H
17b R = CH_3
17c R = CF_3

were initially carried out in DMSO solution. Sensor **16b** showed a broad absorption band centred at 441 nm and a smaller shoulder at 560 nm, which upon addition of anions, such as of AcO^-, $H_2PO_4^-$ and F^-, increased in intensity at the expense of the 441 nm absorption. Furthermore, a new band at 350 nm and two clear isobestic points at 465 and 380 nm were also observed. These changes occurred with a yellow to purple colour change, which was clearly visible to the naked eye. By plotting the changes at 560 nm, as a function of

$-\log[AcO^-]$, a sigmoidal curve was observed that changed over two log units, which is characteristic of 1:1 binding.

It was postulated that the 4-amino moiety may aid in the binding, hence, giving rise to such colour changes, in a similar manner to that seen for **6**. The addition of a large excess of AcO^- or $H_2PO_4^-$ to **16a** and **16b** did not give rise to any additional changes in absorption spectra. However, when excess F^- was used, additional colour changes were observed that were attributed to deprotonation of the 4-amino naphthalimide moiety. The deprotonation was also verified using ^1H NMR titration in DMSO-d_6. The most important result from the studies of **16a** and **16b** was that upon addition of competitive hydrogen bonding solvents, such as MeOH, the colour changes were not reversed. Therefore, titrations were carried out in 1:1 (v/v) EtOH-H_2O buffered solutions at pH 7.1 and pH 7.3 for **16a** and **16b** (Figure 1.14), respectively. On both occasions, titrations with anions gave rise to the same general spectral and colour changes as described in DMSO above. These changes were fitted and it was shown that **16a** had a higher affinity for AcO^- ($\log\beta$ = 3.4 ±0.1)), over $H_2PO_4^-$ ($\log\beta$ = 2.2 (±0.1)) and F^- ($\log\beta$ = 1 (±0.2)). These results clearly demonstrated the feasibility of the use of charge neutral anion receptors in mixed aqueous media, which was a significant stepping stone towards real application of such sensors in competitive media.

In contrast to these results, the urea based sensors **17a-c** were only able to bind anions in aprotic solvents, such as DMSO.[17,129] These three sensors showed similar changes in their absorption spectra to those above upon binding to anions, such as AcO^-,

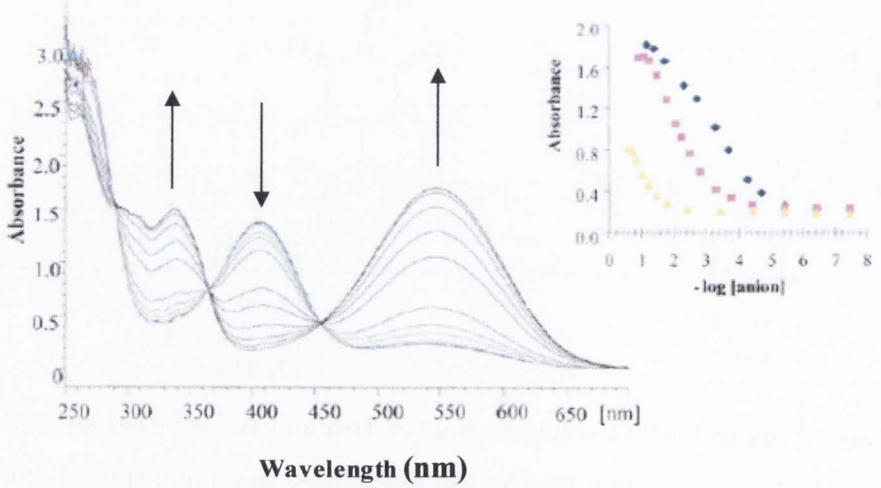


Figure 1.14: The changes in the absorption spectra of **16b** upon addition of F^- in 1:1 EtOH-H_2O. **Insert:** The changes at 548 nm as a function of -log[anion]: •) AcO^-, ■) F^-, and ▲) $H_2PO_4^-$.[128]

$H_2PO_4^-$ and F^- in DMSO, Figure 1.15. Also, upon excitation of the ICT transition, the addition of anions resulted in quenching of the fluorescence emission or a shift to longer

wavelengths. Additionally, ^{1}H NMR titrations in DMSO-d_6 demonstrated that AcO^- was recognised through 'pure' hydrogen bonding while the interactions for $H_2PO_4^-$ and F^- were due to initial hydrogen bonding followed by full or partial deprotonation.

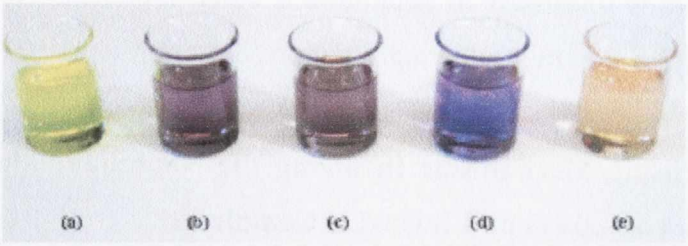


Figure 1.15: The chromogenic response of DMSO solutions of sensor **17c** [1 × 10^{-3} M] upon interaction with various anions: (a) Sensor **17c;** (b) **17c** + 1 eq. AcO^-. (c) **17c** + 1 eq. $H_2PO_4^-$ (d) **17c** + 1 eq. F^- (e) **17c** + F^- (excess).[129]

Fu *et al.*[130] have also utilised the colorimetric and fluorescent properties of 4-hydrazine based naphthalimides in the design and synthesis of sensor, **18**, which showed highly selective fluorescent sensing of pyrophosphate (PPi) in aqueous solution, as determined from fluorescence titrations with anions. The guanidiniocarbonyl pyrrole receptor, which was designed specifically to satisfy the geometrical requirements of PPi, was attached to the 4-amino position *via* a hydrazine spacer, Figure 1.16. Molecular modelling studies showed the appropriate size and geometry of the PPi anion with the receptor of **18**. The titrations were carried out in the competitive media of 90% H_2O-DMSO (v/v, 10 mM HEPES, pH = 7.4) with the Na^+ salts of F^-, Cl^-, AcO^-, NO_3^-, SO_4^-

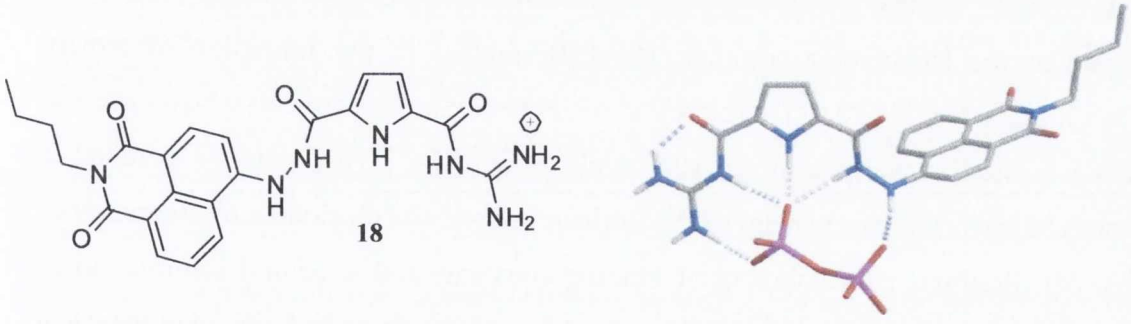


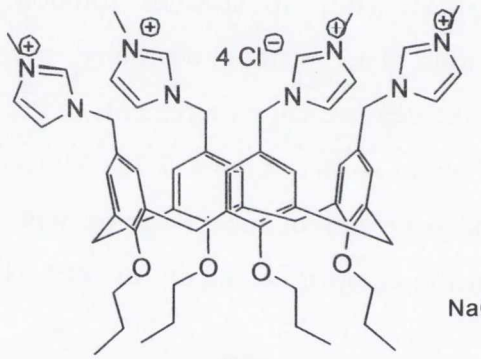
Figure 1.16: (A) The structure of **18** and **(B)** the calculated energy minimized structure for the complex between receptor **18** and PPi.[130]

and HCO_3^-. The biologically important anions ATP, AMP, ADP and PPi were also tested. Excitation of the naphthalimide ICT absorption band of **18** (460 nm) resulted in fluorescence emission at 510 nm, which was enhanced only upon addition of PPi, with a concomitant bathochromic shift from 510 to 514 nm. Job plot analysis indicated the formation of a 1:1 complex with PPi and a binding constant of $\log K_{1:1}$ = 1.9 (± 0.2) was obtained by a nonlinear least-square fitting method.

The 4-hydrazine based naphthalimide based anion sensors and the previously described 4-amino, 4-amido and N-imide naphthalimide-based sensors function *via* the '*binding site-signalling subunit*' approach for which both these entities are covalently attached. However, and as discussed in Section 1.3, other approaches to anion sensing exist, such as those described in the following section.

1.7.5 Alternative Sensing Mechanisms Involving the Naphthalimide Fluorophore: Assemblies, Displacement Assays and Inclusion Complexes

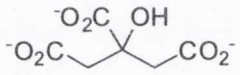
Compounds **19a-c** were utilised by Pishel *et al.*[131] in the assembling of a novel citrate sensing ternary complex. The components of the ternary complex were the water soluble imidizolium-substituted calix[4]arene, **19a**, the fluorescent aminodiacetate derivative of 1,8-naphthalimide, **19b**, and the trianion, citrate, **19c**. The addition of citrate



19a



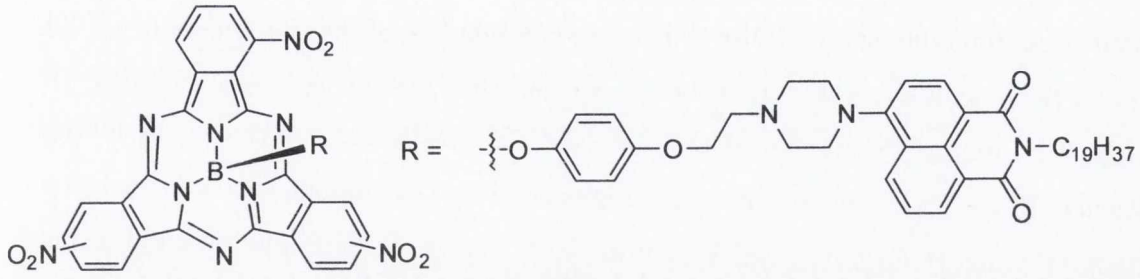
19b



19c

and tartrate to the Host:Guest complex **19a:19b** resulted in the formation of ternary complexes $\log K_{1:1} = 4.79$ (±0.01) and $\log K_{1:1} = 3.99$ (±0.05), respectively, which gave rise to variation in the fluorescence of the **19b**, while AcO^-, SO_4^{2-}, NO_3^- and Cl^- resulted in only minor changes. The mechanism of the intricate sensor was elucidated by fluorescence titrations, pH titrations, establishment of binding constants and structural information as obtained by ^1H NMR spectroscopy. Overall, the authors described the photophysical observations at pH 7 as follows: Complexation of the ammonium form of **19b** by **19a** gave rise to significant amounts of the amino form of **19b**, which caused a strong fluorescence quenching. The addition of citrate or tartrate to the binary complex lead to the recovery of the ammonium form of **19b**, resulting in a fluorescence enhancement.

In an alternative approach to the assembly of the ternary complex above, Tian *et al.* [132] have reported the subphtalocyanine (SubPc) based F^- sensor, **20**, in which F^- resulted in dissociation of the axial coordinated 1,8-naphthalimide based ligand. This sensing mechanism is reminiscent of indicator displacement assays, which were discussed in Section 1.3.



20

Excitation of the ICT absorption maxima of the naphthalimide (390 nm) in THF resulted in a weak emission at 495 nm, while excitation at 500 nm gave rise to a characteristic SubPc fluorescence at 578 nm.[133] The weak naphthalimide fluorescence was postulated as being due to excitation energy transfer (EET) from the naphthalimide chromophore to the SubPc chromophore, as a consequence of spectral overlap. It was reported that the addition of F^- to **20** resulted in the displacement of the naphthalimide moiety, which restored its emission, which in turn resulted in the quenching of the fluorescence emission of the SubPc. These events also gave rise to large changes in the visible region of the absorption spectra of the SubPc. The changes in the absorption spectra for F^- were fitted using the Benesi-Hildebrand equation,[134] which gave a high binding constant of $\log K_{1:1} = 5.11$. As the intensity of the fluorescence at 495 nm increased with a concomitant decrease at 578 nm, sensor **20** can be referred to as a ratiometric anion sensor.

As for the calixarene cavity of **19a**, cyclodextrins, which are a group of naturally occurring cylcic oligomers of D-glucopyranose, have been shown to form inclusion complexes with a variety of organic compounds in aqueous solution. Fu *et al.*. [135] have recently described the fluorescent behaviour of a 4-amino-1,8-naphthalimide derived β-cyclodextrins, **21a** and **21b**, in which the latter displayed large enhancements in its

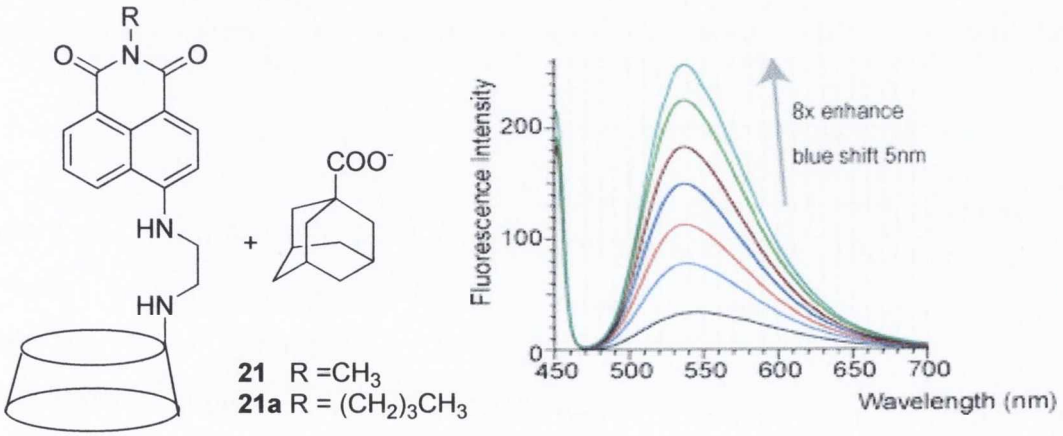


Figure 1.17: The structure of the naphthalimide derived cyclodextrin and adamantine-1-carboxylate and the corresponding changes in the fluorescence of **21a** (10 μM) upon titration with Na^+ adamantine-1-carboxylate in Tris-HCl (20 mM, pH 7.4).[135]

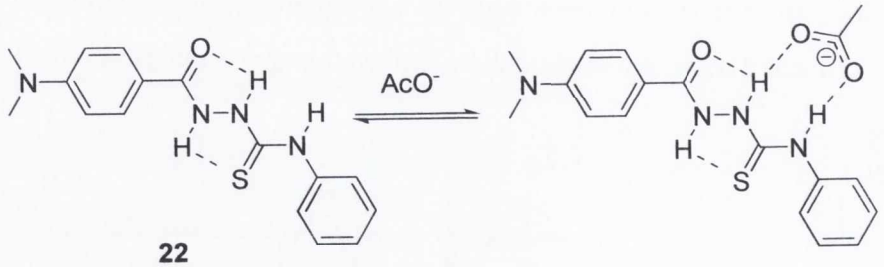
fluorescence upon complexation with various cyclic and acyclic aliphatic acids, such as adamantane-1-carboxylic acid, Figure 1.17. In contrast, the guest induced fluorescent change of **21a** was minor. The conformations of the two systems were also investigated using induced circular dichroism (ICD), 2D NOESY NMR and molecular modelling experiments. From these studies, it was concluded that **21a** adopts the self inclusion conformation while **21** does not, which is most likely due to the hydrophobic butyl group of **21a**. Upon anion binding, exclusion of the fluorophore of **21a** from the cyclodextrin cavity gave rise to an enhancement in its fluorescence emission spectra.

1.8 Neutral Amidourea and Amidothiourea Based Sensors for Anions

As mentioned in Section 1.5.1, the classical urea and thiourea moieties have been combined with an amide, in an attempt to improve on their anion binding capability. In the case of a thiourea, these new anion receptor moieties have been referred to as amidothioureas or *N*-benzamidothioureas. The following sections detail the recent reports within the literature, which make use of this anion receptor moiety for the detection of anions.

1.8.1 Colorimetric and Fluorescent Amidoureas and Thioureas

In 2002 Jiang *et al.*[104] presented the first example of an amidothiourea receptor for anion sensing purposes. The *N*-*p*-(dimethylamino)benzamido-*N'*-phenylthiourea, **22**, consists of a dual fluorescent reporter *p*-(dimethylamino)benzamido (DMABA) which is linked by a rigid hydrazine spacer to a thiourea moiety. AM1 calculations showed that the



22

Figure 1.18: Hydrogen bonding with acetate.[104]

most stable conformation of **22** was one in which two five-membered rings were formed *via* intramolecular hydrogen bonds, as shown for **22** and its corresponding AcO^- complex, Figure 1.18. The absorption spectrum of **22** in MeCN showed a λ_{max} at 311 nm, which upon the addition of certain anions, increased in absorption with concomitant increases and decreases at 360 and 280 nm, respectively (Figure 1.19). Of the various anions titrated (AcO^-, $H_2PO_4^-$, HSO_4^-, ClO_4^-, Cl^-, F^- and Br^-) a high sensitivity and selectivity towards

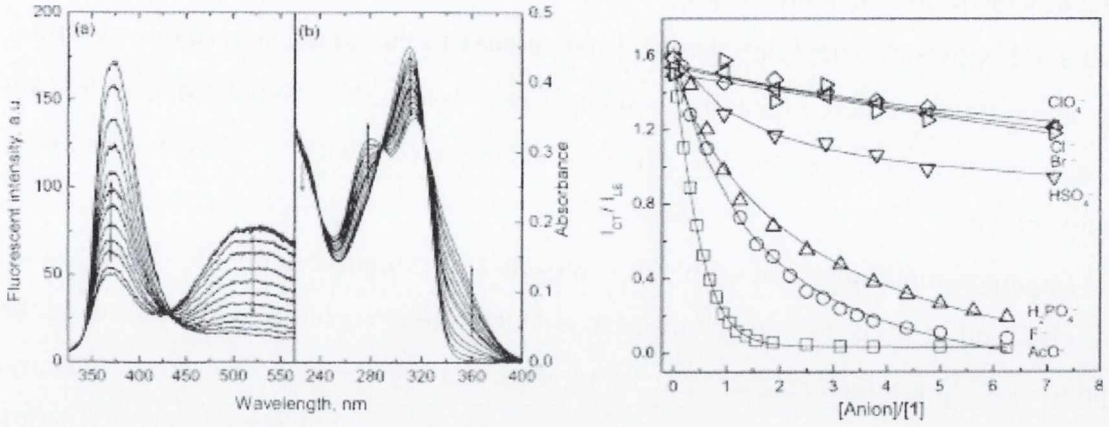
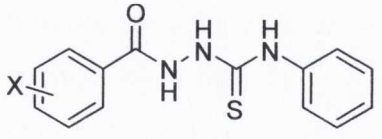


Figure 1.19: The changes in the absorption spectra of **22** upon titration with AcO^- in MeCN and the plots of the LE to CT fluorescence maximum intensity ratio of **22** versus anion concentration, fitted to 1:1 binding stoichiometries.[104]

AcO^- was observed. The fluorescence spectrum of **22** in MeCN, Figure 1.19 (B), showed two bands at 370 and 520 nm, which are due to the locally excited state (LE) and the charge transfer (CT) state of the DMABA fluorophore in equilibrium, respectively. Addition of the aforementioned anions resulted in quenching of the CT emission and concomitant enhancement in the LE emission.

In agreement with the formation of hydrogen bonded complex, downfield shifts were also observed in the ^1H NMR spectrum of **22** upon titration (DMSO-d_6) with AcO^-. Binding constants (K) were obtained by fitting the changes in both the absorption and emission spectra. Some of these constants were of the order of 10^5 mol^{-1} L^{-1}, which are high in comparison to the corresponding *N*-*N*'-phenylthioureas, which are typically in the range of 10^4 mol^{-1} L^{-1}, and has since prompted the incorporation of this receptor moiety into sensors for anions, by various other researchers. [106,136-139]

Continuing their work on such receptors Jiang *et al.*[78] described a series of amidothioureas, which were functionalised on the *N*-benzamido ring, in order to investigate the substituent effect (X) on the anion binding capabilities of **23a-h**.



23

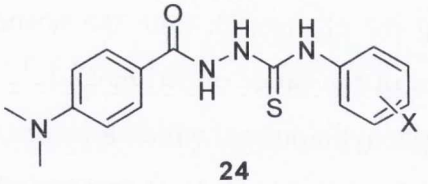
X = (a) *p*-OC_2H_5 (b) *p*-CH_3, (c) *m*-CH_3 (d) H, (e) *p*-Cl, (f) *p*-Br, (g) *m*-Cl, (h) *p*-NO_2

The absorption spectra of **23a-h** in MeCN exhibited λ_{max} at *ca.* 270 nm, which was shifted to longer wavelengths in the presence of anions such as AcO^-, $H_2PO_4^-$ and F^-. As anticipated, these changes were slightly larger than those of the highly electron donating DMABA substituent sensor **22**. The spectra of **23a-h** showed little dependence on the *N*-

benzamido substituent, X. However, the extent of the bathochromic shift upon addition of anions varied with the substituent. This led the authors to the conclusion that a structural change around the twisted hydrazine bond occurred upon anion interaction, therefore, allowing communication and, hence, ground state intramolecular CT between the anion and the receptor.

The anion binding of **23d** with AcO^- was also investigated using ^1H NMR titration in DMSO-d_6 and showed the appearance of a new downfield signal at 10.82 ppm while the N-H protons of **23d**, which resonated at 10.54, 9.82 and 9.72 ppm, decreased in intensity. These changes were assigned to the formation of a hydrogen bonded complex. Binding constants were also determined, by fitting the changes in the absorption spectra to a 1:1 stoichiometry, using nonlinear regression analysis. These values were mostly of the order of magnitude of 10^6 mol^{-1} L^{-1}, which are higher than seen for **22**, due to the presence of the various electron withdrawing moieties.

In a further attempt to improve on the anion binding capabilities of such structures, Jiang *et al.* [79] reported the structurally similar receptors, **24a-g**. In contrast to **22** and **23a-h**, these receptors are functionalised with signal reporters at both ends of the amidothiourea receptor, therefore, allowing their interaction with anions to be studied using both absorption and fluorescence techniques. As seen for **23a-h**, the absorption spectra of **24a-g**



24

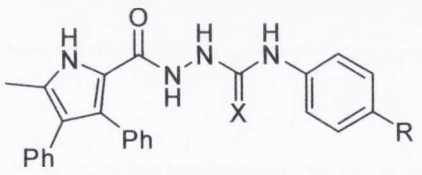
X = (a) *p*-CH_3, (b) H, (c) *p*-Cl, (d) *p*-Br, (e) *m*-Br, (f) *m*-NO_2, (g) *p*-NO_2

were almost independent of the substituent at the *N'*-phenyl ring and of the solvent polarity, as determined by recording the absorption spectra in various organic solvents. Dual fluorescence was observed for **24a-g** in a variety of solvents, which showed the long wavelength emission shifted to the red in highly polar solvents, confirming the occurrence of ICT in these systems. As for **23a-h**, ^1H NMR studies showed that the ICT DMABA fluorophore was electronically decoupled from the thiourea anion binding site. The absorption and emission spectra of these receptors showed large changes upon addition of anions, such as AcO^-, $H_2PO_4^-$ and F^- in MeCN, similarly indicating a conformational change around the N-N bond as proposed for the previous examples. These studies also suggested that the *N'*-phenyl ring substitution pattern tuned the anion binding sensitivity and the strongest interaction was observed between **24g** and AcO^-, with a large value of $K_{1:1} = 1.9 \times 10^8$ mol^{-1} L^{-1}.

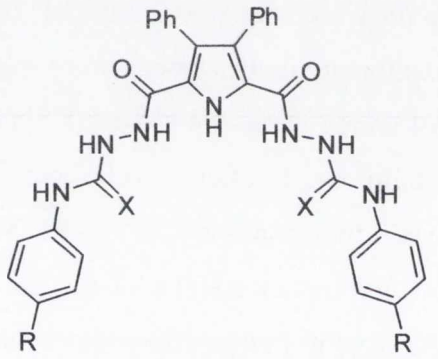
The amidothiourea sensors detailed in this section are structurally similar, with only the phenyl ring substituents being varied. However, heterocycles have also been incorporated into such sensors, therefore, giving rise to the possibility of additional hydrogen bonding interactions in solution. Such sensors are discussed in the following section.

1.8.2 Heterocyclic Based Amidourea and Thioureas

Gale *et al.*[136,140] have investigated the anion binding of a number of pyrrolylamidourea and thiourea compounds *via* absorption and ^{1}H NMR spectroscopy in DMSO and DMSO-d_6, respectively. Compared to the urea receptors, the thiourea receptors, **25c** and **25d**, gave rise to large changes in their absorption spectra upon titration with F^-, AcO^-, $H_2PO_4^-$ and $C_6H_5CO_2^-$ in DMSO, and also in the more competitive solvent system, 9:1 DMSO-H_2O.



25a X = O, R = phenyl
25b X = O, R = 4-nitrophenyl
25c X = S, R = phenyl
25d X = S, R = 4-nitrophenyl



26a X = O, R = phenyl
26b X = O, R = 4-nitrophenyl
26cX = O, R = 3,5-dinitrophenyl

The most interesting result from these studies was the isolation of crystals of **25d**, which were red in colour and grown in the presence of one equivalent of F^-, upon evaporation of a CH_2Cl_2-diethyl ether solution (Figure 1.20). The X-ray crystal structure showed that a deprotonation of the N-H between the thiourea and the amide had occurred. It was also found that the ^{1}H NMR spectra of these crystals was identical to the ^{1}H NMR spectra of **25d** after titration with anions, where only three N-H proton resonances were identifiable. It was concluded that these compounds may fail to form hydrogen bonded complexes due to the non-convergent nature of the N-H protons, which was seen in the X-ray crystal structures of **25b** and **26a**. In general, thiourea receptors functionalised with electron withdrawing groups have been shown to undergo deprotonation in the presence of anions, however, this normally requires at least two equivalents of anion. In contrast, a neat and complete deprotonation of **25d** occurred with just one equivalent of anions, such as F^-,

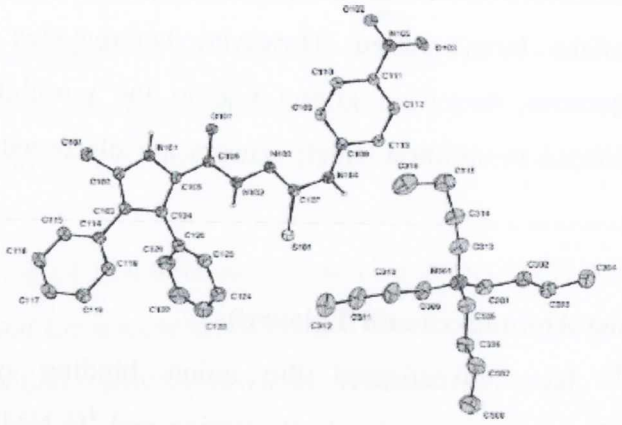
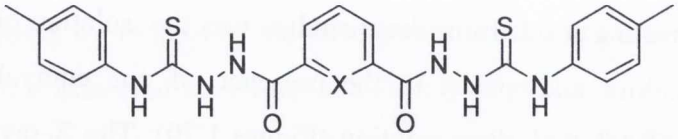


Figure 1.20: The X-ray crystal structure of the TBA^+ salt of the deprotonated receptor **25d**.[136,140]

AcO^- and $H_2PO_4^-$. The ability of the bis-systems, **26a-c**, to sense anions was also investigated by ^1H NMR and absorption spectroscopy. It was anticipated that deprotonation of the amidothiourea receptors may be prevented, due to the presence of the less acidic urea and the possibility for cooperative binding between both arms of the receptor. Although small changes were observed in the absorption spectra upon titration with anions, which were fitted to a 1:1 binding model, the authors clearly stated that there were possibilities of other stoichiometric species in solution. While **26a-c** showed enhanced affinity for anions (*ca.* 10^3-10^4 M^{-1}) in comparison to **25a-d** (10^3 M^{-1}), selective anion detection was not achieved under the experimental conditions.

Heterocyclic pyridine has also been incorporated into an amidothiourea sensor by researchers such as Wei *et al.*.[137] The benzene based sensor, **27a** and the pyridine based sensor, **27b,** showed strong colorimetric detection of anions in DMSO, particularly for F^-.

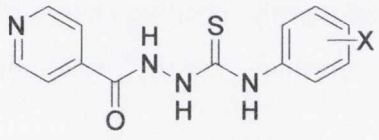


27a X = CH
27b X = N

The absorption spectra of **27a** and **27b** showed a λ_{max} at 266 nm, which upon titration with F^-, was slightly red shifted with the formation of a new transition at 350 nm. These changes occurred with a colour change from colourless to green-yellow and were reversed upon the addition of MeOH. Job plots indicated a 1:2 Host:Guest stoichiometric interaction with sensor **27a** and **27b** with F^-. In the case of AcO^- and $H_2PO_4^-$, a 1:1 binding was observed. The ^1H NMR spectra of **27a** in DMSO-d_6 showed resonances for the N-H protons at 10.60, 9.75 and 9.65 ppm. Upon the addition of two equivalents of F^- the peak

at 10.60 was shifted to 10.80 ppm, while the two other proton resonances combined and were found at 9.70 ppm. These changes were suggested to support the formation of a hydrogen bonded complex. The binding constants for both sensors with the various anions showed that the pyridine derivative bound anions more strongly, possibly due to the nitrogen atom, which could give rise to a preferential anion binding conformation through the formation of intra or intermolecular hydrogen bonding.

Jiang *et al.*[141] have also extended the scope of their neutral amidothiourea sensors through the incorporation of a pyridine moiety, which gave the *N*-(Isonicotinamido)-*N'*-phenylthioureas, **28a-e**. As seen for the previously discussed hydrazine-based



X = (a) *p*-OMe,(b) *p*-Me, (c) H, (d) *m*-Br, (e) *m*-CF_3

naphthalimide sensors (Section 1.7.4), **28c-e** were able to bind anions in aqueous solution. These sensors were designed with the aim of creating a hydrophobic anion binding cleft, which would create a less polar microenvironment, and as such, promoting efficient anion binding in aqueous solution. This was obtained by placing the amidothiourea receptor moiety between two hydrophobic groups, for which an aryl group and a pyridine moiety were chosen. The changes in the absorption spectra upon titration with F^-, AcO^- and $H_2PO_4^-$ were monitored in MeCN (Figure 1.21), 1:1 MeCN-H_2O and H_2O (Figure 1.21), which all showed the formation of a new transition at *ca.* 360 nm. A similar pattern of change was seen in all the solvents, however, the magnitude of the changes decreased with

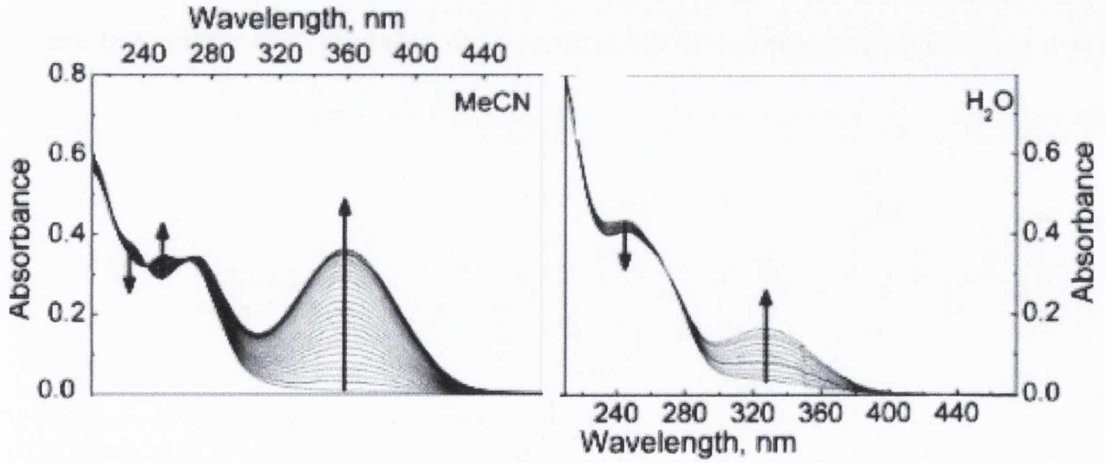


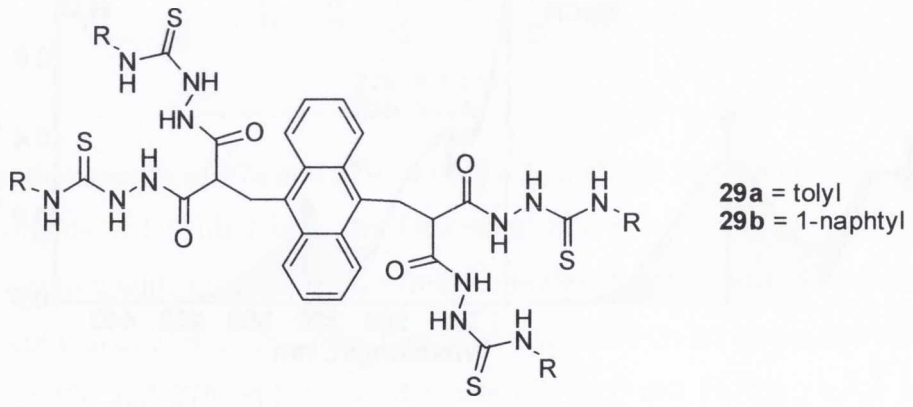
Figure 1.21: The changes in the absorption spectra of **28c** [20 μM] upon titration with the TBA^+ salt of AcO^- in MeCN and similarly, the changes in H_2O upon titration of the NH_4^+ salt. The aqueous solution of pH 5.5 was tuned using NaOH/HCl.[141]

increasing solvent polarity. Furthermore, the binding constant for the **28c**:AcO^- complex decreased with increasing water content. However, despite the polar solvent environment, binding constants as high as 10^3 M^{-1} were determined in H_2O. Evidence for the hydrophobic microenvironment of **28** was also obtained from quantum mechanic calculations, thermodynamic analysis, NMR aromatic current shielding, and comparative anion binding. The nature of the anion receptor site was also found to affect the anion binding in water and only receptors **28c-e** showed anion binding capacity in mixed MeCN-H_2O solution. Furthermore protonation of the pyridine moiety and subsequent anion titrations in 1:1 MeCN-H_2O at pH 3.5 showed no spectral changes in the absorption spectra of **28c** (pK_a = 3.5). Therefore, it was concluded that the positive charge of the pyridinium prevented the approach to the *N*'-phenyl terminal, as the hydrophobic interaction weakened.

This section has shown a variety of simple chromophores attached to amidothiourea moieties which can lead to colorimetric responses in the presence of anions. Apart from the fluorescent DMAB sensor **22**, other fluorophores have since been appended to the amidothiourea receptor moiety and these will be discussed in the following section.

1.8.3 Fluorescent Amidothiourea Based Sensors for Anions

He *et al.*[142] have reported the anion binding capabilities of **29a** and **29b** in DMSO, which bear four amidothiourea binding sites appended to an anthracene fluorophore. Upon addition of dicarboxylate anions (malonate, succinate, glutarate, adipate, suberate and sebacate) to **29a**, the fluorescence intensity was enhanced, while addition of anions to **29b** resulted in the quenching of the fluorescence emission, most likely *via* PET from the electron rich naphthalene receptor unit to the anthracene fluorophore. It was proposed that

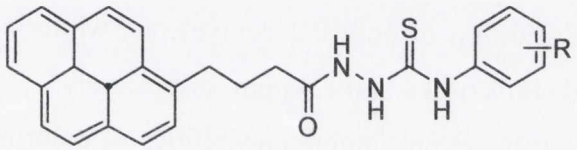


29a = tolyl
29b = 1-naphtyl

the enhancement in the PET may be due to an increase in the rigidity of the receptor upon anion binding. Increases in the absorption spectra of **29a** and **29b** at 400 and 460 nm, respectively, was also observed upon titration of anions. The selectivity for the various

dicarboxylate anions was related to the chain lengths, with both sensors preferentially binding longer chain lengths, such as adipate over the aforementioned carboxylates. The changes in the absorption and fluorescence spectra were best fitted to 1:1 complexation models and the largest values were determined for both sensors with adipate as 3.68 (±0.32) × 10^4 M^{-1} and 1.55 (±0.11) × 10^5 M^{-1}, for **29a** and **29b**, respectively.

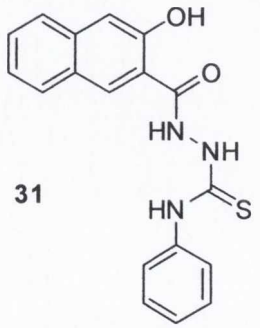
Leading from the work above, Jiang *et al.*[143] have studied the pyrene functionalised amidothioureas, **30a-c**. Titration with AcO^-, F^- and $H_2PO_4^-$ resulted in quenching of the pyrene fluorescence emission in MeCN, due to enhanced PET from the electron rich anion



30a R = *p*-CH_3
30b R = H
30c R = *m*-CF_3

binding site to the fluorophore. As for an 'ideal' PET sensor, no changes were observed in the absorption spectra of the pyrene unit upon addition of anions. High binding constants of 10^5 mol^{-1} L were determined from fitting the changes in the fluorescence emission spectra and the binding constants decreased in the order of **30a** < **30b** < **30c** for $H_2PO_4^-$ in MeCN. Accurate determination of the binding interaction of F^- and AcO^- was not possible. The nature of the interaction was also investigated by ^{1}H NMR anion titration in CD_3CN. Two of the N-H resonances were shifted downfield signifying the formation of hydrogen bonded complex, while the other N-H proton was not visible and resonated at the same chemical shift as the aromatic protons. Consequently, the authors speculated that although the spacer chain was quite long, excited state electron transfer could occur from the electron rich anion complexed amidothiourea to the pyrene fluorophore.

Jiang *et al.*[144] have further extended their studies on fluorescent amidothiourea anion sensors, with the *o*-hydroxynaphthamide based sensor, **31**. Here, large changes were



31

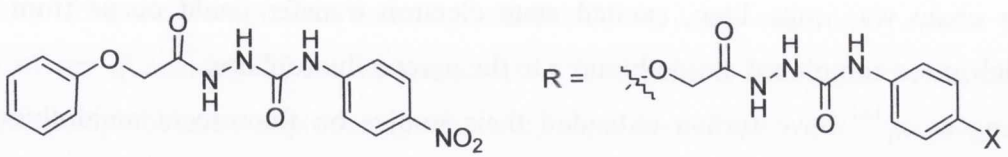
observed in both the absorption and emission spectra of **31** in the presence of anions such as AcO^-, $H_2PO_4^-$ and F^-, for which the absorption data was best fitted using a non linear regression analysis. The values determined from the fitting were of the order 10^6 $mol^{-1}L$

for F^- and AcO^- and 10^5 mol^{-1} L for $H_2PO_4^-$. The fluorescence emission spectra of **31** exhibited a λ_{max} at 400 nm, which upon the addition of anions, was quenched with the concomitant formation of a new transtition at 535 nm. A control molecule, for which the hydroxyl group was replaced with a methoxy group, showed similar changes to **31**, however, the new red shifted emission was not observed upon titration with anions. This indicated that the transition in the fluorescence emission spectra at 535 nm may be due to excited state intramolecular proton transfer (ESIPT). ^1H NMR titrations of **31** with a variety of anions in CD_3CN also indicated the formation of hydrogen bonded complexes for these changes. In the case of AcO^-, the amido N-H, as well as the phenolic OH, broadened and disappeared upon the addition of only 0.2 equivalents, while both of the thiourea protons underwent downfield shifts of 0.4 and 1.4 ppm, respectively.

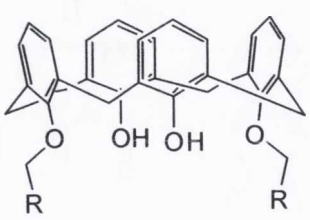
So far, this review has detailed the anion binding capabilities of colorimetric and fluorescent amidothiourea sensors. As with most classical anion receptors, amidothioureas have also been appended to various scaffolds in order to create preorganised hydrogen bonding motifs. Such sensors will be discussed in the following section.

1.8.4 Amidoureas and Thioureas Appended to Scaffolds

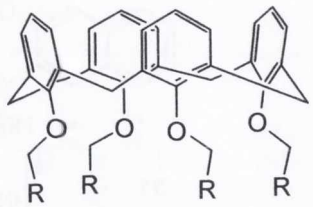
The amidourea sensor **32** was investigated by Gunnlaugsson *et al.*[105] and its interaction with anions such as AcO^-, $H_2PO_4^-$, $HP_2O_7^{3-}$ and F^- were investigated in DMSO. Colorimetric changes in the presence of $HP_2O_7^{3-}$ and F^- prompted the incorporation of **32** into 1,3-disubstituted calix[4]arene scaffolds giving rise to novel bis



32



32a X = NO_2

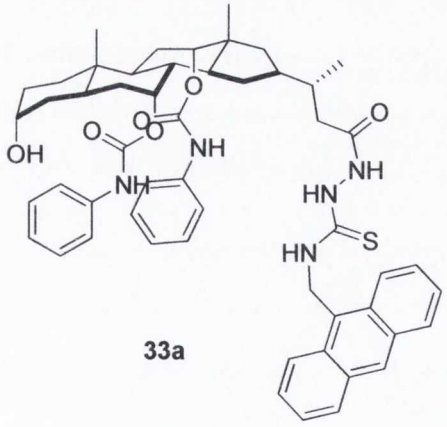


32b X = NO_2
32c X = H

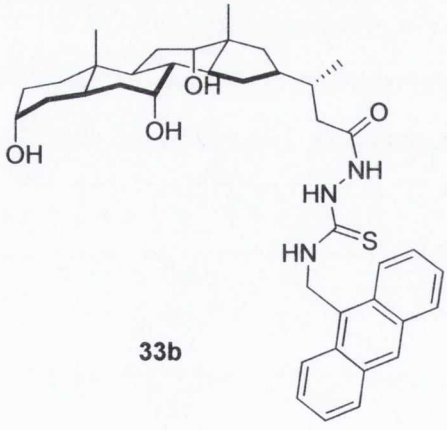
and tetra amidourea-based colorimetric sensors for anions, **32a** and **32b**.[105,106] The ICT transition of the absorption spectra of **32a** and **32b** (*ca.* 335 nm) were shifted to longer wavelengths upon titration with anions in DMSO. In the case of $HP_2O_7^{3-}$ and F^-, colour changes from yellow to purple and colourless to red occurred for **32a** and **32b**,

respectively. For both sensors, strong 1:1 hydrogen bonding of $HP_2O_7^{3-}$ was demonstrated. In the case of F^-, 1:1 hydrogen bonding with **32a** occurred, while deprotonation of **32b** was verified *via* ^1H NMR spectroscopy in DMSO-d_6. Sensor **32c** was synthesised in order to observe more clearly the changes in the ^1H NMR spectra upon titration with anions, as the N-H protons of **32b** disappeared after the addition of just 0.1 equivalent of anion. The ^1H NMR spectra of **32c** upon titration with $H_2PO_4^-$ remained symmetrical, therefore, indicating that binding occurred between all arms of the calixarene. Additionally, the N-H protons were significantly shifted upon the addition of anions.

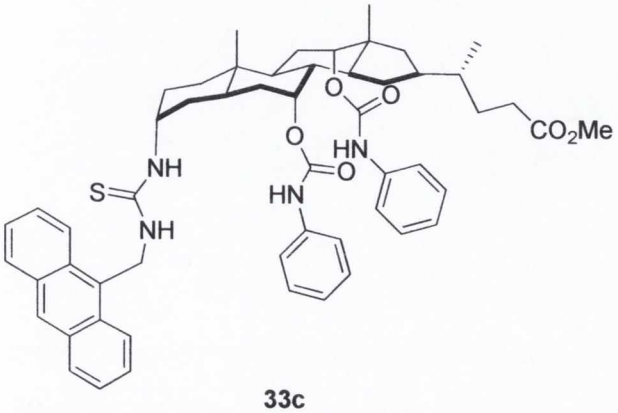
Apart from the work above, only a few other researchers have appended amidothioureas to scaffolds. For instance, Chan *et al.*[138] have reported several amidothiourea PET based sensors, which were developed from cholic acid. Sensors **33a-c** showed strong fluorescent responses towards anions, as well as high sensitivity and selectivity in MeCN. No changes were seen in the absorption spectra of **33a-c** upon titration with anions such as carboxylates, $H_2PO_4^-$ and Br^-. In contrast, excitation at 366 nm resulted in PET quenching of the characteristic anthracene emission, however, in the case of **33a**, an enhancement was observed upon addition of Br^-. These changes were fitted to a 1:1 binding isotherm using non linear regression analysis and the values determined reflect the decreasing bascicity of the various carboxylates studied. In comparison to the



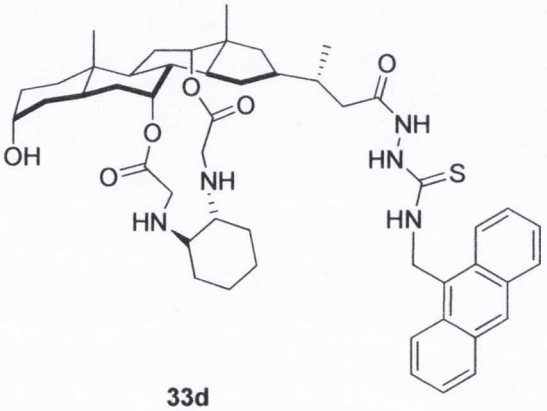
33a



33b



33c



33d

thiourea-based sensor, **33c**, larger binding constants were determined for both of the amidothiourea-based sensors, **33a** and **33b**, which illustrates the higher anion binding affinity of the latter. In comparison to the aforementioned anions, F^- showed a 1:2 Host:Guest stoichiometric interaction with **33a** and **33b**, which was assigned to hydrogen bonding followed by deprotonation. Conversely, deprotonation of **33c** by F^- did not occur and only a 1:1 binding stoichiometry was observed. These results illustrated the higher acidity of such amidothiourea sensors compared to their thiourea analogues.

Extending their cholic acid based sensors, Chan *et al.*[145] have recently incorporated cyclic 1,2-diamino chiral receptive sites into its structure and developed sensor, **33d**. This gave rise to a fluorescent scaffold for the ditopic sensing of amino acids, such as serine, lysine and threonine, in MeCN. Upon the addition of L- and D-serine, the fluorescence emission was quenched on both occasions due to PET from the receptor to the anthracene moiety. Binding constants were established for both diasteriomeric complexes, which indicated preferential binding of D-serine. ^{1}H NMR titrations were also carried out in CD_3CN and the results confirmed a stronger binding affinity with D-serine, with larger upfield shifts for the anthracene methylene protons as well as the α-hydrogen of D-serine, compared to that of L-serine. The sensor also selectively bound ATP over other nucleotides, in a similar manner to the amino acids, with the amidothiourea receptor binding to the phosphate backbone.[146]

He *et al.*[139] have also reported the tripodal scaffold, **34**, which is functionalised with amidothiourea arms. The absorption spectra of **34** in DMSO showed a λ_{max} at 358 nm with a shoulder at *ca.* 440 nm (Figure 1.22). The λ_{max} was shifted to *ca.* 406 nm with the

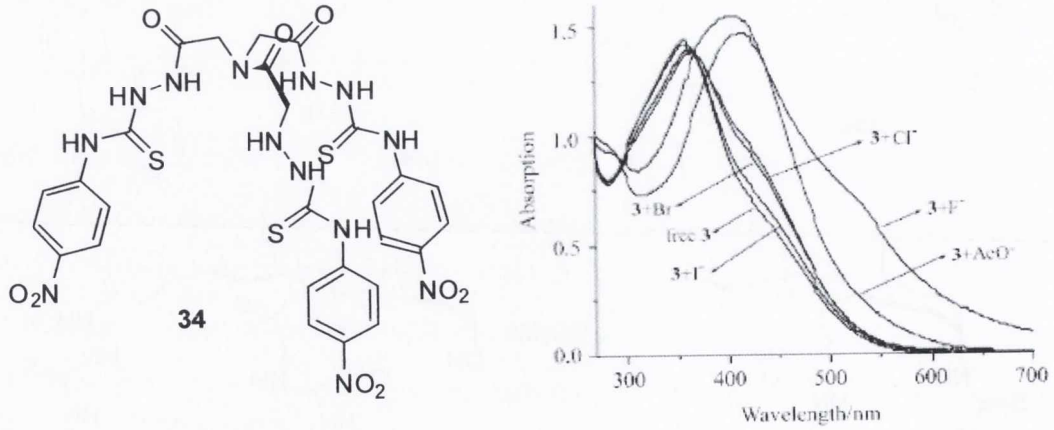


Figure 1.22: The tripodal receptor **34** and the changes in the absorption spectra of **34** [5×10^{-5} M] upon addition of various anions in DMSO.[139]

formation of two isobestic points upon the addition of 1.5 equivalents of AcO^-. Such changes occurred with a colour change from green-yellow to light brown. Further addition

of anion resulted in a slight decrease in the absorption centred at 406 nm and an increase at *ca.* 522 nm, which occurred with the formation of an isobestic point at *ca.* 455 nm. These changes were reversed upon the addition of protic solvent. Similar results were seen for F^-, however, the long wavelength changes resulted in a colour changes from light brown to carmine. The changes in the absorption spectra were also fitted using non linear least squares curve method, which gave rise to higher binding constants for F^- ($K_{1:3}$ = 10.22 ± 0.42) than AcO^- ($k_1 = 1.1 \times 10^4$ $mol^{-1}L$ and $k_2 = 6.0 \times 10^4$ $mol^{-1}L$).

1.9 Work Described Within This Thesis

The focus of Chapter 1 has been to review the many examples within the literature, which make use of either the naphthalimide fluorophore or the amidothiourea moiety, in the construction of sensors for anions. These two topics were discussed, as the objective of this PhD work was to construct anion sensors bearing such motifs. A brief introduction to the work described within this thesis will now be discussed.

Chapter 2 details the synthesis, photophysical properties and anion binding capabilities of the 4-amino-1,8-naphthalimide based thiourea and urea sensors, **4a-c**, in DMSO.[112] As shown in Section 1.7.1, these sensors are structurally similar to those previously reported by Pfeffer and Gunnlaugsson *et al.*[107,111] and it was anticipated that their modified structures would give rise to an enhancement in PET upon anion binding. Such work then led to the synthesis and spectroscopic investigations into the anion binding capabilities of a novel bis-1,8-naphthalimide based thiourea sensor for anions. This is followed by the design and attempted synthesis of a naphthalimide substituted with anion receptor moieties at both the 3- and 4-positions of the fluorophore. It was envisaged that such a structure could give rise to stronger cooperative binding with anions, particularly with $H_2PO_4^-$.

Chapter 3 discusses results from the investigations into the anion binding capabilities of a series of neutral organic bis-amidothiourea sensors in more competitive aqueous based media, such as 4:1 DMSO-H_2O solution.[112] However, some investigations were carried out in MeCN. The amidothiourea receptor moieties were appended to the easily functionalised 2,6-dicarboxypyridine backbone, which has been previously used as a scaffold for the construction of anion sensors by various researchers,[66,147,148] and, hence, allowed a range of signalling subunits to be incorporated. The concept of the design and possible anion interactions are depicted in Figure 1.23, with R representing possible signalling units.

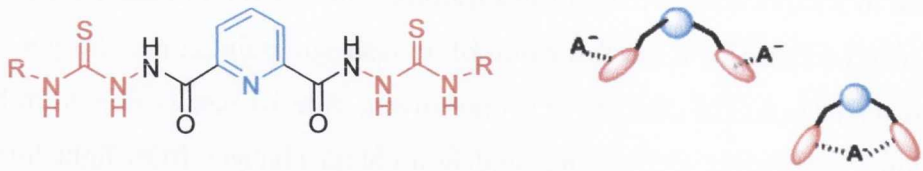


Figure 1.23: Schematic representation of design concept.

Chapter 4 details results from the investigation of amidothiourea anion sensors in highly competitive media, such as 1:1 EtOH-H_2O and 1:1 MeOH-H_2O solutions. The design of these sensors is similar to those described in Chapter 3, however, here glycol chains have been attached at the 4-position of the pyridine moiety in order to enhance their solubility in aqueous media. The glycol chain was also introduced as a means of synthesising tetra amidothiourea sensors, which could be capable of detecting up to four anions in solution, schematic representation, Figure 1.24.

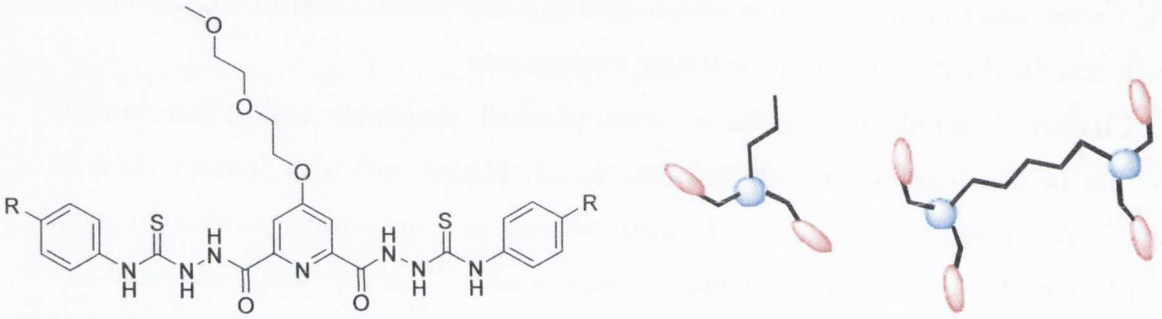


Figure 1.24: (Left) General structure of the bis amidothiourea sensors and **(Right)** Schematic representation of such *bis* and *tetra* amidothiourea pyridine-based sensors, both functionalised with glycol chains at the 4- position.

Chapter 5 gives a brief overview of certain results discussed in Chapters 3 and 4 of this thesis and also compares and contrasts these with that reported within the literature. Additionally, potential future work is discussed.

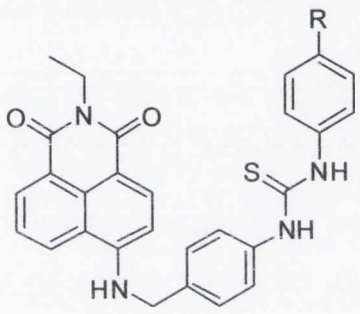
In Chapters 2-4, the anion binding capabilities of the sensors were evaluated using UV-Vis absorption and/or fluorescence emission spectroscopy. The interaction with anions was also investigated, in some cases, using ^{1}H NMR spectroscopy. Control experiments were also carried out using TBAOH, in order to establish if the observed interactions between the receptors of these sensors and the various anions were due to hydrogen bonding or to deprotontion of acidic N-H moieties. The spectroscopic changes observed using these techniques were, when possible, fitted using the non-linear regression analysis program, SPECFIT^{TM}[109,110] (see Appendix A0), whereas the results obtained from the ^{1}H NMR spectroscopy titrations were analysed using programs such as WIN EQ NMR[149] and NMR*TiT*.[150]

Chapter 2

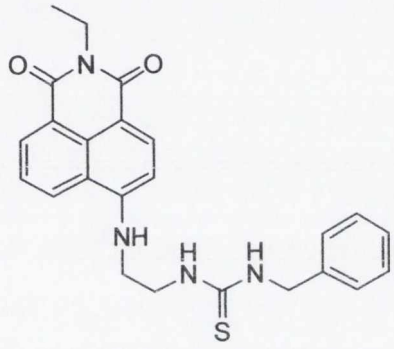
Naphthalimide-Based Thiourea and Urea Sensors for Anions

2.0 Introduction and Objectives of Current Studies

The 4-amino-1,8-naphthalimide fluorophore has been used in the design of sensors for anions by various researchers.[113,116,120,130,151] These sensors were discussed in Chapter 1, with a particular emphasis on the work of the Gunnlaugsson research group, who have reported anion recognition and sensing in both organic and aqueous media using colorimetric and fluorescent naphthalimide based urea and thiourea compounds.[14,15] Some of these have been based on the *'fluorophore-spacer-receptor'* model, such as sensor **3**, that was designed to bind $H_2PO_4^-$ *via* cooperation of the 4-amino N-H moiety of the 1,8-naphthalimide with the thiourea protons of the receptor (Section 1.7.1).[111]



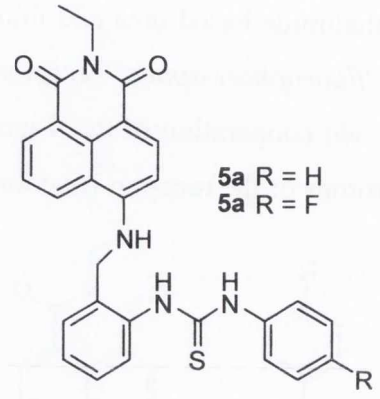
1a R = H
1b R = CF_3



3

The binding constant, (expressed as log*K*), determined using ^{1}H NMR titration of **3** with $H_2PO_4^-$ was $\log K_{1:1} = 3.4$ (±0.1). This binding constant is larger than that obtained for the more electron withdrawing phenyl receptor, **1a** ($\log K_{1:1} = 2.9$ ±0.1), thereby illustrating the influence of the flexible ethyl spacer chain in cooperative binding of the tetrahedral $H_2PO_4^-$ anion. Cooperative binding was further supported by comparison of the binding constants obtained with AcO^-, which was less for **3** than that obtained for its precursor **1a**.[107] Removal of the electron rich aromatic spacer of **1a**, and replacing it with the flexible chain of **3** also reduced the rate of electron transfer between the two parts of the sensor, diminishing the PET. In an attempt to improve on this design, Pfeffer *et al.* evaluated the anion binding capabilities of **5a** and **5b** that were structurally modified to preserve cooperative binding of $H_2PO_4^-$whilst restoring the rate of electron transfer to that seen for **1a**.[115] The electron rich aromatic benzyl spacer maintained pre-organisation and a phenyl receptor was also introduced with the aim of increasing the acidity of the thiourea protons. This design proved somewhat successful and cooperative binding of $H_2PO_4^-$ was achieved. The binding constant was estimated to be ~ $\log K_{1:1} = 3.7$, using ^{1}H NMR titration in DMSO-d_6, as after the addition of three equivalents of anion the resonances for the N-H protons disappeared. However, only minor fluorescence quenching, *ca.* 7%, of **5a** by $H_2PO_4^-$ was observed, in comparison with **1a**, where 67% quenching was observed. The

focus of the work discussed in the following chapter was to further improve the binding and possibly the fluorescent properties of the previously described sensor **3**. It was decided to investigate if the replacement of the benzyl moiety in **3** by a phenyl moiety would result in an improvement in the fluorescent properties of the sensor, rather than replacing the flexible spacer.



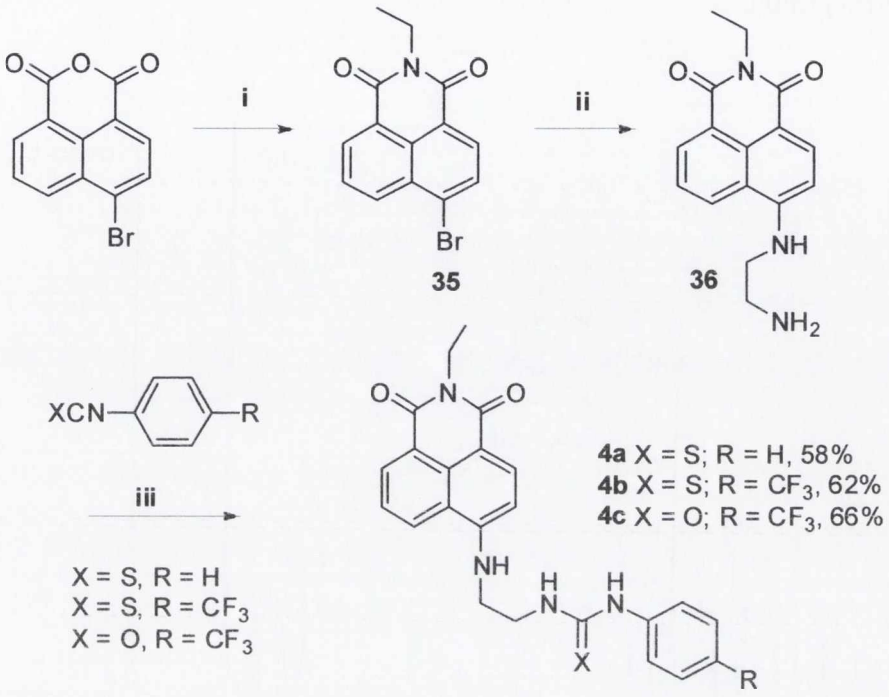
5a R = H
5a R = F

The phenyl group would increase the electron density at the receptor site, therefore, facilitating PET and also increasing the acidity of the thiourea protons, which would result in a higher affinity for anions. Therefore, the structural analogue **4a**, shown in Scheme 2.0, was designed and synthesised, and its ability to sense anions was investigated using various spectroscopic techniques such as ^{1}H NMR, absorption and fluorescence spectroscopy. Other derivatives of this structure, **4b** and **4c**, were also synthesised and studied in order to evaluate the electronic effects of a *para* trifluoromethylphenyl group (CF_3) and the urea, respectively. The results of these studies are detailed in this chapter and were also published in *Tetrahedron Letters*.[112]

2.1 Synthesis and Characterisation of 4-Amino-1,8-Naphthalimide Based Thiourea and Urea Sensors 4a-c

The procedure for the synthesis of 4-amino-1,8-naphthalimides derivatives has been previously devised within the Gunnlaugsson research group.[107] As the basic design is amenable to further modifications, sensors **4a-c** were obtained in three basic steps, as shown in Scheme 2.0. Commercially available 4-bromo-1,8-naphthalic anhydride and 1.2 equivalents of *n*-ethylamine (70 %) were firstly refluxed in 1,4-dioxane for 16 hours. The reaction mixture was then poured into ice-water and the resulting precipitate filtered, washed with water and dried in air to give the imide **35** as an off-white powder in 79% yield. Nucleophilic aromatic substitution of the bromide was accomplished by heating **35** in neat 1,2-diaminoethane at 80°C for 16 hours. The reaction mixture was then poured into ice-water and extracted with CH_2Cl_2 to afford the di-amine **36** as an orange solid in 61%

yield. Sensors **4a-c** were synthesised from the di-amine **36** by reaction with the appropriate isothiocyanate or isocyanate in $CHCl_3$ at room temperature for 16 hours.



Scheme 2.0: i) Ethylamine, 1,4-dioxane, reflux 16 h. ii) 1,2-diaminoethane, 80°C, 16 h. iii) $CHCl_3$, RT, 16 h.

On all occasions the reactions led to the formation of precipitates that were collected by filtration and washed with warm $CHCl_3$ to remove unreacted starting materials, which gave **4a**, **4b** and **4c** as bright yellow solids in 58%, 62% and 66% yields, respectively. There was no need for further purification in the case of **4a**. However, minor impurities were removed from sensors **4b** and **4c** by refluxing the respective products in EtOH, after which the suspended compounds were collected by hot filtration and dried in air to give yellow powders. Compounds **4a-c** were characterised by NMR spectroscopy, infrared spectroscopy, mass spectrometry and elemental analysis. The ^{1}H NMR spectrum of **4a** is shown in Figure 2.0 (600 MHz, DMSO-d_6) and clearly shows the presence of the three N-H proton resonances at 9.74, 7.97 and 7.87 ppm. The signal at 9.74 ppm, N-H_1, is that of the thiourea proton located next to the phenyl moiety, as determined by selective NOE (Nuclear Overhauser Effect). The N-H proton at 7.87 ppm, assigned to the 4-amino-1,8-naphthalimide moiety, has a similar chemical shift to the other thiourea proton, N-H_2. These exchangeable N-H protons were also easily identified by the addition of D_2O to the ^{1}H NMR sample. The replacement of the phenyl group in the receptor part of sensor **4a** with an electron withdrawing *p*-CF_3 phenyl group was clearly visible in the ^{1}H NMR spectrum of **4b**, Figure 2.1, and resulted in significant downfield shifts for both thiourea protons. In comparison to **4a**, N-H_1, which is located next to the *p*-CF_3 phenyl group of **4b**,

was shifted further downfield by 0.26 ppm to 10.0 ppm. The other thiourea proton, N-H_2, was also shifted by 0.31 ppm to 8.28 ppm, which has the same chemical shift as the naphthalimide H_2 proton.

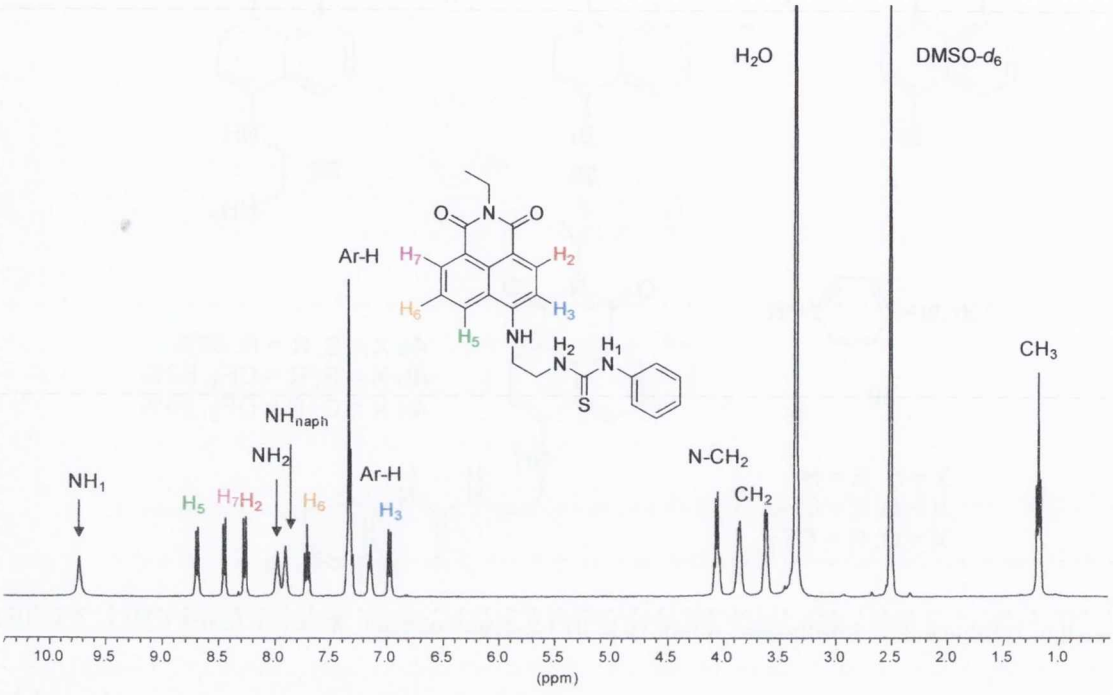


Figure 2.0: ^{1}H NMR (400 MHz, DMSO-d_6) spectrum of **4a.**

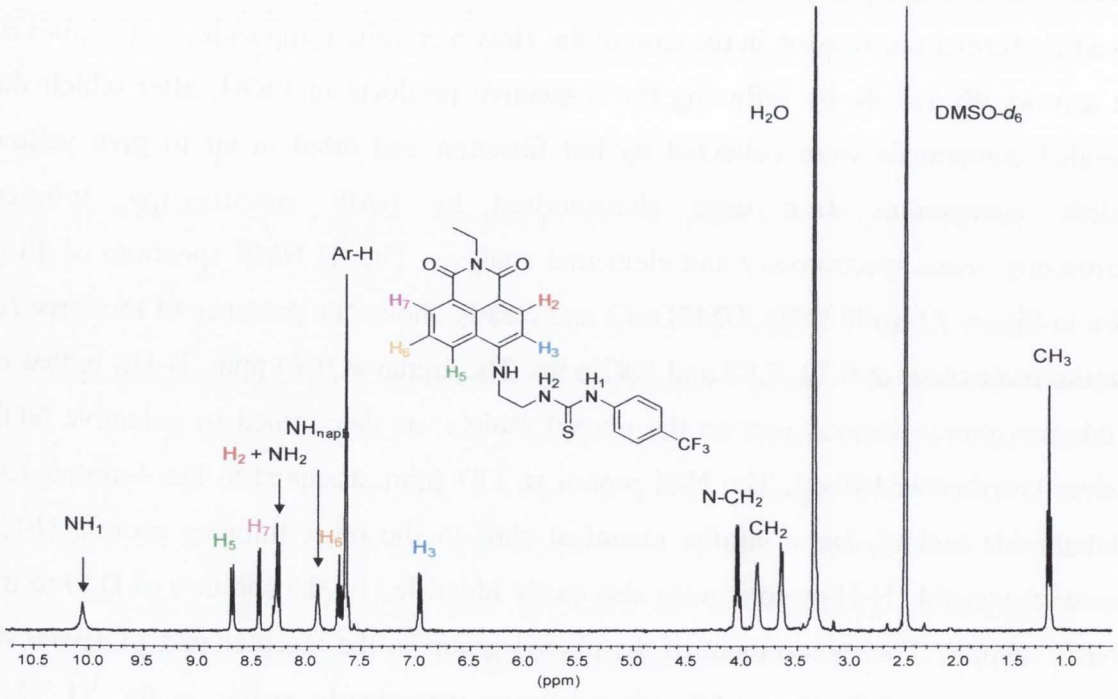


Figure 2.1: ^{1}H NMR (400 MHz, DMSO-d_6) spectrum of **4b.**

Additionally, the ^{19}F NMR spectrum of **4b** showed the presence of the CF_3 group, which resonated at -60.88 ppm. For the urea sensor, **4c**, N-H_1 and N-H_2 resonated at 9.10 ppm and 6.62 ppm, respectively. Despite the presence of the electron withdrawing CF_3 group, the urea protons are located further upfield than those of the phenyl based thiourea receptor **4a**, which is often observed in such structures.[152] The ^{13}C NMR spectrum of **4b** contained the expected number of resonances while both the ^{13}C NMR spectra of **4b** and **4c** showed resonances which were due to the CF_3 moiety and its characteristic quartet multiplicity $J_{^{13}C^{19}F}$ = 270 Hz. Electrospray (ES^+) mass spectra of **4a-c** gave peaks for the [M+H] ions, while the IR spectra of **4a-c** showed medium broad peaks at ~ 3300 cm^{-1} due to the bending and stretching modes of the N-H protons. Several strong sharp peaks were also visible for the carbonyl groups (~1600 cm^{-1}). Having fully characterised these sensors, we next carried out a detailed photophysical analysis of these structures. The results of these investigations are discussed in the next section.

2.2 Photophysical Evaluation of Sensors 4a-c[112]

Previous spectroscopic studies reported within the literature on receptors **1-4** were carried out in DMSO solution.[107,111,115] The changes seen in the absorption and the emission spectra of sensors **1** and **2** in DMSO were fully reversible upon the addition of polar protic solvents, such as MeOH. This reversibility is most likely due to the competitive nature of the solvent breaking apart the hydrogen bonded complex between the receptor and the anion. Because of this, the titrations of sensors **4a-c** were also carried out in DMSO. Prior to these titrations, the molar absorption coefficients (ε) were determined for **4a-c** in DMSO solution. All sensors were found to obey the Beer-Lambert law with ε values of 15,262, 15,370 and 15,387 $M^{-1}cm^{-1}$for **4a**, **4b** and **4c**, respectively. The absorption spectra of all three sensors were similar to each other with a characteristic absorption band centred at 441, 443 and 442 nm for **4a**, **4b** and **4c**, respectively, as shown in Figure 2.2. This band is due to the ICT transition of the naphthalimide fluorophore.[153] A second band also occurred at shorter wavelengths, which was assigned to the naphthalimide moiety as well as the aryl unit of the receptors. Excitation of the sensors at their respective absorption maxima, gave rise to strong emission between 450 and 700 nm (green to the naked eye), which was centred at 530 nm. Excitation of the absorption band at shorter wavelengths (*ca.* 270 nm) also gave rise to such long wavelength emission.

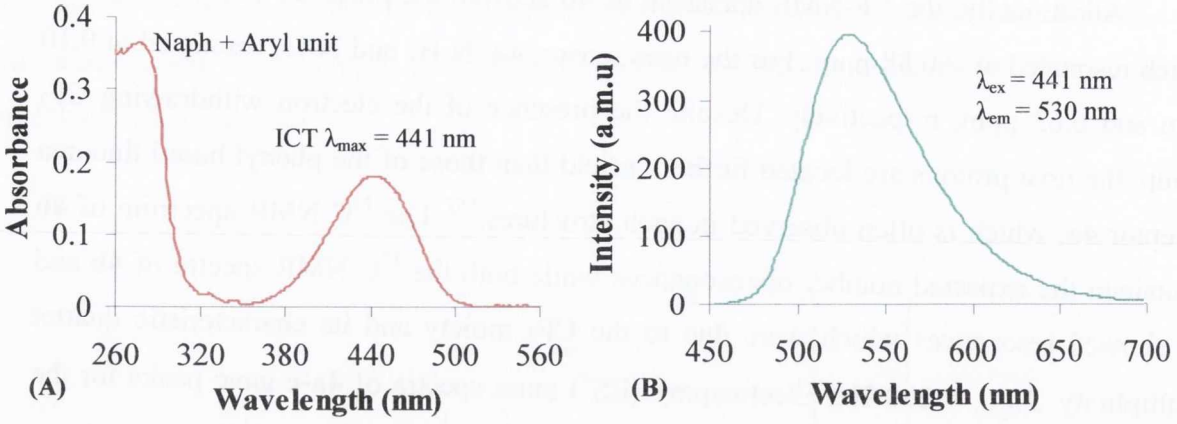


Figure 2.2: (A) The absorption spectrum and the corresponding emission spectrum **(B)** of **4a** [1×10^{-5} M] in DMSO at room temperature (RT).

The fluorescence quantum yields (Φ_F) of **4a-c** were determined using 4-*N*-butyl-*N*'-ethyl-1,8-naphthalimide as a reference[153] and are listed in Table 2.0. These values were calculated by the relative method using Equation (EQ) 1.0, where Q is the quantum yield, A is the absorbance of the solution, E is the corrected emission intensity and n is the average refractive index of the solution.[154] The subscripts R and X refer to the reference and the unknown compounds, respectively. The values determined show that **4a-c** are highly emissive and, hence, their potential for the development of fluorescent sensors.

$$Q_X = Q_R \frac{A_R}{A_X} \times \frac{E_X}{E_R} \times \frac{n_X}{n_R} \qquad \text{(EQ. 1.0)}$$

Table 2.0: Photophysical Properties of **4a-c** in DMSO.

Sensor	λ_{max} (nm)	logε	λ_{em} (nm)	Φ_F (±10%)
4a	441	4.2	530	0.632
4b	443	4.2	530	0.654
4c	442	4.2	530	0.642

The following section will discuss the ability of **4a-c** to sense anions such as AcO^-, $H_2PO_4^-$, F^-, Cl^- and Br^- as their tetrabutylammonium salts in DMSO. Stock solutions of **4a-c** were prepared in DMSO at *ca.* 1×10^{-3} M and then diluted in the cuvette to *ca.* 1×10^{-5} M. Tetrabutylammonium salts of the anions were prepared in DMSO giving three stock solutions of 1×10^{-1} M, 1×10^{-2} M and 1×10^{-3} M (Section 6.2.1). All titrations were repeated to ensure that the results were reproducible.

2.2.1 Absorption and Fluorescence Titration of 4a with AcO^-

Absorption titrations were first carried out with sensor **4a** with AcO^-. In agreement with that observed for sensors **1** and **2**, the changes were only minor (Appendix A, Figure

A1). This was anticipated as the receptor is separated from the fluorophore by the ethyl spacer, therefore, preventing electronic communication between the two counterparts in the ground state. However, excitation of the ICT transition after the addition of AcO^- gave rise to quenching of the long wavelength emission by *ca.* 30%, as shown in Figure 2.3. No other significant changes were observed, such as changes in the shape or position of the λ_{max} of the spectra.

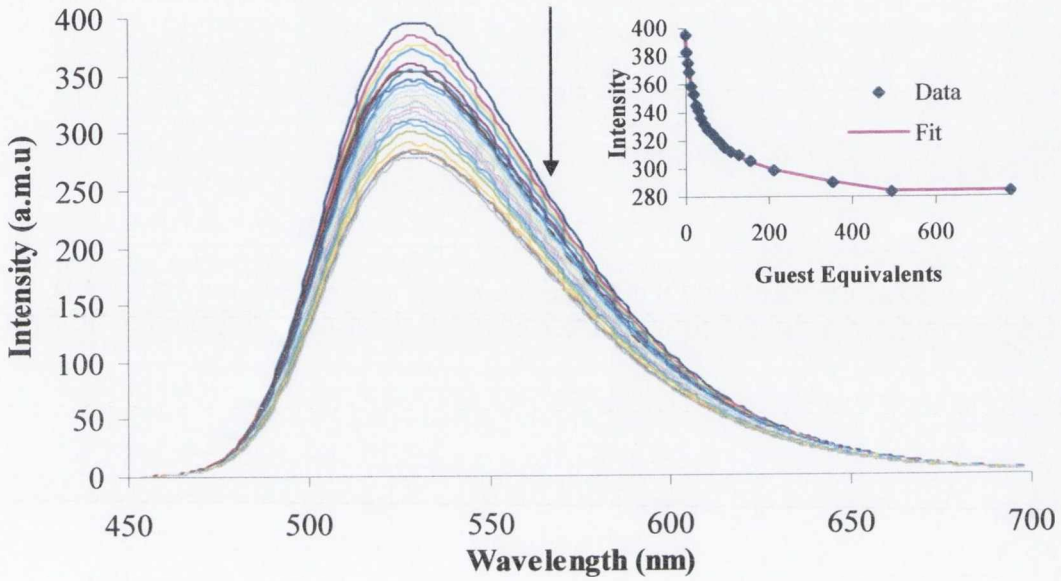
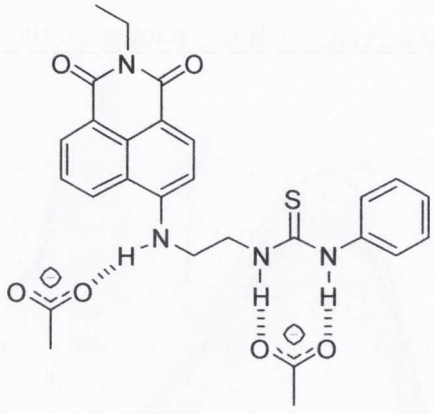


Figure 2.3: The changes in the emission spectra of **4a** [1.2×10^{-5} M] upon titration with AcO^- ($0 \rightarrow 1000$ equivalents, [11mM]). **Insert:** The binding isotherm with fit, which was determined using SPECFIT™, at 530 nm ($0 \rightarrow 400$ equivalents).

This behavior is typical of PET where the emission is quenched due to an electron transfer to the excited state fluorophore from the anion complexed thiourea receptor. However, these changes are quite small indicating that the PET process is not thermodynamically favorable and that the reduction potential of the receptor does not change significantly upon anion binding. Nevertheless, the changes in the fluorescence spectra upon addition of AcO^- were fitted using the non-linear regression analysis program SPECFIT/32™.[109,110] The best fit for the binding isotherm, as shown in the insert of Figure 2.3, was obtained by fitting the data to a 1:1 (Host:Guest) stoichiometry. The fit resulted in a binding constant of $\log K_{1:1} = 3.47$ (± 0.01).[155] The speciation distribution diagram, shown in Figure 2.4, which is depicted from $0 \rightarrow 400$ equivalents of AcO^-, clearly shows that at *ca.* 30 equivalents there was a 50% formation of the 1:1 complex in solution. Not until a very high concentration, *ca.* 300 equivalents of AcO^-, was 95% formation reached. The occurrence of complex with a 1:2 Host:Guest stoichiometry was also investigated, as secondary interactions between AcO^- and the 4-amino moiety could also be envisaged, as shown in Scheme 2.1. Such interactions were anticipated at higher concentrations of AcO^-.

A good fit was also obtained and the speciation distribution diagram, shown as insert in Figure 2.4, depicts concomitant formation of 1:1 and 1:2 complexes, however, at quite low concentrations of AcO^- (68% and 13% at 8 equivalents, respectively). Additionally, the



Scheme 2.1: Possible 1:2 H:G binding interactions occurring between AcO^- and **4a**.

standard deviation for the 1:2 fit was larger than that determined for the 1:1 fit, by a factor

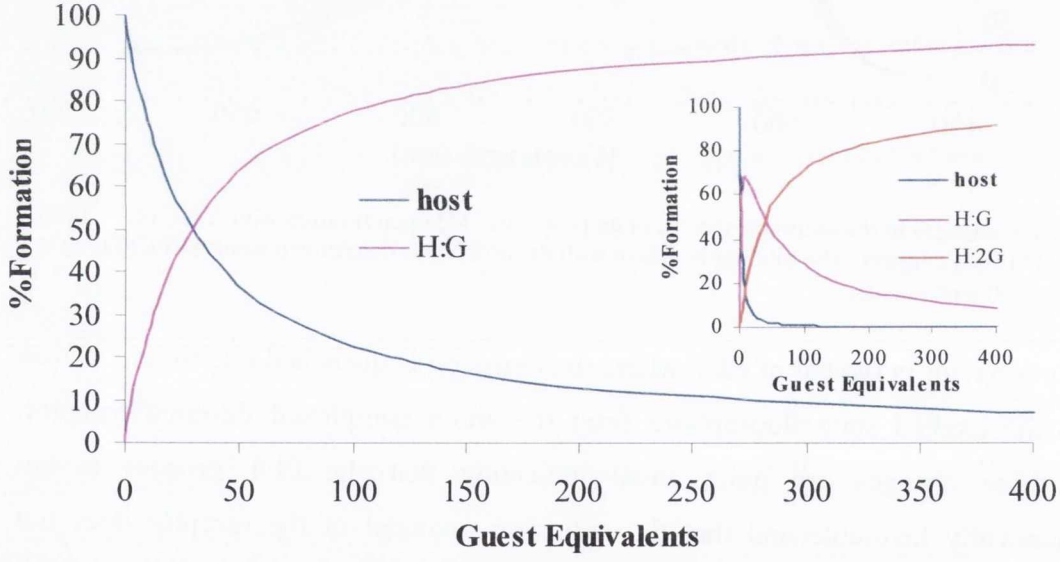


Figure 2.4: The speciation distribution diagram for the binding of **4a** with AcO^-, shown from 0 → 400 equivalents. **Insert:** Similarly, the speciation distribution diagram showing the formation of 1:1 and 1:2 H:G complexes.

of ten. Because of this, and due to the absence of significant changes in the ICT transition of the absorption spectra, the 1:1 fit was preferred.

In an analogous fashion to the above, the binding of $H_2PO_4^-$ to sensor **4a** was next investigated and the results from which will be discussed in the next section.

2.2.2 Absorption and Fluorescence Titration of 4a with $H_2PO_4^-$

In comparison to the lack of changes in the absorption spectra upon addition of AcO^-, a bathochromic shift of *ca.* 6 nm was observed for **4a** upon addition of $H_2PO_4^-$, as

shown in Figure 2.5. This was indicative of perturbation of the ICT transition of the naphthalimide fluorophore, due to the interaction of the 4-amino moiety with $H_2PO_4^-$, most likely through weak hydrogen bonding. The shift could also be due to the fact that the ICT character gives rise to a δ^+ on the 4-amino moiety, which through electrostatic interactions may experience the presence of the complexed anion. A small decrease in the absorbance at shorter wavelengths (280 nm) also occurred. Unfortunately, despite the small changes in the absorption spectra, the quenching of the fluorescence emission of **4a** (Appendix A, Figure A2) was less than that observed with AcO^- (*ca.* 8 → 20% with 3 mM → 34 mM solution, respectively). These changes could not be fitted using the non linear regression analysis program, SPECFIT™.

The differing results in the absorption and fluorescence emission spectra of **4a** upon titration with AcO^- and $H_2PO_4^-$ indicate different modes of interaction with these anions. The quenching of the fluorescence upon addition of AcO^- signifies the recognition of the anion at the receptor site; however, the absence of changes in the ICT transition of the absorption spectra suggests that there is no measurable contribution from the 4-amino moiety. Although the changes in the emission spectra upon titration with $H_2PO_4^-$ are smaller than those observed for AcO^-, it can be concluded that there is an interaction with the 4-amino moiety by the anion.

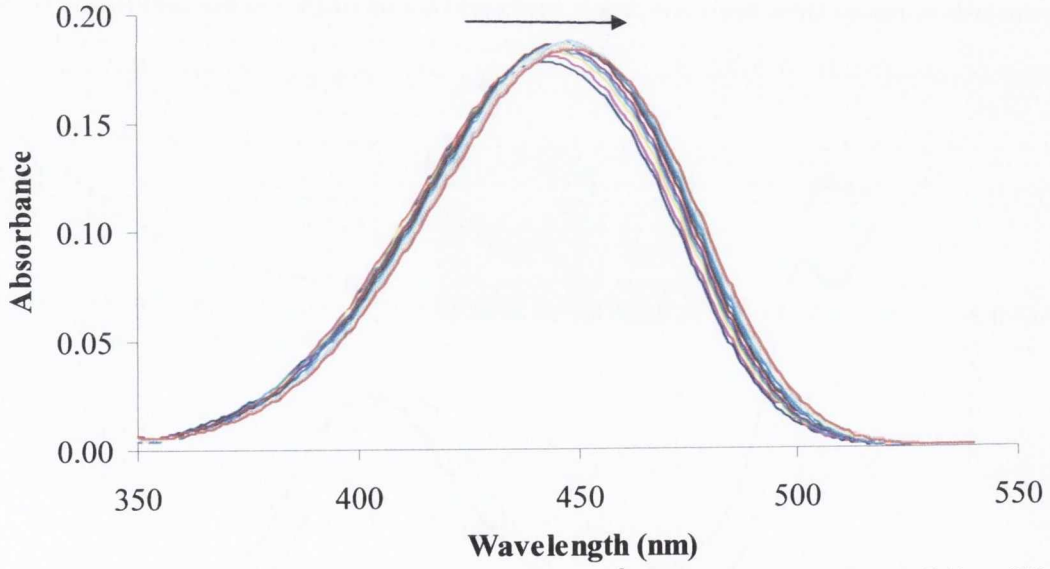


Figure 2.5: The changes in the absorption spectrum of **4a** [1.1×10^{-5} M] upon addition of $H_2PO_4^-$ (0 → 280 equivalents, [3 mM]) in DMSO.

This may suggest the formation of a 1:2 Host:Guest complex, as considered in the fitting in Figure 2.4. However, it is more likely due to 1:1 cooperative binding by all three N-H protons, as previously observed for the structurally similar sensor, **3**[115], therefore,

illustrating that basicity is not a sole deciding factor for anion interaction with sensor **4a**. The higher partial negative charge of AcO^-, in comparison with $H_2PO_4^-$, may also provide an explanation for the absence of quenching with $H_2PO_4^-$ *i.e.* the receptor is less electron rich.[156] The changes upon titration of sensor **4a** with F^- were next investigated.

2.2.3 Titration of 4a with F^-

In contrast to the results obtained upon addition of AcO^- and $H_2PO_4^-$, significant changes were seen in both the absorption and the fluorescence emission spectra of **4a** upon addition of F^-. The absorption spectra upon titration of **4a** with F^-, are depicted in Figure 2.6, and clearly show that the ground state of the receptor is affected by the anion. As for the titration with $H_2PO_4^-$, the ICT transition underwent a bathochromic shift with the formation of an isobestic point at 452 nm, however, this occurred to a greater extent. Furthermore, changes were also observed at shorter wavelengths, in which there was a decrease and an increase in the absorptions at 240 and 340 nm, respectively. These changes occurred with the formation of an isobestic point at 289 nm and are indicative of F^- interaction with the phenyl receptor. The addition of F^- also gave rise to a colour change from bright yellow-green to a darker yellow, Figure 2.6. In this instance, cooperative binding of F^-, as postulated for $H_2PO_4^-$, seems unlikely due to its smaller size. The larger changes observed in the absorption spectra with F^- could either be due to stronger hydrogen bonding than seen for AcO^- and $H_2PO_4^-$ or to the basic nature of F^-, which can cause deprotonation in solution.[31,108]

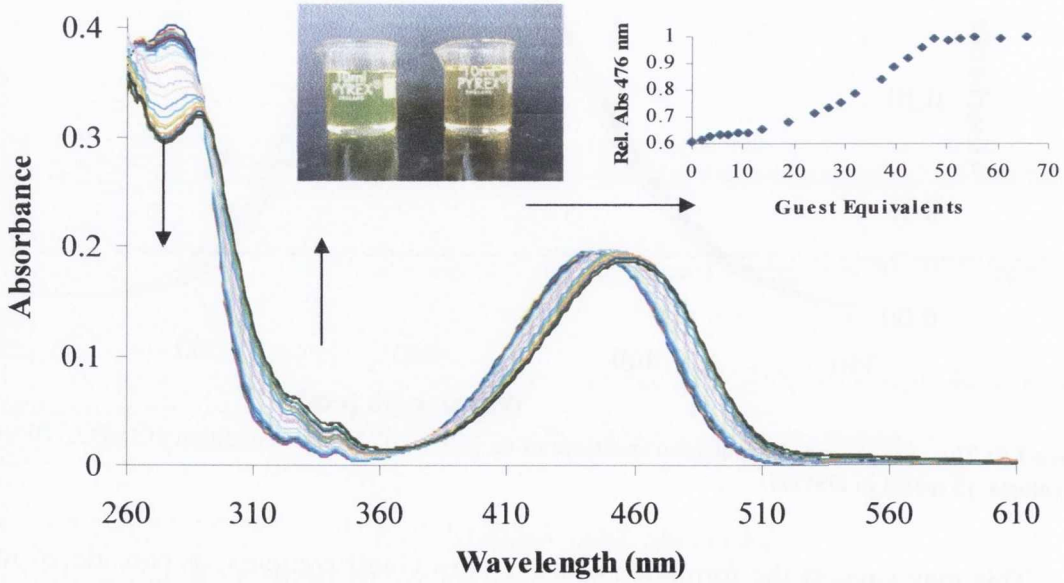


Figure 2.6: The changes in the absorption spectra of **4a** [1.3×10^{-5} M] upon addition of F^- (0 → 86 equivalents, [1 mM]) in DMSO. **Insert:** The relative changes observed at 476 nm against guest equivalents.

Numerous urea and thiourea receptors have been shown to form hydrogen bonded complexes with F^-, [55] however, excess F^- can result in the removal of hydrogen bonded F^- from the complex (HF), which eventually gives rise to the formation of bifluoride (HF_2^-).[107,157] Although AcO^- is more basic than F^-, HF_2^- has a unique stability and is, therefore, the driving force behind the deprotonation.[158] Therefore, deprotonation of the thiourea moiety is likely to occur, as deprotonation of the 4-amino moiety has been shown to result in long wavelength changes in the absorption spectra.[108,123,159] Indeed, upon titration with F^-, changes at long wavelengths were observed for **4a**, as shown in Figure 2.7. However, these changes, which occurred after the addition of *ca.* 50 equivalents of F^-, only reached 0.015 absorbance units after the addition of *ca.* 750 equivalents, [8 mM]. These long

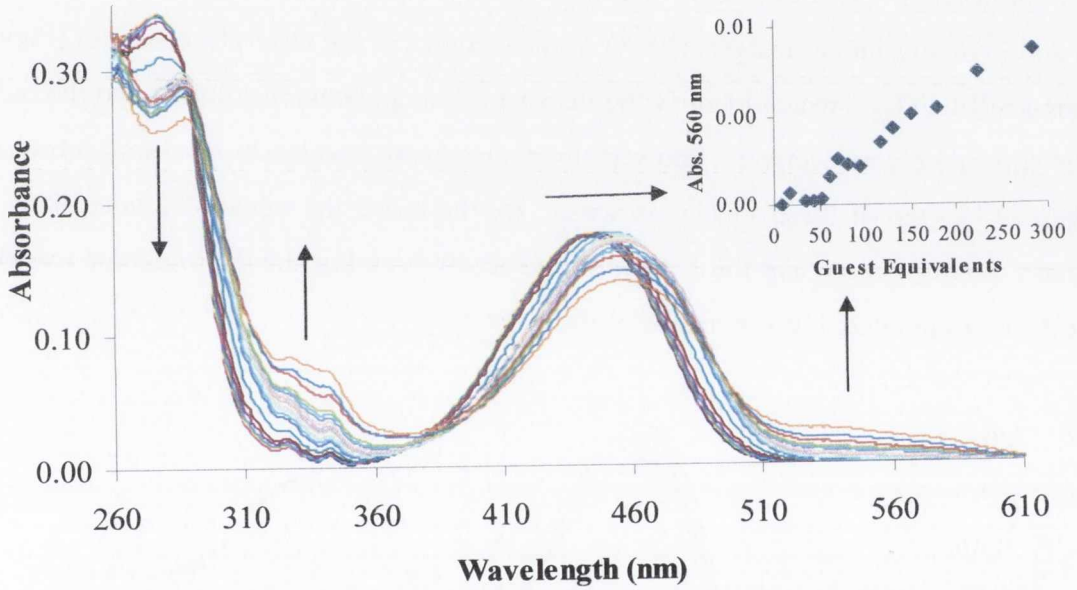


Figure 2.7: The changes in the absorption spectra of **4a** [1.1×10^{-5} M] upon addition of F^- (0 → 750 equivalents, or [8 mM]). **Insert:** The changes at 560 nm against equivalents.

wavelength changes are smaller compared with those reported for **1** upon addition of 5 mM [F^-] and, therefore, indicate that full deprotonation of the 4-amino moiety of **4a** does not occur in the concentration range above. Nevertheless, deprotonation of the 4-amino moiety most likely contributes to the changes in the absorption spectra shown in Figure 2.6, however, only at high concentrations.

In comparison to these changes, the fluorescence emission spectrum of **4a** was dramatically affected by the addition of F^-, as shown in Figure 2.8, occurring over the same concentration range as shown in Figure 2.6. Here the emission was fully quenched upon the addition of 0 → 80 equivalents of the anion with no noticeable changes in the position of the λ_{max}. The changes in the emission were significantly larger than those observed for AcO^- and demonstrate that PET was more effective upon interaction of the

receptor with F^-. Indeed, a combination of hydrogen bonding and deprotonation would make the receptor highly electron rich, resulting in enhancement of the PET quenching of the naphthalimide excited state. Such fluorescence quenching can be described as 'on-off' fluorescence switching. These changes were also fully reversible, as upon addition of protic solvent, such as MeOH, the emission was restored. Additionally, excitation of the long wavelength absorption at *ca.* 540 nm, Figure 2.7, resulted in a new broad and weak emission between 580-800 nm, which is also indicative of the formation of the negatively charged naphthalimide fluorophore ($Naph^-$).[16] The changes in the absorption and fluorescence spectra upon titration with F^- could not be fitted using SPECFIT™. This is likely due to the occurrence of multiple binding, such as shown for AcO^- in Scheme 2.1, and/or deprotonation processes occurring in solution. Despite this, principle factor analysis (PFA) and evolving factor analysis (EFA) of the changes in the absorption spectra (Figure 2.6) using SPECFIT™, which identify the number of components in solution and the order of their appearance, respectively, showed three significant species in solution (Appendix A, Figure A3). One of these species is sensor **4a**, therefore, the other two most likely to occur, of a possible three, are the F^- complexed receptor and/or the deprotonated receptor and/or the deprotonated 4-amino naphthalimide species.

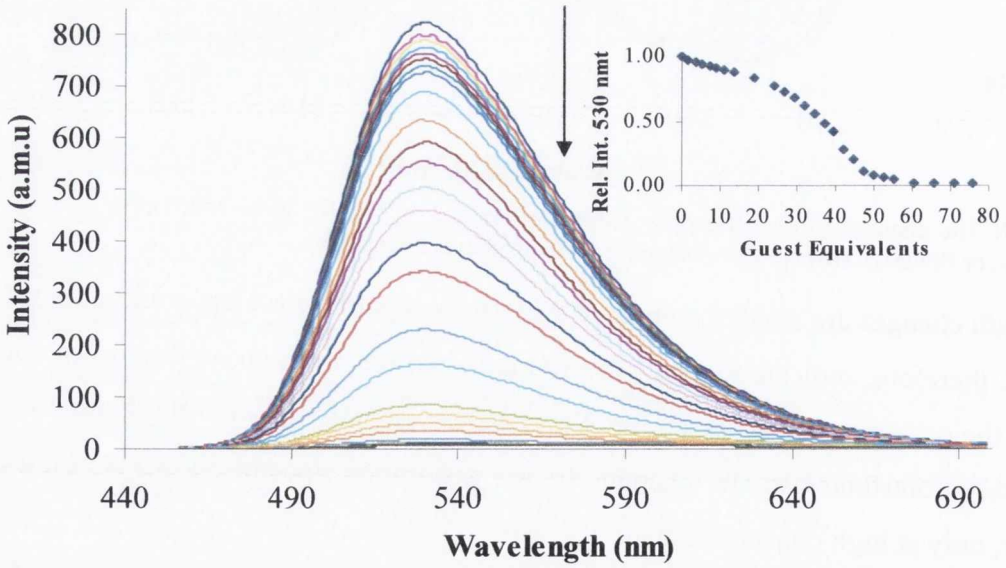


Figure 2.8: The changes in the fluorescence emission spectra of **4a** [1.3×10^{-5} M] upon addition of F^- (0 → 86 equivalents, [1 mM]). **Insert:** The relative changes in the emission at 530 nm.

The overall changes in the relative emission at 530 nm for the three anions discussed herein are shown in Figure 2.9, which clearly shows a selectivity for F^- by **4a**, as only for F^- is the emission modulated in a dramatic way. Additionally, titration of **4a** with the TBA salts of Cl^- and Br^- did not lead to any significant changes in either the absorption

or the emission spectra, possibly due to their larger size and lower charge density. This also indicated that the changes in the fluorescence emission spectra are not due to the heavy atom effect. Additionally, the quantum yield (Φ_F) of sensor **4a** was reduced from 0.632 to 0.010 and 0.465 in the presence of 1 mM [F^-] and 13 mM [AcO^-], respectively. Hence, sensor **4a** shows good selectivity for F^- over other competitive anions. The anion binding capabilities of both sensors **4b** and **4c** were next investigated and are discussed in the following sections.

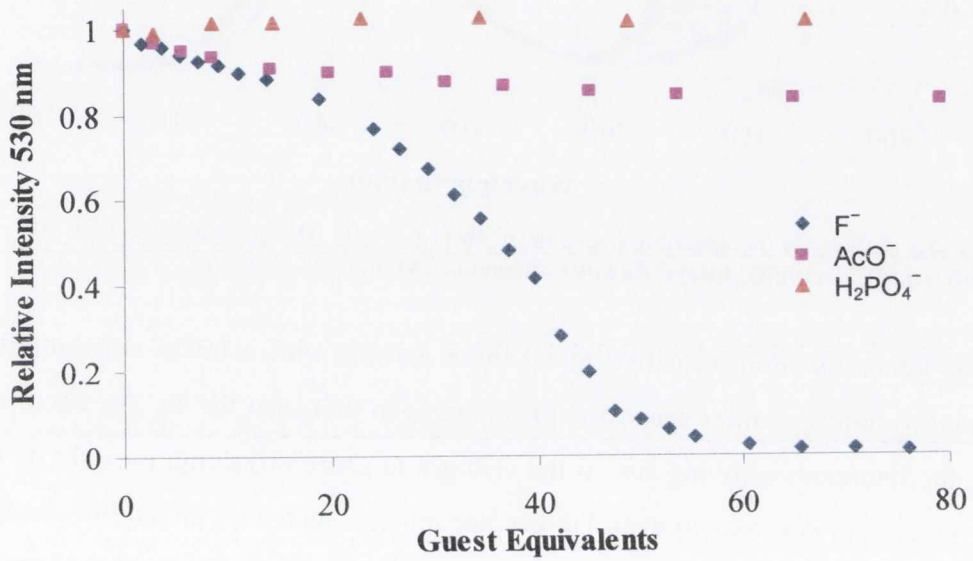


Figure 2.9: The changes in the emission of **4a** at 530 nm upon titration with various anions.

2.3 Absorption and Fluorescence Titration of Sensor 4b with Anions

The results obtained upon titration of sensor **4b** with AcO^-, $H_2PO_4^-$ and F^- were very similar to those obtained for sensor **4a**. The absorption spectrum of **4b** was unaffected upon titration with AcO^- whilst the fluorescence was quenched to a similar extent to that seen for sensor **4a** (Appendix A, Figures A4-5). These changes were also fitted using SPECFIT^{TM} to a 1:1 Host:Guest stoichiometry, which gave a $\log K_{1:1} = 4.56$ (± 0.02). This value is higher than that determined for **4a** and reflects the strong electron withdrawing ability of the *p*-CF_3 receptor moiety. Titration with $H_2PO_4^-$ showed a weak bathochromic shift in the absorption spectra, however, the changes in the emission spectra were only minor (Appendix A, Figures A6-7).

In comparison to sensor **4a** the changes in the absorption spectra, Figure 2.10, of **4b** upon titration with F^- were more pronounced with larger changes occurring at short wavelengths (280 and 340 nm). This is due to the stronger electron withdrawing ability of the CF_3 group, compared to the phenyl based receptor **4a**, which may make the N-H protons more acidic and hence, better hydrogen bonding donors. Therefore, it was found

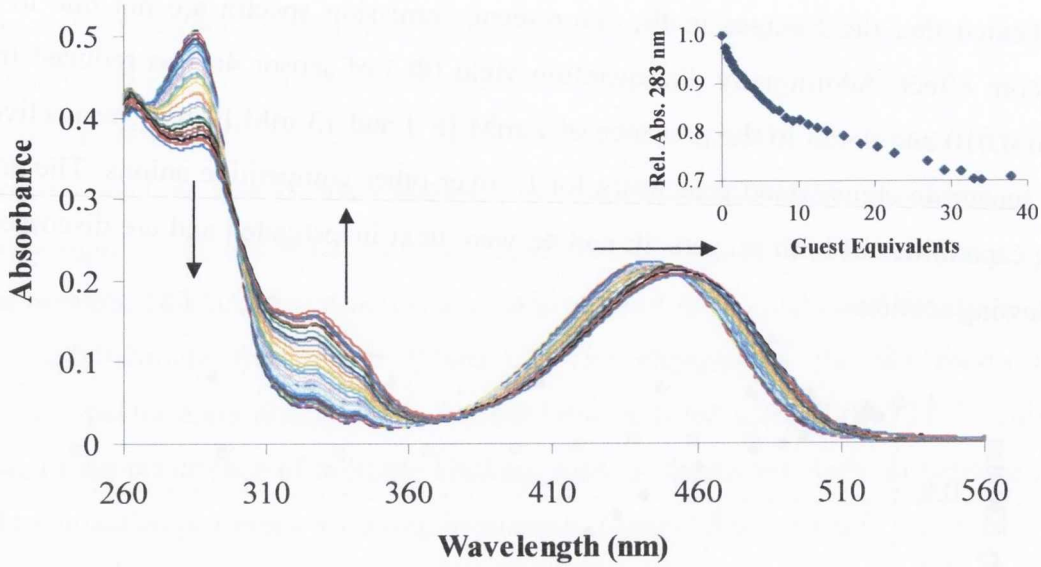
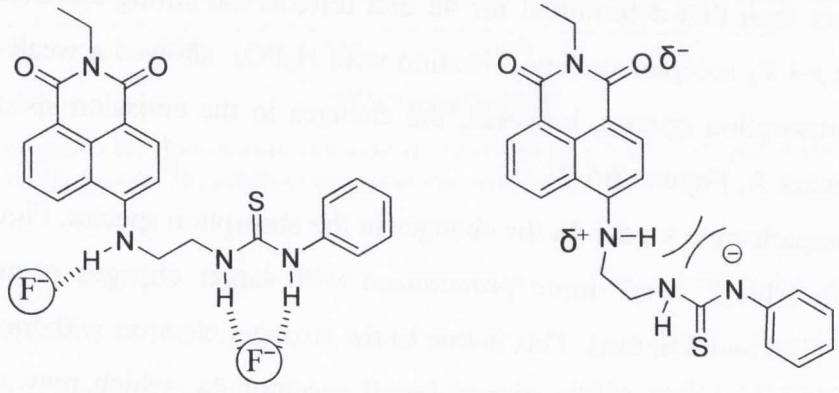


Figure 2.10: The changes in the absorption spectra of **4b** [1.5×10^{-5} M] upon addition of F^- ($0 \rightarrow 38$ equivalents, [0.6 mM]) in DMSO. **Insert:** Relative changes at 283 nm.

that **4b** was generally more sensitive to all three anions, with a lower concentration of anion needed to induce similar spectroscopic changes to that seen for **4a**. As discussed for sensor **4a**, the interactions giving rise to the changes at short wavelengths could be due to hydrogen bonding or deprotonation at the receptor moiety, such as depicted in Scheme 2.2.

The corresponding changes in the emission spectra were identical to those of **4a** (Appendix A, Figure A8). However, full quenching of the emission required a lower concentration of F^- ($0 \rightarrow$ *ca.* 45 equivalents). Additionally, the binding isotherm for **4b** is steeper than that for **4a**, therefore, indicating a stronger interaction with F^- (summarised in Figure 2.12), which is due to the increased acidity of the N-H protons. As observed for **4a**, the Φ_F of **4b** in the presence of F^- underwent a large decrease ($0.654 \rightarrow 0.017$), within the same concentration range. Unfortunately, the changes could not be fitted using SPECFIT™, most likely for the same reasons postulated for the interaction of **4a** with F^-.



Scheme 2.2: (Left) Possible structure of F^- complex occurring in solution and **(Right)** possible electrostatic interactions between the deprotonated receptor and the 4-amino moiety of **4a**.

2.4 Absorption and Fluorescence Titration of Sensor 4c with Anions

Unlike that seen for **4a** and **4b** in Sections 2.2.3 and 2.3, respectively, no significant changes were seen in both the absorption and fluorescence spectra of the urea sensor, **4c**, upon titration with AcO^- or $H_2PO_4^-$, even at high anion concentrations. Additionally, little or no changes were observed in the absorption (Figure 2.11) and fluorescence spectra upon titration with low concentrations of F^-.

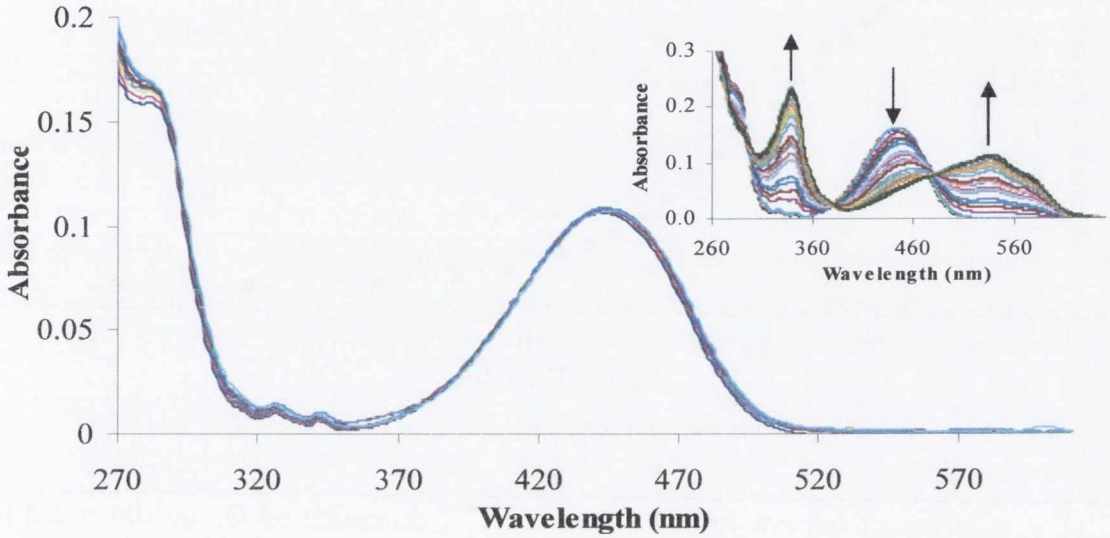


Figure 2.11: The changes in the absorption spectra of **4c** [7.0×10^{-6} M] upon addition of F^- (0 → 53 equivalents). **Insert:** The changes in the absorption spectra of **4c** upon addition of F^- (0 → 840 equivalents).

The lower affinity of sensor **4c** towards anions is perhaps due to the presence of the less electron withdrawing oxygen atom of the urea receptor, which results in the N-H protons being less efficient hydrogen bond donors. Conversely, significant changes were observed in the absorption spectra at higher concentrations of F^-, as shown in the insert of Figure 2.11. These changes occurred after the addition of *ca.* 50 equivalents of F^-, with concomitant quenching of the fluorescence emission, and a further 50 equivalents were required to give rise to *ca.* 30% emission quenching (Appendix A, Figure A9). To obtain full quenching of the emission larger quantities of F^- were required (~840 equivalents, 6.0 mM), as shown in the insert of Figure 2.11. These changes are in contrast with the fluorescence quenching seen for **4a** and **4b**, which occurred at low concentrations (< 0.6-0.8 mM, respectively), and in the absence of long wavelength changes in the absorption spectra. It was anticipated that the interaction observed between **4c** and F^- would be more similar to that for **4a** and **4b**. However, only deprotonation of the 4-amino N-H moiety was clearly observed at high concentrations of F^-.[107] The small changes occurred at short wavelength (*ca.* 280 and 340 nm) and the 3-4 nm shift in the ICT transition may indicate a

weak interaction at the urea receptor at low concentrations. However, this did not give rise to a sufficiently electron rich receptor in order to result in an enhancement of the PET process.

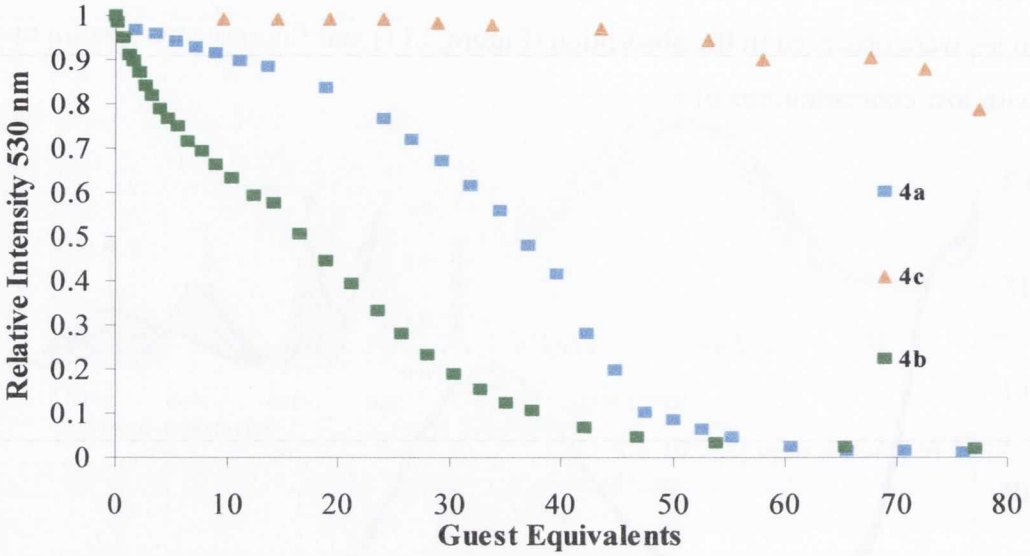


Figure 2.12: The changes in the emission at 530 nm upon titration of **4a-c** with F^- in DMSO.

The affinities of sensors **4a** and **4b** towards F^-, compared to **4c**, are illustrated in Figure 2.12. As shown, the emission of both thiourea-based sensors **4a** and **4c** was fully quenched at low concentrations of F^-, while the urea analogue gave rise to only *ca.* 30% quenching. These results are in good agreement with the fact that a thiourea moiety (pK_a = 21.0) is a better hydrogen bond donor than the corresponding urea (pK_a = 26.9), which would make the interaction of these with F^- stronger.[160] We next attempted to establish if the quenching of the emission was due to hydrogen bonding or to deprotonation, or indeed to a combination of both by titrating sensor **4a** with TBAOH.[161] These results are discussed in the next section.

2.5 Absorption and Fluorescence Titration of Sensor 4a with TBAOH

As discussed in the previous section above, the spectroscopic changes were also evaluated by titration of **4a** with TBAOH. Hydroxide ions can rarely be captured by hydrogen bonding interactions,[162] and usually behaves purely as a Brønsted base. Therefore, TBAOH was expected to directly deprotonate the receptor moiety of **4a**. The changes in the absorption spectra upon titration with TBAOH are shown in Figure 2.13. The initial changes, shown in red, were accompanied by a colour change of the solution from green-yellow to yellow. These changes, which occurred at low concentrations of TBAOH (*ca.* 0 → 80 equivalents), were assigned to deprotonation of the thiourea receptor

moiety of **4a**. Concomitant full quenching of the emission was also observed (Appendix A, Figure A10).

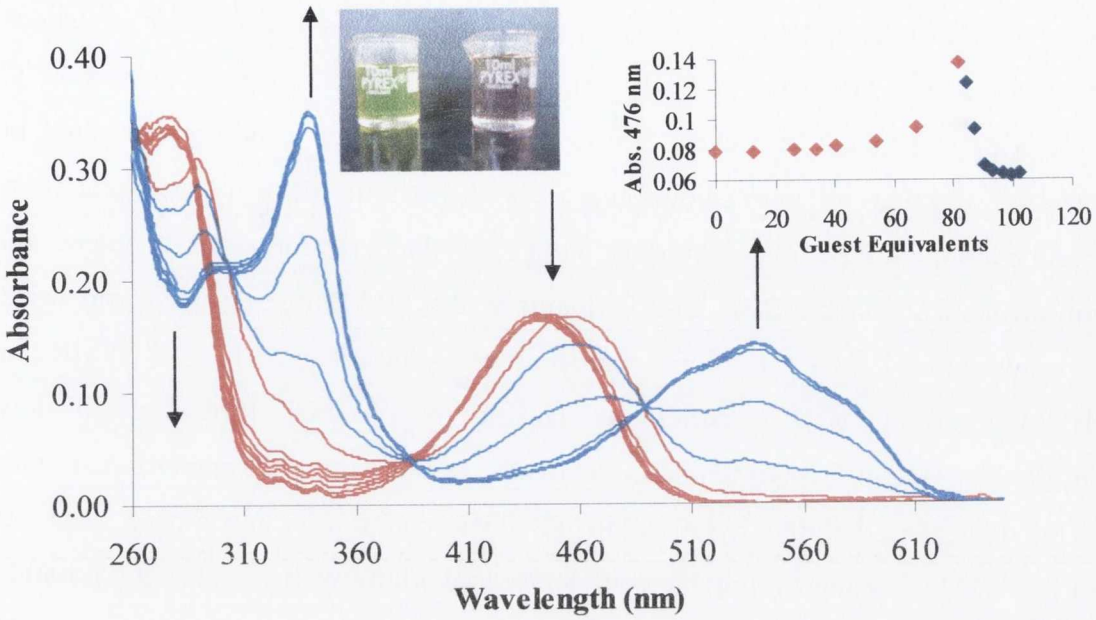


Figure 2.13: The changes in the absorption spectra of **4a** [1×10^{-5} M] upon titration with TBAOH (0→102 equivalents) in DMSO. Insert: The changes in the absorption spectra of **4a** upon addition of TBAOH (0→ 102 equivalents).

After the addition of *ca.* 80 equivalents of TBAOH, the formation of long wavelength transitions occurred (shown in blue), which resulted in a colour change of the solution from yellow to pink-purple, Figure 2.13. These larger changes were assigned to deprotonation of the 4-amino moiety.[107]

No further changes were observed in the absorption spectra after the addition of *ca.* 90 equivalents of TBAOH. The plot of the changes in the ICT transition, shown as an insert in Figure 2.13, clearly show the two-step process occurring. The species formed from deprotonation of the thiourea moiety is not stable, with respect to further TBAOH addition, and the second deprotonation occurs thereafter. Additionally, the changes observed upon titration of **4a** with F^- (Figure 2.6), were similar to the initial changes above with TBAOH, and occurred within a similar concentration range. This indicates that deprotonation of the receptor moiety of **4a** may also occur in the presence of low concentrations of F^-, as previously postulated in Scheme 2.2.

The long wavelength changes in the absorption spectra of **4a** occurred at *ca.* 90 (±10) equivalents of TBAOH. The concentration of TBAOH (*ca.* 90 equivalents) needed to fully quench the fluorescence emission of **4a** was slightly more than needed to quench the fluorescence using F^- (60 equivalents). If deprotonation is occurring with F^-, this implies a possible error in the concentrations of the stock solutions, as TBAOH is a stronger base. The concentration of sensor **4a** was accurate, as the molar absorption coefficient in DMSO

was determined. However, the TBA^+ salts are hygroscopic materials and, hence, are stored in a desiccator over P_2O_5. In comparison to the TBA^+ salts of AcO^-, $H_2PO_4^-$ and HO^-, the F^- used for the previous titrations was a hydrate, in which the number of water molecules was not specified. The TBA salts of AcO^- and $H_2PO_4^-$ were dried under vacuum at 40° C over P_2O_5 prior to titration, however, it was reported that such conditions resulted in decomposition of TBAF.[33] These studies also showed that removal of all the water from TBAF resulted in rapid E2 elimination of the butyl alkyl chain, the formation of butene and the thermodynamically stable HF_2^- ion.[158] Therefore, the TBAF utilised above was dried under vacuum over P_2O_5 at room temperature. Additionally, the ^1H NMR of $TBAOH.30H_2O$ (400 MHz, DMSO-d_6) showed the gradual formation of low concentrations of butene at room temperature, over a 48 hour period (Appendix A, Figure A11). This indicated that the hygroscopic TBAOH, could also decompose, such as reported for TBAF,[33] demonstrating the complexity in working with F^- salts, and possibly hydroxides. This complexity is demonstrated in the following section, in which sensor **4a** was titrated with commercially available $TBAF.3H_2O$. It was thought that these titrations would be more accurate, as the hydration state of the F^- salt was specified.

2.6 Absorption and Fluorescence Titration of Sensor 4a with $TBAF.3H_2O$

Titration with $TBAF.3H_2O$ gave rise to changes in both the absorption and emission spectra of **4a**, which were similar to that reported in the above section (Appendix A, Figures A12-13). Figure 2.14 shows the relative changes observed in the ICT transition

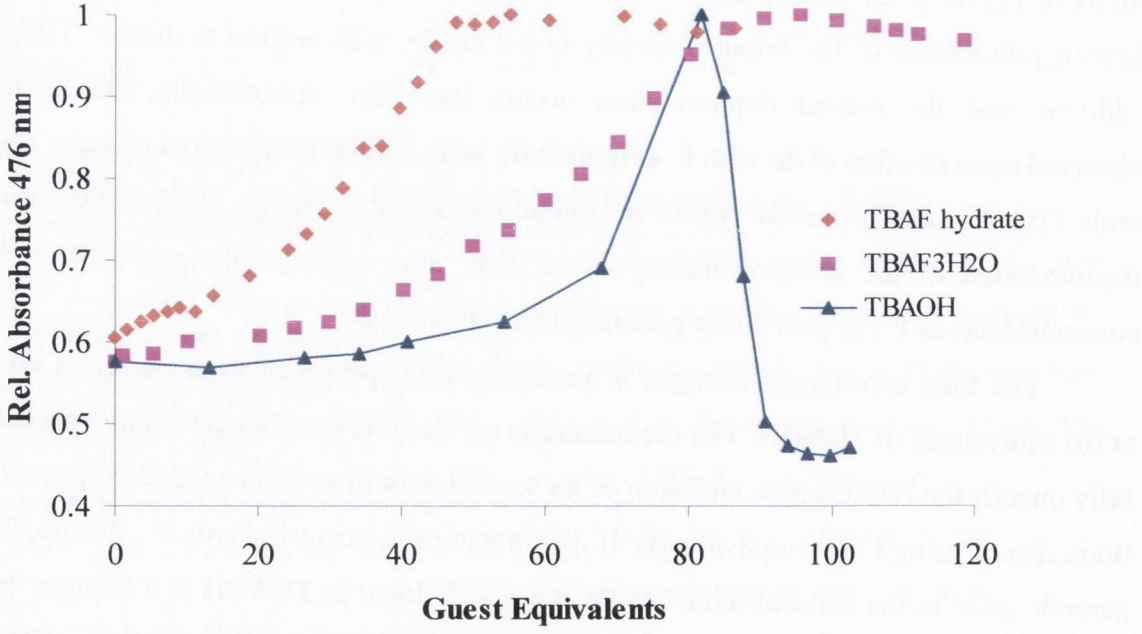


Figure 2.14: The relative changes in absorption spectra of **4a** at 476 nm with various anions

of the absorption spectra, upon titration of both F^- salts, and also the changes observed due to deprotonation, which were discussed above. In comparison with TBAOH, the binding isotherms for both titrations with F^- indicate that a single main process occurs and also that the final species in solution are stable, with respect to further F^- addition, within the concentration range shown. A full quenching of the fluorescence emission was observed (Figure 2.15) for both F^- salts, which also occurred within the same concentration range as above. Additionally, the changes in both the absorption and the emission spectra of **4a** upon titration with both F^- salts were reproducible with a higher affinity observed for the hydrated F^- species on each occasion.

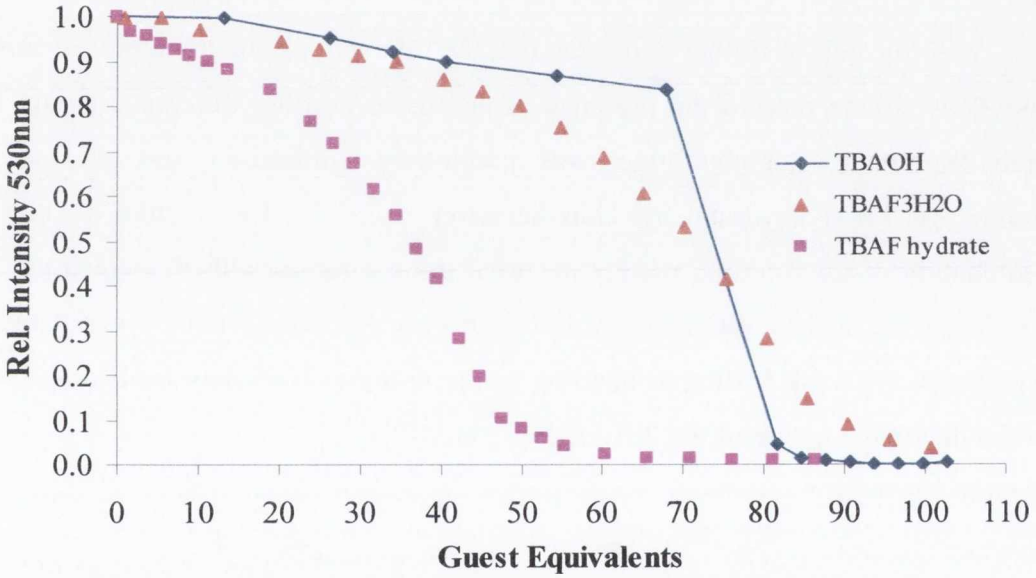


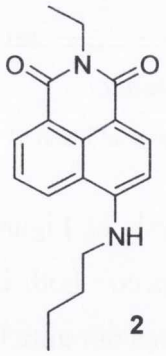
Figure 2.15: The changes in the emission of **4a** upon addition of various anions

Various interpretations can be made from analysis of Figures 2.14 and 2.15. The binding isotherms from the absorption and emission spectra both indicate that sensor **4a** has a higher affinity for the hydrated F^- species. This was not anticipated as 'wet' F^- may have lead to the preparation of stock solutions with a lower F^- content than calculated. The changes in both the absorption and emission spectra of **4a** with the hydrated F^- occurred at a lower concentration than seen with TBAOH, which possibly indicates the formation of a hydrogen bonded complex. Compared with these results, the changes observed with the tri-hydrated F^- and TBAOH occurred over a similar concentration range. In this instance, a deprotonation of the receptor by F^- is indicated. The establishment of the exact nature of the Host:Guest interaction is complicated by the above results. Both F^- titrations may represent different kinds of interactions in solution, *i.e.* the presence of water may promote hydrogen bonding of F^- to the receptor. However, the complexities of working with F^-

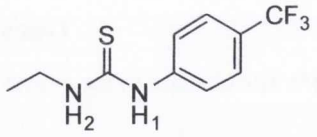
salts, which were discussed in the previous section, could also be the source of these varied changes. The concentrations of the solutions used for the F^- titrations may be inaccurate. Indeed, work carried out by Sessler, Schmidten and Gale, which focused on the effect of solvent and counter-cations in anion binding, mentioned these complexities as the reason why they choose Cl^-, and not F^-, for their studies.[34] In a further attempt to establish the nature of the Host:Guest interactions, reference compounds **2** and **37** were synthesised and their photophysical properties were investigated. These are discussed in the following section.

2.7 Design, Synthesis and Photophysical Properties of Reference Compounds 2 and 37

With the aim of further understanding the interactions above, reference compounds **2** and **37** were analysed in the presence of anions in DMSO. Reference compound **2**, a simple 4-amino-1,8-naphthalimide, was previously synthesised and analysed in the presence of TBAF hydrate by Gunnlaugsson *et al.*[107] These studies showed that deprotonation of the 4-amino moiety occurred upon titration with F^-, which gave rise to large changes in the absorption and emission spectra. Although **2** does not contain an anion receptor moiety, weak hydrogen bonding to the 4-amino N-H may lead to spectroscopic changes due to the nature of the ICT excited state.[120,153]



2



37

Receptor **37** was designed in order to understand more fully the changes in the absorption spectra of the thiourea moieties of sensors **4a** and **4b,** which absorb at short wavelengths. Similar phenyl based urea and thiourea receptors have been reported to bind AcO^- and one equivalent of F^- with deprotonation occurring upon addition of a second equivalent of F^-.[161,163] Receptor **37** was synthesised in a single step by reacting *n*-ethylamine with 4-trifluoromethylphenyl isothiocyanate in $CHCl_3$. After reducing the volume of the reaction, it was also poured into water giving a precipitate which was collected by filtration and dried in air to give a white solid in 80% yield. The ^1H NMR (400 MHz, DMSO-d_6) of **37** showed two thiourea protons, N-H_1 and N-H_2, which

resonated at 9.81 and 8.06 ppm, respectively. Indeed, these chemical shifts are similar to those observed for the thiourea protons of **4b**.

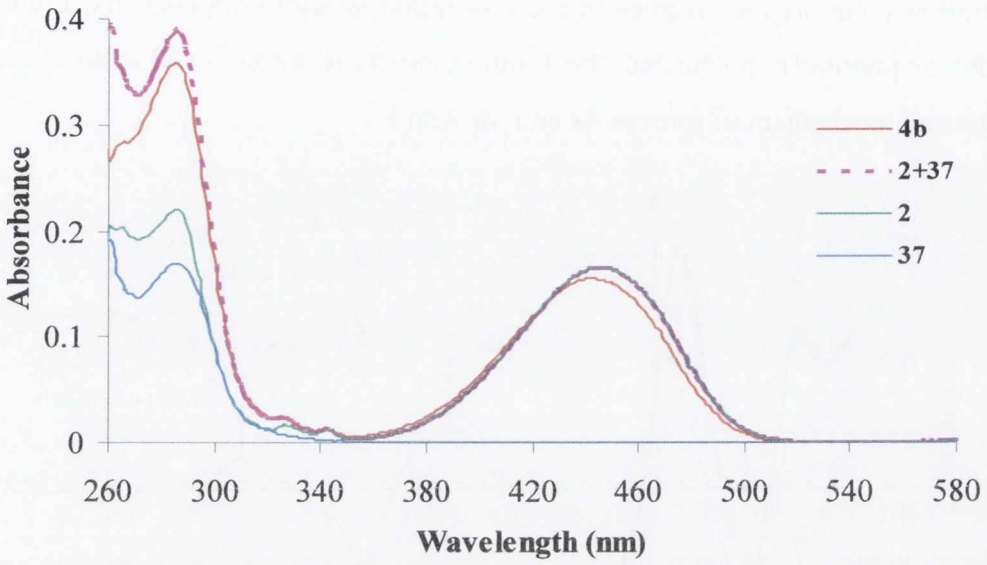


Figure 2.16: The absorption spectra of sensor **4b** and reference compounds at 1×10^{-5} M in DMSO.

The absorption spectra of **2** and **37** in DMSO, as well as the analogous CF_3 based sensor **4b**, are shown in Figure 2.16. The absorption spectrum resulting from the addition of both those of **2** and **37** is also shown and is very similar to that of sensor **4b**, thereby illustrating how titration of the reference compounds may aid to describe the anion interactions with the thiourea receptors and the 4-amino moiety of sensors **4a-c.** It was anticipated that titration of **2** with TBAOH may distinguish between changes due to hydrogen bonding or deprotonation of the 4-amino moiety with F^-.[107] Additionally, titration of receptor **37** with AcO^-, F^- and TBAOH would likely give rise to different changes in the absorption spectra at short wavelengths, which could be compared to those for sensors **4a-c**.

2.7.1 Absorption and Fluorescence Titration of Reference Compound 2 with F^- and TBAOH

In order to understand more the F^- induced changes at the 4-amino moiety of **4a-c**, reference compound **2** (ε = 15083 M^{-1} cm^{-1}) was titrated with both of the F^- salts, TBAF hydrate and TBAF.$3H_2O$, as well as with TBAOH in DMSO.

Upon titration with the hydrated F^-, the appearance of new transitions in the absorption spectra of **2** did not occur until after the addition of *ca.* 60 equivalents (±10), as shown in Figure 2.17. As reported within the literature, these changes, which occur simultaneously at 285, 340, 440 and 540 nm, when the long wavelength ICT transition is

red shifted, are due to deprotonation of the 4-amino moiety.[107] No changes at short wavelengths or a shift in the ICT transition occurred, such as those seen for **4a** in Figure 2.6. Full quenching of the fluorescence emission of **2** occurred within the same concentration range as the changes in the absorption spectra (Appendix A, Figure A14). Therefore, as previously postulated, the 4-amino moiety is not involved to any great extent in the sensing mechanism of sensors **4a** and **4b** with F^-.

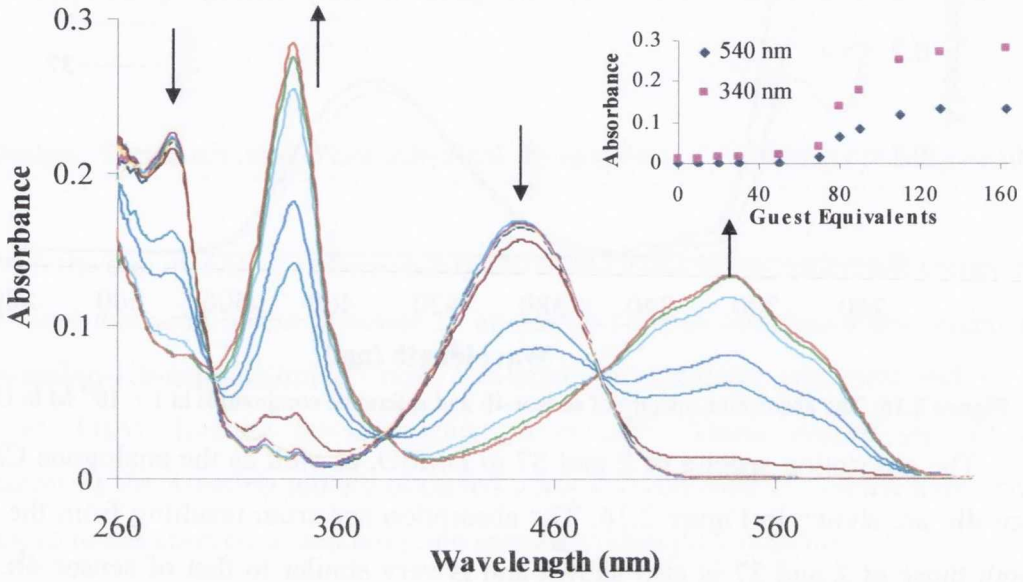


Figure 2.17: The changes in the absorption spectra of **2** [1.0×10^{-5} M] upon addition of F^- (0 → 163 equivalents). **Insert:** The changes at 340 and 540 nm.

Titration of **2** with TBA.F.$3H_2O$ also gave rise to similar changes in the absorption and the emission spectra (Appendix A, Figures A15-16). However, as observed for **4a** in Section 2.6, a larger concentration of TBA.F.$3H_2O$ was required to induce deprotonation (> 230 equivalents) and also for the changes to reach a plateau (> 450 equivalents), in comparison to the hydrated F^-. As discussed above, this is most likely due to the composition of the F^- salts, which was discussed in Sections 2.5 and 2.6.

Titration of **2** with TBAOH mirrored the titrations with both F^- salts. Comparison of the changes in the absorption spectra, at 340 nm, indicated that a one step process occurred in the presence of F^- and TBAOH (Appendix A, Figure A17). This further indicated that there is no measurable hydrogen bonding occurring, between the N-H moiety of **2** and F^-, prior to deprotonation. Therefore, it is likely that a neat deprotonation of the acidic 4-amino moiety occurs with the release of HF, which can then react with further F^- to form the stable self complex, bifluoride (HF_2^-).[157]

2.7.2 Absorption Titration of Reference Compound 37 with AcO^-, F^- and TBAOH.

In order to gain insight into the anion induced changes occurring at the receptor site in sensors **4a** and **4b**, compound **37** (ε = 16074 M^{-1} cm^{-1}) was titrated with AcO^-, TBAOH and both F^- salts in DMSO. Compound **37** is only weakly fluorescent, therefore, only absorption titrations were carried out.

The absorption spectrum of **37** in DMSO exhibited a broad band, centred at 286 nm, tailing into 350 nm. As seen for sensors **4a-c**, no significant changes were observed in the absorption spectra up to the addition of 20 equivalents of AcO^-. Thereafter, a very slight bathochromic shift at 286 nm (*ca.* 3 nm) was observed, most likely indicating the formation of a hydrogen bonded complex with the thiourea receptor moiety[161] (Appendix A, Figure A18).

In contrast, titration of **37** with TBAF hydrate (Figure 2.18) resulted in the appearance of a new transition centred at *ca.* 333 nm, which reached a plateau after the addition of *ca.* 50 equivalents of anion. A concomitant decrease in the absorbance at 285 nm was also observed. These changes gave rise to the formation of a single psuedo isobestic point at *ca.* 302 nm, indicating that there was most likely only two major species present in solution.[155] Although these changes could not be fitted using SPECFIT™, the EFA also indicated the presence of two main species in solution. Titration of **37** with $TBAF.3H_2O$ gave rise to similar changes in the absorption spectra, which occurred over similar concentration ranges (Appendix A, Figure A19). However, some differences were observed between the titrations of **37** with both F^- salts (see later).

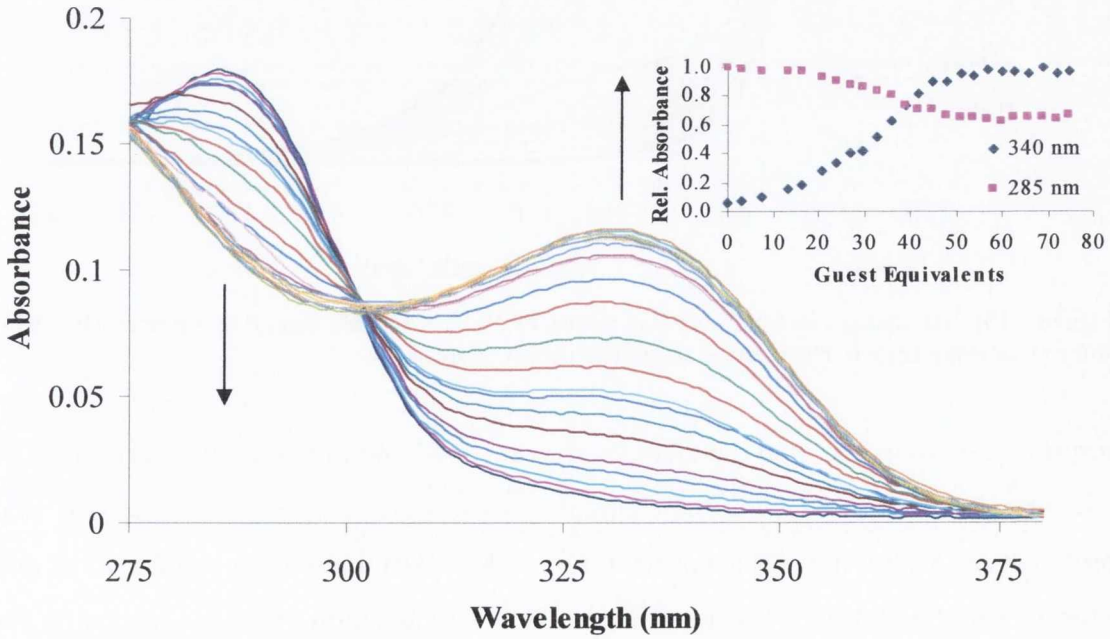


Figure 2.18: The changes in the absorption spectra of **37** [1.1×10^{-5} M] upon addition of TBAF hydrate (0 → 74 equivalents) **Insert:** The relative changes against guest equivalents at 285 and 340 nm.

Titration of **37** with TBAOH resulted in larger changes in the absorption spectra in comparison to those with F^-, as shown in Figure 2.19. The initial changes, shown in red, were only minor but occurred with the formation of a pseudo isobestic point at *ca.* 289 nm. Subsequently, the course of reaction between **37** and TBAOH changed, shown in blue, with the formation of an isobestic point at 302 nm. At high concentrations of TBAOH (> 90 equivalents, 2 mM) further changes (shown in green) were observed, in which an increase in the absorbance occurred with a concomitant blue shift. The changes at 285 nm are shown as insert of Figure 2.19 and clearly indicate the occurrence of these three main processes in solution. These tri-phasic changes suggest a possible deprotonation of both N-H fragments of the thiourea receptor. Yatsimirsky *et al.* have previously reported small initial changes in the ^{1}H NMR spectra of similar receptors, upon titration with TBAOH in DMSO-d_6, which are reportedly due to the existence of both singly and a small amount of doubly deprotonated forms of the receptor, in a slow equilibrium.[161] This results in a strong delocalisation of negative charge giving rise to only minor changes in the chemical shifts of the ^{1}H NMR spectra. If such a process were to occur in the concentration range of

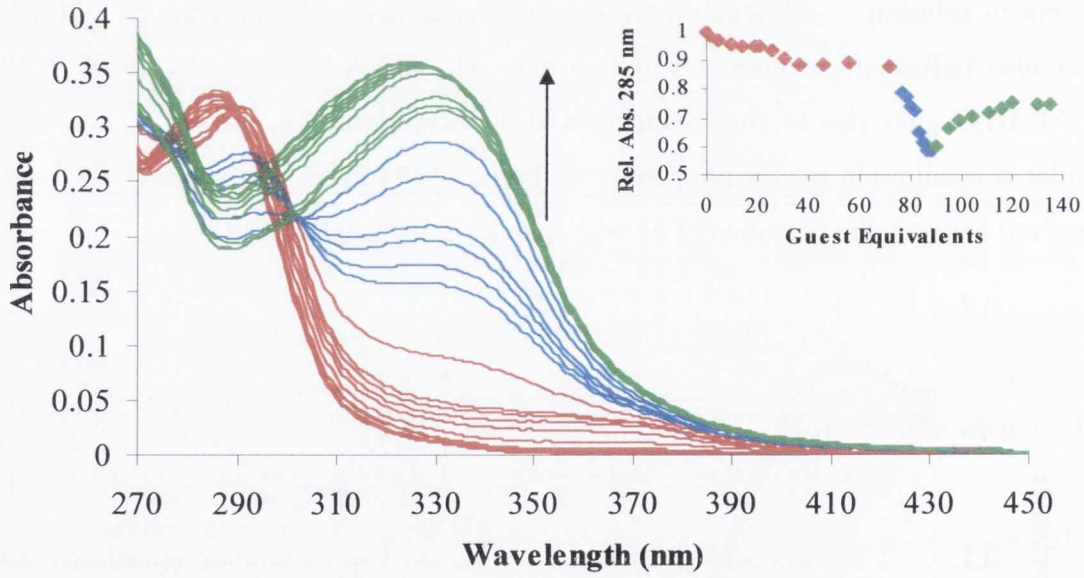


Figure 2.19: The changes in the absorption spectra of **37** [2×10^{-5} M] upon titration with TBAOH (0 → 130 equivalents). **Insert:** The changes at 285 nm against equivalents.

absorption spectroscopy, then the changes shown in red and blue may represent, overall, a single deprotonation of **37**, with the changes shown in green signifying a possible second deprotonation. Additional species present during the TBAOH titration could also be due to the formation of a hydrogen bonded complex between the anion of **37** and its neutral form,

which finally becomes deprotonated at sufficiently high TBAOH concentration. However, the formation of such species is not certain and is only speculative.

The spectroscopic differences between the titrations of **37** with both F^- salts and TBAOH were analysed by plotting the ratio of the absorbances at 332 and 285 nm, as shown in Figure 2.20. This plot clearly shows that there is a difference between the changes observed in both of the F^- titrations. Re-examination of these titrations showed that the new transition, which occurred at *ca.* 333 nm upon the addition of F^-, was equal in magnitude for both F^- salts. However, in contrast, slightly larger changes were observed at 285 nm for the tri-hydrated F^- salt, hence, giving rise to the different ratios. Despite these differences, the plot indicates that a single process occurs upon titration with both F^- salts. In this instance, mono-deprotonation is a likely occurrence, due to the basic nature of F^- and also the large excess added (*ca.* 50 equivalents).

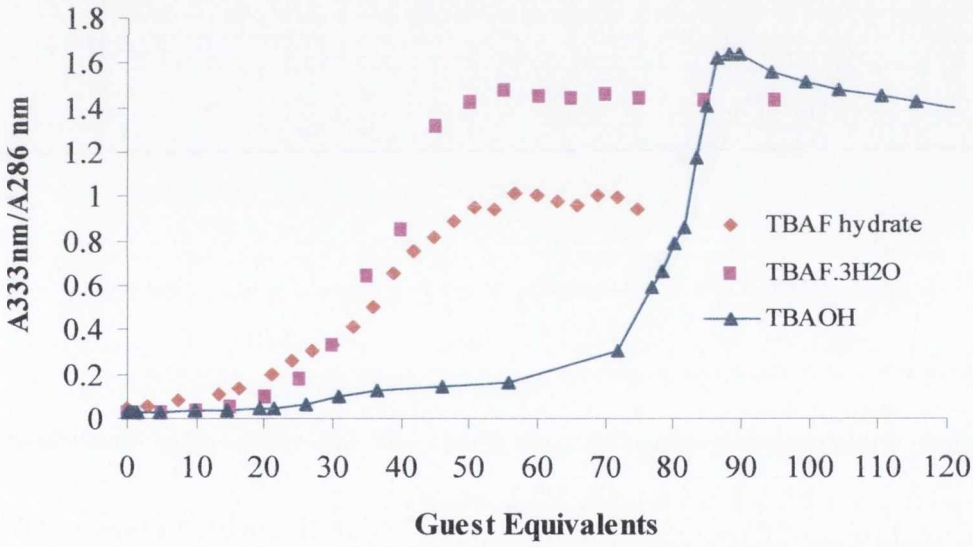


Figure 2.20: The changes in the absorption spectra, $A_{333nm}/A_{286\ nm}$, of **37** upon addition of various anions.

A deprotonation was further supported by the presence of isobestic points at *ca.* 302 nm in both the F^- and TBAOH titrations, which may indicate the occurrence of a common species in solution. Additionally, the binding isotherm at 340 nm, shown as insert in Figure 2.18, shows a minor inflexion point at *ca.* 30 equivalents of F^-. This was observed on more than one occasion and occurred at similar concentrations. This may indicate that hydrogen bonding of F^- occurs up to this point, which is then followed by deprotonation, however, this is not certain and will be further investigated by ^1H NMR titrations.

The results obtained from the titrations of both **2** and **37** with F^- were compared with those for **4b**. Figure 2.21 shows the resulting absorption spectra of **4b**, **2** and **37**, after

titration with F^- (*i.e.* the endpoint). These spectra all show changes at short wavelengths (*ca.* 340 nm) when compared to their spectra prior to titration, Figure 2.16. The changes at *ca.* 340 nm in the absorption spectra of **2** do not occur in the absence of long wavelength changes. Therefore, as previously stated, this shows there is no substantial contribution from the 4-amino moiety in the sensing mechanism of **4a-c**. However, the absorption spectrum resulting from titration of **37** with F^- overlaps the changes in the absorbance at short wavelengths for **4b** with F^-. These changes clearly identify the thiourea receptor as the site of anion interaction and, therefore, also as the source of emission quenching.

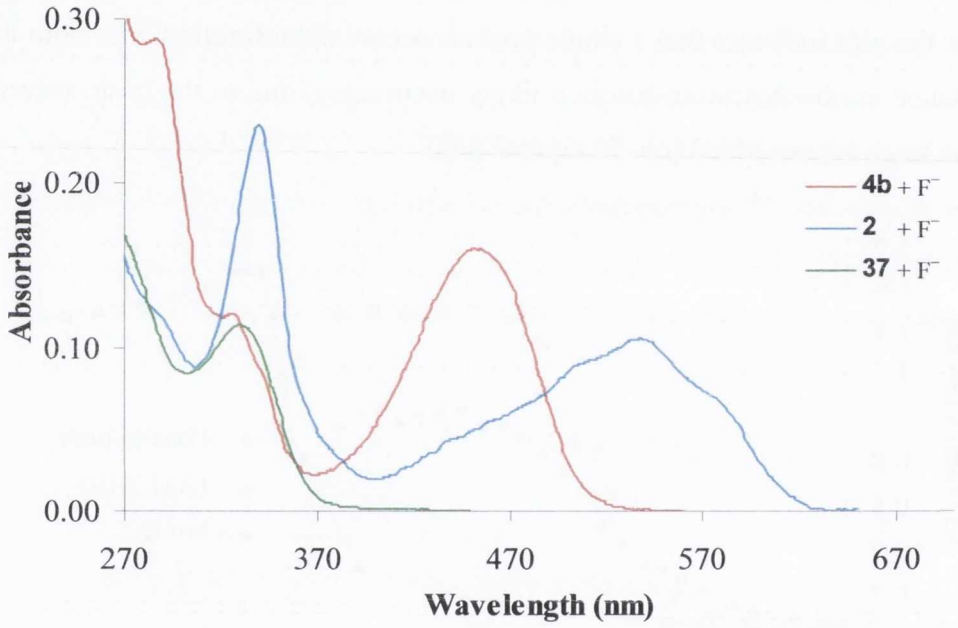


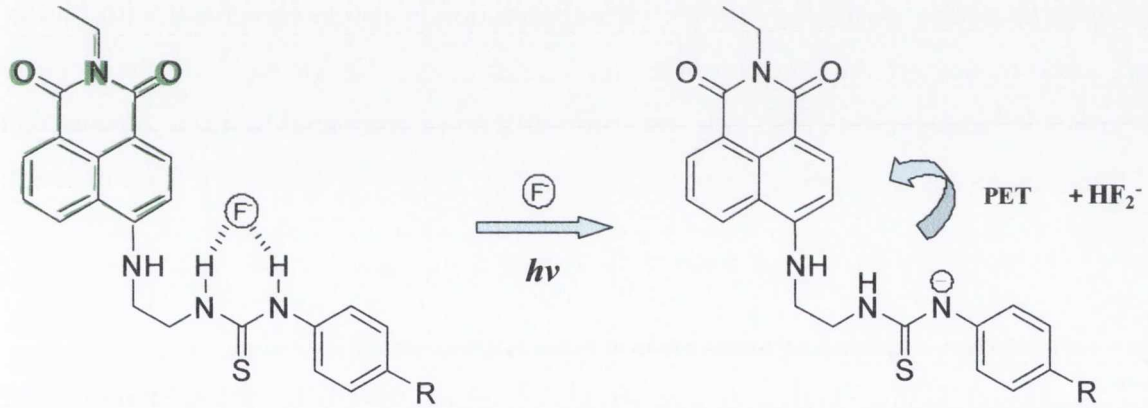
Figure 2.21: The absorption spectra of **4b**, **2** and **37** at [1×10^{-5} M], which resulted from titration with F^- in DMSO.

2.8 Conclusion of Photophysical Measurements of 4a-c with Anions in DMSO

Sensors **4a-c** were developed with the aim of detecting the presence of anions, such as AcO^-, $H_2PO_4^-$ and F^-, *via* PET in DMSO solution. Their design was based on that of structurally similar anion sensors, which have been previously reported within the literature.[111] Indeed, these sensors showed changes of varying degree in both their absorption and emission spectra, upon titration with different concentrations of the aforementioned anions.[112] The largest spectroscopic responses were observed upon titration of sensors **4a-c** with F^-, for which full quenching of their fluorescence emission spectra occurred. Small changes were observed in their absorption spectra, therefore, classifying these sensors as selective fluorescent PET sensors for F^-, as their fluorescence emission was only slightly quenched by AcO^- and $H_2PO_4^-$. Although the fluorescence emission of **4c** was also quenched by F^-, its affinity for the anion was far lower and full quenching required much higher concentrations than for **4a** and **4b**. This is due to the less

electron withdrawing urea receptor of sensor **4c** compared to the thiourea analogues. No quenching of the fluorescence emission of **4a-c** occurred upon addition of other halides (Cl^- and Br^-), which ruled out the heavy atom effect as the mechanism of quenching. The smaller changes observed in both the absorption and emission spectra of **4a** and **4b** with AcO^- and $H_2PO_4^-$, were most likely due to the formation of hydrogen bonded complexes, which in the case of $H_2PO_4^-$ consisted of contributions from the 4-amino moiety as well as the receptor.

The nature of the anion interactions was investigated *via* absorption and fluorescence titration of **4a** with TBAOH and also by titration of the reference compounds **2** and **37** Titration of sensor **4a** with TBAOH indicated that deprotonation of the thiourea receptor moiety leads to a full quenching of the emission. Although such quenching was also observed for **4a** and **4b** with F^-, this may be due to hydrogen bonding, deprotonation or a combination of both, such as depicted in Scheme 2.3.



Scheme 2.3: Schematic representation of possible F^- interactions resulting in quenching of the naphthalimide emission.

The final species in solution after titration of **4a** with F^- is most likely the deprotonated receptor, as similar results were observed for the TBAOH titrations and also because of the excess F^- present in solution. This was supported by the photophysical analysis of receptor **37** in the presence of F^- and TBAOH. A shift of the ICT transition in the absorption spectra of both sensors **4a** and **4b** was observed upon titration with $H_2PO_4^-$. This shift was assigned to cooperative binding of the tetrahedral $H_2PO_4^-$ anion. Similarly, a shift in the ICT transition was observed with F^-, however, cooperative binding with F^- seems unlikely, due to its smaller size. No shift was observed in the ICT transition of **2** upon deprotonation with either F^- or TBAOH. Therefore, we do not anticipate that a hydrogen bonding interaction occurred between F^- and the 4-amino moiety of sensors **4a-c**. Rather, we anticipate that the shift in the ICT transition may be due to through space interactions between the deprotonated receptor and the 4-amino moiety. Such interactions

have been previously postulated for structurally similar sensors.[119] The interactions postulated above will be investigated further in the following section *via* anion titration using ^{1}H NMR spectroscopy in DMSO-d_6.

The work carried out in the previous chapter also highlights some complexities when using the TBA^+ salts of F^- and OH^-. While titration of **4a** with both F^- salts resulted in similar spectroscopic changes, the concentrations required to induce these changes were different. Additionally, slightly different spectroscopic changes were seen for the titration of **37** with both F^- salts. Despite these complexities, these titrations were useful in helping to define the anion interactions with sensors **4a-b**. It is anticipated that the different results for both F^- salts are likely due to the extremely hygroscopic nature of these salts as well as their composition, instability in solution and ability to decompose upon drying.[33]

As outlined in the objectives (Section 2.0), it was shown that removing the benzyl receptor of **3** and replacing it with a phenyl receptor leads to an enhancement in PET upon titration with anions, particularly for F^-. This observation is also in agreement with Pfeffer *et al.*, who have reported quenching of a very similar magnitude for **5a**.[115] As the electron rich aromatic spacer of **5a** is the only structural difference compared to **4a**, it appears that the thiourea receptor is mainly responsible for the enhancement in PET upon anion binding.

2.9 ^{1}H NMR Titrations of Sensors 4a-c with Anions in DMSO-d_6

This section investigates the interactions of sensors **4a-c** with various anions using ^{1}H NMR spectroscopy. The changes in the ^{1}H NMR spectra of DMSO-d_6 solutions were monitored upon the addition of AcO^-, $H_2PO_4^-$, F^- and HO^- as their tetrabutylammonium salts. Sensor **4a** was titrated with both TBAF.hydrate and TBAF.$3H_2O$, as the concentration of F^- present could be corrected upon integration of the TBA^+ peaks relative to the methyl peak of **4a**. The composition of both F^- salts were only briefly investigated by ^{1}H NMR (400 MHz, DMSO-d_6) as an in depth analysis of these salts was not the primary focus of this thesis. It was anticipated that these results would shed some light on the differing results obtained in the absorption and fluorescence titrations. As for the previous sections, sensor **4a** and the reference compound, **37**, were both titrated with TBAOH.

2.9.1 ^{1}H NMR Titration of Sensor 4a with AcO^- in DMSO-d_6

The successive addition of AcO^- to **4a** resulted in a significant change in the chemical shifts of several protons, as shown in Figure 2.22. As expected, the largest shifts

were seen for the two thiourea protons, N-H_1 and N-H_2, both of which experienced significant downfield shifts of *ca.* 2.3 and 3.0 ppm, respectively, which are indicative of strong hydrogen bonding between the receptor and AcO^-. Small shifts were also seen for the phenyl protons of the receptor. However, the 4-amino N-H proton was only shifted by 0.15 ppm. Therefore, it was concluded that the 4-amino proton was not involved in the binding to any great extent, as seen for **3**.

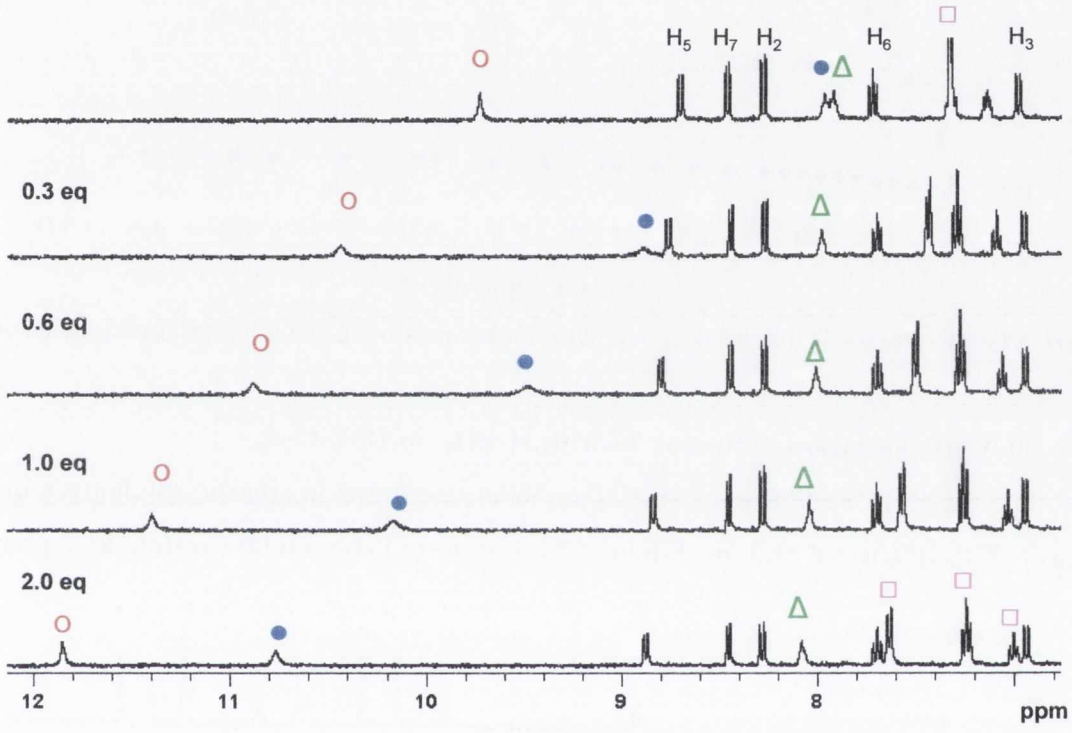


Figure 2.22: Stack plot of ^{1}H NMR spectra (400 MHz, DMSO-d_6) of **4a** [2.4 x 10^{-3} M] after addition of various equivalents of AcO^-. Red ○ and blue ● track thiourea protons N-H_1 and N-H_2, respectively. Green Δ tracks the 4-amino N-H moiety. Pink □ shows phenyl protons of **4a** and their chemical shift at two equivalents

A plot of ΔδH for several protons *vs* equivalents of AcO^- provided the binding isotherms, and is shown in Figure 2.23. The changes for the thiourea protons indicate a 1:1 Host:Guest stoichiometric interaction in solution. Figure 2.23 shows that both thiourea protons of sensor **4a** did not undergo cumulative chemical shifts of similar magnitude in the presence of AcO^-. This is in contrast to that observed for **3** and **5a** and may be due to the different micro-environments of both thiourea protons. Also, the ^{1}H NMR spectrum of **4b** (Section 2.1) showed that the introduction of the CF_3 moiety to **4a** shifted the N-H_2 proton further downfield than the adjacent N-H_1 proton. The nature of the binding of **4a** to AcO^- was investigated further through fitting of the titration data and is discussed in Section 2.12.

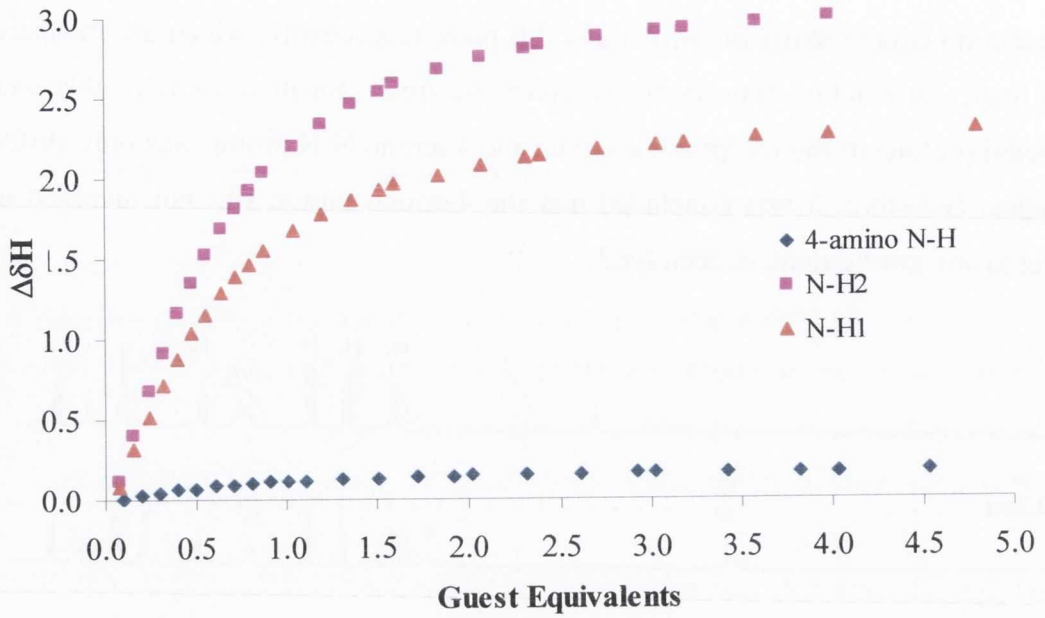


Figure 2.23: The changes in the chemical shift of the N-H protons of **4a** [2.4 x 10^{-3} M] upon addition of AcO^-.

2.9.2 ^{1}H NMR Titration of Sensor 4a with $H_2PO_4^-$ in DMSO-d_6

The successive addition of $H_2PO_4^-$ to **4a** also resulted in significant changes in the chemical shifts of several protons, Figure 2.24. Large shifts of similar magnitude, 2 ppm,

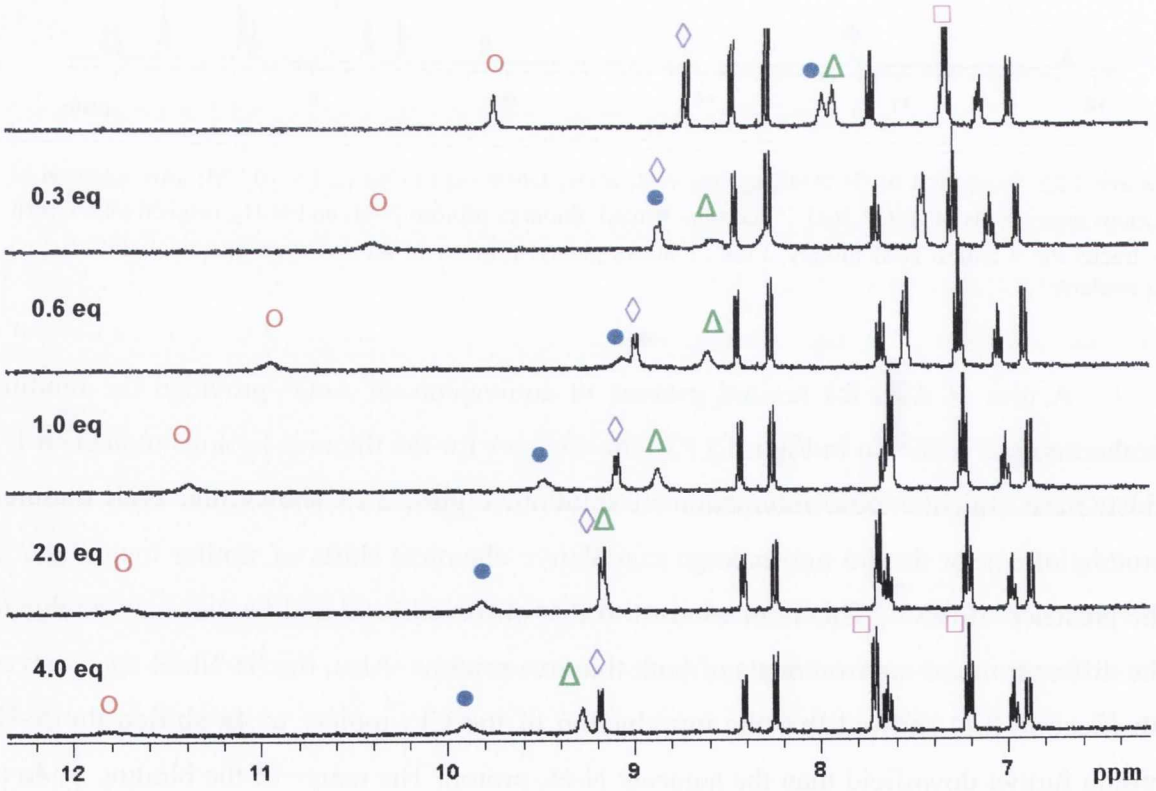


Figure 2.24 Stack plot of ^{1}H NMR spectra (400 MHz, DMSO-d_6) of **4a** [2.4 x 10^{-3} M] after addition of various equivalents of $H_2PO_4^-$. Red ○ and blue ● track thiourea N-H_1 and N-H_2 protons, respectively. Purple ◊ tracks naphthalimide H_5. Green Δ tracks the 4-amino N-H moiety. Pink □ shows the phenyl protons of **4a** and their chemical shift at four equivalents).

were observed for both of the thiourea protons. Slightly larger changes were seen for the phenyl protons, than those observed with AcO^-. However, in direct contrast to the titration of **4a** with AcO^-, the 4-amino proton also shifted downfield by 1.4 ppm, as well as the naphthalimide H_5 proton, which was shifted downfield by 0.5 ppm. In contrast, the H_3 proton only underwent a small downfield shift (*ca.* 0.1 ppm).

These results suggest the formation of a hydrogen bonded complex between the thiourea protons and the 4-amino proton, as seen for **3**.[111] By plotting the $\Delta\delta H$ for several protons *vs* the equivalents of $H_2PO_4^-$, binding isotherms were obtained and are shown in Figure 2.25.

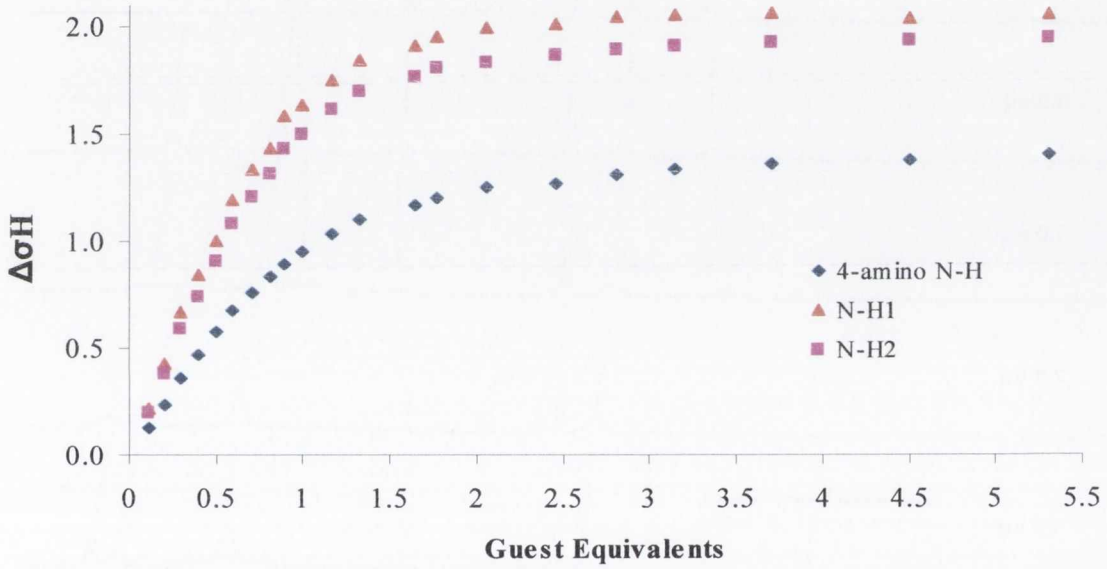


Figure 2.25: The changes in the chemical shift of the N-H protons of **4a** [2.4 x 10^{-3} M] upon addition of $H_2PO_4^-$.

A more definite plateau was also observed in the binding isotherm compared to the titration with AcO^-, indicating that a more stable complex was formed. After the addition of two equivalents of $H_2PO_4^-$, little or no change was observed for both thiourea protons.

2.9.3 ^{1}H NMR Titration of Sensor 4a with F^- salts in DMSO- d_6

Prior to titration with sensor **4a**, both the F^- salts were analysed by ^{1}H NMR and ^{19}F NMR. The corresponding spectra for both F^- salts showed the presence of HF_2^- at very low concentrations but at greater quantities in the hydrated salt.[33] A different batch of the tri-hydrate did not contain signals for HF_2^-, therefore, highlighting the inconsistency in the composition of TBAF salts, which may contribute varying experimental results with sensitive techniques. Nevertheless, ^{1}H NMR titrations of **4a** were carried out using both TBAF hydrate and TBAF.$3H_2O$. In the case of the former, the N-H signals became

significantly broadened after the addition of only a small quantity of the anion and completely disappeared after the addition of *ca.* 0.5 equivalents, as shown in Figure 2.26. The naphthalimide protons were all significantly broadened with H_5 and H_6 disappearing with the addition of *ca.* 2 equivalents. The naphthalimide H_2, H_3 and H_7 protons were least affected by these titrations, with H_2 retaining its multiplicity throughout. This can be reasoned due to their distance from the 4-amino moiety and the thiourea receptor site. In comparison to the titrations of **4a** with AcO^- and $H_2PO_4^-$, there was an upfield shift of the entire spectrum, particularly for the phenyl receptor protons. This implies that an increase

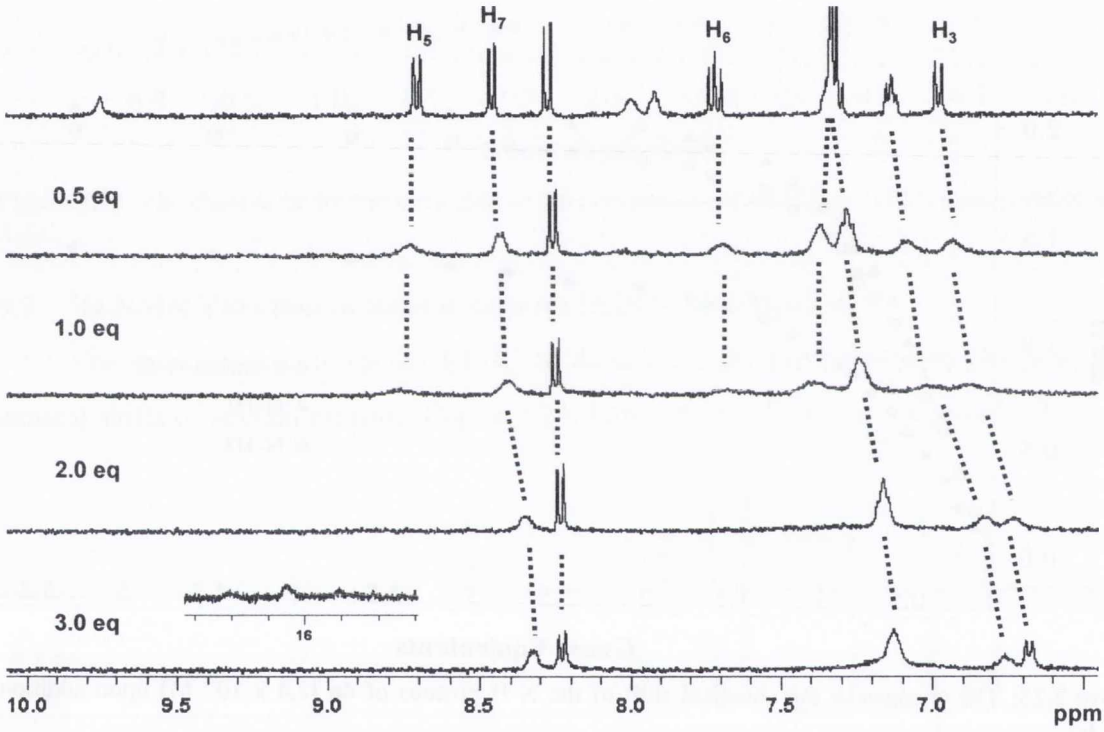


Figure 2.26: Stack plot of ^{1}H NMR spectra (400 MHz, DMSO-d_6) of **4a** [2.1×10^{-3} M] after addition of various equivalents of TBAF hydrate.

in the electron density of the phenyl moiety occurred, which is indicative of deprotonation at the receptor site. After the addition of two equivalents of F^- the formation of a weak broad signal at *ca.*16 ppm was observed, which formed a distinct triplet (J = 123 Hz) upon the addition of further F^-.[33] This occurred with a concomitant colour change from yellow-green to orange. Both these changes were assigned to the formation of HF_2^-, which are consistent with F^- mediated deprotonation. Further broadening and a colour change from orange to deep orange-red was observed, up to the addition of six equivalents of F^-.

In the case of TBAF.$3H_2O$, the changes in the ^{1}H NMR titration were very similar (Appendix A, Figure A20). Upon the addition of two equivalents of F^-, the HF_2^- triplet was observed at 16 ppm, along with a colour change to orange.

Drastic colour changes from yellow to red-purple were previously reported for sensors **3** and **5a**, upon the addition of 0.5 equivalents of F^-.[111,115] In contrast, titration of both F^- salts with **4a** did not give rise to such colour changes. The colour of **4a** in DMSO-d_6 became orange at two equivalents and then a deep orange-red at three equivalents of F^-. The presence of HF_2^- in the ^{1}H NMR spectra, after the addition of two equivalents, indicated that deprotonation of the receptor moiety occurred. As discussed in the absorption titrations of **4a** with TBAOH (Section 2.5), deprotonation of the receptor moiety does not give rise to large colour changes, as the thiourea receptor is a further distance from the naphthalimide chromophore.

2.10 ^{1}H NMR Titration of Sensor 4b with AcO^-, $H_2PO_4^-$ and F^- in DMSO-d_6

Titration of **4b** with AcO^- gave rise to similar changes in the ^{1}H NMR spectra to those observed above (Appendix A, Figure A21). Both N-H_1 and N-H_2 experienced downfield shifts of *ca.* 2.8 and 3.3 ppm, respectively. As expected, these shifts were larger in comparison to those of **4a** and are due to the presence of the electron withdrawing *p*-CF_3 moiety.

The changes in the ^{1}H NMR spectra upon titration with $H_2PO_4^-$ also resulted in similar changes to those seen for AcO^- above (Appendix A, Figure A22). However, the N-H_1 resonance was significantly broadened and disappeared after the addition of *ca.* 1.7 equivalents of $H_2PO_4^-$. Cooperative binding also occurred with sensor **4b**, as the 4-amino proton was shifted downfield by *ca* 1.4 ppm, which was of the same magnitude as seen for sensor **4a** and can be reasoned due to its distance from the electron withdrawing receptor moiety.

Sensor **4b** was solely titrated with TBAF.3H_2O (Appendix A, Figure A23), as no significant differences were observed between the ^{1}H NMR titrations of **4a** with both F^- salts (Section 2.9.3). A similar pattern of change to that seen for sensor **4a** was seen in the ^{1}H NMR titrations of **4b** with F^-. After the addition of two equivalents of F^-, the HF_2^- resonance at 16 ppm appeared along with a colour change from yellow to orange, which indicated that deprotonation also occurred.

2.11 ^{1}H NMR Titration of Sensor 4c with TBAF.3H_2O in DMSO-d_6

Although no significant changes were observed in the absorption or emission spectra of **4c** upon titration with AcO^- and $H_2PO_4^-$, changes were observed in the ^{1}H NMR spectra upon addition of these anions (Appendix, Figure A24 and 25). These changes

followed the same trend to those of **4a** and **4b** and, therefore, indicated the formation of hydrogen bonded complexes with the urea based sensor **4c**.

In contrast, the changes observed upon titration with F^- were slightly different to those observed with sensors **4a** and **4b**, Figure 2.27. Downfield shifts of *ca.* 0.5 ppm, for both urea N-H protons, were clearly visible up to the addition of 0.45 equivalent of F^-. Such clear downfield shifts of the receptor N-H protons were not observed for the thiourea derivatives, however, this is likely due to the presence of the less electron withdrawing oxygen atom of the urea moiety of **4c**, which makes the N-H protons less acidic and, hence, less efficient hydrogen bond donors. These changes occurred with a concomitant downfield shift (0.2 ppm) of the 4-amino proton. Additionally, the aromatic protons and their multiplicities were clearly visible up to the addition of one equivalent of F^-. Further addition of anion resulted in broadening of the naphthalimide resonances, however, the phenyl protons were clearly visible throughout the titration. Despite the lower acidity of the urea receptor the addition of two equivalents of F^- resulted in the formation of HF_2^-, as for titration with sensors **4a** and **4b**. The initial changes in the N-H and H_5 protons were of a similar trend to those observed with $H_2PO_4^-$, however, the downfield shifts were of a smaller magnitude.

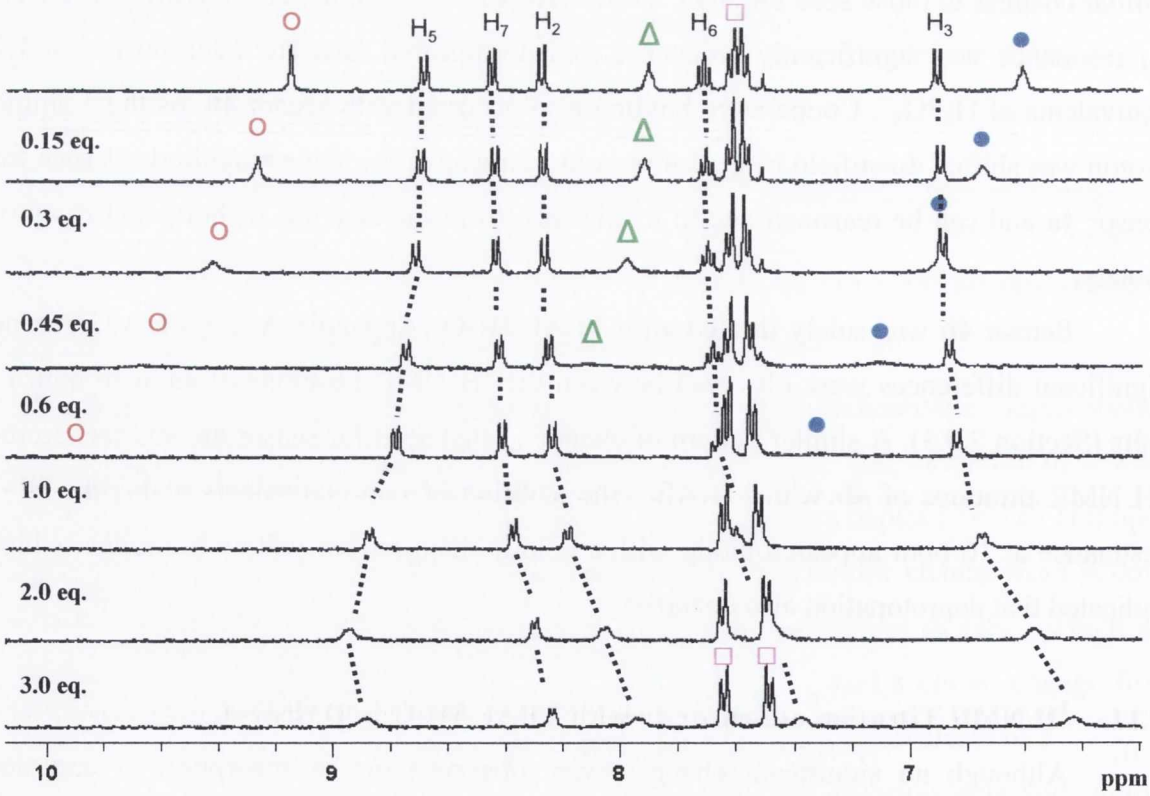


Figure 2.27 Stack plot of the ^1H NMR spectra (400 MHz, DMSO-d_6) of **4c** [2 x 10^{-3} M] after addition of various quantities of F^-. Red ○ and blue ● track thiourea N-H_1 and N-H_2 protons, respectively. Green Δ tracks the naphthalimide N-H moiety. Pink □ shows phenyl protons of **4c** and their chemical shift at three equivalents)

These changes indicate the formation of a hydrogen bonded complex with the urea sensor **4c**, which may involve a contribution from the 4-amino moiety, up to the addition of one equivalent. These results are in contrast to the absorption and fluorescence titrations, in which little or no changes were observed at low concentration of F^-.

2.12 Determination of Binding Constants for 4a and 4b upon titration with AcO^- and $H_2PO_4^-$ using ^1H NMR Spectroscopy

Binding constants were determined for both sensors **4a** and **4b** with AcO^- and $H_2PO_4^-$, as their N-H protons underwent large chemical shifts. The changes in the ^1H NMR spectra of **4a-c** upon addition of F^- were not fitted, due to the observed broadening and smaller chemical shifts of the signals. The ^1H NMR data was fitted using *NMRTit HG*, which fits the data to a 1:1 binding isotherm, and also with *NMRTit HGG* and NMR*TitHHG* which fits to 1:2 and 2:1 binding isotherms, respectively, by an iterative procedure.[164] The binding of $H_2PO_4^-$ to **4a** was firstly analysed using *NMRTit HG*. The changes in the chemical shifts of all three N-H protons fitted well to a 1:1 stoichiometric interaction. The fit generated for N-H_1, the most downfield thiourea proton, at 9.7 ppm is shown in Figure 2.28, for which a binding constant of $\log K_{1:1}$ = 3.8 was determined. Similarly, a $\log K_{1:1}$ of 3.7 was determined upon fitting the changes seen for the N-H_2 proton (Appendix A, Figure A26).

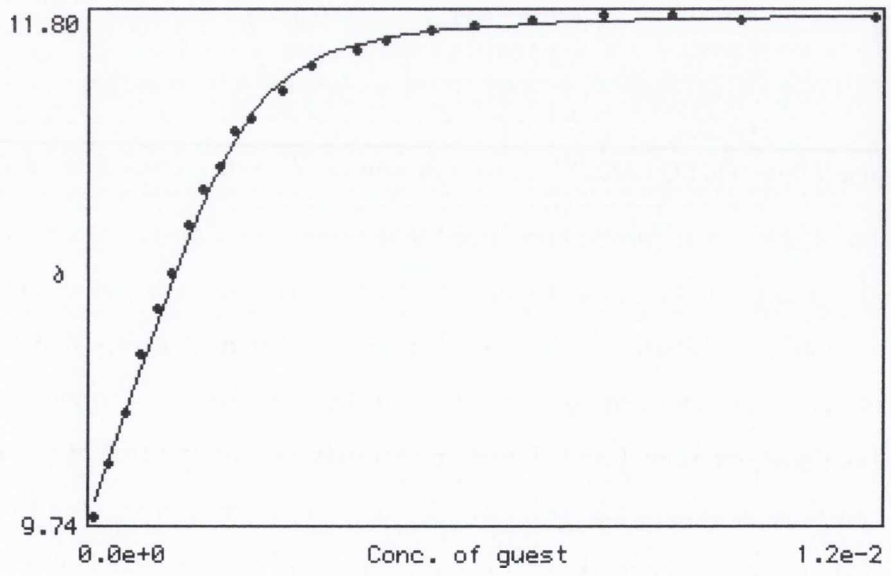


Figure 2.28: The binding isotherm and fit obtained for **4a** upon fitting of the changes in the chemical shift of N-H_1 to a 1:1 complexation model, upon addition of $H_2PO_4^-$.

The changes in the chemical shift of the 4-amino proton also fit well to the 1:1 stoichiometric model, with a $\log K_{1:1}$ of 3.3 (Appendix A, Figure A27). This is a slightly

lower constant than that obtained for the thiourea protons, however, the 4-amino moiety underwent a smaller cumulative chemical shift upon binding. Only the N-H_2 and the 4-amino protons of sensor **4b** were fit upon titration with $H_2PO_4^-$, as after one equivalent the N-H_1 resonance disappeared. The binding constants determined for a 1:1 stoichiometric interaction were $\log K_{1:1}$ = 4.4 and 3.7, respectively. (Appendix A, Figure A28-29). As expected, these constants were higher than those determined for the phenyl receptor, **4a**. The changes for sensor **4a** with AcO^- also fit well to the 1:1 stoichiometric model, which resulted in $\log K_{1:1}$ = 3.5, for both thiourea protons (Appendix A, Figure A30-31). This value is the same as that determined from the fluorescence measurements of **4a** with AcO^- ($\log K_{1:1}$ = 3.5 ± 0.01). In a similar manner, the changes for sensor **4b** with AcO^- fitted well to the 1:1 model and binding constants of $\log K_{1:1}$ = 3.9 were determined for both thiourea protons (Appendix, Figure A32-33). These results are summarised in Table 2.1 and are compared to those previously reported in the literature, by Gunnlaugsson and Pfeffer *et al.*[111,115]

Table 2.1: Cumulative chemical shifts and stability constants determined from fitting the changes in the N-H_2 proton of **4a-b** in DMSO-d_6.

Receptor	Anion	Log$K_{1:1}$	$\Delta\delta H_{naph}$(pm)	$\Delta\delta H_1$(ppm)	$\Delta\delta H_2$(ppm)
3*	AcO^-	3.6 (± 0.1)	-	2.5	2.5
	$H_2PO_4^-$	3.4 (± 0.1)	1.6	1.8	1.8
5a*[a]	AcO^-	2.8 (± 0.1)	< 0.5	3.5	3.5
	$H_2PO_4^-$	3.7[a]	1.4	1.9	1.9
4a[b]	AcO^-	3.5 (± 0.1)	0.1	2.3	3.0
	$H_2PO_4^-$	3.7 (± 0.1)	1.4	2	2
4b[b]	AcO^-	3.9		2.8	3.3
	$H_2PO_4^-$	4.4	1.4	2.4	2.0

*Values obtained from Win EQ NMR. [149] [a]Value is an estimate. [115] [b]Values obtained using *NMR*tit.

From Table 2.1 it can be concluded that replacement of the benzyl moiety in **3** by the phenyl moiety in **4a** leads to an increase in the $\log K_{1:1}$ value obtained for the cooperative binding of $H_2PO_4^-$, which is also comparable to that reported for receptor **5a**. The binding constant obtained for the 1:1 fit of **4a** with AcO^- is larger than obtained for **5a**, but less than that seen for **3**. It was previously postulated that the reduction in the binding constant obtained for **5a** may be due to steric constrain introduced by the preorganised aromatic spacer. However, removal of the benzyl spacer of **3** also resulted in a slight decrease in the binding constant. The N-H_2 proton of both sensors **4a** and **4b** was shifted further downfield than N-H_1 in the presence of AcO^-, which indicates that this proton is not sterically hindered by the naphthalimide moiety.

2.13 ^{1}H NMR Titration of Sensor 4a with TBAOH in DMSO-d_6

As for the absorption and fluorescence titrations of sensor **4a**, ^{1}H NMR titrations of **4a** with TBAOH were also carried out. Similarly to that seen for F^-, there was a complete disappearance of the N-H peaks. However, this occurred with the addition of only 0.1 equivalent of TBAOH, Figure 2.29. The subsequent changes were also similar to those seen for F^-, but again, only up to the addition of one equivalent of TBAOH. After the addition of 1.5 equivalents, the spectrum was broadened and the naphthalimide protons were no longer visible. This occurred with a concomitant colour change from orange to deep red. Upon the addition of two equivalents a second colour change from red to deep purple was observed, in a similar manner to that seen upon titration of **3** and **5a** with F^-. The corresponding ^{1}H NMR spectrum exhibits sharp peaks in the aromatic region, which have been shifted upfield, and integrate for ten protons. The naphthalimide H_2 and H_3 protons were shifted the furthest upfield, which indicates that deprotonation of the 4-amino moiety occurred.

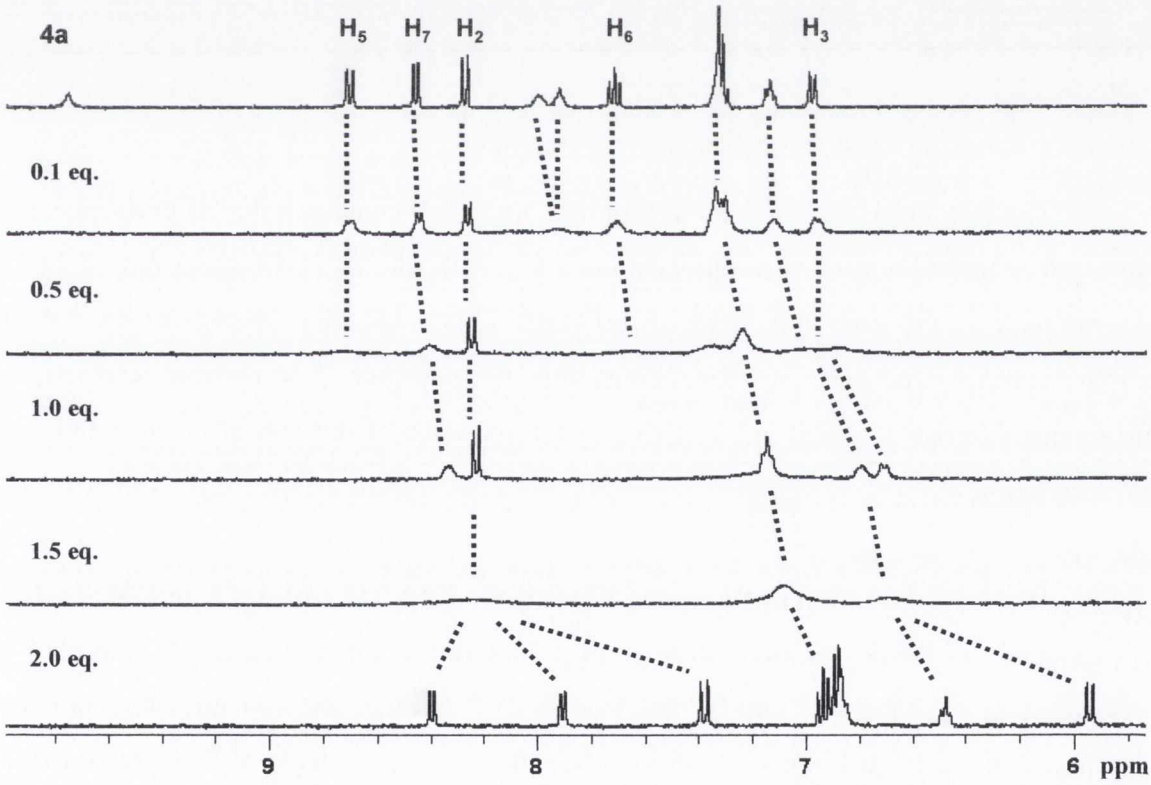


Figure 2.29: Stack plot of ^{1}H NMR spectra (400 MHz, DMSO-d_6) of **4a** [2.1 x 10^{-3} M] upon addition of various equivalents of TBAOH.30H_2O

However, despite the addition of two equivalents of TBAOH, which likely leads to the deprotonation of two N-H moieties, a remaining N-H could be not be located using ^{15}N-^{1}H COSY NMR experiments. The ^{1}H NMR spectrum at two equivalents is also similar to that observed upon addition of two equivalents of F^- to reference compound **2**.[107] This

further supports our proposal that the 4-amino proton was removed from sensor **4a** using TBAOH.[16] Additionally, the NMR spectrum observed after the addition of one equivalent of TBAOH to **4a** is very similar to that seen upon addition of two to three equivalents of F^- (Figure 2.26) and, hence, further supports that deprotonation of the receptor moiety occurred.

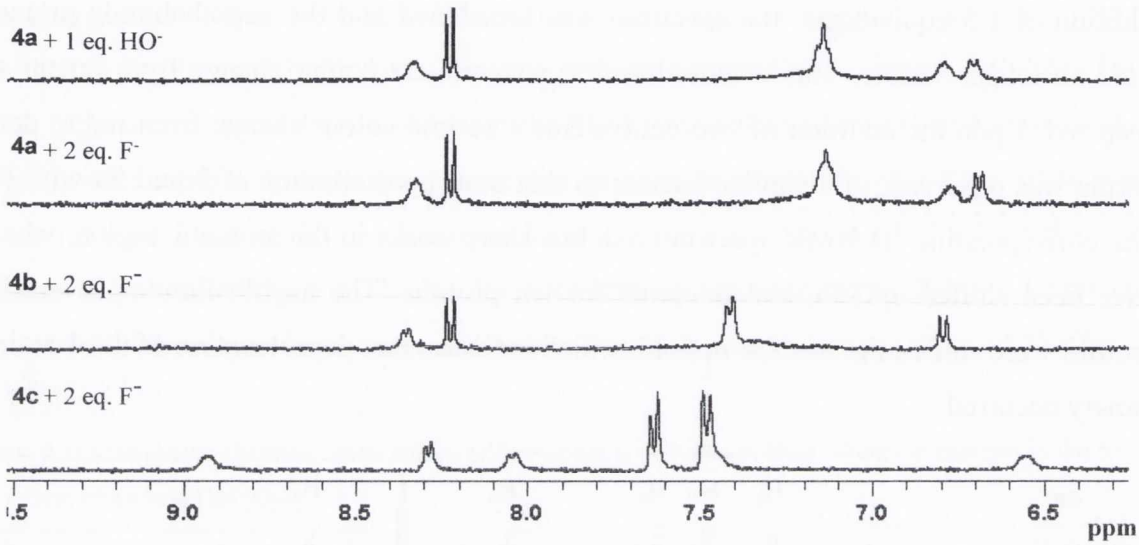


Figure 2.30: Stack plot comparing the ^{1}H NMR spectra of the deprotonated sensor **4a** with the ^{1}H NMR spectra of sensors **4a-c** after the addition of two equivalents of F^-.

The results are summarised in Figure 2.30, which compares the ^{1}H NMR spectra of **4a-c** after the addition of two equivalents of F^-, with the ^{1}H NMR spectrum of **4a** after deprotonation with one equivalent of TBAOH. This stack plot clearly shows that very similar species were generated for **4a** and **4b**. The spectrum of **4c** is more resolved, with more signals visible, which is likely due to the presence of the less electron withdrawing urea receptor.

2.14 ^{1}H NMR Titration of Receptor 37 with F^-, TBAOH and AcO^- in DMSO-d_6

The ^{1}H NMR titration of reference compound **2** was previously reported and discussed in the thesis of Dr. Gillian Hussey [16,107], which showed no interaction upon titration with AcO^- or $H_2PO_4^-$. Additionally, when two equivalents of F^- were added to **2**, a similar spectrum to that observed for sensor **4a** with two equivalents of TBAOH resulted. The downfield region of the ^{1}H NMR (400 MHz, DMSO-d_6) spectrum of **37** showed two broad peaks for the thiourea protons resonating at 9.81 and 8.07 ppm and two signals at *ca.* 7.70 ppm, assigned to the phenyl CF_3 moiety (shown in Figure 2.31).

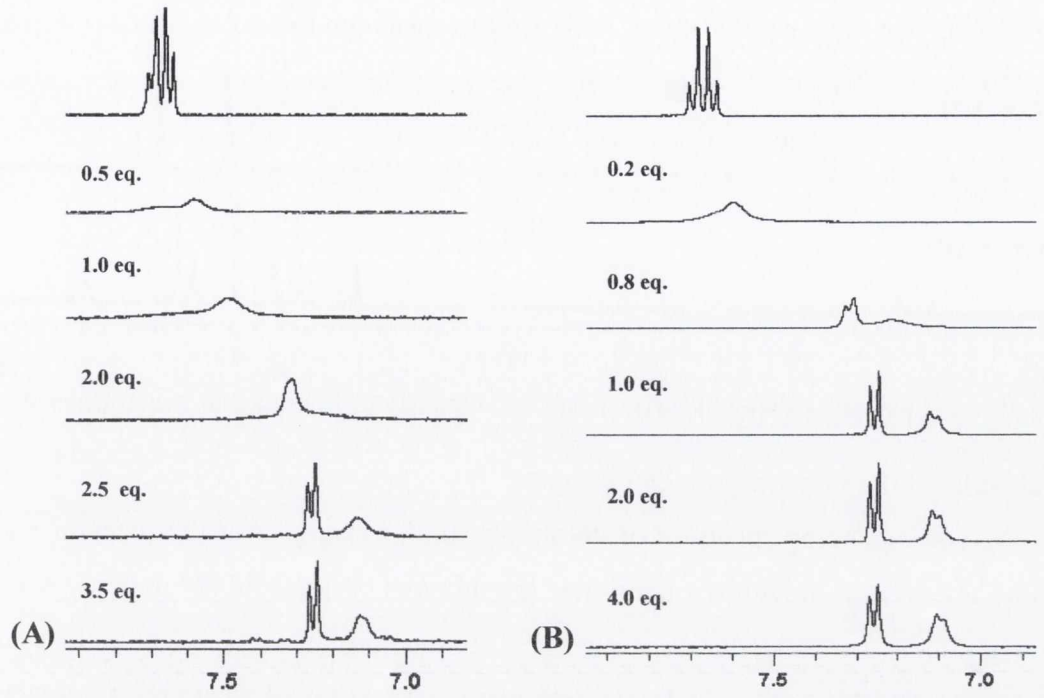


Figure 2.31: Stack plot of changes in the ^{1}H NMR spectra of the phenyl protons of **37** upon titration with **(A)** F^- and **(B)** TBAOH in DMSO-d_6.

Addition of F^- resulted in the disappearance of the N-H resonances (*ca.* 0.4 equivalents) with concomitant broadening and an upfield shift of the phenyl protons (Figure 2.31(A)). After the addition of two equivalents a new species was formed, at which point the HF_2^- triplet was also seen at 16 ppm, indicating that deprotonation had occurred. There were no further changes up to the addition of 3.5 equivalents. The spectrum at 2.5 equivalents contains a doublet at *ca* 7.25 ppm, which resembles the signal for the phenyl receptor protons of the CF_3 based sensor **4b**, after the addition of two equivalents of F^- (Figure 2.30). This indicates a similar species was generated at the receptor moiety of sensor **4b**.

Upon addition of TBAOH to **37** the N-H protons also broadened and disappeared. The ^{1}H NMR titration of **37** with one equivalent of TBAOH, Figure 2.31 (B), showed a very similar species to that seen upon addition of > two equivalents of F^- to **37**. No further changes were observed up to the addition of eight equivalents, which indicates that only one N-H proton was removed from the receptor at low concentrations of TBAOH.

Titrations were also carried out with **37** and AcO^- in order to see if the thiourea protons underwent cumulative chemical shifts of similar magnitude upon binding of AcO^-. As seen for **4a**, titration of **37** (Appendix A, Figure A34) with AcO^- resulted in the formation of a hydrogen bonded complex. Figure 2.32 shows the ^{1}H NMR of **37**, after the addition of two equivalents of AcO^-, for which both N-H protons underwent cumulative

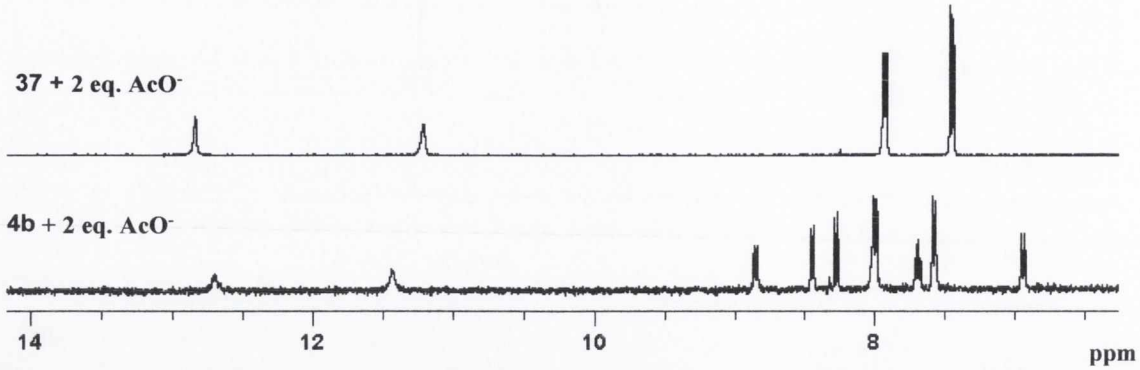


Figure 2.32: Stack plot of ^{1}H NMR (400 MHz, DMSO-d_6) titration of **37** and **4a** with 2 equivalents of AcO^-

chemical shifts of the same magnitude (~3 ppm).

The corresponding spectrum of **4b** shows similar changes for the receptor part of the sensor, however, as previously mentioned the thiourea protons did not undergo shifts of similar magnitude. As good fits were obtained for the formation of 1:1 complexes with sensors **4a** and **4b** with AcO^-, we do not anticipate that additional Host:Guest interactions occur in solution. The different cumulative chemical shifts may be due to the solvated state of the receptor, however, it is difficult to postulate a reason for this, particularly in the absence of crystal structures.

2.15 Conclusion of ^{1}H NMR Titrations of 4a-c with Anions in DMSO-d_6.

In agreement with the absorption and fluorescence titrations of both sensors **4a** and **4b**, hydrogen bonded complexes with AcO^- and $H_2PO_4^-$ were also observed using ^{1}H NMR titrations. The formation of 1:1 hydrogen bonded complexes with $H_2PO_4^-$ was confirmed, with the 4-amino moiety participating in the binding. The binding constants were higher than those determined with AcO^-, therefore, demonstrating that charge density is not the sole deciding factor for the preferential interaction with these receptors. Additionally, the binding constant determined for **4a** with $H_2PO_4^-$ was larger than that obtained for the structural precursor **3**, indicating the ability of the phenyl moiety to increase the acidity of the thiourea protons. In the case of AcO^-, the constant determined for the 1:1 complex with **4a** was comparable to that previously reported for the precursor **3**.[111,115] In contrast to AcO^- and $H_2PO_4^-$, the titrations of sensor **4a** with F^- clearly showed that a different process was occurring in solution, in which the end product was very similar to the resulting spectrum upon deprotonation of **4a**, with one equivalent of TBAOH. The ^{1}H NMR titrations of **4b** with F^- also indicated a similar species to that seen for **4a** was generated. Therefore, we propose that a single deprotonation of the receptor part of sensors **4a** and **4b** occurred, and also likely for sensor **4c**. As discussed in Section

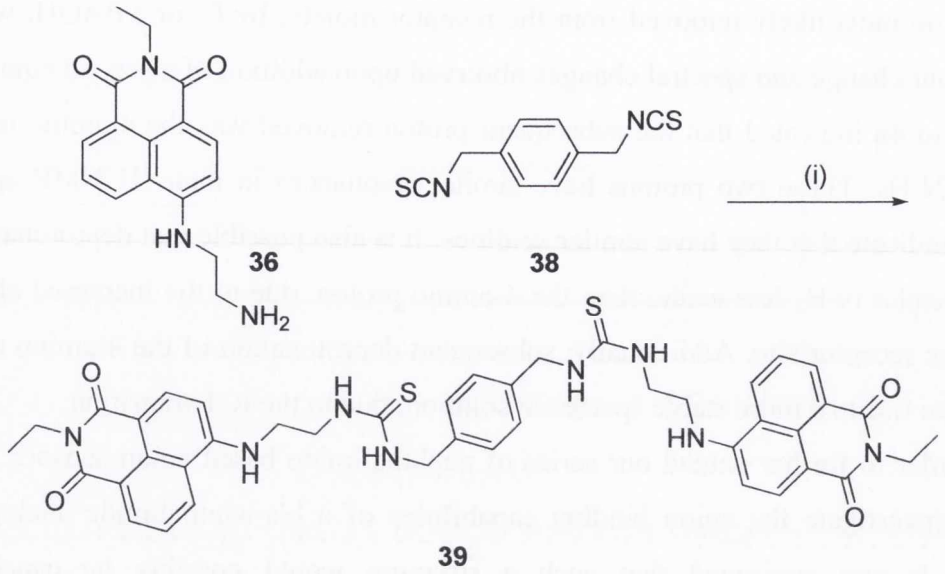
2.5, the proton most likely removed from the receptor moiety, by F^- or TBAOH, was N-H_1. The colour change and spectral changes observed upon addition of a second equivalent of TBAOH to **4a** indicated that the subsequent proton removed was the 4-amino moiety, rather than N-H_2. These two protons have similar resonances in their ^{1}H NMR spectra, which may indicate that they have similar acidities. It is also possible that deprotonation of N-H_1 may render N-H_2 less acidic than the 4-amino proton, due to the increased electron density at the receptor site. Additionally, subsequent deprotonation of the 4-amino moiety may also give rise to a more stable species in solution, due to the ICT transition.

In order to further extend our series of naphthalimide based anion sensors, it was decided to investigate the anion binding capabilities of a bis-napthalimide analogue of sensor **4a**. It was envisaged that such a structure would possibly be capable of cooperatively binding $H_2PO_4^-$ anions, in a similar manner to that observed for **4a.** Additionally, such a sensor may exhibit different responses in its absorption and fluorescence emission spectra, compared to those seen for **4a**, upon the addition of anions in DMSO. The presence of two thiourea receptors could also give rise to a sensor which could cooperatively bind other anionic species, such as bis-carboxylates.[165,166] Therefore, the following section will first discuss the synthesis of the bis-naphthalimide-based anion sensor, **39** (Scheme 2.4), which will be followed by the preliminary investigations into its sensing capabilities.

2.16 Synthesis of the Bis-Naphthalimide Sensor 39

The synthesis of **39** was carried out in a few steps according to the synthetic pathway shown in Scheme 2.4. In comparison to sensor **4a**, the receptor moieties of **39** contained methylene groups rather than a phenyl group. It was envisaged that this structural modification would make the sensor more flexible, which could facilitate cooperative binding between both the thiourea moieties and anions.

The synthesis of the bis-isothiocyanate, **38**, has been previously reported within the literature[167] and was synthesised from 1,4-phenylenedimethanamine using thiophosgene ($CSCl_2$). Two equivalents of **36** and one equivalent of **38** were then stirred in DMF at room temperature under an atmosphere of argon. After seven days, a yellow precipitate formed in solution. The reaction was then left stirring for a further two days after which the precipitate was isolated by suction filtration and then dried under vacuum to give **39** as a bright yellow solid in 8% yield. The crude ^{1}H NMR (400 MHz, DMSO-d_6) spectrum of **39**



Scheme 2.4: Synthesis of **39** from **36** and **38**. **Reagents and conditions:** DMF, RT, 9 days.

showed that the desired product was obtained, Figure 2.33. The volume of the filtrate was then concentrated under reduced pressure, which was then precipitated into ice-water. This gave an orange solid, which was collected and dried by suction filtration. Subsequent ^{1}H NMR (400 MHz, DMSO-d_6) analysis of this solid also showed the presence of **39**, however, the starting materials, **36** and **38** were also present. It is possible that longer

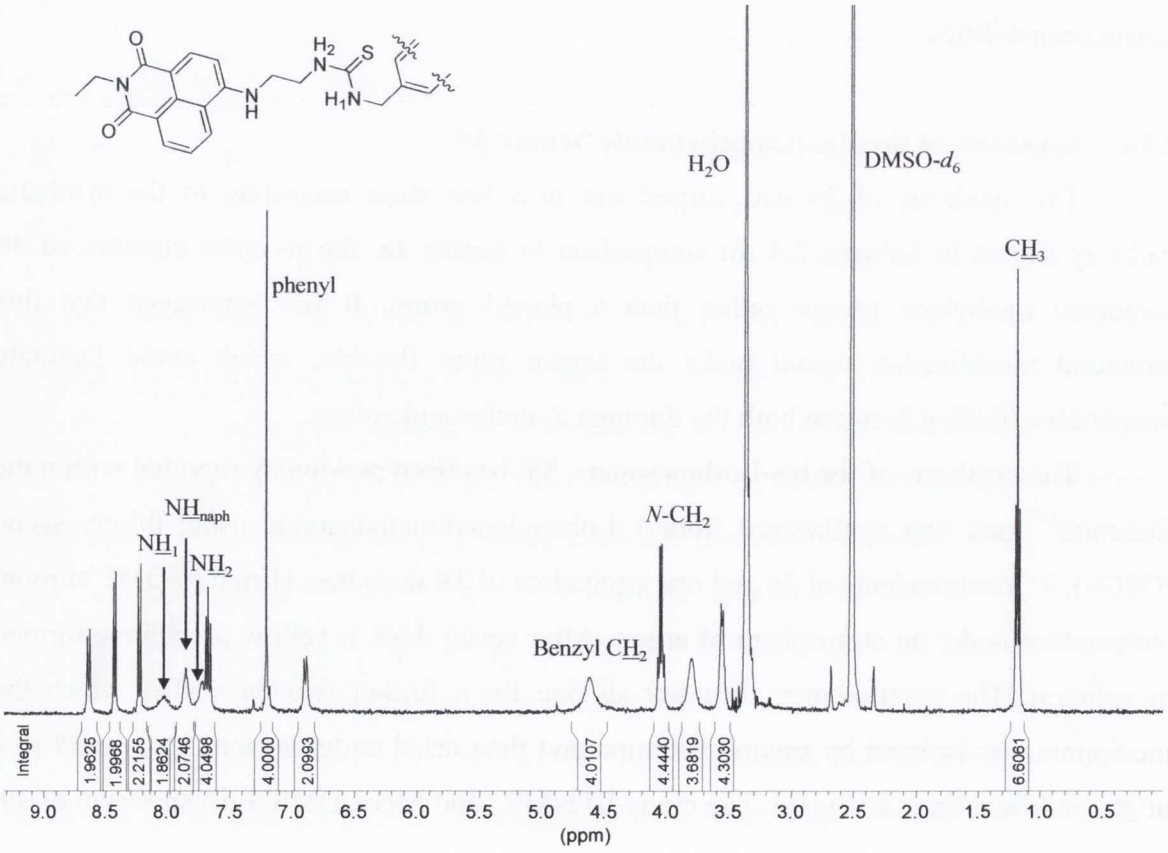


Figure 2.33: The crude ^{1}H NMR (400 MHz, in DMSO-d_6) spectrum of **39**

reaction times or increasing the temperature of this reaction could lead to higher yields, however, due to time constraints, the reaction conditions were not optimised.

As shown in Figure 2.33, the N-H protons resonated at 8.02, 7.84 and 7.71 ppm and were assigned to the N-H_1, 4-amino moiety and N-H_2 protons, respectively, using selective NOE analysis. These chemical shifts were similar to those observed for the N-H protons of the benzyl-based naphthalimide sensor **3**, which was discussed in Chapter 1, Section 1.7.1. The broad singlet at 4.61 ppm was assigned to the methylene groups of the phenyl spacer (7.20 ppm), also by selective NOE. The ^{13}C NMR spectrum (100 MHz, DMSO-d_6) showed the expected number of peaks and the $[M+H]^+$ ion was also observed using ES-MS. Despite the low yield obtained, enough material was synthesised in order to carry out preliminary anion titrations with sensor **39**. Although minor unidentified impurities were present in the ^1H NMR spectrum of **39** (7.30, 4.87 ppm), these were less than 10%. The results from the absorption and fluorescence emission titrations are discussed in the following section.

2.17 Preliminary Absorption and Fluorescence Titrations of 39 with Anions

The absorption spectrum of **39**, shown in Figure 2.34, was similar to that seen for sensor **4a** (Figure 2.2(A)) in DMSO. Additionally, the absorption of the ICT transition of **39** was approximately twice that of **4a** at similar concentrations, due to the presence of the two naphthalimide fluorophores. Although not shown, in a similar manner to **4a**, excitation of the ICT transition or the absorption at 284 nm gave rise to a broad emission centred at 531 nm.

Sensor **39** was titrated with anions such as AcO^-, $H_2PO_4^-$ and F^- (TBAF·$3H_2O$) in DMSO. The changes in the absorption spectrum of **39** with these anions were similar to those observed for **4a**, whereby minor changes were observed for AcO^-, a slight bathochromic shift of the ICT transition was observed with $H_2PO_4^-$ and F^- (Figure 2.34) gave rise to large changes at high concentration (> 200 equivalents).

In comparison to the changes in the absorption spectra of **4a** at low concentration of F^-, Figure 2.6, little or no changes occurred at low concentration with **39**, insert Figure 2.34. This may be due to the fact that the receptor moieties of **39** are less acidic than that of **4a**. Hence, the pK_a value of the most acidic thiourea proton of **39** may be close to that of the 4-amino moiety. Therefore, in the case of **39**, the spectral changes due to deprotonation of the thiourea moieties may overlap with those resulting from deprotonation of the 4-amino proton.

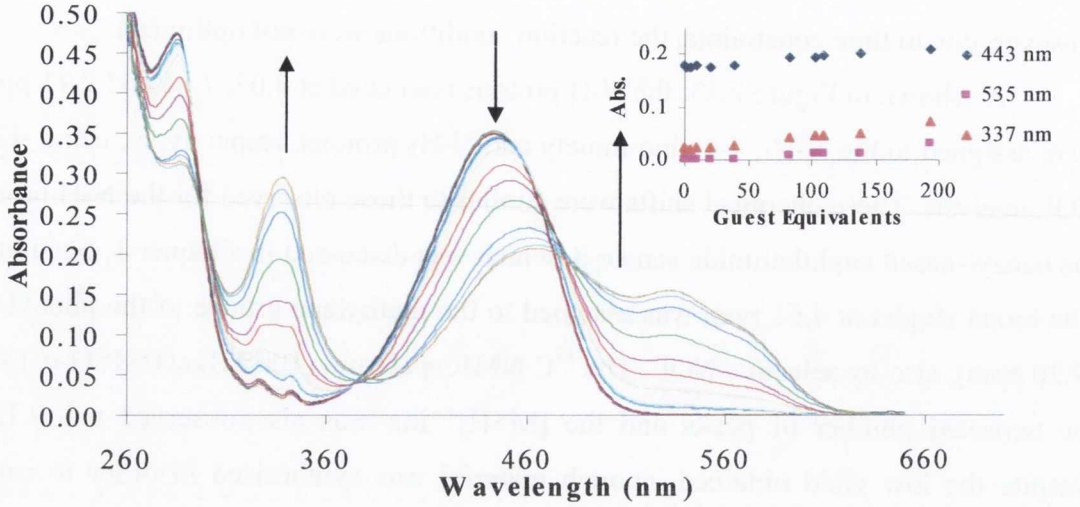


Figure 2.34: The changes in the absorption spectra of **39** [1.2×10^{-5} M] upon addition of F^- (0→ 3000 equivalents) in DMSO. **Insert:** Plot showing little or no changes at low concentration of F^-.

A similar trend to that seen for **4a** was also observed in the fluorescence emission spectra of **39**, whereby only minor quenching of the emission intensity was observed upon titration with AcO^- and $H_2PO_4^-$. Conversely, full quenching of the emission was observed with F^- (Appendix A, Figure A35). In contrast to the quenching observed upon titration of **4a** with F^- (Figure 2.8), little or no quenching of the emission of **39** was seen until after the addition of *ca.* 50 equivalents of F^- *ie.* when the changes at long wavelengths (540 nm) in the absorption spectrum slowly began to occur. Full quenching of the emission was achieved after the addition of *ca.* 1000 equivalents of F^-. Therefore, the quenching of the emission was most likely due to a combination of hydrogen bonding to the thiourea receptors followed by their deprotonation, as well as deprotonation of the 4-amino moiety.

It was anticipated that **39** could possibly bind larger anions such as Cl^- and HSO_4^-. However, titration of **39** with these anions did not give rise to any significant changes in either the absorption or the fluorescence emission spectra of **39**. Sensor **39** was also titrated with the larger anion, $HP_2O_7^{3-}$, and the resulting changes in the absorption spectra were similar to those seen with F^- in Figure 2.34 (Appendix A, Figure A36). Moreover, the quenching of the fluorescence emission was also similar to that observed for **39** with F^-. As the overall changes with F^- were assigned to hydrogen bonding followed by deprotonation, the changes in the presence of $HP_2O_7^{3-}$ indicated a similar mechanism for the anion sensing.

As mentioned above, a bathochromic shift was observed in the absorption spectrum of **39** upon titration with $H_2PO_4^-$. For this reason, it was decided to carry out preliminary

^{1}H NMR titrations with this anion and the results from these investigations will be discussed in the following section.

2.18 Preliminary ^{1}H NMR Titrations of Sensor 39 with $H_2PO_4^-$ in DMSO-d_6

The results from the titration of **39** with $H_2PO_4^-$ in DMSO-d_6 are shown below in Figure 2.35. In a similar manner to that observed for the titration with **4a**, the successive addition of $H_2PO_4^-$ resulted in significant changes in the chemical shifts of the N-H protons, as well as for the H_5 naphthalimide proton. As expected, these changes were similar to those reported by Pfeffer *et al.* for the mono-analogue, **3**.[168] In addition to these

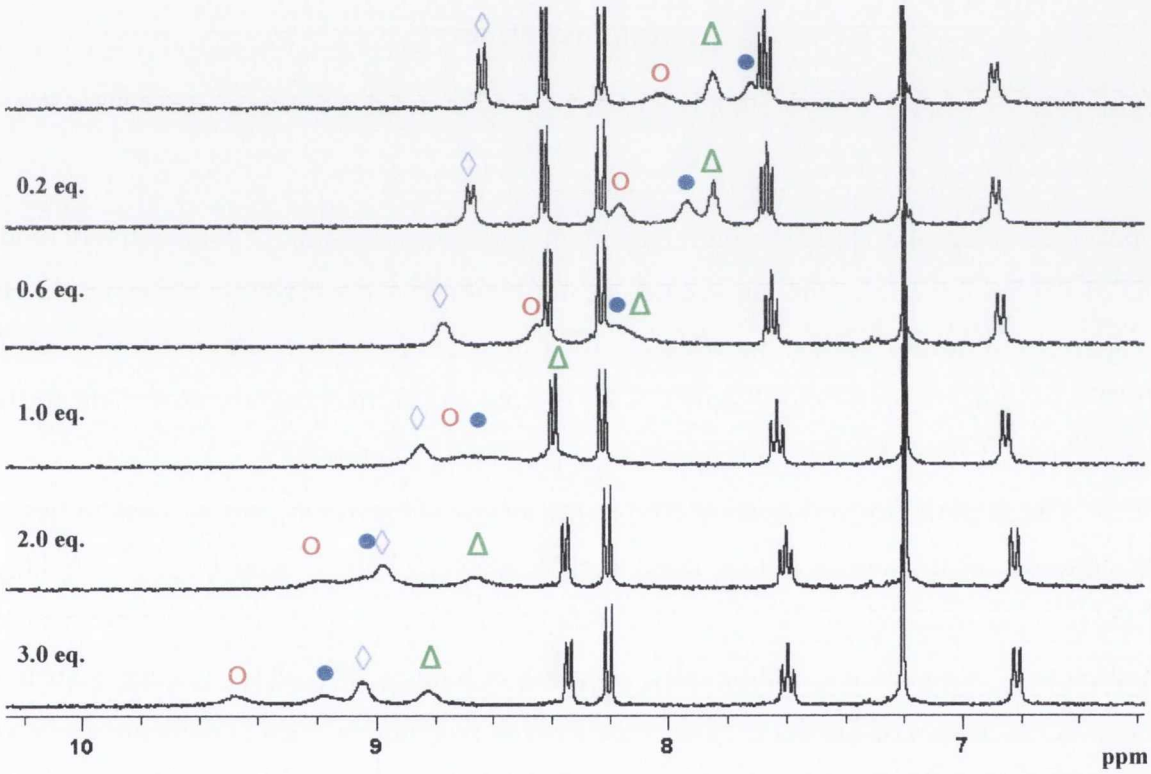


Figure 2.35 Stack plot of ^{1}H NMR spectra (400 MHz, DMSO-d_6) of **39** [3 x 10^{-3} M] after addition of various equivalents of $H_2PO_4^-$. Red ○ and blue ● track thiourea N-H_1 and N-H_2 protons, respectively. Purple ◊ tracks naphthalimide H_5. Green Δ tracks the 4-amino N-H moiety.

changes, the broad signal for the methylene protons of the phenyl spacer sharpened and was also shifted slightly upfield by *ca.* 0.1 ppm (not shown).

By plotting the $\Delta\delta$H for the N-H protons and the naphthalimide H_5 proton, binding isotherms were obtained and are shown in Figure 2.36. The cumulative chemical shifts for each proton were similar in magnitude to those reported for **3**.[111] Both the N-H_1 and N-H_2 protons were shifted by 1.6 and 1.7 ppm, respectively, which was indicative of strong hydrogen bonding to the receptor moieties. From Figure 2.36, the binding interaction

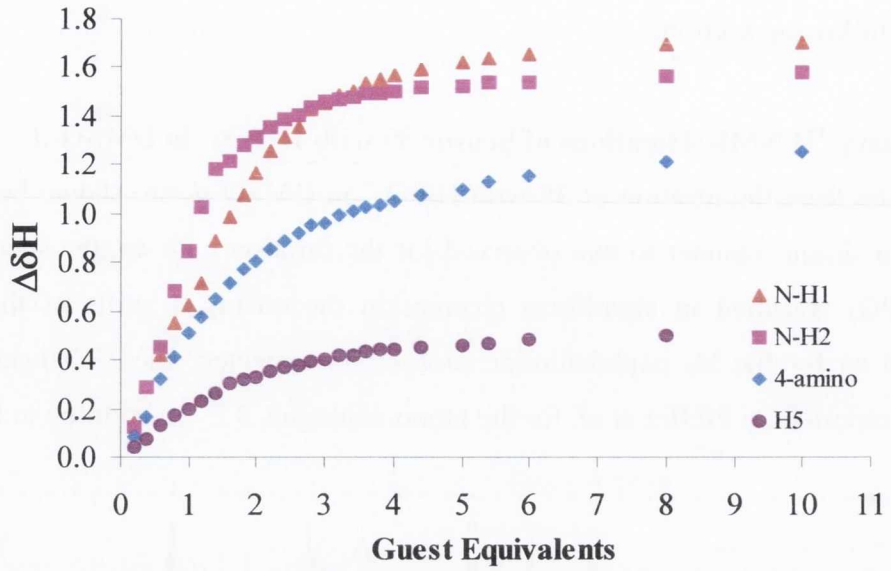


Figure 2.36: The changes in the chemical shift of the N-H and H_5 naphthalimide protons of **39** [3 x 10^{-3} M] upon addition of $H_2PO_4^-$.

appears to be that of a 1:2 Host:Guest stoichiometry, indicating that **39** cooperatively binds two $H_2PO_4^-$ anions in a similar manner to the binding of one $H_2PO_4^-$ anion by **4a**. In comparison to these changes, the addition of Cl^- resulted in only minor changes in the ^1H NMR spectrum, whereby the thiourea N-H_2 proton was shifted slightly downfield to the same chemical shift of the 4-amino proton (Appendix A, Figure A37).

The preliminary spectroscopic investigations into the anion sensing capabilities of **39** showed that the sensor could detect the presence of both F^- and $HP_2O_7^{3-}$, as large changes were observed in both the absorption and fluorescence emission spectra upon titration with these anions. Additionally, cooperative binding of $H_2PO_4^-$ was also shown to occur. With the aim of further exploring the sensing potential of such naphthalimide-based thiourea sensors, the development of sensors functionalised with anion receptor moieties at the 3 position was undertaken. Another family was developed functionalized at both the 3- and 4-positions of the fluorophore with H-bond donors. The results from these studies are discussed in the following sections.

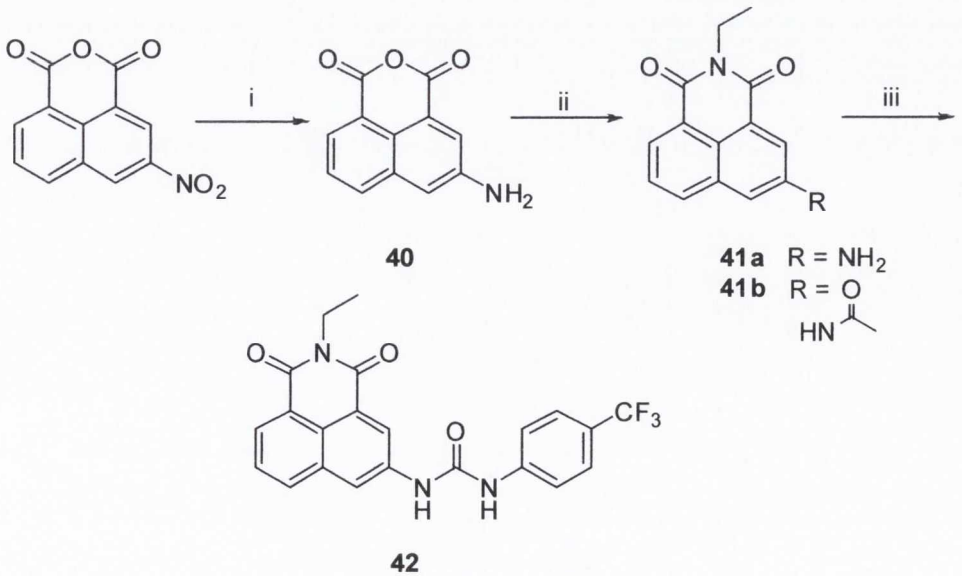
2.19 Development of 3,4-Substituted Naphthalimide-Based Sensors

As shown in Chapter 1, the majority of naphthalimide-based anion sensors developed to date are functionalised with an anion receptor moiety at the four position of the naphthalene ring, due to the possibility for modulation of the ICT character of the fluorophore upon anion sensing, as well as their synthetic accessibility.[14,127] However,

modulation of the ICT transition is also possible by substitution at the three position of the fluorophore. In the past we have investigated the anion sensing capabilities of **42** (Scheme 2.5), which was substituted with a urea receptor at the 3-position of the fluorophore. Investigations into the anion sensing capabilities of **42** showed the selective detection of F^- over AcO^- and $H_2PO_4^-$ in DMSO. Therefore, these results will be presented in the following section. Then, with the sensing potential of a 3-substituted naphthalimide established, it was decided to investigate the sensing capabilities of a naphthalimide functionalised with anion receptor moieties at both the 3 and 4 positions of the naphthyl ring. It was anticipated that such a sensor could also cooperatively bind anions. Therefore, the attempted synthesis of a novel 3,4-substituted naphthalimide derivative, **47,** will also be discussed in the following sections (Scheme 2.6).

2.19.1 Synthesis and Characterisation of the Urea Sensor 42

The synthesis of compound **42** was achieved in three steps and is shown in Scheme 2.5. The nitro group of the commercially available 3-nitro-1,8-naphthalic anhydride was reduced at room temperature using catalytic hydrogenation in the presence of Pd/C at 3 atm in DMF.[169] The product was isolated upon pouring the reaction mixture into ice-water and the resulting precipitate was then collected and dried in air by suction filtration. The ^1H NMR (400 MHz, DMSO-d_6) spectrum of **40** showed a broad singlet pertaining to the amino group at 6.10 ppm and a downfield shift of the naphthalimide protons was also observed. Compound **40** was then refluxed in the presence of 70% ethylamine in 1,4-dioxane for 16 hours and the imide **41a** was isolated in a similar manner to that described



Scheme 2.5: Synthesis of **42** from 3-nitro naphthalic anhydride. **Reagents and conditions** (i) H_2, Pd/C, DMF, 16 h, RT (ii) ethylamine, dioxane, reflux, 16 h. (iii) 4-(Trifluoromethyl)phenyl isocyanate, MeCN, reflux, 16h.

for **40**, as an orange solid in 51% yield. The ^{1}H NMR (400 MHz, DMSO-d_6) spectrum of **41a** exhibited a quartet and a triplet at 4.04 and 1.18 ppm, respectively, which were assigned to the *N*-ethyl group. The acetamide derivative of **41a** was also synthesised in order to compare the absorption and fluorescence emission spectra with that of **42**. Therefore, compound **41b** was synthesised using a procedure previously reported for similar derivatives,[169] whereby **40** was refluxed in the presence of acetic anhydride and acetic acid for one hour. The precipitate formed was collected and dried by suction filtration to give a beige solid in 80% yield.

The ^{1}H NMR (400 MHz, DMSO-d_6) spectrum of **41b** showed that the amide proton resonated at 10.53 ppm and a singlet pertaining to the acetamide methyl group was found at 2.15 ppm. Subsequent refluxing of **41a** with one equivalent of 4-trifluoromethylphenyl isocyanate in MeCN for 16 hours resulted in the precipitation of the desired product, which was collected and dried in air by suction filtration to give **42** as a beige solid in 83% yield. The ^{1}H NMR (400 Hz, DMSO-d_6) spectrum of **42** showed two broad singlets at 9.41 and 9.22 ppm, characteristic of urea protons, Figure 2.37. The ^{13}C NMR (100 Hz, DMSO-d_6) spectra showed the expected number of resonances, while the $[M+H]^+$ ion was also observed using ES-MS. With sensor **42** fully characterised by conventional methods, its anion sensing capabilities were next investigated and the results will be discussed in the following section.

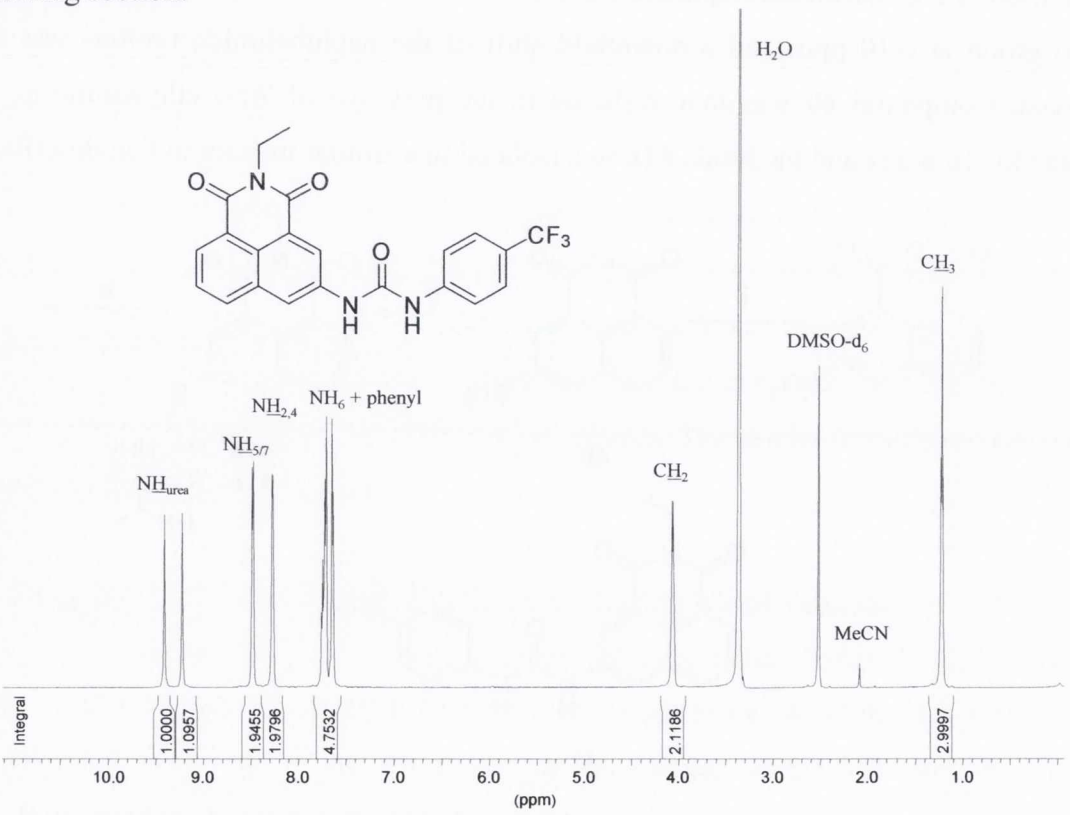


Figure 2.37: The ^{1}H NMR (400 Hz, DMSO-d_6) spectrum of **42**.

2.20 Photophysical Properties of Sensor 42 in DMSO

The absorption spectrum of compounds **42**, **41b** and **4a** in DMSO are shown in Figure 2.38. Sensor **42** exhibited three main absorption bands at *ca.* 285, 340 and 394 nm, for which the latter transition at longer wavelengths was assigned to the ICT transition of the fluorophore.[170] In comparison to **4a** (450 nm), the ICT transition of **42** was shifted to shorter wavelengths, which reflects the weaker ICT of such 3-subsituted derivatives. The transition at 285 nm was assigned to the naphthalimide fluorophore as well as the *p*-CF_3 phenyl group, as deduced from the absorption spectrum of **41b**.

Excitation of **42** at both 394 nm and 340 nm gave rise to a broad emission centred at 453 nm, which was similar to that observed for **4a** (λ_{em} 530 nm), (Appendix A, Figure A38). The anion binding capabilities of **42** were next investigated using absorption and fluorescence emission spectroscopy.

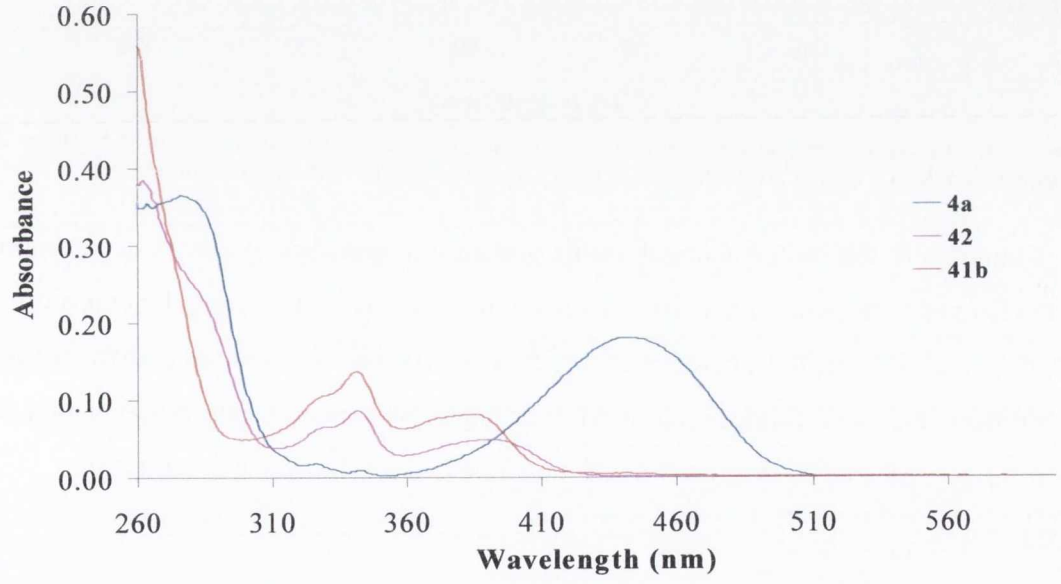


Figure 2.38: The absorption spectra of **42** [1.2×10^{-5} M], **4a** [1.2×10^{-5} M] and **41b** in DMSO.

2.20.1 Absorption and Fluorescent Anion Titrations of 42 in DMSO

In a similar manner to the behaviour of sensor **4a**, preliminary titrations showed that little or no changes occurred in the absorption and fluorescence emission spectra of **42** upon titration with the TBA salts of AcO^- and $H_2PO_4^-$. However, upon titration of **42** with F^- (TBAF·$3H_2O$) a minor increase in the absorption spectrum at short wavelengths resulted (*ca.* 329), indicating the interaction of F^- at the receptor site (Figure 2.39). These changes also occurred with a bathochromic shift in the ICT transition. In contrast to these changes, after the addition of *ca.* 25 equivalents of F^-, large enhancements were observed in the

absorption spectra at both short and long wavelengths (insert Figure 2.39). These changes were similar to those which occurred upon deprotonation of the 4-amino moiety of **4a**, therefore indicating that a deprotonation of the urea proton adjacent to the naphthalimide occurred at high concentrations of F^-. Additionally these changes were reversed upon the addition of protic solvents such as MeOH or H_2O.

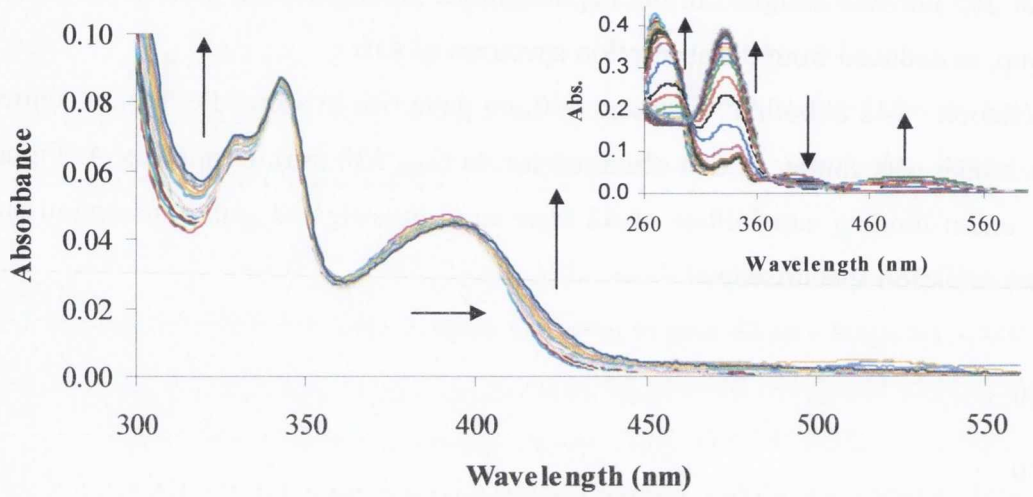


Figure 2.39: The changes in the absorption spectra of **42** [1.2×10^{-5} M] upon addition of F^- ($0 \rightarrow 25$ equivalents) in DMSO. **Insert :** The changes at high concentration of F^- ($0 \rightarrow 300$ equivalents).

Converse to the minor changes in the absorption spectrum at low concentration of F^-, large changes were seen in the fluorescence emission spectrum. Here, the emission was quenched by *ca.* 75% in the presence of *ca.* 50 equivalents of anion, as shown in Figure 2.40. Additionally, these changes occurred over a similar concentration range to that seen for **4a** in the presence of F^- (Figure 2.8). The changes in the fluorescence emission

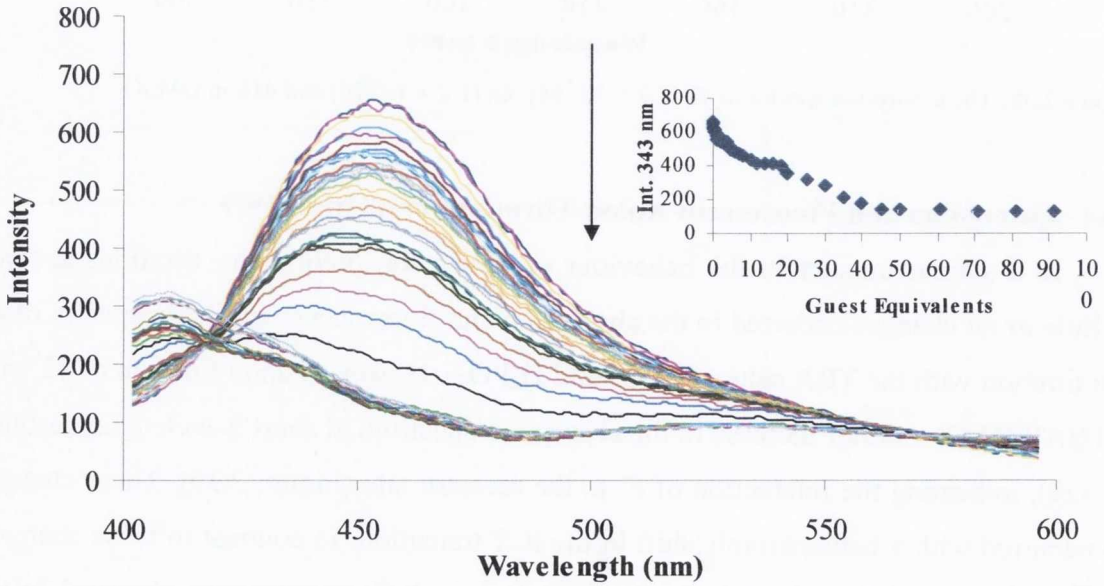


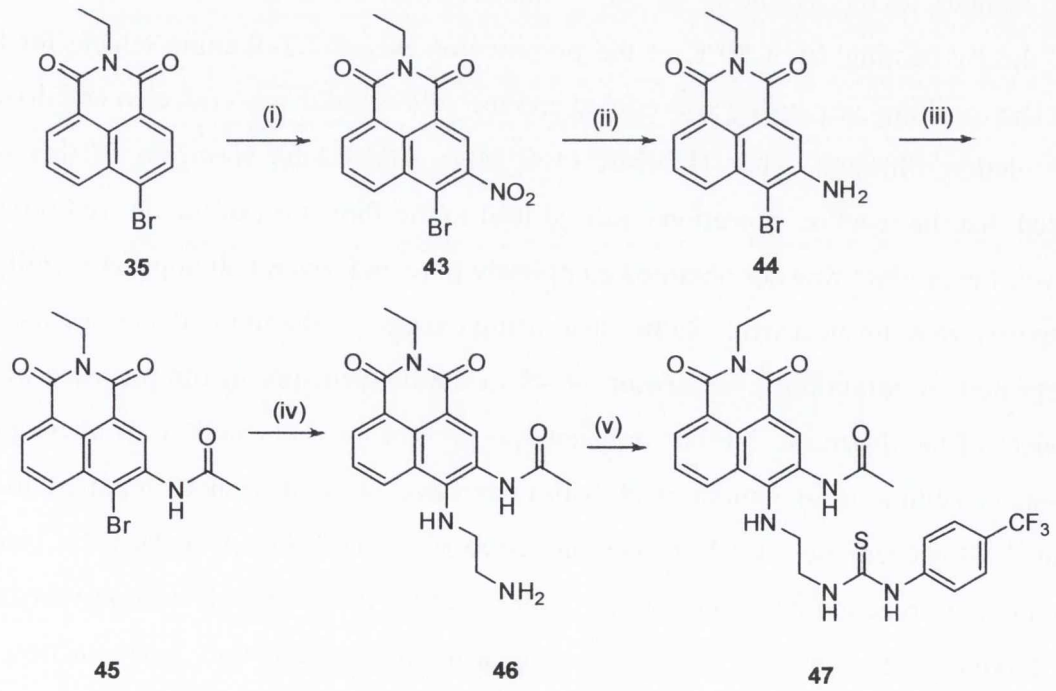
Figure 2.40: The changes in the fluorescence emission spectra of **45** [1.2×10^{-5} M] upon addition of F^- ($0 \rightarrow 300$ equivalents) in DMSO. **Insert:** The changes at 455 nm as a function of equivalents added.

intensity as a function of anion equivalents are shown in the insert of Figure 2.40. These changes indicated that a two-step process occurred, which was most likely due to hydrogen bonding to the urea receptor followed by deprotonation.

Overall, the changes in both the absorption and emission spectra of **42** showed that naphthalimides substituted with an anion receptor at the 3-position could signal the presence of basic anions, such as F^- in DMSO. Therefore, it was anticipated that the incorporation of a similar functional group into sensor **4a** could possibly improve its anion sensing capabilities. Therefore, the synthesis of **47** was attempted (Scheme 2.6), whereby an acetamide was introduced at the 3-position, providing an additional hydrogen bond donor for anion binding. Rather than introducing a urea at the 3-position of **4a**, as in the case of **42**, it was anticipated that an acetamide group would be more suitable in order to avoid steric hindrance with the thiourea receptor at the 4-position. Therefore, it was envisaged that hydrogen bonding interactions between the 4-amino moiety, the 3-acetamide moiety and the thiourea receptor and anions could occur, particularly in the case of $H_2PO_4^-$. The attempted synthesis of **47** will be described in the following section.

2.21 Attempted Synthesis of the 3,4-Substituted Naphthalimide Sensor, 47

The synthesis of sensor **47** was first attempted according to Scheme 2.6. Nitration at the 3-position was achieved by dissolving compound **35** in a mixture of neat nitric and sulfuric acid, which was then stirred at room temperature for 20 minutes. The reaction



Scheme 2.6: i) HNO_3, H_2SO_4, 20 min, RT ii) SnCl, HCl, 85 °C 1 h. iii) $(Ac)_2O$, AcOH, 6 h, reflux. iv) 1,2-diamino ethane, $CHCl_3$, 3h, RT. v) 4-(Trifluoromethyl)phenylisothiocyanate, $CHCl_3$, reflux.

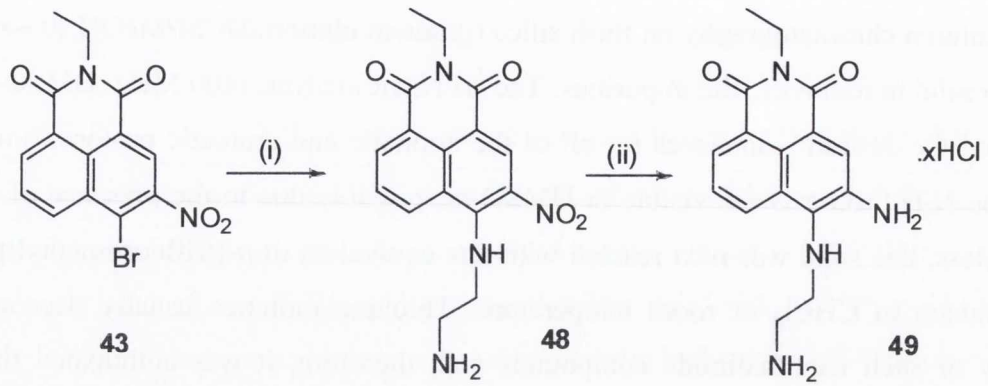
mixture was then precipitated into water and the solid was collected and dried in air by suction filtration to give a pale yellow solid.

The crude ^{1}H NMR (400 MHz, DMSO-d_6) spectrum showed a singlet at 8.81 ppm, which was assigned to the naphthalimide H_2 proton and, hence, indicated that the reaction was successful. However, the starting material, **35**, and most likely a di-nitrated product were also visible in the spectrum. These impurities were removed by recrystallising the residue several times from EtOH, which gave a yellow solid, **43**, in 54% yield. Initially, reduction of the nitro group was attempted using catalytic hydrogenation in the presence of Pd/C in MeOH at 1 atm. However, this resulted in the decomposition of the compound, as determined by ^{1}H NMR spectroscopy in DMSO-d_6. Degradation also occurred when the reaction was carried out in DMF. The reduction of the nitro group was further attempted by stirring a mixture of **43** with five equivalents of $SnCl_4$ in HCl at 85 °C for one hour. These conditions were successful, however, a side product, *N*-ethyl-3-amino-1,8-naphthalimide, was also formed. This was easily removed by column chromotography on flash silica using gradient elution (DCM/MeOH 0→10%), giving **44** as a yellow solid in 88% yield.

The ^{1}H NMR (400 MHz, DMSO-d_6) spectrum of **44** showed a broad singlet at 6.24 ppm pertaining to the amino group and the naphthalimide H_2 proton was also shifted upfield relative to that seen for **43**. The amino group was then acetylated by refluxing a suspension of **44** in acetic acid with acetic anhydride for six hours.[169] The product was collected and dried by suction filtration to give a pale yellow solid, **45**, in 68% yield. In a similar manner to the synthesis of **36**,[111] nucleophilic aromatic substitution was then carried out by heating **45** at 80°C in the presence of excess 1,2-diamino ethane for four hours. The resulting suspension was cooled and the yellow solid was collected and dried in air by suction filtration. The ^{1}H NMR (400 MHz, DMSO-d_6) spectrum of this solid indicated that the reaction conditions utilised lead to the formation of the desired product. However, the product was not obtained completely pure and several attempts at identifying the impurity were unsuccessful. Rather than using excess 1,2-diamino ethane, the reaction was repeated by refluxing a suspension of **45** in 2-ethoxyethanol in the presence of one equivalent of the di-amine. 2-Ethoxyethanol was chosen for this reaction, as nucleophilic aromatic substitutions of similar naphthalimides have been previously reported in this solvent.[117] However, the ^{1}H NMR spectrum (400 MHz, DMSO-d_6) of the solid isolated showed that no reaction had occurred. In order to access if the lack of reaction was due to steric hindrance caused by the neighbouring acetamide group, the same reaction was carried out on compound **44**. However, once again, the ^{1}H NMR (400 MHz, DMSO-d_6) spectrum showed that no reaction had occurred. Therefore, attempts were made to purify

the mixture obtained from the reaction carried out in the presence of excess diamine. Indeed, column chromatography on flash silica (gradient elution, DCM/MeOH (0 → 50%) was successful in removing the impurities. The ^{1}H NMR analysis (400 MHz, DMSO-d_6) of **46** showed the desired resonances for all of the aliphatic and aromatic protons, however, not all the N-H protons were visible in DMSO-d_6, possibly due to the presence of water. Nevertheless, this solid was next reacted with one equivalent of *p*-(trifluoromethyl)phenyl isothiocyanate in $CHCl_3$ at room temperature. Thiourea moieties usually decrease the solubility of such naphthalimide compounds and, therefore, it was anticipated that the product would precipitate out of organic solution upon formation. However, no precipitate formed and analysis of the reaction mixture *via* ^{1}H NMR (400 MHz, DMSO-d_6) showed only the presence of the starting materials. The reaction was carried out again by refluxing the reagents in $CHCl_3$. A precipitate was formed, which was collected by suction filtration and dried under vacuum to give a yellow solid. The crude ^{1}H NMR (400 MHz, DMSO-d_6) spectrum of the residue indicated that **47** was present, as broad singlets indicative of N-H thiourea protons were visible downfield, however, impurities were also present in the spectrum. Therefore, the crude product was first recrystallised from EtOAc, followed by column chromatography on flash silica with an eluting phase of 1:1 EtOAc-Hexane. However, these attempts were both unsuccessful in removing the impurities. Additionally, the ^{1}H NMR (400 MHz, DMSO-d_6) spectrum of the product obtained from the attempted purifications indicated that at least two napthalimide-based compounds were present. Most noticeable about the spectrum was that the resonances of the *N*-ethyl group were no longer visible, indicating that decomposition may have occurred. This was more clearly observed upon recording the ^{1}H NMR spectrum in MeOH-d_4.

Due to the difficulties in the synthesis of compounds **46** and **47**, an alternative pathway for the synthesis of **47** was considered, Scheme 2.7. Here, it was anticipated that the alkyl amine of **49** would be more reactive than the aromatic amine and, therefore, could be selectively reacted with the isothiocyanate, followed by subsequent acetylation of the aromatic amine. Nucleophilic aromatic substitution of the bromo group of 4-bromo-3-nitro-1,8-naphthalimides has been previously reported within the literature.[171] Indeed, nucleophilic substitution of the bromo group of **43** was achieved in the presence of just 1.5 equivalents of 1,2-diamino ethane by stirring at room temperature in $CHCl_3$. The product precipitated out of solution upon formation and was then collected and dried by suction filtration to give **48** as a yellow solid in 68% yield.



Scheme 2.7: i) 1.5 Equivalents of 1,2-diamino ethane, $CHCl_3$, RT, 3 h ii) Pd/C, H_2, MeOH, HCl

The ^{1}H NMR (400 MHz, DMSO-d_6) spectrum of **48** showed the presence of the desired product, and the $[M+H]^+$ ion was also observed using ES-MS. The nitro group was then reduced by stirring a suspension of **48** in MeOH under 2 atm of H_2 in the presence of Pd/C and HCl for one hour.[171] The catalyst was removed by filtering through celite and the filtrate was evaporated to dryness under reduced pressure to give a hygroscopic oily red solid. The ^{1}H NMR (400 MHz, DMSO-d_6) spectrum of **49** showed that the reduction was successful as a broad singlet was observed at 8.20 ppm, which was assigned to the 3-amino protons. Additionally, the $[M+H]^+$ ion of **49** was also observed using ES-MS. However, unidentified impurities were also visible in the ^{1}H NMR spectrum of **49**. Nevertheless, several different reaction conditions were then used to try and react the alkyl amine of **49** with the desired isothiocyante, however, these were all unsuccessful. Reactions carried out at room temperature in MeCN, MeOH, THF-H_2O and DCM in the presence of one equivalent of isothiocyante led to the recovery of both starting materials as well as unidentified impurities. Compound **49** was also refluxed in MeCN and $CHCl_3$ in the presence of excess isothiocyante, however, both these reactions appeared to have led to decomposition, as multiple peaks were observed in the aromatic region by ^{1}H NMR analysis.

In summary, in all of the attempts to react **49** with the desired isothiocyanate, the starting materials were recovered or the ^{1}H NMR spectrum indicated that decomposition had occurred. Additionally, the ^{1}H NMR (400 MHz, DMSO-d_6) spectrum of **48** showed the appearance of new minor signals in the spectrum over a period of 16 hours. This was also observed in the ^{1}H NMR (400 MHz, DMSO-d_6) spectrum of compound **49**. Unfortunately, time restrictions did not allow for further attempts of this reaction.

2.22 Overall Conclusion

This chapter has detailed the synthesis and characterisation of a new series of naphthalimide based fluorescent sensors, **4a-c**, for anions. Their anion recognition ability was investigated by various spectroscopic methods such as absorption, fluorescence and ^{1}H NMR spectroscopy in DMSO and DMSO-d_6 solutions, respectively. A small structural modification of the precedents set out in the literature resulted in an enhancement in PET, which led to a full quenching of the naphthalimide fluorescence emission by F^-. The quenching of the fluorescence emission of **4a-b** occurred at low concentrations of F^- and in the absence of significant changes in the absorption spectra. Sensor **4b** showed a slightly higher affinity than **4a** towards F^-, most likely due to the presence of the electron withdrawing *p*-CF_3 receptor moiety. Conversely, a far higher concentration of F^- was required to quench the fluorescence emission of **4c**, which also occurred with large concomitant changes in the absorption spectra. Hence, **4a-b** were shown to be selective fluorescent PET sensors for F^-.

Quenching of the fluorescence emission of **4a** and **4b,** was also observed upon titration with AcO^- and $H_2PO_4^-$, however, to a much lesser extent than seen for F^- ($F^- > AcO^- > H_2PO_4^-$). While no significant changes were seen in the absorption spectra of these sensors with AcO^-, both the absorption spectra of **4a** and **4b** showed a shift in the ICT transition upon addition of $H_2PO_4^-$. This shift indicated pertubation of the 4-amino N-H moiety and, hence, cooperative binding between the tetrahedral $H_2PO_4^-$ anion and all three N-H protons of **4a-b**. In contrast, the urea receptor, **4c**, did not show any significant changes in its absorption or fluorescence emission spectra upon titration with AcO^- and $H_2PO_4^-$, most likely as it is a weaker hydrogen bond donor.

Using ^{1}H NMR titrations it was confirmed that the changes observed in the absorption and/or emsssion spectra of **4a** and **4b** were due to the formation of hydrogen bonded complexes with AcO^- and $H_2PO_4^-$. Significant downfield shifts of both of the N-H thiourea protons were observed and, in the case of $H_2PO_4^-$, the 4-amino proton was also shifted downfield. The changes in the ^{1}H NMR spectra of **4a** and **4b** were fitted and binding constants were determined, which for **4a** and $H_2PO_4^-$, was higher than reported for the precursor, **3**. Therefore, as anticipated the removal of the benzyl receptor in **3** and replacing it with the phenyl receptor gave rise to a stronger cooperative binding of $H_2PO_4^-$. As seen for the absorption and the fluorescence titrations, higher anion affinities were observed by ^{1}H NMR titration for the *p*-CF_3 derivative, **4b**. Despite the absence of significant changes in both the absorption and fluorescence emission spectra of **4c**, the ^{1}H NMR titrations with AcO^- and $H_2PO_4^-$clearly showed the formation of hydrogen bonded

complexes. Therefore, complexation of these anions by **4c** does not result in significant change in the reduction potential of the receptor moiety and consequently no enhancement in PET occurs.

In the case of F^-, efforts were made to establish the nature of the interaction at the receptor sites of **4a-c** *via* absorption, fluorescence and ^{1}H NMR titrations of **4a**, **2** and **37** with F^-, as well as with TBAOH. Titration of **2** with F^- and TBAOH indicated that a neat deprotonation of the 4-amino moiety occurred in the presence of F^- and also that the deprotonation does not contribute, to any great extent, to the sensing mechanism of **4a-b**. The ^{1}H NMR titration of **37** with F^- and TBAOH showed similar species at 2.5 and one equivalents, respectively. Therefore, as reported within the literature for similar thiourea receptors,[161,163] deprotonation of **37** does not occur until after the addition of two equivalents of F^-. This indicates that hydrogen bonding followed by deprotonation most likely occurs between **37** and F^-, and, therefore, also for sensors **4a-b**. This is further supported by the appearance of the HF_2^- triplet at 16 ppm, which is indicative of deprotonation, and was observed upon addition of *ca.* two equivalents of F^- to **4a-b** and **37**.

The final section of this chapter focused on the preliminary spectroscopic investigations into the anion sensing capabilities of a novel bis-1,8-naphthalimide, as well as the attempted synthesis of a 3,4-substituted naphthalimide based sensor for anions.

The novel bis-1,8-naphthalimide-based thiourea sensor **39** was synthesised and characterised by NMR, MS and IR. The preliminary results obtained from the absorption and fluorescence titrations of **39** with anions, such as AcO^-, $H_2PO_4^-$, and F^-, in DMSO gave rise to similar changes to those observed for **4a**. In the case of F^-, a quenching of the fluorescence emission was observed, which was assigned to hydrogen bonding followed by deprotonation. At higher concentrations of F^-, large changes at long wavelengths were observed in the absorption spectra, which were accompanied by a colour change from yellow to pink. These changes gave rise to full quenching of the fluorescence emission and were assigned to deprotonation of the 4-amino moiety. In a similar manner, titration of **39** with $HP_2O_7^{3-}$ gave rise to large changes in both the absorption and fluorescence emission spectra, indicating a similar mechanism of anion interaction. Additionally, the preliminary ^{1}H NMR (400 MHz, DMSO-d_6) titrations indicated that **39** could cooperatively bind two $H_2PO_4^-$ anions, in a similar manner to that seen for the previously reported mono derivative, **3**. Potential future work on this sensor would involve further ^{1}H NMR titrations with AcO^- and F^- as well as spectroscopic titrations with bis carboxylates, such as succinate and glutarate.

The synthesis and anion binding capabilities of a naphthalimide substituted with a urea at the 3-position was also discussed. The selective detection of F^- over AcO^- and $H_2PO_4^-$ was also shown, as large changes occurred in the absorption and fluorescence emission spectrum of **42** in DMSO. The spectroscopic investigations of **42** in the presence of anions led to the design of the novel 3,4-substituted naphthalimide, **47**. Two different synthetic pathways were investigated for the synthesis of this compound, however, these were both unsuccessful and the synthesis was more problematic than envisaged.

Chapter 3

Amidothiourea-Based Sensors for Anions

3.0 Introduction and Objectives

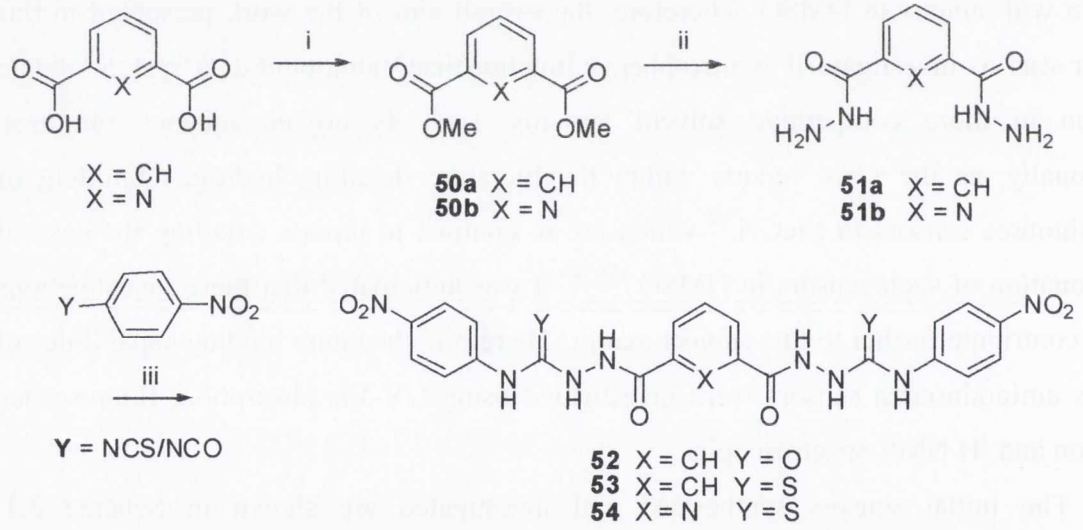
The emergence of a new class of anion receptors referred to as amidoureas and amidothioureas were discussed in detail in Chapter 1.[79,104,106,136,137,146] Inspired by this work and by the scope for the synthetic modification of the 2,6-dicarboxyamidopyridine scaffold, we initially focused on appending *p*-nitro-phenyl chromophores to the amidothiourea receptor.[137,140,172-175] Nitro-phenyl groups are present in many synthetic anion receptors, as when attached directly to ureas and thioureas, they can enhance anion binding due to the electron withdrawing effect of the nitro group.[163,176-178] Therefore, ICT of the *p*-nitro-phenyl chromophore provides a simple way of easily introducing a colorimetric signalling mechanism into synthetic receptors. As, shown in Chapter 1, Section 1.8.2, Wei *et al.*[137] have previously described such pyridine-based amidothiourea sensors, in which a *p*-tolyl signalling moiety was utilised to monitor the anion binding in DMSO. The Gunnlaugsson group[105] have also previously shown that calixarene-based amidoureas can give rise to selective and dramatic changes in their absorption spectra upon titration with anions in DMSO. Therefore, the overall aim of the work presented in this chapter was to investigate if *p*-nitro-phenyl functionalised amidothiourea systems could function in more competitive solvent systems, such as organic-aqueous mixtures. Additionally, as there are reports within the literature detailing hydrogen bonding of amidothiourea sensors in MeCN,[79] which are in contrast to reports detailing the ease of deprotonation of such sensors in DMSO,[136,140] it was anticipated that these investigations would contribute further to this subject matter. Therefore, the anion binding capabilities of various amidothiourea sensors were investigated using UV-Vis absorption, fluorescence emission and ^{1}H NMR spectroscopies.

The initial sensors synthesised and investigated are shown in Scheme 3.1. Aforementioned, the 2,6-dicarboxyamidopyridine unit was chosen to function as a scaffold for the attachment of the *p*-nitro-phenyl-based receptor moieties (Chapter 1, Section 1.9). In addition to the well established synthetic chemistry of such pyridine derivatives, the nitrogen atom of 2,6-dicarboxyamidopyridine can form hydrogen bonds with the adjacent amide groups, which can result in pre-organisation of appended receptor moieties for sensing purposes.[179,180] Therefore, sensor **54**, which is shown in Scheme 3.1, was the first synthetic target for the anion binding studies discussed in this chapter. As can be seen, the corresponding benzene-based amidothiourea and amidourea sensors, **53** and **52**, respectively, were also synthesised for the sake of comparison.

3.1 Synthesis of *p*-Nitro Phenyl-Based Amidoureas/Thioureas 52-54

The synthesis of sensors **52-54** is shown in Scheme 3.1. Sensors **53** and **54** have previously been referred to as a control in the studies of the tripodal sensor **34**,[139] which was discussed in Chapter 1, Section 1.8.4. However, these studies did not report the synthesis of **53** and **54** and absorption titrations were solely carried out in the presence of AcO^- in DMSO. Therefore, these sensors were characterised and their potential to detect various anions in more competitive media was investigated.

Sensors **52-54** were formed by stepwise synthesis from the commercially available dicarboxylic acids, 2,6-pyridine dicarboxylic acid and 1,3-benzene dicarboxylic acid. Esterification was acid catalysed and achieved in high yields using literature procedures for both **50a** and **50b**.[181,182] Addition of hydrazine monohydrate to both esters in methanol at room temperature resulted in almost immediate precipitation of white solids, which were filtered and dried in air to give the hydrazides **51a** and **51b** in 65 and 86% yields, respectively, as reported within the literature.[137]



Scheme 3.1: i) H_2SO_4, MeOH, reflux. ii) $N_2H_4 \cdot H_2O$, MeOH, RT. iii) MeCN, reflux, 16 h.

Sensors **52-54** were then formed by heating these hydrazides and the corresponding *p*-nitro-phenyl isocyanate or isothiocyanate in MeCN. In all cases, the reactions resulted in the formation of pale yellow precipitates, which were collected by suction filtration and dried in air, giving **52**, **53** and **54** in 92, 70 and 98% yields, respectively.

3.2 Characterisation of Sensors 52-54

Compounds **52-54** were characterised by NMR, IR and MS. The ^{1}H NMR (600 MHz, DMSO-d_6) spectra of both **52** and **54** are shown in Figures 3.1 and 3.2, respectively, to illustrate the differences between these two types of sensors. The downfield region of

the spectrum of **52**, Figure 3.1, displayed C_2 symmetry, in which the three N-H proton resonances occurred at 10.52, 9.65 and 8.65 ppm, and integrated for two protons each. The signal at 10.52 ppm was assigned to the amide N-H protons, while the remaining two resonances were assigned to the urea protons using ^{1}H-^{1}H and ^{15}N-^{1}H COSY NMR. In contrast to that seen in the ^{1}H NMR spectrum of **52**, the N-H protons of **53** were located further downfield at 10.81 and 10.21 ppm, due to the more electron withdrawing effect of the thiourea receptor (Appendix B, Figure B1). Furthermore, in comparison to **52**, the ^{1}H NMR spectrum of **53** showed that there were only two chemically distinct N-H environments, as the thiourea protons occurred at similar chemical shifts. The downfield region of the ^{1}H NMR spectrum of **54** is shown in Figure 3.2, which clearly shows the N-H protons were shifted further downfield than seen for **53**, most likely due the introduction of the pyridine ring. The N-H resonances of **54** were also more complex than seen for **52** and **53**, as there were three broad and major resonances as well as some minor ones present.

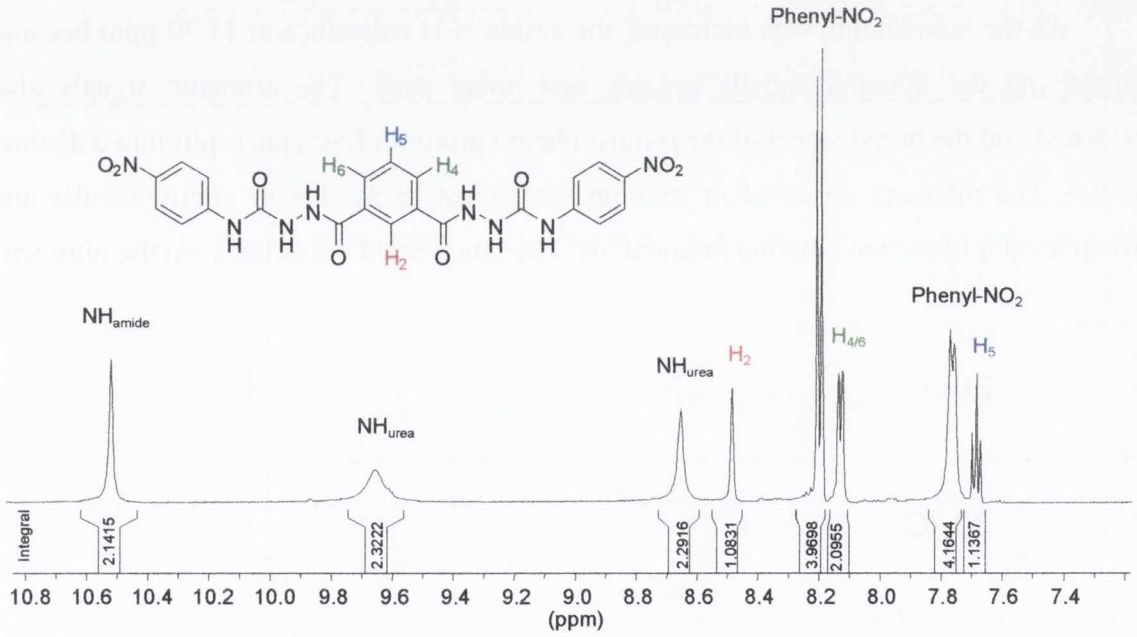


Figure 3.1: The downfield region of the H^1 NMR (600 MHz, DMSO-d_6) spectrum of **52**.

The major N-H resonances, which occurred at 11.30, 10.37 and 10.20 ppm, integrated for two protons each and were assigned to the amide and the two thiourea protons, respectively. The ^{1}H NMR spectrum of **53** also contained minor resonances, however, these were less prominent than those observed in the ^{1}H NMR spectrum of **54**. Investigation into the cause of these minor resonances showed that they were in fact due to rotamers at room temperature in DMSO-d_6, as upon heating, a single species was observed. The changes observed in the variable temperature (VT) ^{1}H NMR experiments of **54** are shown in Figure 3.3 and were reversible for every temperature increment.

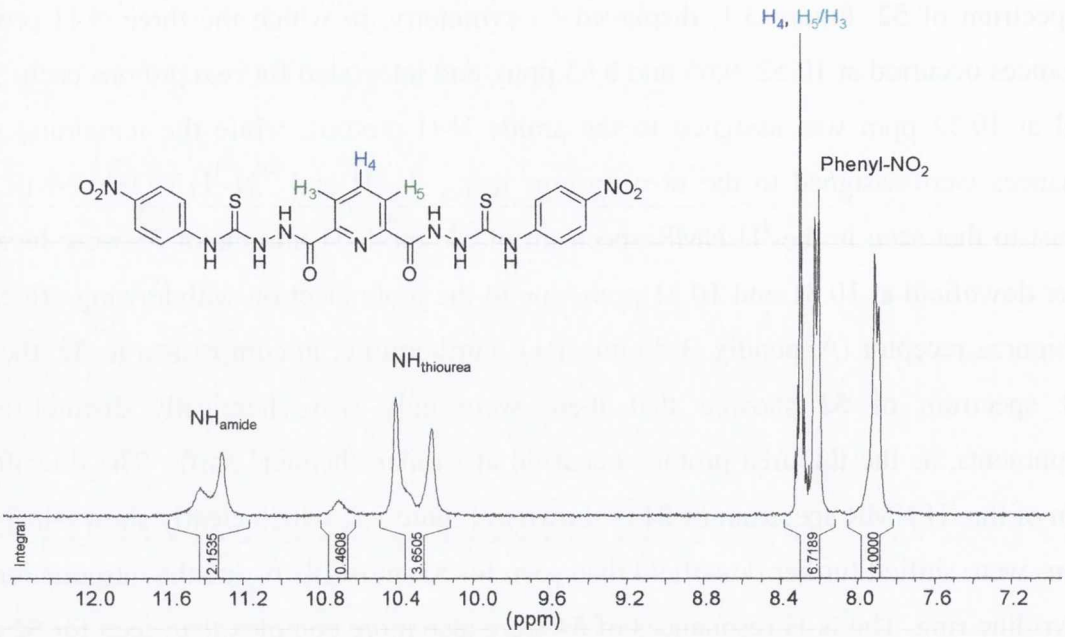


Figure 3.2: The downfield region of the H^1 NMR (600 MHz, DMSO-d_6) spectrum of **54**.

As the temperature was increased, the amide N-H resonance at 11.30 ppm became sharper and the thiourea signals became one broad peak. The aromatic signals also sharpened and the broad signal of the *p*-nitro-phenyl protons (7.90 ppm) split into a distinct doublet. The rotamers observed in solution were most likely due to intermolecular and intramolecular hydrogen bonding interactions. The latter could occur between the nitrogen

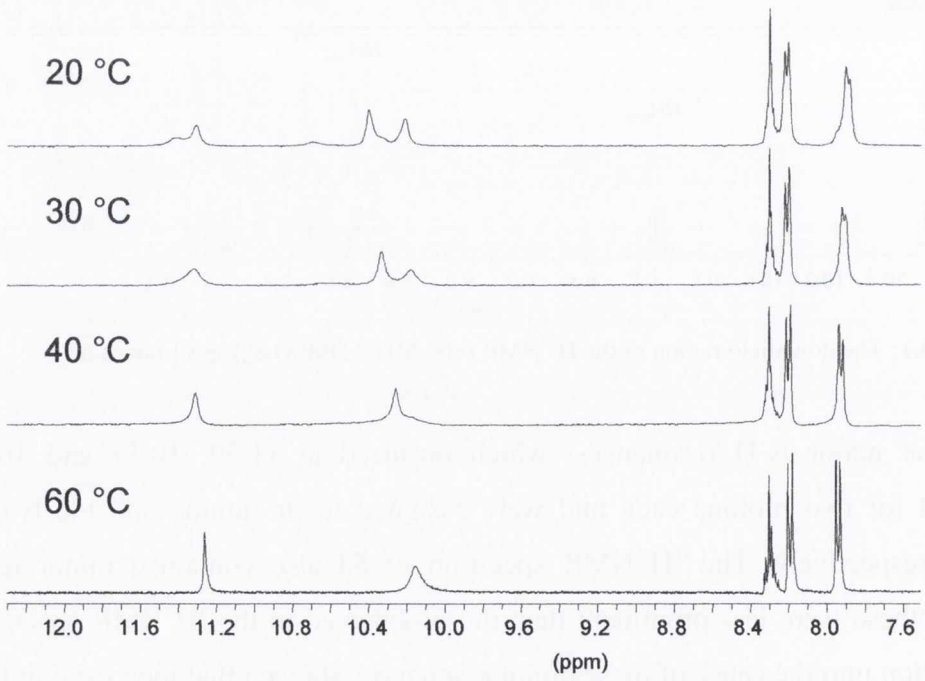


Figure 3.3: VT ^{1}H NMR (400 MHz, DMSO-d_6) spectra of **54**

of the pyridine centre and the amide N-H protons at the 2- and 6-positions. Indeed, rotamers were also visible in the ^{15}N-^{1}H COSY spectrum, which is shown in Figure 3.4.

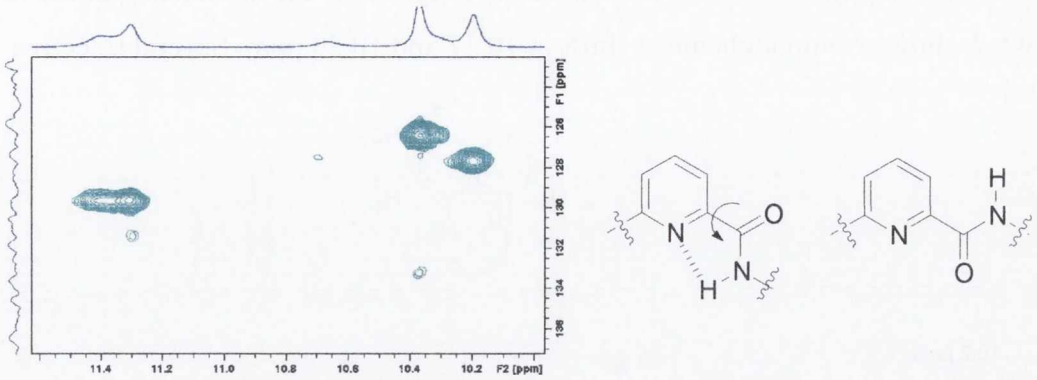


Figure 3.4: (Left) The ^{15}N-^{1}H COSY NMR spectrum of **54** (600 MHz, DMSO-d_6) and **(Right)** the possible conformers in solution.

The resonances of the amide protons at *ca.* 11.30 ppm showed a shoulder in the ^{1}H NMR spectrum, which was absent in the corresponding benzene-amidourea derivative, **52**. However, a minor shoulder was also observed for the benzene-amidothiourea derivative, **53**. This illustrated that the rotamers were more prevalent in the thiourea analogues, which may reflect the intrinsic higher acidity of these moieties and therefore, their ability to engage in a higher extent of hydrogen bonding. In contrast to the ^{1}H NMR spectrum of **54** in DMSO-d_6, the spectrum of **54** in DMF-d_7 (600 MHz), Figure 3.5, showed the presence of a single conformer in solution, thus illustrating the effect different solvents may have on the conformation of these sensors in solution. This may be important for the formation of Host:Guest interactions, as strong intramolecular hydrogen bonds have been shown to promote or prevent complexation.[59,183-185]

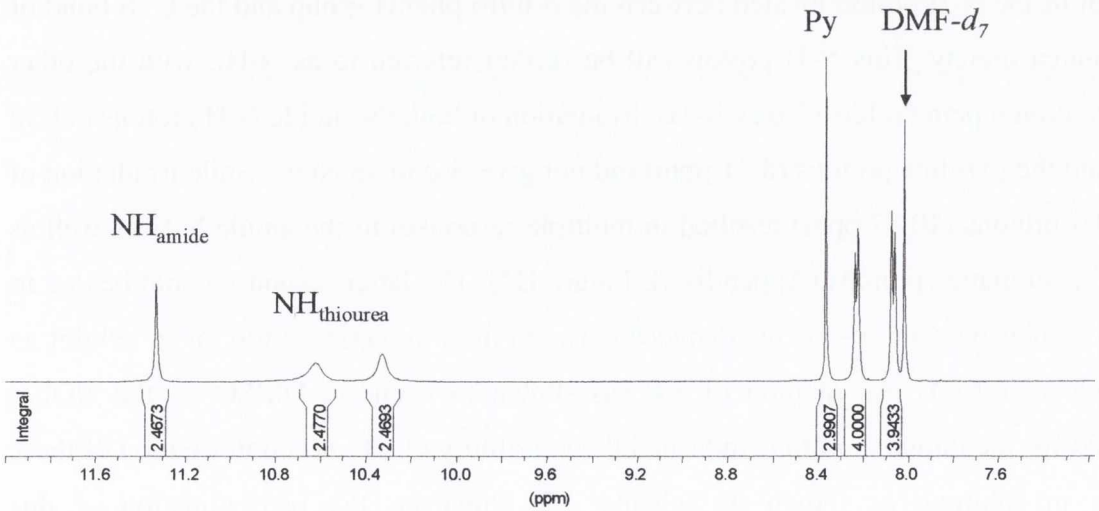


Figure 3.5: ^{1}H NMR (600 MHz, DMF-d_7) spectrum of **54**.

In contrast to **52**, exact assignment of the thiourea protons of **54** in DMSO-d_6 or DMF-d_7 (600 MHz) was difficult, most likely due to the presence of multiple inter- and intramolecular hydrogen bonds. As shown in Figure 3.2, the thiourea protons of **54** in DMSO-d_6 showed similar chemical shifts at 10.37 and 10.20 ppm. Several selective

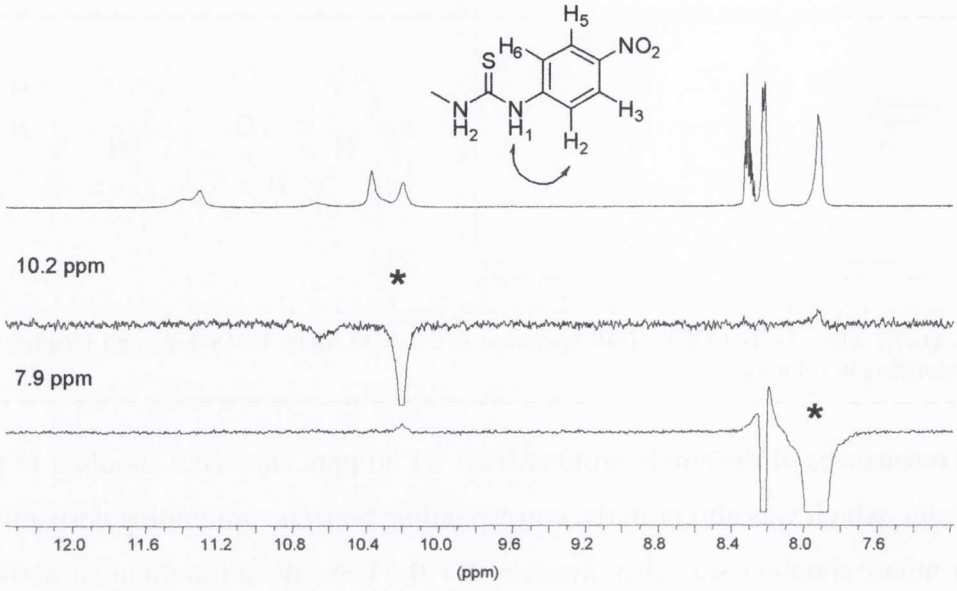
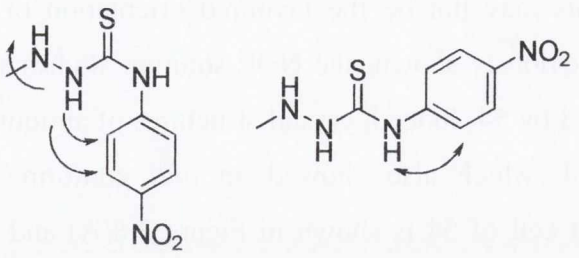


Figure 3.6: Selective ROESY ^{1}H NMR (600 MHz, DMSO-d_6) spectra of **54**.

Rotational nuclear Overhauser Effect Spectroscopy (ROESY) NMR experiments were carried out in an attempt to unambiguously assign these protons, as shown in Figure 3.6. Irradiation of the aromatic *p*-nitro-phenyl protons at 7.90 ppm resulted in a response from the N-H protons at 10.20 ppm. Reversibly, a response at 7.90 ppm was observed upon irradiation of the N-H protons at 10.20 ppm. This indicated that the *p*-nitro-phenyl protons at 7.90 ppm were most likely H_2 and H_6 and therefore, the N-H resonance at 10.20 ppm was that of the N-H proton located between the *p*-nitro phenyl group and the C=S bond of the thiourea moiety. This N-H proton will be further referred to as N-H_1, with the other thiourea proton being referred to as N-H_2. Irradiation of both the amide N-H protons (11.30 ppm) and the pyridine protons (8.31 ppm) did not give rise to an NOE, while irradiation of the N-H_2 protons (10.37 ppm) resulted in multiple responses to the amide N-H as well as all of the aromatics protons (Appendix B, Figure B2). The latter response could be due to intermolecular interactions, as the distance between these moieties is too far to exhibit an intramolecular NOE. As rotation of **54** was shown to occur in DMSO-d_6, the NOE's observed for the thiourea protons indicated the possibility of an *anti*-conformation of these protons in solution, as shown in Scheme 3.2. However, the predomination of this conformer cannot be said for certain and the NOE's above were only discussed to emphasise that the conformation of **54** in solution is complicated.



Anti *Syn*

Scheme 3.2: Schematic representation of the thiourea fragment of **54** with NOE's observed and possible conformations in solution

The ^{13}C NMR spectra of **52-54** in DMSO-d_6 showed the expected number of resonances, while the $[M+H]^+$ ion of each compound was observed using ES-MS. The IR spectra of all sensors showed strong sharp bands from *ca.* 1300-1700 cm^{-1}, due to the carbonyl and nitro group stretches. Both thiourea derivatives, **53** and **54**, showed weak broad vibrations centred at *ca.* 3000 cm^{-1}, due to the stretching of the N-H moieties. In comparison to **53** and **54**, the urea derivative displayed a slightly sharper and stronger vibration in this region.

Flat plate-like crystals of **54**, suitable for X-ray crystallographic analysis, were grown in both DMSO and DMSO-d_6, from which the crystal structure was solved by Dr. T. McCabe (Trinity College Dublin). The crystals obtained from both solvents gave rise to a similar data set and the crystal structure obtained from DMSO-d_6 is shown in Figure 3.7, with selected bond lengths and angles detailed in Table 3.0. As can be seen from Figure 3.7, the N-H protons of the thiourea receptor are in an *anti*-conformation.

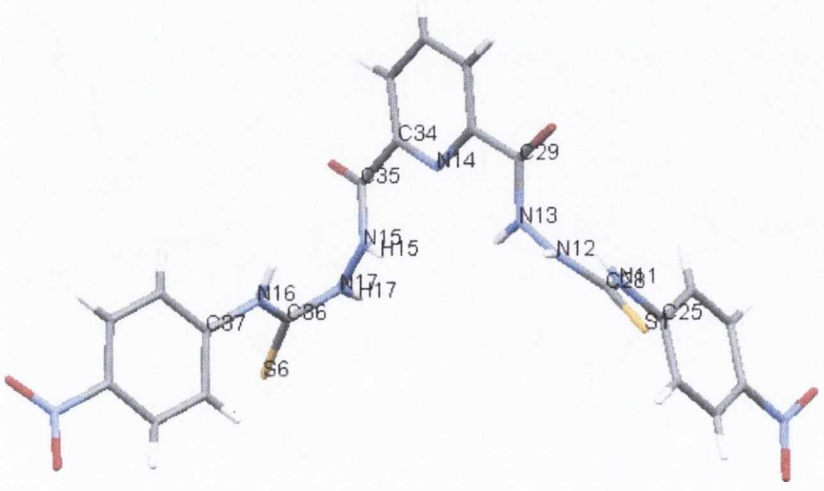


Figure 3.7: The X-ray crystal structure of **54**.

While this is not the suitable geometry for directional hydrogen bonding between an anion and a urea moiety,[186] this may not be the favoured orientation of the N-H protons in solution. However, as previously shown, the NOE solution studies suggested that such a conformation was adopted by **54**. Indeed, crystal structures of amidothiourea sensors have previously been reported, which also showed an *anti* conformation of the thiourea protons.[128,137,140] The unit cell of **54** is shown in Figure 3.8(A) and here the asymmetric unit consisted of two molecules of **54** and six DMSO molecules. A trifurcated DMSO molecule was observed, which was hydrogen bonded to both of the amide N-H's of a

Table 3.0: Selected bond lengths and bond angles for **54**

Bond	Length (A)	Bond	Angle (°)
C(36)-S(6)	1.664	S(1)-C(28)-N(13)	117.36
C(28)-S(1)	1.679	S(1)-C(28)-N(11)	126.49
N(13)-N(12)	1.396	C(25)-H(11)-C(28)	128.53
N(15)-N(17)	1.392	C(36)-N(15)-N(13)	122.06
C(29)-N(13)	1.352	N(14)-C(34)-C(35)	116.62
C(35)-N(15)	1.361	H(17)-N(17)-C(36)	113.99
N(16)-C(37)	1.426	H(15)-N(15)-N(17)	120.63

single molecule, while the third hydrogen bond was formed with the N-H_2 proton on the adjacent molecule.[187] The multiple hydrogen bonds observed in the solid state shed some light on the NOE NMR results observed in solution. While similar interactions between the solvent and the sensor may not have occurred in the solid and solution states, both techniques indicated that **54** was involved in multiple intermolecular hydrogen bonds.

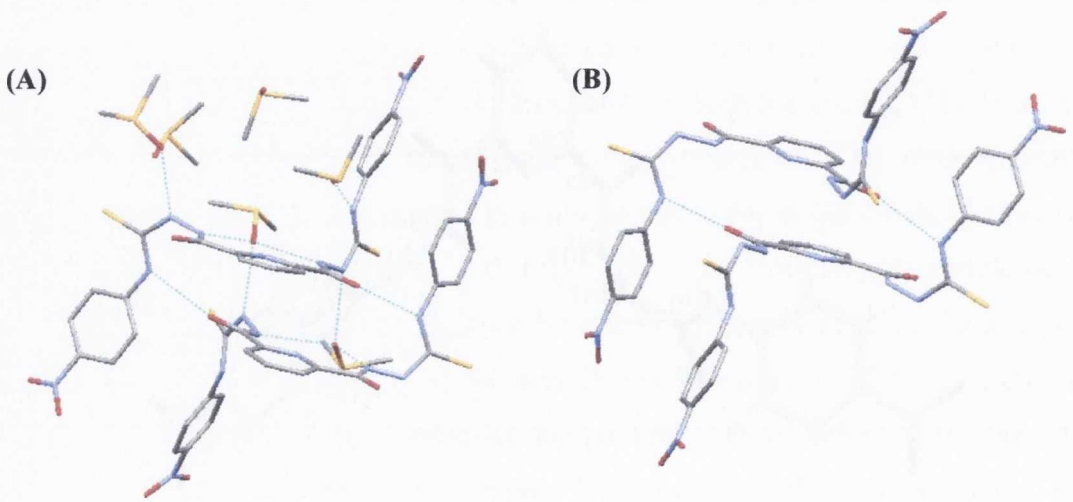


Figure 3.8: A) The X-ray crystal structure of **54** showing six hydrogen bonded DMSO molecules. **B)** The unit cell dimer with intermolecular hydrogen bonds. Hydrogen atoms are omitted for clarity.

Indeed, as well as the hydrogen bonding observed with the DMSO solvent molecules, Figure 3.7 (B) shows that the unit cell contained an intermolecular hydrogen bond from the carbonyl oxygen on one arm of each molecule to the N-H_1 on the adjacent molecule. The three dimensional (3D) packing of **54** for two crystallographic axes are shown in Figure 3.9. These structures illustrate the combination of hydrogen bonding and π-π stacking, which gives rise to an elaborate 3D network that is perforated with DMSO solvent filled channels.

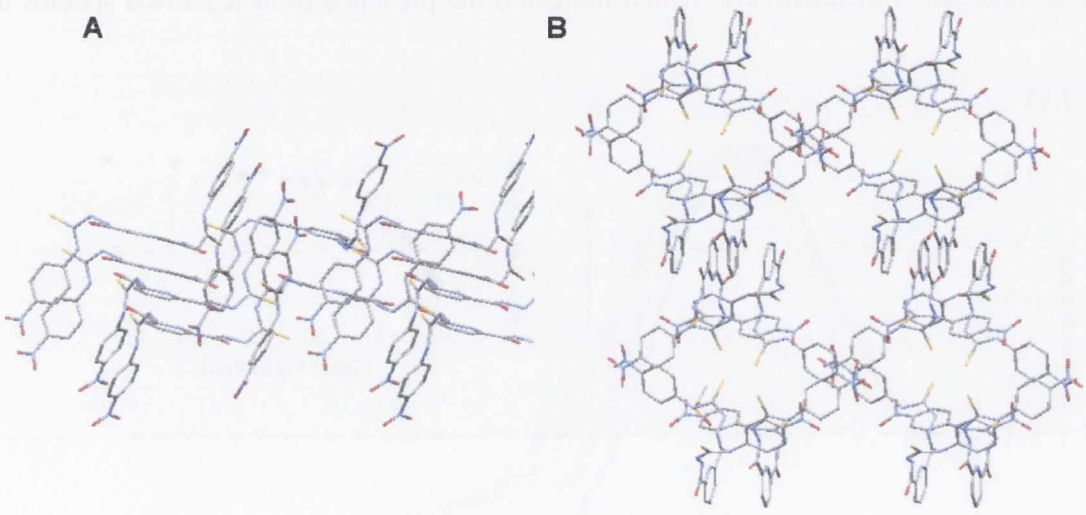


Figure 3.9: (A) View along the b* crystallographic axis. **(B)** View along the c crystallographic axis. Hydrogen atoms and solvent molecules are omitted for clarity.

3.3 Absorption Titrations of 52-54 with Anions in DMSO

In order to gain an understanding of the anion interactions for these sensors, compounds **52-54** were first titrated in DMSO using various different anions. Molar absorption coefficients (ε) were determined at the respective λ_{max} for **52**, **53** and **54** in DMSO, as 32,500 M^{-1} cm^{-1}, 21,749 M^{-1} cm^{-1} and 21,270 M^{-1} cm^{-1}, respectively. Stock solutions of the sensors were prepared at *ca.* [1×10^{-3} M], which were then diluted to *ca.* 1-2×10^{-5} M prior to titration. Stock solutions of the various anions were also prepared at varying concentrations of *ca.* [1×10^{-1}], [1×10^{-2}] and [1×10^{-3}] M in DMSO. Additionally, these solutions were prepared using only Pyrex glass as sensor **54** was shown to interact with ions present in soda-glass based materials. Such phenomenon has previously been observed for the hydrazine based sensors, **16a-b**, discussed in Chapter 1.[128] This observation will be discussed further in Section 3.9.

The absorption spectra of **52-54** in DMSO were all similar, with a characteristic absorption band at λ_{max} = 341 nm for **52**, 350 nm for **53** and 348 nm for **54**, which were assigned to the *p*-nitro-phenyl chromophores. The spectrum of **54** also exhibited a shoulder

at *ca.* 280 nm, which was assigned to the pyridine moiety. Preliminary absorption titrations in DMSO were first carried out with compounds **52-54** using the TBA salt of $H_2PO_4^-$ and the results for **52** and **54** are shown in Figure 3.10. Each of these sensors displayed a bathochromic shift, in which the λ_{max} was shifted to longer wavelengths, upon increasing the anion concentration. In the case of **53** and **54**, a new absorption band was observed, centred at *ca.* 425 nm, which tailed into *ca.* 560 nm. No clear isobestic points were observed in these titrations but 'pseudo' isobestic points were observed at *ca.* 344 and 353 nm for **52** and **53-54**, respectively, which indicated the presence of at least two species in

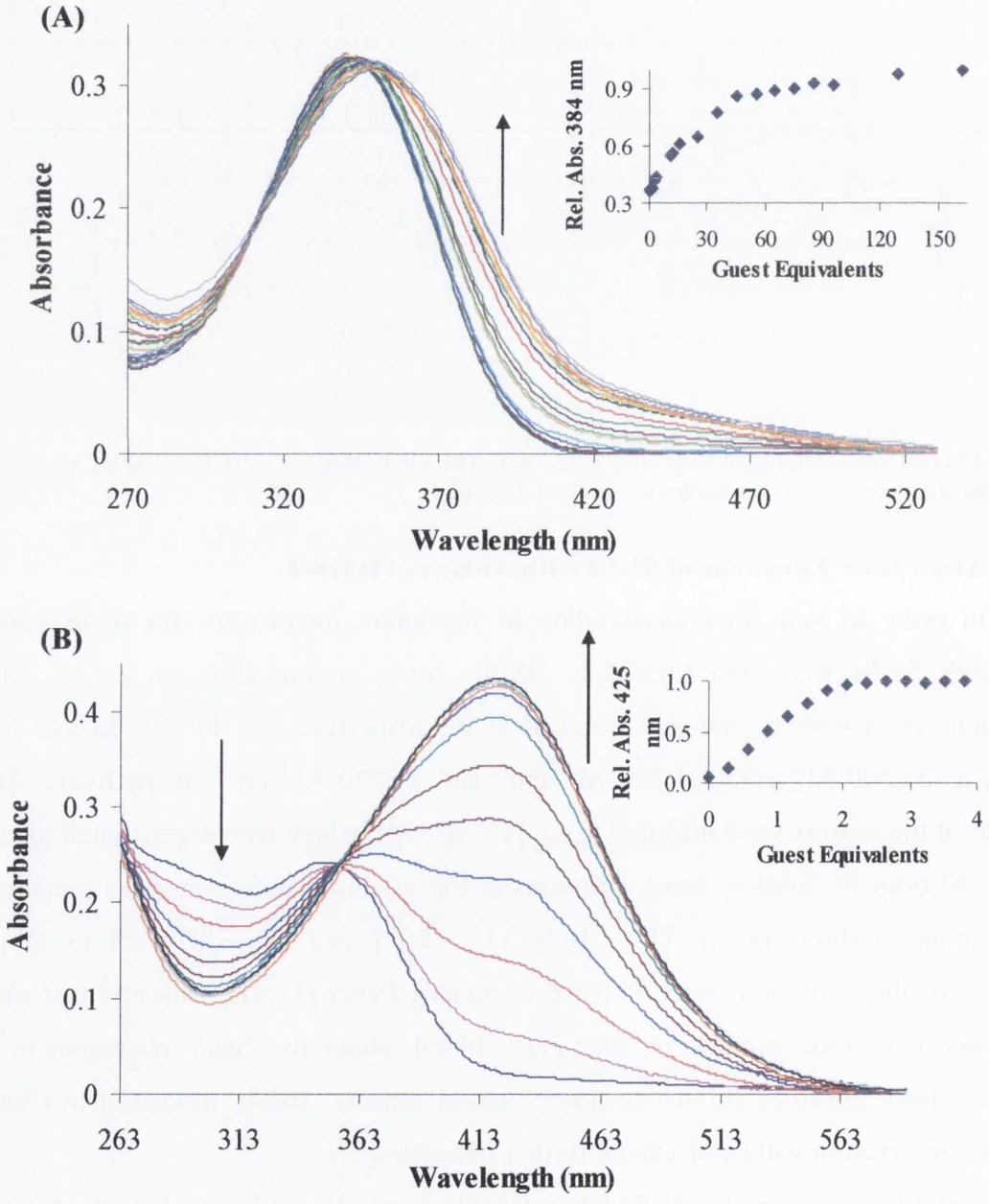


Figure 3.10: (A) The changes in the absorption spectra of **52** [1×10^{-5} M] upon addition of $H_2PO_4^-$ (0 → 162 equivalents) in DMSO. **Insert:** The relative changes in the absorbance at 384 nm against equivalents. **(B)** The changes in the absorption spectra of **54** [1×10^{-5}M] upon addition of $H_2PO_4^-$ (0 → 5 equivalents) in DMSO. **Insert:** The relative changes in the absorbance at 384 nm against equivalents.

solution. Additionally, the changes observed in the absorption spectra of **52-54** resulted in a colour change from colourless to yellow.[188-191] By comparing the titration profiles in Figure 3.10, it can be seen that **54** showed more significant changes in its absorption spectra, as well as a much higher affinity for $H_2PO_4^-$ than the urea analogue, **52**. While *ca.* 50 equivalents of $H_2PO_4^-$ were required to reach a plateau with **52**, only two equivalents were required in the case of **54**. The changes in the absorption spectra of **53**, as well as the observed stoichiometry (Appendix B, Figure B3) were very similar to that observed for **54**. Overall, the changes observed indicated that $H_2PO_4^-$ interacted with the amidourea and thiourea receptors, which are in conjugation with the *p*-nitro-phenyl chromophores. This gave rise to enhanced ICT character and subsequently shifted the spectra to longer wavelengths, hence, giving rise to the appearance of the yellow colour. Additionally, on comparing the benzene derivative, **53**, with the pyridine derivative, **54**, a slightly higher affinity for anions was observed with the latter, as a slightly lower concentration of anion was required to reach a plateau (Appendix B, Figure B4). This may be due to hydrogen bonding between the pyridine nitrogen and the adjacent N-H protons forming a preorganised conformation or a cleft-like environment, which can interact with anions more favorably, as previously postulated by Wei *et al.*[137]

Due to the higher affinity of **54** for $H_2PO_4^-$, further titrations were carried out with the TBA salts of $HP_2O_7^{3-}$, F^- and AcO^-. Similar changes were observed in the absorption spectra for all these anions, with $HP_2O_7^{3-}$ being detected most strongly in a 1:1 stoichiometry, as shown in Figure 3.11. Additionally, as for $H_2PO_4^-$, a 1:2 Host:Guest

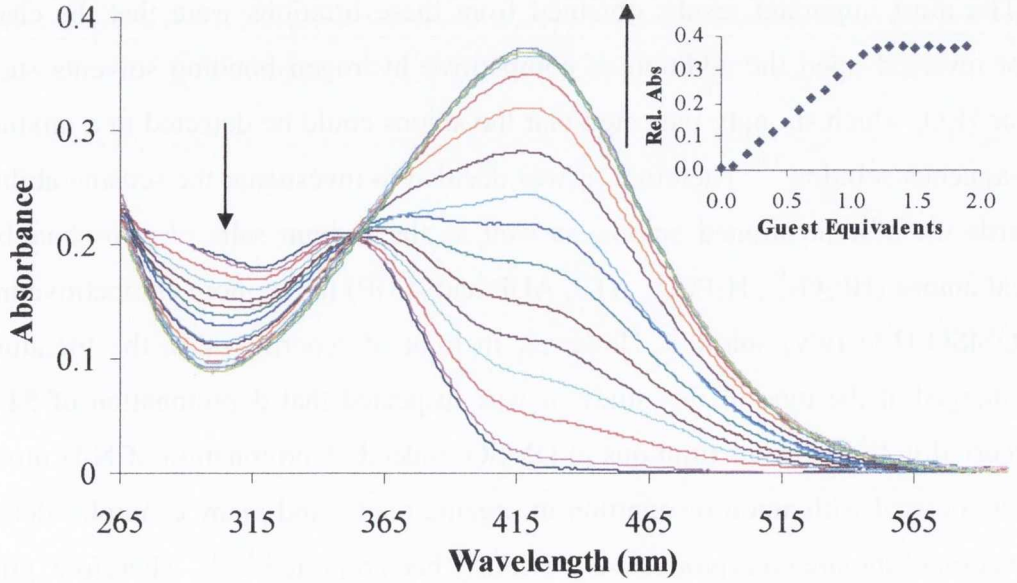


Figure 3.11: The changes in the absorption spectra of **54** [1×10^{-5} M] in DMSO upon addition of $HP_2O_7^{3-}$ (0→ 2 equivalents). **Insert:** Changes in UV-vis at 425 nm with increasing anion additions.

stoichiometry was observed with F^- and AcO^-. The relative changes in the absorption spectra of **54**, shown in Figure 3.12, indicate that $H_2PO_4^-$, $F^-$and AcO^- may form hydrogen bonded complexes with each amidothiourea arm of the sensor, as a plateau was observed after the addition of *ca.* two equivalents of each of these anions. Conversely, it was envisaged that $HP_2O_7^{3-}$ may bridge both arms of the sensor, thus, giving rise to theobserved 1:1 stoichiometry. In contrast to these results, titrations of **54** with Cl^- gave rise to only very minor changes in the absorption spectra, within the same concentration range, while Br^- did not give rise to any significant changes.

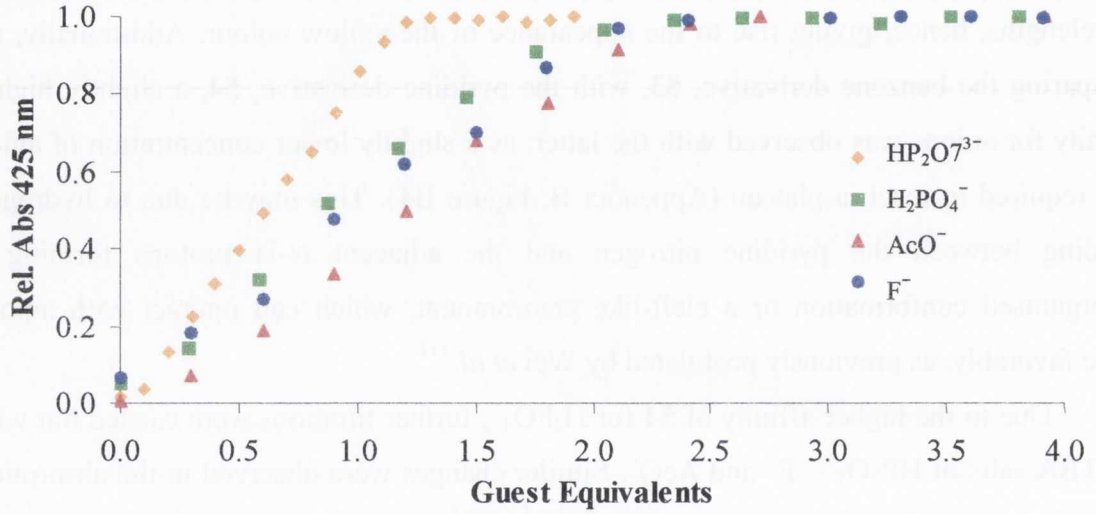


Figure 3.12: The relative changes in the absorption spectra of **54** [1×10^{-5} M] at 425 nm upon addition of various anions in DMSO.

The most important results obtained from these titrations were that the changes were not reversed upon the addition of competitive hydrogen bonding solvents such as MeOH or H_2O, which strongly indicated that the anions could be detected in a mixture of organic-aqueous solution.[128] Therefore, it was decided to investigate the sensing ability of **54** towards the aforementioned anions, as well as the sodium salts of phosphate-based biological anions ($HP_2O_7^{3-}$, $H_2PO_4^-$, ATP, ADP and AMP) in the more competitive media of 4:1 DMSO-H_2O (v/v) solution. However, in light of reports within the literature,[136] which emerged at the time of this study, it was suspected that deprotonation of **54** may have occurred in the previous titrations in DMSO. Indeed, deprotonation of N-H moieties is often associated with anion recognition in organic media and many examples detailing deprotonation of thiourea receptors have previously been reported.[152,161] Therefore, prior to the spectroscopic investigations of **54** with anions in 4:1 DMSO-H_2O, titrations with base were firstly carried out, in order to observe the changes resulting from any possible

deprotonation. The various titrations carried out in this solvent system are discussed in the following sections.

3.4 Absorption Titrations of 54 with Base and the TBA salts of Various Anions in 4:1 DMSO-H_2O Solution

The changes in the absorption spectra of **54** upon titration with NaOH in 4:1 DMSO-H_2O are shown in Figure 3.13. The λ_{max} of **54** was shifted slightly from 348 nm in DMSO to 344 nm in the partially aqueous solvent system. From Figure 3.13, it is clear that substantial changes occurred in the absorption spectrum as a function of pH. In a similar manner to the titrations discussed above, a bathochromic shift to *ca.* 412 nm was observed upon the addition of NaOH. These changes were clearly visible to the naked eye as the solution changed from pale yellow to deep yellow. The changes in the absorption spectra of **54** as a function of the equivalents of OH^- added are shown as an insert in Figure 3.13. The bi-phasic plot indicated that the first deprotonation was completed upon the addition of one equivalent of OH^-, while approximately 14 equivalents more were required to remove the second N-H proton. Comparison of Figure 3.13 with Figures 3.10(B) and 3.11, shows that the changes in the presence of OH^- were very similar to the changes which occurred in the presence of anions in DMSO. Due to these similarities, it is reasonable to assume that deprotonation of **54** by the various anions may have occurred in DMSO solution.

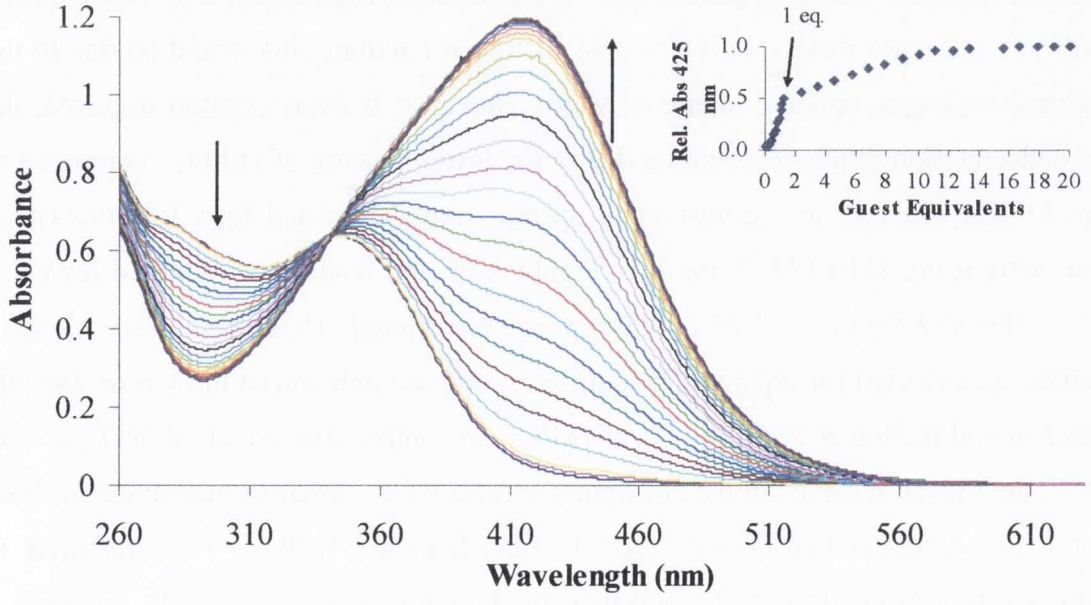


Figure 3.13: The changes in the absorption spectra of **54** [3×10^{-5} M] in DMSO upon addition of NaOH (0 → 25 equivalents). **Insert:** The relative changes at 425 nm plotted *vs.* –log [NaOH].

Having established that NaOH gave rise to significant changes in the absorption spectra of **54**, the changes upon addition of the aforementioned anions were next investigated. Figure 3.14 shows the changes in the absorption spectra of **54** upon titration with the TBA salt of $H_2PO_4^-$ in 4:1 DMSO-H_2O. Under these solvent conditions, **54** displayed similar changes to that shown for the titration with NaOH, Figure 3.13, in which the spectra were shifted to longer wavelengths upon interaction with $H_2PO_4^-$. Once more, no clear isosbestic point was observed for these changes. However a pseudo isosbestic

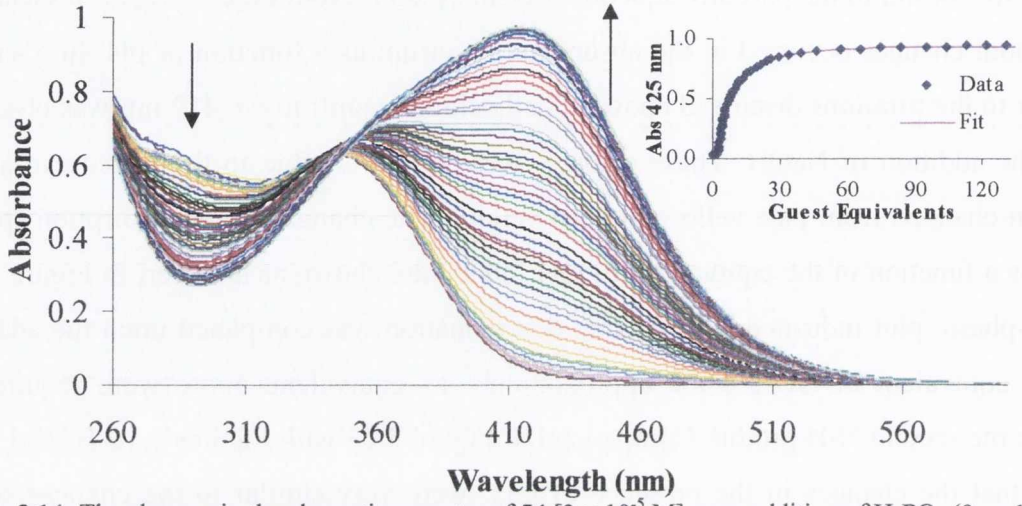


Figure 3.14: The changes in the absorption spectra of **54** [3×10^{-5} M] upon addition of H_2PO_4 (0 → 133 equivalents) in 4:1 DMSO-H_2O. **Insert:** The binding isotherm at 425 nm and corresponding fit obtained using SPECFIT™.

point was seen at *ca.* 340 nm. As shown in the insert in Figure 3.14, the number of equivalents required to reach a plateau (*ca.* 30 equivalents) were higher than that required in DMSO (*ca.* 2 equivalents). In the case of hydrogen bonding, this would be due to the competitive hydrogen bonding nature of water. However, if deprotonation occurred, the higher concentration required would be due to the lower bascitiy of $H_2PO_4^-$, compared to hydroxide. The changes in the absorption spectra were best fitted to a 1:2 Host:Guest stoichiometry using SPECFIT™, insert in Figure 3.14, and binding constants of $\log K_{1:1}$ = 4.24 (± 0.06) and $\log K_{1:2}$ = 4.07 (± 0.04) were determined. These values are close in magnitude, as expected for separated binding sites, one on each arm of the sensor. Despite the good fit and the lower basicity[192,193] of $H_2PO_4^-$ in comparison to that of AcO^-, F^- and $HP_2O_7^{3-}$, the overall changes in the absorption spectra were similar in magnitude to those seen for the deprotonation above. As 30 equivalents of $H_2PO_4^-$ were required to deprotonate the sensor, it could be said that the deprotonation was 'forced', however, a measureable element of hydrogen bonding prior to deprotonation was not observed. In the case of thiourea sensors, reported hydrogen bonding of basic anions is often followed by deprotonation.[156,161] In general, hydrogen bonding and deprotonation can give rise to

overlapping spectral changes, nevertheless, these two interactions are normally distinguished by observing the changes at a single wavelength as a function of concentration. *i.e* a stable hydrogen bonded complex initially forms up to a certain concentration, which is subsequently deprotonated upon the addition of further anion. While changes due to hydrogen bonding and deprotonation for such amidothiourea sensors would most likely overlap, no such two-step process was observed in the case of **54** with $H_2PO_4^-$.

Nevertheless, as many elegant sensors, which function *via* deprotonation have been reported in the literature,[194-196] further titrations of **54** with anions were carried out and the results are shown in Figure 3.15. Clearly, the presence of water affected the Host:Guest interactions and the affinity of **54** for the various anions tested was quite different to that previously observed in DMSO, Figure 3.12. Both AcO^- and F^- showed

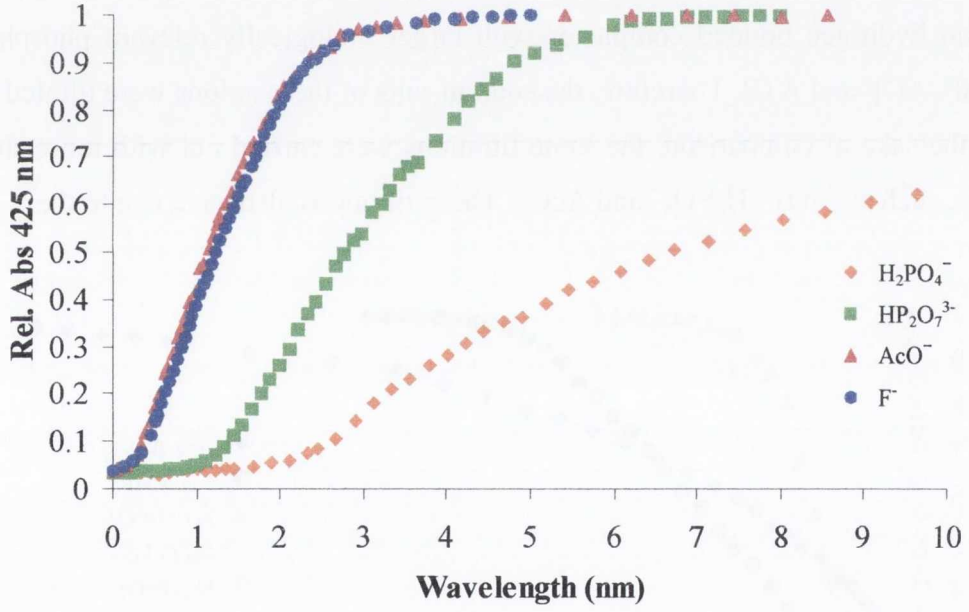


Figure 3.15: The relative changes in the absorption spectra of **54** [3×10^{-5} M] at 425 nm upon addition of various anions in 4:1 DMSO-H_2O

similar high affinities for **54**, while the phosphates, particularly $H_2PO_4^-$, showed lower affinities ($F^- \approx AcO^- > HP_2O_7^{3-} > H_2PO_4^-$). This change in the order of affinity could possibly be due to different solvation of the anions and/or ion-pairing of the TBA salts in the aqueous-based solvent system, compared to that in DMSO. Indeed, the $H_2PO_4^-$ anion is a kosmotropic[197] anion that shows high hydration energies, which may explain the lower affinity in the presence of water.[2] Also noticeable from Figure 3.15 is that no changes occurred at low concentration of these anions, which was more pronounced for the phosphate salts. This unexpected behaviour can be speculated as being due to a solvent effect and/or a concentration effect. In the case of the former, the interaction of anions with

54, may require displacement of hydrogen bonded solvent molecules from the anion and/or the sensor and, therefore, only when a certain threshold has been reached, an interaction can occur. In the case of the latter, titration of **54** at a concentration of 1×10^{-5} M in 4:1 DMSO-H_2O showed that a higher number of equivalents of both the phosphate salts were required to give rise to spectroscopic changes, compared to the titrations carried out at 3×10^{-5} M (Appendix B, Figure B5, B6). Due to this phenomenon, the titrations of **54** in 4:1 DMSO-H_2O were carried out at *ca.* [3×10^{-5} M], compared to those at 1×10^{-5} M in DMSO. The absorption titrations of **54** with phosphate-based biological anions in 4:1 DMSO-H_2O are discussed in the next section.

3.5 Absorption Titrations of 54 with Phosphate-Based Biological Anions in 4:1 DMSO-H_2O Solution

Due to the lower affinity of **54** towards the phosphate salts, it was envisaged that **54** may form hydrogen bonded complexes with larger biologically relevant phosphates, such as AMP, ADP and ATP. Therefore, the sodium salts of these anions were titrated with **54** and for the sake of comparison, the same titrations were carried out with more simple sodium salts, such as $P_2O_7^-$, $H_2PO_4^-$ and AcO^-. These titrations also gave rise to the

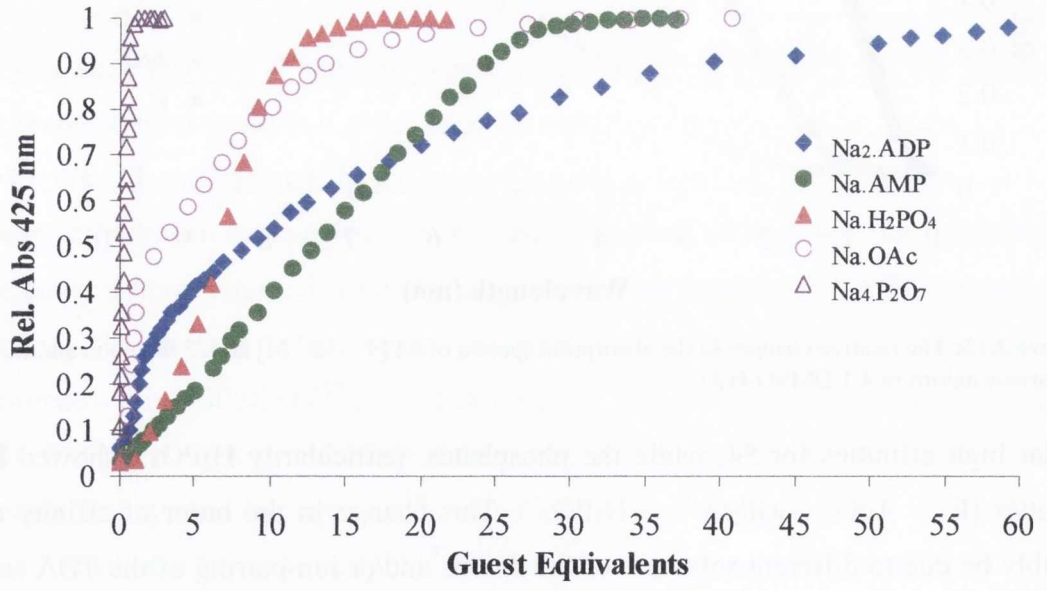


Figure 3.16: The changes in the absorption spectra of **54** [3×10^{-5} M] at 425 nm upon addition of various anions in 4:1 DMSO-H_2O.

formation of a new transition in the absorption spectra at long wavelengths, similar to that seen for the TBA salts and for NaOH in 4:1 DMSO-H_2O solution. Once again, these changes were visible to the naked-eye and the spectral changes indicated a common mechanism of interaction of **54** with these anions (Appendix B, Figure B7). In contrast to

the TBA salts in Figure 3.15, the sodium-based anions gave rise to immediate changes in the absorption spectra in 4:1 DMSO-H_2O solution. This clearly illustrated the sensitivity of **54** towards changes in the local environment and also showed that the choice of counter-cation effected the Host:Guest interactions.[198]

By plotting the relative changes in the absorption spectra of **54** at 425 nm, as a function of the number of equivalents of anions added, binding isotherms were obtained, which can be seen in Figure 3.16. In comparison to that seen for the TBA salt of pyrophosphate, the sodium salt showed a very strong 1:1 interaction in 4:1 DMSO-H_2O solution. However, the stoichiometries of both salts differed and the sodium-based pyrophosphate anion was more highly charged and, therefore, more basic. This most likely explains the higher affinity observed between **54** and this salt. In contrast to the titrations with AMP and ADP, no changes were observed in the presence of ATP (not shown). The changes in Figure 3.16 also clearly showed a two-step interaction with both AcO^- and ADP. These binding isotherms resemble those observed upon titration of **54** with NaOH, Figure 3.13, and once more indicated that the overall interaction was most likely due to deprotonation of both amidothiourea receptor moieties of **54**.

At this point, buffering of the 4:1 DMSO-H_2O solution with HEPES was considered. However, dissolution of **54** in a mixture of 4:1 DMSO-H_2O (HEPES, 0.1 M) resulted in the solution becoming more yellow, indicating an interaction of the sensor with the buffer, most likely the anionic sulfate component. Tris-HCl was also considered, as no interaction between **54** and Cl^- was previously observed in 4:1 DMSO-H_2O. Reports within the literature have shown that the pH of Tris-HCl was not influenced by the presence of up to 0.30 mole fraction of DMSO.[199] However, the mole fraction of DMSO in 4:1 DMSO:H_2O is *ca.* 0.5. Therefore, the pH of such a solution could not be accurately determined or considered as reliable and, hence, no further attempt was made to buffer the 4:1 DMSO-H_2O solutions.

To quantify the interaction of **54** with the various anions above, the changes in 4:1 DMSO-H_2O were analysed using SPECFIT^{TM}, in a similar manner to that previously shown for $H_2PO_4^-$. These results are discussed in the following section.

3.6 Fitting of the Absorption Titrations of 54 with Anions in 4:1 DMSO-H_2O using SPECFIT™

As the pH of **54** in 4:1 DMSO-H_2O, before, during and after anion titration could not be accurately determined (due to the percentage of DMSO present), the protonation/deprotonation model from SPECFIT™ was not suitable in order to determine association/dissociation constants. Therefore, a Host:Guest model was utilised for a numerical estimation, on the interactions occurring in solution. While the model is based purely on metal-ligand interactions, it was thought that the different spectroscopic species would be recognised, regardless of whether they were the product of a binding event or a deprotonation. From this fitting, 'apparent' affinity constants (log*K*) could be estimated for certain anions, Table 3.1, from which the species distribution in solution could be obtained. In all cases, the changes were fitted to various combinations of Host:Guest stoichiometries, including 1:1, 1:2 and 1:3. As previously discussed for $H_2PO_4^-$ (Section 3.4), Table 3.1 shows that for each anion, the log*K* values determined for each stoichiometric species were similar in magnitude. Figure 3.17 shows the species distribution diagram, which was obtained from the 1:2 Host:Guest fit for the titration of **54** with $H_2PO_4^-$, previously shown

Table 3.1: Binding constants obtained from fitting the changes upon titration of 54 with various anions in 4:1 DMSO-H_2O using SPECFIT™.

Anion Salt	Host:Guest	Log*β*	St. Dev	Log*K*
TBA.H_2PO_4	1:1	4.24	(± 0.07)	4.2
	1:2	8.31	(± 0.05)	4.1
$TBA_3.HP_2O_7$	1:1	6.53	(± 0.3)	6.5
	1:2	-	-	-
	1:3	15.5	(± 0.3)	-
Na_2.ADP	1:1	2.4	(± 0.6)	3.62
	1:2	6.0	(± 0.4)	3.8
	1:3	10.43	(± 0.07)	3.4
TBA.AcO	1:1	5.7	(± 0.2)	5.7
	1:2	11.3	(± 0.1)	5.6

in Figure 3.14. This clearly shows the simultaneous formation of the 1:1 and 1:2 stoichiometric species in solution, with the 1:2 species becoming the main species at higher concentrations of the anion. Considering the similarities in the titrations with anions and base, it is possible that the 1:1 species corresponds to a deprotonation, with the 1:2 species corresponding to the removal of a second N-H proton. The fits and corresponding speciation plots for $HP_2O_7^{3-}$ and AcO^- are shown in Appendix B, Figures B8-9, B10-11.

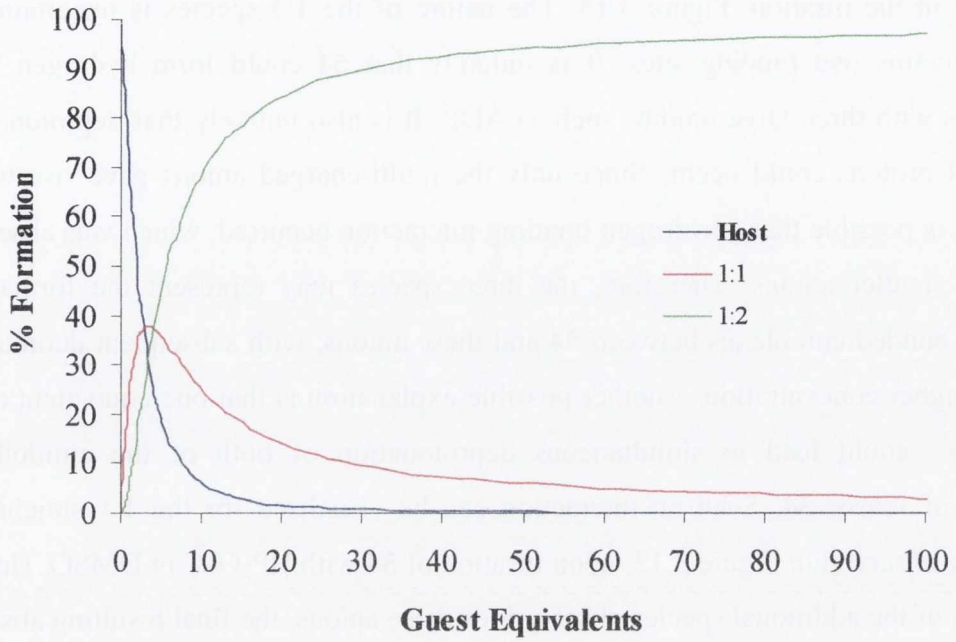


Figure 3.17: The species distribution diagram of **54** [3 × 10^{-5} M] upon addition of $H_2PO_4^-$ (0 → 133 equivalents) in 4:1 DMSO-H_2O.

The best fit for the $HP_2O_7^{3-}$ titration was obtained by allowing for the formation of a 1:1 and a 1:3 species in solution, which in the case of the former, gave a high binding constant of $\log K_{1:1}$ = 6.5 (± 0.3). As a good fit could not be obtained by including a 1:2 stoichiometry, this indicated that the 1:2 species did not reach more than 10% formation during the course of the titration. In a similar manner to $HP_2O_7^{3-}$, a 1:3 species was also observed for the interaction of **54** with ADP (See Appendix B, Figure B12 for fit). In the case of ADP, the errors obtained for the 1:1 and 1:2 species were quite high, however, the

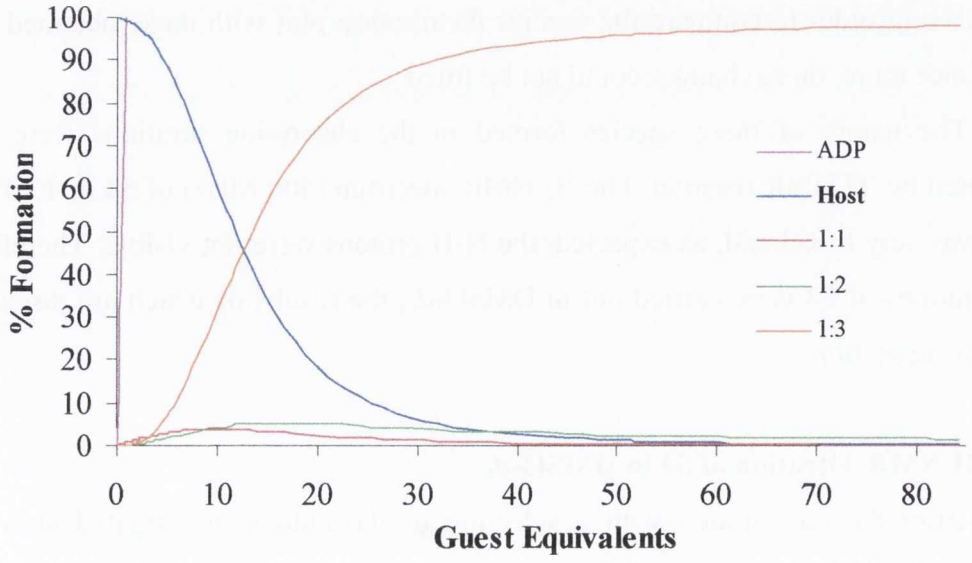


Figure 3.18: The species distribution plot of **54** [3 × 10^{-5} M] upon addition ADP (0 → 88 eq) in 4:1 DMSO-H_2O

species distribution diagram showed that these species did not reach more than 10% formation in the titration, Figure 3.18. The nature of the 1:3 species is uncertain as the sensor contains two binding sites. It is unlikely that **54** could form hydrogen bonded complexes with three large anions, such as ADP. It is also unlikely that deprotonation of three N-H protons could occur. Since only the multi-charged anions gave rise to a 1:3 species, it is possible that a hydrogen bonding interaction occurred, which was absent with the other smaller anions. Therefore, the three species may represent the formation of hydrogen bonded complexes between **54** and these anions, with subsequent deprotonation of **54** at higher concentration. Another possible explanation is that one equivalent of ADP or $HP_2O_7^{3-}$ could lead to simultaneous deprotonation of both of the amidothiourea receptors of sensor **54**. Such an interaction can be visualised for the 1:1 stoichiometry previously observed in Figure 3.12, upon titration of **54** with $HP_2O_7^{3-}$ in DMSO. However, regardless of the additional species observed for these anions, the final resulting absorption spectra in all titrations was similar, as well as the magnitude of the changes, which indicated that the main interaction resulted in deprotonation of sensor **54**. The changes in the absorption spectra upon titration with the TBA salt of F^- could not be fitted using SPECFIT™. However, the binding isotherm for F^-, shown in Figure 3.15, was almost identical to the isotherm observed for AcO^-. Therefore, it can be assumed that the strength of the interaction with F^- was similar in magnitude to that for AcO^-. The changes in the absorption spectra upon titration with the sodium salts of AcO^-, $H_2PO_4^-$ and $HP_2O_7^{3-}$ were also analysed using SPECFIT™, however, these changes could not be fitted. In the case of the latter, this was most likely due to the steep slope of the titration curve. Attempts were also made to fit the changes in the absorption spectra upon deprotonation of the sensor with NaOH, in order to compare the species distribution plot with those obtained for the anions. Once more, these changes could not be fitted.

The nature of these species formed in the absorption titrations were further investigated by ^{1}H NMR titration. The ^{1}H NMR spectrum (400 MHz) of **54** in 4:1 DMSO-d_6:D_2O was very broad and, as expected, the N-H protons were not visible. Therefore, ^{1}H NMR titrations of **54** were carried out in DMSO-d_6, the results of which are discussed in the following section.

3.7 ^{1}H NMR Titration of 54 in DMSO-d_6

Sensor **54** was titrated with a selection of the anions investigated above. The changes in the ^{1}H NMR spectra of **54** upon titration with $H_2PO_4^-$ in DMSO-d_6 are shown in Figure 3.19 and give an indication of the general trend observed for these titrations. The

first addition of $H_2PO_4^-$ (0.2 equivalents, not shown) resulted in the broadening of all the proton resonances. The intensity of the N-H amide proton, 11.30 ppm, decreased and new broad resonance was also observed slightly further downfield at *ca.* 11.8 ppm. Both thiourea protons also broadened, before completely disappearing after two equivalents of anion, along with the new signal at 11.8 ppm. At one equivalent of $H_2PO_4^-$ a new signal

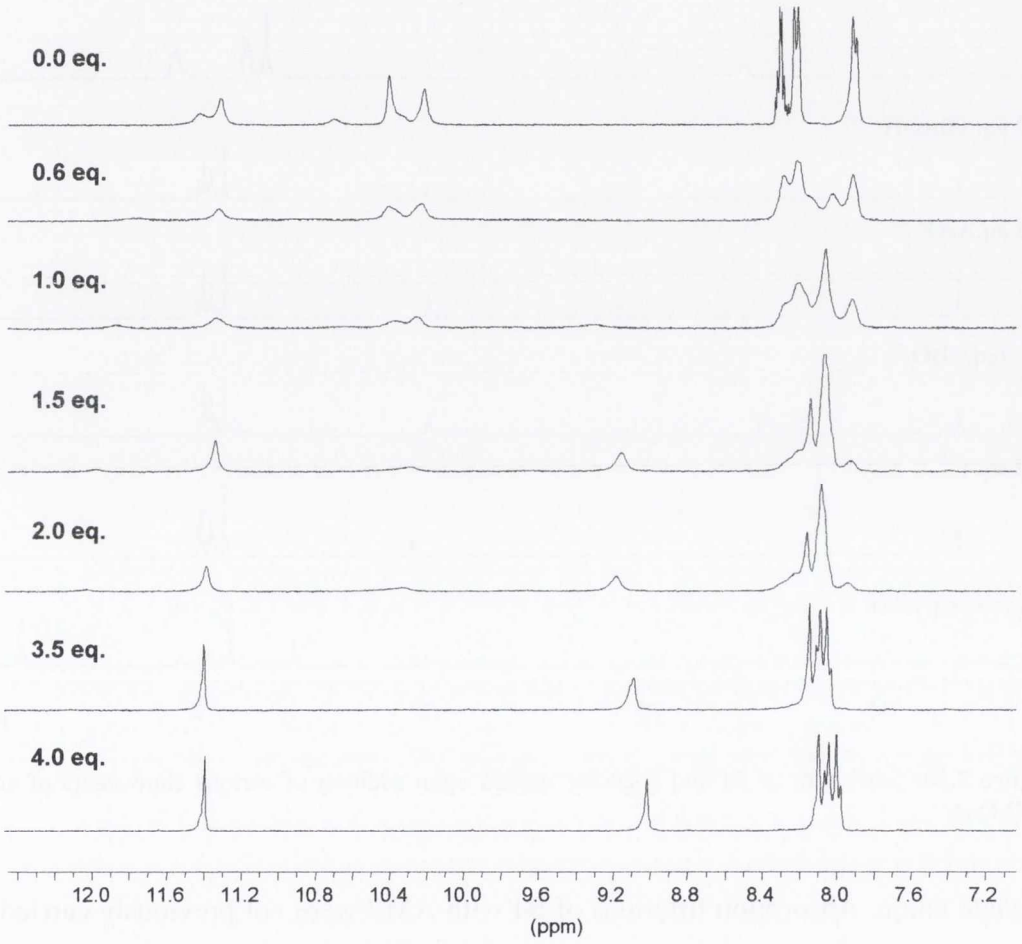


Figure 3.19: The ^{1}H NMR (400 MHz, DMSO-d_6) titration of **54** [9.5 mM] with $H_2PO_4^-$.

also appeared at *ca.* 8.9 ppm, which gradually sharpened, along with the amide N-H signal, as the titration progressed. The resulting sharp resonances at 11.36 and 8.95 ppm were identified as N-H protons by ^{15}N-^{1}H COSY NMR and both signals integrated for two protons each. In the case of the aromatic protons, the signals for the pyridine protons, as well as the *p*-nitro-phenyl protons at *ca.* 8.22 ppm, were shifted upfield, while the *p*-nitro-phenyl signal at 7.90 ppm was shifted downfield. Overall, these types of changes were indicative of deprotonation, as only four N-H protons were identified in the final spectrum. Additionally, similar deprotonation patterns with pyrrole-amidothioureas have also been reported by Gale *et al.*[136] Figure 3.20 shows that titration of **54** with AcO^-, F^-, AMP^-,

$HP_2O_7^{3-}$ and TBAOH also gave rise to similar spectra to that seen for $H_2PO_4^-$ above. Figure 3.20 also shows the number of equivalents of each anion that were required to produce the spectra above. Apart from $H_2PO_4^-$, these results are in close agreement with the number of equivalents required to reach a plateau in the absorption titrations in DMSO, shown previously in Figure 3.12. At the endpoint of the titration with AMP, the protons of **54** were more difficult to observe, due to the overlapping signals of the adenosine-based

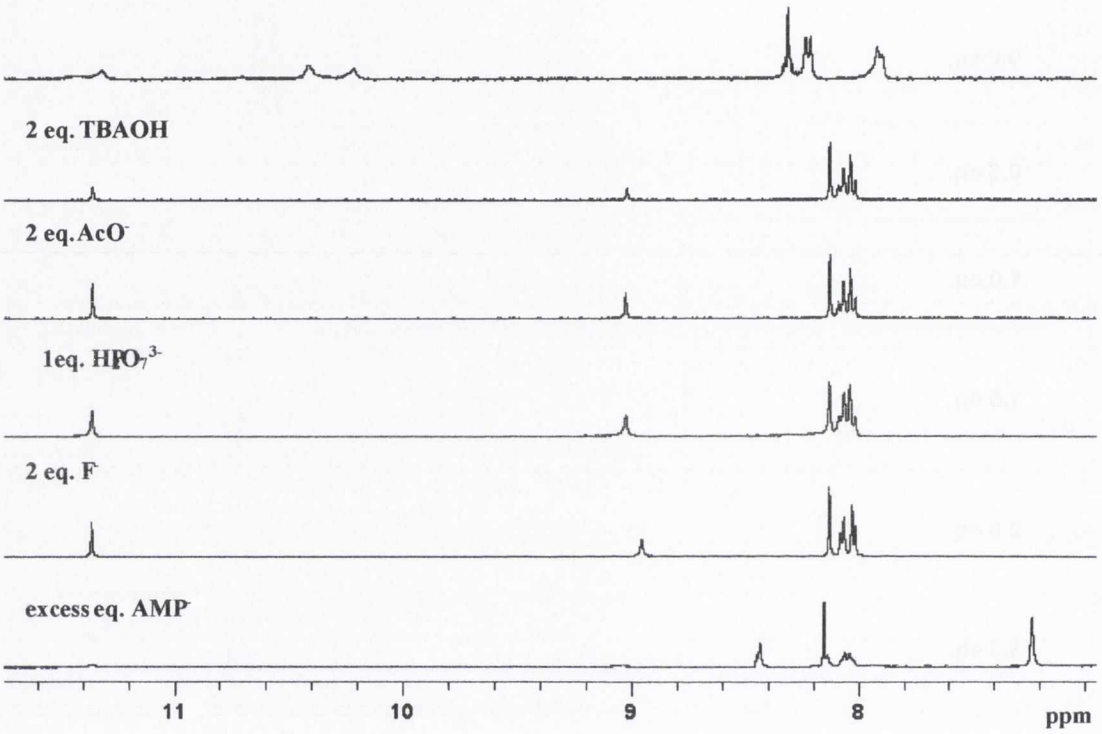


Figure 3.20: Stack plot of **54** and resulting spectra upon addition of various equivalents of anions in DMSO-d_6.

phosphate anion. Absorption titrations of **54** with AMP were not previously carried out in DMSO solution. However, in a similar manner the absorption titrations in 4:1 DMSO-H_2O, the ^1H NMR titrations showed that a higher concentration of AMP was required to reach a plateau in comparison to the smaller anions analysed (Figure 3.16). As the changes in the ^1H NMR titrations with anions clearly indicated that a deprotonation occurred, we did not attempt to fit the titration data. However, several selective ROESY NMR experiments (600 MHz, DMSO-d_6) in the presence of 2.5 equivalents of F^- were carried out, with the aim of identifying the structure of the species generated above, Figure 3.21.

Irradiation of the N-H resonance at 11.36 ppm resulted in a weak response from the pyridine moiety while irradiation of the other N-H resonance at 8.95 ppm resulted in a response from the aromatic protons of the *p*-nitro-phenyl groups. This verified that the remaining N-H resonance at 11.36 ppm, was that of the amido protons, as anticipated, and

that the other signal at 8.95 ppm was that of N-H_1 protons. It was originally thought that N-H_1 protons would be the most acidic, due to their location between the *p*-nitro-phenyl group and the thiourea. The ^{1}H NMR spectrum of **54** also showed that both thiourea protons had similar chemical shifts, which indicated that they may have similar pK_a values. Therefore, the large changes in the absorption and ^{1}H NMR titrations indicated that there is a high degree of conjugation within the sensor, whereby deprotonation of N-H_2 was

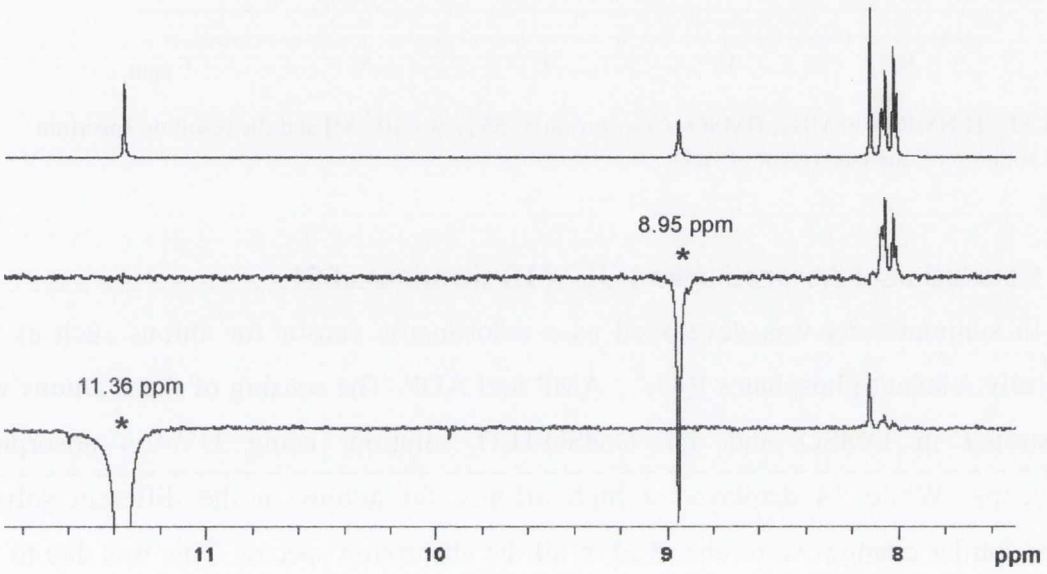


Figure 3.21: Selective ROESY NMR (600 MHz, DMSO-d_6) experiments on **54** [3.7×10^{-3} M] after the addition of 2.5 equivalents of F^-.

communicated to the *p*-nitro-phenyl chromophore. As mentioned in Chapter 1, and also in further support of the ROESY NMR experiments, Gale *et al.*[136,140] have reported the crystal structure of **25d**, a similar compound in which the corresponding N-H_2 was removed by one equivalent of F^-.

The mono-amidothiourea, **55**, was also synthesised in order to observe the ^{1}H NMR spectrum after the addition of one equivalent of anion, Figure 3.22. The benzene derivative was synthesised rather than the pyridine derivative, as it was more synthetically accessible. Indeed, the ^{1}H NMR (DMSO-d_6) spectrum of **55** after the addition of one equivalent of AcO^-, Figure 3.22, clearly shows the generation of a similar species to that observed for **54**. The broad singlets at 10.80 and 9.05 ppm both integrated for one proton each, indicating that one proton was removed from the compound by the anion.

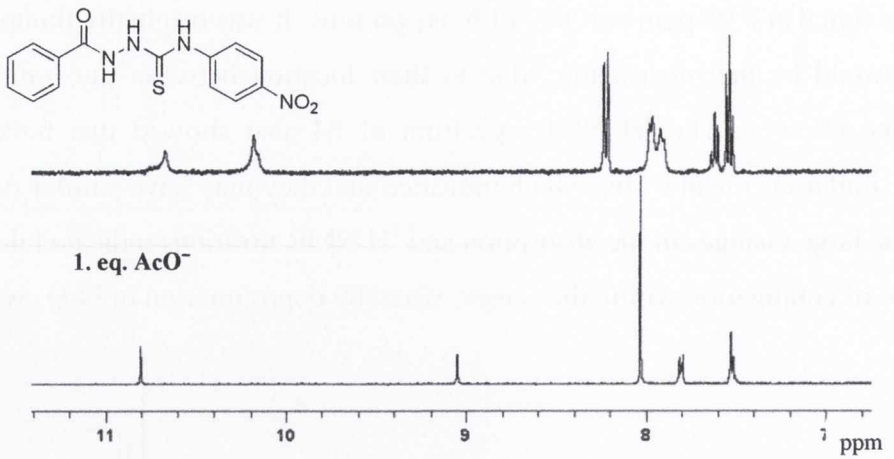


Figure 3.22: ^{1}H NMR (400 MHz, DMSO-d_6) spectrum of **55** [1.9×10^{-3} M] and the resulting spectrum upon the addition of one equivalent of AcO^-.

3.8 Conclusion of Absorption and ^{1}H NMR titrations of 54

In summary, **54** was developed as a colorimetric sensor for anions such as the biologically relevant phosphates $P_2O_7^{4-}$, AMP and ADP. The sensing of these anions was demonstrated in DMSO and 4:1 DMSO-H_2O solution, using UV-Vis absorption spectroscopy. While **54** displayed a high affinity for anions in the different solvent systems, similar changes were observed in all the absorption spectra. This was due to the fact that the main interaction between **54** and all anions was a deprotonation, as verified by titration using NaOH. Therefore, while **54** was shown to be very sensitive to the presence of anions in solution; selectivity was not achieved in terms of anion specific spectroscopic changes. However, a large affinity for the sodium salt of pyrophosphate was observed in 4:1 DMSO-H_2O, when compared to the other biological salts analysed. The nature of the anion interaction was also investigated by ^{1}H NMR titration of **54** in DMSO-d_6, which showed that indeed a deprotonation occurred in solution.

As previously mentioned, these results are in accordance with studies carried out by Gale *et al.*[136] on pyrrole-amidothioureas in DMSO-H_2O solution. However, Chapter 1 of this thesis also discussed the research by Jiang *et al.*,[79] which showed the formation of hydrogen bonded complexes between anions and sensors similar to **54** in MeCN. Due to the high affinity observed between **54** and anions, it was decided to investigate if the structure could be slightly modified in order to tilt the balance from deprotonation towards hydrogen bonding. This was carried out by varying the chromophore appended to the amidothiourea receptor of sensor **54** and the results from this investigation are discussed in Section 3.10 and 3.17.

However, before discussing the derivatives of **54**, which were synthesised and studied, the sensitivity of **54** towards its environment in solution is illustrated in the following section, as such sensitivity often led to difficulties when carrying out the anion titrations.

3.9 Sensitivity of Sensor 54

As mentioned in Section 3.3, stock solutions for the titrations of **54** with anions were prepared in Pyrex glass (Borosilicate). Sensor **54** (~10^{-5} M) was dissolved in DMSO within a Pyrex beaker and the solution was then placed in a soda-glass beaker, which resulted in a colour change from colourless to yellow. This also occurred in a 4:1 DMSO-H_2O mixture of the sensor. Figure 3.23 shows the absorption spectrum of **54** in DMSO, for which the solution was prepared in a Pyrex glass beaker, and the changes observed upon contact with a glass Pasteur pipette. As can be seen, the resulting changes in the absorption spectrum were significant, when compared to the anion induced changes discussed in the previous sections. It was concluded that an interaction most likely occurred between the sensor solutions and the soda glass based materials, such as Pasteur pipettes, beakers and sample tubes.

In addition, the DMSO solvent (Sigma Aldrich D5879, ≥ 99.5% GC) used for the titrations was also supplied in a plastic container. Spectrophotometric grade DMSO (Fluka 41641, ≥ 99.8% GC) was also purchased, which was packaged in a glass bottle. However, titration solutions prepared in this solvent resulted in a colour change of the sensor solutions, similar to that seen above. Figure 3.23 also shows a slight 'shoulder' present at

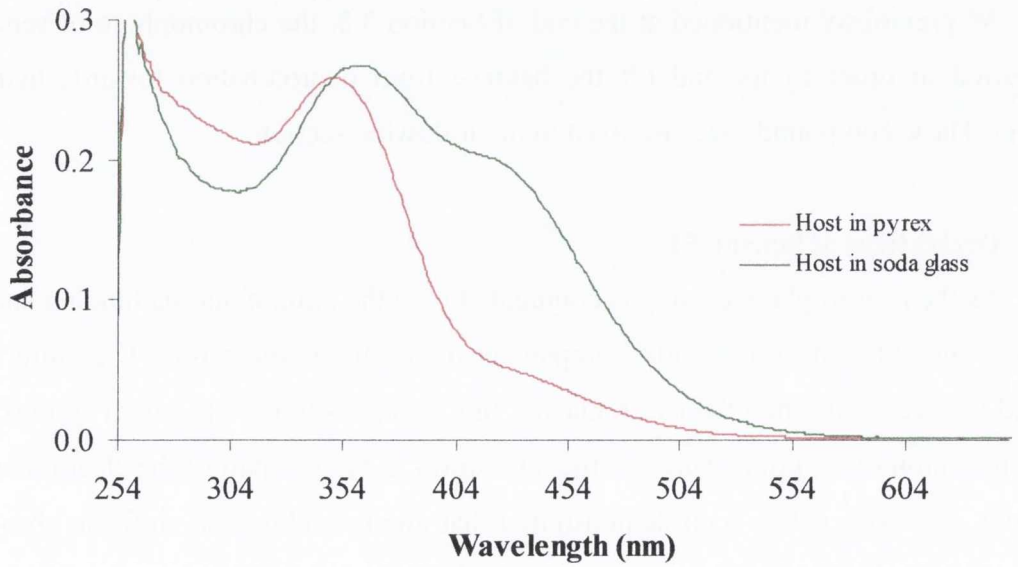


Figure 3.23: The absorption spectrum of **54** in DMSO and the resulting spectrum from pipetting with a glass pasteur pipette.

ca. 430 nm in the absorption spectrum of **54**. This was not present in the previous examples, however, the spectrum shown in Figure 3.23 was prepared from a different batch of DMSO solvent. This seems to indicate that **54** was quite sensitive to small differences existing between different batches of DMSO (≥ 99.5%+GC). As the shoulder present in the absorption spectrum overlapped with the wavelengths where the changes occurred upon addition of anions for **54**, this often led to difficulties in reproducing some of the results previously obtained. As anticipated, titration of **54** with anions, when such a shoulder was initially present, did not result in a plateau at the same number equivalents of anion as observed when no shoulder was present. Therefore, the titrations which are carried out in DMSO in the following sections are those whereby no shoulder was present in the absorption spectrum prior to titration and, hence, no such complications were encountered.

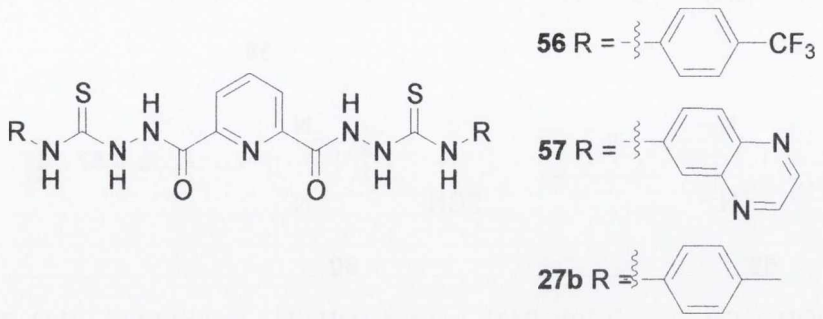
In an attempt to overcome this problem, the absorption spectrum of **54** was recorded in 1% DMSO in MeCN, as the sensor was not fully soluble in 100% MeCN. In this less competitive solvent system, no shoulder at *ca.* 430 nm was observed. Sensor **54** was titrated with AcO^- in this solution and, as anticipated, the spectroscopic changes were similar to those observed in 100% DMSO and 4:1 DMSO-H_2O solution. However, a plateau at one equivalent of AcO^- was observed (Appendix B, Figure B13). This is in contrast to the titrations in 100% DMSO, which required two equivalents of AcO^-. A 1:1 stoichiometry between **54** and AcO^- could be visualised if the new solvent system allowed cooperative hydrogen bonding of the anion to both arms of the sensor.[192] This result will be discussed further in Section 3.11, alongside titrations of similar compounds, which were also titrated in 1% DMSO in MeCN.

As previously mentioned at the end of Section 3.8, the chromophore of sensor **54** was varied in order to try and tilt the balance from deprotonation towards hydrogen bonding. These compounds are discussed in the following section.

3.10 Derivatives of Sensor 54

As the *p*-nitro phenyl group is conjugated with the amidothiourea binding site, it is therefore one of the most influential components on the anion interaction. Therefore, it was decided to investigate the effect of replacing this group with a *p*-CF_3-phenyl group, as in **56**, on the anion recognition. This substituent absorbs in the UV part of the electromagnetic spectrum, however, it has been demonstrated that anion binding can shift the absorption spectrum towards the visible region, in a similar manner to that seen for **54** above.[80] Additionally, the *p*-CF_3 phenyl group is also electron withdrawing, but contrary to the *p*-

nitro-phenyl group, it withdraws electrons *via* the inductive effect. Therefore, **56** was synthesised and its anion binding capabilities were analysed in 4:1 DMSO-H_2O.

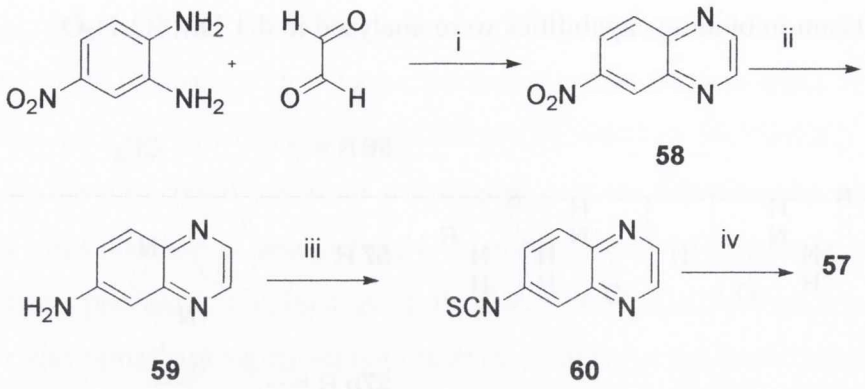


It was also decided that an alternative signalling moiety, whereby the anion interaction could be followed by both absorption and fluorescence emission spectroscopy, would be useful in defining the interaction of such amidothiourea sensors with anions.[200-204] Consequently, a 6-aminoquinoxaline fluorophore was chosen for this purpose, giving **57**. Furthermore, in order to compare the effect of an electron donating group on the acidity of the receptor, the previously described tolyl derivative, **27b**, was also synthesised to be used as a control in 4:1 DMSO-H_2O titrations.[137] Additionally, as hydrogen bonding for such compounds has been reported in MeCN,[79] the anion binding capabilities of **56** and **57** in this solvent were also investigated. The synthesis of **56**, **57** and **27b** will be discussed in the following section.

3.11 Synthesis of Sensors 56, 57 and 27b

Sensors **56** and **27b** were synthesised according to the procedure detailed in Scheme 3.1 using the commercially available *p*-CF_3-phenyl and *p*-tolyl isothiocyanates, respectively. In the case of **27b**, an excess of the isothiocyanate was used due its lower reactivity as a consequence of the electron donating methyl group. Both **56** and **27b** were isolated as white solids in 77 and 55% yields, respectively.

Sensor **57** was also synthesised in a similar manner to **54**, **56** and **27b**, however, as 6-quinoxaline isothiocyanate was not commercially available, it was synthesised in three simple steps according to literature procedures, as shown in Scheme 3.2.[205,206] Firstly, 4-nitrobenzene-1,2-diamine and glyoxal (40%) were refluxed in EtOH for three hours. The resulting precipitate was then isolated by suction filtration and recrystallised from isopropanol, which gave **58** as light brown needles in 70% yield.[206] The nitro group of **58** was then reduced using 10% Pd/C with H_2 in MeOH.[205] The crude product was then basified and extracted with ethyl acetate to give **59** as an orange solid in 73% yield.



Scheme 3.3: (i) EtOH, reflux, 3h. (ii) 10% Pd/C, 1 atm, MeOH, RT, 4h. (iii) $CSCl_2$, H_2O, RT. (iv) **51b**, MeCN, reflux, 16h.

Compound **59** was then reacted with 1.5 equivalents of thiophosgene ($CSCl_2$) in H_2O for one hour and the resulting orange precipitate was collected by suction filtration and dried in air.[205] The isothiocyanate, **60**, was not characterised and was used without further purification by addition to a suspension of **51b** in MeCN. The suspension was refluxed overnight and the resulting solid was isolated by suction filtration. Minor impurities were removed from the crude product by refluxing a suspension of **57** in EtOH overnight. The suspension was then filtered hot and the solid was dried under vacuum, which gave sensor **57** as an orange solid in 81% yield.

3.12 Characterisation of Sensors 56, 57 and 27b

The ^{1}H NMR spectra of **56**, **57** and **27b** (400 MHz, DMSO-d_6) are shown in Appendix B, Figures B14-16. Similar to that seen for **54**, the N-H protons of **56** also showed the presence of rotamers in solution. Additionally, the signals at 11.28, 10.24 and 10.07 ppm were assigned to the amide and both thiourea protons, respectively. As previously discussed for **53**, only two N-H environments were observed for **56**, in which both thiourea protons resonated at 10.28 ppm. The ^{1}H NMR spectra of **56** and **57** indicated that their N-H protons may also be quite acidic, as their chemical shifts were similar to those of **54**. In contrast to **54**, **56** and **57**, the electron donating nature of the tolyl group in **27b** was clearly illustrated in the chemical shifts of the thiourea resonances, as they were shifted upfield to 9.92 and 9.78 ppm.

The ^{13}C NMR spectra of **56**, **57** and **27b** displayed the expected number of resonances. The ES-MS analysis of **57** and **27b** showed peaks at m/z = 570.1254 and 494.1454 for the respective $[M+H]^+$ ions, while the $[M-H]^-$ ion of **56** was observed at m/z = 600.0686. The IR spectra of the novel compounds, **56** and **57**, showed medium broad vibrations at *ca.* 2900 and 3100 cm^{-1}, due to N-H stretches. Both spectra also showed

strong sharp bands at *ca.* 1700, 1550 and 1450 cm^{-1}, which were assigned to the carbonyl groups, as well as N-H bending.

The anion binding capabilities of the *p*-CF_3-phenyl derivative, **56**, were next investigated, the results of which are discussed in the following sections.

3.13 Absorption and ^1H NMR Titrations of 56 with Anions in 4:1 DMSO-H_2O Solution

The absorption spectrum of **56** in 4:1 DMSO-H_2O showed a single band with a λ_{max} at 276 nm, which was assigned to both the *p*-CF_3-phenyl and the pyridine moieties. Upon addition of AcO^-, a new transition was formed at 357 nm and a concomitant colour change from colourless to yellow was observed, Figure 3.24. While the spectroscopic changes were quite significant they were not, however, as pronounced as those observed for the *p*-nitro-phenyl derivative, **54**. Additionally, a higher number of equivalents of AcO^- (*ca.* 50 equivalents), was needed to reach a plateau in the titration, than required with **54** (*ca.* 3 equivalents). This indicated a potential reduction in the acidity of the receptor protons in this sensor *vs.* **54**. In a similar manner to **54**, the titration of **56** with AcO^- showed that no

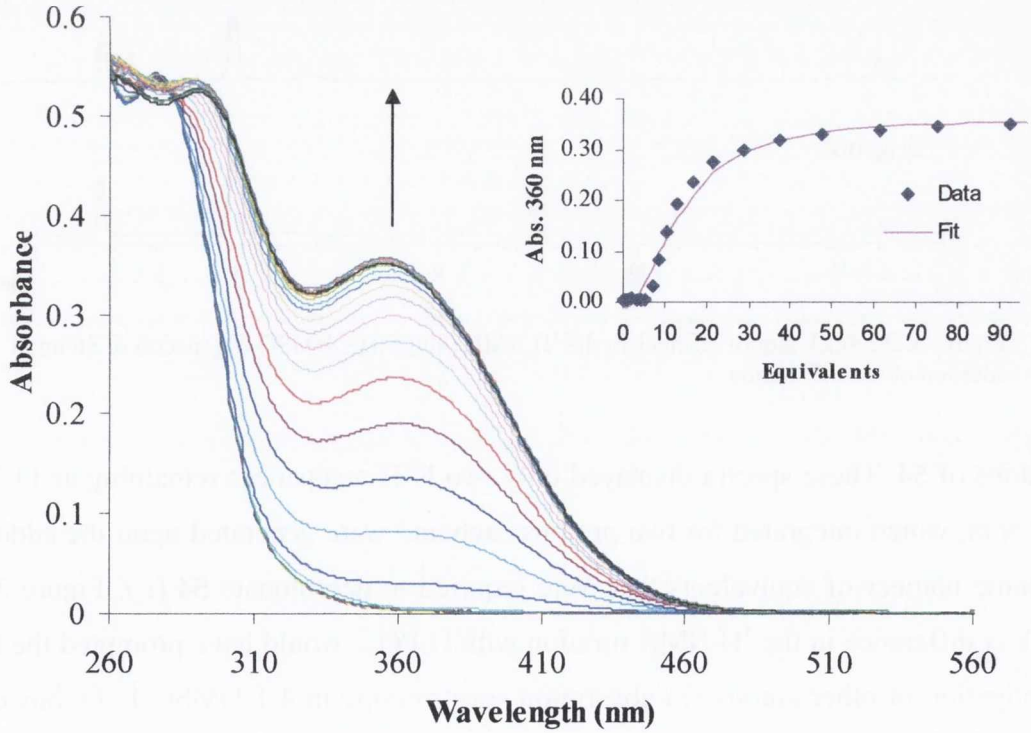


Figure 3.24: The changes in the absorption spectra of **56** [1.9×10^{-5} M] upon addition of AcO^- (0 → 325 equivalents) in 4:1 DMSO-H_2O. **Insert**: The changes at 360 nm against equivalents, with 1:2 fit. (0 → 90 equivalents)

changes occurred at low concentrations of anion, within 0→5 equivalents, and that the changes in the absorption spectrum of **56** upon titration with TBAOH mirrored those with

AcO^-, which indicated that deprotonation of **56** also occurred (Appendix B, Figure B17). Consequently, absorption titrations of **56** with other anions were not carried out. The changes observed in the absorption spectra upon titration with AcO^- could only be fitted for 1:2 Host:Guest species in solution, which gave a $\log\beta_{1:2} = 7.21$ (± 0.03). This value is significantly lower than that reported for **54** for the same stoichiometry with AcO^- ($\log\beta_{1:2} = 11.3$ (± 0.1), which indicates a low formation constant for the 1:1 species and, hence, supports the favourable formation of the doubly deprotonated (1:2) species in solution.

The ^{1}H NMR spectra of **56** (400 MHz, DMSO-d_6) after the addition of various equivalents of TBAOH, AcO^- and $H_2PO_4^-$ (see Appendix B, Figure B18) are shown in Figure 3.25 and indicate the generation of similar species to those observed in the ^{1}H NMR

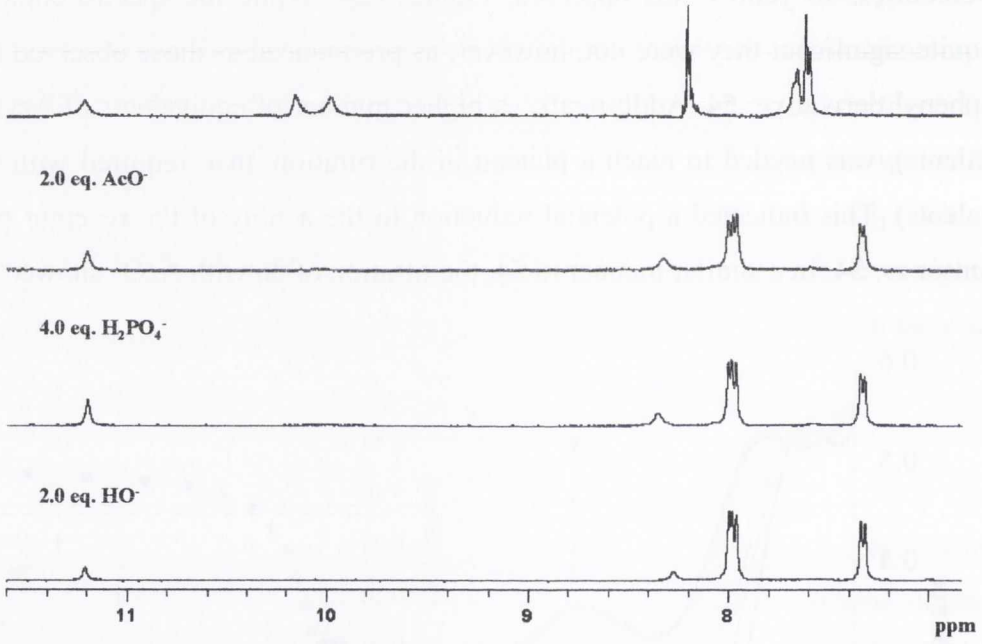


Figure 3.25: Stack plot of changes in the ^{1}H NMR (400 MHz, DMSO-d_6) spectra of **56** upon addition of various anions.

titrations of **54**. These spectra displayed only two N-H resonances remaining at 11.20 and 8.28 ppm, which integrated for two protons each and were generated upon the addition of the same number of equivalents that were required to deprotonate **54** (*c.f.* Figure 3.19 or 3.20). A difference in the ^{1}H NMR titration with $H_2PO_4^-$ would have prompted the further investigation of other anions *via* absorption spectroscopy in 4:1 DMSO-H_2O, however, it appeared that **56** was behaving in a similar manner to that previously seen for **54**.

In further support of deprotonation, the bis-TBA salt of **56** was synthesised by adding two equivalents of TBAOH·30H_2O to a suspension of **56** in MeOH. The suspended white solid gradually turned yellow and became soluble, indicating that a reaction had occurred and, hence, the formation of a soluble charged product. The solvent was then

removed, giving a yellow solid, which was analysed by ^{1}H NMR spectroscopy. Indeed, the ^{1}H NMR (400 MHz, DMSO-d_6) spectrum of this solid was identical to that observed in the ^{1}H NMR titrations above in Figure 3.25 (Appendix B, Figure B19).

Due to the reports within the literature of hydrogen bonding for such sensors in MeCN, the anion binding capabilities of **56** and **57** were next investigated in this solvent.

3.14 Absorption Titrations of 56 and 57 in 1% DMSO in MeCN (v/v)

Sensors **56-57** were found to be insoluble in MeCN. As detailed in Section 3.11, their synthesis was carried out in MeCN whereby the products precipitated out of solution. Therefore, for these experiments, **56** was first dissolved in DMSO and then diluted to the required concentration using MeCN, such that the overall volume of DMSO did not exceed 1%. Titrations with TBAOH and AcO^- were then carried out in this solvent mixture. The changes in the absorption spectra of **56** were similar to those seen above in the 4:1 DMSO-H_2O solution (Appendix B, Figure B20-21). The relative changes in the absorption spectra of **56** at 350 nm for both anions in 1% DMSO-MeCN are shown in Figure 3.26. As anticipated, compared with the titrations in 4:1 DMSO-H_2O, a lower concentration of anion was required to deprotonate the sensor in this less competitive solvent system, with

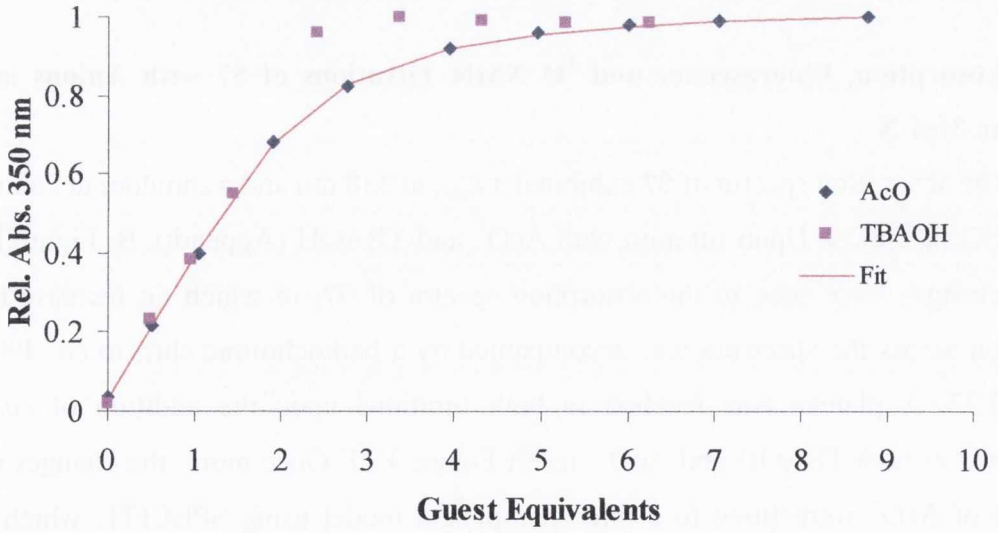


Figure 3.26: The changes in the absorption spectra of **56** (2×10^{-5} M) at 350 nm, upon titration with TBAOH and AcO^- (with 1:2 H:G fit) in 1% DMSO in MeCN.

an approximate 1:2 Host:Guest interaction clearly visible for both anions. Additionally, the changes observed in MeCN occurred from the first addition of anion, unlike that seen in the 4:1 DMSO-H_2O solution. Therefore, the absence of initial changes in the case of **54** in 4:1 DMSO-H_2O, confirm that this effect may be partly due to solvent interactions.

The changes in the absorption spectra of **56** upon titration with AcO^- were best fitted to a 1:2 stoichiometric binding model by including two coloured species, namely 1:1 and 1:2 Host:Guest species, Figure 3.26. As observed for **54** (Table 3.1), similar values with $\log K_{1:1}$ = 5.7 ± (0.2) and $\log K_{1:2}$ = 5.0 ± (0.2) were determined from this analysis. Furthermore the $\log\beta_{1:2}$ value (10.7 ± 0.2) observed in this solvent was larger than that estimated in 4:1 DMSO-H_2O, which reflected the less competitive nature of MeCN. The species distribution diagram also showed simultaneous formation of both species (Appendix B, Figure B22).

The titration of **54** in 1% DMSO in MeCN was previously discussed in Section 3.9. This titration showed a 1:1 Host:Guest stoichiometry with AcO^-, in contrast to the 1:2 stoichiometry with **56** shown in Figure 3.26. Considering that deprotonation of **56** occurred in the presence of AcO^- above, it is unlikely that 1:1 hydrogen bonding occurred in the case of **54**. Therefore, it seems more likely that the 1:1 Host:Guest stoichiometry observed was a result of external factors, the sensitivity of **54** having been already demonstrated (Section 3.9).

As discussed in Section 3.10, the anion binding capabilities of the quinoxaline based sensor, **57**, was also followed by fluorescence emission spectroscopy, the results of which are discussed in the following section.

3.15 Absorption, Fluorescence and ^{1}H NMR Titrations of 57 with Anions in 1% DMSO in MeCN

The absorption spectra of **57** exhibited a λ_{max} at 338 nm and a shoulder at 260 nm in 1% DMSO in MeCN. Upon titration with AcO^- and TBAOH (Appendix B, Figure B23), similar changes were seen in the absorption spectra of **57**, in which an increase in the absorption across the spectrum was accompanied by a bathochromic shift to *ca.* 490 nm, Figure 3.27. A plateau was reached in both titrations upon the addition of *ca.* two equivalents of both TBAOH and AcO^-, insert Figure 3.27. Once more, the changes in the presence of AcO^- were fitted to a three component model using SPECFIT, which gave high binding constants of $\log K_{1:1}$ = 6.4 ± (0.2) and $\log K_{1:2}$ = 6.4 ± (0.1), which were equal in magnitude. Again, the species distribution diagram showed simultaneous formation of both species indicating simultaneous deprotonation of both arms of the sensor (Appendix B, Figure B24).

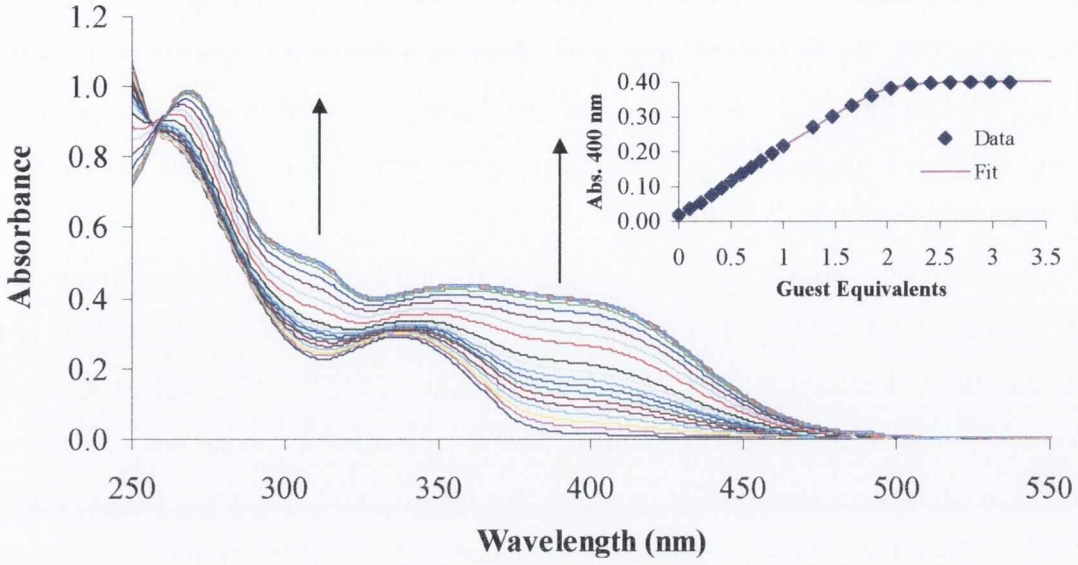


Figure 3.27: The changes in the absorption spectra of **57** in 1% DMSO in MeCN [2×10^{-5} M] upon addition of AcO^- ($0 \rightarrow 3.5$ equivalents) **Insert:** The changes at 400 nm with 1:2 fit.

The changes in the fluorescence emission were also monitored during the course of the titrations. Excitation of the absorption bands at 338 and 262 nm led to similar broad emission spectra centred at 464 and 477 nm, respectively (Appendix B, Figure B25). However, the emission at 477 nm was of a higher intensity. Figure 3.28 shows that the fluorescence emission at 464 nm was quenched by 62% upon the addition of *ca.* two equivalents of AcO^-. In a similar manner, the fluorescence emission at 477 nm was quenched by 48%. After the addition of *ca.* one equivalent of AcO^-, the emission spectrum

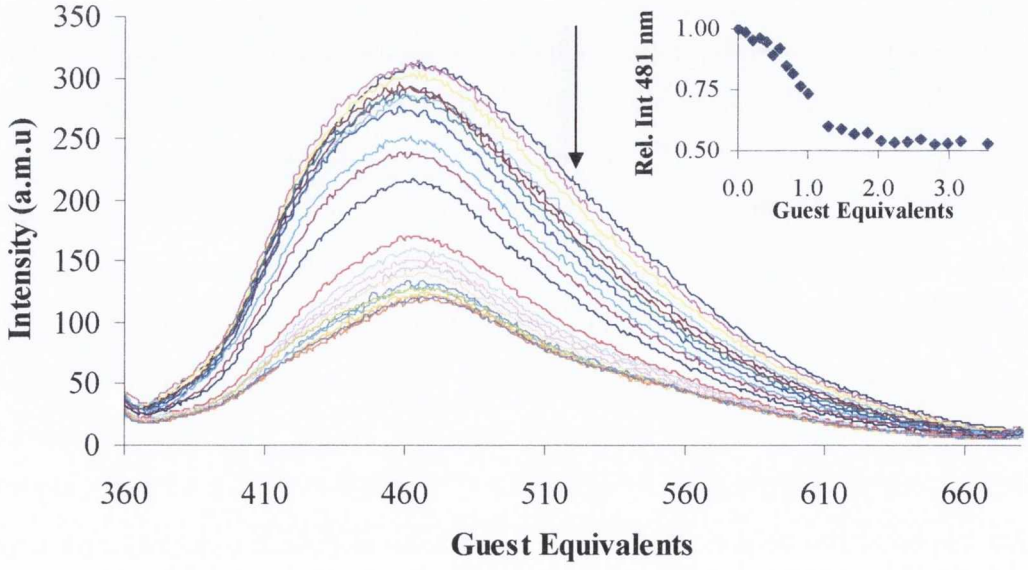


Figure 3.28: The changes in the emission spectra (λ_{ex} = 338 nm) of **57** [2×10^{-5} M] upon addition of AcO^- ($0 \rightarrow 3.5$ equivalents) in 1% DMSO in MeCN. **Insert**: The relative changes in intensity at 481 nm.

also exhibited a change in the shape of its emission band, with the appearance of a slight shoulder around 545 nm. In agreement with the absorption titrations, a plateau was reached at two equivalents of anion, however, most of the changes occurred from 0→1 equivalent. An overall bathochromic shift of *ca.* 5 nm was also observed. These changes indicated the formation of a new species in solution.

The ^{1}H NMR (400 MHz, DMSO-d_6) titrations of **57** also showed the formation of similar species in solution upon titration with TBAOH and AcO^-, whereby two N-H protons had been deprotonated (Appendix B, Figures B26-27). ^{1}H NMR (600 MHz) titrations of **57** with AcO^- in 5% DMSO-d_6 in MeCN-d_3 were also carried out and showed the formation of species very similar to those observed in pure DMSO-d_6 (Appendix B, Figure B28). Therefore, the absorption, fluorescence and ^{1}H NMR titrations combined, indicated that both **56** and **57** underwent deprotonation in the presence of AcO^-, in mainly MeCN solution.

The results discussed for **54** and **56** show that deprotonation of the electron withdrawing substituted amidothioureas occurred in the presence of basic anions in 4:1 DMSO-H_2O. In comparison to work carried out by Jiang *et al.*,[79] deprotonation of **56** and **57** in *ca.* 99% MeCN also occurred. As a result of these studies, it was decided to investigate the previously reported amidothiourea, **27b**, which was functionalised with an electron donating tolyl group.[137] These results are discussed in the following section.

3.16 Absorption and ^{1}H NMR Titrations of 27b with Anions in 4:1 DMSO-H_2O Solution

The synthesis, photophysical properties and anion binding capabilities of the tolyl derivative, **27b**, in DMSO have been previously described within the literature by Wei *et al.*[137] In order to obtain a clearer picture of the Host:Guest interactions in our derivative, sensor **27b** was titrated with AcO^- and TBAOH in 4:1 DMSO-H_2O, in an identical manner to that done for **54**, **56** and **57**. The absorption spectrum of **27b** exhibited a λ_{max} at 255 nm, which upon titration with AcO^- in 4:1 DMSO-H_2O gave rise to a new transition centred at *ca.* 350 nm, Figure 3.29. Contrary to these results, titration of **27b** with TBAOH gave rise to more pronounced changes in the absorption spectrum, Figure 3.30, where the increase in the absorption was at least three times as intense to that seen in Figure 3.29. These changes were also bi-phasic, as shown for **54**, and a hypsochromic shift was observed after the addition of *ca* 4 equivalents of OH^-. These results indicated that hydrogen bonding may have occurred upon titration of **27b** with AcO^-. Therefore, the changes in the presence of

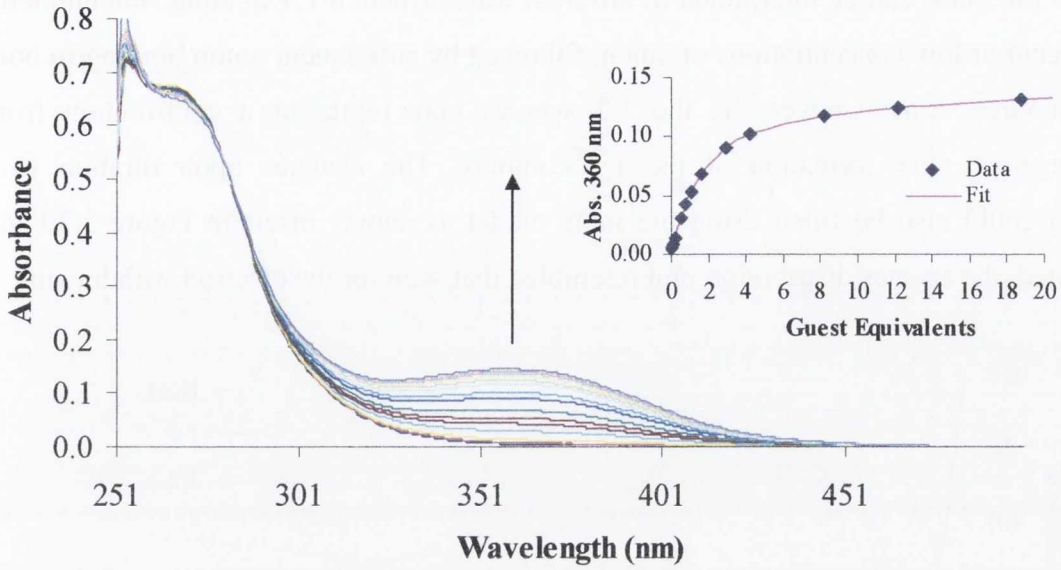


Figure 3.29: The changes in the absorption spectra of **27b** [2.5×10^{-5} M] upon addition of AcO^- (0 → 47 equivalents) in 4:1 DMSO-H_2O. **Insert:** The changes at 360 nm with 1:2 fit, shown from (0 → 19 equivalents).

AcO^- were fitted to a three component system using SPECFIT^{TM}, which is shown as an insert in Figure 3.29. The binding constants determined for this fit were $\log K_{1:1} = 4.67$ (± 0.06) and $\log K_{1:2} = 3.10$ (± 0.23). The difference in the magnitude of these binding constants is quite large compared to the values previously reported for sensors **54**, **56** and **57** in Sections 3.6 and 3.14-3.15. Additionally, the species distribution plot shows that the two species do not form simultaneously, or at least not to the same extent as was seen for the electron withdrawing derivatives **54**, **56** and **57**, Figure 3.31. The species distribution

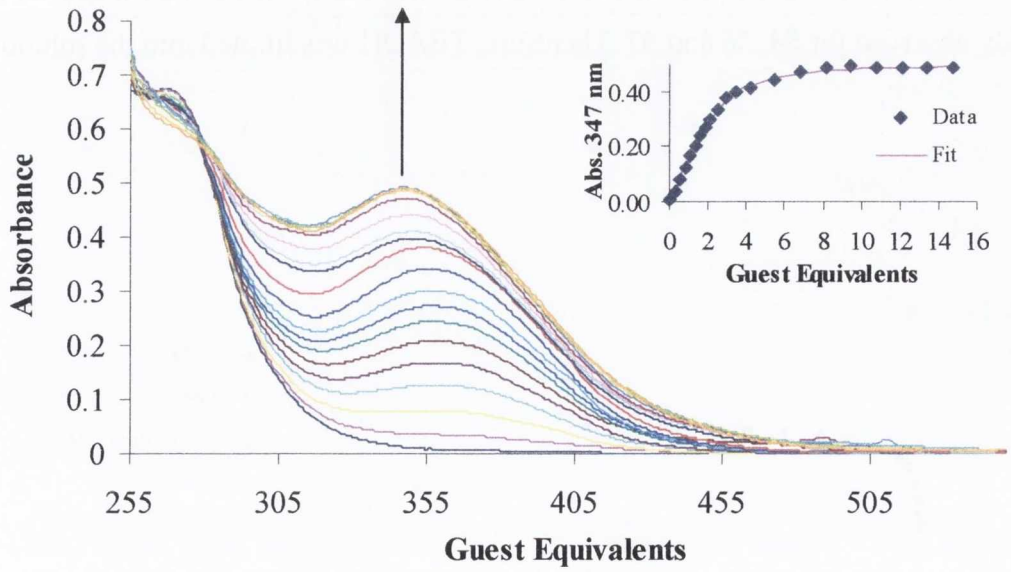


Figure 3.30: The changes in the absorption spectra of **27b** [2.5×10^{-5} M] upon addition of TBAOH (0 → 16 equivalents) in 4:1 DMSO-H_2O. **Insert**: The changes at 347 nm.

diagram for AcO^- can be interpreted in different ways, where a 1:1 binding stoichiometry could occur at low concentrations of anion, followed by subsequent anion binding to both amidothiourea arms. Conversely, the 1:2 species may represent a contribution from deprotonation, after formation of the 1:1 complex. The changes upon titration with TBAOH could also be fitted using the same model as above, insert in Figure 3.30. As anticipated, the species distribution plot resembled that seen for the electron withdrawing

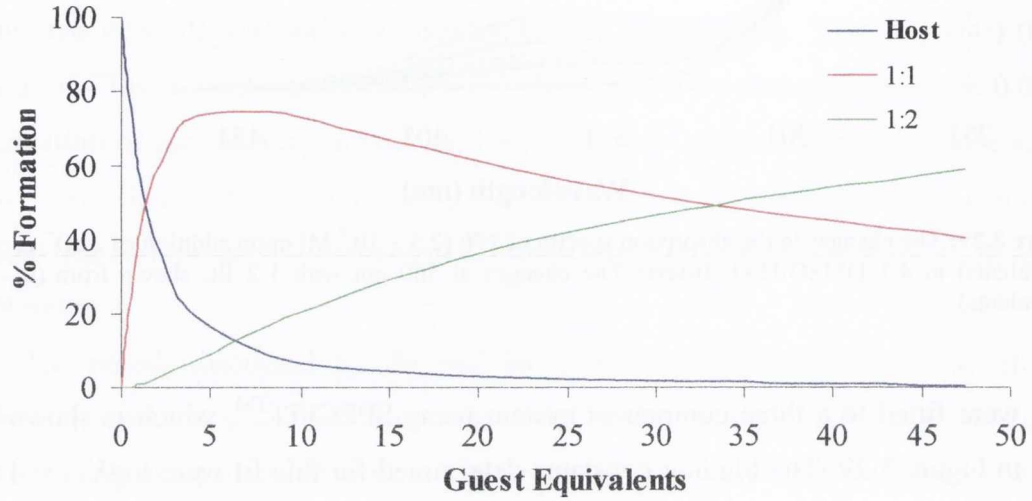


Figure 3.31: The species distribution plot of **27b** [2.5 x 10^{-5} M] upon addition of AcO^- (0 → 47 equivalents) in 4:1 DMSO-H_2O.

derivatives, **54**, **56** and **57** (Appendix B2, Figure B29). Here, both the 1:1 and 1:2 species formed simultaneously at low concentrations, from which similar binding constants of $\log K_{1:1} = 4.6$ (± 0.2) and $\log K_{1:2} = 4.8$ (± 0.1) were determined.

The plateau obtained upon titration of **27b** with AcO^- was not as linear as those previously observed for **54**, **56** and **57**. Therefore, TBAOH was titrated into the solution

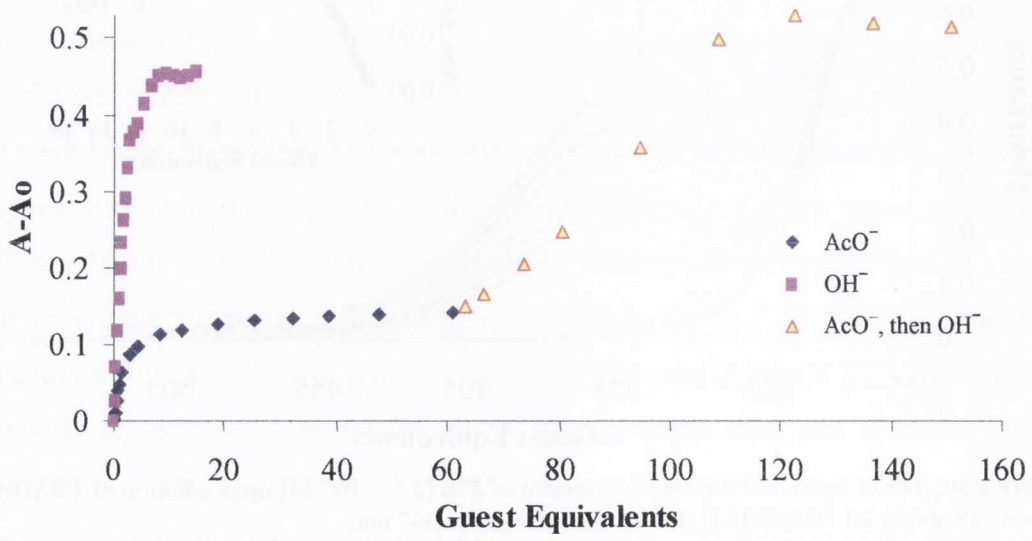


Figure 3.32: The changes in the absorption spectra of **27b** [2.5 × 10^{-5} M] upon titration with AcO^- and TBAOH in 4:1 DMSO-H_2O. A_0 = Initial absorbance.

after the addition of *ca.* 70 equivalents of AcO^-, Figure 3.32. The resulting changes in the absorption spectra of **27b** were similar in magnitude to that of the TBAOH titration, hence indicating that a partial deprotonation most likely occurred in the presence of AcO^-.

The interaction of **27b** with various anions was also investigated using ^1H NMR titration in DMSO-d_6. Figure 3.33 shows the resulting spectra after the addition of various equivalents of AcO^-, $H_2PO_4^-$ and TBAOH. The spectra in the presence of AcO^- and $H_2PO_4^-$ exhibit similarities to the spectrum resulting from deprotonation. However, minor broad resonances were also present in these spectra (*), most likely due to the fact that a larger excess of anion would be required to deprotonate the less electron withdrawing receptor moieties of **27b**, in comparison to those of **54, 56** and **57**. The ^{15}N-^1H COSY NMR experiments of **27b** after the addition of three equivalents of AcO^- clearly identified a thiourea N-H proton at 7.60 ppm (*), while the signal at 11.30 ppm was assigned to the amide N-H (Appendix B, Figure B30). Additionally, upon heating this sample to 60 °C, the minor resonances as well as the N-H protons broadened and some signals were no longer visible. Similar behaviour was observed upon heating **27b** after the addition of two equivalents of AcO^- (Appendix B, Figure B31). This indicated the presence of both a major and a minor species in solution.

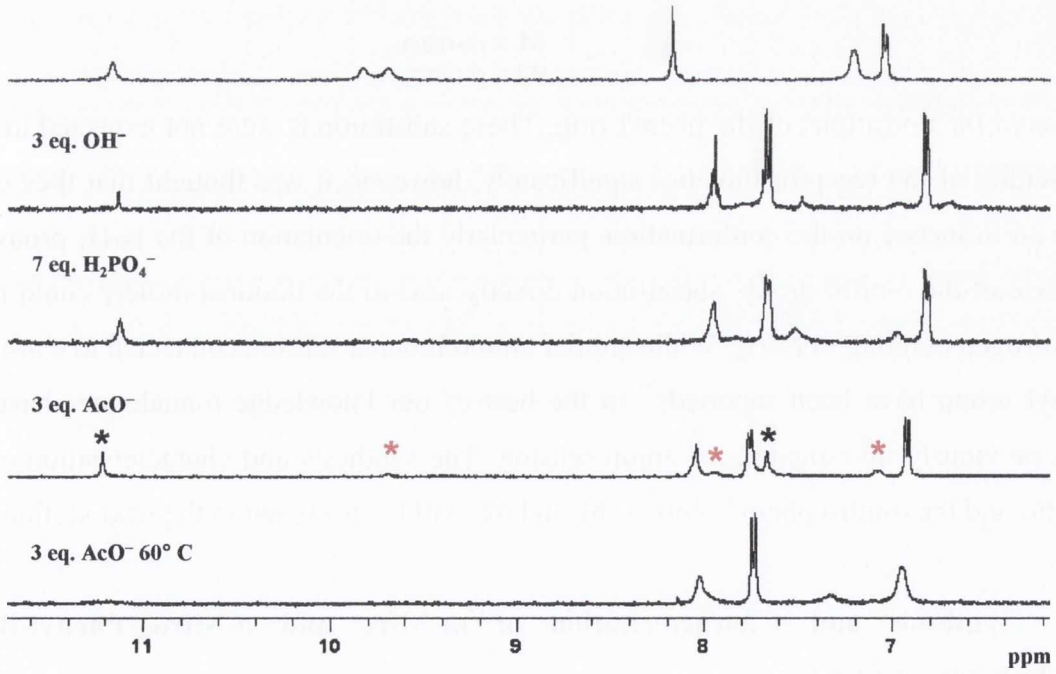


Figure 3.33: ^1H NMR (400 MHz, DMSO-d_6) spectra of **27b** [1.9×10^{-3} M] upon the addition of various equivalents of anions. * The thiourea proton identified by ^{15}N-^1H COSY NMR. *The minor species in solution.

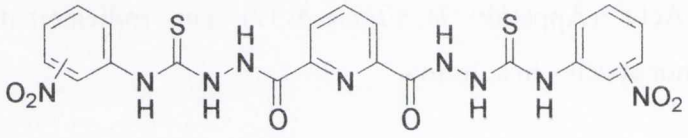
In summary, there was an obvious difference in the changes in the absorption spectra of **27b**, upon titration with TBAOH and AcO^- in 4:1 DMSO-H_2O. The ^1H NMR

spectra in the presence of both anions and OH^- showed the formation of similar species, however, minor resonances were also observed in the anion titrations suggesting different interactions in solution. Therefore, the exact nature of the interactions was difficult to establish. In contrast to this, similar interactions were observed in the absorption and ^1H NMR titrations of **54**, **56** and **57** with both anions and TBAOH, despite the different solvent conditions used for the two techniques.

In a further attempt to achieve hydrogen bonding between anions and amidothiourea sensors functionalised with electron withdrawing groups, structural isomers of the *p*-nitro-phenyl derivative, **54**, were investigated. The results from these studies are discussed in the following section.

3.17 Structural Isomers of Sensor 54: *m*-Nitro and *o*-Nitro-Phenyl-Based Sensors

As the *p*-nitro-phenyl group was easily appended to the pyridine scaffold and also gave rise to large spectroscopic changes, it was decided that structural isomers of **54** would be synthesised and investigated, whereby the nitro group was placed at the *ortho* (*o*-)



61 = *m*-nitro
62 = *o*-nitro

and *meta* (*m*-) positions of the phenyl ring. These substitutions were not expected to alter the acidity of the receptor moieties significantly, however, it was thought that they could have an influence on the conformation, particularly the orientation of the N-H_1 proton. In the case of the *o*-nitro group, substitution directly next to the thiourea moiety could result in hydrogen bonding to N-H_1. While similar amidothiourea sensors connected to a *m*-nitro-phenyl group have been reported,[79] to the best of our knowledge *o*-analogues have not been previously investigated for anion sensing. The synthesis and charactersiation of the *m*-nitro and the *o*-nitro phenyl sensors, **61** and **62**, will be discussed in the next section.

3.18 Synthesis and Characterisation of *m*-Nitro and *o*-Nitro Phenyl-Based Amidothioureas 61-62

Sensors **61** and **62** were synthesised using the same procedure described in Scheme 3.1, whereby the dihydrazide **51b** was condensed with the commercially available 3-nitro or 2-nitro-phenyl isothiocyanate in MeCN. In the case of the *ortho*- derivative, an excess of the isothiocyanate was used as to avoid unreactivity due to possible steric hindrance. The

meta- derivative, **61**, was obtained as a white solid in 78% yield while the *o*- derivative, **62,** was obtained as a bright yellow solid in 67% yield. There was no need for further purification of either sensor.

Sensors **61-62** were characterised by NMR, MS, IR and elemental analysis. Both ^{1}H NMR (DMSO-d_6) spectra of **61** and **62** showed the presence of rotamers in solution, as determined by VT ^{1}H NMR (Appendix B, Figures B32-33). As expected, the chemical shifts of the N-H protons of **61** and **62**, Figure 3.34, were similar to **54**. In the case of **61** the broad resonances of the N-H protons as well as the aromatic protons, H_2, H_4 and H_6, indicated a slow rotation around the C-N bond. In contrast, the ^{1}H NMR spectrum of **62** showed sharper resonances, possibly indicating a more rigid structure in solution. The ^{13}C NMR (DMSO-d_6) spectra of **61** and **62** showed the expected number of resonances, while HRMS (ES^+) of both sensors displayed the desired $[M+H]^+$ peaks. Additionally, the N-H region of the IR spectrum of **62** showed sharp and strong vibrations in comparison to the weaker peaks observed in the spectra of **54** and **61**. While crystals of **61** were grown in DMSO-d_6, unfortunately, these were not suitable for X-ray crystallographic analysis. With sensors **61** and **62** fully characterised, their anion binding capabilities were next investigated.

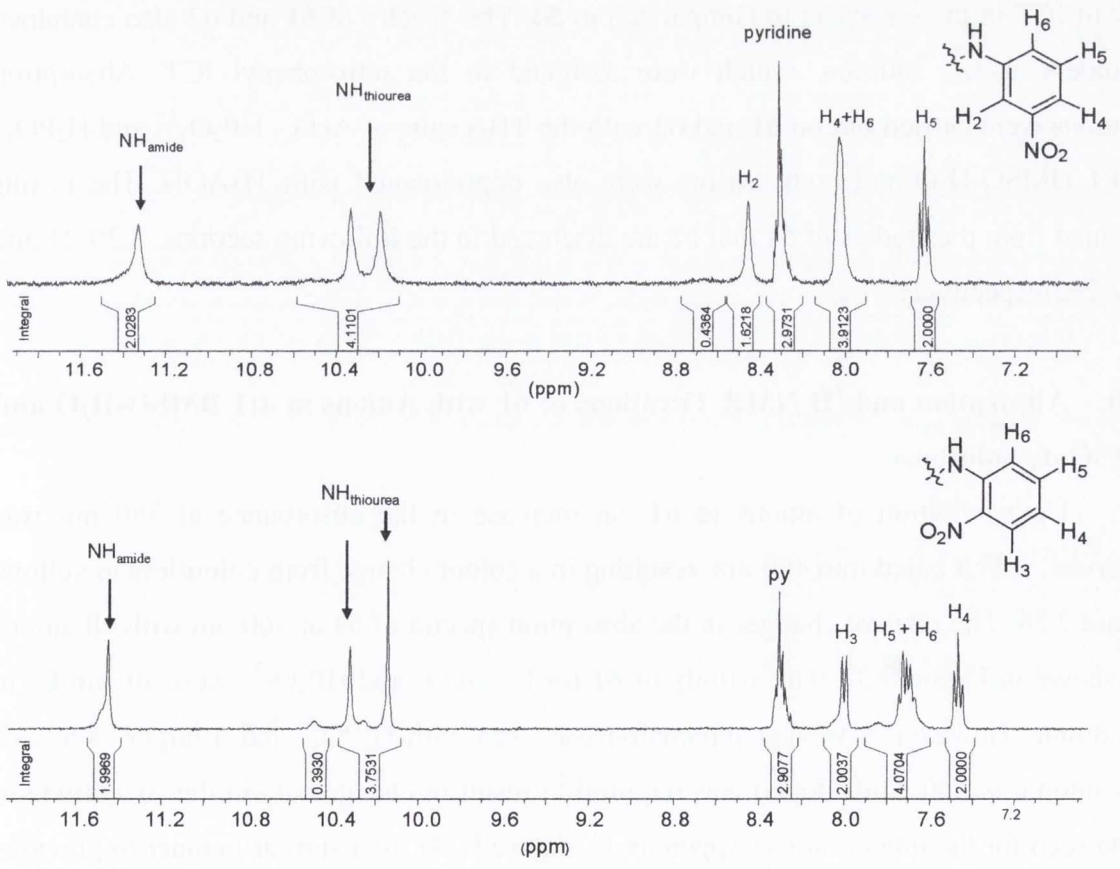


Figure 3.34: The downfield region of ^{1}H NMR (600 MHz, DMSO-d_6) spectra of **61** (top) and **62** (bottom) at RT. Structures show assignment of *p*-nitro-phenyl group protons.

3.19. Absorption Spectra of 54, 61 and 62 in 4:1 DMSO-H_2O

The absorption spectra of **61** and **62** in 4:1 DMSO-H_2O were quite different from that recorded for **54**, with λ_{max} at 272 nm (ε = 35774 M^{-1} cm^{-1}) and 255 nm (ε = 25,266 M^{-1} cm^{-1}), respectively. Both spectra are shown in Figure 3.35, which clearly demonstrates the

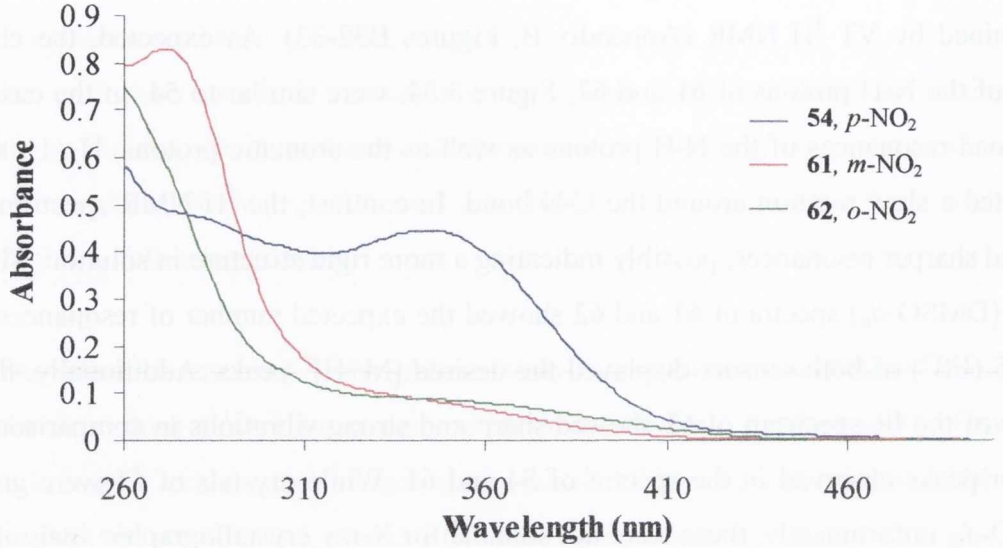


Figure 3.35: The absorption spectra of **54** [2.1 × 10^{-5} M], **61** [2.3 × 10^{-5} M] and **62** [2.4 × 10^{-5} M] in 4:1 DMSO-H_2O.

lack of ICT in these sensors in comparison to **54**. The spectra of **61** and **62** also contained shoulders at *ca.* 360 nm, which were assigned to the nitro-phenyl ICT. Absorption titrations were carried out on **61** and **62** with the TBA salts of AcO^-, $HP_2O_7^{3-}$ and $H_2PO_4^-$ in 4:1 DMSO-H_2O and both sensors were also deprotonated with TBAOH. The results obtained from the studies of **61** and **62** are discussed in the following sections, 3.20-21 and 3.22-23, respectively.

3.20 Absorption and ^1H NMR Titrations of 61 with Anions in 4:1 DMSO-H_2O and DMSO-d_6 Solutions

Upon addition of anions to **61**, an increase in the absorbance at 360 nm was observed, which tailed into 460 nm, resulting in a colour change from colourless to yellow, Figure 3.36. The relative changes in the absorption spectra of **61** at 360 nm with all anions are shown in Figure 3.37. The affinity of **61** for F^-, AcO^- and $HP_2O_7^{3-}$ were all similar in magnitude. However, a weaker interaction was seen with $H_2PO_4^-$ and a larger excess of this anion (*ca.* 150 equivalents) was required to result in changes of similar magnitude to those seen for the other anions (Appendix B, Figure B34). In a similar manner to previous titrations in this solvent system, no significant changes were observed until after the

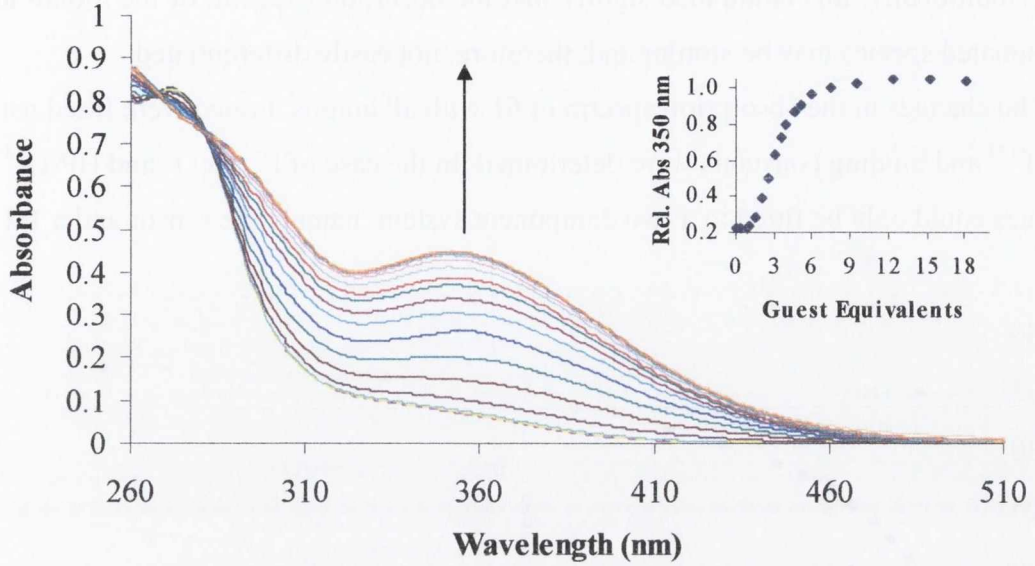


Figure 3.36: The changes in the absorption spectra of **61** (2.3×10^{-5} M] upon addition of $HP_2O_7^{3-}$ in 4:1 DMSO-H_2O (0 → 40 equivalents). **Insert:** The relative changes at 350 nm against equivalents.

addition of *ca.* one equivalent of anion. As for the previous sensors studied, **61** was also directly deprotonated with TBAOH, which showed similar changes in the absorption spectra to those seen upon titration with anions. These changes occurred from the first aliquot of TBAOH, with just over two equivalents required to reach a plateau (Appendix B, Figure B35). By plotting the changes in the absorption spectrum at a single wavelength

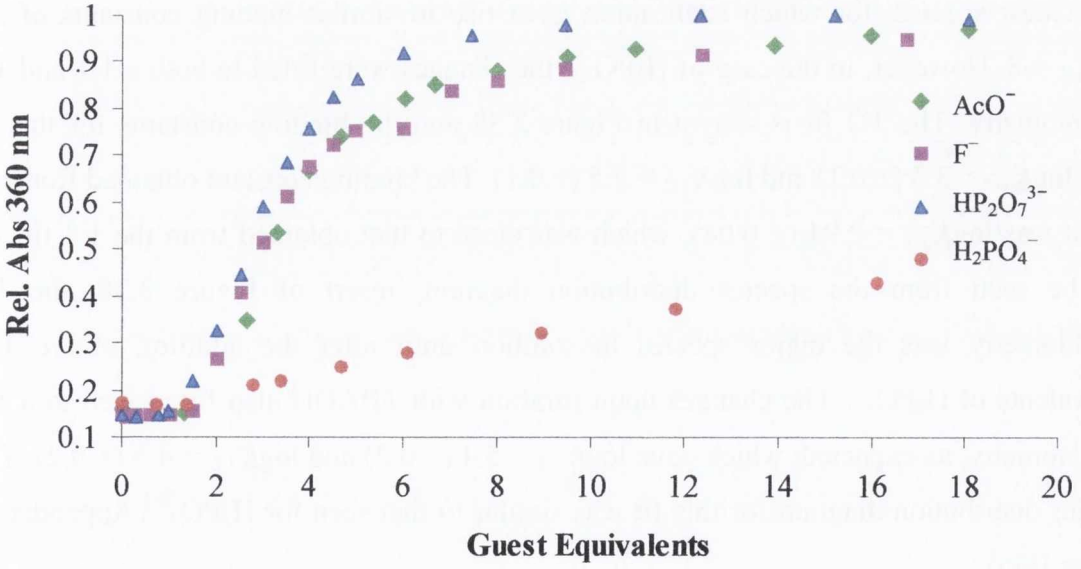


Figure 3.37: The relative changes in the absorption spectra of **61** at 360 nm upon addition of various anions in 4:1 DMSO-H_2O.

as a function of OH^-, the changes for **61** appeared mono-phasic. This was in contrast to the titration of **54** with OH^- (insert of Figure 3.13). The fact that two different processes were not easily distinguished could be due to sensor **54** having more similar pK_a's for its N-H_2

protons. Additionally, this could also signify that the absorption spectra of the mono- and di-deprotonated species may be similar and, therefore, not easily differentiated.

The changes in the absorption spectra of **61** with all anions titrated were fitted using SPECFIT™ and binding constants were determined. In the case of F^-, AcO^- and $HP_2O_7^{3-}$ the changes could only be fitted to a two component system, namely the sensor and a 1:2

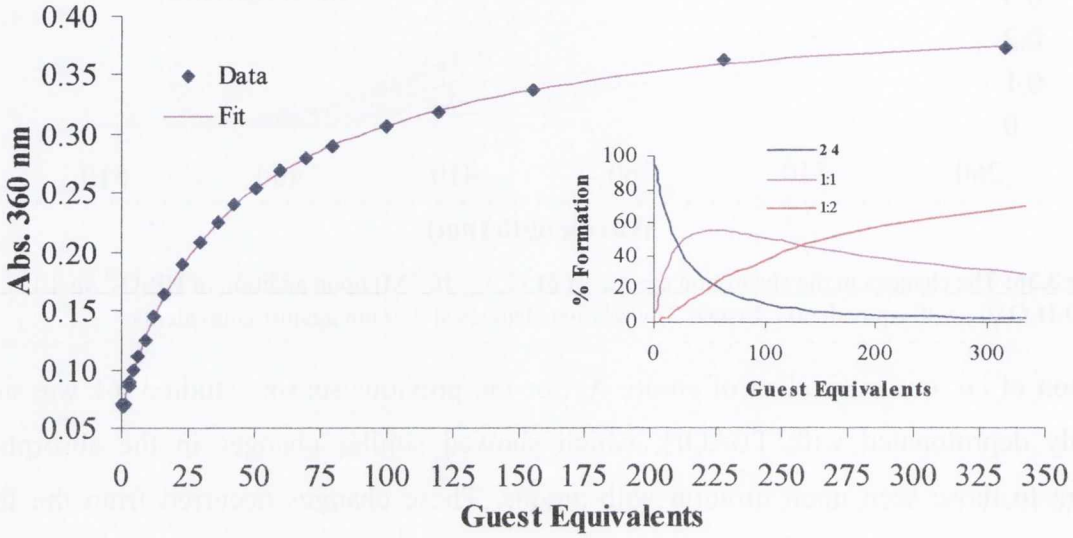


Figure 3.38: The 1:2 fit obtained from fitting the changes in the absorption spectrum of **61** upon titration with $H_2PO_4^-$ **Insert:** The corresponding species distribution diagram.

Host:Guest species, for which each anion gave rise to similar binding constants of *ca.* $\log\beta_{1:2} = 8$. However, in the case of $H_2PO_4^-$, the changes were fitted to both a 1:1 and 1:2 stoichiometry. The 1:2 fit is shown in Figure 3.38 and the binding constants for this fit were $\log K_{1:1} = 3.3$ (± 0.1) and $\log K_{1:2} = 2.5$ (± 0.1). The binding constant obtained from the 1:1 fit was $\log K_{1:1} = 2.94$ (± 0.04), which was close to that obtained from the 1:2 fit. As can be seen from the species distribution diagram, insert of Figure 3.38, the 1:1 stoichiometry was the major species in solution until after the addition of *ca.* 150 equivalents of $H_2PO_4^-$. The changes upon titration with TBAOH also fitted well to a 1:2 stoichiometry, as expected, which gave $\log K_{1:1} = 5.4$ (± 0.2) and $\log K_{1:2} = 4.5$ (± 0.2). The species distribution diagram for this fit was similar to that seen for $H_2PO_4^-$ (Appendix B, Figure B36)

In conclusion, the weaker affinity of **61** for $H_2PO_4^-$ compared to the other anions indicated that hydrogen bonding may have occurred, however, the species distribution diagram for $H_2PO_4^-$ was very similar to that obtained from fitting the OH^- titration. This suggested that the overall interaction in the presence of $H_2PO_4^-$ was due to deprotonation. Therefore, despite the structural change, it is possible that the thiourea protons of **61** may

also adopt an *anti* conformation in solution, as seen in the crystal structure of **54**. Nevertheless ^{1}H NMR titrations were carried out in order to establish the nature of the species forming in solution.

3.21 ^{1}H NMR titration of 61 in DMSO-d_6

Sensor **61** was titrated with F^-, AcO^- and $H_2PO_4^-$ as well as with TBAOH in DMSO-d_6 solution. A similar pattern of changes were observed to those seen in the ^{1}H NMR titrations of **54** (Appendix B, Figure B37). In the case of $H_2PO_4^-$, after the addition

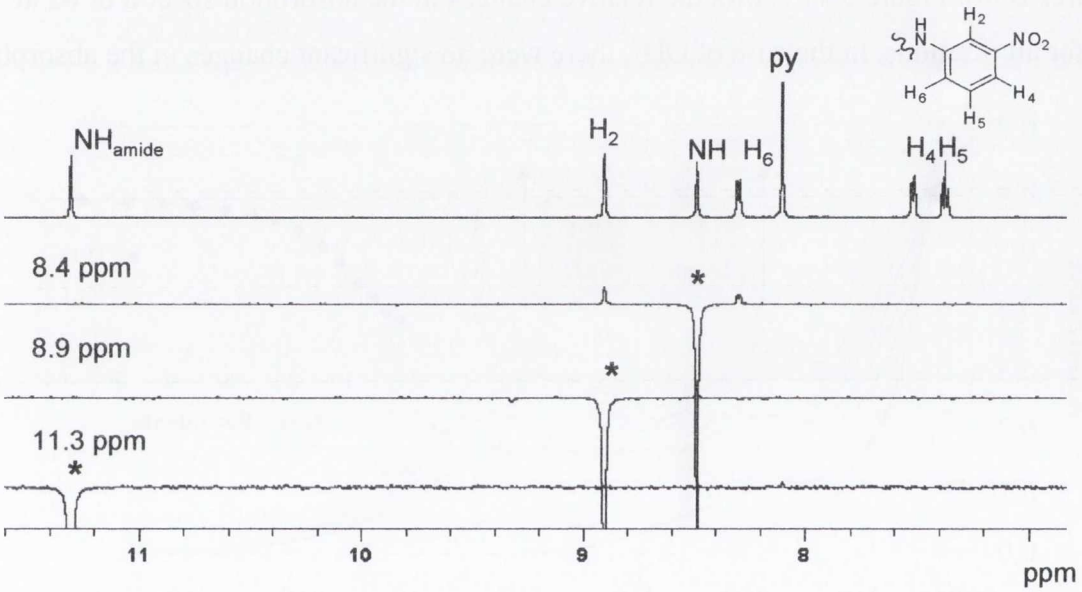


Figure 3.39: Selective ROE (600 MHz, DMSO-d_6) of **61** (1.8 mM) upon the addition of two equivalents of TBAOH.

of four equivalents of the anion, a new species was clearly evident in the ^{1}H NMR spectrum, in which only two N-H signals were present, both integrating for two protons each. The trend observed upon titration of **61** with AcO^- and F^- was the same, with identical species formed upon the addition of two equivalents of these anions. This was due to the higher basicity of AcO^- and F^- in comparison to $H_2PO_4^-$.[156,193] Indeed, as anticipated from the absorption titrations, the addition of TBAOH resulted in an identical spectrum to those seen for the anions, at two equivalents, Figure 3.39. Additionally, the ^{15}N-^{1}H COSY NMR identified the remaining N-H protons at 11.30 (amide) and 8.55 (N-H_1) ppm and selective ROESY NMR experiments, Figure 3.39, at two equivalents of TBAOH clearly indicated that the thiourea proton removed was N-H_2, as postulated for **54**. In a similar manner to above, the *o*-derivative was next investigated.

3.22 Absorption Titration of 62 with Anions in 4:1 DMSO-H_2O

Absorption titrations of **62** were carried out in 4:1 DMSO-H_2O using the TBA salts of AcO^- and $H_2PO_4^-$ and the sensor was also deprotonated using TBAOH. The absorption spectrum of **62** exhibited a transition at *ca.* 360 nm, which upon the addition of these anions, gave rise to a significant increase in the absorption centred at 350 nm, with the concomitant formation of a new transition centred at *ca.* 460 nm. This transition tailed into *ca.* 610 nm, therefore, giving rise to a colour change from yellow to pale orange, Figure 3.40. Similar changes were observed upon titration with AcO^- and OH^- (Appendix B, Figures B38). Figure 3.41 shows the relative changes in the absorption spectra of **62** at 350 nm for all titrations. In the case of OH^-, there were no significant changes in the absorption

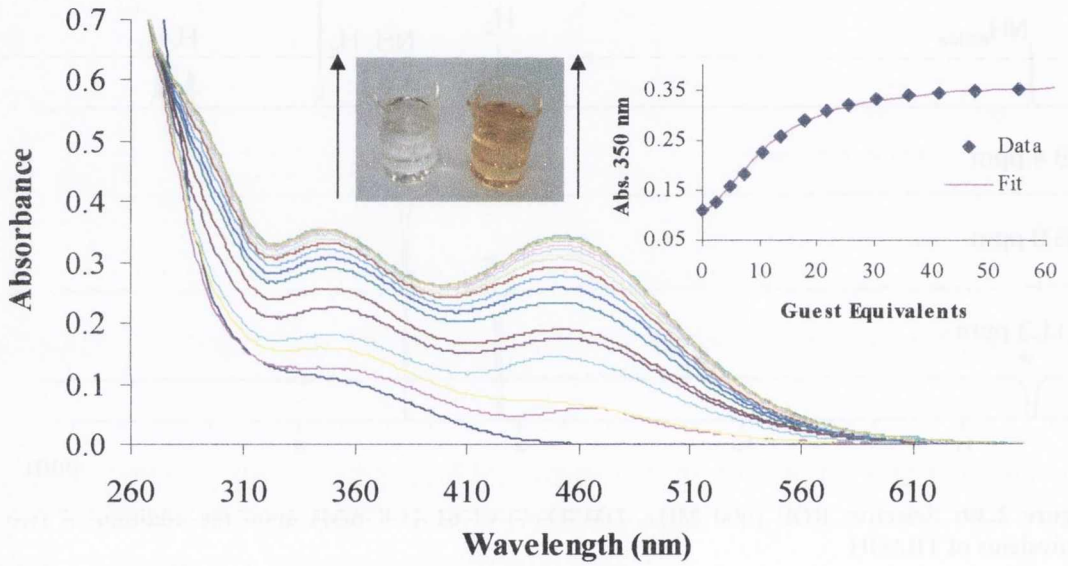


Figure 3.40: The changes in the absorption spectra of **62** [4×10^{-5} M] upon addition of $H_2PO_4^-$ in 4:1 DMSO-H_2O (0 → 155 equivalents). **Insert:** The changes at 350 nm with 1:2 fit.

spectrum until after the addition of *ca.* three equivalents of OH^- and a further four equivalents were required to deprotonate the sensor. In contrast, instantaneous changes occurred in the absorption spectrum of **62** upon titration with AcO^- and $H_2PO_4^-$. For AcO^-, the larger part of the changes were observed up to the addition of two equivalents, however, similarly to **54** and **61**, a larger excess of $H_2PO_4^-$ was required to reach a plateau (*ca.* 50 equivalents) in the absorption spectrum.

The changes in the presence of all anions were analysed using SPECFIT™. In the case of OH^-, attempts to fit the data to 1:1 or 1:2 stoichiometries did not lead to satisfying results and convergence was not reached. This was attributed, most likely, to the absence of initial changes in the absorption spectra. The changes in the absorption spectra of **62** upon titration with $H_2PO_4^-$ were best fitted to a 1:2 stoichiometry, which gave $\log K_{1:1} = 3.2$ ($\pm$ 0.1) and $\log K_{1:2} = 3.6$ ($\pm$ 0.1), insert Figure 3.40. Although not as good a fit, the titration

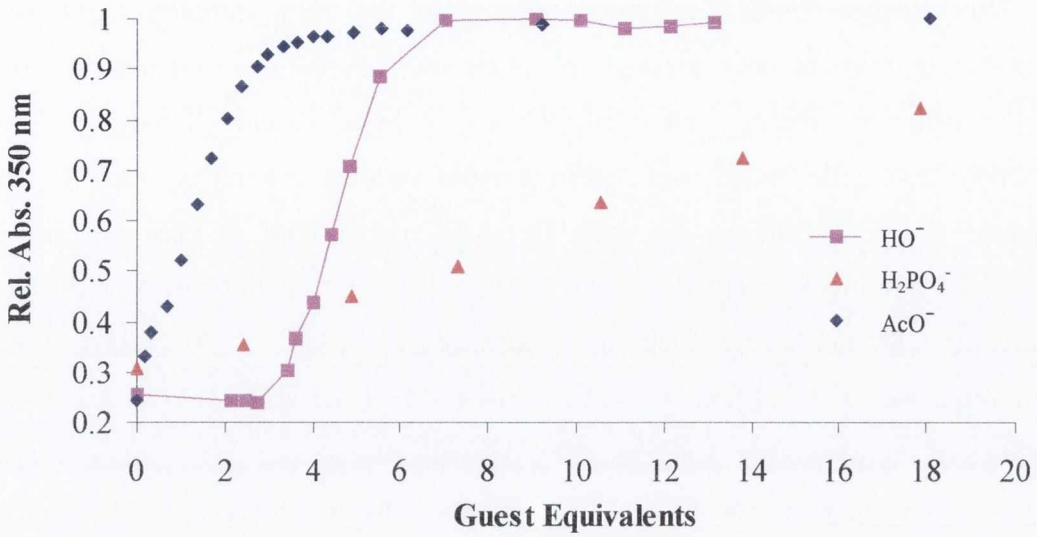


Figure 3.41: The relative changes in the absorption spectra of **62** at 360 nm upon addition of various anions in 4:1 DMSO-H_2O.

data could also be fitted to a 1:1 stoichiometry, giving a $\log K_{1:1}$ of 3.25 (± 0.06). Additionally, fitting the data to a model consisting of just **62** and a 1:2 species, gave a $\log \beta_{1:2}$ = 6.6 ((± 0.05). As can be seen, the binding constants obtained from these three different fits are comparable. Conversely, in the case of AcO^-, the changes could only be fitted to a 1:1 stoichiometry, which resulted in a larger 1:1 binding constant than seen for $H_2PO_4^-$ ($\log K_{1:1}$ = 5.10 (± 0.04)).

As a plateau at the same absorbance units was observed for both AcO^- and OH^-, it is likely that this was as a result of similar interactions *.i.e* deprotonation. The formation of a 1:1 **62**:AcO^- complex would not be expected to result in spectroscopic changes of the same magnitude to those observed upon deprotonation. Additionally, an eventual plateau at the same absorption units was also observed for $H_2PO_4^-$, indicating that the overall interaction was due to deprotonation. However, it is possible that a hydrogen bonded complex initially formed. Nevertheless, the species in solution were next investigated by ^{1}H NMR spectroscopy in DMSO-d_6, which is discussed in the following section.

3.23 ^{1}H NMR titrations of 62 with Anions in DMSO-d_6

The ^{1}H NMR titrations of **62** with the various anions (Appendix B, Figure B39) also showed the formation of a new species in solution. Only two N-H resonances at 11.30 and 9.98 ppm remained, which integrated for two protons each. The latter proton was identified by ^{15}N-^{1}H COSY NMR. Again, two equivalents of AcO^- and TBAOH were required to produce this new species, while four equivalents of $H_2PO_4^-$ were required.

3.24 Overall Conclusion

This chapter detailed an investigation into the anion binding capabilities of pyridine-based amidothiourea sensors. The anion interactions of the various sensors were studied in different solvents, such as DMSO, 4:1 DMSO-H_2O and 1% DMSO in MeCN. Their interaction with anions was analysed using various techniques, such as UV-Vis absorption, fluorescence emission and ^{1}H NMR spectroscopies. The chapter mainly focused on the anion interaction with amidothioureas functionalised with electron withdrawing chromophores, such as *p*-nitro-phenyl (**54**), *p*-CF_3-phenyl (**56**), 6-aminoquinoxaline (**57**) and finally *o*- and *m*-nitro-phenyl (**61** and **62**). The anion binding capabilities of the previously described tolyl derivative were also investigated, in order to compare its behaviour to that of the aforementioned sensors. The receptor moieties of the various sensors were also deprotonated using hydroxide, in order to compare to the interaction with anions. This was carried out, as deprotonation of structurally related sensors have been reported by Gale *et al.*[136]

Sensors **56**, **61** and **62** were found to be the most efficient colorimetric sensors as they displayed clear colour changes at low concentrations (10^{-5} M), from colourless to yellow, with the latter changing from yellow to pale orange upon addition of anions, in 4:1 DMSO-H_2O. While **54** [1×10^{-5} M] displayed a clear colour change from colourless to yellow in DMSO, the titrations at [3×10^{-5} M] in 4:1 DMSO-H_2O did not display such a change, as the solution was already pale yellow prior to titration.

The main interaction which occurred between **54**, **56**, **57** and **61-62** and the various anions in all solvent systems, was established as deprotonation. The first sensor studied, **54**, displayed similar changes in its absorption spectra and similar affinities for AcO^-, F^- and $H_2PO_4^-$ in the polar aprotic solvent, DMSO, whereby two equivalents of the aforementioned anions were required to deprotonate the sensor. Only one equivalent of $HP_2O_7^{3-}$ was required, most likely due to the additional charge on the anion, which could lead to simultaneous deprotonation of both N-H protons. These results indicated a low pK_a of the receptor moieties of **54**, as similar responses were seen for all anions, which have varying basicity.[31,193] The changes in the ^{1}H NMR (400 MHz, DMSO-d_6) spectra of **54** were also similar for each anion titrated and a new species was identified at the end of the titrations, in which only four N-H protons remained. Selective ROESY NMR experiments established that the protons removed were the thiourea N-H_2 protons.

In the more competitive organic-aqueous solvent mixture of 4:1 DMSO-H_2O, the interaction of **54** with anions varied slightly. A lower affinity was observed for $H_2PO_4^-$ compared to the other anions investigated. This was potentially due to the introduction of

water to the system, which may have affected various interactions in solution, as well as the properties of both the anion and the ligand. Titrations of **54** with the sodium salts of biologically relevant anions were also carried out and a high affinity was observed for pyrophosphate. Large changes were also observed in the absorption spectrum of **54** upon titration with AMP and ADP, however, no response was observed for ATP. In a similar manner to the titrations carried out in DMSO, the overall changes in the absorption spectra of **54** upon titration with anions in 4:1 DMSO-H_2O, were once more assigned to deprotonation. This was verified by titration with TBAOH. Similar results were also obtained from the spectroscopic investigations of **54**, **61** and **62** with anions in 4:1 DMSO-H_2O and DMSO-d_6.

Absorption titrations of **56** and **57** with AcO^- and TBAOH were also carried out in the non competitive solvent, MeCN as hydrogen bonding of structurally similar sensors has been reported in this solvent. These titrations showed that the solvation of the sensors was different as an immediate response was observed upon the addition of these aforementioned anions. However, as for the titrations of **54** in 4:1 DMSO-H_2O, similar changes were observed in the absorption titrations of **56** with AcO^- and TBAOH in 1% DMSO in MeCN. For sensor **57**, the absorption and the ^1H NMR titrations also showed that the spectroscopic changes were due to deprotonation. Furthermore, ^1H NMR titrations of **57** with AcO^- in 5% DMSO-d_6 in MeCN-d_3 showed the formation of a similar species to those observed in DMSO-d_6.

The studies on the methyl derivative, **27b**, which has previously been reported within the literature, were more inconclusive than the results obtained for the electron withdrawing derivatives. There was a clear difference in the results obtained in the absorption titrations with OH^- and AcO^- in 4:1 DMSO-H_2O. As the ^1H NMR titrations of **27b** in DMSO-d_6 showed similar spectra upon titration with AcO^- and OH^-, it is difficult to say whether the changes in the absorption spectra were due to a partial deprotonation or the formation of a hydrogen bonded complex.

In conclusion, it is possible that the N-H thiourea protons of these sensors do not orientate '*syn*' in order to allow the formation of hydrogen bonded complexes in DMSO, 4:1 DMSO-H_2O or MeCN. It may be reasonable to suggest that the intrinsic acidity of the amidothiourea moiety makes it unsuitable as an anion binding receptor. While large spectroscopic changes may be achieved when this moiety is appended to electron withdrawing chromophores or fluorophores, the results herein show that such changes are due to deprotonation. Therefore, while these sensors show high affinity for anions, they do not appear to be selective in the studied environments. However, it is envisaged that far

more competitive solvent systems, such as alcohol and water mixtures could give rise to hydrogen bonding between anions and amidothiourea sensors. We anticipated that the amidothiourea arms of such sensors could be forced to constrict together in the presence of water, possibly forming a hydrophobic pocket.[141] This approach was investigated and is discussed in the following chapter of this thesis.

Chapter 4

Glycol-Based Amidothiourea Sensors

4.0 Introduction and Objectives

The design and synthesis of several amidothiourea-based sensors were discussed in detail in Chapter 3 and their anion binding capabilities were assessed in DMSO, MeCN and 4:1 DMSO-H_2O solutions. These studies showed that deprotonation of these sensors by anions such as AcO^-, F^- and $H_2PO_4^-$, was the main interaction that occurred in solution. Hence, while the effect of varying the chromophore appended to the amidothiourea receptor was investigated in Chapter 3, this chapter focuses on the design, synthesis and anion binding capabilities of several amidothiourea sensors, which are soluble in more competitive media, such as mixtures of alcohol and water. To achieve this, the pyridine moieties of sensors **54** and **56** were functionalised with a polyoxyethylene chain. The *p*-tolyl derivative, **27b**, was not considered for the studies within this chapter as it was envisaged that a chromophore capable of participating in a strong ICT, or an electron withdrawing chromophore, would be necessary to signal a binding event in such a competitive media. It was anticipated that these polyoxyethylene-based amidothiourea sensors would engage in hydrogen bonding with various anions in mixtures of alcohol and water solution. The synthesis of these polyoxyethylene functionalised amidothiourea sensors, as well as their anion sensing abilities, will be discussed in the following sections.

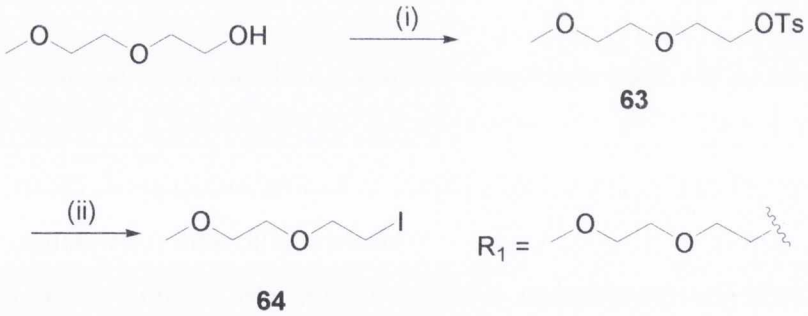
4.1 Synthesis of the Polyoxyethylene-Based Amidothiourea Sensors 70, 71, 74 and 75

As discussed in Section 1.9 of Chapter 1, various substituents can be introduced at the hydroxyl group of 4-hydroxypyridine-2,6-dicarboxylic acid (chelidamic acid).[173,207-210] Additionally, such functionalisation can also be utilised to link two pyridine moieties together,[207] allowing for the synthesis of polyoxyethylene-based tetra-amidothiourea analogues of sensors **54** and **56**. Once the polyoxyethylene chains were attached to the pyridine scaffold, similar synthetic pathways to those shown in Chapter 3 (Scheme 3.1) were followed to obtain the desired bis-amidothiourea sensors, **70** and **71** (Scheme 4.3), as well as the tetra-amidothiourea sensors, **74** and **75** (Scheme 4.4), respectively. However, the iodo functionalised polyoxyethylene chains, **64** and **66**, were initially synthesised (Schemes 4.1 and 4.2, respectively) and will firstly be discussed in the following section.

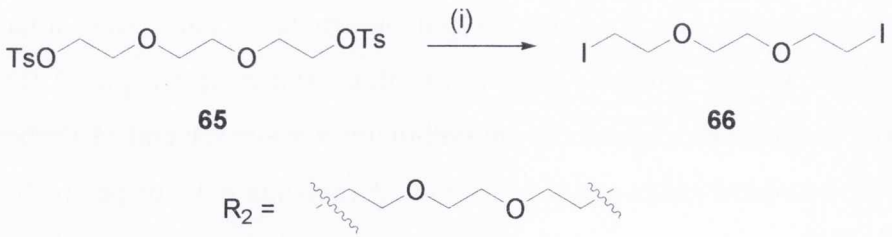
4.1.1 Synthesis of the Iodo-Polyoxyethylene Chains 64 and 66

The formation of the iodo-polyoxyethylene chain, **64**, was achieved in a few synthetic steps and high yields were obtained, Scheme 4.1.[211] Diethylene glycol monomethyl ether was first converted to the corresponding tosylate (Ts), **63**, by reacting it

with 1.5 equivalents of NaOH and 1.1 equivalents of *p*-toluenesulfonyl chloride (TsCl) in a mixture of THF and water for 16 hours at room temperature. The solvent was then removed under reduced pressure and the resulting residue was extracted with $CHCl_3$, washed with water and dried over $MgSO_4$. Removal of the solvent under reduced pressure gave a colourless oil, **63**, in 50% yield. The ^1H NMR (400 MHz, $CDCl_3$) spectrum of **63** showed the presence of the expected aromatic and methyl tosyl resonances at 7.82, 7.36 and 3.71 ppm, respectively. Compound **63** was then reacted further by refluxing it in acetone in the presence of 1.5 equivalents of NaI. This led to the formation of a precipitate that was isolated by suction filtration, washed with acetone and the filtrate was then evaporated to dryness under reduced pressure. The resulting residue was then dissolved in $CHCl_3$ and washed with water, brine, and finally dried over $MgSO_4$. Subsequent removal of the solvent under reduced pressure gave **64** as an orange oil in 77% yield. As anticipated, the ^1H NMR (400 MHz, $CDCl_3$) spectrum of **64** no longer showed the presence of the tosyl resonances and a slight shift of the neighbouring methylene peaks was also observed. Once attached to the pyridine scaffold, the polyoxyethylene chain, **64**, will be abbreviated as 'R_1' in the following synthetic schemes.



Scheme 4.1: (i) NaOH, TsCl, THF, H_2O, 16 h, RT. (ii) NaI, Acetone, reflux, 16 h.



Scheme 4.2: (i) NaI, Acetone, reflux, 16 h.

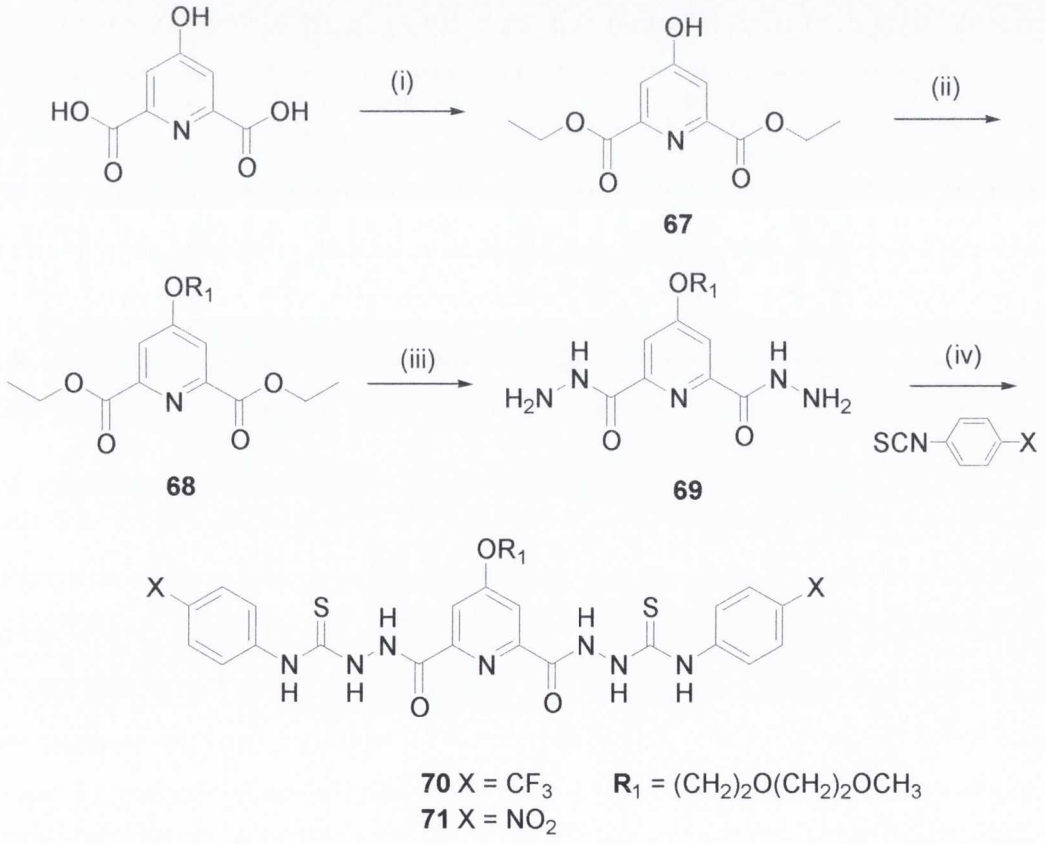
The synthesis of the polyoxyethylene chain which was utilised for the formation of the tetra-amidothiourea sensors **74** and **75** is shown in Scheme 4.2. The di-tosylate, **65**, was previously synthesised within the Gunnlaugsson group by Mr. Christophe Lincheneau, in a similar manner to that of **63**.[212] The di-iodo derivative, **66**, was then achieved in 53% yield,

using the same procedure to that of **64**. The ^{1}H NMR (400 MHz, $CDCl_3$) spectra of both **65** and **66** displayed the expected C_2 symmetry. In a similar manner to **64**, compound **66** will be abbreviated as 'R_2' in Scheme 4.4, which details the synthesis of the tetra-amidothiourea sensors.

In addition to the ^{1}H NMR analysis of **63-66**, these compounds were also characterised by ^{13}C NMR (400 MHz, $CDCl_3$) spectroscopy and the $[M+Na]^+$ ion of each compound was observed using ES-MS. The synthesis of the bis-amidothiourea sensors, **70** and **71**, using compound **64**, will be discussed in the following section.

4.1.2 Synthesis of the Bis-Amidothiourea Sensors 70 and 71

The first step in the synthesis of **70** and **71** was the esterification of chelidamic acid to the ethyl ester, **67**, Scheme 4.3.[173] This was achieved by refluxing the acid in the presence of excess H_2SO_4 in EtOH for four hours. The solvent was then removed under reduced pressure and the residue was directly basified to pH 8 using saturated $NaHCO_3$ solution. The product was then extracted into CH_2Cl_2, dried over $MgSO_4$ and the solvent



Scheme 4.3: (i) H_2SO_4, EtOH, 4 h, reflux. (ii) **64**, K_2CO_3, DMF, 80 °C, 16 h. (iii) $N_2H_4{\cdot}H_2O$, EtOH, reflux, 16 h. (iv) X = CF_3 or NO_2, MeCN, reflux, 16 h.

was then removed under reduced pressure. This initially gave **67** as a yellow oil, which upon drying turned into a white solid, giving **67** in 50% yield. The synthesis of **68** from **67** was first attempted using the Mitsunobu reaction, as reported within the literature.[173,209] However, several flash silica columns were required to separate **68** from the triphenylphosphine oxide side product of this reaction. Therefore, an alternative method was used, in which **67** was initially dissolved in DMF in the presence of one equivalent of K_2CO_3 and stirred at room temperature for 15 minutes.[207] Subsequently, the polyoxyethylene chain, **64**, was added to the suspension, which was then heated at 80 °C for 16 hours. The solvent was then removed under reduced pressure and the resulting residue was dissolved in CH_2Cl_2, washed with a solution of 1% acetic acid and water. After drying over $MgSO_4$, removal of the organic solvent under reduced pressure gave **68** as a yellow oil in 67% yield. Successful coupling of **66** to the pyridine moiety of **67** was confirmed by ^{1}H NMR (400 MHz, $CDCl_3$), which showed that the methylene protons of the polyoxyethylene chain were shifted slightly, relative to that seen in the ^{1}H NMR spectrum of **64**. Compound **68** was then refluxed in EtOH in the presence of excess hydrazine for 16 hours, which upon cooling resulted in the formation of a precipitate. This solid was isolated by suction filtration and upon drying in air gave **69** as a white solid in 51% yield. The ^{1}H NMR spectrum (400 MHz, DMSO-d_6) of **69** showed the presence of two broad N-H resonances at 10.59 and 4.61 ppm, which were assigned to the amide and amine protons, respectively. Upon refluxing **69** with two equivalents of the desired isothiocyanate in MeCN, an off-white precipitate was formed. This was isolated by suction filtration and dried in air to give the *p*-CF_3-phenyl derivative, **70**, as a white solid in 66% yield, and the corresponding *p*-NO_2 phenyl derivative, **71**, as a pale yellow solid in 98% yield. Sensors **70** and **71** were fully characterised using ^{1}H and ^{13}C NMR, IR, MS and elemental analysis, the results of which are shown in Chapter 6.

The ^{1}H NMR spectrum of **70** in DMSO-d_6 is shown in Figure 4.1 and, as anticipated, the downfield region of the spectrum is similar to that seen for the precursor, **56** (Appendix B, Figure B14). However, the eight *p*-CF_3-phenyl protons resonated at the same chemical shift as the pyridine moiety. A similar ^{1}H NMR spectrum to that seen for **54** was also observed for the *p*-NO_2-phenyl derivative **71**, however, here the aromatic and N-H protons were shifted further downfield. The ^{13}C NMR (100 MHz, DMSO-d_6) spectra of both **70** and **71** showed the expected number of resonances, while the MALDI mass spectrometry analysis identified **70**, with a *m/z* peak for the $[M+H]^+$ ion at 720.1533, whereas a peak for the $[M+Na]^+$ ion of **71**, *m/z* = 696.1240, was observed using HRMS.

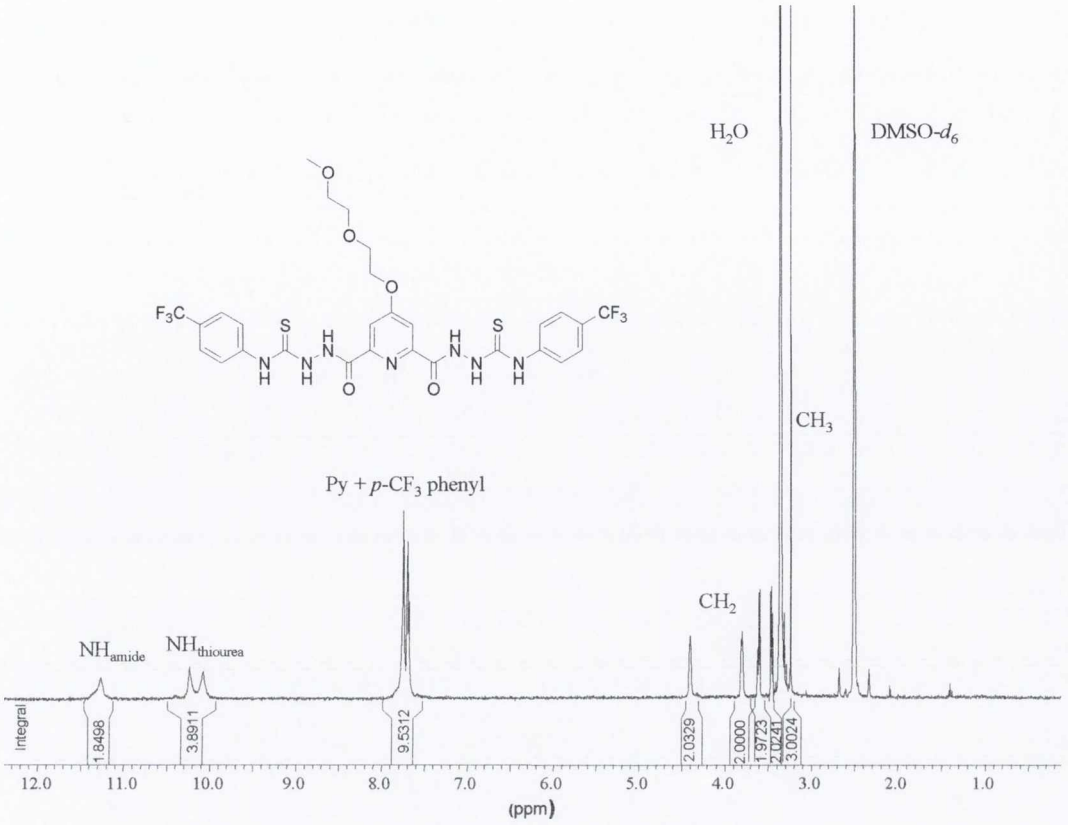
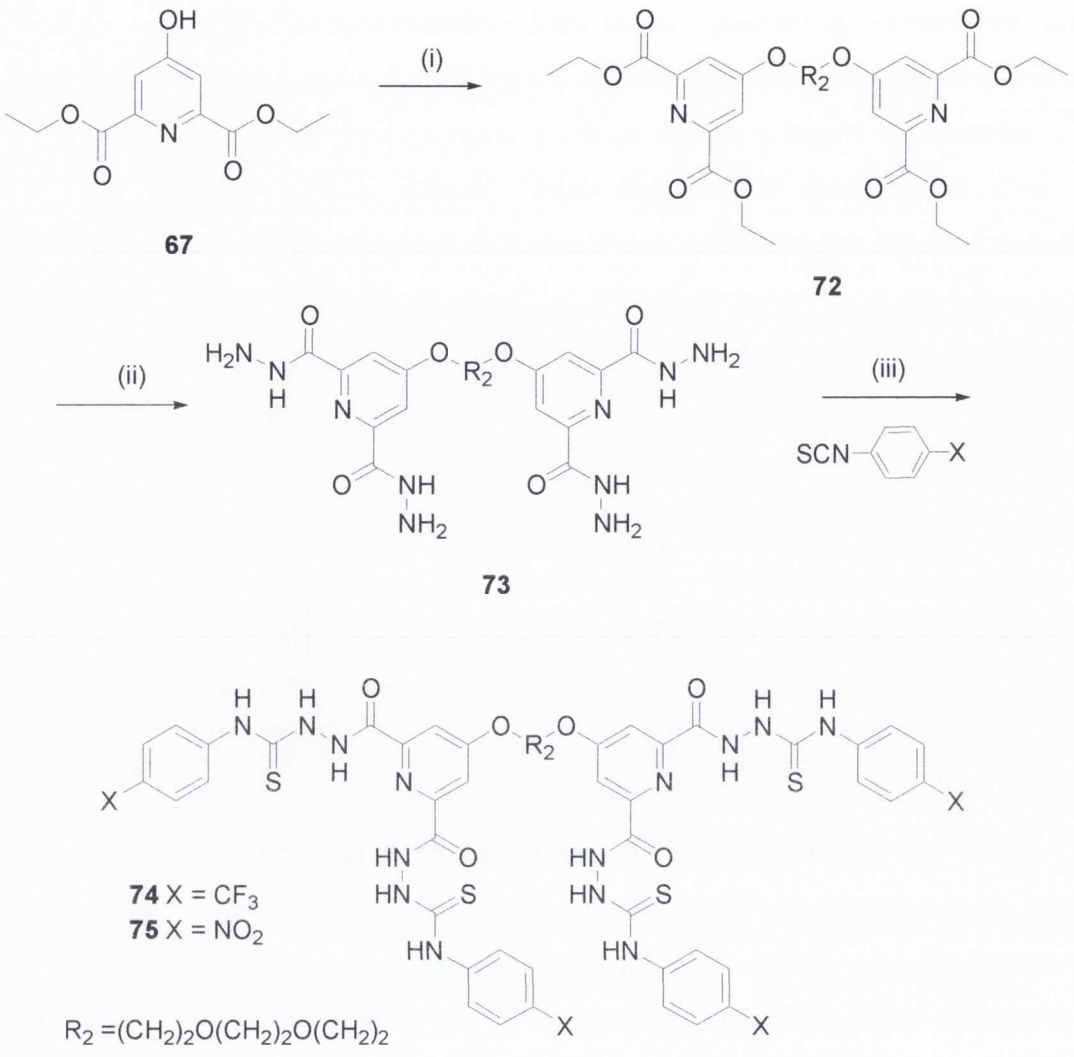


Figure 4.1: ^{1}H NMR (400 MHz, DMSO-d_6) of **70**

Colourless needle-like crystals of **70** were grown from DMSO-d_6 solution, however, these were not found to be suitable for X-ray crystallographic analysis. Several further attempts were made to grow crystals by slow evaporation of either **70** or **71** from various solvents and solvent mixtures, such as DMSO, DMSO-d_6, MeOH and EtOH. Unfortunately, none of these solvent systems resulted in high quality crystals suitable for X-ray crystallographic analysis. Having successfully formed the desired products **70** and **71**, the synthesis of the tetra-amidothiourea analogues, **74** and **75**, will be discussed in the following section.

4.1.3 Synthesis of the Tetra-Amidothiourea Sensors 74 and 75

In a similar manner to that discussed above in Section 4.1.2, the polyoxyethylene chain **66** was reacted with the diester **67**, Scheme 4.4, giving the desired bis-pyridine **72** as a yellow oil. Minor impurities, which were visible in the crude ^{1}H NMR (400 MHz, $CDCl_3$) spectrum of **72**, were removed upon recrystalisation of **72** from EtOH, giving the desired product as a white solid in 73% yield.



Scheme 4.4: (i) **66**, K_2CO_3, DMF, 80 °C, 16 h. (ii) $N_2H_4 \cdot H_2O$, EtOH, reflux, 16 h. (iii) X = CF_3 or NO_2, MeCN, reflux, 16 h.

The hydrazide **73** and the desired amidothioureas **74** and **75** were also synthesised using the same synthetic procedure described for the bis systems above. This gave the tetra-amidothioureas **74** and **75** as white and pale yellow solids in 68% and 42% yields, respectively. Sensors **74** and **75** were both characterised using conventional methods, the results of which can be found in Chapter 6. As an example, the ^{1}H NMR spectrum of **74** in DMSO-d_6 is shown in Figure 4.2 and clearly shows broad resonances for all the protons, in a similar manner to that seen for sensor **56** (Chapter 3). A similar ^{1}H NMR (400 MHz, DMSO-d_6) spectrum was observed for **75**, however, and as expected, the resonances for the aromatic and N-H protons were shifted further downfield, due to the presence of the nitro groups. Furthermore, VT ^{1}H NMR (400 MHz, DMSO-d_6) experiments of **75** showed the presence of rotamers in solutions, such as those shown for **54** in Chapter 3 (Appendix C, Figure C1). The ^{13}C NMR spectra of both sensors showed the expected number of

resonances, while HRMS showed the presence of the $[M+H]^+$ ions for both sensors, giving m/z = 1349.2284 and 1257.2189 for **74** and **75**, respectively. The IR spectra of **74** and **75** displayed broad vibrations in the N-H regions, significant of hydrogen bonding.

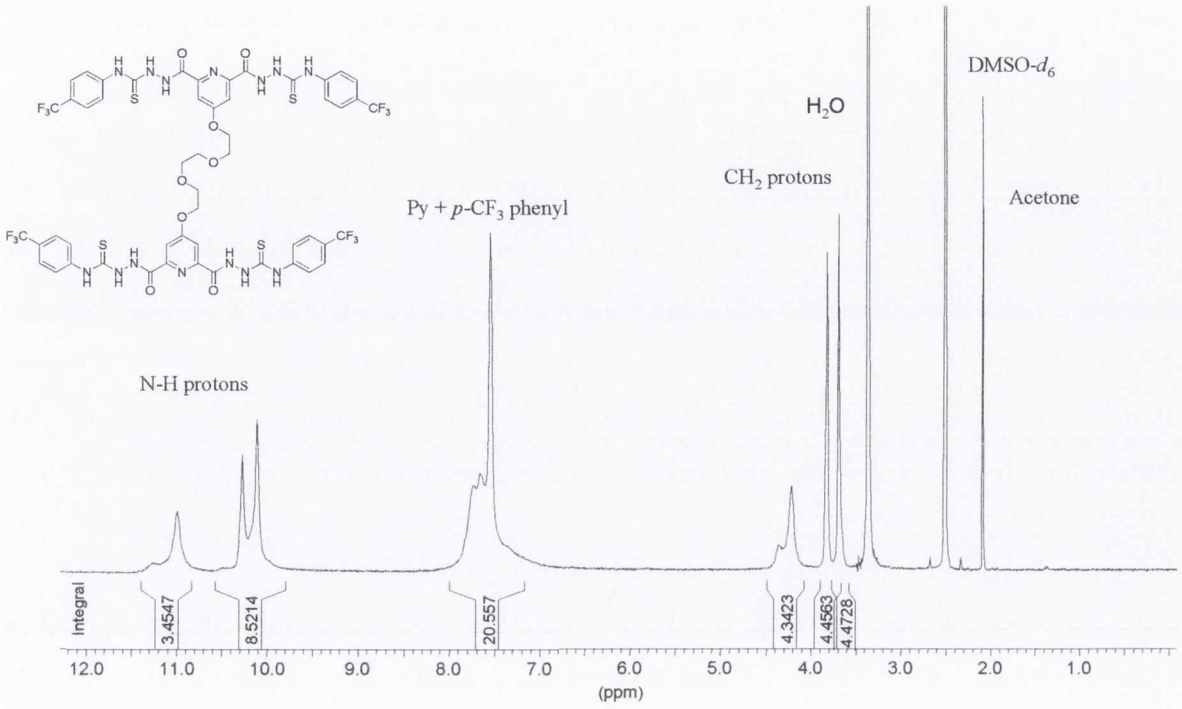


Figure 4.2: ^{1}H NMR (400 MHz, DMSO-d_6) of **74**

Pale yellow crystals of **75** were grown from a solution of EtOH and DMSO-d_6, which were found to be suitable for X-ray crystallographic analysis. The data were collected by Dr. T. McCabe and the resulting structure is shown in Figure 4.3. However, the structure produced could only be partially assigned. Despite this, it is clear from this

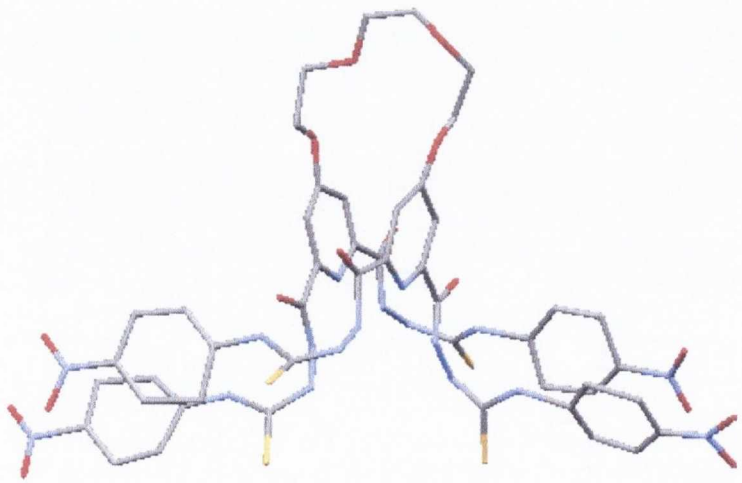


Figure 4.3: The X-ray crystal structure of **75.**

structure that the two pyridine moieties were π-π stacked with the polyoxyethylene chain forming a 'crown-ether' type loop between them, Figure 4.3. The close proximity of the four amidothiourea receptor moieties indicated that cooperative binding of anions may be possible if such a conformation was adopted in solution. Having characterised sensors **70** and **71** as well as **74** and **75**, their anion binding capabilities were next investigated using UV-Vis absorption spectroscopy, in a similar manner to that detailed in Chapter 3.

As previously mentioned in Section 4.0, these titrations were not carried out in DMSO solution, due to the occurrence of deprotonation with this solvent. Therefore, the following titrations were carried out in alcohol or mixtures of alcohol and water solution. In order to gain a further understanding of the Host:Guest interactions in solution between sensors **70** and **71** and anions, they were initially investigated in MeOH. As for previous anion titrations, stock solutions of the sensors in MeOH were prepared at *ca.* 2×10^{-3} M, which were then diluted in the titration cell to a final concentration of *ca.* 2×10^{-5} M.

4.2 Absorption Titrations of 70 and 71 with Anions in MeOH

The absorption spectrum of **70** (ε = 26,200 $M^{-1}cm^{-1}$, 275 nm) when recorded in MeOH is displayed in Figure 4.4 and shows several transitions centred at 210, 240, 275 and 350 nm. The band centred at *ca.* 275 nm was assigned to the n-π* transitions of the pyridine moiety, while the band at 240 nm was most likely due to the π-π* transitions of both the pyridine and the *p*-CF_3-phenyl moieties. The transition at lower energy, centred at 350 nm, was assigned to ICT of the *p*-CF_3-phenyl chromophore.

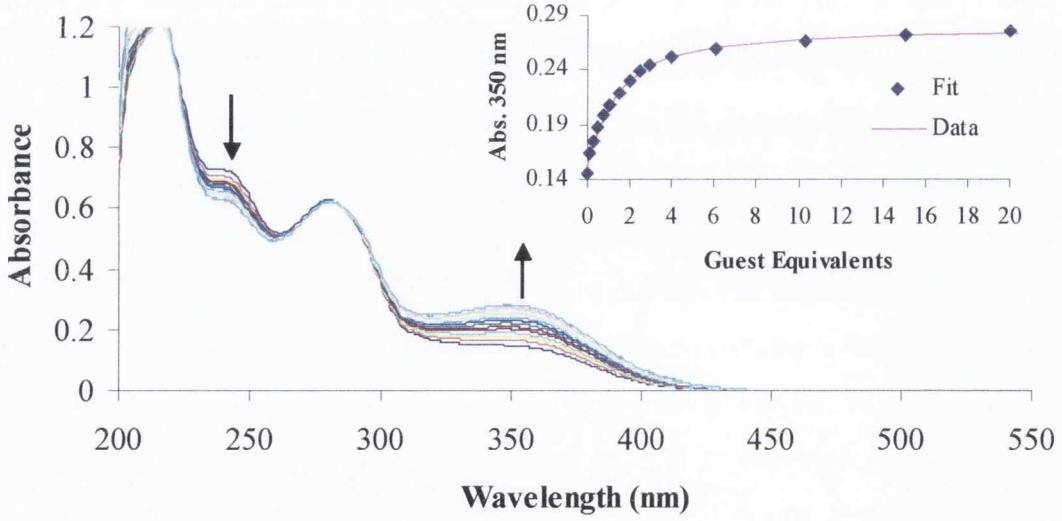


Figure 4.4: The changes in the absorption spectra of **70** [2.4×10^{-5} M] upon titration with AcO^- (0 → 50 equivalents) in MeOH. **Insert**: The changes at 350 nm with 1:2 H:G fit obtained from SPECFIT™.

The addition of AcO^- to **70** in MeOH resulted in an increase in the absorption band at *ca.* 350 nm, with a small concomitant decrease in the band centred at 240 nm, Figure 4.4. In contrast, no changes were observed in the pyridine transition (275 nm), therefore, indicating that the spectral changes were due to the interaction of AcO^- with the amidothiourea receptor moieties of **70**.

The changes in the absorption spectrum at 350 nm as a function of the equivalents added are shown as an insert in Figure 4.4. In comparison to the 1:2 Host:Guest stoichiometry observed upon titration of **56** with AcO^- in either 4:1 DMSO-H_2O or MeCN solutions (Chapter 3, Figure 3.26), these spectral changes reached a plateau after the addition of only one equivalent of AcO^-. This suggested that **70** may cooperatively bind AcO^-, as a result of the anion bridging both arms of the amidothiourea sensor through hydrogen bonding with the various N-H donors. Therefore, in order to fully understand these interactions, the changes in the absorption spectrum of **70** were analysed using SPECFIT™, for which the data was fitted best to a 1:2 Host:Guest stoichiometry, insert Figure 4.4.

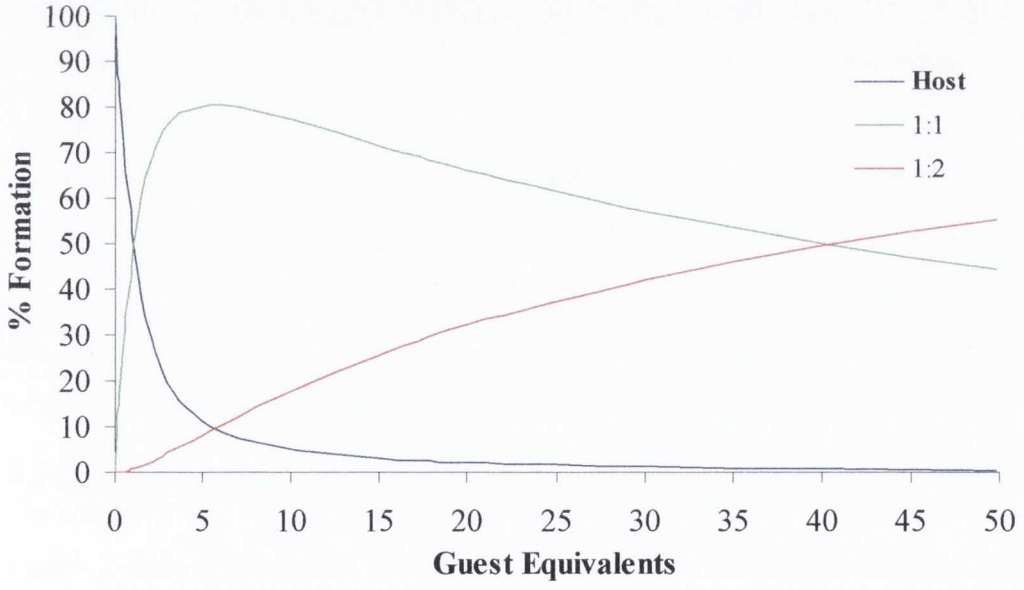


Figure 4.5: Species distribution diagram upon fitting the titration of **70** with AcO^- in MeOH to a 1:2 H:G binding model.

This fit resulted in binding constants of $\log K_{1:1} = 4.9$ (± 0.1) and $\log K_{1:2} = 3.0$ (± 0.4). As can be seen, the former value is large considering the competitive nature of the solvent environment. This data could also be fitted to a 1:1 stoichiometry ($\log K_{1:1} = 4.6$ (± 0.1)), however, a better fit was obtained by allowing for the occurrence of a second minor species in solution. Nevertheless, the inclusion of this minor species did not result in a

large change in the $\log K_{1:1}$ value compared to that of the 1:1 fit. Indeed, the species distribution diagram for the 1:2 fit shows that the 1:1 stoichiometric species was the most abundant in solution up to the addition of 40 equivalents of AcO^- and that the 1:2 species was only formed in significant quantities at high anion concentrations, Figure 4.5. Therefore, it is possible that the 1:1 species represents the formation of a hydrogen bonded complex, which is subsequently deprotonated at higher concentrations, or the 1:2 species could also indicate a second binding interaction. The binding constants and, hence, the species distribution diagram, obtained for the 1:2 stoichiometric interaction of AcO^- with **70** in MeOH were similar to those determined for **27b** in 4:1 DMSO-H_2O (Chapter 3, Figure 3.31). These results were promising as the changes in the absorption spectra of **27b** upon titration with anions, as well as the species distribution diagram, were significantly different to those observed for compounds **54**, **56** and **57**, for which the spectroscopic investigations showed unambiguously that a deprotonation occurred in 4:1 DMSO-H_2O solution (Chapter 3).

Due to the high binding affinity observed for AcO^-, sensor **70** was also titrated with the TBA salts of F^- and $H_2PO_4^-$. Similar changes to those observed with AcO^- occurred in the presence of F^-, however, these changes were smaller in magnitude (*ca.* 50%) and did not reach a plateau until after the addition of *ca.* 5 equivalents of anion (Appendix C, Figure C2). Titration of **70** with $H_2PO_4^-$ resulted in a minor increase in the ICT transition, which, after the addition of five equivalents, began to decrease in absorption with a concomitant minor bathochromic shift (Appendix C, Figure C3). Unfortunately, the changes in the presence of F^- and $H_2PO_4^-$ could not be fitted using SPECFIT™.

In summary, the largest spectral changes were observed upon titration of **70** with AcO^- in MeOH and, therefore, it can be said that **70** showed a higher affinity for this anion over F^- and $H_2PO_4^-$.

In a similar manner to the sensors studied in Chapter 3, the occurrence of deprotonation was not discounted and, therefore, sensor **70** was titrated with a stronger base in MeOH. The changes in the absorption spectrum of **70** in the presence of hydroxide, Figure 4.6, were considerably larger than those seen upon titration with AcO^-. Large changes occurred at both transitions centred at 240 and 350 nm, and a hypsochromic shift was observed for the ICT transitions after the addition of *ca.* six equivalents of base. These changes also occurred with the formation of an isobestic point at *ca.* 266 nm, indicating the presence of two species in solution.[155] The relative changes in the absorption spectra of **70** at 350 nm upon titration with OH^- and AcO^- in MeOH are shown as an insert in Figure 4.6. These changes demonstrated that in the case of OH^-, a two-step process occurred,

which indicated that deprotonation of the two amidothiourea N-H protons occurred, in a similar manner to that detailed in Chapter 3 (Section 3.4).

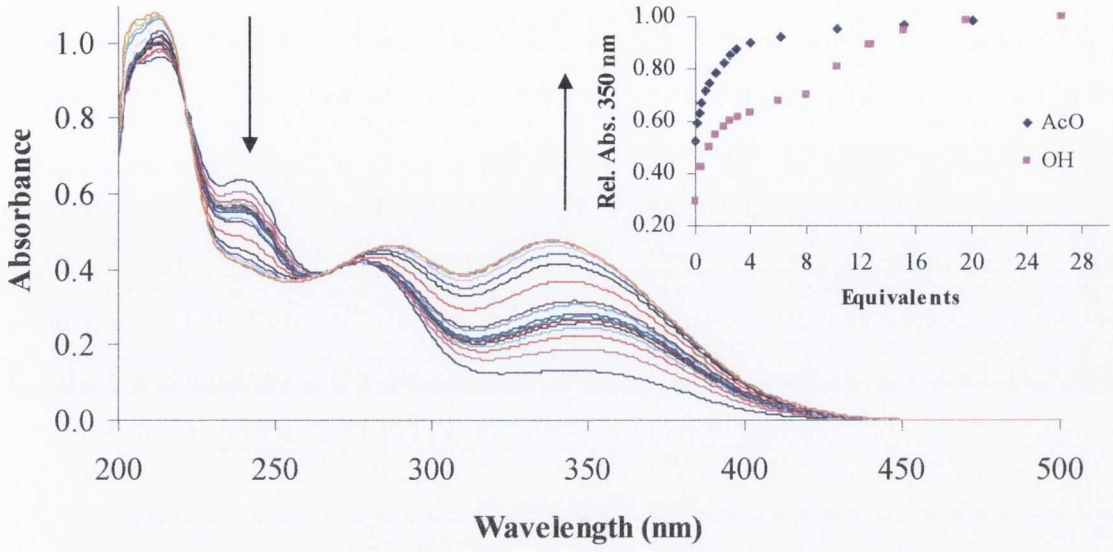


Figure 4.6: The changes in the absorption spectra of **70** upon titration with OH^-. **Insert:** The relative changes at 350 nm upon titration with AcO^- and OH^- as a function of equivalents.

Despite the fact that the changes in the presence of stronger base were larger than that seen for AcO^-, the initial spectral changes in both titrations were quite similar. Therefore, a partial deprotonation of the receptor was also considered a possibility, which could give rise to the changes observed in the absorption spectrum of **70** with AcO^-. This will be discussed further in Section 4.6, subsequent to the discussion of the spectroscopic pH titrations of **70** and **71**.

The interaction of sensor **70** with AcO^- was also investigated using ^1H NMR spectroscopy in MeOH-d_3. Although the N-H protons were not visible in this solvent, one of the signals for the *p*-CF_3-phenyl protons was shifted slightly downfield (*ca.* 0.1 ppm) to the same chemical shift of the pyridine moiety upon the addition of AcO^- (Appendix C, Figure C6). While downfield shifts are usually indicative of hydrogen bonding, the overall changes in the ^1H NMR spectra were only minor and, therefore, did not aid much in the assessment of the Host:Guest interactions.

4.2.1 Absorption Titrations of 71 with Anions in MeOH

In a similar manner to the titrations above, the nitro derivative, **71** (ε = 36,950 $M^{-1}cm^{-1}$, 339 nm), was also titrated with AcO^-, F^- and $H_2PO_4^-$ in MeOH solution. The absorption spectrum of **71** is shown in Figure 4.7 and clearly demonstrates a high energy transition centred at 210 nm as well as a broad transition centred at 339 nm, which tailed

into 500 nm. The addition of anions such as AcO^- and F^- (shown in Figure 4.7) to this solution resulted in an increase in the absorption band centred at *ca.* 400 nm and a concomitant small decrease at *ca.* 270 nm. In the case of AcO^-, the largest changes occurred up to the addition of one equivalent of AcO^-, which then reached a plateau after the addition of *ca.* two equivalents of anion, whereas in the case of F^-, *ca.* 3 equivalents were required to reach a plateau (insert Figure 4.7).

As previously discussed for sensor **70**, titration of **71** with $H_2PO_4^-$ gave rise to only minor changes in the absorption spectrum, compared to those seen for either AcO^- or F^-. These minor spectral changes were similar to those seen for **70** with $H_2PO_4^-$ (Appendix C, Figure C3), however, in the case of **71**, the changes were more pronounced, Figure 4.8. The changes at 387 nm as a function of the equivalents of $H_2PO_4^-$ added are shown in

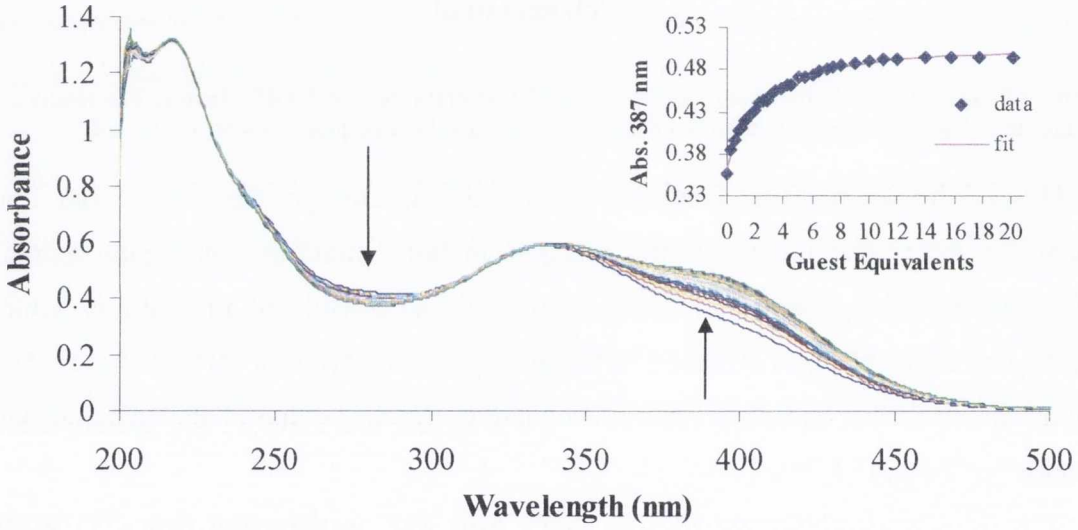


Figure 4.7: The changes in the absorption spectra of **71** [1.6×10^{-5} M] upon titration with F^- ($0 \rightarrow 20$ equivalents) in MeOH. **Insert**: The changes at 387 nm with 1:2 fit obtained from SPECFIT™.

Figure 4.8 and clearly illustrate the difference in the spectral changes compared to those seen for AcO^- and F^-. The initial changes ($0 \rightarrow 5$ equivalents) were similar to those observed for AcO^- and F^-, however, after further addition of $H_2PO_4^-$ a decrease in the absorption spectrum at 387 nm occurred ($5 \rightarrow 10$ equivalents). These changes suggested the presence of more than one species in solution over the course of the titration. The different spectral response towards the $H_2PO_4^-$ anion in comparison to the other anions tested could be due to its larger size and tetrahedral geometry, resulting in a more varied hydrogen bond network between the sensor and the anion.

The changes in the presence of AcO^- and F^- were fitted best to a 1:2 Host:Guest stoichiometry using SPECFIT™, which gave binding constants of $\log K_{1:1} = 5.60$ (± 0.07) and $\log K_{1:2} = 3.6$ (± 0.1) for AcO^- and $\log K_{1:1} = 4.8$ (± 0.1) and $\log K_{1:2} = 3.6$ (± 0.2) for F^-,

respectively. In comparison to the fitting of **70** with AcO^-, the species distribution diagrams for **71** upon titration with both AcO^- and F^- showed a larger contribution from

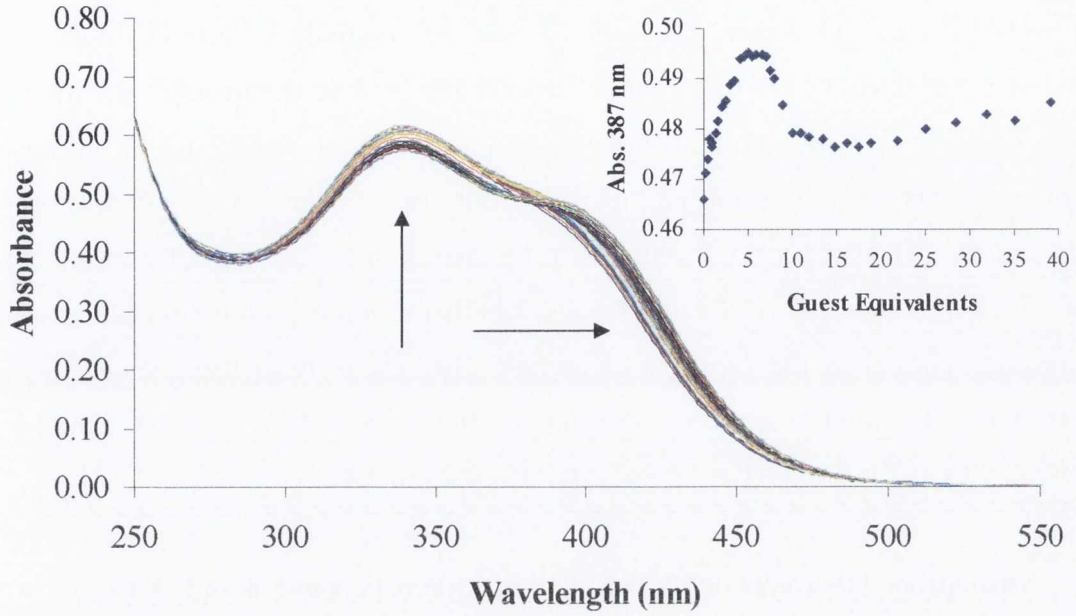


Figure 4.8: The changes in the ICT transiton of the absorption spectra of **71** [1.64×10^{-5} M] upon titration with $H_2PO_4^-$ (0 → 52 equivalents) in MeOH. **Insert**: The changes at 387 nm.

the 1:2 species (Appendix C, Figures C4 and C5). This could be due to the presence of the nitro groups, which make the N-H protons more acidic and, hence, better hydrogen bond donors, or conversely, more easy to deprotonate. Analysis of the changes in the presence of $H_2PO_4^-$ using SPECFIT™ did not result in a fit within the acceptable error limits, most likely due to the more complex nature of the changes.

4.2.2 Absorption Titrations of 70 in EtOH

Sensor **70** was also titrated with AcO^- in EtOH solution. As expected, the absorption spectrum was similar to that recorded in MeOH and the addition of AcO^- resulted in similar spectral changes to those observed above (Appendix C, Figure C7). These changes also reached a plateau after the addition of *ca.* one equivalent of AcO^-, however, in contrast to the titrations in MeOH, the overall changes in EtOH were slightly larger in magnitude, *ca.* 15%. The changes in the absorption spectrum of **70** upon titration in EtOH were also best fitted to a 1:2 Host:Guest stoichiometry, which gave a large 1:1 binding constant of $\log K_{1:1} = 6.0$ (± 0.1). The 1:2 species, $\log K_{1:2} = 2.8$ (± 0.3), was a minor species throughout the titration and did not reach more than 30% formation up to the addition of 60 equivalents of AcO^-. Overall, each fit obtained for the titrations of compounds **70** and **71** with AcO^- and F^- were best fitted to a 1:2 stoichiometry, with the 1:1 species being the major species present at low concentrations of the anion.

With these results at hand, the anion binding capabilities of **70** and **71** were next assessed in even more competitive media. As larger spectral changes were observed for **70** in EtOH solution, it was decided to carry out the subsequent titrations of **70** in a mixture of 1:1 EtOH-H_2O (v/v). However, as sensor **71** was only partially soluble in EtOH, it was titrated in 1:1 MeOH-H_2O (v/v) solution. These results will be discussed in the following section. Most importantly, as the following titrations will be carried out in an aqueous environment, this will allow the pK_a of the sensors to be determined *via* spectroscopic means and the pH of the sensor solutions to be measured before and after titration with anions. Such measurements will help to assign whether or not deprotonation contributed to the spectral changes in the presence of anions. The results from these studies will be discussed after the preliminary investigations of **70** and **71** with AcO^-, $H_2PO_4^-$ and F^- in 1:1 EtOH-H_2O and 1:1 MeOH-H_2O, respectively (Section 4.4).

4.3 Absorption Titrations of 70 and 71 with Anions in Alcohol and Water

The absorption spectrum of **70** (ε = 25,950 $M^{-1}cm^{-1}$, 280 nm) in 1:1 EtOH-H_2O solution is shown in Figure 4.9 and was similar to that observed in EtOH solution. As before, the addition of anions such as AcO^-, $H_2PO_4^-$ and F^- to this solution resulted in a modulation of the ICT transition of the sensor, which, interestingly, was most pronounced for the titration with $H_2PO_4^-$, Figure 4.9.

The insert of Figure 4.9 shows that the largest changes occurred up to the addition of one equivalent of $H_2PO_4^-$, with two equivalents necessary to reach a plateau. These changes were best fitted to a 1:1 binding stoichiometry using SPECFIT™ and in this case,

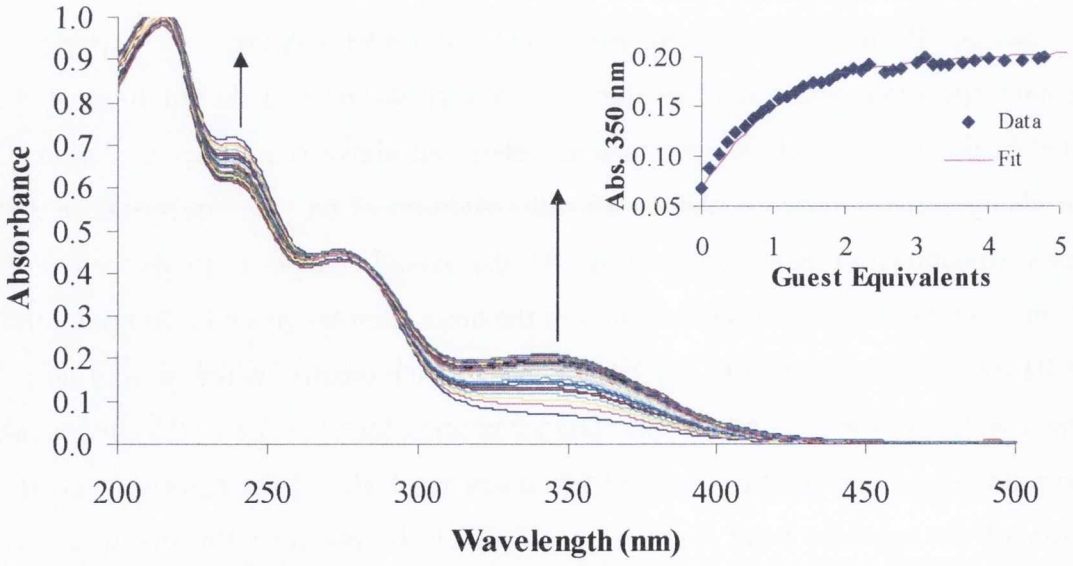


Figure 4.9: The changes in the absorption spectra of **70** [1.65×10^{-5} M] upon titration with $H_2PO_4^-$ (0 → 8.5 equivalents) in 1:1 EtOH-H_2O. **Insert**: The changes at 350 nm with 1:1 fit obtained from SPECFIT™.

no 1:2 species was observed. The binding constant determined from the fit was $\log K_{1:1}$ = 5.12 (±0.09), indicating strong binding of phosphate. Similar changes were seen in the absorption spectrum of **70** upon titration with AcO^-, with *ca.* two equivalents of anion also required to reach a plateau (Appendix C, Figures C8). In the case of F^-, a larger excess of anion was required to reach a plateau (*ca.* 15 equivalents), which was most likely due to the hydrated nature of F^- in water (Appendix C, Figure C9).

The changes in the absorption spectrum of **70** with F^- and AcO^- were analysed using SPECFIT™ and were also best fitted to a 1:1 stoichiometry. The binding constants determined for F^- and AcO^- in this solvent system were $\log K_{1:1} = 4.61$ (± 0.04) and $\log K_{1:1}$ = 4.58 (± 0.05), respectively, demonstrating that the sensor did not show any clear selectivity for these anions.

The species distribution diagram obtained from the 1:1 fit with $H_2PO_4^-$ is shown in Figure 4.10. Similarly to the species distribution diagram observed in MeOH (Figure 4.5), the 1:1 species was the major species in solution after the addition of one equivalent of $H_2PO_4^-$. If this species is due to the formation of a hydrogen bonded complex between the

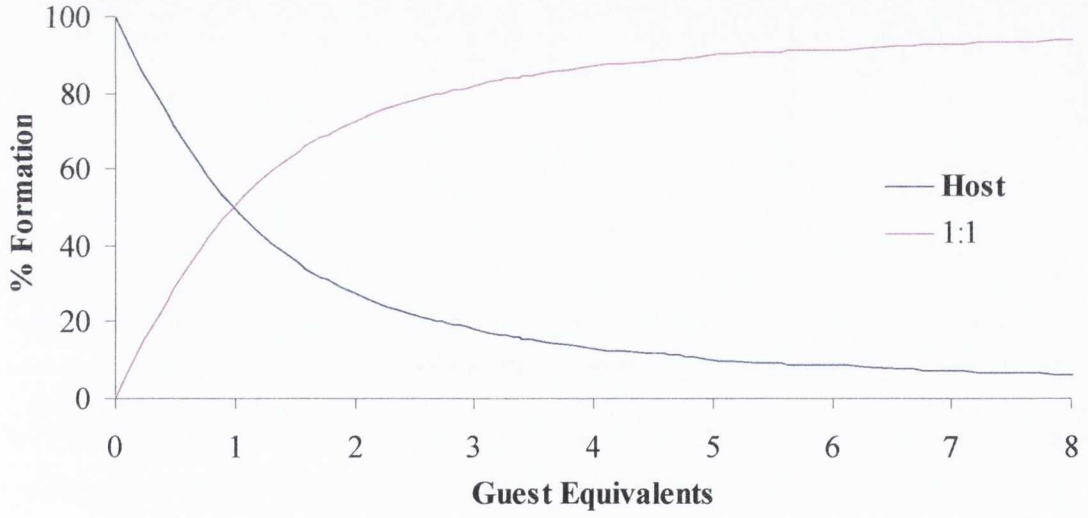


Figure 4.10: Species distribution upon fitting the titration of **70** with $H_2PO_4^-$ in 1:1 EtOH-H_2O to a 1:1 binding stoichiometry

sensor and this anion, it is possible that the 1:1 binding stoichiometry was favoured due to the formation of a hydrophobic cleft within the structure of **70**, as previously postulated by Jiang *et al.* for mono-amidothiourea sensors (Chapter 1, Section 1.8.2).[141] Despite the more competitive solvent system employed here, the binding constant determined for AcO^- was similar to that determined in MeOH. The strong interaction with $H_2PO_4^-$ may be due to the fact that the tetrahedral anion could more easily bridge both arms of the sensor, in comparison to the planar AcO^- anion or the small spherical F^- anion, which is more

hydrated in this solvent system. In contrast to these changes, no changes were seen in the absorption spectrum of **70** upon titration with Cl^-, Br^- and I^-.

The absorption spectrum of **71** in 1:1 MeOH-H_2O solution was similar to that observed in MeOH and similar spectral changes occurred upon titration with AcO^- (Figure 4.11), $H_2PO_4^-$ and F^- (Appendix C, Figures C10 and C11). The titrations with AcO^- and $H_2PO_4^-$ reached a plateau after the addition of *ca.* two equivalents, while titration with F^- required *ca.* four equivalents. Although the latter was quite different to that reported for **70** with F^-, there is an error associated when titrating F^-, as was addressed in Chapter 2. The data from these titrations was also analysed using SPECFIT™ and in all cases the titrations were best fitted to a 1:1 stoichiometry. This gave large binding constants of $\log K_{1:1} = 5.65$ (± 0.06), 5.46 (± 0.07) and 5.17 (± 0.06) for AcO^-, $H_2PO_4^-$ and F^-, respectively, demonstrating no strong preference for one specific anion, in this competitive mixed solvent system.

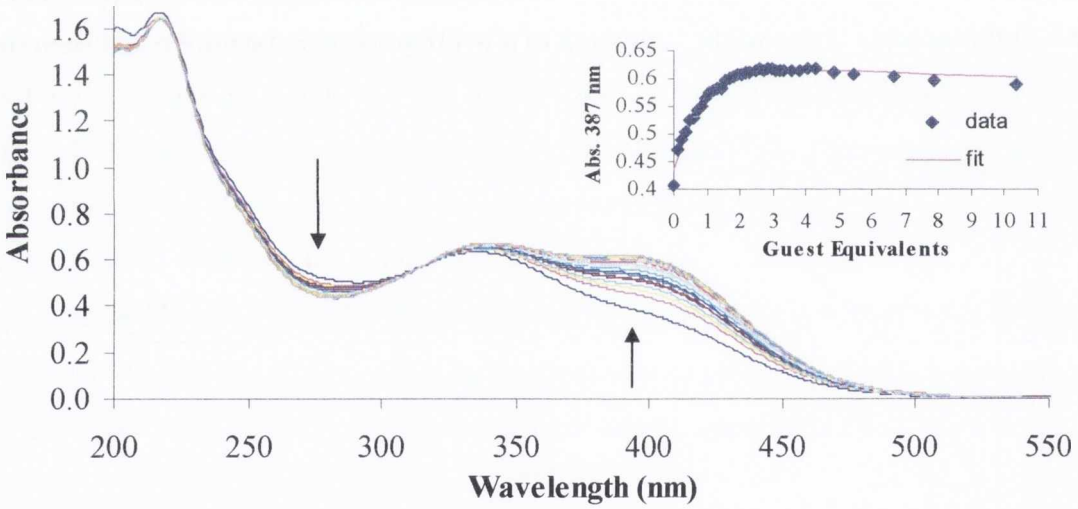


Figure 4.11: The changes in the absorption spectra of **71** [1.85×10^{-5} M] upon titration with AcO^- (0→ 10.3 equivalents) in 1:1 MeOH-H_2O. **Insert**: The changes at 387 nm with 1:1 fit obtained from SPECFIT™

Due to the high affinity observed between **70** and **71** and the various anions titrated, as well as the selectivity of **70** for $H_2PO_4^-$, we set out to determine the response of these sensors to other biologically important phosphates such as $HP_2O_7^{3-}$, AMP, ADP and ATP. This will be discussed in Section 4.6. However, in order to better understand the nature of the interaction between **70** and **71** and the various anions titrated, spectroscopic pH titrations were first carried out on **70** and **71** in both 1:1 EtOH-H_2O and 1:1 MeOH-H_2O solution, respectively, and the outcome of these will be firstly discussed in the following section.

4.4 Absorption pH titrations of 70 and 71 in Mixtures of Alcohol and Water Solutions

Absorption pH titrations of **70** were carried out in 1:1 EtOH-H_2O (0.01M NaCl) solution. The pH of a solution of **70** in 1:1 EtOH-H_2O was measured as 6.8. This solution was then acidified to pH 2 using HCl and then gradually basified to pH 12 using NaOH. For each pH adjustment, the absorption spectrum was recorded. In a similar manner, the basic solution was then acidified to pH 2 and the changes were shown to be reversible, to a greater extent. The overall changes in the absorption spectra from pH 2-12 are shown in Figure 4.12, as well as the changes at various wavelengths as a function of pH. The largest changes were observed for the ICT transition centred at 350 nm and also for the transition at 240 nm, which were assigned to protonation and subsequent deprotonation of the amidothiourea *p*-CF_3 phenyl receptor moieties of **70**.

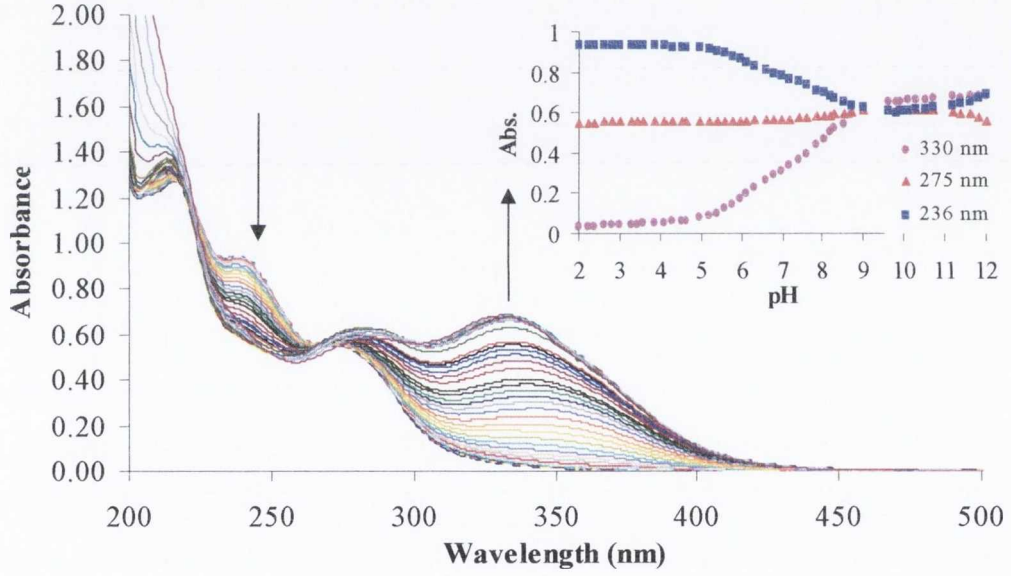


Figure 4.12: The changes in the absorption spectra of **70** [2.1×10^{-5} M] upon titration with NaOH from pH 2-12 in 1:1 EtOH-H_2O (0.01M NaCl). **Insert:** The changes at 330, 275 and 236 nm as a function of pH.

These changes occurred over the range of pH 5 to pH 9. In comparison to these changes, smaller changes were seen for the pyridine n-π^* transition. Additionally, at more alkaline pH, a hypsochromic shift was observed in the ICT transition, indicating the formation of a new species at high pH. Figure 4.12 also shows that initial acidification of the 1:1 EtOH-H_2O solution of **70** resulted in the disappearance of the ICT transition, which subsequently reappeared upon increasing the pH to *ca.* 5. In comparison to the changes in the presence of acid and base, the changes in the absorption spectrum of **70** upon titration with anions in this solvent system were far smaller in magnitude (see Figure 4.9).

The changes in the absorption spectrum of **70** were fitted using a Ligand/H^+ speciation model from SPECFIT™, allowing the protonation constants of **70** and **71** to be determined. Figure 4.13 shows the titration curve of **70** for the changes at 332 nm as a function of pH, in which two inflexion points are clearly visible, as well as the fit obtained from SPECFIT™. Therefore, from the titration data, at least two deprotonations were expected.

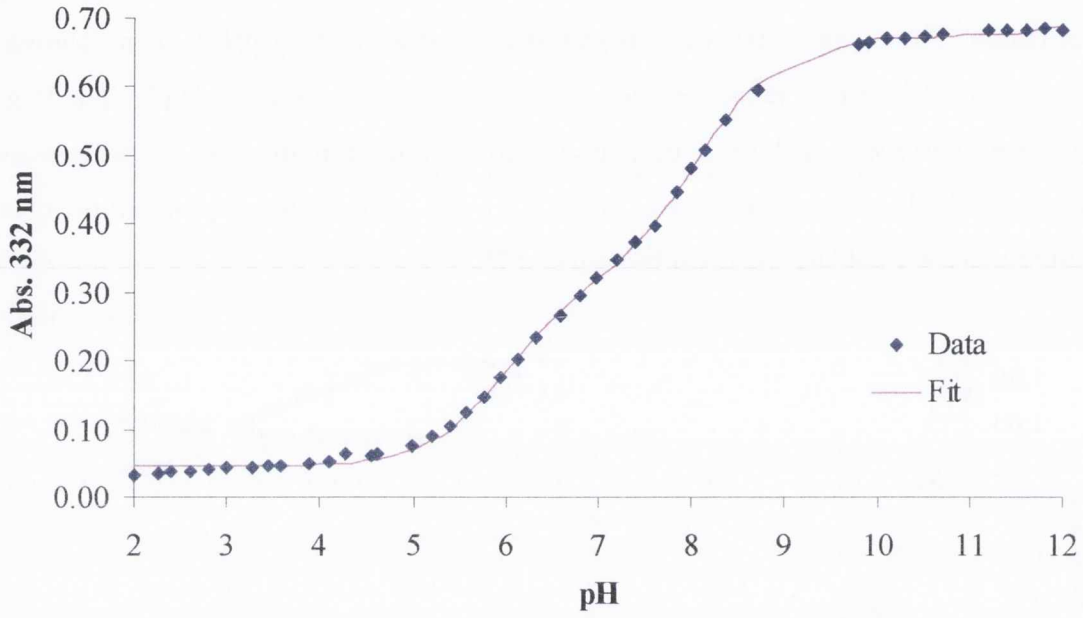


Figure 4.13: The changes in the absorption spectra of **70** as a function of pH and the fit at 332 nm obtained from SPECFIT™.

The best fit was obtained using a model that involved the occurrence of four coloured species, and thus three deprotonations. The species distribution diagram, Figure 4.14, illustrates the effect of pH on the species in solution, and shows the four coloured species, where LH_6 is the fully protonated sensor, **70**. Not including LH_6, this plot shows three other coloured species, two major and one minor species, the latter occurring above pH 11, which was most likely significant of the hypsochromic shift observed in the pH absorption titrations.

Although six pK_a values can be expected for the six N-H protons of sensor **70**, only two are clearly visible from the speciation plot, with another pK_a probable at pH values above 12. The step by step deprotonation of **70** can be described by Equations 4.0 and 4.1 and these represent the main processes occurring in Figure 4.14. The global deprotonation process, Equation 4.2, is represented by the overall binding constant β_{mn}, which describes all deprotonations in solution and is the product of the step by step protonation constants.

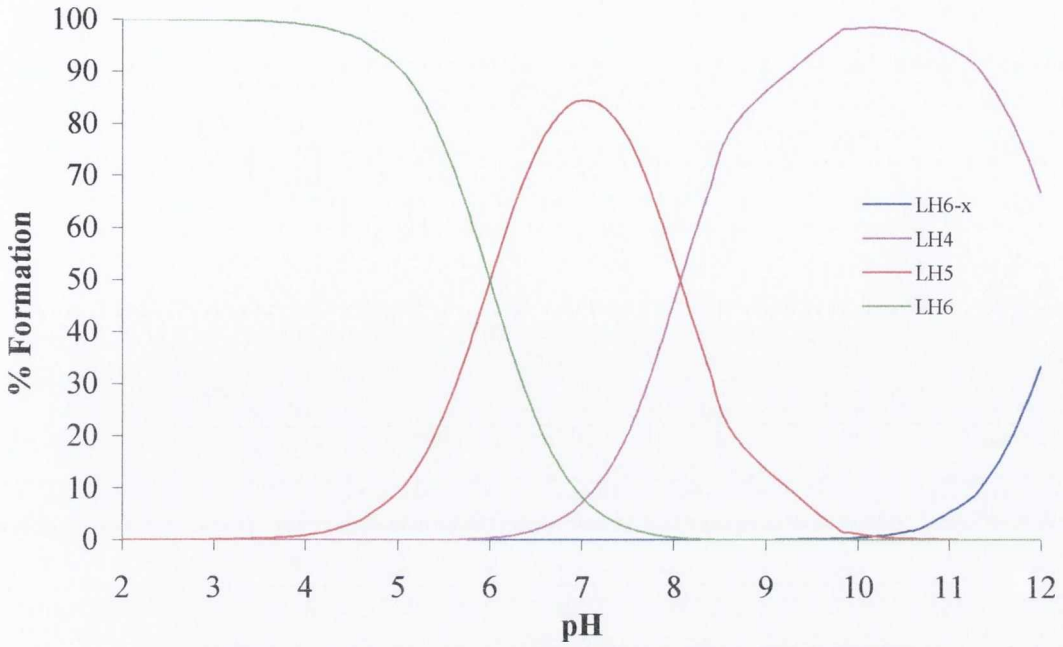


Figure 4.14: The species distribution plot of **70** as a function of pH

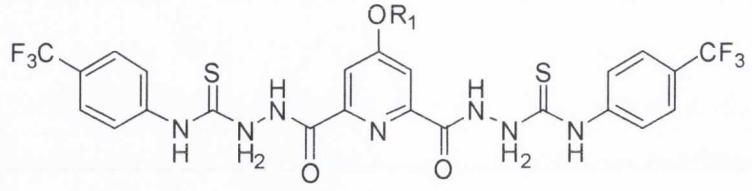
Eq 4.0: $LH_6 \xleftrightarrow{K_1} LH_5^- + H^+$ $\qquad K_1 = \dfrac{[LH_5^-][H^+]}{[LH_6]}$

Eq 4.1: $LH_5^- \xleftrightarrow{K_2} LH_4^{2-} + H^+$ $\qquad K_2 = \dfrac{[LH_4^{2-}][H^+]}{[LH_5^-]}$

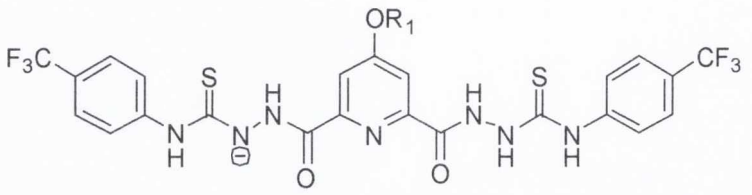
Eq 4.2: $LH_n \xleftrightarrow{\beta_{nm}} LH_{n-m}^{m-} + m\,H^+$ $\qquad \beta_{nm} = \dfrac{[LH_{n-m}^{m-}][H^+]}{[LH_n]}$

As shown in Chapter 3, the N-H_2 proton of compounds **54**, **61** and **62** was shown to be the most acidic N-H receptor proton in organic solution. Therefore, the LH_5^- and LH_4^{2-} species depicted in Figure 4.14 can possibly be attributed to the mono- and the di-deprotonated sensor, respectively, where the N-H_2 proton has been removed from each amidothiourea arm. The proposed structures of the LH_5^- and LH_4^{2-} species, as well as their corresponding pK_a values of 5.99 (± 0.06) and 8.07 (± 0.05), respectively, are shown in Figure 4.15. Although grown from organic solutions, the crystal structures of a mono deprotonated amidothiourea (compound **25d**, Chapter 1),[136,140] as well as the crystal structure of a mono deprotonated urea derivative have been reported within the literature.[156,177]

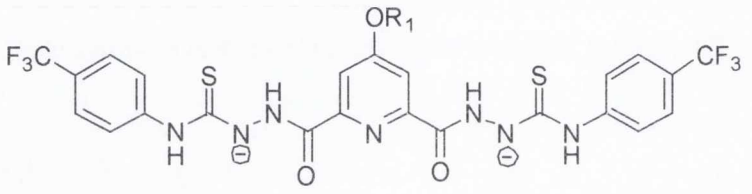
As previously mentioned, another pK_a was possibly present above pH 12 and due to the uncertainty in the structure of this species, it has been denoted as LH_{6-x} within Figure 4.14. The LH_{6-x} species could correspond to a LH_3^{3-} species, whereby another proton has



LH_6



LH_5^- $pK_{a1} = 5.99$ (+/- 0.06)



LH_4^{2-} $pK_{a2} = 8.07$ (+/- 0.05)

Figure 4.15: The proposed species generated upon titration of LH_6 (**70**) with OH^- in 1:1 EtOH-H_2O.

been removed from the thiourea receptor. However, it can be envisaged that it would be quite difficult to generate such a species from this sensor. No pK_a was observed at low pH of the titration, indicating that the pyridine moiety of **70** was not protonated over the course of the titration (the pK_a of picolinamide[213] and *N*,*N*-bis(2-aminoethyl)dipicolinc acid diamide[214] have been reported as 2.10 and 1.82, respectively).

Absorption pH titrations were also carried out with **71** in 1:1 MeOH-H_2O solution (Appendix C, Figure C12). Similar changes were observed in the absorption spectrum and data analysis using SPECFIT™ also showed the occurrence of similar species in solution (Appendix C, Figure C13). However, in contrast to **70**, the more electron withdrawing nitro derivative, **71**, showed a higher percentage formation of the LH_{6-x} species at high pH. The pK_a values determined for LH_5^- and LH_4^{2-} were 5.80 (± 0.07) and 7.62 (± 0.06), respectively, which are slightly lower than those of **70**, as was to be expected.

The first pK_a of **70** and **71** in the solvent mixtures studied were much lower than what was anticipated. With such a low pK_{a1} in these solvent mixtures, deprotonation of the receptor by anions may possibly occur. Additionally, the species distribution diagrams indicated that a substantial percentage of the mono deprotonated form of the ligand, (LH_5^-)

existed in solution at the beginning of the various anion titrations, *ca.* 84% (pH 6.8) and 80% (pH 7) in the case of **70** and **71**, respectively. Therefore, in the previous anion titrations only *ca.* 5% and less than 7% of the overall charge neutral LH_6 species of **70** and **71** were present at the start of the titrations, respectively. Nevertheless, the changes in the absorption spectra as a function of pH upon addition of anions to **70** and **71** were re-investigated. These results will be discussed in the following section.

4.5 pH Measurements of 70 and 71 with Anions in Aqueous-Based Solution

Stock solutions of **70** and **71** were prepared in 1:1 EtOH-H_2O and 1:1 MeOH-H_2O, respectively, and the pH of each solution was measured. On several occasions, the pH of **70** and **71** were recorded as 7.2 (± 0.1) and 6.9 (± 0.1) using a glass electrode. However, using the same stock solutions, these values were shown to occasionally vary by up to 0.4 pH units. These variations only led to very minor changes in the absorption spectra. It is most likely that these fluctuations were due to the close proximity of the pK_a values to the pH of the ligand solution.

Table 4.0 lists the pH values of several solutions of **70** and **71** and the subsequent changes in the pH measured upon the addition of one, two, three and ten equivalents of AcO^-, $H_2PO_4^-$ and F^-. These are compared with the pH values measured upon the addition of the same number of equivalents of TBAOH to both sensors. These results clearly demonstrate that only minor changes occurred in the pH of **70** and **71** upon addition of AcO^-, $H_2PO_4^-$ and F^-. Overall, the changes from the initial pH were no more than 0.3 pH units and in each case a decrease in the pH occurred. Indeed, Jiang *et al.*[141] have reported

Table 4.0: The changes in the pH (± 0.1) of **70** [1.6×10^{-5} M] and **71** [1.7×10^{-5} M] upon addition of various equivalents of anions in 1:1 EtOH-H_2O and 1:1 MeOH-H_2O mixtures, respectively.* uncertainty in value due to fluctuation in pH measured.

70	AcO^-	$H_2PO_4^-$	F^-	OH^-
0 eq	7.2	7.5	7.2	7.3
1 eq.	7.2	7.4	7.3	7.8
2 eq.	7.2	7.4	7.2	8.2
3 eq.	7.1	7.3	7.2	8.5
10 eq.	7.0	7.2	7.1	11
71	AcO^-	$H_2PO_4^-$	F^-	OH^-
0 eq	6.9	6.8	6.8	6.5
1 eq.	6.8	6.8	7.0	7.2
2 eq.	6.8	6.8	7.0	7.4*
3 eq.	6.7	6.7	6.9	7.7
10 eq.	6.6	6.6	6.7	10.0

similar pH changes for amidothiourea sensors in water. In the case of TBAOH, significantly larger changes in the pH were measured, as anticipated. For example, the addition of three equivalents of OH^- to both **70** and **71** gave rise to similar changes in the absorption spectrum to those observed in the presence of anions, however, the changes in the presence of OH^- were accompanied by an overall increase in the pH of 1.2 units. Despite the results observed in the pH speciation plots for **70** and **71**, these pH measurements suggested that hydrogen bonding occurred in the presence of the various anions in mixtures of alcohol and water.

With this information in hand, sensors **70** and **71** were titrated with biologically relevant phosphate-based anions such as $HP_2O_7^{3-}$, AMP, ADP and ATP. These results will be discussed in the following section.

4.6 Absorption Titrations of Sensors 70 and 71 with Biologically Relevant Phosphate-Based Anions in Alcohol and Water Solutions

Sensor **70** was first titrated with the TBA salt of $HP_2O_7^{3-}$, Figure 4.16. This gave rise to large changes in the absorption spectrum, which were similar to those observed in the presence of OH^-, Section 4.4. The insert of Figure 4.16 shows that the largest changes occurred up to the addition of just two equivalents of $HP_2O_7^{3-}$, with a further 18 equivalents were required to reach a plateau. The pH of the solution prior to titration was measured as 7.2, while the pH at the end of the titration was measured as 8.3. This verified that the overall changes upon titration with $HP_2O_7^{3-}$ were due to deprotonation. Additionally, in order to compare the pH changes in the presence of $HP_2O_7^{3-}$ with the

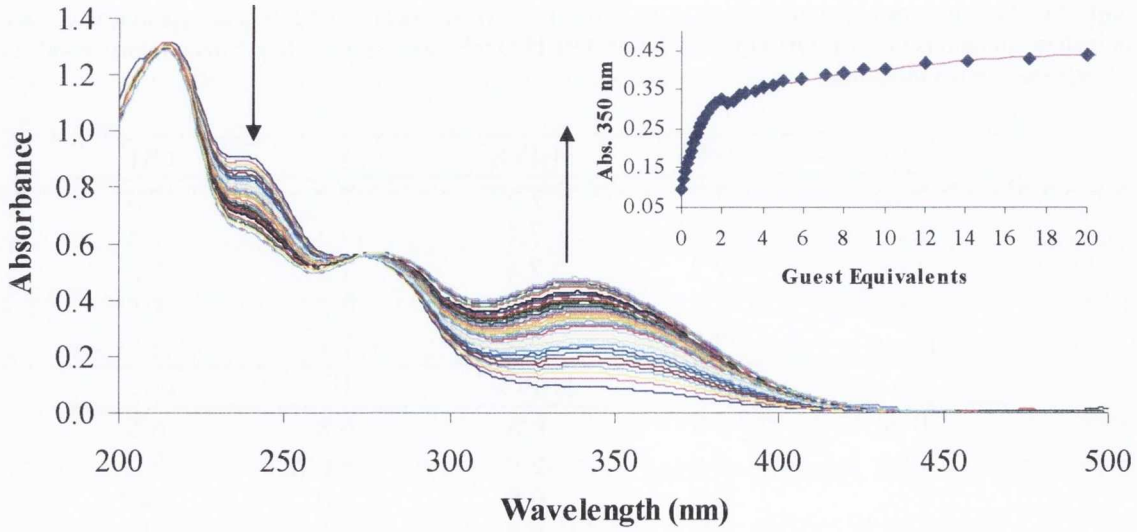


Figure 4.16: The changes in the absorption spectra of **70** [2.1×10^{-5} M] upon titration with $HP_2O_7^{3-}$ ($0 \rightarrow 130$ equivalents) in 1:1 EtOH-H_2O. **Insert:** The binding isotherm and 1:2 fit at 350 nm, shown from ($0 \rightarrow 20$ equivalents)

values shown in Table 4.0, the pH of **70** after the addition of just three equivalents of $HP_2O_7^{3-}$ was also measured. The pH change (0.7 units) was larger that that observed for the anions in Table 4.0 (0.3 units), indicating that deprotonation occurred in the presence of three equivalents of the anion.

In comparison to the previous anions employed in this solvent mixture, the changes in the absorption spectrum were best fitted to a 1:2 Host:Guest stoichiometry using SPECFIT™ (insert Figure 4.16), which gave $\log K_{1:1} = 5.58$ (± 0.07) and $\log K_{1:2}$ 3.64 (± 0.09). The species distribution diagram, Figure 4.17, as well as the binding constants, indicated the formation of a stable 1:1 species, which was the major species in solution up to the addition of 10 equivalents of $HP_2O_7^{3-}$. A second species then occurred, which became the major species after the addition of *ca.* 12 equivalents of $HP_2O_7^{3-}$. These species most likely correspond to the deprotonation of two N-H protons of the amidothiourea receptor moieties, as detailed in Section 4.4.

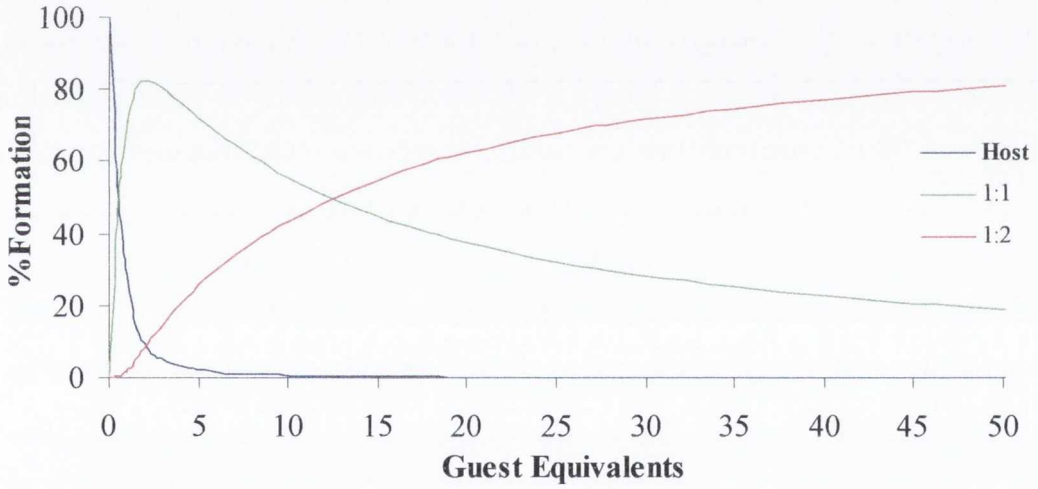


Figure 4.17: The species distribution plot of **70** [2.1×10^{-5} M] upon titration with $HP_2O_7^{3-}$ (0 → 10 equivalents) in 1:1 EtOH-H_2O.

Sensor **70** was next titrated with the sodium salt of AMP in 1:1 EtOH-H_2O solution, Figure 4.18. The changes in the absorption spectra of **70** at long wavelengths were similar to those seen for the previously discussed anions, such as AcO^-, $H_2PO_4^-$ and F^-. However, a plateau was only reached after the addition of *ca.* 6 equivalents of AMP, compared to just two equivalents previously seen for $H_2PO_4^-$ (Section 4.3). Similar changes were also observed for ADP (Appendix C, Figure C14). Both the titrations with AMP and ADP were best fitted to a 1:1 stoichiometry using SPECFIT™, which gave $\log K_{1:1} = 4.02$ (± 0.12) and 3.63 (± 0.12), respectively. Additionally, only minor changes in the pH of these solutions were observed (*ca.* 0.2 pH units), suggesting that the changes

observed were more likely due to the formation of hydrogen bonded complexes than the occurrence of deprotonation.

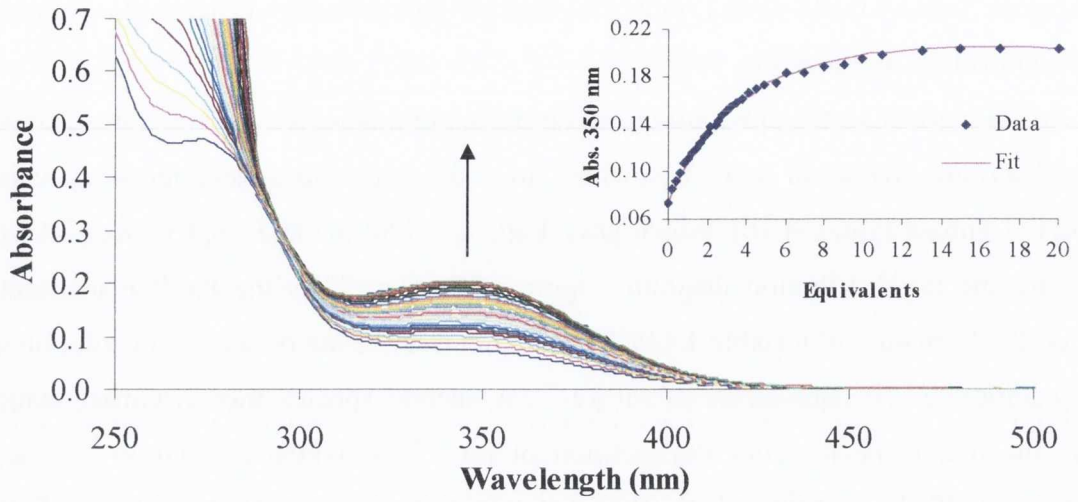


Figure 4.18: The changes in the absorption spectra of **70** [1.80 × 10^{-5} M] at long wavelengths upon titration with AMP (0 → 27 equivalents) in 1:1 EtOH-H_2O. **Insert:** The binding isotherm and 1:1 fit at 350 nm.

In contrast to these changes, titration of **70** with ATP resulted in a decrease in the absorption at 350 nm, as shown in Figure 4.19, which was similar to that observed upon acidification of **70**. Investigation into the nature of aqueous ATP solutions revealed that such solutions are in fact mildly acidic. This indicated that these changes were due to protonation of the receptor moieties of **70**, as shown in the pH titrations in Section 4.4. A similar spectral response was also observed upon the addition of the TBA salt of HSO_4^- to a solution of **70**, which is also acidic (pK_a = -3.1).[192] In addition to these results, after the addition of ATP and HSO_4^- to **70**, the pH was measured as 4.5 (± 0.1) and 4.2 (± 0.1),

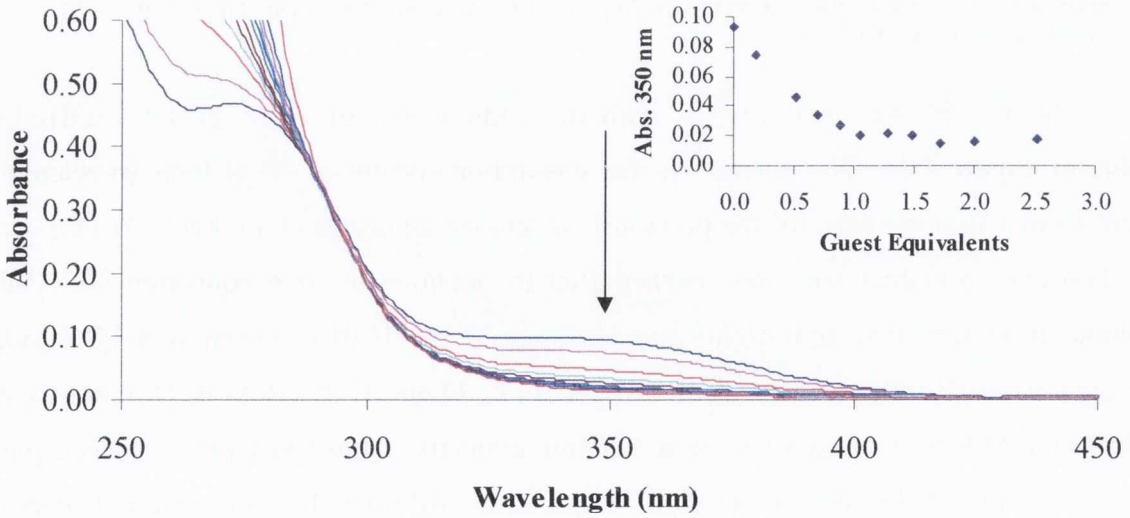


Figure 4.19: The changes in the absorption spectra of **70** [1.80 × 10^{-5} M] at long wavelengths upon titration with ATP (0 → 5 equivalents) in 1:1 EtOH-H_2O. **Insert:** The changes at 350 nm.

respectively, showing that these changes were indeed due to protonation of the receptor moieties of **70**.

In summary, sensor **70** could distinguish between ATP and $HP_2O_7^{3-}$ in 1:1 EtOH-H_2O solution, as these anions resulted in protonation and deprotonation of the receptor moieties. In contrast, smaller changes were observed in the absorption spectra of **70** upon titration with $H_2PO_4^-$, AMP and ADP. Although the spectral changes were similar for these three anions, the log$K_{1:1}$ value determined, *ca.* 5.1, 4.0 and 3.5, respectively, suggested that the order of affinity may correspond to the size of these anions. The simultaneous addition of one equivalent of AMP, ADP and ATP to **70** in a 1:1 EtOH-H_2O resulted in a decrease in the absorbance of the ICT transition, showing that **70** was protonated by ATP in the presence of the other phosphate anions.

Full absorption titrations of **71** with the various biological salts in 1:1 MeOH-H_2O were not carried out. However, the addition of 1, 2, 3, 10, 20 and 30 equivalents of AMP, ADP and $HP_2O_7^{3-}$ to **71** each gave rise to increases in the absorption spectra centred at 400 nm, in a similar manner to that seen for AcO^-, F^- and $H_2PO_4^-$ (Section 4.3). The addition of AMP and ADP resulted in small increases, which were accompanied by minor changes in the pH, of *ca.* 0.2 units, (Appendix C, Figure C15). In contrast to these changes, the addition of $HP_2O_7^{3-}$ resulted in large increases in the absorption spectra at long wavelengths and also large changes in the pH of the solution, an increase by 1 pH unit after the addition of 10 equivalents of the anion. Sensor **71** was also titrated with ATP, which resulted in a decrease in the absorption spectrum at long wavelengths, Figure 4.20, as seen for **70**. However, in contrast to that seen for **70**, the decrease in the absorption was accompanied by a colour change from yellow to colourless, hence, giving rise to

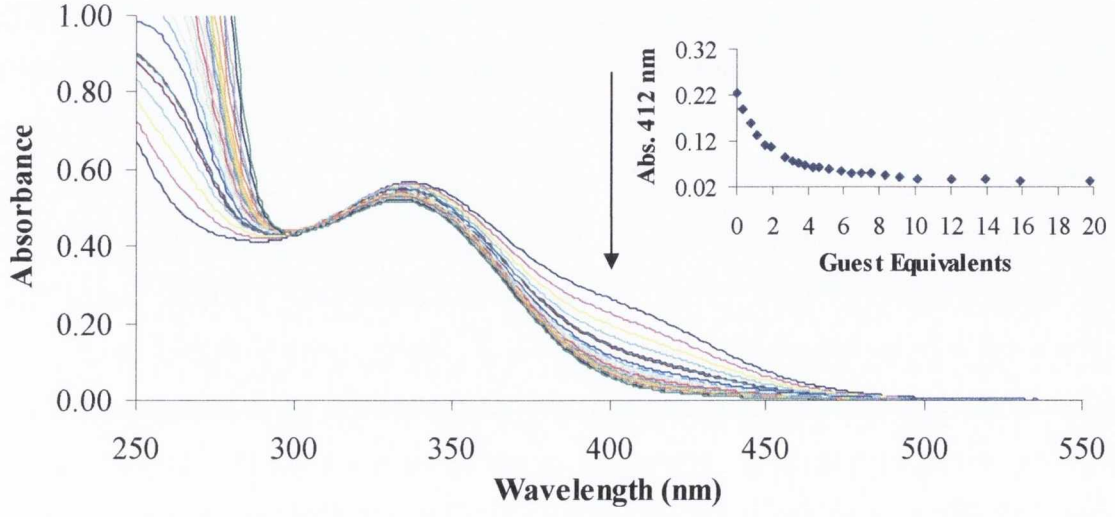


Figure 4.20: The changes in the absorption spectra of **71** [1.80×10^{-5} M] at long wavelengths upon titration with ATP (0 → 5 equivalents) in 1:1 MeOH-H_2O. **Insert:** The changes at 412 nm.



Figure 4.21: The colour change upon the addition of ATP to a solution of **71** [*ca.* 2×10^{-5} M] in 1:1 MeOH-H_2O. **(Left) 71 (Right) 71 + ATP** (15 equivalents).

colorimetric detection of ATP, Figure 4.21. In a similar manner to that seen upon titration of **70** with ATP, a decrease in the pH of **71** was also measured (pH 6.8 to 5.1). Also, as demonstrated for **70**, the simultaneous addition of ADP, AMP and ATP to **71** in 1:1 MeOH-H_2O resulted in a decrease in the ICT transition of the absorption spectrum and the same colour change as shown in Figure 4.21.

In summary, the results shown in Table 4.0 suggest that **70** and **71** form hydrogen bonded complexes with AcO^-, $H_2PO_4^-$ and F^-. Additionally, only minor changes in the pH of **70** and **71** were observed upon titration with AMP and ADP. Therefore, it was decided to investigate the sensing capabilities of **70** in buffered solution. The results from these studies will be discussed in the following section.

4.7 Buffer Studies with Sensor 70

With the changes in the absorption spectra as a function of pH and the pK_a values of both **70** and **71** established, it was decided to investigate the effects of buffer on the sensing mechanism of **70**. Indeed, the sensing of anions by charge neutral hydrazine-based sensors has previously been demonstrated in 1:1 EtOH-H_2O buffered solution.[128]

Due to the anionic content of all buffers, the buffers chosen for these studies were those for which the anionic counterparts were Cl^- and SO_4^-. Absorption titrations of **70** with Cl^- in 1:1 EtOH-H_2O previously showed that no spectral changes occurred in the presence of this anion and, in the case of HSO_4^-, the changes were smaller than those seen for anions such as AcO^- and $H_2PO_4^-$ (Figure 4.16). Therefore, the buffers selected for these studies were MES (2-*N*-(morpholino)ethanesulfonic acid) and TRIS (Tris(hydroxymethyl)aminoethane). The former was chosen as the buffering range is pH 5.5-6.7 and the species distribution diagram, shown in Figure 4.14, indicated that **70** was fully protonated at this pH (LH_6). Therefore, the pH of **70** in 1:1 EtOH-H_2O was buffered at 5.5 (0.1 M MES), as well as at pH 7.0 and 8.5 using TRIS (0.1M). Figure 4.22 shows the

absorption spectrum of **70** (1:1 EtOH-H_2O) and the resulting spectra upon buffering at the chosen pH values.

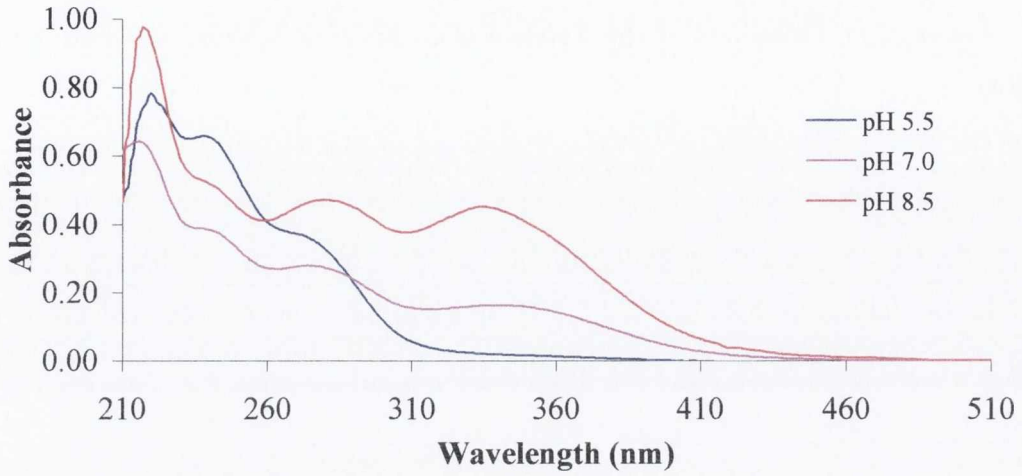


Figure 4.22: The absorption spectra of **70** [1.4×10^{-5} M] upon buffering (0.1 M) at pH 5.5, 7.0 and 8.5 in 1:1 EtOH-H_2O.

As can be seen from Figure 4.22, the spectrum at pH 5.5 resembles that seen at acidic pH in the absorption pH titrations in Section 4.4. Furthermore, the spectra which were buffered at pH 7 and 8.5 also resembled those seen at similar pH values in Section 4.4. Therefore, these results further supported the pK_a values previously determined for **70**. Comparison of the spectrum recorded at pH 8.5 (0.1 M) TRIS with the pH titrations indicated that the sensor was almost fully deprotonated by the TRIS base. Therefore, changes in the absorption spectrum were not anticipated upon the addition of anions. Indeed, the addition of AcO^- and $H_2PO_4^-$ (excess) did not give rise to any significant spectral changes. Similarly, no changes were observed upon the addition of AcO^- and $H_2PO_4^-$ to the solutions buffered at pH 5.5 and pH 7.0. In the case of the former, these results were unexpected as the sensor was in the fully protonated state, LH_6, and, hence, all of the N-H protons were available to engage in hydrogen bonding interactions. Therefore, the absence of spectral changes in the buffered solutions indicate that the changes previously observed upon titration with anions such as AcO^-, $H_2PO_4^-$, F^-, AMP and ADP were as a result of deprotonation, rather than anion binding. However, the results shown in Table 3.0, Section 4.4, suggested that the spectral changes were as a result of hydrogen bonding, as only minor changes in the pH of these un-buffered solutions occurred.[141] It can be speculated that the buffer, which is present at high concentrations (0.1 M), could interfere with the formation of a hydrogen bonded complex. However, this cannot be said for certain. Because of the uncertainty that the buffers plays in these measurements, any

remaining titrations that were carried out in aqueous solutions were done in the absence of any buffer.

4.8 Absorption Titrations of the Tetra-Amidothiourea Sensor, 74, with Anions in Alcohol.

The absorption spectrum of **74** was recorded in MeOH and EtOH solutions, which both showed similar spectra to those observed for the bis derivative **70** in these two solvents. Sensor **75** was only partially soluble in EtOH, however, the absorption spectrum in MeOH was similar to that observed for **71**. In a similar manner to the analysis of **70** and **71**, the *p*-CF_3 derivative, **74**, was first investigated.

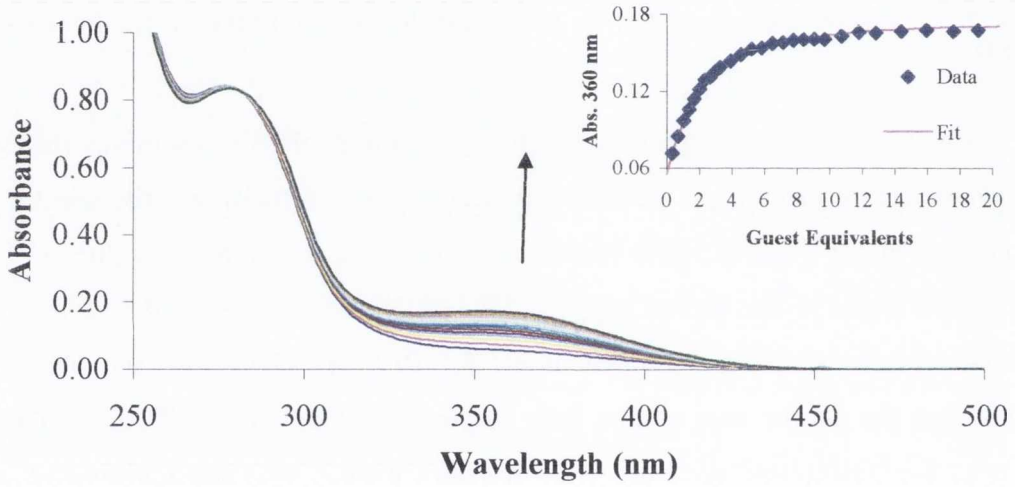


Figure 4.23: The changes in the ICT transition of the absorption spectra of **74** [1.55 x 10^{-5} M] in EtOH upon titration with $H_2PO_4^-$ (0 → 32 equivalents). **Insert:** The changes at 360 nm with 1:1 fit (0 → 20 equivalents).

The addition of $H_2PO_4^-$ to **74** in EtOH gave rise to small changes in the ICT transition of the absorption spectrum, as shown in Figure 4.23. Here, the largest changes occurred up to the addition of one equivalent of $H_2PO_4^-$ and reached a plateau at *ca.* two equivalents. Similar changes were observed upon titration of **74** with AcO^- and F^-. The spectroscopic changes for all anions were analysed using SPECFIT™. In the case of $H_2PO_4^-$, the changes were best fitted to a 1:1 Host:Guest stoichiometry, which gave a binding constant of $\log K_{1:1}$= 4.55 (± 0.03). The AcO^- and F^- titrations were also best fitted to a 1:1 stoichometric model, which resulted in binding constants of $\log K_{1:1}$= 6.3 (± 0.3) and $\log K_{1:1}$= 5.3 (± 0.2), respectively (Appendix C, Figure C16 and Figure C17, respectively). However, the fit obtained for AcO^- was not as good as those previously

obtained (*e.g.* Section 4.3, Figures 4.3 and 4.7) and, therefore, this value was considered only an as estimation. Nevertheless, this $\log K_{1:1}$ value was close in magnitude to that determined for **70** with AcO^- in EtOH, Section 4.3. Therefore, despite the anticipated possibility of cooperative anion binding for **74**, the changes in the absorption spectra were smaller than those observed with **70** and similar binding constants were obtained for both **74** and **70** with AcO^- in EtOH, Section 4.3.

Sensor **74** was also titrated with AMP, ADP and ATP in EtOH. In the case of AMP, slightly larger changes were seen in the ICT transition of the absorption spectrum compared to those seen for AcO^-, $H_2PO_4^-$ and F^-. However, these changes did not reach a plateau until after the addition of *ca.* 80 equivalents of AMP, at which point the absorption of the AMP began to overlap with the changes in the ICT transition of **74** (Appendix C, Figure C18).

The changes in the presence of AMP were fitted using SPECFIT™, from which the best fit was for a 1:1 stoichiometry, giving $\log K_{1:1} = 3.67 (\pm 0.03)$ for the binding of AMP. In comparison to the changes in the presence of AMP, only minor changes occurred in the presence of ADP and titration with ATP did not result in a decrease in the absorption of the ICT transition, as had been seen for the previous sensors. In the case of hydrogen bonding, the absence of any significant spectral changes suggested that ADP may be too large to interact in a favourable manner with the sensor. This may indicate that a cavity or 'binding pocket' was formed by the sensor in solution, such as that seen in the crystal structure of **75**.

The increase in the absorption of the ICT transition of **74** upon titration with anions in EtOH indicated a common mechanism of anion interaction to that seen for sensors **70** and **71**. Indeed, titration of **74** with $HP_2O_7^{3-}$ in EtOH gave rise to large changes in the absorption spectrum, the magnitude of which compared to those of the aforementioned anions is shown in Figure 4.24.

The spectral changes in the presence of $HP_2O_7^{3-}$ were similar to those observed upon titration of **70** with $HP_2O_7^{3-}$ and TBAOH in 1:1 EtOH-H_2O solution, Figures 4.16 and 4.12, respectively. These changes were previously assigned to deprotonation of the receptor moieties of **70**, as a large increase in the pH of the solution was measured (Section 4.7). Therefore, it is quite likely that the overall changes in the absorption spectrum of **74** upon titration with $HP_2O_7^{3-}$ were also due to deprotonation of the N-H_2 protons. Although these changes could not be fitted using SPECFIT™, the evolving factor analysis (EFA) estimated the presence of three coloured species in solution, including sensor **74**. The other

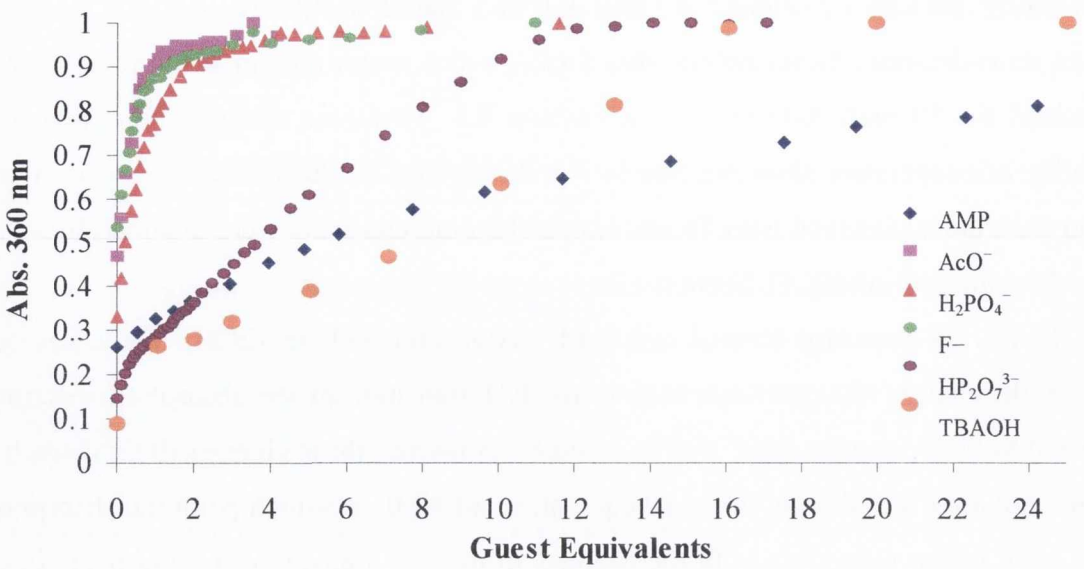


Figure 4.24: The relative changes in the absorption spectra of **74** upon titration with various anions in EtOH.

two species present most likely resulted from the deprotonation of the receptor moieties of **74**. In support of the latter explanation, the titration of **74** with TBAOH resulted in large changes in the absorption spectrum, the magnitude of which were similar to those seen in the presence of $HP_2O_7^{3-}$, Figure 4.24. Conversely, titration of **74** with the TBA salt of HSO_4^- resulted in a decrease in the absorption spectrum at 360 nm, which was indicative of protonation of the receptor moieties (Appendix C, Figure C19).

Due to the presence of four receptor moieties within sensor **74**, as well as the flexible polyoxyethylene chain, it was decided to investigate if sensor **74** could cooperatively bind larger anions such as Cl^-, Br^- and I^-. Unfortunately, no changes were seen in the absorption spectra of **75** upon titration with these anions.

In summary, comparison of the $\log K_{1:1}$ binding constants determined for both **70** and **74** with AcO^- in EtOH did not imply that cooperative binding occurred. However, it was noticed that for each titration of **74** that was analysed using SPECFIT™, the 1:1 stoichiometry (excluding $HP_2O_7^{3}$) gave rise to the best fit on all occasions. This was in contrast to the titrations of **70** and **71** in 100% alcohol, which were best fitted to a 1:2 binding stoichiometry. Although, the main species in these titrations was also shown to be a 1:1 species, a second minor species occurred at high concentrations. In a similar manner to the investigations of sensors **70** and **71** in the previous sections, the sensing capabilities of **75** in MeOH were next investigated.

4.8.1 Absorption Titrations of Sensor 75 with Anions in Alcohol

Sensor **75** was titrated with AcO^- in MeOH, which gave rise to similar changes to those seen in the absorption spectra of **71** (Appendix C, Figure C20). In contrast to **74**, these changes were best fitted to a 1:2 stoichiometry using SPECFIT^{TM}, which gave binding constants of $\log K_{1:1}$= 5.00 (± 0.04) and $\log K_{1:2}$= 3.1 (± 0.1). These values are lower than those determined for **71** upon titration with AcO^- in MeOH (Section 4.2.1). Sensor **75** was also titrated with TBAOH and HSO_4^- in MeOH, which resulted in a large increase and decrease in the ICT transition of the absorption spectra. This is most likely due to deprotonation and protonation of the receptor moieties by these anions, respectively. The overall changes in the absorption spectra of **75** upon titration with AcO^-, TBAOH and HSO_4^- in MeOH are shown in Figure 4.25.

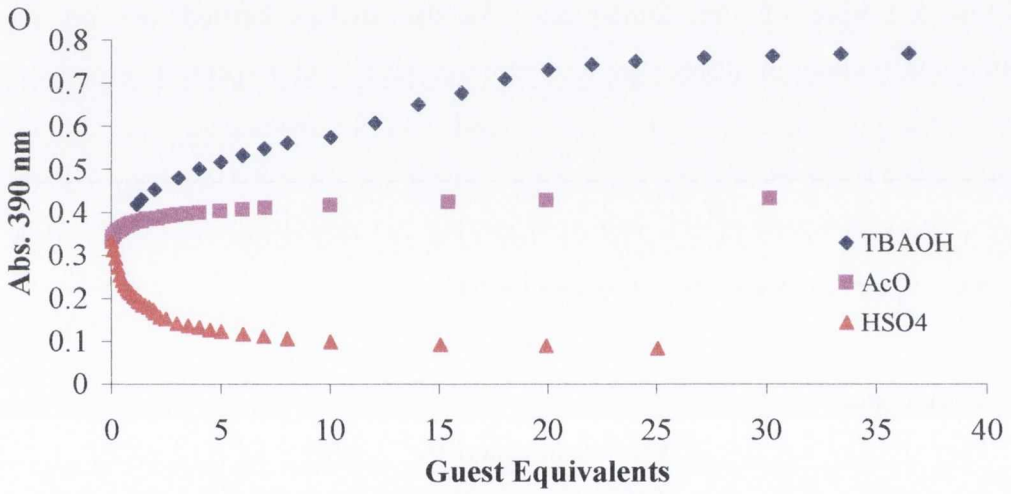


Figure 4.25: The changes in the absorption spectra of **75** [1 × 10^{-5} M] at 390 nm upon titration with various anions in MeOH.

Once again, these results confirmed the common spectral responses of all the sensors detailed in this chapter upon titration with anions. In a similar manner to compound **71**, the addition of HSO_4^- to **75** resulted in a colour change of the solution from yellow to colourless (Section 4.6). Indeed, the addition of ATP to **75** also resulted in the same colour change. Due to time constraints, further titrations of **75** with anions such as $H_2PO_4^-$, F^-, $HP_2O_7^{3-}$, AMP and ADP were not carried out and the sensing capabilities of **74** and **75** were next investigated in more competitive media.

4.8.2 Absorption Titrations of 74 and 75 with Anions in Alcohol and Water Solutions

The absorption spectra of **74** and **75** in 1:1 EtOH-H_2O (v/v) and 1:1 MeOH-H_2O (v/v) solutions, respectively, were similar to their corresponding spectra in alcohol. Titration of **74** with $H_2PO_4^-$ resulted in a different pattern of change to that observed for the previous sensors and a decrease in the absorptions centred at 210, 240 and 280 nm was observed. However, upon the addition of 0.8 equivalents of $H_2PO_4^-$, a white precipitate was visible in solution. This indicated that the initial decreases in the absorption spectrum were also as a result of precipitation of the sensor from solution. The solubility of sensors **74** and **75** in alcohol were lower than that of **70** and **71**. While, it was anticipated that an 'anion binding pocket' may be formed in solution by the tetra-amidothiourea sensors, such interactions may also result in an increase of stacking interactions in solution and, hence, lower the solubility of the compounds. As the studies carried out on the tetra-amidothiourea sensors in alcohol showed more or less similar spectral responses to their corresponding bis analogues, it was decided not to investigate the anion binding capabilities of **74** and **75** in more competitive media any further. However, the addition of ATP to a solution of **75** in 1:1 MeOH-H_2O also showed colorimetric detection of this anion, in a similar manner to that observed for **71**.

4.9 Conclusion

This chapter has detailed the design and the synthesis of four novel glycol-based amidothiourea sensors for anions, **70**, **71**, **74** and **75**, which were characterised by conventional spectroscopic methods. These sensors were functionalised with polyoxyethylene chains with the aim of improving their solubility in competitive hydrogen bonding solvents, such as MeOH and EtOH, as well as in mixtures of alcohol and water solutions. Indeed this proved successful for the bis systems, as both **70** and **71** were titrated with various anions in both alcohol and alcohol-water mixtures. Conversely, the tetra systems **74** and **75** were partially soluble in alcohol-water mixtures and, hence, were only titrated in alcohol solutions.

The anion binding capabilities of **70** and **71** were initially assessed in either or both MeOH and EtOH solution, by titrating these compounds with AcO^-, $H_2PO_4^-$ and F^-. The results from these titrations showed that both sensors interacted most strongly with AcO^-, with large 1:1 binding constants determined using SPECFIT^{TM}. Additionally, the control titrations carried out with base suggested that these changes could be due to the formation of hydrogen bonded complexes, as the changes in the presence of base were far larger in

magnitude. In comparison to the changes observed in the absorption spectra of both **70** and **71** with AcO^- and F^-, the spectral changes in the presence of $H_2PO_4^-$ were different, whereby an increase in the absorption followed by a decrease and bathochromic shift occurred. This indicated that the nature of the hydrogen bonded complex formed with the tetrahedral anion was quite different to that of AcO^- and F^-.

Working towards achieving anion binding in highly competitive media, compounds **70** and **71** were then titrated with the aforementioned anions in mixtures of alcohol and water (1:1 EtOH-H_2O and 1:1 MeOH-H_2O) solutions. These titrations resulted, on all occasions, in an increase in the ICT transition of both **70** and **71** in the presence of AcO^-, $H_2PO_4^-$ and F^-. In the case of **70**, strong recognition of $H_2PO_4^-$ was shown to occur in 1:1 EtOH-H_2O solution, as a high binding constant was determined using SPECFIT™.

In order to better understand the anion interactions of **70** and **71** in 1:1 EtOH-H_2O and 1:1 MeOH-H_2O solutions, spectroscopic pH titrations were carried out. The results from these titrations gave a further understanding of these sensors in solution and the effect that pH had on the changes in the absorption spectra. These experiments showed that the pK_{a1} values of these sensors were quite low (*ca.* 6 for both **70** and **71**). These values initially caused concern that the receptor moieties of **70** and **71** may be deprotonated by anions too easily. However, despite the low pK_{a1} determined, only minor changes in the pH (*ca.* 0.3) were measured upon the addition of anions such as AcO^-, $H_2PO_4^-$ and F^- to mixed alcohol-water solutions of **70** and **71**. These results supported the formation of hydrogen bonded complexes in these solvent systems. Additionally, the changes observed in these titrations were fitted to 1:1 stoichiometries, while those in 100% alcohol were fitted to 1:2 stoichiometries. This may indicate that there was minor contribution from deprotonation in the less competitive alcohol solutions, however, as the pH of these solutions could not be measured, this cannot be said for certain.

Compounds **70** and **71** were also titrated with biologically important phosphate-based anions, such as AMP, ADP, ATP and $HP_2O_7^{3-}$. In the case of the latter, large spectral changes, as well as changes in the pH were observed. Therefore, the overall changes in the presence of $HP_2O_7^{3-}$ were assigned to deprotonation of the receptors in both **70** and **71**. In contrast to these changes, smaller spectral changes were seen in the ICT transitions of **70** and **71** upon addition of AMP and ADP. These changes gave rise to minor changes in the pH of *ca.* 0.2 pH units and in the case of **70**, were best fitted to a 1:1 stoichiometry. In contrast to these results, the addition of ATP resulted in a decrease in the ICT transition of the absorption spectra of both **70** and **71**, as well as a substantial decrease in the pH. However, in the case of **71**, the decrease in the absorption spectrum was more

pronounced and, hence, a colour change from yellow to colourless was observed. The addition of one equivalent of AMP, ADP and ATP to **71** resulted in the same colour change, showing that **71** could sense the presence of ATP, due to protonation of the receptor moieties of **71**.

Titrations of the tetra-amidothiourea sensors, **74** and **75**, with various anions also gave rise to an increase in the ICT band in the absorption spectra, in a similar manner to that seen for **70** and **71** in EtOH and MeOH, respectively. However, the changes in the presence of AcO^-, $H_2PO_4^-$ and F^- were smaller in magnitude when compared to those seen for **70** and **71**. It was hoped that these sensors could detect the presence of anions more strongly than **70** and **71** due to the cooperative binding of anions by all four receptor moieties within a 'binding pocket'. The main species observed upon fitting the titrations of **74** with AcO^-, $H_2PO_4^-$, F^- and AMP was a 1:1 stoichiometric species, as had been seen for the bis systems earlier. In the case of AcO^-, the binding constant with **74** was comparable to that observed for **70** in EtOH. Hence, these binding constants did not indicate a cooperative effect for the recognition of AcO^-. As previously mentioned, the solubility of these compounds in 1:1 alcohol-water solutions was lower than anticipated, making the preparation of such solutions difficult. Due to solubility issues and the fact that the general trends of the spectroscopic changes were similar to those observed for the **70** and **71**, the anion sensing capabilities of these sensors were not investigated in alcohol and water. However, in the case of ATP, similar colorimetric detection by **75** in 1:1 MeOH-H_2O was observed, as the solution changed from yellow to colourless upon addition of this anion, which was clearly visible to the naked eye.

Chapter 5

Overview of Thesis and Future Work

5.0 Overview of Thesis: Introduction

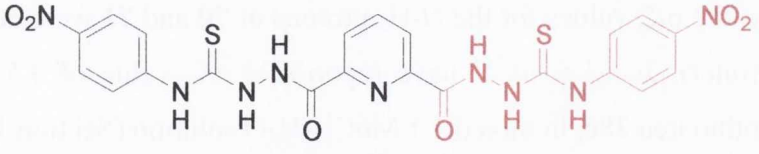
In light of the results discussed in Chapters 3 and 4 of this thesis, the focus of the following section is to compare and contrast these results to specific reports within the literature. Additionally, the most important results from these chapters will be outlined.

As mentioned throughout this thesis, there are reports detailing hydrogen bonding between anions and amidothioureas but there are also reports detailing anion induced deprotonation of these sensors (detailed in Chapter 1). Therefore, certain amidothioureas within the literature, which have structurally similar receptor moieties to those discussed in this thesis, are discussed below in order to allow simple comparison.

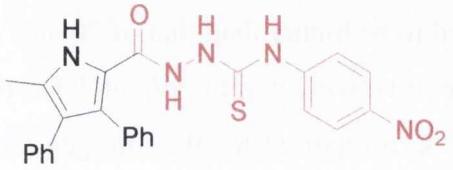
Conversely, the spectroscopic results from the investigations of the naphthalimide-based anion sensors in Chapter 2 were in agreement with those previously reported within the literature and, hence, these sensors will not be discussed further. As previously mentioned in Section 2.22, future work could be carried out on the sensing capabilities of the bis-naphthalimide **39** with di-anions, such as bis-carboxylates.

5.1 Amidothioureas Functionalised with Electron Withdrawing Groups

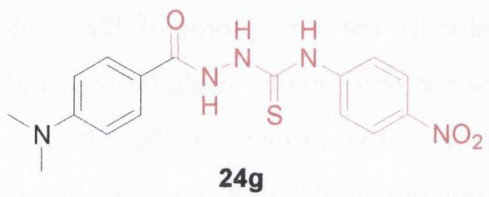
Chapter 3 of this thesis discussed the UV-Vis absorption and ^{1}H NMR anion titrations of several amidothiourea compounds, including the *p*-nitro-phenyl-based sensor, **54**. The titrations of **54** with anions and OH^- in 4:1 DMSO-H_2O showed that anions gave rise to deprotonation of the receptor moieties of **54** (Section 3.4). Aforementioned, these results are in agreement with the solution studies of the *p*-nitro-phenyl-based sensor **25d** in similar conditions, which were carried out by Gale *et al.*[136] (Section 1.8.2). Additionally, the crystal structure of **25d**, which showed that deprotonation occurred in the presence of one equivalent of F^-, strongly supports our findings.



54



25d



24g

Despite the fact that **24g** also contains an electron withdrawing *p*-nitro-phenyl-based receptor, Jiang *et al.*[79] have reported that this sensor forms hydrogen bonded complexes with anions in MeCN (Section 1.8.1). The changes in the UV-Vis spectrum of **24g** in MeCN upon deprotonation with OH^- were not investigated. However, these results were reported prior to the studies of **25d** in DMSO and, therefore, anion induced deprotonation may not have been considered a possible outcome.

As a consequence of the results reported by Jiang *et al.*[79], this thesis detailed titrations of **56** (*p*-CF_3-phenyl-based receptor) and **57** (quinoxaline-based receptor) with anions and OH^- in 1% DMSO-MeCN solution, as it is plausible that different solvents may lead to different Host:Guest interactions in solution. However, these titrations also indicated that deprotonation occurred in the presence of anions (Section 3.14).

5.2 Amidothioureas Functionalised with Electron Donating Groups

The sensors discussed above were functionalised with electron withdrawing receptor moieties. In contrast, many of the amidothiourea sensors previously reported to bind anions have been functionalised with simple phenyl groups or with electron donating phenyl groups (*e.g* Chapter 1; **23a-c**, **24a**, **27a-b**, **28a-b**, **29a**).[78,79,137,141,142] As discussed in Section 3.16, this prompted our investigations of **27b**, which showed that anions and OH^- did not lead to spectroscopic changes of the same magnitude, in a similar manner to that seen for the electron withdrawing derivatives. Therefore, it is acknowledged that hydrogen bonding between these sensors and anions may occur.

5.3 Amidothioureas in Aqueous-Based Solution

Chapter 4 of this thesis discussed the sensing capabilities of the *p*-nitro-phenyl and *p*-CF_3-phenyl substituted amidothioureas, **70** and **71**, in mixtures of 1:1 alcohol and water. Most importantly, the pK_a values for the N-H_2 protons of **70** and **71** were determined (*ca.* 6 in alcohol and water). Jiang *et al.*[141] have reported a pK_a value of 3.5 for the phenyl substituted amidothiourea **28c**, in mixed 1:1 MeCN-H_2O solution (Section 1.8.2). Although **28c** was studied in a different mixture of aqueous media compared to **70** and **71**, the pK_a value for the N-H_2 proton of **28c** would be expected to be higher than that of **70** and **71**, as the receptor moiety would be less acidic. Therefore, it is likely that the pK_a at 3.5 is that of the pyridine nitrogen of **28c**. Similar values have been reported for the nitrogen atom of isonicotinamides in water.[213] Consequently, it would be interesting to know the pK_a value for the N-H_2 proton of **28c**. However, no further pK_a values were reported for **28c** or for the electron withdrawing derivatives **28d-e** (*m*-Br and *m*-CF_3). Neither were titrations with

OH^- carried out for the sake of comparison, despite these results being published after those of Gale *et al.*[136] Titrations with OH^- may not have been considered necessary as only minor changes in the pH of **28c** were reported upon titration with anions.

In the case of **70** and **71**, assignment of the exact nature of the interaction with anions was difficult, for several reasons, some of which are outlined below:

- The low pK_a values of **70** and **71** indicated that the sensors were quite acidic and, hence, partially deprotonated in 1:1 alcohol-water, prior to titration with anions (Section 4.4). However, despite this, it is reasonable to suggest that there are enough hydrogen bond donors remaining, which could engage in hydrogen bonding interactions with anions.
- As seen for **28c**, the changes in the pH of solutions of **70** and **71** upon addition of various anions (Table 4.0) were only minor, indicating that hydrogen bonding occurred in solution.
- Upon buffering solutions of **70** at pH 5 (sensor fully protonated, LH_6), no changes occurred in the absorption spectrum upon titration with anions. These results suggested that the spectroscopic changes in the presence of anions could be due to changes in pH (Section 4.7).

As a consequence of the points outlined above, amidothioureas will not be further pursued within the Gunnlaugsson group for the purpose of anion binding in aqueous media. In the case of **70** and **71**, hydrogen bonding may have occurred, however, it is thought that the pH window between the occurrence of hydrogen bonding and deprotonation is small and overlaps, hence, making assignment of the interaction more complicated.

5.4 Future Work

The sensors detailed in this thesis have all contained a central diamido pyridine unit, which has been well established as a tridentate unit that can self assemble with lanthanide metal cations, forming 1:3 Metal:Ligand (M:L) complexes.[215-217] Apart from the work detailed in this thesis, sensor **56** was titrated with the perchlorate salt of Tb^{3+} by Mr. Christophe Lincheneau (of the Gunnlaugsson Group) and has been shown to selectively form 1:1 and 1:3 M:L complexes (**Tb.56** and **Tb.56$_3$**, respectively). Solution studies of the complexation process were carried out in various solvent systems. Preliminary results showed that only minor changes occurred in the UV-Vis absorption spectra of **56** upon

addition of Tb^{3+} in 4:1 DMSO-H_2O, however, a large increase in the Tb^{3+} luminescence was observed. Conversely, in MeOH large changes occurred in both the UV-Vis absorption and emission spectrum. Furthermore, the addition of AcO^- gave rise to an increase in the emission spectra of **Tb.56** and **Tb.56$_3$,** while the addition of $H_2PO_4^-$ quenched the emission of the complexes. Additional studies are underway on the various other amidothiourea ligands which were synthesised in this thesis. The preliminary results discussed above indicate that such Tb^{3+} sensors may be suitable for the sensing of anions.

Chapter 6

Experimental Procedures

6.0 General Experimental Details

All chemicals were obtained from Sigma-Aldrich, Fluka and Novabiochem and unless otherwise specified were used without further purification. Deuterated solvents for NMR analysis were purchased from Apollo Scientific. Solvents for synthetic purposes were used at GPR or HPLC grade unless otherwise stated. Analytical TLC was performed using Merck Kieselgel 60 F_{254} silica plates. Visualisation was by UV light (254 nm). NMR spectra were recorded using a Bruker Spectrospin DPX-400 instrument, operating at 400.13 MHz for ^{1}H NMR, 100.6 MHz for ^{13}C NMR, 376.4 MHz for ^{19}F NMR and 161.9 MHz for ^{31}P NMR. NMR spectra were also recorded using a Bruker AV-600 MHz, operating at 600.1 MHz for ^{1}H NMR and 150.9 MHz for ^{13}C NMR. Shifts were referenced relevant to the internal solvent signals, with chemical shifts expressed in parts per million (ppm) downfield from the standard. Multiplicities are abbreviated as follows: singlet (s), doublet (d), triplet (t), quintet (q), multiplet (m) and broad (br). Aromatic naphthalimide protons are numbered according to that shown in Figure 5.1. All NMR spectra and titrations were performed at 293 K, unless otherwise specified. Mass Spectra were determined by detection using electrospray on a Mass Lynx NT V 3.4 on a Waters 600 Controller connected to a 996 photodiode array detector with HPLC-grade methanol, water or acetonitrile as carrier solvents. Accurate molecular weights were determined by a peak-matching method, using leucine enkephaline (H-Try-Gly-Gly-Phe-Leu-OH) as the standard internal reference (m/z = 556.2771); all accurate mass were calculated to ≤ 5 ppm. Samples were prepared as solutions in methanol or acetonitrile. Melting points were determined using an Electrothermal IA9000 digital melting point apparatus in an unsealed capillary tube. Infrared spectra were recorded on a Perkin Elmer Spectrum One FT-IR spectrometer fitted with a universal ATR sampling accessory. Elemental analysis was carried out at the microanalysis laboratory, School of Chemistry and Chemical Biology, University College Dublin. X-ray diffraction analysis was carried out by Dr. Thomas McCabe, School of Chemistry, Trinity College Dublin.

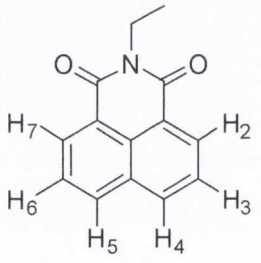


Figure 5.1: Aromatic protons of 1,8-naphthalimide.

6.1 NMR Titrations

^{1}H NMR titrations were carried out on a Bruker Spectrospin DPX-400 instrument at 25 °C. Data analysis was conducted using Microsoft Excel 2003®, TopSpin, NMR*tit*[150] and WinEQNMR.[149] All titrations were repeated to ensure reproducibility.

6.1.1 Preparation of Solutions for NMR Titrations with Anions

Host solutions were prepared using deuterated solvents (Apollo: DMSO-d_6 DE60H and MeCN-d_3 DE20H) whereby the concentration ranged between 1×10^{-3} M and 5×10^{-3} M. The volume of host solution titrated was between 0.6 and 0.8 mL. The TBA (Aldrich: AcO^- 335991, OH^- 86866, $HP_2O_7^{3-}$ 93397; Fluka: $H_2PO_4^-$ 86867) and Na salts of the various anions used were $\geq$ 97% in purity. All TBA salts were dried over P_2O_5 at 40 °C under vacuum, except for TBAF hydrate (Alrich 241512) and TBAF.$3H_2O$ (Aldrich 86872), which were dried under vacuum at room temperature.[33] The concentrations of these guest solutions were prepared such that 2-5µl would give *ca.* 0.1 or 0.2 molar equivalents of anion, with the dilution volume not exceeding more than 10%. Each addition was delivered using a 10 µl gastight syringe (Supelco, 26256).

6.2 UV-Visible Absorption and Fluorescence Titrations

UV-Visible absorption and fluorescence titrations were carried out at 25 °C on a Varian Cary 50 and Eclipse spectrometers, respectively. Data analysis was conducted using Microsoft Excel 2003® and SPECFIT/32™ (Appendix A0).[109,110] The pH titrations were carried out using a glass electrode (Orion Ross SureFlow 8172 BN combination electrode). All titrations were repeated to ensure reproducibility.

6.2.1 Preparation of Solutions for UV-Visible Absorption and Fluorescence Titrations with Anions

The DMSO solvent used was purchased from Sigma Aldrich (D5879, $\geq$ 99.5% GC). HPLC grade MeCN (Sigma Aldrich, 34851), EtOH (Merck, K40023527 920) and MeOH (Sigma Aldrich, 34860) solvents were used for titrations. The aqueous-based solutions were prepared using Millipore water. The TBA and Na anion salts used in the titrations were purchased and dried as detailed in Section 6.1.1. Solutions of these salts were prepared in the desired solvent at varying concentrations of *ca.* 1 M, 1×10^{-1} M, 1×10^{-2} M and 1×10^{-3} M. Host solutions were prepared between 1×10^{-3} M and 3×10^{-3} M and were then diluted to the desired concentration prior to titration (*ca.* $1 - 3 \times 10^{-5}$ M). The volume of host solution titrated was 3 mL, with the dilution volume not exceeding more than 10%.

After each addition of anion the titration solution was stirred for *ca.* 3 minutes. As for the NMR titrations, each addition was delivered using a 10 μl gastight syringe. For the pH absorption titrations (Section 4.4), *ca.* 50 mL of host solution was prepared and the pH was adjusted using acid and base solutions.

6.3 General Synthetic Procedures

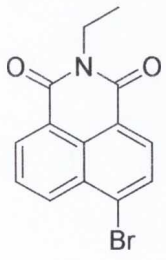
6.3.1 Procedure 1: Synthesis of Naphthalimide-based Ureas and Thioureas

A solution of the isocyanate or thiocyanate (1 equivalent) in $CHCl_3$ was added to a solution of the amine (1 equivalent) in $CHCl_3$. The reaction mixture was stirred at room temperature under argon for 16 h. The precipitate was then isolated by suction filtration and washed several times with $CHCl_3$. The solid was dried under vacuum.

6.3.2 Procedure 2: Synthesis of Amidoureas and Amidothioureas

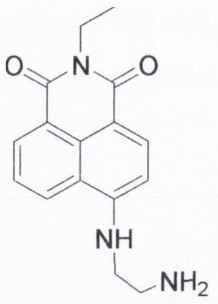
A solution of the isocyanate or isothiocyanate (2 equivalents) in MeCN was added to a solution of the amine (1 equivalent) in MeCN. The reaction mixture was refluxed under argon for 16 h. The precipitate was then isolated by suction filtration and washed several times with warm MeCN. The solid was dried under vacuum.

6-Bromo-2-ethyl-benzo[*de*]isoquinoline-1,3-dione (35)[107]



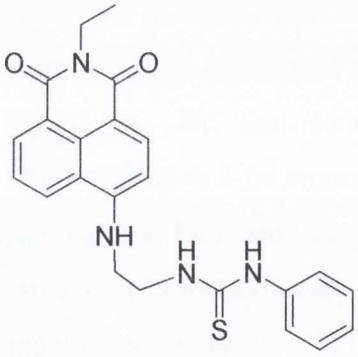
4-Bromonaphthalic anhydride (2.03 g, 7.21 mmol) and 70% ethylamine (0.39 g, 8.66 mmol) were heated at reflux overnight in 1,4-dioxane (100 mL). The reaction mixture was poured into water and the solid product was isolated by vacuum filtration. The solid was then dissolved in CH_2Cl_2 (100 mL), washed with H_2O (2 × 20 mL) and 1M HCl (2 × 20 mL). The solvent was removed under reduced pressure to give **35** as a pale yellow solid (1.76g, 79%). m.p. 160-162 °C (Lit.m.p.[218] 160-161 °C); δ_H (400 MHz, $CDCl_3$), 8.62 (1H, d, J = 7.5 Hz, Naph-$\underline{H}_5$), 8.50 (1H, d, J = 8.5 Hz, Naph-$\underline{H}_7$), 8.38 (1H, d, J = 8.0 Hz, Naph-$\underline{H}_2$), 8.00 (1H, d, J = 8.0 Hz, Naph-$\underline{H}_3$), 7.82 (1H, dd, J = 7.8 Hz, 8.0 Hz, Naph-$\underline{H}_6$), 4.24 (2H, q, J = 7.0 Hz, $C\underline{H}_2$), 1.34 (3H, t, J = 7.0 Hz, $C\underline{H}_3$); δ_C (100 MHz, $CDCl_3$), 162.9 (C=O), 162.8 (C=O), 132.6 (CH), 131.4 (CH), 130.6 (CH), 130.5 (CH), 130.1 (q), 129.6 (q), 128.5 (q), 127.5 (CH), 122.7 (q), 121.9 (q), 35.2 (CH_2), 12.8 (CH_3).

2-Ethyl-6-diaminoethyl-benzo[*de*]isoquinoline-1,3-dione (36)



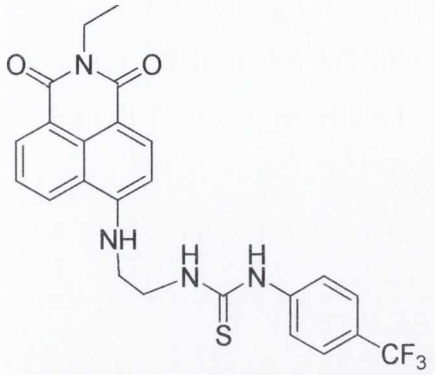
Diaminoethylene (excess) was added to **35** (1.84 g, 6.07 mmol). The reaction mixture was stirred neat at 80 °C for 16 h. The reaction mixture was then poured into water, forming a precipitate which was collected by suction filtration. The solid was dissolved in CH_2Cl_2 (100 mL), washed with H_2O (2 × 20 mL) and the organic layer was then dried over $MgSO_4$. The solvent was removed under reduced pressure to give **36** as an orange solid (1.12 g, 61%). m.p. 105-108 °C; HRMS: (ES^+) Calculated for $C_{16}H_{18}N_3O_2$ $[M+H]^+$: 284.1399; found: 284.1299; δ_H (600 MHz, $CDCl_3$), 8.70 (1H, d, J = 8.28, Naph-$\underline{H}_5$), 8.41 (1H, d, J = 6.78 Hz, Naph-$\underline{H}_7$), 8.24 (1H, d, J = 8.28, Naph-$\underline{H}_2$), 7.66 (1H, dd, J = 7.56 and 7.14 Hz, Naph-$\underline{H}_6$), 6.79 (1H, d, J = 8.28 Hz, Naph-$\underline{H}_3$), 4.05 (2H, q, J = 7.2 Hz, NC$\underline{H}_2$), 3.40 (2H, br s, C$\underline{H}_2$), 2.90 (2H, br s, C$\underline{H}_2$), 1.18 (3H, t, J = 7.14, C$\underline{H}_3$); δ_C (150 MHz, $CDCl_3$), 163.8 (C=O), 163.0 (C=O), 151.1 (q), 134.4 (CH), 130.8 (CH), 129.6 (q), 128.9 (CH), 124.4 (CH), 122.1 (q), 120.4 (q),107.9 (q), 104.1 (CH), 46.4 (CH_2), 40.4 (CH_2), 34.5 (CH_2), 13.6 (CH_3); IR υ_{max} (cm^{-1}) 3458, 3337, 2936, 1675, 1629, 1574, 1366, 1343, 1246, 1066.

2-Ethyl-6-[(4-phenylthiocarbamoyl)ethylamino]-benzo[*de*]iso-quinoline-1,3-dione (4a)



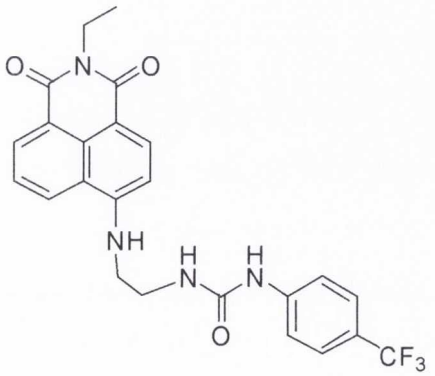
Compound **4a** was synthesised according to **Procedure 1** using **36** (0.299 g, 2.21 mmol) and phenylisothiocyanate (0.628 g, 0.26 mL, 2.21 mmol,) in $CHCl_3$ (60 mL). The product was obtained as a bright yellow solid (0.53 g, 58%). m.p. 238-240 °C; Calculated for $C_{23}H_{22}N_4O_2S$ .04 $CHCl_3$: C, 65.35; H, 5.24; N, 13.27%; found: C, 65.36; H, 5.31; N, 13.11%; HRMS: (ES^+) Calculated for $C_{23}H_{23}N_4O_2S$ $[M+H]^+$: 419.1542; found: 419.1539; δ_H (600 MHz, DMSO-d_6), 9.74 (1H, br s, N$\underline{H}_{urea}$), 8.69 (1H, d, J = 8.3 Hz, Naph-$\underline{H}_5$) 8.45 (1H, d, J = 7.14 Hz, Naph-$\underline{H}_7$), 8.27 (1H, d, J = 8.7 Hz, Naph-$\underline{H}_2$), 7.97 (1H, br s, N$\underline{H}_{urea}$), 7.87 (1H, br s, $NH_{\underline{naph}}$), 7.77 (1H, t, J = 7.7 Hz, Naph-$\underline{H}_6$), 7.36-7.30 (4H, m, Ar-$\underline{H}_{2,3,}$ $\underline{H}_{5,6}$), 7.14 (1H, t, Ar-$\underline{H}_4$), 6.99 (1H, d, J = 8.7 Hz, Naph-$\underline{H}_3$), 4.08 (2H, q, J = 6.78, NC$\underline{H}_2$), 3.88 (2H, br s, C$\underline{H}_2$), 3.64 (2H, br s, $NH_{naph}C\underline{H}_2$), 1.19 (3H, t, J = 7.2 Hz, C$\underline{H}_3$); δ_C (150 MHz, DMSO-d_6), 180.4 (C=S), 163.8 (C=O), 163.0 (C=O), 150.9 (q), 139.0 (q), 134.3 (CH), 130.9 (CH), 129.6 (CH), 129.1 (q), 128.8 (CH), 124.9 (CH), 124.6 (CH), 123.8 (CH), 122.2 (q), 120.4 (q), 108.3 (q), 104.3 (CH), 42.5 (CH_2), 42.5 (CH_2), 34.5 (CH_2), 13.6 (CH_3); IR υ_{max} (cm^{-1}) 3354, 3231, 3173, 1683, 1642, 1587, 1540, 1430, 1396, 1369, 1343, 1247, 1190, 1108.

2-Ethyl-6-[(4-trifluoromethylphenylthiocarbamoyl)ethylamino]-benzo[*de*]isoquinoline-1,3-dione (4b)



Compound **4b** was synthesised according to **Procedure 1** using **36** (0.102 g, 0.33 mmol) and 4-trifluoromethylphenyl isothiocyanate (0.068 g, 0.33 mmol,) in $CHCl_3$ (30 mL). The solid obtained was suspended in MeOH (40 mL) and refluxed overnight to remove minor impurities. The product was filtered and dried under vacuum to give **4b** as a bright yellow solid (0.102 g, 62%). m.p. 226-228 °C; Calculated for $C_{24}H_{21}F_3N_4O_2S{\cdot}0.2CHCl_3$: C, 56.95; H, 4.19; N, 10.98%; found: C, 56.98; H, 4.10; N, 11.01%; HRMS (ES^+): Calculated for $C_{24}H_{22}F_3N_4O_2S$: 486.1416 $[M+H]^+$; found: 487.1439; δ_H (400 MHz, DMSO-d_6), 10.0 (1H, br s, NH_{urea}), 8.70 (1H, d, J = 9.0 Hz, Naph-$\underline{H}_5$) 8.46 (1H, d, J = 8.0 Hz, Naph-$\underline{H}_7$), 8.28 (2H, m, $N\underline{H}_{urea}$, Naph-$\underline{H}_2$), 7.91 (1H, br s, $N\underline{H}_{naph}$), 7.73 (1H, t, J = 8.0 Hz, Naph-$\underline{H}_6$), 7.64 (4H, br s, Ar-H), 6.98 (1H, d, J = 8.0 Hz, Naph-$\underline{H}_3$), 4.05 (2H, q, J = 7.0 Hz, $NC\underline{H}_2$), 3.87 (2H, q, J = 5.0 Hz, $C\underline{H}_2$,), 3.64 (2H, m, $NH_{naph}C\underline{H}_2$), 1.18 (3H, t, J = 7.03 Hz, $C\underline{H}_3$); δ_C (100 MHz, DMSO-d_6), 181.4 (C=S), 164.3 (C=O), 163.5 (C=O), 151.4 (q), 143.7 (q), 134.8 (CH), 131.5 (CH), 130.1 (q), 129.3 (CH), 126.6 (CH), 125.1 (CH), 124.3 (q), 123.1 (CF_3, $J_{^{13}C^{19}F}$ = 272.1 Hz), 123.8 (q, $J_{^{13}C^{19}F}$ = 27.0 Hz), 122.7 (q), 120.9 (q), 108.0 (q), 104.0 (CH), 42.2 (CH_2), 41.8 (CH_2), 34.2 (CH_2), 13.3 (CH_3); δ_F (376 MHz, DMSO-d_6) – 60; IR υ_{max} (cm^{-1}) 3383, 3259, 1672, 1639, 1614, 1586, 1527, 1396, 1371, 1343, 1328, 1319, 1244, 1156, 1110, 1065, 1053, 1015, 840, 773, 757.

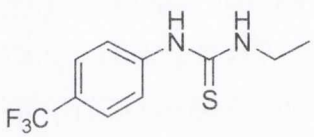
2-Ethyl-6-[(4-trifluoromethylphenylureidocarbamoyl)ethylamino]-benzo[*de*]isoquinoline-1,3-dione (4c)



Compound **4c** was synthesised according to **Procedure 1** using **36** (0.100 g, 0.32 mmol) and 4-trifluorophenyl isocyanate (0.061 g, 0.046 mL, 0.32 mmol) in $CHCl_3$ (30 mL). The solid obtained was suspended in MeOH (40 mL) and refluxed overnight to remove minor impurities. The product was filtered and dried under vacuum to give a bright yellow solid (0.155 g, 66%). m.p. 270-272 °C; Calculated for $C_{24}H_{21}F_3N_4O_3{\cdot}0.1$ $CHCl_3$: C, 60.01; H, 4.41; N, 11.61%; found: C, 59.87; H, 4.54; N, 11.56%; HRMS (ES^+):

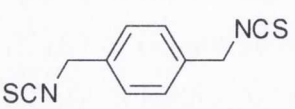
Calculated for $C_{24}H_{22}N_4O_3F_3$ $[M+H]^+$: 471.1644; found: 471.1654; δ_H (400 MHz, DMSO-d_6), 9.16 (1H, br s, NH_{urea}), 8.67 (1H, d, J = 8.5 Hz, Naph-$\underline{H}_5$) 8.43 (1H, d, J = 7.0 Hz, Naph-$\underline{H}_7$), 8.26 (1H, d, J = 8.5 Hz, Naph-$\underline{H}_2$), 7.89 (1H, br s, $N\underline{H}_{urea}$), 7.69 (1H, t, J = 8.5, Naph-$\underline{H}_6$), 7.62 (2H, d, J = 8.5 Hz, Ar-$\underline{H}$), 7.57 (2H, d, J = 9.1 Hz, Ar-$\underline{H}$), 6.89 (1H, d, J = 8.5 Hz, Naph-$\underline{H}_3$), 6.62 (1H, br s, $N\underline{H}_{naph}$), 4.08 (2H, q, J = 7.03, $NC\underline{H}_2$), 3.51-3.46 (4H, m, $C\underline{H}_2$), 1.18 (3H, t, J = 7.0 Hz, $C\underline{H}_3$); δ_C (100 MHz, DMSO-d_6), 163.9 (C=O), 163.1 (C=O), 155.8 (q), 151.1 (q), 144.5 (q), 134.6 (CH), 131.1 (CH), 128.8 (CH), 126.4 (CH, $J_C{}^{13}{}_F{}^{19}$ = 3.8 Hz), 125.1 (CF_3, $J_{^{13}C^{19}F}$ = 270.0 Hz), 124.8 (CH), 123.7 (q), 122.4 (q), 121.5 (q, $J_{^{13}C^{19}F}$ =31.0 Hz), 120.5 (q), 117.8 (CH), 108.3 (q), 104.3 (CH), 43.6 (CH_2), 38.3 (CH_2), 34.7 (CH_2), 13.7 (CH_3); IR υ_{max} (cm^{-1}) 3396, 3302, 1685, 1650, 1628, 1589, 1542, 1373, 1347, 1325, 1249, 1166, 1119, 1107, 1067, 1016, 837, 822, 774, 759.

Thiourea, *N*-ethyl-*N'*-[4-(trifluoromethyl)phenyl]- (37)



4-Trifluoromethylphenyl isothiocyanate (0.300 g, 1.47 mmol) and *N*-Ethylamine (0.066 g, 0.077 mL, 1.47 mmol) were stirred in $CHCl_3$ (30 mL) at room temperature for 16 h. The solvent was removed under reduced pressure to give **37** as a white solid (0.308 g, 84.6%). m.p. 145-146 °C; HRMS $(ES)^+$: Calculated for $C_{10}H_{12}N_2F_3S$ $[M+H]^+$: 249.0673; found 249.0699; δ_H (400 MHz, DMSO-d_6), 9.79 (1H, br s, NH_{urea}), 8.04 (1H, br s, NH_{urea}), 7.69 (2H, d, J = 8.8 Hz, Ar-H), 7.64 (2H, d, J = 8.8 Hz, Ar-H), 2.51 (2H, br q, J = 1.7 Hz, $C\underline{H}_2$,) 1.14 (3H, t, J = 7.04 Hz, $C\underline{H}_3$); δ_C (100 MHz, DMSO-d_6), 180.4 (C=S), 143.8 (q), 126.0 (CH), 124.8 (CF_3, $J_{^{13}C^{19}F}$ = 270.0 Hz), 123.9 (q), 123.3 (CH), 40.0 (CH_2), 14.4 (CH_3); IR υ_{max} (cm^{-1}) 3299, 3183, 3146, 2972, 1665, 1623, 1595, 1587, 1574, 1551, 1495, 1330, 1291, 1224, 1176, 1160, 1112, 852, 842, 751, 700, 684.

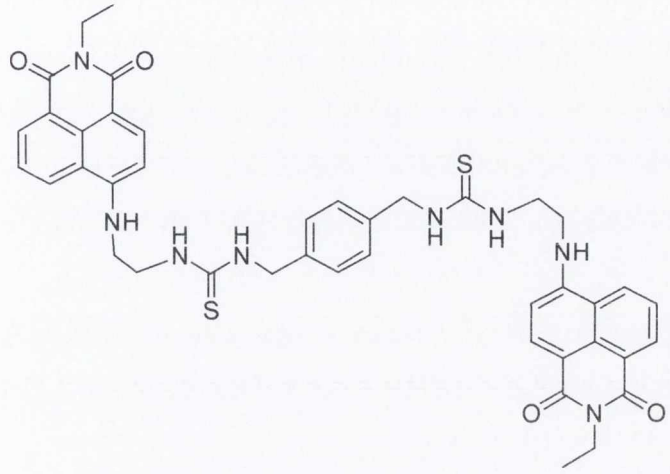
1,4-bis(isothiocyantomethyl)benzene (38)[219]



α,α-Diamino-*p*-xylene (1.00 g, 7.34 mmol) and thiophosgene ($CSCl_2$) (1.01 g, 0.67 mL 8.81 mmol) were stirred in CH_2Cl_2 (50 mL) at room temperature overnight. The organic solution was then washed with water (2 × 20 mL), dried over $MgSO_4$ and the solvent was then allowed to evaporate at room temperature. The solid obtained was then dried under vacuum to give **38** as a pale yellow solid (0.22 g, 17%). m.p. 54-58 °C (Lit m.p.[167] 64 °C); HRMS $(ES)^+$: Calculated for $C_{10}H_8N_2S_2$ $[M]^+$: 220.0129; found 220.0129; δ_H (400 MHz, DMSO-d_6), 7.43 (4H, br s, $C\underline{H}$), 4.96 (4H, br s, $C\underline{H}_2$); δ_C (100 MHz, DMSO-d_6), 134.7 (q), 129.3 (N=C=S)

127.7 (CH), 47.6 (CH_2); IR υ_{max} (cm^{-1}), 2969, 2894, 2179, 2090, 1516, 1419, 1329, 798, 738, 714.

Bis-{2-Ethyl-6-[(4-trifluoromethylphenylthiocarbamoyl)ethylamino]-benzo[*de*]isoquinoline-1,3-dione} (39)



Compound **38** (0.106 g, 0.48 mmol,) and **36** (0.272 g, 0.96 mmol) were stirred under argon in DMF (8 mL) at room temperature for 9 days. The precipitate formed was collected by suction filtration to give a bright yellow solid (0.030 g, 8%). m.p. 226-228 °C; HRMS $(ES)^+$: Calculated for $C_{42}H_{43}N_8O_4S_2$ $[M+H]^+$: 787.2849, found 787.2814; δ_H (600 MHz, DMSO-d_6), 8.64 (2H, d, J = 8.5 Hz, Naph-$\underline{H}_5$), 8.42 (2H, d, J = 7.5 Hz, Naph-$\underline{H}_7$), 8.23 (2H, d, J = 8.7 Hz, Naph-$\underline{H}_2$), 8.02 (2H, br s, N$\underline{H}$), 7.84 (2H, br s, N$\underline{H}_{naph}$), 7.71 (2H, br s, N$\underline{H}$), 7.67 (2H, t, J = 8.0 Hz, Naph-$\underline{H}6$), 7.20 (4H, s, Ar-H), 6.89 (2H, d, 7.7, J = 8.5 Hz, Naph-H$\underline{3}$), 4.62 (4H, br s, $\underline{CH_2}$), 4.04 (4H, q, J = 7.0, Ar- NC$\underline{H_2}$), 3.79 (4H, br s, C$\underline{H_2}$), 3.55 (4H, d, J = 5.5 Hz, C$\underline{H_2}$), 1.19 (3H, t, J = 7.0 Hz, C$\underline{H_3}$); δ_C (150 MHz, DMSO-d_6), 184.3 (C=S), 163.8 (C=O), 163.0 (C=O), 153.0 (q), 150.9 (q), 134.4 (CH), 130.9 (CH), 129.6 (q), 128.8 (CH), 127.5 (CH), 124.6 (CH), 122.2 (q), 120.4 (q), 108.2 (q), 104.2 (CH), 47.1 (CH_2), 43.0 (CH_2), 42.4 (CH_2), 34.5 (NCH_2), 13.6 (CH_3); IR υ_{max} (cm^{-1}) 3239, 1682, 1633, 1586, 1543, 1370, 1345, 1244, 1108, 1063, 882, 771, 756.

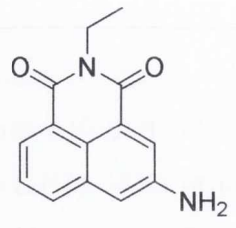
5-Amino-benzo[*de*]isoquinoline-1,3-dione (40)[169]



3-Nitro-1,8-naphthalic anhydride (5.0 g, 20.5 mmol) and 10% Pd/C (0.50 g) in DMF were shaken under hydrogen at 3 atm for 16 h. The catalyst was then filtered off through celite and washed with DMF. The filtrate was concentrated under reduced pressure and water was added. The resulting precipitate was then filtered and washed with water to give **40** as a mustard brown solid (0.38 g, 88%). m.p. 304-306 °C (Lit. m.p.[169] > 300 °C) δ_H (600 MHz, DMSO-d_6), 8.12, (2H, m, Naph-$\underline{H}_5$, $\underline{H}_7$) 7.97 (1H, s, Naph-$\underline{H}_2$), 7.66 (1H, dd, J = 7.8 and 7.5 Hz, Naph-$\underline{H}_6$) 7.37 (1H, s, Naph-$\underline{H}_4$), 6.10 (2H, br s, N$\underline{H}_2$); δ_c (150 MHz, DMSO-d_6)

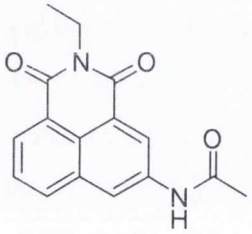
161.3 (C=O), 161.2 (C=O), 148.5 (q), 133.9 (q), 132.8 (CH), 127.6 (CH), 127.5 (CH), 123.4 (CH), 123.2 (q), 119.6 (q), 118.7 (q), 112.9 (CH).

2-Ethyl-5-amino-benzo[*de*]isoquinoline-1,3-dione (41a)[220]



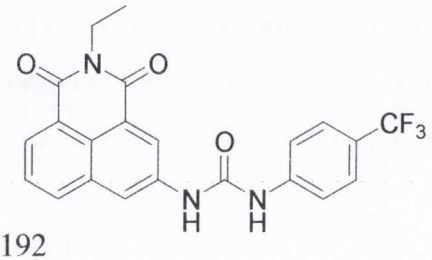
3-Amino-1,8-naphthalic anhydride (0.25 g, 1.18 mmol) and 70% ethylamine were refluxed in 1,4-dioxane for 16h. The reaction mixture was poured into water and the precipitate was isolated by suction filtration to give **41a** as an orange solid (0.14 g, 51%). m.p. 275-277 °C (Lit. m.p.[220] 276 °C); δ_H (400 MHz, DMSO-d_6), 8.07 (1H, d, J = 7.0 Hz, Naph-$\underline{H}_7$), 8.02 (1H, d, J = 7.6, Naph-$\underline{H}_5$), 7.96 (1H, s, Naph-$\underline{H}_2$), 7.60 (1H, dd, J = 8.16 and 7.60 Hz, Naph-$\underline{H}_6$), 7.27 (1H, s, Naph-$\underline{H}_4$), 6.00 (2H, br s, N$\underline{H}_2$) 4.04 (2H, q, J = 7.0 Hz, NC$\underline{H}_2$) 1.18 (3H, t, J = 7.0 Hz, C$\underline{H}_3$); δ_c (100 MHz, DMSO-d_6), 163.8 (C=O), 163.7 (C=O), 148.1 (q), 133.8 (q), 131.7 (CH), 127.3 (CH), 125.6 (CH), 122.9 (q), 122.1 (CH), 121.9 (q), 120.8 (q), 112.0 (CH), 34.9 (CH_2), 13.4 (CH_3).

2-Ethyl-5-acetamide-benzo[*de*]isoquinoline-1,3-dione (41b)



Compound **41b** was synthesised by treating **41a** (0.078 g, 0.319 mmol) in acetic acid (3.0 mL) with acetic anhydride (0.40 ml) and the whole stirred at reflux for 2 hours. The suspension was cooled and collected by suction filtration to yield **41b** as a beige solid (0.072 g, 80%). m.p. decomposed at 230 °C; δ_H (400 MHz, DMSO-d_6), 10.75 (1H, s, N$\underline{H}$), 8.71 (1H, d, J = 1.2 Hz, Naph-$\underline{H}_2$), 8.55 (1H, d, J = 1.2 Hz, Naph-$\underline{H}_4$), 8.32 (1H, d, J = 7.2 Hz, Naph-$\underline{H}_7$), 8.31(1H, J = 8.4 Hz, Naph-$\underline{H}_5$), 7.77 (1H, t, J = 7.5 Hz, Naph-$\underline{H}_6$), 4.06 (2H, q, J = 4.7 Hz, NC$\underline{H}_2$), 2.15 (3H, s, (C=O)C$\underline{H}_3$), 1.21 (3H, t, J = 4.7 Hz, C$\underline{H}_3$); δ_c (100 MHz, DMSO-d_6), 169.4 (C=O), 163.4 (C=O), 163.2, (C=O) 138.3 (q), 133.9 (CH), 132.3 (q), 129.1 (CH), 127.8 (CH), 124.1 (q), 123.9 (CH), 122.9 (q), 122.1 (q), 120.7 (CH), 35.1 (CH_2), 24.3 (C=OCH_3), 13.4 (CH_3) ; IR υ_{max} (cm^{-1}) 3295, 3129, 2975, 2935, 1699, 1665, 1655, 1628, 1596, 1565, 1509, 1465, 1428, 1378, 1348, 1329, 1277, 1262, 1240, 1164, 1131, 1090, 1061,1043, 1017, 979, 938, 908, 878, 821, 782, 762, 745, 736, 698, 654.

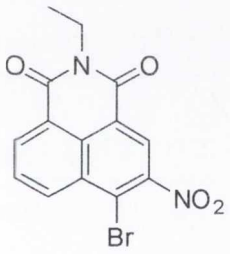
2-Ethyl-5-[(4-trifluoromethylphenyl)ureidocarbamoyl)]-benzo[*de*]iso-quinoline-1,3-dione (42)



Compound **41a** (0.380 g, 1.58 mmol) and 4-trifluoromethylphenyl isocyanate (0.296 g, 1.58 mmol) were refluxed in MeCN for 24 h. The precipitate was

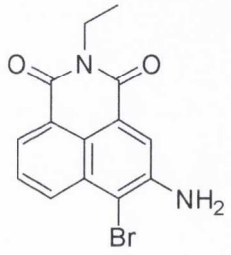
isolated by suction filtration to give a beige solid (0.515 g, 76%). m.p. 337-339 °C; Calculated for $C_{22}H_{17}N_3O_3F_3$: C, 61.83; H, 3.77; N, 9.83%; found: C, 61.65; H, 3.81; N, 9.65%; HRMS (ES^+): Calculated for $C_{22}H_{17}N_3O_3F_3$ $[M+H]^+$: 428.1222; found: 428.1242; δ_H (600 MHz, DMSO-d_6), 9.41 (1H, s, N$\underline{H}_{urea}$), 9.22 (1H, s, N$\underline{H}_{urea}$), 8.48 (2H, d, J = 8.2 Hz, Naph-$\underline{H}_{7,5}$), 8.27 (2H, d, J = 7.5 Hz, Naph-$\underline{H}_{2,4}$), 7.77-7.70 (3H, m, Naph-$\underline{H}_6$, Ar-H), 7.64 (2H, d, J = 7.9 Hz, Ar-$\underline{H}$), 4.05 (2H, q, J = 6.7 Hz, NCH_2), 1.22 (3H, t, J = 6.7 Hz, CH_3); δ_c (150 MHz, DMSO-d_6) 163.4 (C=O), 163.2 (C=O), 152.6 (q), 143.4 (q), 138.5 (q), 133.6 (CH), 132.4 (q), 128.7 (CH), 127.7 (CH), 126.3 (CH), 124.9 (q, $J_{^{13}C^{19}F}$ = 270 Hz), 123.7 (q), 123.6 (CH) , 122.8 (q), 122.4 (CF_3, $J_{^{13}C^{19}F}$ = 32 Hz), 122.1 (q), 120.1 (CH), 119.8 (CH), 35.0 (CH_2), 13.4 (CH_3); δ_N (60 MHz, DMSO-d_6), 111.0, 111.6; IR υ_{max} (cm^{-1}) 3371, 3304, 1656, 1555, 1326, 1231, 1154, 1110, 1068, 1055, 1017, 843, 787, 686.

6-Bromo-2-ethyl-5-nitro-benzo[de]isoquinoline-1,3-dione (43)



Compound **43** was synthesised by gradually treating **35** (4.0 g, 13.5 mmol) in sulphuric acid (26.5 ml) at room temperature with a mixture of nitric acid (0.66 mL) and sulphuric acid (13.4 mL) and the reaction mixture was stirred for 30 minutes at room temperature. The reaction mixture was precipitated into ice and the product was isolated by suction filtration. The residue was recrystallised twice from EtOH to give **43** as a pale yellow solid (2.5 g, 54%). m.p. 178-179 °C; HRMS (ES^+): Calculated for $C_{14}H_{10}BrN_2O_4$ $[M+H]^+$: 348.9745; found 348.9825; δ_H (400 MHz, DMSO-d_6), 8.81 (1H, s, Naph-$\underline{H}_2$), 8.75 (1H, d, J = 8.5 Hz, Naph-$\underline{H}_7$), 8.69 (1H, d, J = 7.5 Hz, Naph-$\underline{H}_5$), 8.14 (1H, t, J = 8.0 Hz, Naph-$\underline{H}_6$), 4.07 (2H, q, J = 7.0 Hz, $C\underline{H}_2$), 1.22 (3H, t, J = 7.0 Hz, $C\underline{H}_3$); δ_c (100 MHz, DMSO-d_6), 162.1 (C=O), 161.4 (C=O), 149.0 (q), 134.2 (CH), 133.3 (CH), 130.6 (CH), 130.2 (q), 128.2 (q), 124.2 (CH), 123.4 (q), 122.9 (q), 120.8 (q), 35.2 (CH_2), 12.9 (CH_3); IR υ_{max} (cm^{-1}) 1654, 1534, 1330, 1242, 784.

5-amino-6-bromo-2-ethyl-1*H*-benzo[de]isoquinoline-1,3(2*H*)-dione (44)



Compound **44** was synthesised by treating **43** (0.6 g, 1.72 mmol) with a mixture of stannous chloride (1.94 g, 8.59 mmol) and concentrated hydrochloric acid (2 mL). The reaction mixture was stirred at 85 °C for 1h. The suspension was cooled and collected by suction filtered to yield **44** as a yellow solid (0.48 g, 88%), after purification by column chromatography on flash silica (using gradient elution, DCM/MeOH 0→10%). m.p. 146-147 °C; HRMS (ES^+):

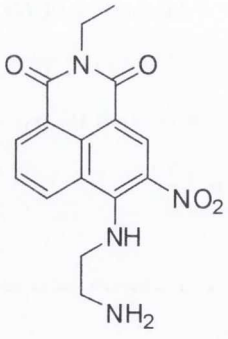
Calculated for $C_{14}H_{11}BrN_2O_2$ $[M+H]^+$: 319.0096; found 319.0082; δ_H (400 MHz, DMSO-d_6), 8.23 (1H, d, J = 8.5 Hz Naph-$\underline{H}_7$), 8.17 (1H, d, J = 7.0 Hz, Naph-$\underline{H}_5$), 8.13 (1H, s, Naph-$\underline{H}_2$), 7.81 (1H, t, J = 7.5 Hz, Naph-$\underline{H}_6$), 6.34 (2H, br s, N$\underline{H}_2$), 4.04 (2H, q, J = 7.0 Hz, C$\underline{H}_2$), 1.19 (3H, t, J = 7.0 Hz, C$\underline{H}_3$); δ_c (100 MHz, DMSO-d_6), 163.1 (C=O), 162.8 (C=O), 145.4 (q), 133.6, 129.8 (CH), 128.5 (CH), 125.8 (CH), 122.4 (CH), 122.1 (q), 121.8 (q), 120.5 (q), 106.5 (q), 34.8 (CH_2), 13.1 (CH_3); IR υ_{max} (cm^{-1}) 3351, 2750, 1630, 1321, 1241, 782.

N-(6-bromo-2-ethyl-1,3-dioxo-2,3-dihydro-1H-benzo[de]isoquinolin-5-yl)acetamide (45)



Compound **45** was synthesised by treating **44** (1.8 g, 5.64 mmol) in acetic acid (22.5 mL) with acetic anhydride (0.4 ml), which was then stirred at reflux for 6 hours. The suspension was cooled and collected by suction filtration to yield **45** as a white solid (1.35 g, 68%). m.p. 268-269 °C; HRMS (ES^+): Calculated for $C_{16}H_{13}BrN_2O_3Na$ $[M+Na]^+$ 383.0018; found 383.0007; δ_H (400 MHz, DMSO-d_6), 10.09 (1H, s, N$\underline{H}$), 8.65 (1H, s, Naph-$\underline{H}_2$), 8.54 (1H, d, J = 8.5 Hz, Naph-H_5), 8.48 (1H, d, J = 7.5 Hz, Naph-H_7), 7.95 (1H, t, J = 7.5 Hz, Naph-$\underline{H}_6$), 4.06 (2H, q, J = 7.0 Hz, NC$\underline{H}_2$), 2.22 (3H, s, (C=O)C$\underline{H}_3$), 1.21 (3H, t, J = 7.0 Hz, C$\underline{H}_3$); δ_c (100 MHz, DMSO-d_6), 169.2 (C=O), 162.7 (C=O), 162.4, (C=O) 136.3 (q), 132.6 (CH), 130.8 (q), 130.3 (CH), 128.0 (CH), 128.7 (CH), 125.3 (q), 123.7 (q), 122.6 (q), 121.7 (q), 34.9 (CH_2), 23.3 (CH_3), 13.0 (CH_3); IR υ_{max} (cm^{-1}) 3246, 1708, 1658, 1319, 1242, 787.

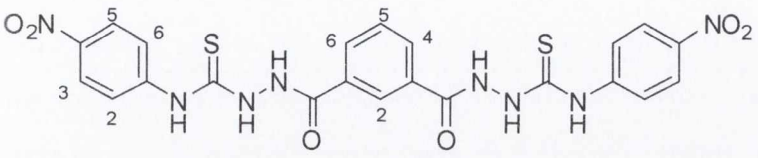
5-Nitro-6-bromo-2-ethyl-1*H*-benzo[de]isoquinoline-1,3(2*H*)-dione (48)



Compound **48** was synthesised by reacting **43** (0.468 g, 1.34 mmol) with 1,2-diaminoethane (0.120 g, 0.134 mL, 2.01 mmol) in $CHCl_3$ at room temperature for 3 h. A precipitate was formed, which was isolated by suction filtration. The residue was titurated in hot $CHCl_3$ and MeOH and then filtered to give **48** as a yellow solid, which was then dried under vacuum (1.35 g, 68%). m.p. > 300 °C; HRMS (ES^+): Calculated for $C_{16}H_{17}N_4O_4$ 329.1249 $[M+H]^+$; found 329.1250; δ_H (600 MHz, DMSO-d_6), 8.86 (1H, s, Naph-$\underline{H}_2$,), 8.85 (1H, d, J = 7.5 Hz, Naph-$\underline{H}_7$,), 8.50 (1H, d, J = 7.2 Hz, Naph-$\underline{H}_5$), 7.75 (1H, t, J = 7.8 Hz, Naph-$\underline{H}_6$), 5.06 (3H, br s, N$\underline{H}$, N$\underline{H}_2$), 4.05 (2H, q, J = 7.0 Hz, C$\underline{H}_2$CH$_3$), 3.67 (2H, br t, J = 5.5 Hz, C$\underline{H}_2$), 2.92 (2H, t, J = 5.7 Hz, C$\underline{H}_2$), 1.19 (3H, t, J = 7.0 Hz, C$\underline{H}_3$); δ_c (150 MHz, DMSO-d_6), 163.3 (C=O), 162.2 (C=O), 150.5 (q), 133.4 (CH), 132.6 (CH), 131.5 (q), 130.2 (CH), 128.7 (q), 125.8 (CH), 125.1 (q), 122.2 (q), 108.1(q), 51.7 (CH_2), 41.3 (CH_2),

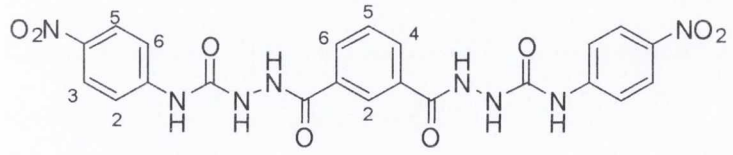
34.9 (CH_2), 13.4 (CH_3); IR υ_{max} (cm^{-1}) 3394, 3086, 2980, 2871, 1687, 1643, 1588, 1569, 1537, 1383, 1330, 1215, 1076, 764.

1,3–Bis-[4-nitrophenyl(thioureidocarbomoyl)]-Benzene (53)



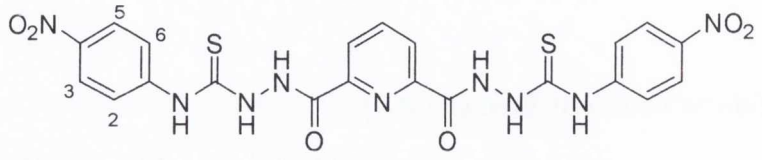
Compound **53** was synthesised according to **Procedure 2** using **51a** (0.20 g, 1.03 mmol) and 4-nitrophenyl isothiocyanate (0.37 g, 2.06 mmol) in MeCN (50 mL). A pale yellow solid was obtained (0.53 g, 92%). m.p. 206-208 °C; HRMS (ES^+): Calculated for $C_{22}H_{19}N_8O_6S_2$ $[M+H]^+$: 555.0869; found: 555.0891; δ_H (400 MHz, DMSO-d_6), 10.82 (2H, br s, N$\underline{H}_{amide}$), 10.22 (4H, br s, N$\underline{H}_{urea}$), 8.53 (1H, br s, $\underline{H}_2$-benz.), 8.22 (4H, d, J = 9.0 Hz, Ar-$\underline{H}_{3,5}$), 8.17 (2H, d, J = 7.5 Hz, $\underline{H}_{4,6}$-benz.), 7.91 (4H, br s, Ar-$\underline{H}_{2,6}$), 7.69 (1H, t, J = 7.5 Hz, $\underline{H}_5$-benz.); δ_C (100 MHz, DMSO-d_6), 180.8 (C=S), 165.4 (C=O), 145.7 (q), 143.6 (q), 132.8 (q), 131.1 (CH), 128.6 (CH), 127.9 (CH), 125.0 (CH), 123.6 (CH); δ_N (60 MHz, DMSO-d_6), 132.0, 128.2, 127.6; IR υ_{max} (cm^{-1}) 3290, 3122, 2965, 1668, 1615, 1579, 1597, 1556, 1507, 1416, 1333, 1300, 1235, 1178, 1139, 1112, 1014, 933, 894, 873, 849, 819, 780, 728, 702, 687.

1,3-Bis-[4-nitrophenyl(ureidocarbomoyl)-Benzene (52)



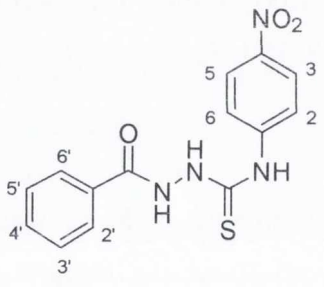
Compound **52** was synthesised according to **Procedure 2** using **51a** (0.10 g, 0.51 mmol) and 4- nitro-phenylisocyanate (0.16 g, 1.03 mmol) in MeCN (40 mL). A pale yellow solid was obtained (0.14 g, 70%). m.p. 235-238 °C; HRMS (ES^+): Calculated for $C_{22}H_{19}N_8O_8$ $[M+H]^+$: 523.1326; found: 523.1342; δ_H (600 MHz, DMSO-d_6), 10.52 (2H, br s, N$\underline{H}_{amide}$), 9.65 (2H, br s, N$\underline{H}_{urea}$), 8.65 (2H, br s, N$\underline{H}_{urea}$), 8.48 (1H, br s, $\underline{H}_2$-benz.), 8.19 (4H, d, J = 9.3 Hz, Ar-$\underline{H}_{3,5}$), 8.12 (2H, d, J = 7.6 Hz, $\underline{H}_{4,6}$-benz), 7.76 (4H, d, J = 8.2 Hz, Ar-$\underline{H}_{2,6}$), 7.68 (1H, t, J = 7.6 Hz, $\underline{H}_5$-benz); δ_C (150 MHz, DMSO-d_6), 165.8 (C=O), 155.3 (C=O), 146.4 (q), 141.1 (q), 132.7 (q), 130.6 (CH), 128.7 (CH), 125.0 (CH), 124.7 (CH) 117.8 (CH); δ_N (60 MHz, DMSO-d_6), 132, 128.2, 127.6; IR υ_{max} (cm^{-1}) 3315, 1717, 1661, 1619, 573, 1503, 1334, 1352, 1304, 1235, 1116, 869, 848, 748, 682.

2,6-Bis-[4-nitrophenyl(thioureidocarbomoyl)]-Pyridine (54)



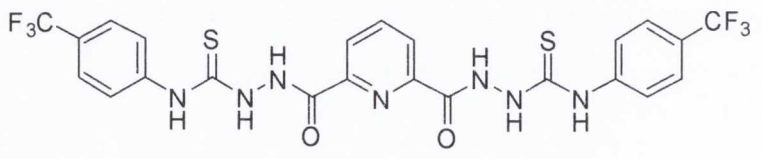
Compound **54** was synthesised according to **Procedure 2** using **51b** (0.281 g, 1.03 mmol) and 4-nitro- phenylisothiocyanate (0.518 g, 2.88 mmol) in MeCN (50 mL). A pale yellow solid was obtained (0.784 g, 98%). m.p. 203-205 °C; HRMS (ES^+): Calculated for $C_{21}H_{18}N_9O_6S_2$ [M+H]: 556.0821; found: 556.0822; δ_H (600 MHz, DMSO-d_6), 11.30 (2H, br s, N$\underline{H}_{amide}$), 10.37 (2H, br s, N$\underline{H}_{urea}$), 10.20 (2H, br s, N$\underline{H}_{urea}$), 8.31 (3H, br s, $\underline{H}_{py}$), 8.22 (4H, br s, Ar-$\underline{H}_{3,5}$), 7.92 (4H, br s, Ar-$\underline{H}_{2,6}$); δ_C (150 MHz, DMSO-d_6), 181.1 (C=S), 162.8 (C=O), 147.8 (q), 145.7 (q), 143.6 (q), 139.8 (CH), 125.6 (CH), 125.2 (CH), 123.9 (CH); δ_N (600 MHz, DMSO-d_6) 129.6, 127.7, 126.2; IR υ_{max} (cm^{-1}) 3128, 2962, 1704, 1597, 1549, 1506, 1469, 1345, 1278, 1219, 1157, 1002, 887, 851, 745, 698.

Benzoic acid, 2-[[(4-nitrophenyl)amino]thioxomethyl]hydrazide (55)



Benzohydrazide (0.069 g, 0.504 mmol) and 4-nitrophenyl isothiocyanate (0.091 g, 0.504 mmol) were stirred at room temperature in MeCN (30 mL) for 16h. The precipitate was isolated by suction filtration and washed with acetonitrile to give a white solid (0.118 g, 73%). m.p. 205-209°C; HRMS (ES^+): Calculated for $C_{14}H_{12}N_4O_3S$ $[M+Na]^+$: 339.0528; found 339.0528; δ_H (400 MHz, DMSO-d_6), 10.65 (1H, br s, N$\underline{H}_{amide}$), 10.17 (2H, br s, N$\underline{H}_{urea}$), 8.21 (2H, d, J = 6.0 Hz, Ar-$\underline{H}_{3,5}$), 7.96 (2H, d, J = 7.0 Hz, Ar-$\underline{H}_{2',6'}$), 7.90 (2H, d, J = 6.5 Hz, Ar-$\underline{H}_{2,6}$), 7.54 (3H, m, Ar-$\underline{H}_{3',4',5'}$); δ_C (100 MHz, DMSO-d_6), 181.1 (C=S), 166.3 (C=O) 146.1 (q), 143.7 (q), 132.6 (q), 132.3 (CH), 128.6 (CH), 128.2 (CH), 125.1 (CH), 123.8 (CH); δ_N (60 MHz, DMSO-d_6), 131.2, 128.7, 127.2; IR υ_{max} (cm^{-1}) 3299, 3183, 3146, 2972, 1665, 1623, 1595, 1587, 1574, 1551, 1495, 1330, 1291, 1224, 1176, 1160, 1112, 852, 842, 751, 700, 684.

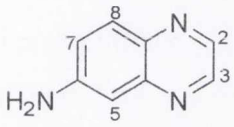
2,6–Bis-[4-trifluoromethylphenyl(thioureidocarbomoyl)]-Pyridine (56)



Compound **56** was synthesised according to **Procedure 2** using **51b** (0.150 g, 0.769 mmol) and 4-

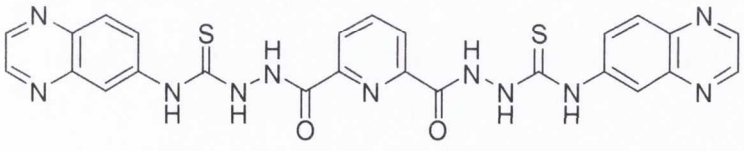
trifluoromethylphenyl isothiocyanate (0.312 g, 1.53 mol) in MeCN (50 mL), yielding **56** as a white solid (0.360 g, 77%). m.p. > 300°C; Calculated for $C_{23}H_{17}F_6N_7O_2S_2$: C, 45.92; H, 2.85; N, 16.30%; found: C, 45.79; H, 2.88; N, 16.10%; HRMS (ES^-): Calculated for $C_{23}H_{16}N_7O_2S_2F_6$ $[M-H]^-$: 600.0711; found: 600.0686; δ_H (400 MHz, DMSO-d_6), 11.30 (2H, br s, N<u>H</u>$_{amide}$), 10.24 (2H, br s, N<u>H</u>$_{urea}$), 10.06 (2H, br s, N<u>H</u>$_{urea}$), 8.21-8.17 (3H, m, <u>H</u>$_{py}$), 7.67-7.74 (8H, m, Ar-<u>H</u>); δ_C (100 MHz, DMSO-d_6), 181.1 (C=S), 162.8 (C=O), 147.7 (q), 142.9 (q), 139.6 (CH), 126.1 (CH), 125.5 (CH), 125.4 (CH), 124.2 (CF_3, $J_{^{13}C^{19}F}$ = 273.1 Hz), 122.2 (q); δ_N (60 MHz, DMSO-d_6), 129.3, 124.2, 126.6; δ_F (162 MHz DMSO-d_6); -61.0; IR υ_{max} (cm^{-1}) 3368, 3134, 2962, 1705, 1617, 1601, 1541, 1463, 1415, 1328, 1278, 1217, 1156, 1105, 1065, 1016, 1000, 931, 886, 838, 786, 745, 725, 685.

6-Amino-quinoxaline (59)[205]



6-Nitroquinoxaline (0.919 g, 6.33 mmol) was hydrogenated at room temperature under 1 atm H_2 with 10% Pd/C (0.091g) in MeOH for 4 h. The catalyst was filtered off and the MeOH was removed under reduced pressure to give a dark red/black solid. The solid was dissolved in water (20 mL) and basified to pH 8 using $NaHCO_3$. The aqueous phase was extracted with ethyl acetate (2 × 30 mL) and dried with $MgSO_4$. The solvent was removed under reduced pressure to give **59** as an orange solid (0.532 g, 73%). m.p. 158-160 °C (Lit. m.p.[221] 156-157 °C); HRMS (ES^+): Calculated for $C_8H_8N_3$ $[M+H]^+$: 146.0718; found: 146.0729; δ_H (400 MHz, DMSO-d_6), 8.60 (1H, br d, J = 1.9 Hz, Ar-<u>H</u>$_3$), 8.44 (1H, br d, J = 1.9 Hz, Ar-<u>H</u>$_2$), 7.74 (1H, d, J = 9.0 Hz, Ar-<u>H</u>$_8$), 7.23 (1H, dd, J = 9.0 and 2.5 Hz, Ar-<u>H</u>$_7$), 6.91 (1H, br s, J = 2.5 Hz, Ar-<u>H</u>$_5$), 6.08 (2H, br s, NH_2); δ_c (100 MHz, DMSO-d_6) 150.9 (q), 145.4 (CH), 145.3 (q), 140.1 (CH), 136.9 (CH), 130.1 (CH), 122.8 (CH), 105.4 (CH).

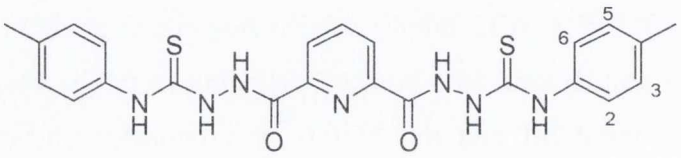
1,6–Bis-[6-aminoquinoxaline(thioureidocarbomoyl)]-Pyridine (57)



6-Aminoquinoxaline (0.200 g, 1.3 mmol) was stirred vigourously in water (5 mL). $CSCl_2$ (0.174 g, 1.5 mmol) was then added dropwise with stirring and the reaction mixture was stirred at room temperature for 2 h. The resulting orange solid was isolated by suction filtration and then added to a suspension of **51b** (0.258 g, 1.3 mmol) in MeCN (30 mL). The reaction mixture was refluxed for 16 h and the solid was then isolated by suction filtration. Minor impurities were removed by refluxing a suspension of the solid in EtOH

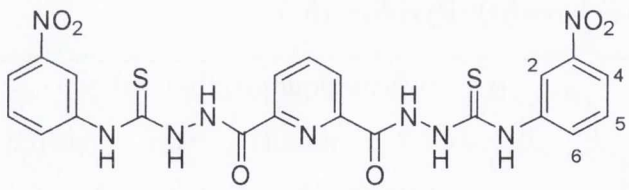
overnight. The compound was collected and dried by suction filtration, giving **57** as an orange solid (0.316 g, 80.8 %). m.p. 214-216 °C; HRMS (ES^+): Calculated for $C_{23}H_{20}N_{11}O_2S_2$ $[M+H]^+$: 570.1243; found: 570.1254; δ_H (600 MHz, DMSO-d_6), 11.38 (2H, br s, N$\underline{H}_{amido}$), 10. 32 (4H, br s, N$\underline{H}_{urea}$), 8.90 (2H, br d, J = 2.0 Hz, C$\underline{H}_{quin}$), 8.87 (2H, br d, J = 2.0 Hz, C$\underline{H}_{quin}$), 8.40-8.20 (5H, br m, C$\underline{H}_{py}$, C$\underline{H}_{quin}$), 8.04-8.02 (4H, br m, C$\underline{H}_{quin}$); δ_C (150 MHz, DMSO-d_6), 181.1 (C=S), 162.8 (C=O), 147.8 (q), 145.7 (CH), 144.8 (CH), 142.1 (q), 140.6 (q), 139.9 (CH), 139.6 (q), 129.1 (CH), 128.0 (CH), 125.0 (CH), 122.6 (CH); δ_N (60 MHz, DMSO-d_6), 129.4, 126.5, 124.0; IR υ_{max} (cm^{-1}) 3147, 2943, 1699, 1619, 1521, 1470, 1367, 1304, 1267, 1219, 1151, 1024, 999, 949, 889, 861, 831, 730, 650, 591, 545, 525.

2,6–Bis-[6-tolyl (thioureidocarbomoyl)]-Pyridine (27b)



Compound **51b** (0.150 g, 0.770 mmol) and *p*-tolylphenyl isothiocyanate (0.453 g, 3.03 mmol) were refluxed together in MeCN (50 mL) for 16 h. The precipitate was isolated by suction filtration and washed with acetonitrile to give **27b** as a white solid (0.210 g, 55%). m.p. decomposed > 300 °C (Lit. m.p.[137] decomposed >200 °C); HRMS (ES^+): Calculated for $C_{23}H_{24}N_7O_2S_2$ $[M+H]^+$: 494.1433; found: 494.1454; δ_H (400 MHz, DMSO-d_6), 11.24 (2H, br s, N$\underline{H}_{amide}$), 9.91 (2H, br s, N$\underline{H}_{urea}$), 9.79 (2H, br s, N$\underline{H}_{urea}$), 8.23 (3H, s, C$\underline{H}_{py}$), 7.28 (4H, br s, Ar-C$\underline{H}_{2,6}$) 7.12 (4H, br d, J = 8.0 Hz, Ar-C$\underline{H}_{3,5}$), 2.28 (6H, s, CH_3); δ_C (100 MHz, DMSO-d_6), 181.1 (C=S), 162.3 (C=O), 148.2 (q), 139.2 (CH), 136.4 (q), 134.2 (q), 128.3 (CH), 125.5 (CH), 124.6 (CH), 20.5 (CH_3); δ_N (60 MHz, DMSO-d_6), 129.5, 126.3, 121.5.

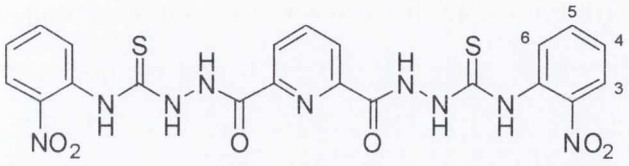
1,6–Bis-[3-nitrophenyl(thioureidocarbomoyl)]-Pyridine (61)



Compound **61** was synthesised according to **Procedure 2** using **51b** (0.053 g, 0.275 mmol) and 3-nitro-phenyl isothiocyanate (0.099 g, 0.551 mmol) in MeCN (40 mL). A white solid was obtained (0.120 g, 78%). m.p. 222-223 °C; Calculated for $C_{21}H_{17}N_9O_6S_2$: C, 45.40; H, 3.08; N, 22.69%; found: C, 45.10; H, 3.06; N, 22.45%. HRMS (ES^-): Calculated for $C_{21}H_{16}N_9O_6S_2$ $[M-H]^-$: 554.0665; found: 554.0651; δ_H (600 MHz, DMSO-d_6), 11.32 (2H, br s, N$\underline{H}_{amide}$), 10. 30 (2H, br s, N$\underline{H}_{urea}$), 10.16 (2H, br s, N$\underline{H}_{urea}$), 8.46 (2H, br s, Ar-$\underline{H}_2$), 8.31-8.25 (3H, m, $\underline{H}_{py}$), 8.02 (4H, br s, Ar-$\underline{H}_{4,6}$), 7.62

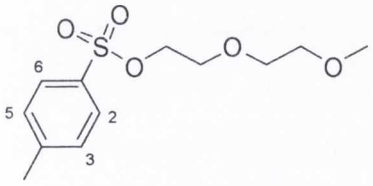
(2H, t, J = 8.04 Hz, Ar-$\underline{H}_5$); δ_C (150 MHz DMSO-d_6), 181.0 (C=S), 162.8 (C=O), 147.8 (q), 149.9 (q), 140.2 (q), 140.1 (CH), 131.9 (CH) 129.6 (CH), 125.3 (CH), 120.0 (CH), 119.8 (CH); IR υ_{max} (cm^{-1}) 3129, 2956, 1702, 1524, 1473, 1435, 1343, 1284, 1267, 1220, 1159, 1001, 890, 862, 806, 746, 670, 689.

2,6–Bis-[2-nitrophenyl(thioureidocarbomoyl)]-Pyridine (62)



Compound **62** was synthesised according to **Procedure 2** using **51b** (0.102 g, 0.528 mmol) and 2-nitrophenylisothiocyanate (0.369 g, 2.11 mmol) in MeCN (50 mL). A bright yellow solid was obtained (0.197 g, 67.2%). m.p. 201-204 °C; Calculated for $C_{21}H_{17}N_9O_6S_2$ C, 45.40; H, 3.08; N, 22.69%; found: C, 45.16; H, 3.06; N, 22.39%; HRMS (ES^-): Calculated for $C_{21}H_{16}N_9O_6S_2$ $[M-H]^-$: 554.0665; found: 554.0687; δ_H (600 MHz, DMSO-d_6), 11.44 (2H, br s, N$\underline{H}_{amide}$), 10.30 (2H, br s, N$\underline{H}_{urea}$), 10.13 (2H, s, N$\underline{H}_{urea}$), 8.32-8.26 (3H, m, $\underline{H}_{py}$), 8.00 (2H, d, J = 7.3 Hz, Ar-$\underline{H}_3$), 7.74-7.67 (4H, m, Ar-$\underline{H}_{5,6}$), 7.46 (2H, t, J = 8.1 Hz, Ar-$\underline{H}_4$); δ_C (150 MHz, DMSO-d_6), 181.5 (C=S), 163.0 (C=O), 147.8 (q), 144.7 (q), 139.8 (CH), 133.5 (q), 133.3 (CH), 130.1 (CH), 126.9 (CH), 125.4 (CH), 124.7 (CH); δ_N (60 MHz, DMSO-d_6), 129.1, 124.1, 119.4; IR υ_{max} (cm^{-1}) 3300, 3205, 3103, 1666, 1604, 1584, 1558, 1501, 1480, 1457, 1443, 1426, 1336, 1261, 1145, 1074, 1000, 959, 915, 875, 843, 788, 754, 731, 712, 671, 641, 620, 543.

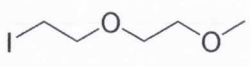
2-(2-Methoxyethoxy)ethyl 4-tosylate (63)[211]



Diethylene glycol monomethyl ether (10.0 g, 83.2 mmol, 9.8 mL) in THF (30 mL) was added to a solution of NaOH (4.9 g, 124 mmol) in H_2O (50 mL) at 0 °C. Tosylchloride (17.4 g, 91.5 mmol) was added to the solution and the mixture was allowed to warm to room temperature. The reaction was then left stirring for 2 days. The THF was removed under reduced pressure and the aqueous solution was extracted with $CHCl_3$ and dried over $MgSO_4$. The solvent was removed under reduced pressure to give **63** as a colourless oil (11.3 g, 50 %); HRMS (ES^+): Calculated for $C_{12}H_{18}O_5Na$ $[M+Na]^+$: 297.0773; found: 297.0775; δ_H (400 MHz, $CDCl_3$), 7.82 (2H, d, J = 8.5 Hz, Ar-$\underline{H}_{2,6}$), 7.36 (2H, J = 8.0 Hz, Ar-$\underline{H}_{3,5}$), 4.19 (2H, t, J = 5.0 Hz, C$\underline{H}_2$), 3.71 (2H, t, J = 5.0 Hz, C$\underline{H}_2$), 3.61-3.58 (2H, m, C$\underline{H}_2$), 3.51-3.48 (2H, m, C$\underline{H}_2$), 3.37 (3H, s, OC$\underline{H}_3$), 2.47 (3H, s, C$\underline{H}_3$); δ_C (100 MHz, $CDCl_3$), 144.3 (q), 132.4 (q), 129.3 (CH), 127.5 (CH),

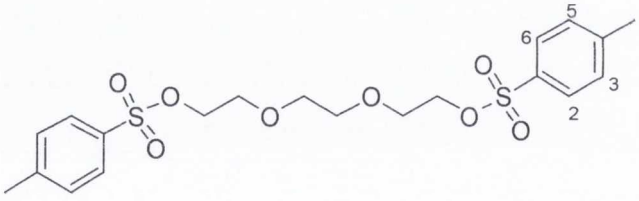
71.3 (CH_2), 70.2 (CH_2), 68.7 (CH_2), 68.2 (CH_2), 58.6 (OCH_3), 21.2 (CH_3); IR υ_{max} (cm^{-1}) 2879, 1597, 1451, 1352, 1174, 917, 815, 773, 662.

1-Iodo-2-(2-methoxyethoxy)ethane (64)[211]



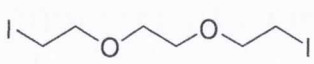
Compound **63** (11.22 g, 40.8 mmol) and NaI (8.63 g, 57.6 mmol) were refluxed in acetone (15 mL) for 16 h. The white precipitate which formed was removed by suction filtration and the solvent was removed under reduced pressure. The residue was then dissolved in 50 mL of $CHCl_3$ and washed with H_2O (2 × 10 mL), brine (10 mL) and dried over $MgSO_4$. The solvent was removed under reduced pressure to give **64** as an orange/brown oil (7.32 g, 77%); HRMS (ES^+): Calculated for $C_5H_{11}O_2INa$ $[M+Na]^+$: 252.9702; found: 252.9693; δ_H (400 MHz, $CDCl_3$), 3.78 (2H, t, J = 7.0 Hz, C$\underline{H}_2$CH$_2$I), 3.69-3.66 (2H, m, C$\underline{H}_2$), 3.59-3.57 (2H, m, C$\underline{H}_2$OCH$_3$), 3.41 (3H, s, OC$\underline{H}_3$), 3.29 (2H, t, J = 7.2 Hz, C$\underline{H}_2$I); δ_C (100 MHz, $CDCl_3$), 72.0 (CH_2), 71.8 (CH_2), 70.1(CH_2), 59.1 (OCH_3), 2.7 (CH_2I); IR υ_{max} (cm^{-1}) 2874, 1453, 1353, 1197, 1092, 1031, 977, 849.

Di-(Tosyl-ethoxy)ethane (65)[212]



Di-(hydroxy-ethoxy)ethane (54.06 g, 0.36 mol), was added to a solution of NaOH (39.99 g, 0.99 mol) in H_2O (150 mL) at 0 °C. Tosylchloride (146.08 g, 0.77 mol) in THF (200 mL) was added dropwise over 4h. The reaction was left stirring for a further 3 h. At this point a white precipitate was visible. The suspension was poured onto an ice water mixture. Toluene (300 mL) was then added and the precipitate was isolated by filtration yielding a white crystalline solid (134.04 g, 81%); m.p. 77-79 °C (Lit m.p.[222] 80-81 °C); HRMS (ES^+): Calculated for $C_{20}H_{26}O_8S_2Na$ $[M+Na]^+$: 481.0967; found: 481.0966; δ_H (400 MHz, $CDCl_3$), 7.80 (4H, d, J = 8.0 Hz, Ar-$\underline{H}_{2,6}$), 7.35 (4H, s, J = 8.0 Hz, Ar-$\underline{H}_{3,5}$), 4.14 (4H, t, J = 4.6 Hz, C$\underline{H}_2$), 3.66 (4H, t, J = 4.8 Hz, C$\underline{H}_2$), 3.53 (4H, s, C$\underline{H}_2$), 2.45 (6H, s, C$\underline{H}_3$). δ_C (100 MHz, $CDCl_3$), 144.4 (q) 132.4 (q), 129.4 (CH), 127.4 (CH); 70.2 (CH_2), 68.7 (CH_2), 68.2 (CH_2), 21.2 (CH_3).

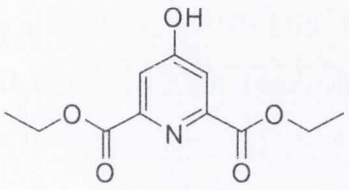
Di-(Iodo-ethoxy)ethane (66)[211]



Compound **65** (3.34 g, 2.18 mmol) and NaI (1.64 g, 3.27 mmol) were refluxed in acetone (50 mL) for 16 h. The white precipitate

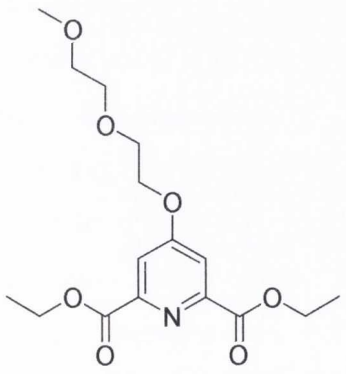
which formed was removed by suction filtration and the solvent was removed under reduced pressure. The residue was dissolved in 50 mL of $CHCl_3$ and then washed with H_2O (2 × 20 mL), brine (20 mL) and dried over $MgSO_4$. The solvent was removed under reduced pressure to give **66** as an orange/yellow liquid (1.40 g, 53 %); HRMS (ES^+): Calculated for $C_6H_{12}O_2I_2Na$ $[M+Na]^+$: 392.8825; found: 392.8820; δ_H (400 MHz, $CDCl_3$), 3.79 (4H, t, J = 7.0 Hz, C$\underline{H}_2$), 3.69 (4H, br s, C$\underline{H}_2$), 3.29 (4H, t, J = 7.0 Hz, C$\underline{H}_2$); δ_C (100 MHz, $CDCl_3$) 71.5 (CH_2) 69.7 (CH_2), 2.4 (CH_2I); IR υ_{max} 2864, 1722, 1460, 1412, 1350, 1262, 1188, 1168, 1089.

Diethyl 4-hydroxypyridine-2,6-dicarboxylate (67)[173]



4-Hydroxypyridine-2,6-dicarboxylic acid (2.00 g, 10.9 mmol) and H_2SO_4 (7.81 g, 79.7 mmol) were refluxed together in EtOH for 4 h. The EtOH was removed under vacuum and the residue was neutralised using $NaHCO_3$. The aqueous solution was extracted with CH_2Cl_2. The organic layer was then dried over $MgSO_4$ and the solvent was removed under vacuum to give a pale yellow oil, **67**, which solidified upon drying under vacuum (1.59 g, 61%). m.p. 120-122 °C (Lit. m.p[174] 122-124 °C); HRMS (ES^+): Calculated for $C_{11}H_{13}NO_5Na$ $[M+Na]^+$: 262.0691; found: 262.0685; δ_H (400 MHz, $CDCl_3$), 7.32 (2H, br s, $\underline{H}_{py}$), 4.48 (4H, q, J = 7.3, C$\underline{H}_2$), 1.44 (6H, t, J = 7.3, C$\underline{H}_3$); δ_C (100 MHz, $CDCl_3$), 162.0 (C=O), 150.1 (C-OH), 138.9 (q), 119.8 (Ar-CH), 63.4 (CH_2), 14.0 (CH_3); IR υ_{max} (cm^{-1}) 3425 , (OH), 2974, 2676, 1728, 1600, 1569, 1444, 1366, 1236, 1160, 1103, 1018, 995, 888, 865, 788, 703.

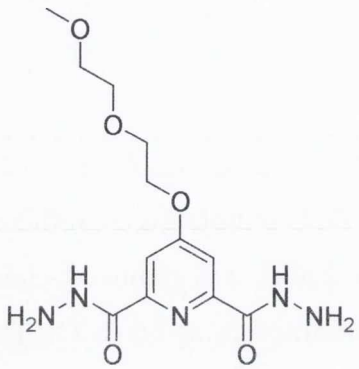
Diethyl 4-(2-(2-methoxyethoxy)ethoxy)pyridine-2,6-dicarboxylate (68)



Compound **67** (0.300 g, 1.26 mmol) and anhydrous K_2CO_3 (0.174 g, 1.26 mmol) were stirred in anhydrous DMF (9 mL) at 25°C for 0.5 h. Compound **64** (0.264 g, 1.14 mmol) was added and the solution was heated at 50 ° C for 50 h. The solvent was then removed under reduced pressure and DCM (20 mL) was added to the residue. The organic layer was washed with 1% acetic acid (5 mL) and H_2O (5 mL). The organic layer was dried over $MgSO_4$ and the solvent was removed under reduced pressure to give **69** as a white solid (0.263 g, 67%); m.p. decomposed at 200-203 °C; HRMS (ES^+): Calculated for $[M+H]^+$: $C_{16}H_{24}NO_7$: 342.1548; found: 342.1553; δ_H (400 MHz, $CDCl_3$),

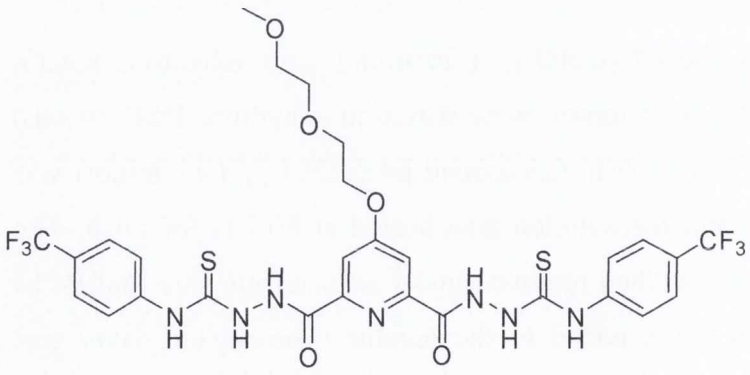
7.82 (2H, s, C$\underline{H}_{py}$), 4.48 (4H, q, J = 7.0 Hz, C$\underline{H}_{2ester}$), 4.33 (2H, t, J = 4.5 Hz, C$\underline{H}_2$), 3.93 (2H, t, J = 4.5 Hz, C$\underline{H}_2$), 3.73-3.72 (2H, m, C$\underline{H}_2$), 3.59 (2H, t, J = 4.5 Hz, C$\underline{H}_2$) 3.40 (3 H, s, OC$\underline{H}_3$), 1.47 (6 H, t, J = 7.0 Hz, C$\underline{H}_3$); δ_C (100 MHz, $CDCl_3$), 166.7 (q), 162.5 (C=O), 150.1 (q), 114.4 (CH), 71.9 (CH_2), 70.9 (CH_2), 69.1 (CH_2), 68.2 (CH_2), 62.4 (OCH_2), 59.1 (OCH_3), 14.2 (CH_3).

4-(2-(2-Methoxyethoxy)ethoxy)pyridine-2,6-dicarbohydrazide (69)



Compound **68** (0.263 g, 0.770 mmol) and hydrazine monohydrate (0.197 g, 6.16 mmol, 0.19 mL) were stirred at reflux in EtOH (40 mL) overnight. The resulting precipitate was isolated by suction filtration and washed with EtOH (2 × 20 mL) to give **69** as a white solid (0.094 g, 51%). m.p. 137-140 °C; HRMS (ES^+): Calculated for $C_{12}H_{19}N_5O_5Na$ $[M+Na]^+$: 336.1284; found: 336.1278; δ_H (400 MHz, DMSO-d_6), 10.60 (2H, br s, N$\underline{H}_{amide}$), 7.60 (2H, s, C$\underline{H}_{py}$), 4.62 (4H, br s, N$\underline{H}_2$), 4.32 (2H, t, J = 4.1 Hz, C$\underline{H}_2$), 3.77 (2H, t, J= 4.5 Hz C$\underline{H}_2$), 3.60-3.58 (2H, m, C$\underline{H}_2$), 3.46-3.43 (2H, m, C$\underline{H}_2$), 3.23 (3H, s, OC$\underline{H}_3$); δ_c (400 MHz, DMSO-d_6), 166.9 (q), 161.6 (C=O), 150.5 (q), 109.6 (CH), 71.2 (CH_2), 69.7 (CH_2), 68.4 (CH_2), 68.0 (CH_2), 58.0 (CH_3); IR υ_{max} (cm^{-1}) 3489, 3321, 3100, 2904, 1651, 1596, 1536, 1511, 1442, 1365, 1348, 1285, 1257, 1165, 1135, 1112, 1096, 1048, 996, 933, 880, 826, 746, 688.

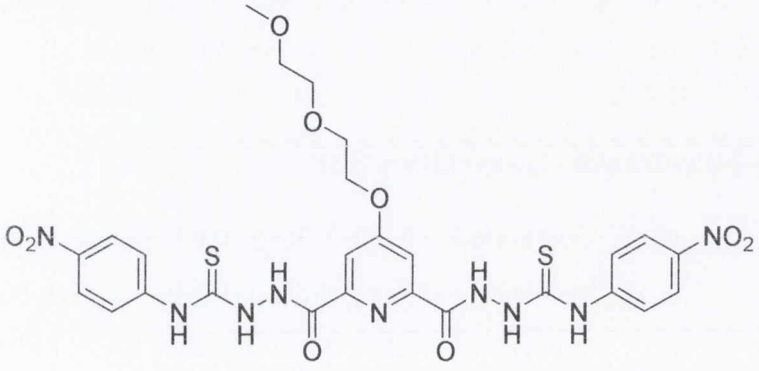
4-(2-(2-Methoxyethoxy)ethoxy)-2,6–Bis-[4-trifluoromethylphenyl (thioureidocarbomoyl)]-Pyridine (70)



Compound **70** was synthesised according to **Procedure 2** using **69** (0.113 g, 0.360 mmol) and 4-trifluormethylphenyl isothiocyanate (0.144 g, 0.720 mmol) in MeCN (20 mL). A white solid was obtained (0.172 g, 66.4%); m.p. decomposed at 200-212 °C; Calculated for $C_{28}H_{27}F_6N_7O_5S_2$: C, 46.73 H, 3.78 N, 13.57%; found C, 46.43; H, 3.69; N, 13.57%; HRMS ($MALDI^+$): Calculated for $C_{28}H_{28}N_7O_5F_6S_2$ $[M+H]^+$: 720.1498; found: 720.1533; δ_H (400 MHz, DMSO-d_6), 11.25 (2H, br s, N$\underline{H}_{amide}$), 10.19 (2H, br s, N$\underline{H}_{urea}$), 10.04 (2H, br s, N$\underline{H}_{urea}$), 7.67 – 7.74 (10H, br m, Ar-H), 4.39

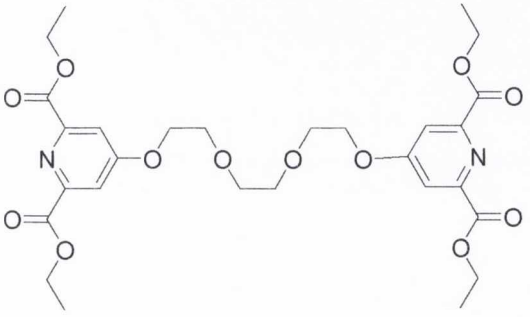
(2H, br s, C$\underline{H}_2$), 3.80 (2H, br s, C$\underline{H}_2$), 3.60 (2H, m, C$\underline{H}_2$), 3.46 (2H, m, C$\underline{H}_2$), 3.24 (3H, s, OC$\underline{H}_3$); δ_C (100 MHz, DMSO-d_6), 181.5 (C=S), 167.4 (q), 162.9 (C=O), 150.2 (q), 143.2 (q), 126.0 (CH), 125.5 (CH), 125.3 (CH), 124.6 (CF_3, $J_{^{13}C^{19}F}$ = 273.1 Hz), 122.5 (q), 111.3 (CH), 71.5 (CH_2), 70.5 (CH_2), 68.8 (CH_2), 58.3 (OCH_3); δ_F (376 MHz, DMSO-d_6), -61.0 (C$\underline{F}_3$); IR υ_{max} (cm^{-1}) 3139, 2947, 1711, 1602, 1583, 1479, 1321, 1277, 1108, 1066, 892, 839.

4-(2-(2-Methoxyethoxy)ethoxy)-2,6–Bis-[4-nitrophenyl (thioureidocarbomoyl)]-Pyridine (71)



Compound **71** was synthesised according to **Procedure 2** using **69** (0.113 g, 1.03 mmol) and 4-nitrophenyl isothiocyanate (0.518 g, 2.88 mmol) in MeCN (20 mL). A pale yellow solid was obtained (0.784 g, 98%). m.p. 188-190 °C. Calculated for $C_{29}H_{27}N_9O_9S_2$: C, 46.35; H, 4.04; N, 18.71%; found: C, 46.19; H, 3.93; N, 18.72%; HRMS (ES^+): Calculated for $C_{26}H_{27}N_9O_9S_2Na$ $[M+Na]^+$; 696.1271; found: 696.1240; δ_H (400 MHz, DMSO-d_6), 11.38-11.25 (2H, br m, N$\underline{H}_{amide}$), 10.68-10.22 (4H, br m, N$\underline{H}_{urea}$), 8.20 (4H, br s, Ar-$\underline{H}$), 7.90 (4H, br s, Ar-$\underline{H}$), 7.75 (2H, br s, $\underline{H}_{py}$), 4.39 (2H, br s, C$\underline{H}_2$,), 3.80 (2H, br s, C$\underline{H}_2$), 3.61 (2H, m, C$\underline{H}_2$), 3.46 (2H, m, C$\underline{H}_2$), 3.24 (3H, s, OC$\underline{H}_3$); δ_C (100 MHz, DMSO-d_6), 181.1 (C=S), 167.6 (q), 163.1 (C=O), 155.6 (q), 150.2 (q), 146.0 (q), 125.3 (CH), 124.0 (CH), 111.5 (CH), 71.7 (CH_2), 70.2 (CH_2), 68.9 (CH_2), 68.8 (CH_2), 58.5 (CH_3); IR υ_{max} (cm^{-1}); 3215, 2933, 1689, 1596, 1548, 1505, 1411, 1336, 1271, 1211, 1146, 1109, 1041, 996, 928, 878, 851, 775, 746, 698.

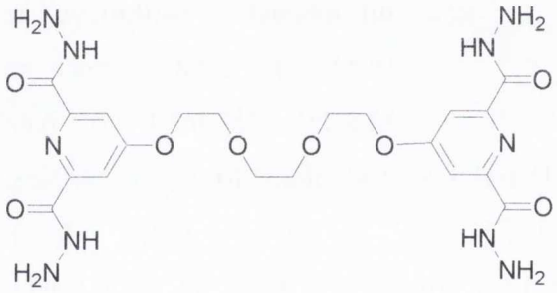
4,4'-((Ethoxy)-ethoxy)ethyl)bis-[diethylester-2,6-pyridine] (72)



Compound **67** (0.200 g, 0.836 mmol) and anhydrous K_2CO_3 (0.115 g, 0.836 mmol) were stirred in anhydrous DMF (60 mL) at 25 °C for 0.5 h. Compound **66** (0.154 g, 0.418 mmol) was added and the solution was heated at 50 ° C for 50 h. The solvent was then removed under

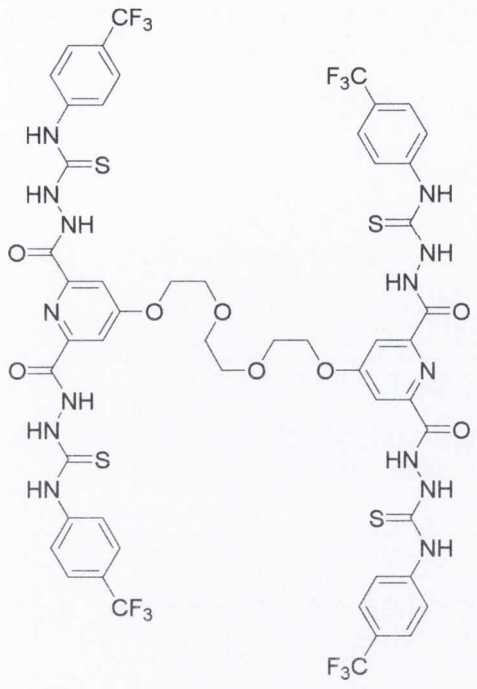
reduced pressure and DCM (50 mL) was added to the residue. The organic layer was washed with 1% acetic acid (25 mL) followed by H_2O (25 mL). The organic layer was dried with $MgSO_4$ and the solvent was removed under reduced pressure to give a yellow oil. The crude product was recrystallised from EtOH giving **72** as a white solid (0.147 g, 41%); m.p. 75-76 °C; HRMS (ES^+): Calculated for $C_{28}H_{36}N_2O_{12}Na$ $[M+Na]^+$: 615.2166; found: 615.2169. δ_H (400 MHz, $CDCl_3$), 7.78 (4H, s, C<u>H</u>$_{py}$), 4.42 (8H, q, J = 7.0 Hz, C<u>H</u>$_2$OCH$_3$), 4.28 (4H, t, J = 4.5 Hz, C<u>H</u>$_2$), 3.88 (4H, t, J = 4.4 Hz, C<u>H</u>$_2$), 3.72 (4H, s, C<u>H</u>$_2$), 1.41 (12 H, t, J = 7.2 Hz, C<u>H</u>$_3$); δ_C (100 MHz, $CDCl_3$), 166.7 (q), 164.6 (C=O), 150.1 (q), 114.4 (CH), 70.9 (CH_2), 69.2 (CH_2), 68.2 (CH_2), 62.4 (CH_2), 14.1 (CH_3); IR υ_{max} (cm^{-1}) 3076, 2983, 2933, 2905, 1742, 1706, 1594, 1567, 1478, 1435, 1369, 1371, 1342, 1328, 1244, 1230, 1158, 1134, 1102, 1067, 1023, 994, 938, 887, 866, 817, 786, 732, 701;

4,4'-((Ethoxy)-ethoxy)ethyl)bis-[dihydrazide-2,6-pyridine] (73)



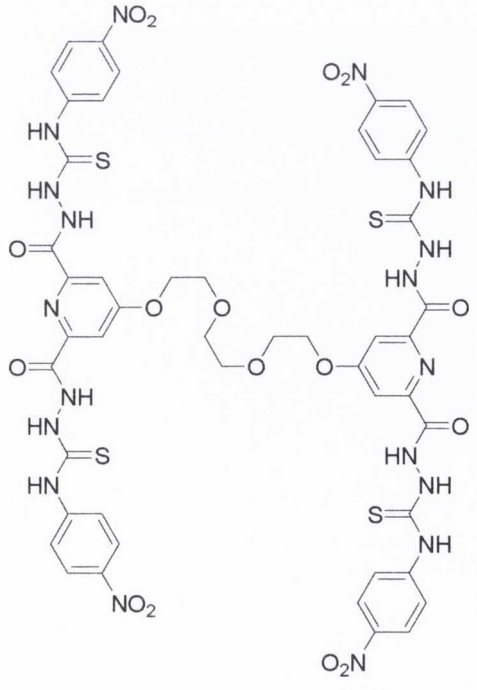
Compound **72** (0.500 g, 0.84 mmol) and hydrazine monohydrate (0.540 g, 16.86 mmol) were refluxed in anhydrous EtOH (300 mL) for 2 days. The white precipitate was collected by suction filtration giving **73** as a white solid (0.367 g, 81%). m.p. decomposed at 200-203 °C. δ_H (400 MHz, DMSO-d_6), 10.59 (4H, br s, N<u>H</u>$_{amide}$), 7.59 (4H, s, C<u>H</u>$_{py}$), 4.61 (8H, br s, N<u>H</u>$_2$), 4.32 (4H, br s, C<u>H</u>$_2$), 3.78 (4H, br s, C<u>H</u>$_2$), 3.62 (4H, s, C<u>H</u>$_2$); δ_C (100 MHz, DMSO-d_6), 167.4 (q), 162.1 (C=O), 150.9 (q), 110.1 (CH), 70.4 (CH_2), 69.0 (CH_2), 68.5 (CH_2); δ_N (60 MHz, DMSO-d_6), 129.6, 135.6; IR υ_{max} (cm^{-1}) 3304 , 3078, 2929, 1654, 1587, 1520, 1434, 1374, 1352, 1322, 1244, 1170, 1124, 1109, 1062, 1050, 992, 946, 912, 889, 823, 747.

4,4'-((Ethoxy)-ethoxy)ethyl) 2,6–Bis-[4-trifluoromethylphenyl(thioureidocarbomoyl)]-Pyridine] (74)



Compound **73** (0.059 g, 0.114 mmol) and 4-trifluoromethyl-phenyl isothiocyanate (0.089 g, 0.447 mmol) were refluxed in MeCN (5 mL) for 20 h. The resulting precipitate was collected and dried by suction filtration, giving **74** as a white solid (0.101 g, 68 %). m.p. > 300 °C; HRMS (ES^+): Calculated for $C_{52}H_{45}N_{14}O_8F_{12}S_4$ $[M+H]^+$: 139.2236; found 139.2284; δ_H (400 MHz, DMSO-d_6), 10.99 (4H, br s, N<u>H</u>$_{amide}$), 10.27 (4H, br s, N<u>H</u>$_{urea}$), 10.11 (4H, br s, N<u>H</u>$_{urea}$), 7.67–7.55 (20H, br m, Ar-<u>H</u>), 4.37-4.22 (4H, br m, C<u>H</u>$_2$), 3.82 (4H, br s, C<u>H</u>$_2$), 3.69 (4H, br s, C<u>H</u>$_2$); δ_C (100 MHz, DMSO-d_6,), 180.9 (C=S), 167.1 (q), 162.7 (C=O), 149.1 (q), 142.6 (q), 125.4 (CH), 124.7 (CH), 124.8 (CH), 124.4 (CF_3, $J_{^{13}C^{19}F}$ = 273.1 Hz), 110.6 (q), 70.3 (CH_2), 68.9 (CH_2), 68.3 (CH_2); IR υ_{max} (cm^{-1}) 3133, 2956, 1702 (C=O), 1602, 1548, 1480, 1416, 1324 (C=S), 1278, 1158, 1106, 1066, 1017, 997, 883, 838.

4,4'-((Ethoxy)-ethoxy)ethyl) 2,6–Bis-[4-nitrophenyl (thioureidocarbomoyl)]-Pyridine] (75)



Compound **73** (0.106 g, 0.19 mmol) and 4-nitrophenyl isothiocyanate (0.142 g, 0.79 mmol) were refluxed in MeCN (5 mL) for 20 h. The precipitate was collected and dried by suction filtration, giving **75** as a pale yellow solid (0.215g, 45%). m.p. 178-179 °C; HRMS (ES^+) Calculated for $C_{48}H_{45}N_{18}O_{16}S_4$ [M+H]: 1257.2144; found 1257.2189; δ_H (400 MHz, DMSO-d_6) 11.00 (4H, br s, N<u>H</u>$_{amide}$), 10.35 (4H, br s, N<u>H</u>$_{urea}$), 10.32 (4H, br s, N<u>H</u>$_{urea}$), 8.18–7.44 (20H, br m, Ar-<u>H</u>), 4.37-4.25 (4H, br m, C<u>H</u>$_2$), 3.83 (4H, br s, C<u>H</u>$_2$), 3.64 (4H, br s, C<u>H</u>$_2$); δ_C (100 MHz, DMSO-d_6) 181.0 (C=S), 167.7 (q), 163.2 (C=O), 149.5 (q), 145.5 (q), 143.8

(q), 124.7 (CH), 123.7 (CH), 123.6 (CH), 68.9 (CH_2), 69.4 (CH_2), 70.8 (CH_2); IR υ_{max} (cm^{-1}) 3215, 2933, 1689, 1596, 1548, 1505, 1411, 1336, 1271, 1211, 1146, 1109, 1041, 996, 928, 878, 851, 746, 698.

References

(1) Dodzuick, H. *Introduction to Supramolecular Chemistry*; Springer, 2002.
(2) Steed, J. W.; Atwood, J. L. *Supramolecular Chemistry*; Wiley: Chichester, 2000.
(3) Lehn, J. M. *Science* **1985**, *227*, 849-856.
(4) Pedersen, C. J. *J. Am. Chem. Soc.* **1967**, *89*, 7017-7036.
(5) Kyba, E. P.; Helgeson, R. C.; Madan, K.; Gokel, G. W.; Tarnowski, T. L.; Moore, S. S.; Cram, D. J. *J. Am. Chem. Soc.* **1977**, *99*, 2564-2571.
(6) Lehn, J. M. *Angew. Chem. Int. Ed.* **1988**, *27*, 89-112.
(7) *Chem. Soc. Rev.* **2009**, *38*, 1509-1701 Special issue for Jean-Pierre Sauvage.
(8) Lehn, J. M. *Supramolecular Chemistry*; Wiley-VCH: Weinheim, 1995.
(9) deSilva, A. P.; Gunaratne, H. Q. N.; Gunnlaugsson, T.; Huxley, A. J. M.; McCoy, C. P.; Rademacher, J. T.; Rice, T. E. *Chem. Rev.* **1997**, *97*, 1515-1566.
(10) *Coord. Chem. Rev.* **2006**, *250*, Special issue on anion receptor chemistry.
(11) James, T. D.; Phillips, M., D.; Shinkai, S. *Boronic Acids in Saccharide Recognition*; Royal Society of Chemistry, 2006.
(12) Gale, P. A.; Sessler, J. L.; Cho, W.-S. *Anion Receptor Chemistry*; Royal Society of Chemistry: Cambridge, 2006.
(13) Bell, K., J.; Westra, A., N. ; Warr, R., J. ; Chartres, J.; Ellis, R.; Tong, C., C.; Blake, A., J.; Tasker, P., A. ; Schröder, M. *Angew. Chem. Int. Ed.* **2008**, *47*, 1745-1748.
(14) Gunnlaugsson, T.; Glynn, M.; Tocci, M. G.; Kruger, P. E.; Pfeffer, F. M. *Coord. Chem. Rev.* **2006**, *250*, 3094-3117.
(15) Gunnlaugsson, T.; Ali, H. D. P.; Glynn, M.; Kruger, P. E.; Hussey, G. M.; Pfeffer, F. M.; dos Santos, C. M. G.; Tierney, J. *J. Fluoresc.* **2005**, *15*, 287-299.
(16) Hussey., G. *Ph.D Thesis, Trinity College, Dublin* **2003**.
(17) Ali., H. D. P. *Ph.D Thesis, Trinity College, Dublin* **2006**.
(18) Quinlan., E. *Ph. D Thesis Trinity College, Dublin* **2006**.
(19) Rich, D. P.; Gregory, R. J.; Anderson, M. P.; Manavalan, P.; Smith, A. E.; Welsh, M. J. *Science* **1991**, *253*, 202.
(20) Simon, B. D.; Bindra, R. S.; Mansfield, T. A.; Nelson-Williams, C.; Mendonca, E.; Stone, R.; Schuram, S.; Nayir, A.; Alplay, H.; Bakkaloglu, A.; Rodriguez-Soriano, J.; Morales, J. M.; Sanjad, S. A.; Taylor, C. M.; Pilz, D.; Brem, A.; Trachtman, H.; Griswold, W.; Richard, G. E.; John, E.; Lifton, R. P. *Nat. Genet.* **1997**, *17*, 171.
(21) Devuyst, O.; Christie, P. T.; Courtoy, P. J.; Beawens, R.; Thakker, R. *Hum. Mol. Genet.* **1999**, *8*, 247-257.
(22) Karniski, P. L.; Sheffield, V. C.; Kerman, T. M.; Wang, R.; Scott, D. A. *Nat. Genet.* **1999**, *21*, 440-443.
(23) Yoshida, A.; Taniguchi, S.; Hisatome, I.; Royaux, I. E.; Green, E. D.; Kohn, L. D.; Suzuki, K. *J. Clin. Endo. Metab.* **2002**, *87*, 3356.
(24) Kornak, U.; Kasper, D.; Bosl, M. R.; Kaiser, E.; Schweizer, M.; Schulz, A.; Friedrich, W.; Delling, G.; Jentsch, T. J. *Cell* **2001**, *104*, 205.
(25) Chantalat, L.; Nicholson, J. M.; Lambert, S. J.; Reid, A. J.; Donavan, M. J.; Reynolds, C. D.; Wood, C. M.; Baldwin, J. P. *Acta Cryst.* **2003**, *D59*, 139525.
(26) Dutzler, B.; Campbell, E.; Cadene, M.; Chait , B. T.; MacKinnon, R. *Nature* **2002**, *415*, 287.
(27) Myasoedov, B. F.; Rovnyi, S. I.; Tananaev, I. G.; Popova, N. N. *Russ. Chem. Rev.* **2003**, *72*, 101-121.
(28) Wallace, K. J.; Fagberni, R. I.; Folmer-Anderson, F. J.; Morey, J.; Lynth, V. M.; Anslyn, E. V. *Chem. Commun.* **2006**, *37*, 3886-3888.
(29) Connett, P. *Fluoride* **2007**, *40*, 155-158: 229-237: 39: 163-172.
(30) Shannon, R. D. *Acta. Cryst.* **1976**, *A32*, 751.
(31) Amendola, V.; Esteban-Gomez, D.; Fabbrizzi, L.; Licchelli, M. *Acc. Chem. Res.* **2006**, *39*, 343-353.

(32) Alunni, S.; Pero, A.; Reichenback, G. *J. Chem. Soc. Perkin Trans. 2* **1998**, 1747.
(33) Sharma, R. K.; Fry, J. L. *J. Org. Chem.* **1983**, *48*, 2112-2114.
(34) Sessler, J. L.; Gross, D. E.; Cho, W.-S.; Lynch, V. M.; Schmidtchen, F. P.; Bates, G. W.; Light, M. E.; Gale, P. A. *J. Am. Chem. Soc.* **2006**, *128*, 12281-12288.
(35) Danil de Namor, A. F.; Abbas, I.; Hammud, H. H. *J. Phys. Chem. B.* **2006**, *110*, 2142-2149.
(36) Hunter, C. A. *Angew. Chem. Int. Ed.* **2004**, *43*, 5310.
(37) Caltagirone, C.; Gale, P. A. *Chem. Soc. Rev.* **2009**, *38*, 520-563.
(38) Garcia-Acosta, B.; Martinez-Manez, R.; Sancenon, F.; Soto, J.; Rurack, K.; Spieles, M.; Garcia-Breijo, E.; Gil, L. *Inorg. Chem.* **2007**, *46*, 3123-3135.
(39) Tasker, P. A.; Tong, C. C.; Westra, A. N. *Coord. Chem. Rev.* **2007**, *251*, 1868-1877.
(40) Suksai, C.; Tuntulani, T. *Chem. Soc. Rev.* **2003**, 192-202.
(41) Martinez-Manez, R.; Sancenon, F. *J. Fluoresc.* **2005**, *15*, 267-285.
(42) Antonisse, M.; Reinhoudt, D. N. *Electranal.* **1999**, *11*, 1035-1048.
(43) Czarnik, A. W. *Acc. Chem. Res.* **1994**, *27*, 302.
(44) Min Su, H.; Dong, H. K. *Angwe. Chem. Int. Ed.* **2002**, *41*, 3809-3811.
(45) Wiskur, S. L.; Ati-Haddou, H.; Lavigne, J. J.; Anslyn, E. V. *Acc. Chem. Res.* **2001**, *34*, 963.
(46) Cho, D. G.; Sessler, J. L. *Chem. Soc. Rev.* **2009**, *38*, 1647-1662.
(47) Park, C. H.; Simmons, H. E. *J. Am. Chem. Soc.* **1968**, 2431.
(48) Gale, P. A.; Garcia-Garrido, S. E.; Garric, J. *Chem. Soc. Rev.* **2008**, *37*, 151-190.
(49) Garcia-Espana, E.; Diaz, P.; Llinares, J. M.; Bianchi, A. *Coord.Chem. Rev.* **2006**, *250*, 2952-2986.
(50) Sung Ok Kang; Rowshan Ara Begum; Bowman-James, K. *Angew. Chem. Int. Ed.* **2006**, *45*, 7882-7894.
(51) Gale, P. A. *Chem. Commun.* **2005**, 3761-3772.
(52) Filby, M. H.; Steed, J. W. *Coord. Chem. Rev.* **2006**, *250*, 3200-3218.
(53) O'Neil, E. J.; Smith, B. D. *Coord. Chem. Rev.* **2006**, *250*, 3068-3080.
(54) Katayev, E. A.; Ustynyuk, Y. A.; Sessler, J. L. *Coord. Chem. Rev* **2006**, *250*, 3004-3037.
(55) Cametti, M.; Rissanen, K. *Chem. Commun.* **2009**, 2809-2829.
(56) Llinares, J. M.; Powell, D.; Bowman-James, K. *Coord. Chem. Rev.* **2003**, *240*, 57-75.
(57) Schmuck, C. *Coord. Chem. Rev.* **2006**, *250*, 3053-3067.
(58) Yoon, J.; Kim, S. K.; Singh, N. J.; Kim, K. S. *Chem. Soc. Rev.* **2006**, *35*, 355-360.
(59) Kubik, S. *Chem. Soc. Rev.* **2009**, *38*, 585-605.
(60) Bowman-James, K. *Acc. Chem. Res.* **2005**, *38*, 671-678.
(61) Yoon, D. W.; Gross, D. E.; Lynch, V. M.; Lee, C. H.; Bennett, P. C.; Sessler, J. L. *Chem. Commun.* **2009**, 1109-1111.
(62) Yoon, D. W.; Gross, D. E.; Lynch, V. M.; Sessler, J. L.; Hay, B. P.; Lee, C. H. *Angew. Chem. Int. Ed.* **2008**, *47*, 5038-5042.
(63) Wintergerst, M. P.; Levitskaia, T. G.; Moyer, B. A.; Sessler, J. L.; Delmau, L. H. *J. Am. Chem. Soc.* **2008**, *130*, 4129-4139.
(64) Garcia-Garrido, S. E.; Caltagirone, C.; Light, M. E.; Gale, P. A. *Chem. Commun.* **2007**, 1450-1452.
(65) Brooks, S. L.; Garcia-Garrido, S. E.; Light, M. E.; Cole, P. A.; Gale, P. A. *Chem. - Eur. J.* **2007**, *13*, 3320-3329.
(66) Bates, G. W.; Gale, P. A.; Light, M. E. *Chem. Commun.* **2007**, 2121-2123.
(67) Caltagirone, C.; Hiscock, J. R.; Hursthouse, M. B.; Light, M. E.; Gale, P. A. *Chem. - Eur. J.* **2008**, *14*, 10236-10243.

(68) Brooks, S. J.; Caltagirone, C.; Cossins, A. J.; Gale, P. A.; Light, M. *Supramol. Chem.* **2008**, *20*, 349-355.
(69) Hiscock, J. R.; Caltagirone, C.; Light, M. E.; Hursthouse, M. B.; Gale, P. A. *Org. Biomol. Chem.* **2009**, *7*, 1781-1783.
(70) Caltagirone, C.; Bates, G. W.; Gale, P. A.; Light, M. E. *Chem. Commun.* **2008**, 61-63.
(71) Pfeffer, F. M.; Lim, K. F.; Sedgwick, K. J. *Org. Biomol. Chem.* **2007**, *11*, 1795-1799.
(72) Lowe, A. J.; Pfeffer, F. M. *Chem. Commun.* **2008**, *16*, 1871-1873.
(73) Nguyen, B. T.; Anslyn, E. V. *Coord. Chem. Rev.* **2006**, *250*, 3118-3127.
(74) Bonizzoni, M.; Fabbrizzi, L.; Taglietti, A.; Tiengo, F. *E. J. Org. Chem.* **2006**, 3567-3574.
(75) Hamilton, A. D. *Coord. Chem. Rev.* **2003**, *240*, 101-110.
(76) Matthews, S. E.; Beer, P. D. *Supramol. Chem.* **2005**, *17*, 411.
(77) Davis, A. P. *Coord. Chem. Rev.* **2006**, *250*, 2939-2951.
(78) Nie, L.; Li, Z.; Han, J.; Zhang, X.; Yang, R.; Liu, W.-X.; Wu, F.-Y.; Xie, J.-W.; Zhao, Y.-F.; Jiang, Y.-B. *J. Org. Chem.* **2004**, *69*, 6449-6454.
(79) Wu, F.-Y.; Li, Z.; Guo, L.; Wang, X.; Lin, M.-H.; Zhao, Y.-F.; Jiang, Y.-B. *Org. Biomol. Chem.* **2006**, *4*, 624-630.
(80) Dos Santos, C. M. G.; Mc Cabe, T.; Watson, G., E.,; Kruger, P. E.; Gunnlaugsson, T. *J. Org. Chem.* **2008**, *73*, 9235-9244.
(81) Steed, J. W. *Chem. Soc. Rev.* **2009**, *38*, 506-519.
(82) Amendola, V.; Fabbrizzi, L. *Chem. Commun.* **2009**, 513-531.
(83) Massue, J.; Quinn, S. J.; Gunnlaugsson, T. *J. Am. Chem. Soc.* **2008**, *130*, 6900-6901.
(84) Dos Santos, C. M. G.; McCabe, T.; Gunnlaugsson, T. *Tetrahedron Lett.* **2007**, *48*, 3135-3139.
(85) Plush, S. E.; Gunnlaugsson, T. *Org. Lett.* **2007**, *9*, 1919-1922.
(86) Junhua, Y.; David, P. *Eur. J. Org. Chem.* **2005**, *2005*, 4249-4252.
(87) Pal, R.; Parker, D.; Costello, L. C. *Org. Biomol. Chem.* **2009**, *7*, 1525-1528.
(88) Wedge, F. J.; Hawthorne, M. F. *Coord. Chem. Rev.* **2003**, *240*, 111-128.
(89) Galbraith, E.; Fyles, T. M.; Marken, F.; Davidson, M. G.; James, T. D. *Inorg. Chem.* **2008**, *47*, 6236-6244.
(90) Kubo, Y.; Kobayashi, A.; Ishida, T.; Misawa, Y.; James, T. D. *Chem. Commun.* **2005**, 2846-2848.
(91) Ward, C. J.; Patel, P.; James, T. D. *Chem. Lett.* **2001**, *30*.
(92) Arimori, S.; Davidson, M. G.; Fyles, T. M.; Hibbert, T. G.; James, T. D.; Kociok-Kohn, G. I. *Chem. Commun.* **2004**, 1640-1641.
(93) Nonaka, A.; Horie, S.; James, T. D.; Kubo, Y. *Org. Biomol. Chem.* **2008**, *6*, 3621-3625.
(94) Estroff, L. A.; Hamilton, A. D. *Chem. Rev.* **2004**, *104*, 1201-1218.
(95) Maeda, M. *Chem. - Eur. J.* **2008**, *14*, 11274-11282.
(96) Palacios, M. A.; Nishiyabu, R.; Marquez, M.; Anzenbacher, P. J. *J. Am. Chem. Soc.* **2007**, *129*, 7538-7544.
(97) Chen, B.; Wang, L.; Zapata, F.; Qian, G.; Lobkovsy, E. B. *J. Am. Chem. Soc.* **2008**, *130*, 6718-6719.
(98) Cametti, M.; Dalla Cort, A.; Bartik, K. *ChemPhysChem.* **2008**, *9*, 2168-2171.
(99) Kim, E.; Kim, H. J.; Bae, D. R.; Lee, S. J.; Cho, E. J.; Seo, M. R.; Kim, J. S.; Jung, J. H. *New. J. Chem.* **2008**, *32*, 1003.
(100) Comes, M.; Marcos, M. D.; Martinez-Manez, R.; Sancenon, F.; Soto, J.; Villaescusa, L. A.; Amoros, P. *Chem. Commun.* **2008**, 3639-3641.

(101) Climent, E.; Casasus, R.; Marcos, M. D.; Martinez-Manez, R.; Sancenon, F.; Soto, J. *Dalton Trans.* **2009**, 4806-4814.
(102) Smith, P. J.; Reddington, M. V.; Wilcox, C. S. *Tetrahedron Lett.* **1992**, *33*, 6085-6088.
(103) Saha, S.; Samanta, A. *J. Phys. Chem. A.* **2002**, *106*, 4763-4771.
(104) Wu, F.-Y.; Li, Z.; Wen, Z.-C.; Zhou, N.; Zhao, Y.-F.; Jiang, Y.-B. *Org. Lett.* **2002**, *4*, 3203-3205.
(105) Quinlan, E.; Matthews, S. E.; Gunnlaugsson, T. *Tetrahedron Lett.* **2006**, *47*, 9333-9338.
(106) Quinlan, E.; Matthews, S. E.; Gunnlaugsson, T. *J. Org. Chem.* **2007**, *72*, 7497-7503.
(107) Gunnlaugsson, T.; Kruger, P. E.; Lee, T. C.; Parkesh, R.; Pfeffer, F. M.; Hussey, G. M. *Tetrahedron Lett.* **2003**, *44*, 6575-6578.
(108) Gunnlaugsson, T.; Kruger, P. E.; Jensen, P.; Pfeffer, F. M.; Hussey, G. M. *Tetrahedron Lett.* **2003**, *44*, 8909-8913.
(109) Gampp, H.; Maeder, M.; Meyer, S. J.; Zuberbhler, A., D. *Talanta* **1985**, *32*, 9501.
(110) Maeder, M.; Zuberbhler, A., D. *Anal. Chem.* **1990**, *62*, 2220-2224.
(111) Pfeffer, F. M.; Buschgens, A. M.; Barnett, N. W.; Gunnlaugsson, T.; Kruger, P. E. *Tetrahedron Lett.* **2005**, *46*, 6579-6584.
(112) Duke, R. M.; Gunnlaugsson, T. *Tetrahedron Lett.* **2007**, *48*, 8043-8047.
(113) Bao, X. P.; Wang, L.; Wu, L.; Li, Z. Y. *Supramol. Chem.* **2008**, *20*, 467-472.
(114) Singh, N.; Kaur, N.; Dunn, J.; Behan, R.; Malrooney, R. C.; Callan, J., F. *Eur. Poly. J.* **2009**, *45*, 272-277.
(115) Pfeffer, F. M.; Seter, M.; Lewcenko, N.; Barnett, N. W. *Tetrahedron Lett.* **2006**, *47*, 5241-5245.
(116) Esteban-Gomez, D.; Fabbrizzi, L.; Liechelli, M. *J. Org. Chem.* **2005**, *70*, 5717-5720.
(117) Yoon, J.; Qian, X.; Kim, J. S.; Lee, C.; Han, S. J.; Kim, N. H.; Kim, S.; Xu, Z. *Tetrahedron. Lett.* **2007**, *48*, 9151-9154.
(118) Veale, E. B.; Gunnlaugsson, T. *J. Org. Chem.* **2008**, *73*, 8073-8076.
(119) Veale, E. B.; Tocci, M. G.; Pfeffer, F. M.; Kruger, P. E.; Gunnlaugsson, T. *Org. Biomol. Chem.* **2009**, *7*, 3447.
(120) de Silva, A. P.; Rice, T. E. *Chem. Commun.* **1999**, 163.
(121) Kluciar, M.; Ferreira, R.; de Castro, B.; Pischel, U. *J. Org. Chem.* **2008**, *73*, 6079-6085.
(122) Pischel, U.; Remon, P.; Ferreira, R. *J. Phys. Chem. C.* **2009**, *113*, 5805-5811.
(123) Tian, H.; Liu, B. *J. Mater.Chem.* **2005**, *15*, 2681-2686.
(124) Qu, Y.; Hua, J. L.; Jiang, Y. H.; Tian, H. *J. Poly. Sci. Part A* **2009**, *47*, 1544-1552.
(125) Li, Y.; Cao, L.; Tian, H. *J. Org. Chem.* **2006**, *71*, 8279-8282.
(126) Milgrom, L. R. *The Colours of Life: An introduction to the chemistry of porphyrins and related compounds.*; Oxford University Press, 1997.
(127) Xu, Z.; Tang, J.; Tian, H. *Chin. Chem. Lett.* **2008**, *19*, 1353-1357.
(128) Gunnlaugsson, T.; Kruger, P. E.; Jensen, P.; Tierney, J.; Ali, H. D. P.; Hussey, M. G. *J. Org. Chem.* **2005**, *70*, 10875-10878.
(129) Ali, H. D. P.; Kruger, P. E.; Gunnlaugsson, T. *New J. Chem.* **2008**, *32*, 1153-1161.
(130) Sun, Y. M.; Zhong, C.; Gong, R.; Fu, E. Q. *Org. Biomol. Chem.* **2008**, *6*, 3044-3047.
(131) Koner, A. L.; Schatz, J.; Nau, W. M.; Pischel, U. *J. Org. Chem.* **2007**, *72*, 3889-3895.
(132) Li, Y.; Xu, S.; Li, X.; Chen, K. C.; Tian, H. *Chem. Lett.* **2007**, *36*, 664-665.
(133) Claessens, C. G.; Gonzales-Rodriguez, D.; Torres, T. *Chem. Rev.* **2002**, *102*, 835.
(134) Benesi, H. A.; Hildebrand, J. H. *J. Am. Chem. Soc.* **1949**, *71*, 2703.

(135) Zhong, C.; Mu, T.; Wang, L.; Fu, E.; Qin, J. *Chem. Commun.* **2009**, 4091-4093.
(136) Evans, L. S.; Gale, P. A.; Light, M. E.; Quesada, R. *New J. Chem.* **2006**, *30*, 1019-1025.
(137) Wei, L.-H.; He, Y.-B.; Wu, J.-L.; Wu, X.-J.; Meng, L.-Z.; Yang, X. *Supramol. Chem.* **2004**, *16*, 561-567.
.(138) Fang, L.; Chan, W.-H.; He, Y.-B.; Kwong, D. W. J.; Lee, A. W. M. *J. Org. Chem* **2005**, *70*, 7640-7646.
(139) Wei, L.-H.; He, Y.-B.; Wu, J.-L.; Qin, H.-J.; Xu, K.-X.; Meng, L.-Z. *Chin. J. Chem.* **2005**, *23*, 608-612.
(140) Evans, L. S.; Gale, P. A.; Light, M. E.; Quesada, R. *Chem. Commun.* **2006**, 965-967.
(141) Yang, R.; Liu, W.-X.; Shen, H.; Huang, H.-H.; Jiang, Y.-B. *J. Phys. Chem. B.* **2008**, *112*, 5105-5110.
(142) Zhen-Ya, Z.; He, Y.-B.; Wu, J.-L.; Wei, L.-H.; Liu, X.; Meng, L.-Z.; Yang, X. *Eur. J. Org. Chem.* **2004**, 2888-2893.
(143) Liu, W.-X.; Jiang, Y.-B. *Org. Biomol. Chem.* **2007**, *5*, 1771-1775.
(144) Li, Z.; Chen, Y. H.; Jiang, Y. B. *Science in China Series B-Chemistry* **2009**, *52*, 786-792.
(145) Wang, H.; Chan, W.-H.; Lee, A. W. M. *Org. Biomol. Chem.* **2008**, *6*, 929-934.
(146) Wang, H.; Chan, W.-H. *Org. Biomol. Chem.* **2008**, *6*, 162-168.
(147) Schmuck, C.; Machon, U. *Chem. Eur. J.* **2005**, *11*, 1109-1118.
(148) Sessler, J. L.; Barkey, N. M.; Pantos, G. D.; Lynch, V. M. *N. J. Chem.* **2007**, *31*, 646-654.
(149) Hynes, M. J. *J. Chem. Soc., Dalton Trans.* **1993**, 311-312.
(150) Bisson, A. P.; Hunter, C. A.; Morales, J. C.; Young, K. *Chem. Eur. J.* **1998**, *4*, 845-851.
(151) Liu, B.; Tian, H. *J. Mater.Chem.* **2005**, *15*, 2681-2686.
(152) Gomez, D. E.; Fabbrizzi, L.; Licchelli, M.; Monzani, E. *Org. Biomol. Chem.* **2005**, *3*, 1495-1500.
(153) de Silva, A. P.; Gunaratne, H. Q.; Habib-Jiwan, J.-L.; McCoy, C. P.; Rice, T. E.; Soumillion, J.-P. *Angew. Chem. Int. Ed. Engl.* **1995**, *34*, 1728-1731.
(154) Ehys Williams, A. T.; Winfield. S. A.; Miller, J. N. *Analyst* **1983**, *108*, 1067.
(155) Connors, K. A. *Binding Constants*; John Wiley & Sons: New York, 1987.
(156) Arnendola, V.; Bonizzoni, M.; Esteban-Gomez, D.; Fabbrizzi, L.; Licchelli, M.; Sancenon, F.; Taglietti, A. *Coord. Chem. Rev.* **2006**, *250*, 1451-1470.
(157) Fabbrizzi, L. *Coord. Chem. Rev.* **2006**, *250*, 1209-1209.
(158) Emsley, J.; Miller, J. M.; Overill, R. E.; Waddilove, R. A. *J. Am. Chem. Soc.* **1981**, *103*, 24.
(159) Li, Z.; Zhang, J. *Chem. Phys.* **2006**, *331*, 159-163.
(160) Bordwell, F., G; Algrim, D., J; Harrelson, J. A., Jr *J. Am. Chem. Soc.* **1988**, *110*, 5903.
(161) Perez-Casas, C.; Yatsimirisky, A. K. *J. Org. Chem.* **2008**, *73*, 2275-2284.
(162) Amendola, V.; Boiocchi, M.; Fabbrizzi, L.; Palchetti, A. *Chem. - Eur. J.* **2005**, *11*, 5648-5660.
(163) Kato, R.; Nishizawa, S.; Hayashita, T.; Teramae, N. *Tetrahedron Lett.* **2001**, *42*, 5053-5056.
(164) Hunter, C. A.; Bisson, A. P.; Morales, J. C.; Young, K. *Chem. Eur. J* **1998**, *5*, 845.
(165) Yen, Y.-P.; Ho, K.-W. *Tetrahedron Lett.* **2006**, *47*, 1193-1196.
(166) Tseng, Y.-P.; Tu, G.-M.; Lin, C.-H.; Chang, C.-T.; Lin, C.-Y.; Yen, Y.-P. *Org. Biomol. Chem.* **2007**, *5*, 3592-3598.
(167) Shibanuma, T.; Shiono, M.; Mukaiyama, T. *Chem. Lett.* **1977**, 573-547.

(168) Pfeffer, F. M.; Gunnlaugsson, T.; Jensen, P.; Kruger, P. E. *Org. Lett.* **2005**, *7*, 5357-5360.
(169) Wardman, P. J.; Middleton, R. W. *J. Heterocyclic Chem.* **1986**, *23*, 849.
(170) Coronado, J. L. G.; Martin, E.; Montero, L. A.; Fierro, J. L. G.; Garcia de La Vega, J. M. *J. Phys. Chem. A.* **2007**, *11*, 9724-9732.
(171) Ippolito, A.; Volpini, R.; Diego Dal, B.; Lambertucci, C.; Cristalli, G. *Biorg. Med. Chem.* **2008**, *16*, 8440-8446.
(172) Kavallieratos, K.; de Gala, S. R.; Austin, D. J.; Crabtree, R. H. *J. Am. Chem. Soc.* **1997**, *119*, 2325-2326.
(173) Vandevyver, C. D. B.; Chauvin, A. S.; Comby, S.; Bunzli, J. C. *Chem. Commun.* **2007**, 1716-1718.
(174) Froidevaux, P.; Harrowfield, J. M.; Sobolev, A. N. *Inorg. Chem.* **2000**, 4678-4687.
(175) Hiromasa Kurosaki; Rakesh Kumar Sharma; Sachiko Aoki; Teruhiko Inoue; Yoshinari Okamoto; Yukio Sugiura; Mitsunobu Doi; Toshimasa Ishida; Otsukac, M.; Goto, M. *J. Chem. Soc., Dalton Trans.* **2001**, 441-447.
(176) Lee, D. H.; Lee, H. Y.; Lee, K. H.; Hong, J.-I. *Chem. Commun.* **2001**, 1188-1189.
(177) Boiocchi, M.; DelBoca, L.; Gomez, D. E.; Fabbrizzi, L.; Licchelli, M.; Monzani, E. *J. Am. Chem. Soc.* **2004**, *126*, 16507-16514.
(178) Martínez-Máñez, R.; Sancenón, F. *Chem. Rev.* **2003**, *103*, 4419-4476.
(179) Chmielewski, M.; Jurczak, J. *Tetrahedron Lett.* **2004**, *45*, 6007-6010.
(180) Micha; lstrok; Chmielewski, J.; Janusz, J. *Chem. - Eur. J.* **2006**, *12*, 7652-7667.
(181) Zhang, W.; Liu, J.; Zhu, H.; Gao, W.; Sun, L. *Synthetic Commun.* **2007**, *19*, 3393-3402.
(182) Newton, A. *J. Am. Chem. Soc.* **1943**, *65*, 320-323.
(183) Goswami, S.; Jana, S.; Dey, S.; Sen, D.; Fun, H.-K.; Chantrapromma, S. *Tetrahedron* **2008**, *64*, 6426-6433.
(184) B.-Q. Su; L. Xian; H.-B. Song; Sheng, L. *Acta Cryst.* **2004**, *C60*, m661-m662
(185) Kovalchuk, A.; Bricks, J. L.; Reck, G.; Rurack, K.; Schulz, B.; Szumna, A.; Wei *Chem. Commun.* **2004**, 1946-1947.
(186) Hay, B. P.; Firman, T. K.; Moyer, B. A. *J. Am. Chem. Soc.* **2005**, *127*, 1810-1819.
(187) Steiner, T. *Angew. Chem. Int. Ed.* **2002**, *41*, 48-76.
(188) Chawla, H. M.; Singh, S. P. *Tetrahedron* **2008**, *64*, 741-748.
(189) Liu, C.; Qian, X.; Wang, J.; Li, Z. *Tetrahedron Lett.* **2008**, *49*, 1087-1090.
(190) Saravanakumar, D.; Devaraj, S.; Iyyampillai, S.; Mohandoss, K.; Kandaswamy, M. *Tetrahedron Lett.* **2008**, *49*, 127-132.
(191) Nishiyabu, R.; Anzenbacher, P. *J. Am. Chem. Soc.* **2005**, *127*, 8270-8271.
(192) Nishizawa, S.; Buhlmann, P.; Iwao, M.; Umezawa, Y. *Tetrahedron Lett.* **1995**, *36*, 6483-6486.
(193) Jose, D. A.; Singh, A.; Das, A.; Ganguly, B. *Tetrahedron Lett.* **2007**, *48*, 3695-3698.
(194) Ros-Lis, J. V.; Martínez-Máñez, R.; Sancenón, F.; Soto, J.; Rurack, K.; Weißhoff, H. *Eur. J. Org. Chem.* **2007**, *2007*, 2449-2458.
(195) Feng, H.; Yuhui, B.; Zhigang, Y.; Thomas, M. F.; Jianzhang, Z.; Xiaojun, P.; Jiangli, F.; Yunkou, W.; Shiguo, S. *Chem.-Eur. J.* **2007**, *13*, 2880-2892.
(196) Hu, S.; Guo, Y.; Xu, J.; Shao, S. *Spectrochimica Acta Part A* **2009**, *72*, 1043-1046.
(197) Tobias, D. J.; Hemminger, J. C. *Science* **2008**, *319*, 1197-1198.
(198) Bordwell, F., G *Acc. Chem. Res.* **1988**, *21*, 456-463.
(199) Mukerjee, P.; Ostrow, D. J. *Tetrahedron Lett.* **1998**, *39*, 423-426.
(200) Shang, X.-F.; Li, J.; Lin, H.; Jiang, P.; Caia, Z.-S.; Lin, H.-K. *Dalton Trans.* **2009**, 2096-2102.
(201) Sessler, J. L.; Maeda, H.; Mizuno, T.; Lynch, V. M.; Furuta, H. *Chem. Commun.* **2002**, 862-863.

(202) Shevchuk, S. V.; Lynch, V. M.; Sessler, J. L. *Tetrahedron* **2004**, *60*, 11283-11291.
(203) Matsumura, Y.; Katoh, A. *J. Luminescence* **2008**, *128*, 625-630.
(204) Yoo, J.; Kim, M.-S.; Hong, S.-J.; Sessler, J. L.; Lee, C.-H. *J. Org. Chem.* **2009**, *74*, 1065-1069.
(205) Vicker, N.; Xiandong, S.; Ganeshapillai, D.; Purohit, A.; Reed, M., John,; Potter, B., Victor Llyod. *PCT. Int. Appl.* **2005**, WO2005042513 (A1)
(206) Nasielski-Hinkens, R.; Benedek-Vamos, M.; Maetens, D. *J. Heterocyclic Chem.* **1980**, *17*, 873-875.
(207) Yin, X.-H.; Tan, M.-Y. *Syn. Commun.* **2003**, *33*, 1113-1119.
(208) Lamture, J. B.; Hong Zhou, Z.; Suresh Kumar, A.; Wensel, T. G. *Inorg. Chem.* **1995**, *34*, 864-869.
(209) Rohr, K.; Vogel, S. *ChemBioChem.* **2006**, *7*, 463-40.
(210) Hiromasa, K.; Rakesh, K. S.; Sachiko, A.; Teruhiko, I.; Yoshinari, O.; Yukio, S.; Mitsunobu, D.; Toshimasa, I.; Masami, O.; Masafumi, G. *J. Chem. Soc., Dalton Trans.* **2001**, 441-447.
(211) Arnaud, A.; Belleney, J.; Boue, F.; Bouteiller, L.; Carrot, G.; Wintgens, V. *Angew. Chem. Int. Ed.* **2004**, *43*, 1718-1721.
(212) Leonard, J. P. *Ph.D Thesis, Trinity College Dublin* **2003**.
(213) Jellinek, H. H. G.; Urwin, J. R. *J. Phys. Chem. B* **1954**, *58*, 548-550.
(214) Motekaitis, R. J.; Martell, A. *Inorg. Chem.* **1988**, *27*, 2718-2724.
(215) Stomeo, F.; Lincheneau, C.; Leonard, J. P.; O'Brien, J. E.; Peacock, R. D.; McCoy, C. P.; Gunnlaugsson, T. *J. Am. Chem. Soc.* **2009**, *131*, 9636-9637.
(216) Comby, S.; Stomeo, F.; McCoy, C. P.; Gunnlaugsson, T. *Helv. Chim. Acta* **2009**, *92*, 2461-2473.
(217) Leonard, J. P.; Jensen, P.; McCabe, T.; O'Brien, J. E.; Peacock, R. D.; Kruger, P. E.; Gunnlaugsson, T. *J. Am. Chem. Soc.* **2007**, *129*, 10986-+.
(218) Konstantinova, T.; Spirieva, A.; Petkova, T. *Dyes and Pigments* **2000**, *45*, 125-129.
(219) Sasaki, S.-I.; Citterio, D.; Ozawa, S.; Suzuki, K. *J. Chem. Soc., Perkins Trans. 2* **2001**, 2309-2313.
(220) Pardo, A.; Martin, E.; Poyato, J. M. L.; Camacho, J. J. *J. Photoch. Photobio. A* **1987**, *41*, 69-78.
(221) Strier, M. P.; Cavagnol, J. C. *J. Am. Chem. Soc.* **1958**, *80*, 1565.
(222) Ouchi, M.; Inoue, Y.; Liu, Y.; Nogamune, S.; Wada, K.; Hakushi, T. *Bull. Chem. Soc. Jpn.* **1990**, *63*, 1260-1262.

Appendices

Binding Constants (log *K*) determination

Within this body of work, the binding constants have been determined by using the nonlinear least-squares program SPECFIT/32™, which is a multivariate data analysis program for modeling and fitting experimental data sets (such as chemical kinetics and equilibrium titrations) obtained from multivariate spectrophotometric measurements. The fitting methodology, which relies on the use of various mathematical parameters,[109] uses the Levenberg-Marquardt procedure to minimise the least-squares residuals between the data set and the model system.[110] In order to solve the number of species (speciation) present at equilibrium, SPECFIT takes advantage of the Newton-Raphson method. The model used specifies various states of interaction, for instance complexation between Host and Guest species, in terms of the overall stability constants (β). Considering the two stepwise equilibrium process involved in the binding interaction between a host (M) and a guest (L), the equilibrium constants K_1 and K_2 implicated in the interaction can be expressed using Equation **A0.1** and Equation **A0.2**.

$$M + L \overset{K_1}{\rightleftharpoons} [ML] \qquad \text{Equation } \mathbf{A0.1}$$

$$[ML] + L \overset{K_2}{\rightleftharpoons} [ML_2] \qquad \text{Equation } \mathbf{A0.2}$$

The stepwise binding constants K_1 and K_2 can be determined using Equations **A0.3** and **A0.4**.

$$K_1 = \frac{[ML]}{[M]\,[L]} \qquad \text{Equation } \mathbf{A0.3}$$

$$K_2 = \frac{[ML_2]}{[ML]\,[L]} \qquad \text{Equation } \mathbf{A0.4}$$

The overall equilibrium constant for this process, β, is the product of the two stepwise constants K_1 and K_2 ($\beta = K_1.K_2$). SPECFIT yields binding constants as cumulative log β values. So, for the 1:2 ($M:L_2$) equilibrium process this is translated by the log $\beta_{1:2}$, which represents the sum of the individual constants ($\log \beta_{1:2} = \log K_1 + \log K_2$). Therefore, for any multi-step equilibrium, by subtraction of successive log β values, the log K for each

equilibrium step can then be determined. This program automatically scales its calculations with the supplied initial concentrations (allowing for dilution).

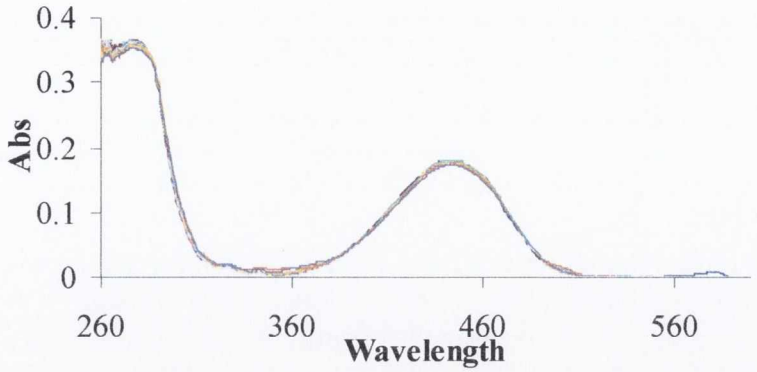


Figure A1: The changes in the absorption spectra of **4a** [1.2×10^{-5} M] upon addition of AcO^- (0 → 1200 equivalents).

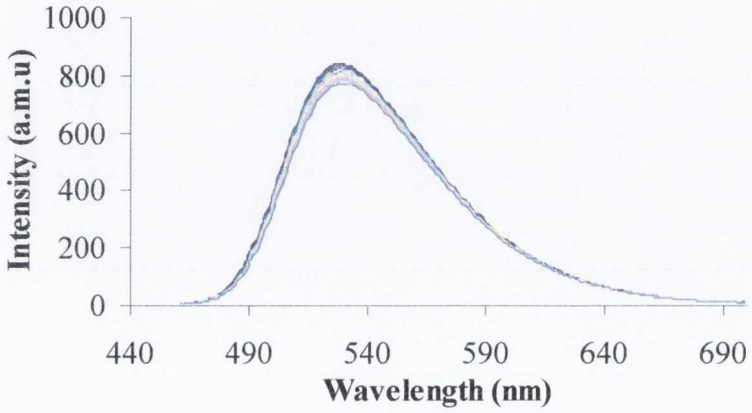


Figure A2: The changes in the emission spectra of **4a** [1.1×10^{-5} M] upon addition of $H_2PO_4^-$ (0 → 280 equivalents).

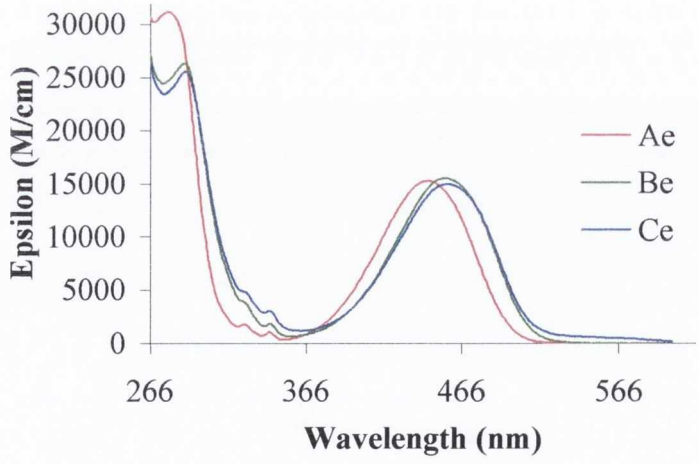


Figure A3: The iterative EFA for sequential species present in solution upon UV-Vis titration of **4a** with F^-.

Table A 1: Values obtained from the principle factor analysis of titration of **4a** with F^-.

#	Eigenvalue	Square Sum	Residual	Prediction
1	1.648E+02	2.235E+00	1.544E-02	Data Vector
2	2.218E+00	1.784E-02	1.379E-03	Data Vector
3	1.402E-02	3.826E-03	6.388E-04	Data Vector
4	1.580E-03	2.247E-03	4.895E-04	Probably Noise
5	5.951E-04	1.651E-03	4.197E-04	Probably Noise
6	3.529E-04	1.299E-03	3.722E-04	Probably Noise

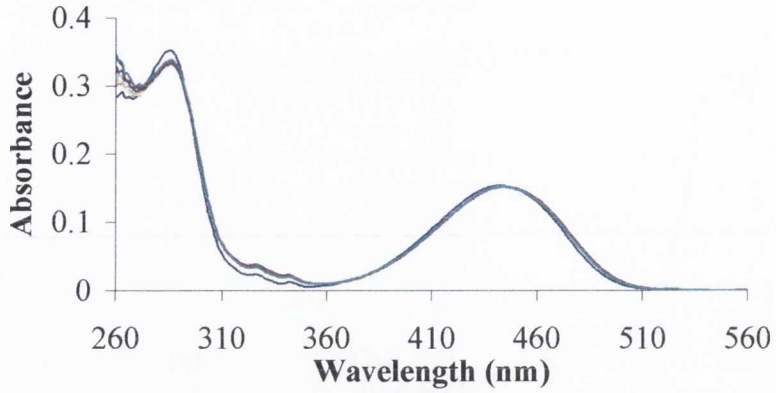


Figure A4: The changes in the absorption spectra of **4b** [9.7×10^{-6} M] upon addition of AcO^- (0 → 71 eq).

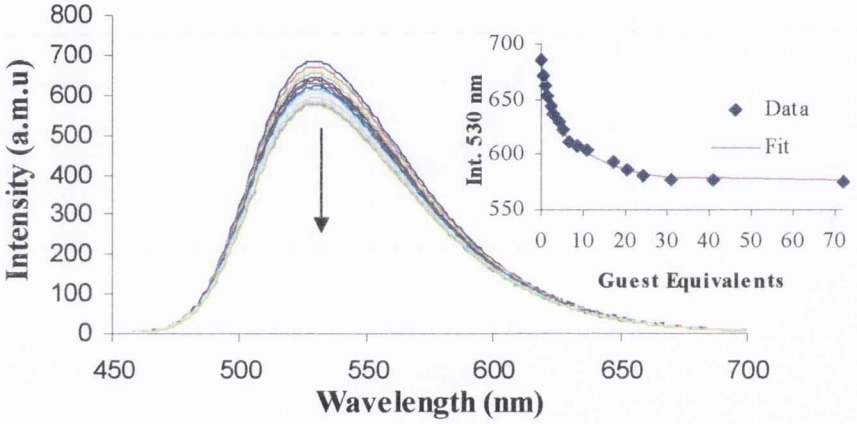


Figure A5: The changes in the emission spectra of **4b** [9.7×10^{-6} M] upon addition of AcO^- (0 → 71 equivalents).

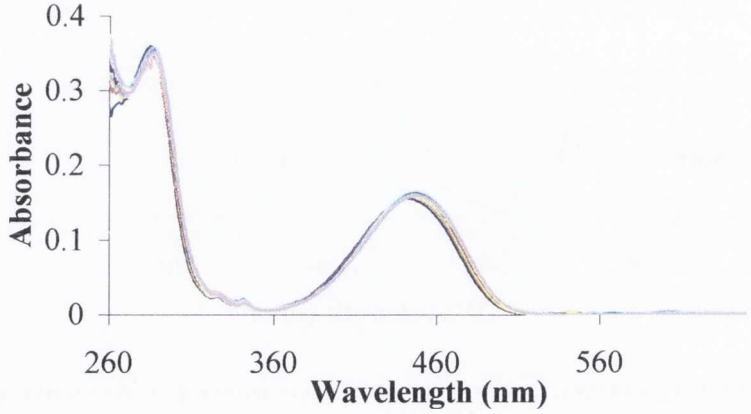


Figure.A6: The changes in the absorption spectra of **4b** [1.0×10^{-5} M] upon addition of $H_2PO_4^-$ (0 → 168 equivalents).

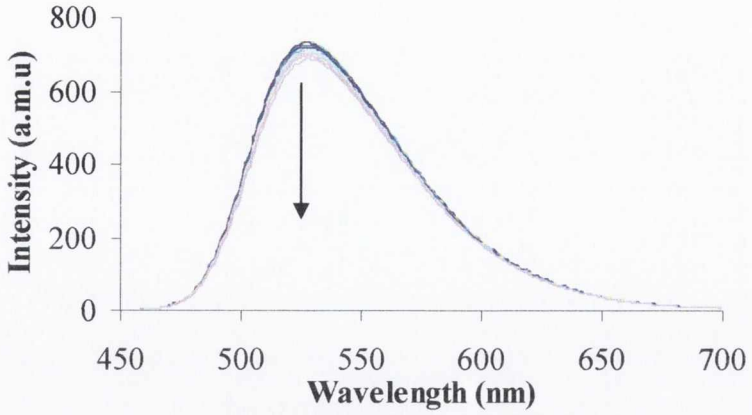


Figure A7: The changes in the emission spectra of **4b** [1.0×10^{-5} M] upon addition of $H_2PO_4^-$ (0 → 168 equivalents).

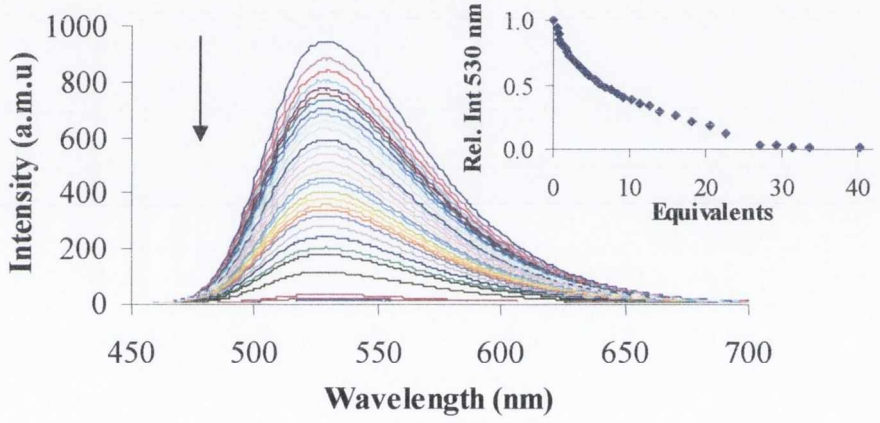


Figure A8: The changes in the emission spectra of **4b** [1.5×10^{-5} M] upon addition of F^- (0 → 45 equivalents). **Insert:** The changes in relative intensity at 530 nm against equivalents; λ_{ex} 443 nm.

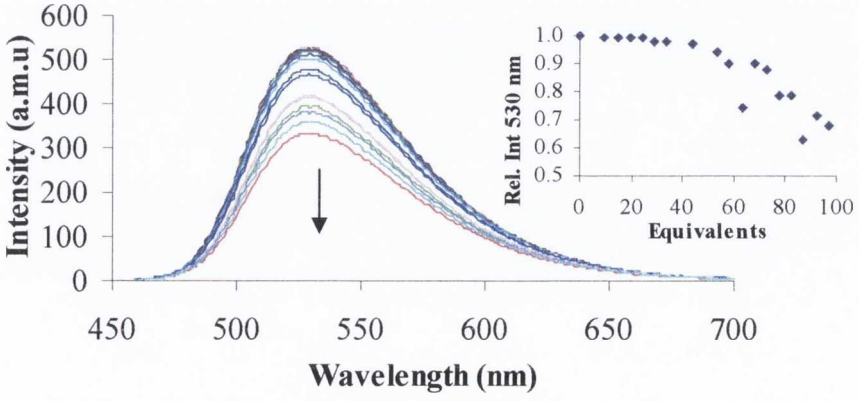


Figure A9: The changes in the emission spectra of **4c** [7×10^{-6} M] upon addition of F (0 → 96 equivalents). **Insert:** The relative changes at 530 nm against equivalents.

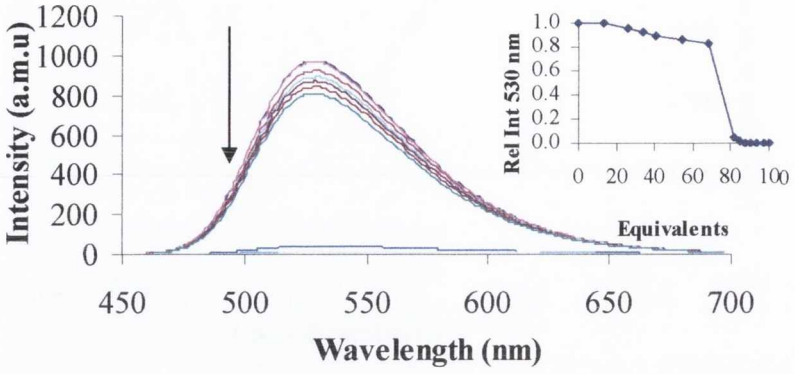


Figure A10: The changes in the emission spectra of **4a** [1×10^{-5} M] upon addition of TBAOH (0 → 96 equivalents). **Insert:** The changes in the relative intensity at 530 nm against equivalents.

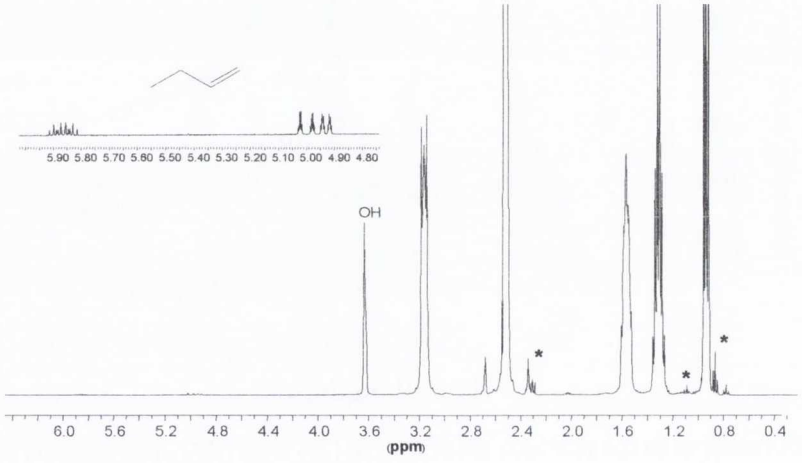


Figure A11: The ^{1}H NMR (400 MHz, DMSO-d_6) spectrum of TBAOH.30H_2O after 48 h in solution. * New peaks formed in solution. **Insert:** Formation of butene at *ca.* 4.9 - 5.9 ppm.

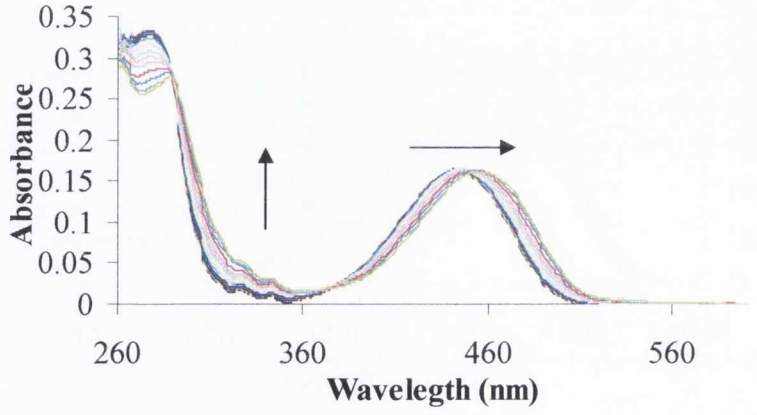


Figure A12: The changes in the absorption spectra of **4a** [1×10^{-5} M] upon titration with TBAF.3H_2O (0 → 90 equivalents) in DMSO.

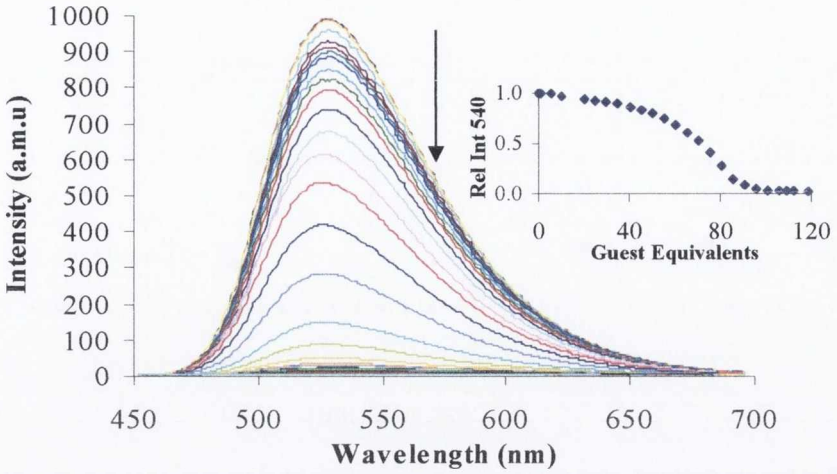


Figure A13: The changes in the absorption spectra of **4a** [1×10^{-5} M] upon titration with TBAF.$3H_2O$ (0 → 120 equivalents) in DMSO. **Insert:** The changes in the relative emission at 530 nm, λ_{ex} 442 nm.

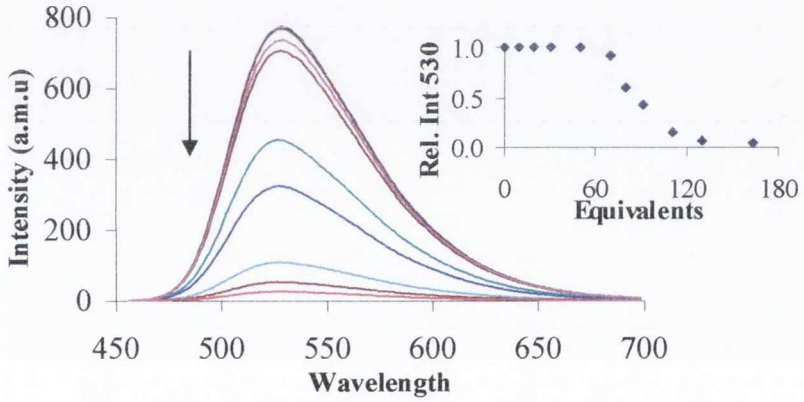


Figure A14: The changes in the emission spectra of **2** [1.0×10^{-5} M] upon addition of TBAF hydrate (0 → 163 equivalents). **Insert:** The relative changes at 530 nm against equivalents, λ_{ex} 445 nm.

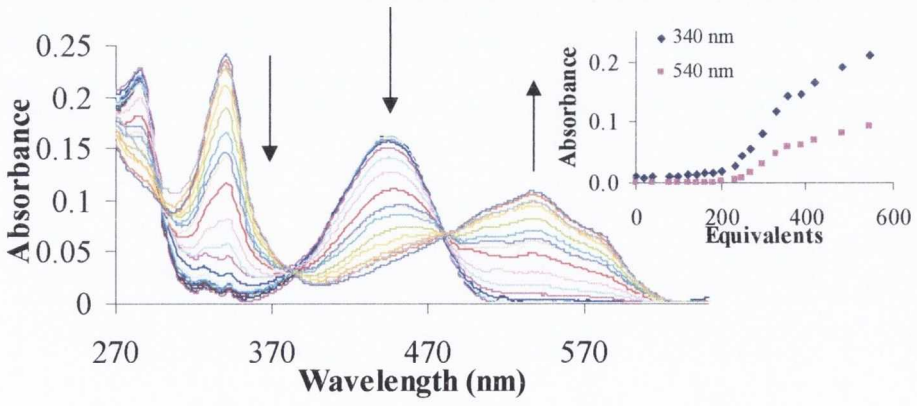


Figure A15: The changes in the absorption spectra of **2** [1.0×10^{-5} M] upon addition of TBAF.$3H_2O$ (0 → 790 equivalents). **Insert:** The simultaneous changes in absorptions at 340 nm and 540 nm from 0 → 600 equivalents.

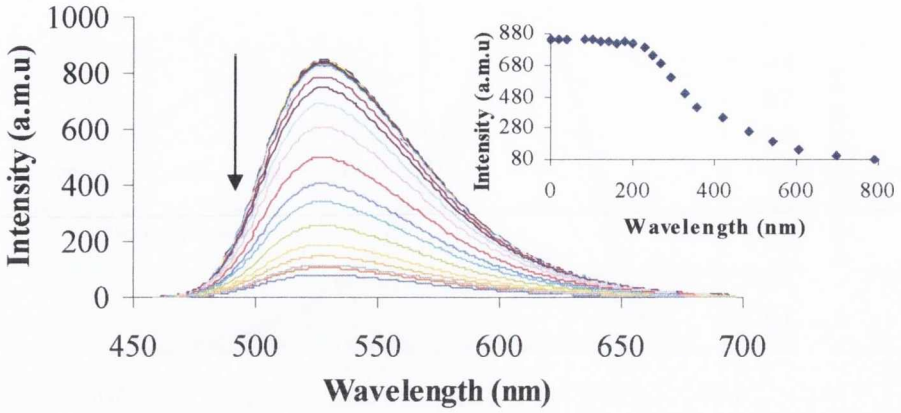


Figure A16: The changes in the emission spectra of **2** [1.0×10^{-5} M] upon addition of TBAF.$3H_2O$ (0 → 790eq). **Insert:** The relative changes at 530 nm against equivalents, λ_{ex} 445 nm.

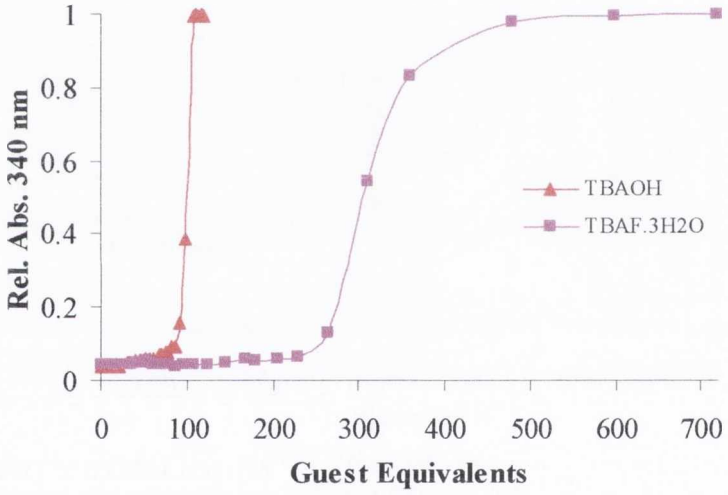


Figure A17: The relative changes in the absorption spectra at 340 nm of **2** [1.0×10^{-5} M] upon titration with TBAF.$3H_2O$ and TBAOH.$30H_2O$ in DMSO.

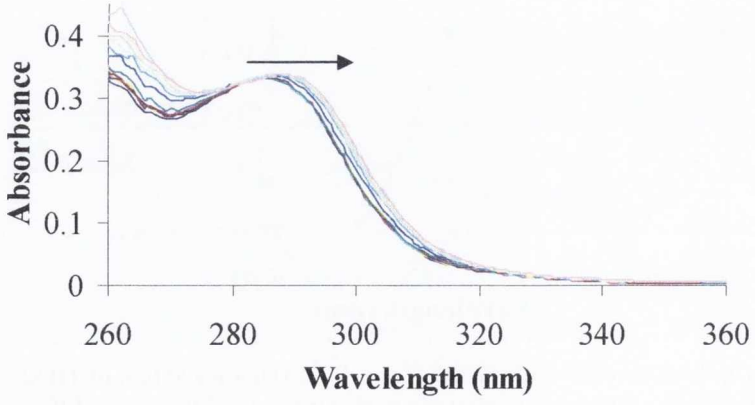


Figure A18: The changes in the absorption spectra of **37** (2×10^{-5} M) upon titration with AcO^- (0 → 100 equivalents).

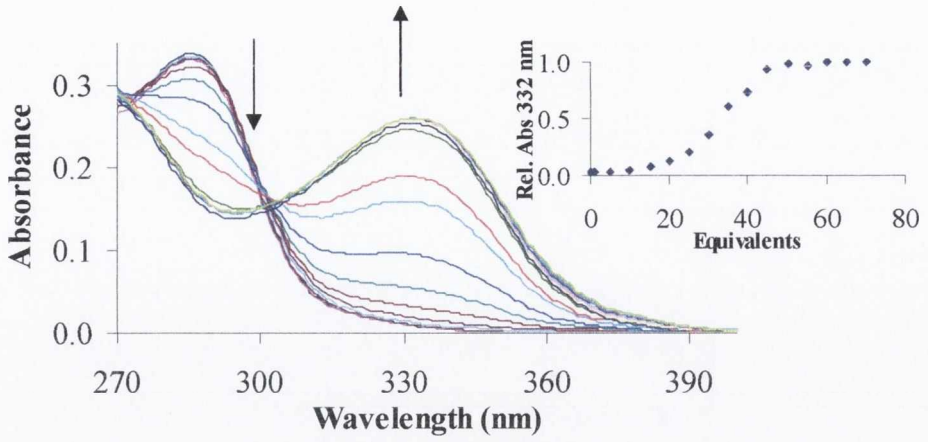


Figure A19: The changes in the absorption spectra of **37** [2.1 × 10^{-5} M] upon titration with TBAF.$3H_2O$ (0 → 105 equivalents). **Insert:** The changes in the relative absorbance at 332 nm.

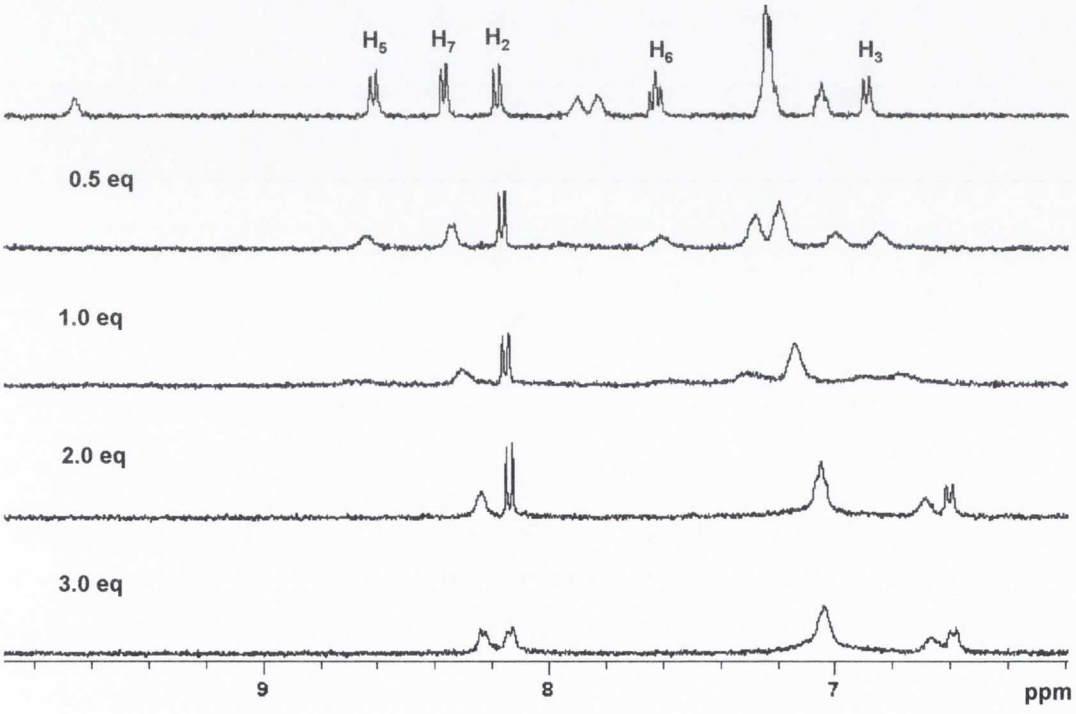


Figure A20: Stack plot of ^{1}H NMR spectra (400 MHz, DMSO-d_6) of **4a** [2.1 x 10^{-3} M] after addition of various equivalents of TBAF $3H_2O$.

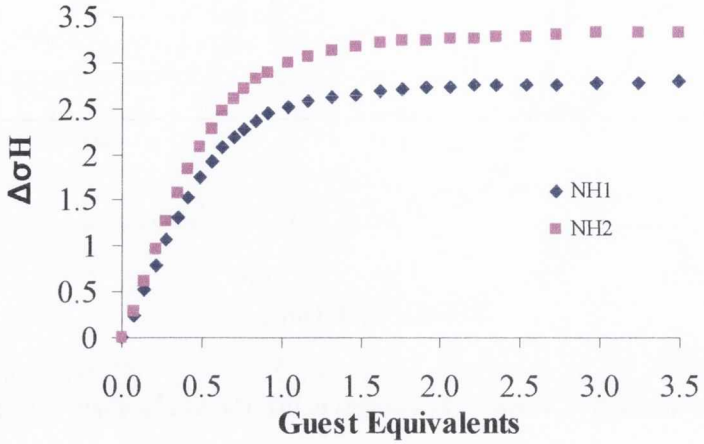


Figure A21: The changes in the chemical shift of the N-H protons of **4b** [2×10^{-5} M] upon titration with AcO^-.

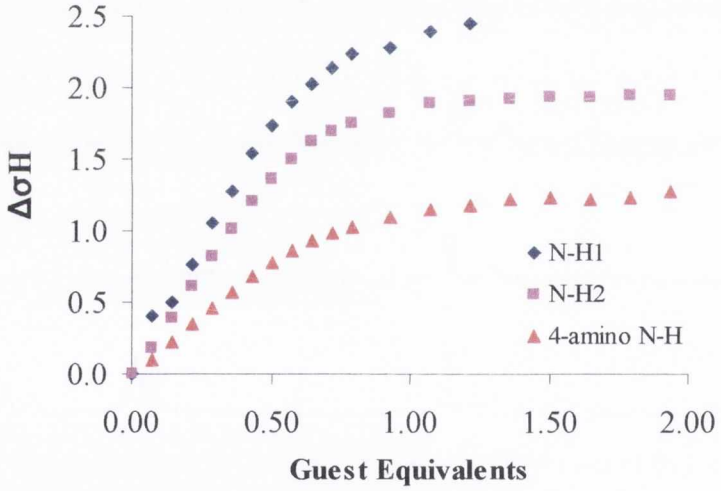


Figure A22: The changes in the chemical shift of N-H protons of **4b** [2×10^{-5} M] upon titration with $H_2PO_4^-$.

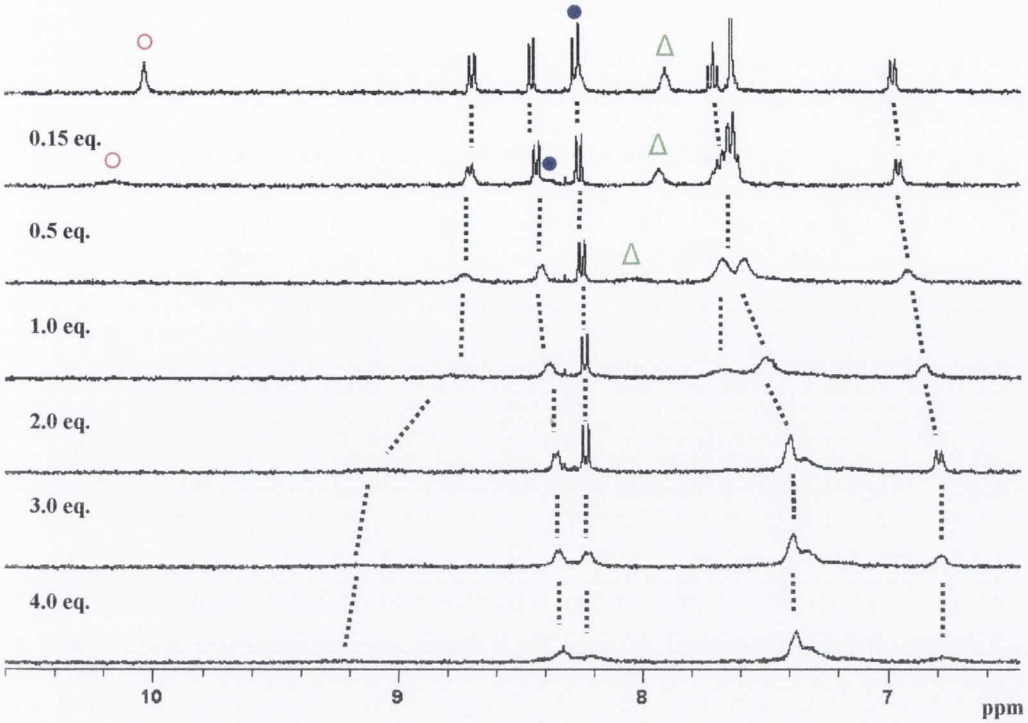


Figure A23: Stack plot of ^{1}H NMR spectra (400 MHz, DMSO-d_6) of **4b** [2 x 10^{-3} M] after addition of various equivalents of TBAF $3H_2O$.

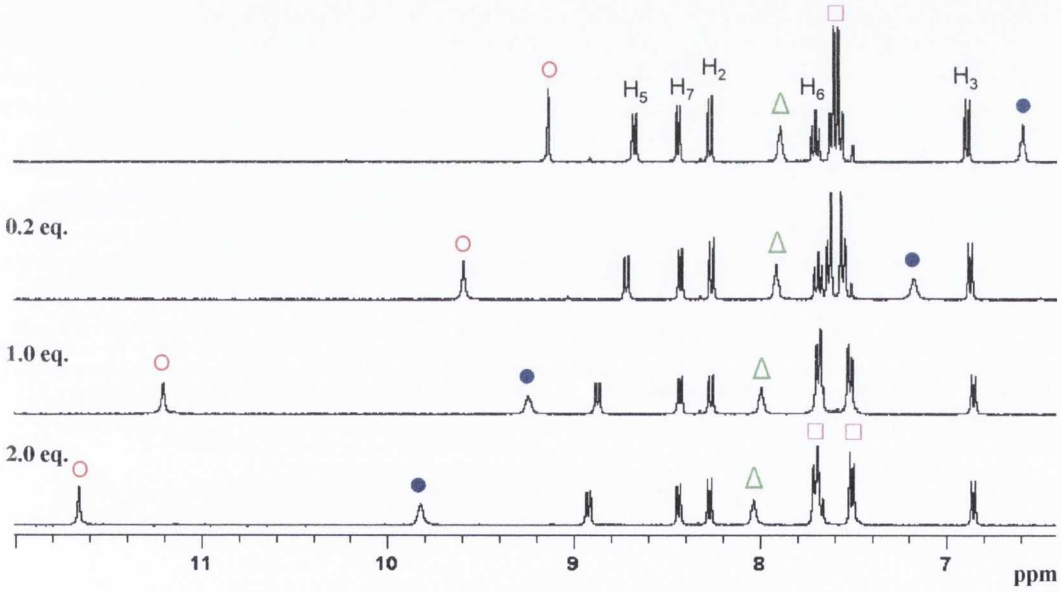


Figure A24: Stack plot of ^{1}H NMR spectra (400 MHz, DMSO-d_6) of **4c** after addition of various equivalents of AcO^-.

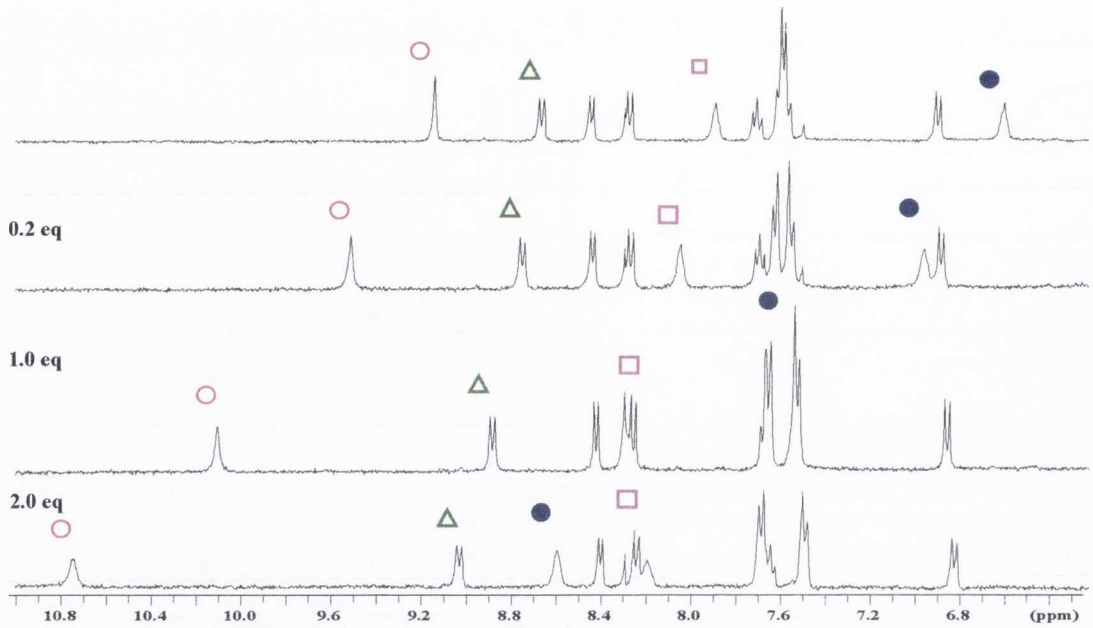


Figure A25: Stack plot of ^{1}H NMR spectra (400 MHz, DMSO-d_6) of **4c** after addition of various equivalents of $H_2PO_4^-$.

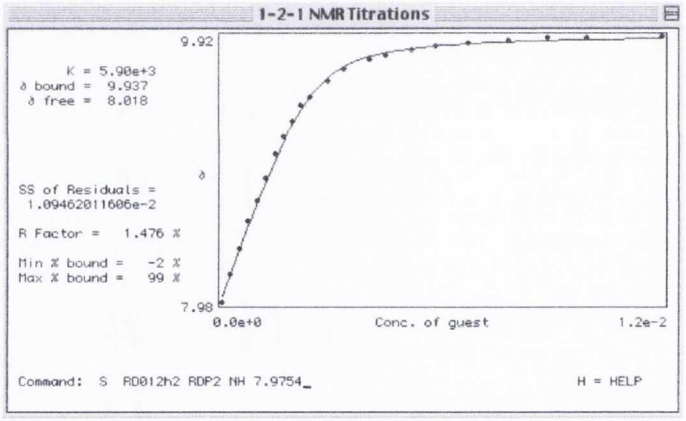


Figure A26: The binding isotherm with fit of **4a** for the changes in the chemical shift of the N-H proton at 7.97 ppm upon titration with $H_2PO_4^-$ in DMSO-d_6.

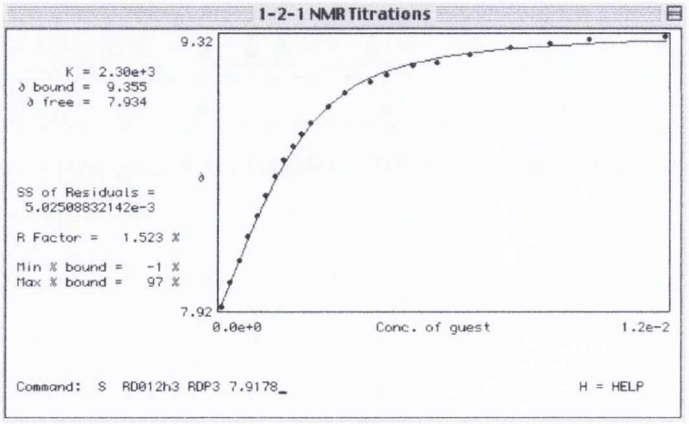


Figure A27: The binding isotherm with fit of **4a** for the changes in the chemical shift of the 4-amino N-H proton at 7.91 ppm upon titration with $H_2PO_4^-$ in DMSO-d_6.

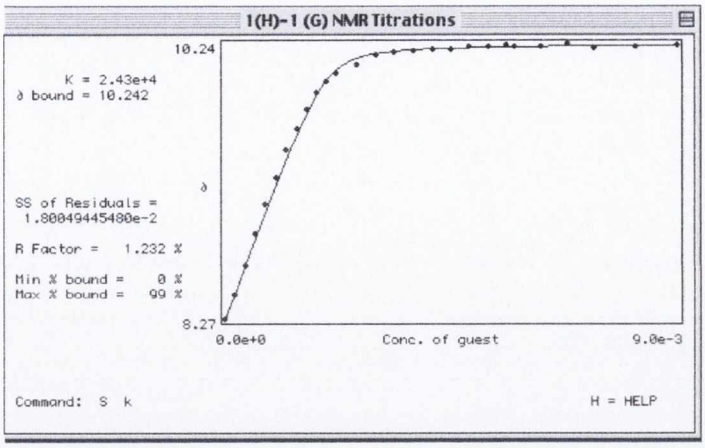


Figure A28: The binding isotherm with fit of **4b** for the changes in the chemical shift of the N-H proton at 8.27 ppm upon titration with $H_2PO_4^-$ in DMSO-d_6.

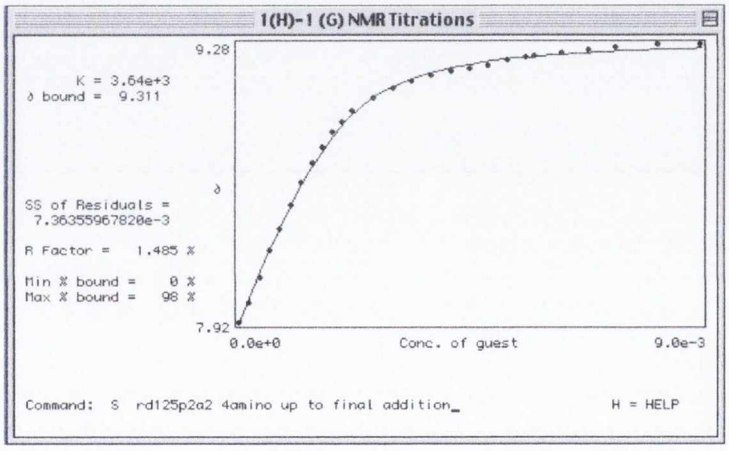


Figure A29: The binding isotherm with fit of **4b** for the changes in the chemical shift of the 4-amino proton at 7.92 ppm upon titration with $H_2PO_4^-$ in DMSO-d_6.

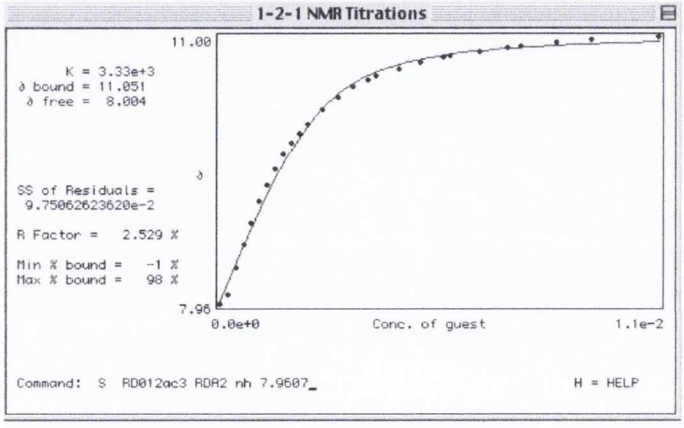


Figure A30: The binding Isotherm with fit of **4a** for the changes in the chemical shift of the N-H proton at 7.96 ppm upon titration with AcO^- in DMSO-d_6

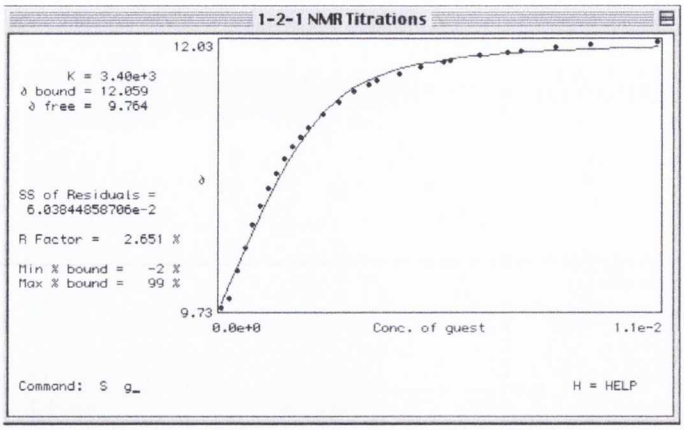


Figure A31: The binding Isotherm with fit of **4a** for the changes in the chemical shift of the N-H proton at 9.72 ppm upon titration with AcO^- in DMSO-d_6

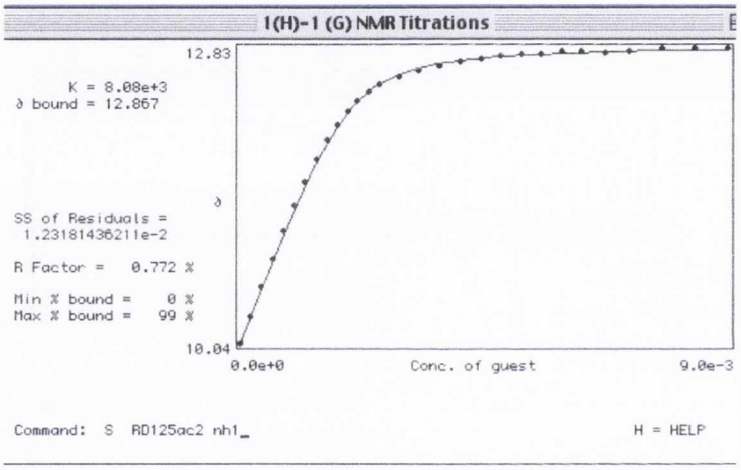


Figure A32: The binding isotherm with fit for the changes in the chemical shift of the N-H_1 proton of **4b** upon titration with AcO^- in DMSO-d_6.

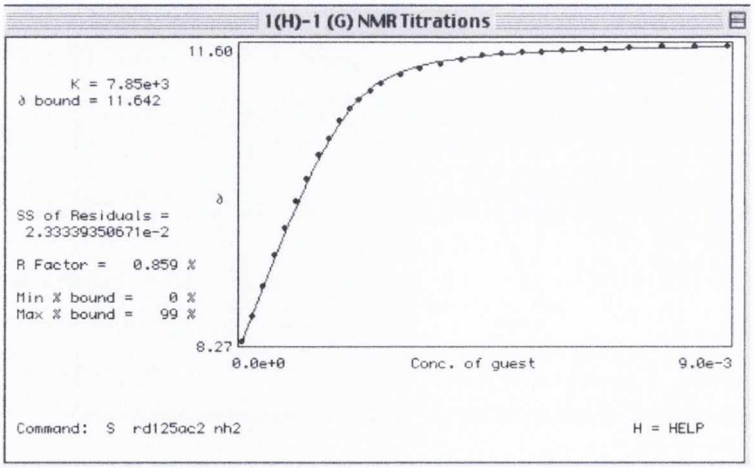


Figure A33: The binding isotherm with fit for the changes in the chemical shift of the N-H_2 proton of **4b** upon titration with AcO^- in DMSO-d_6.

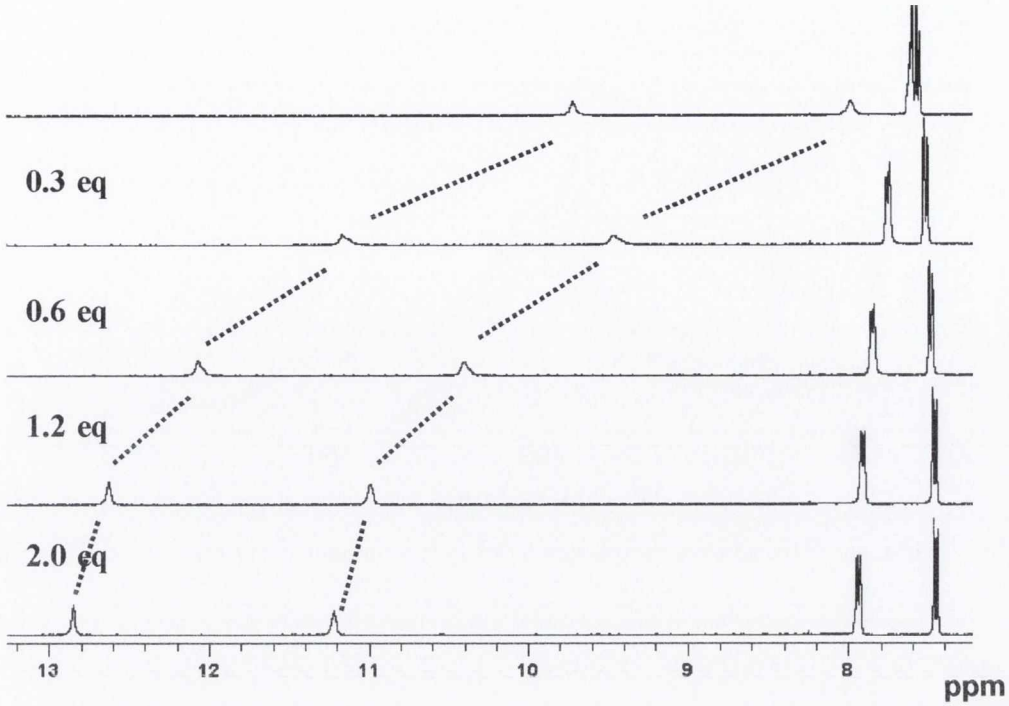


Figure A34: A stack plot of the ^{1}H NMR spectra (400 MHz, DMSO-d_6) of **37** [1.2 x 10^{-2} M] upon the addition of various equivalents of AcO^-.

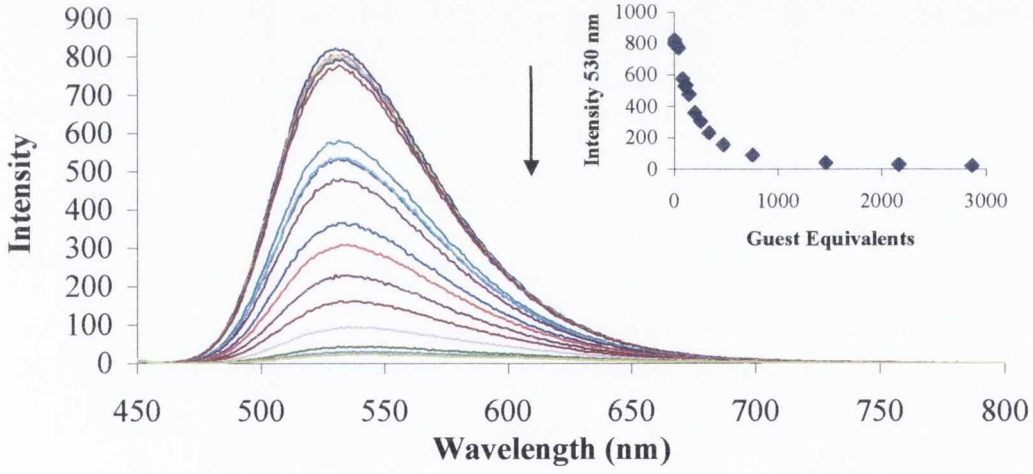


Figure A35: The changes in the emission spectrum of **39** upon titration with F^- (0→3000 equivalents) in DMSO. **Insert**: The changes at 530 nm.

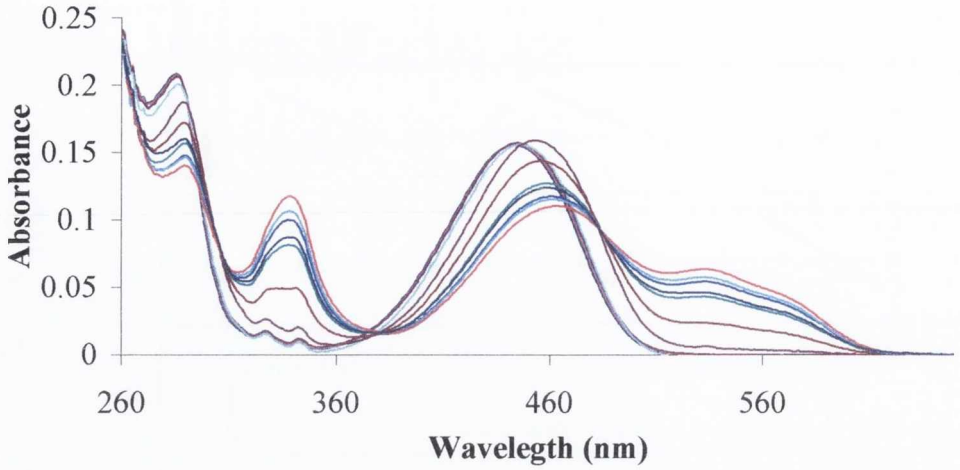


Figure A36: The changes in the absorption spectrum of **39** upon titration with $HP_2O_7^{3-}$ (0→146 equivalents) in DMSO.

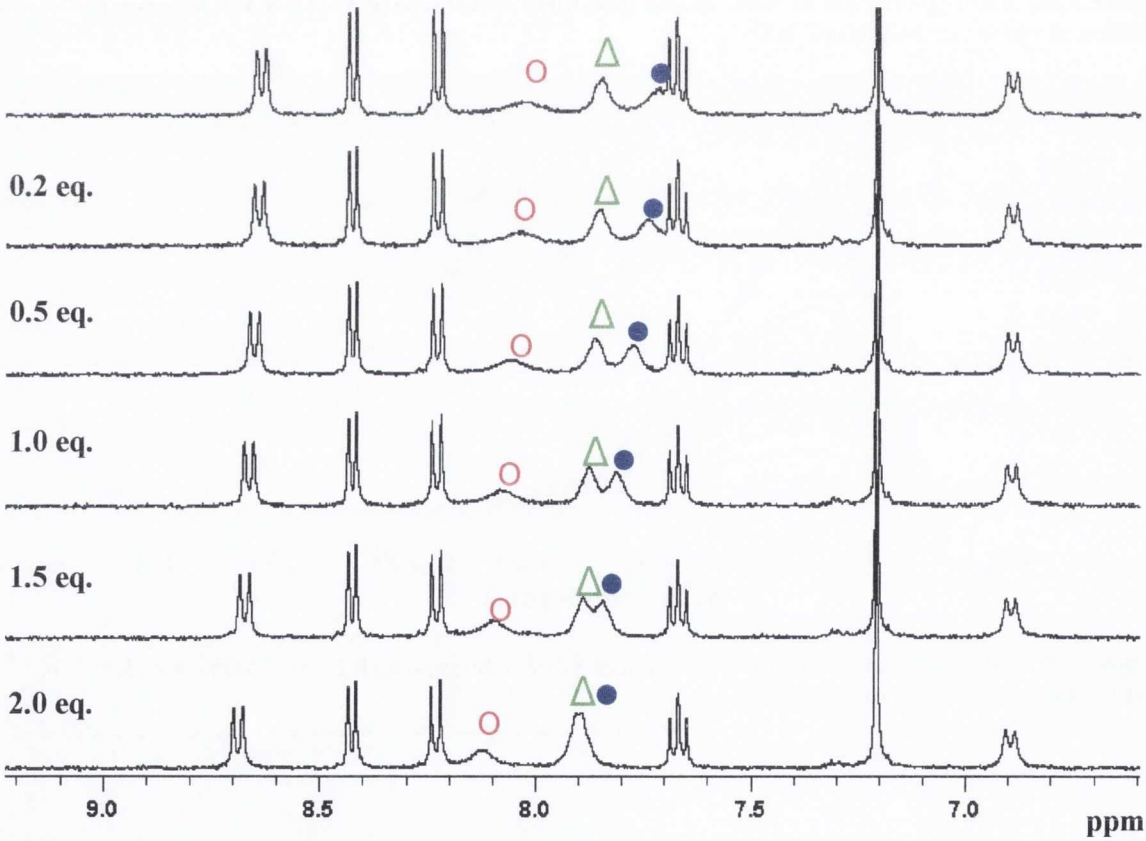


Figure A37: Stack plot of ^{1}H NMR spectra (400 MHz, DMSO-*d6*) of **39** after addition of various equivalents of Cl^-.

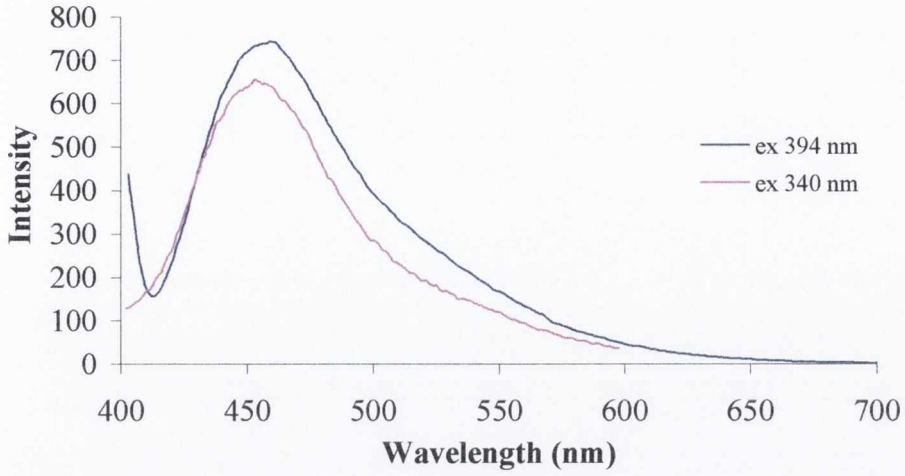


Figure A38: The fluorescence emission spectra of **42** upon excitation at various wavelengths in DMSO.

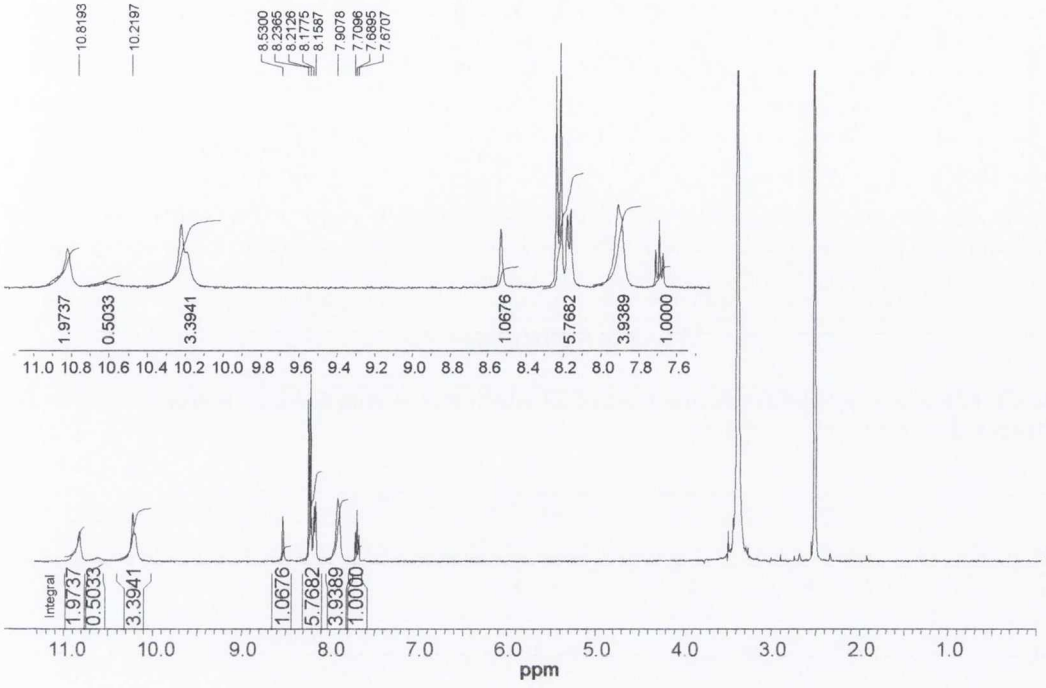


Figure B1: ^{1}H NMR (400MHz, DMSO-d_6) of **53**.

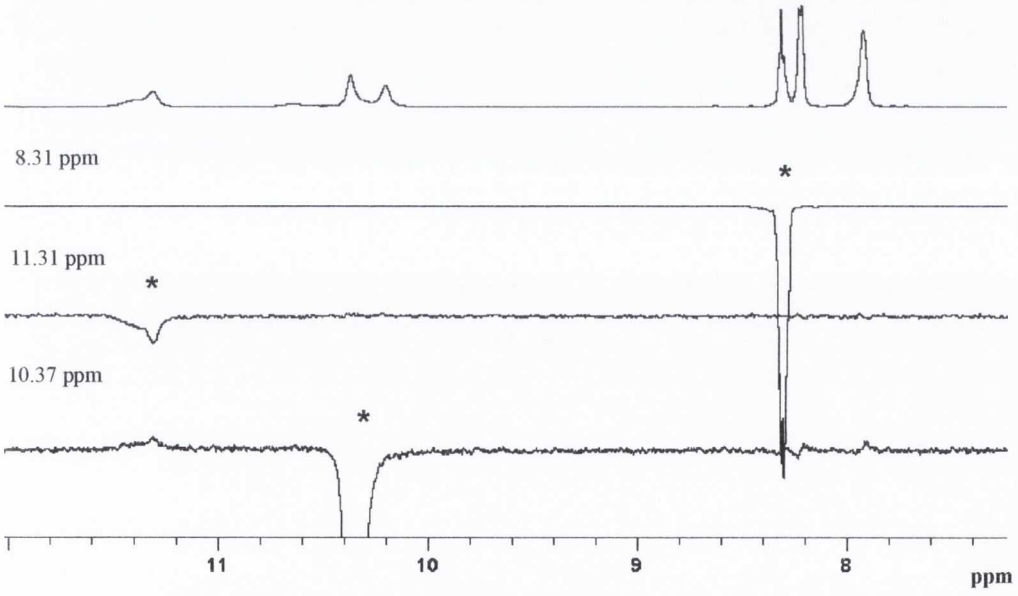


Figure B2: Selective ROESY NMR (600 MHz, DMSO-d_6) of **54**

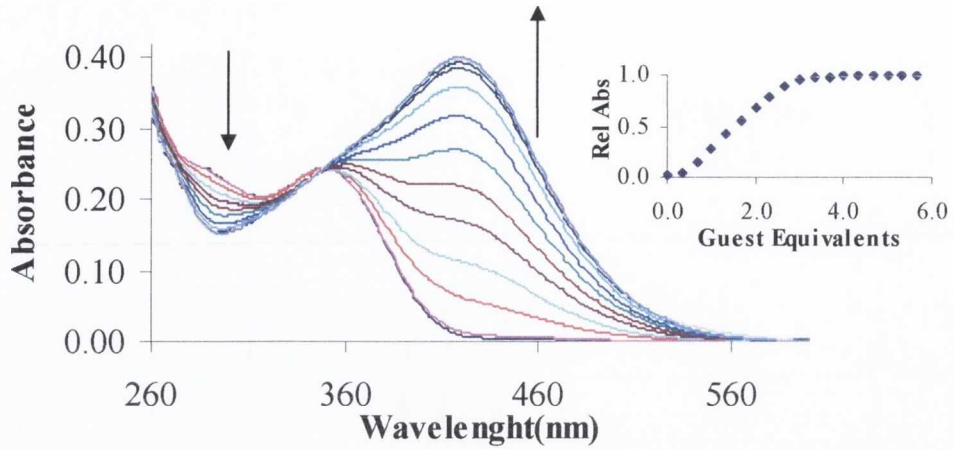


Figure B3: The changes in the absorption spectrum of **53** upon titration with $H_2PO_4^-$. **Insert:** Relative changes at 420 nm.

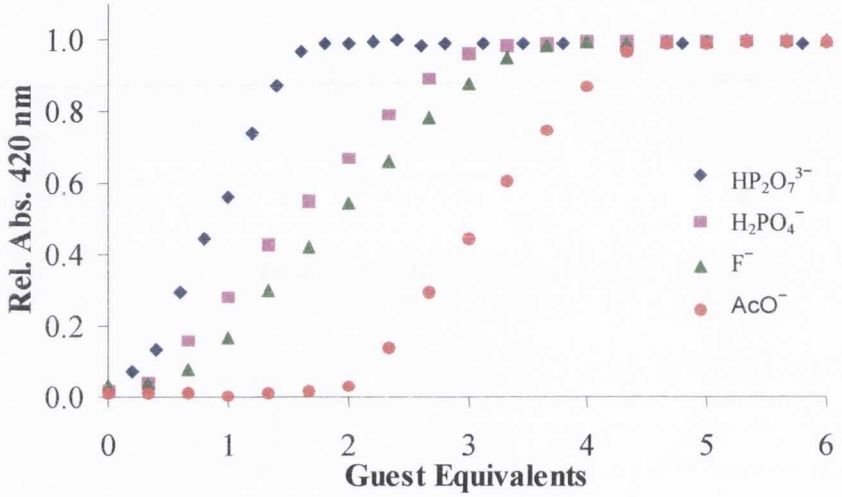


Figure B4: Relative changes in absorption spectrum of **53** [1×10^{-5} M] at 420 nm upon titration with various anions in DMSO.

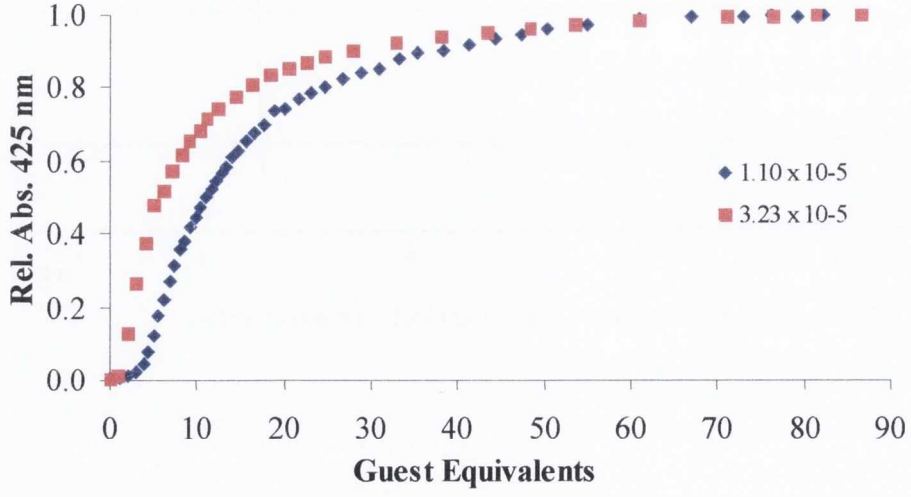


Figure B5: The relative changes in the absorption spectrum of **54** at varying concentrations upon titration with $H_2PO_4^-$ in 4:1 DMSO-H_2O.

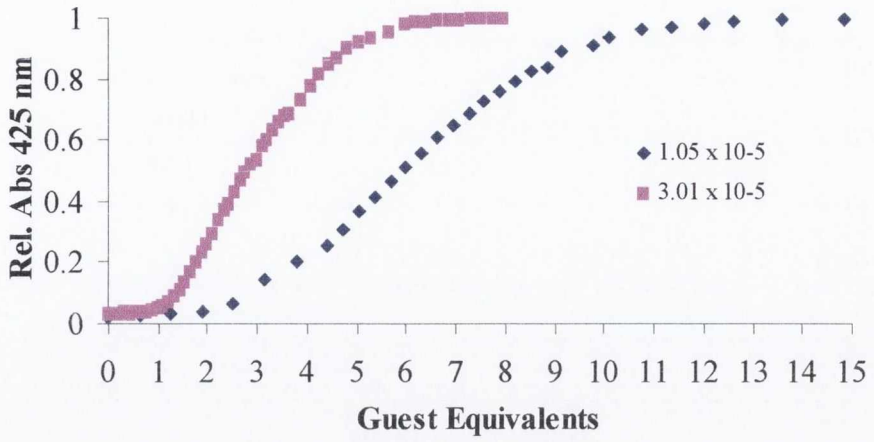


Figure B6: The relative changes in the absorption spectrum of **54** at varying concentrations upon titration with $HP_2O_7^{3-}$ in 4:1 DMSO-H_2O.

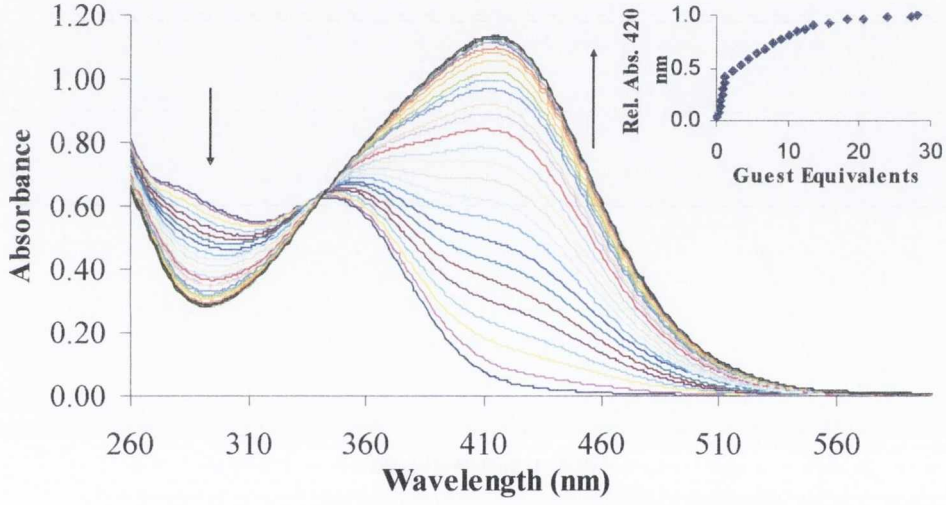


Figure B7: The changes in the absorption spectrum of **54** [3×10^{-5} M] upon titration with NaOAc in 4:1 DMSO-H_2O.

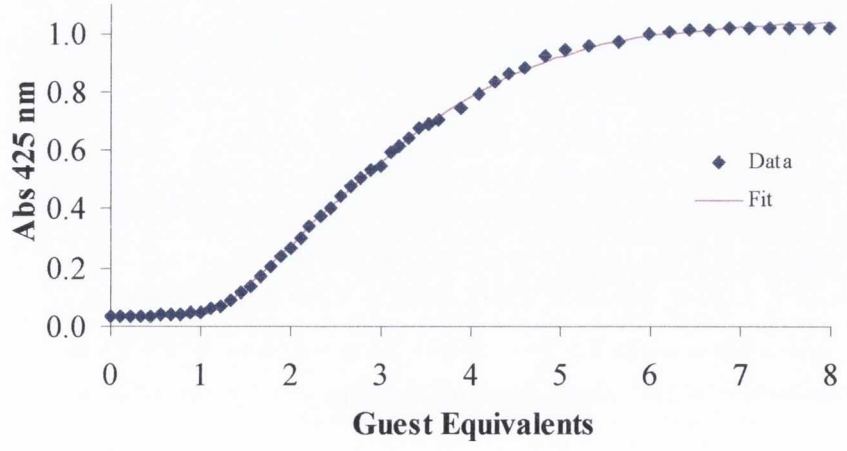


Figure B8: Binding Isotherm with fit of **54** [3×10^{-5} M] upon titration with TBA.$HP_2O_7^{3-}$ in 4:1 DMSO-H_2O.

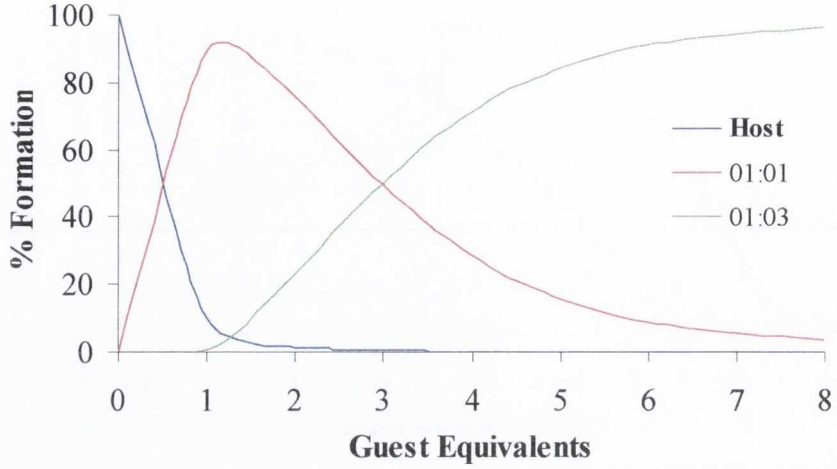


Figure B9: Species distribution diagram of **54** [3×10^{-5} M] upon addition of TBA.HP_2O_7 (0 → 8 eq) in 4:1 DMSO-H_2O.

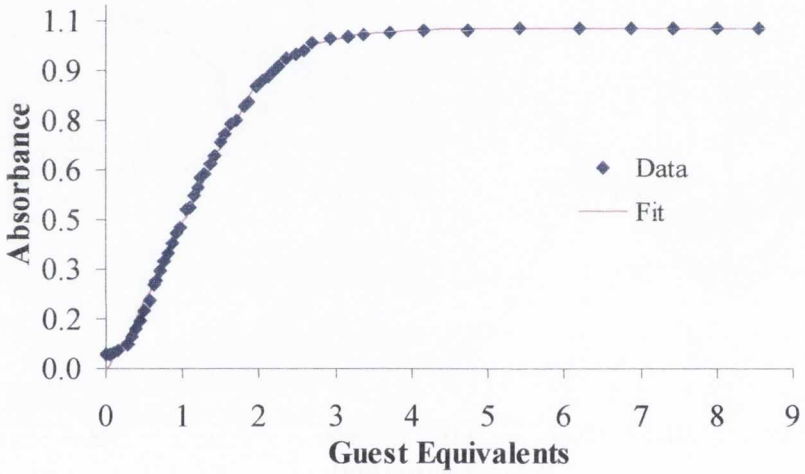


Figure B10: Binding Isotherm with fit of **54** [3×10^{-5} M] upon titration with TBA.OAc in 4:1 DMSO-H_2O.

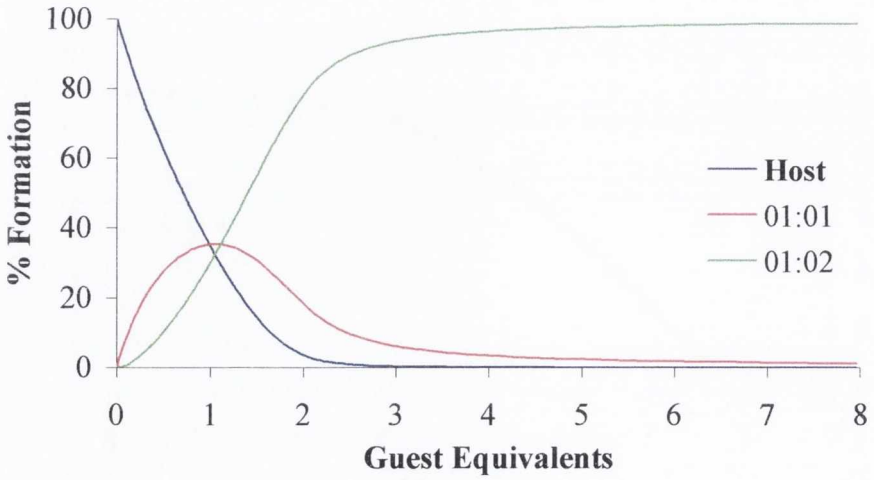


Figure B11: Species distribution diagram of **54** [3×10^{-5} M] upon addition TBA.OAc (0 → 8 eq) in 4:1 DMSO-H_2O.

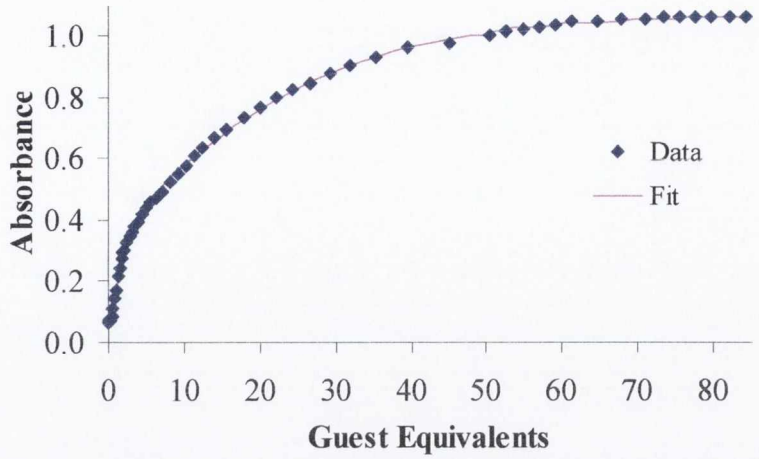


Figure B12: Binding Isotherm with fit of **54** [3×10^{-5} M] upon titration with ADP.Na_2 in 4:1 DMSO-H_2O.

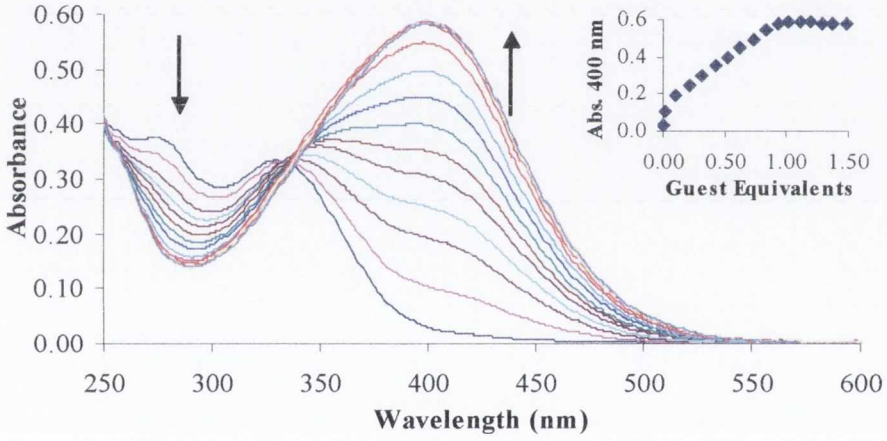


Figure B13: The changes in the absorption spectrum of **54** [2×10^{-5} M] upon titration with AcO^- in 1% DMSO in MeCN.

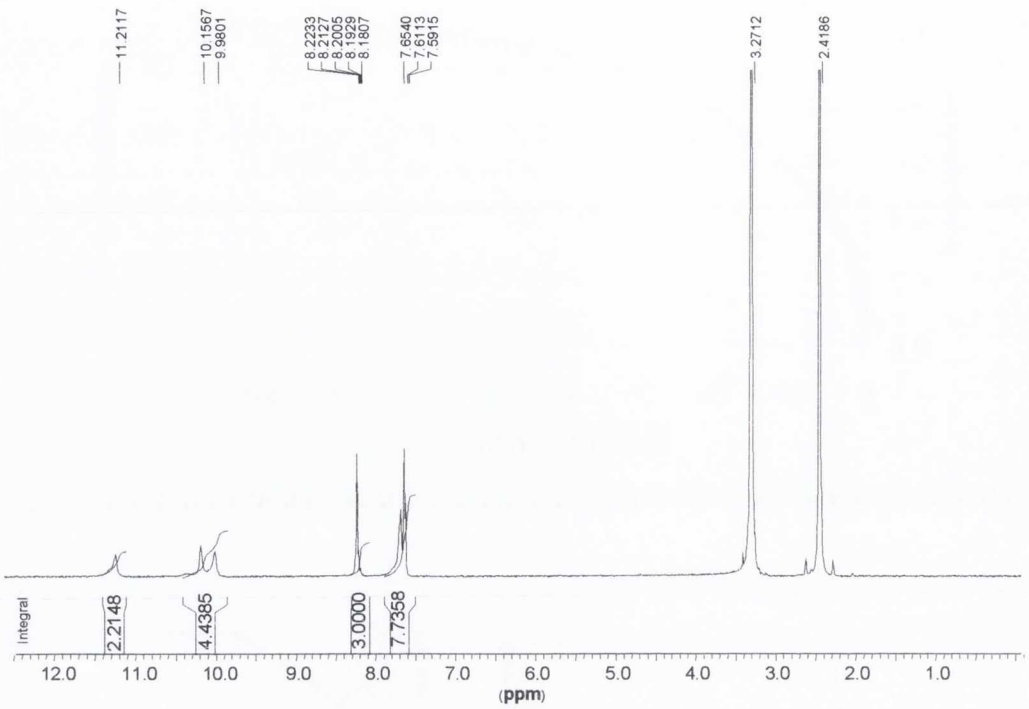


Figure B14: ^{1}H NMR (400 MHz, DMSO-d_6) spectrum of **56**.

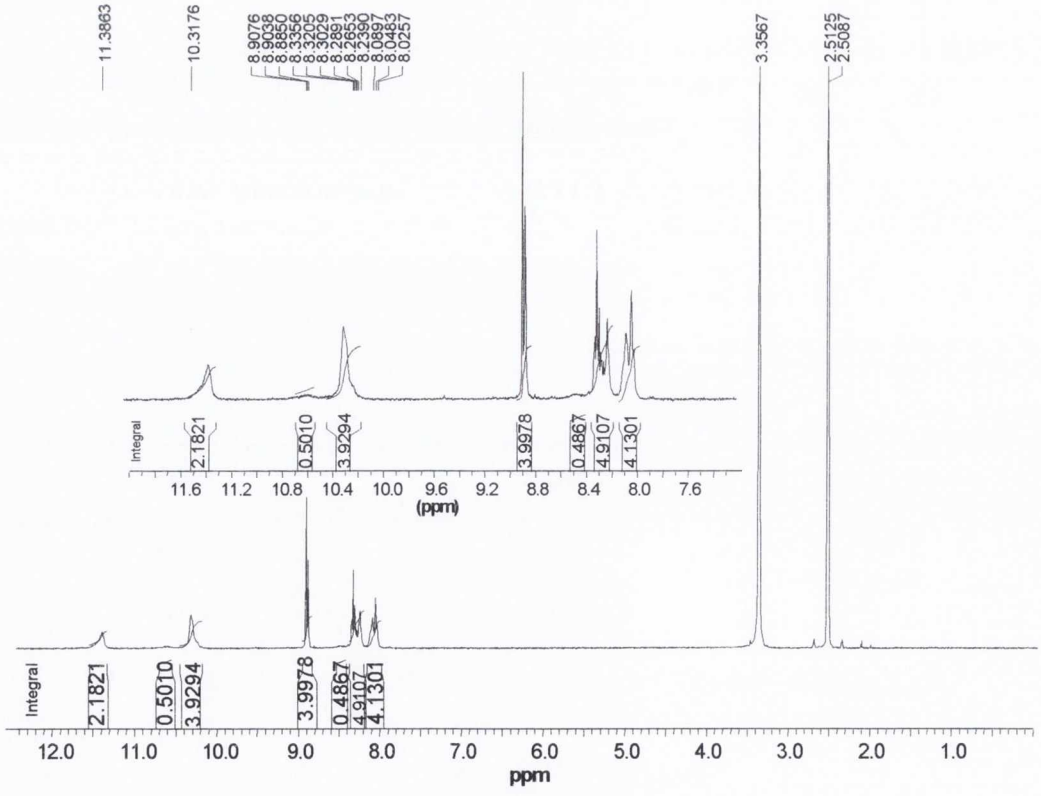


Figure B15: ^{1}H NMR (400 MHz, DMSO-d_6) spectrum of **57**.

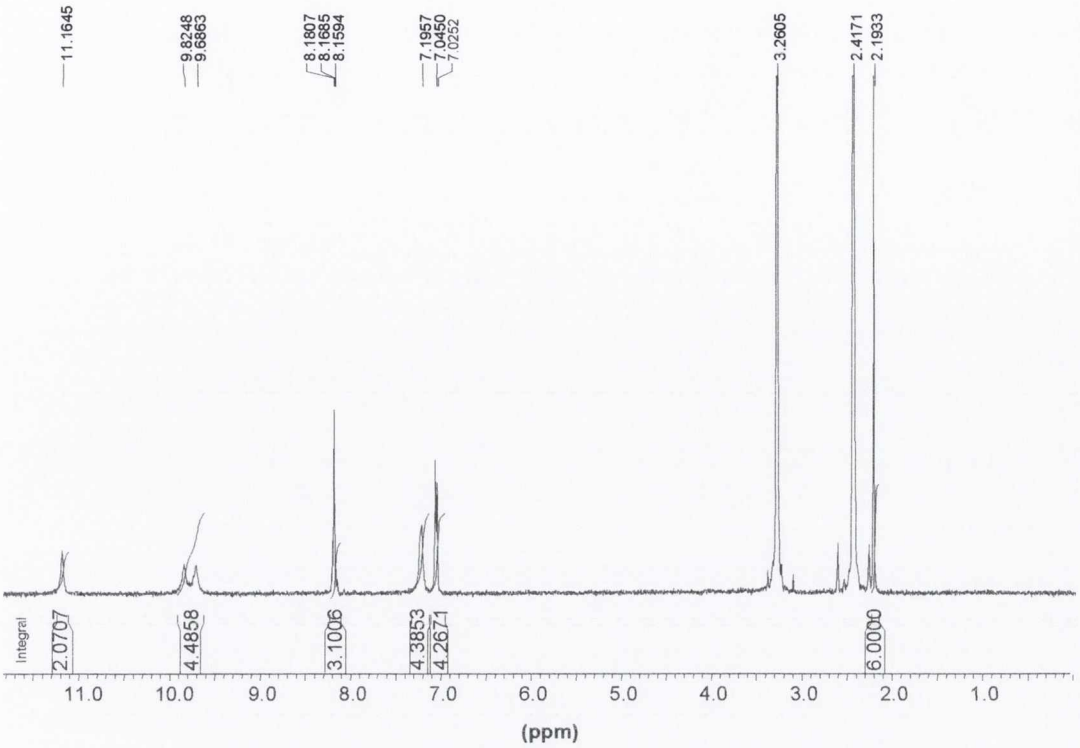


Figure B16: ^{1}H NMR (400 MHz, DMSO-d_6) spectrum of **27b**.

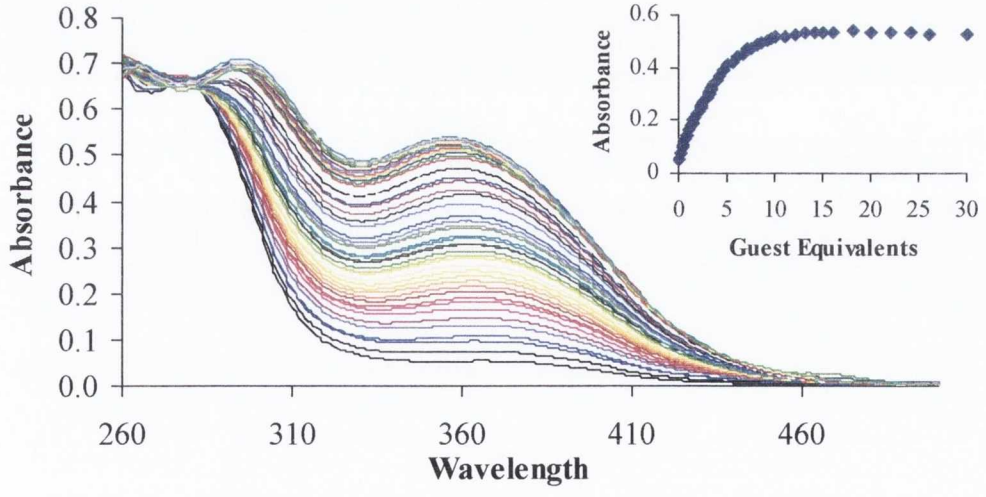


Figure B17: The changes in the absorption spectrum of **56** [2.0×10^{-5} M] upon titration with TBAOH 0→30 equivalents) in 4:1 DMSO-H_2O.

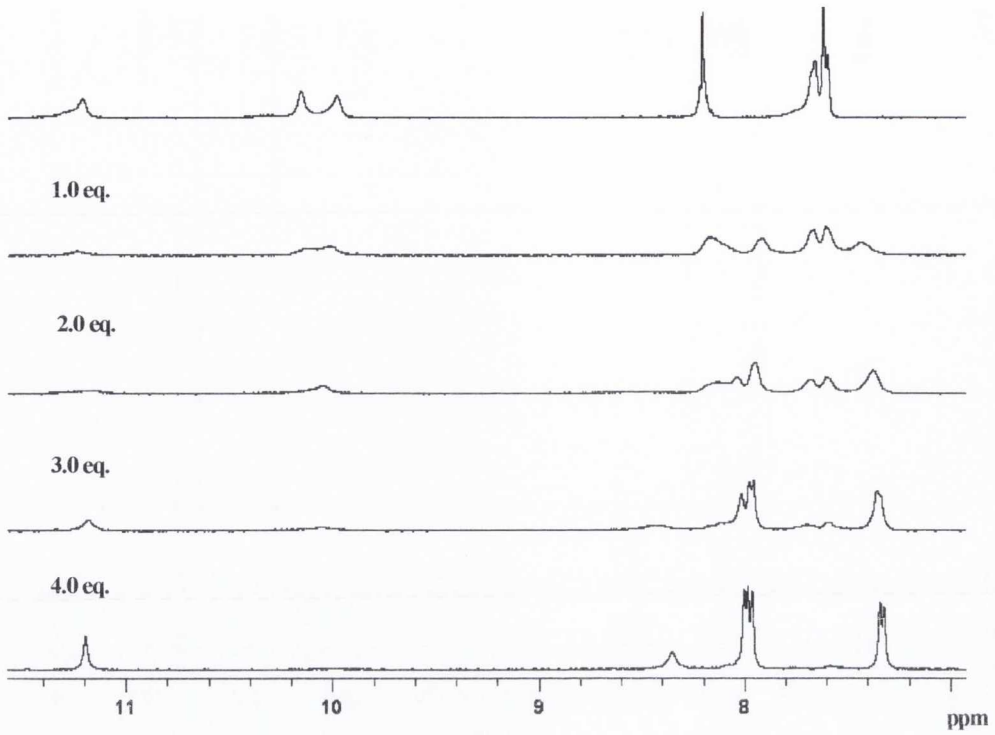


Figure B18: ^{1}H NMR (400 MHz, DMSO-d_6) titration of **56** [3.3×10^{-3} M] with $H_2PO_4^-$.

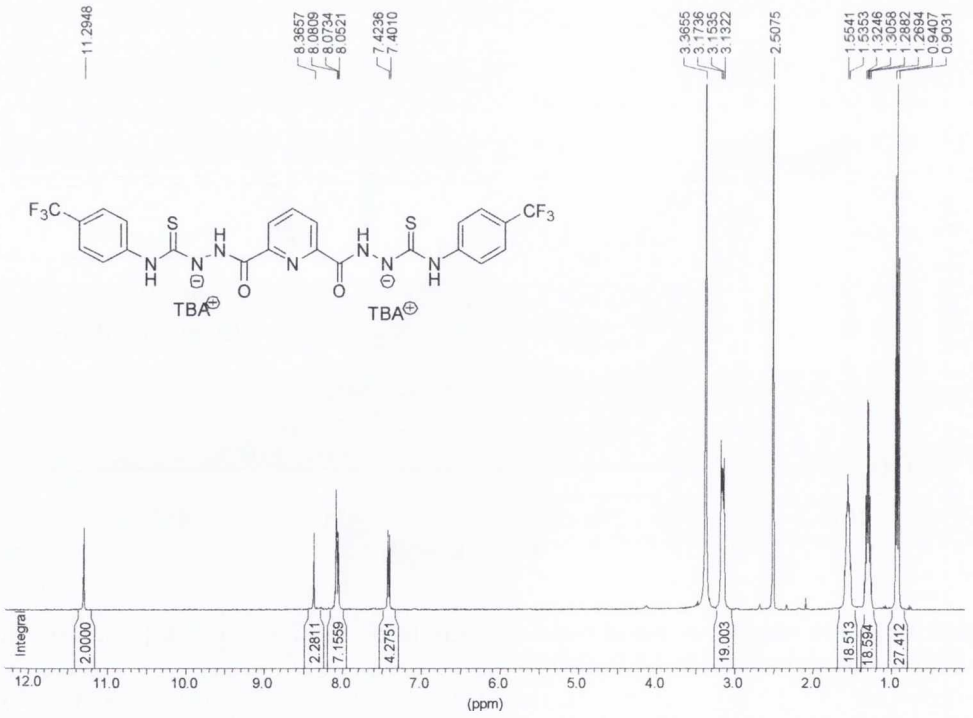


Figure B19: ^{1}H NMR (400MHz, DMSO-d_6) spectrum of **56** after the addition of *ca.* 2 equivalents of TBAOH.

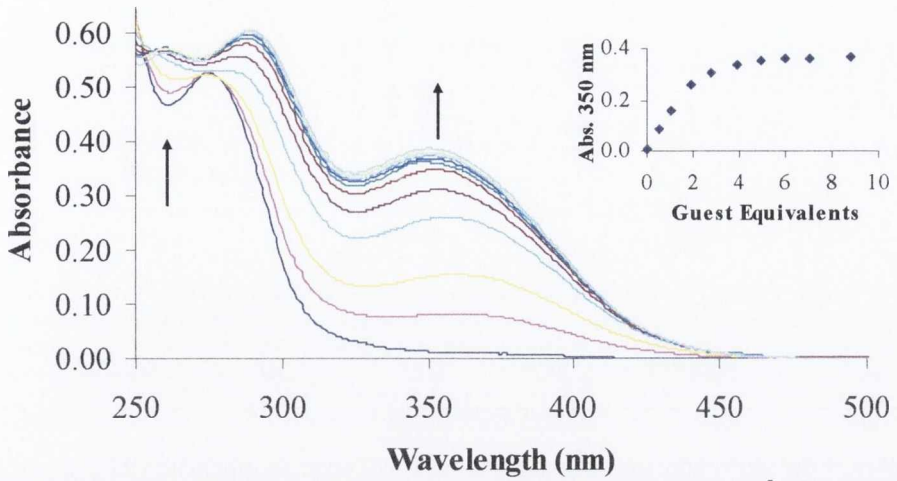


Figure B20: The changes in the absorption spectrum of **56** [1.9×10^{-5} M] upon titration with AcO^- (0 → 9 equivalents) in 1% DMSO in MeCN. **Insert**: The changes at 350 nm.

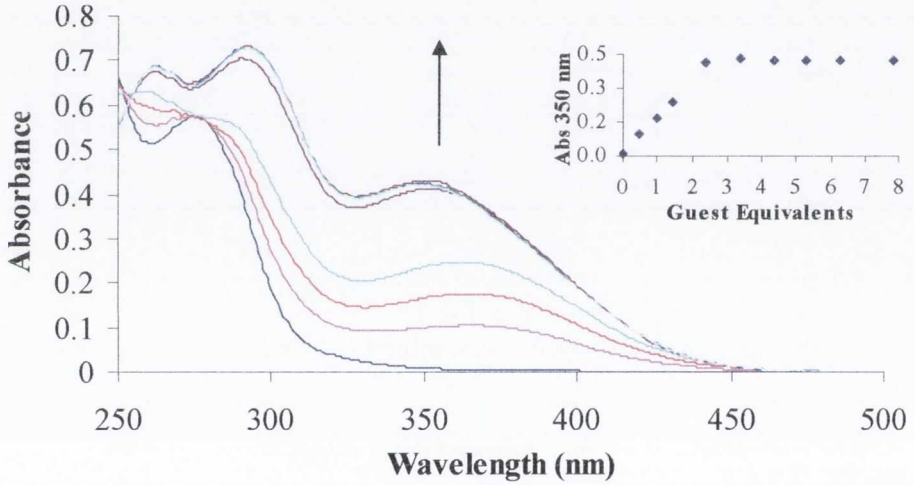


Figure B21: The changes in the absorption spectrum of **56** [2×10^{-5} M] upon titration with OH^- (0 → 9 equivalents) in 1% DMSO in MeCN. **Insert**: The changes at 360 nm against equivalents.

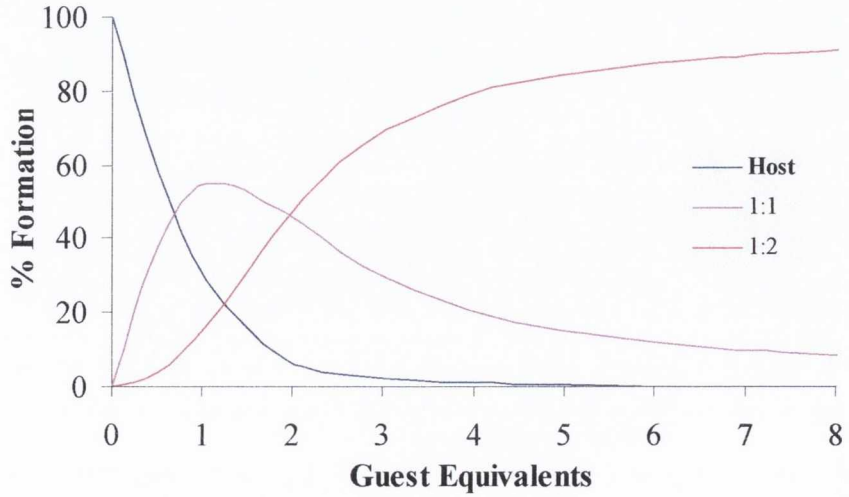


Figure B22: Species distribution diagram of **56** [3×10^{-5} M] upon titration with AcO^- (0 → 8 eq) in 1% DMSO in MeCN.

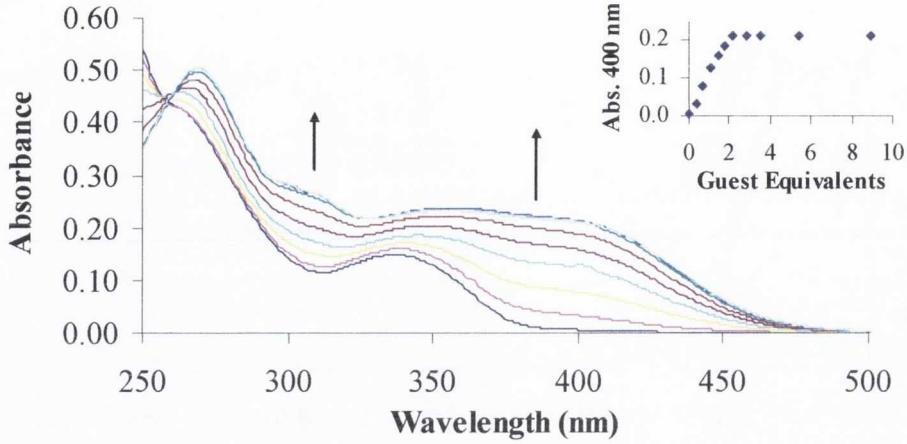


Figure B23: The changes in the absorption spectrum of **57** [1×10^{-5} M] upon titration with OH^- ($0 \rightarrow 9$ equivalents) in 1% DMSO in MeCN. **Insert**: The changes at 360 nm against equivalents.

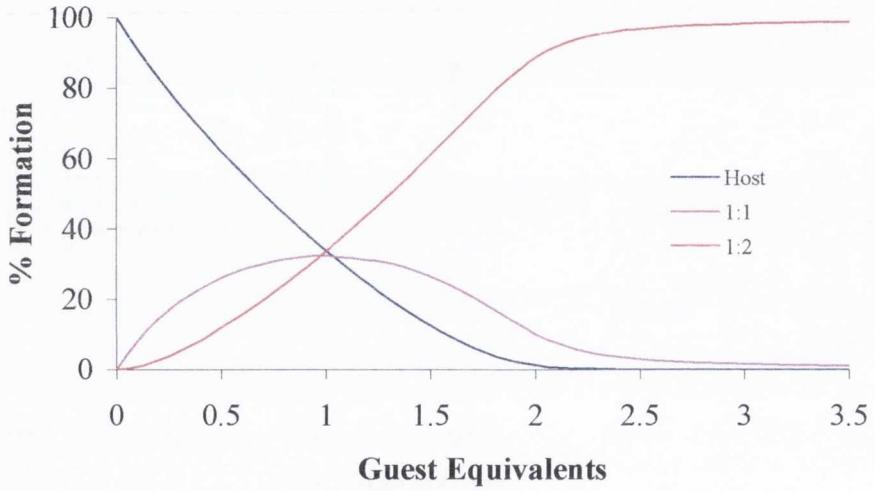


Figure B24: Species distribution diagram of **57** [2×10^{-5} M] upon titration with AcO^- ($0 \rightarrow 3.5$ equivalents) in 1% DMSO in MeCN.

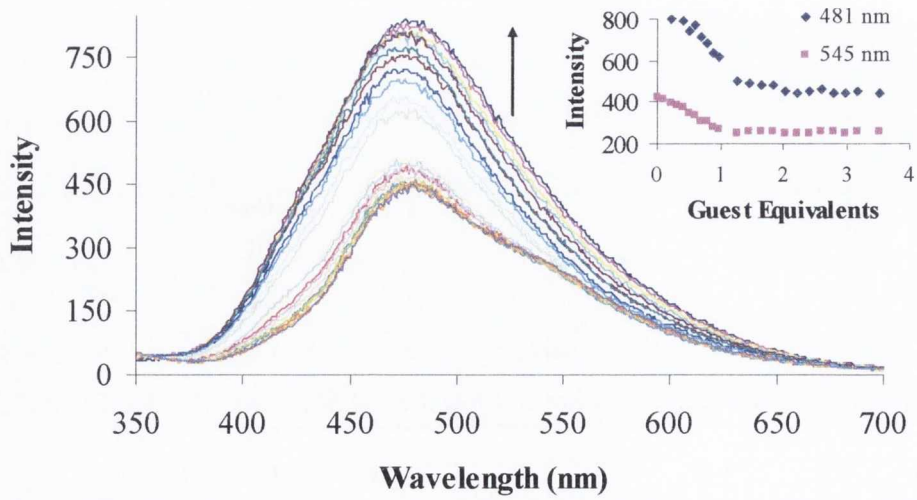


Figure B25: The changes in the emission spectrum (λ_{ex} =262 nm, λ_{em} = 477 nm) of **57** [1.9×10^{-5} M] upon addition of AcO ($0 \rightarrow 3.5$ eq.) in 1% DMSO in MeCN. **Insert**: The changes in intensity at 481 nm and 545 nm.

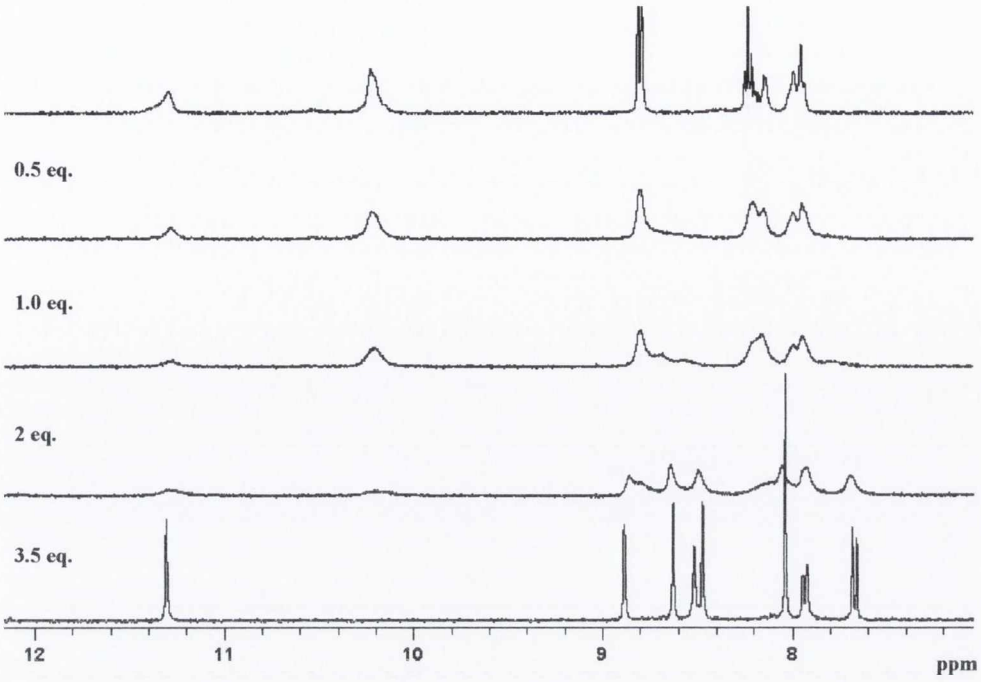


Figure B26: ^{1}H NMR (400 MHz, DMSO-d_6) titration of **57** [3 × 10^{-3} M] with AcO^{-}.

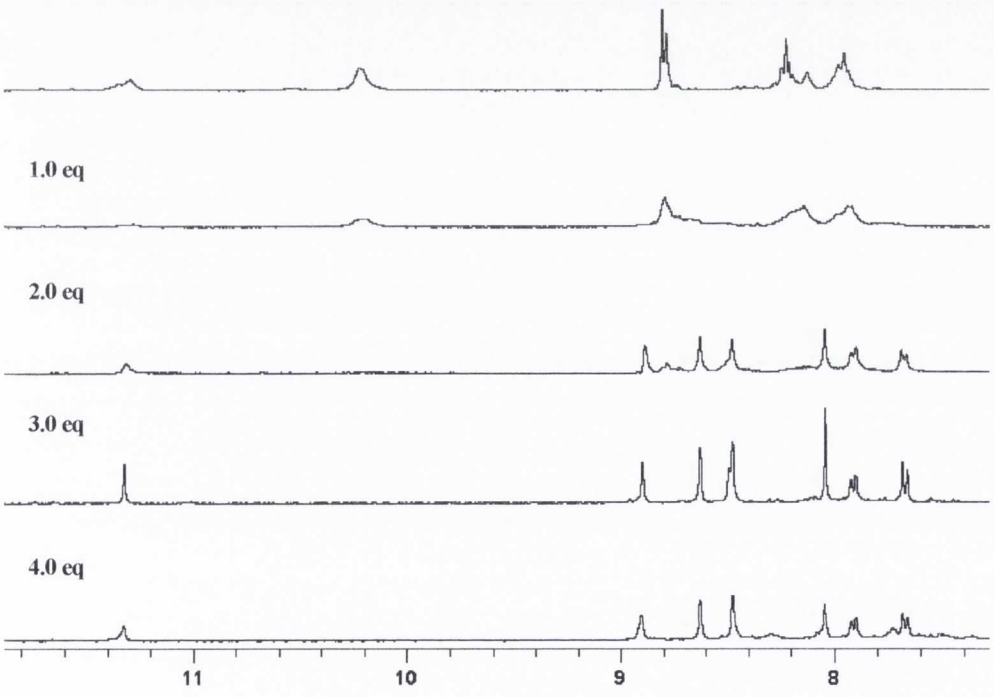


Figure B27: ^{1}H NMR (400 MHz, DMSO-d_6) titration of **57** [3 × 10^{-3} M] with TBAOH.

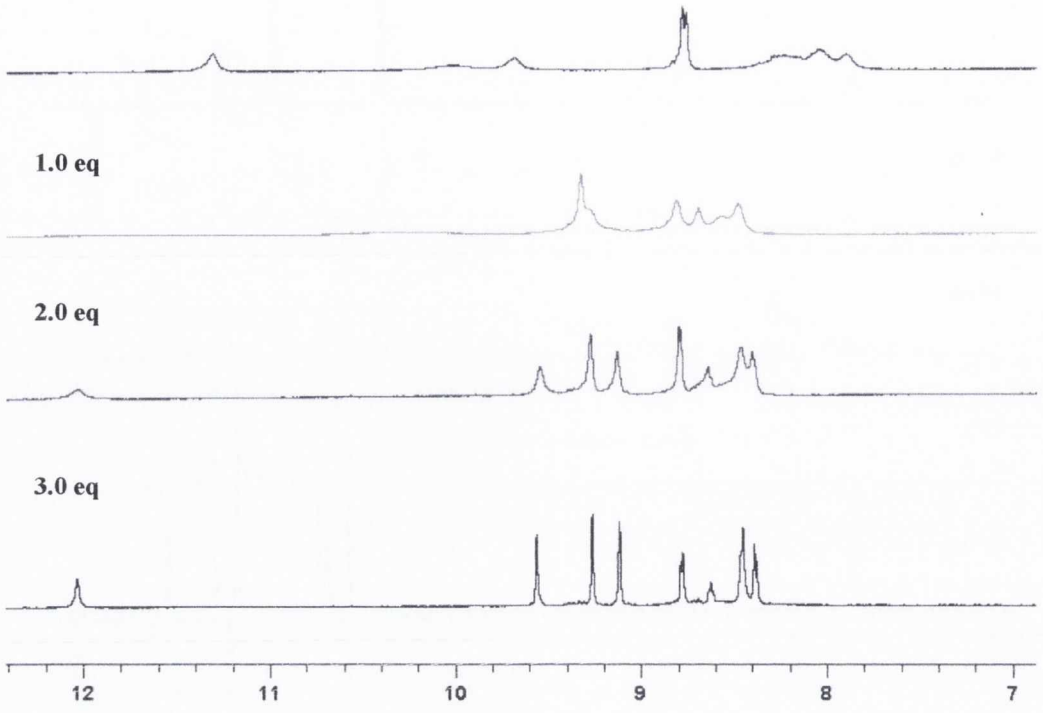


Figure B28: ^{1}H NMR (400 MHz, 5% DMSO-d_6 in MeCN-d_7) titration of **57** [1 $\times 10^{-3}$ M] with AcO^-.

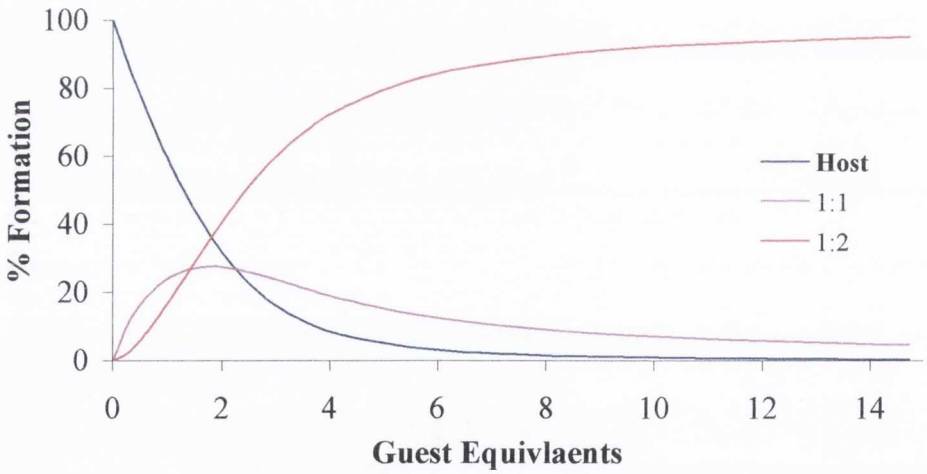


Figure B29: Species distribution diagram of **27b** [2.5 $\times$ 10^{-5} M] upon titration with TBAOH (0 $\rightarrow$ 14.7 equivalents) in 4:1 DMSO-H_2O.

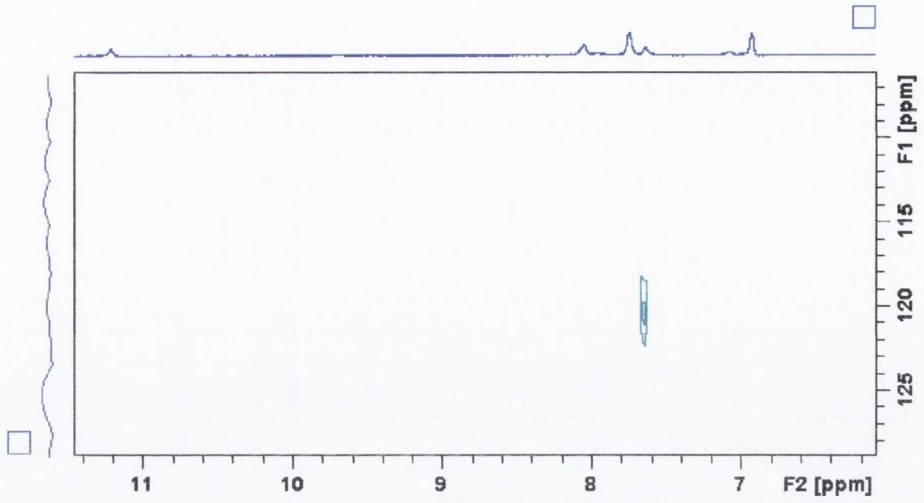


Figure B30: ^{15}N-^{1}H COSY (600 MHz, DMSO-d_6) of **27b** upon the addition of 3.5 equivalents of AcO^-.

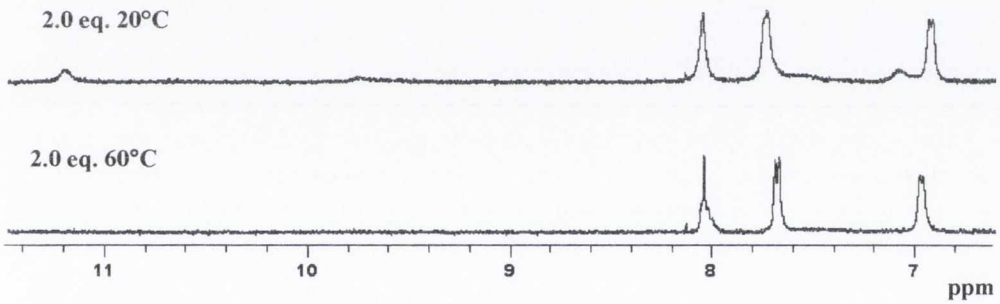


Figure B31: VT ^{1}H NMR (400 MHz, DMSO-d_6) of **27b** upon the addition of 2 equivalents of AcO^-.

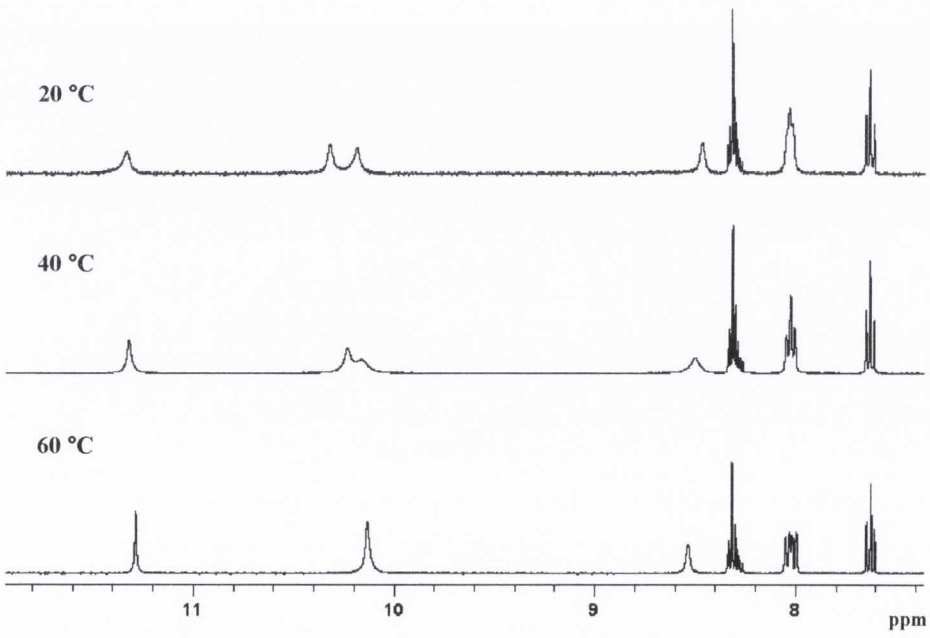


Figure B32: VT ^{1}H NMR (400 MHz, DMSO-d_6) of **61**.

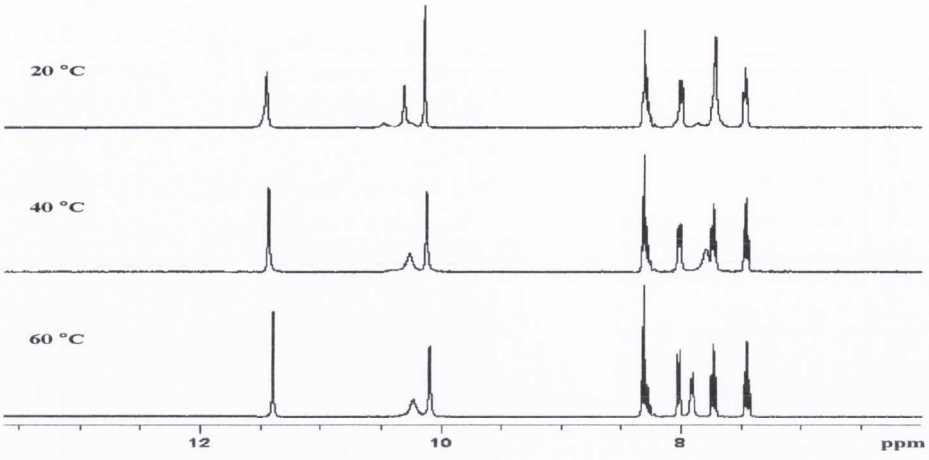


Figure B33: VT ^{1}H NMR (400 MHz, DMSO-d_6) of **62**.

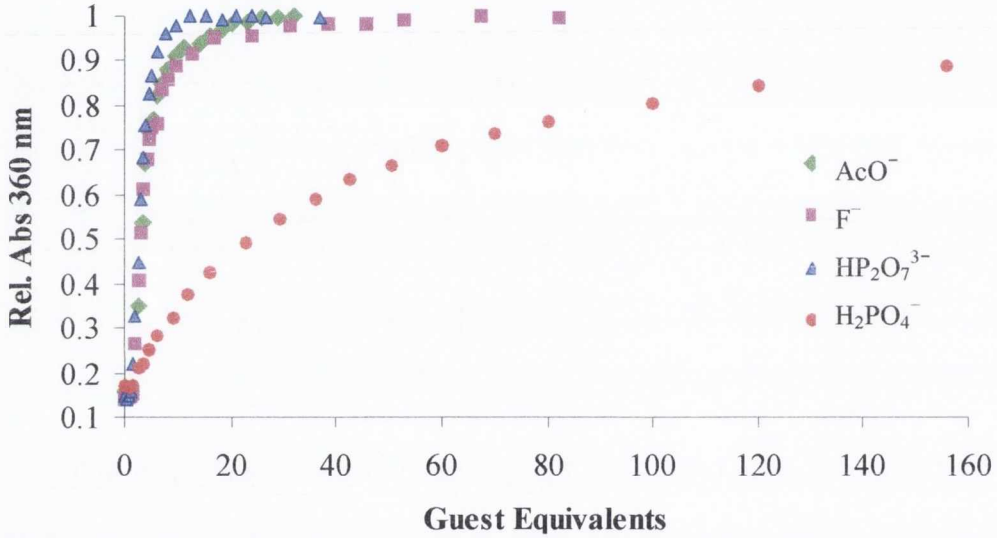


Figure B34: The relative changes in the absorption spectra of **61** at 360 nm upon addition of various anions in 4:1 DMSO-H_2O.

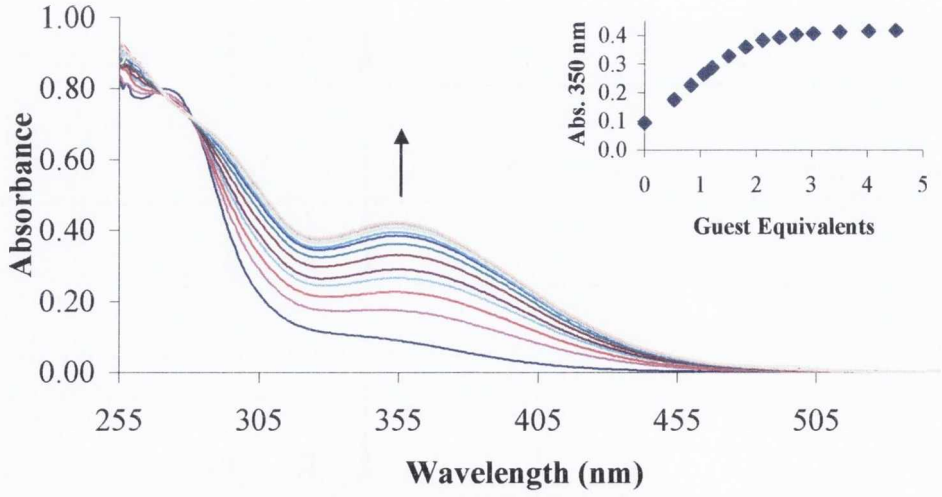


Figure B35: The changes in the absorption spectrum of **61** upon titration with TBAOH (0 → 7.3 equivalents) in 4:1 DMSO-H_2O. **Insert:** The changes at 350 nm.

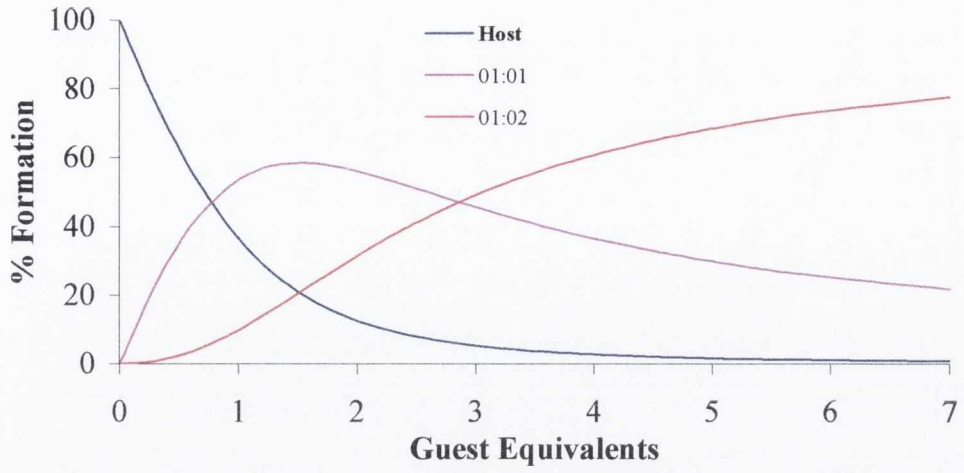


Figure B36: Species distribution diagram of **61** [2.2×10^{-5} M] upon titration with TBAOH (0 → 7 equivalents) in 4:1 DMSO-H_2O.

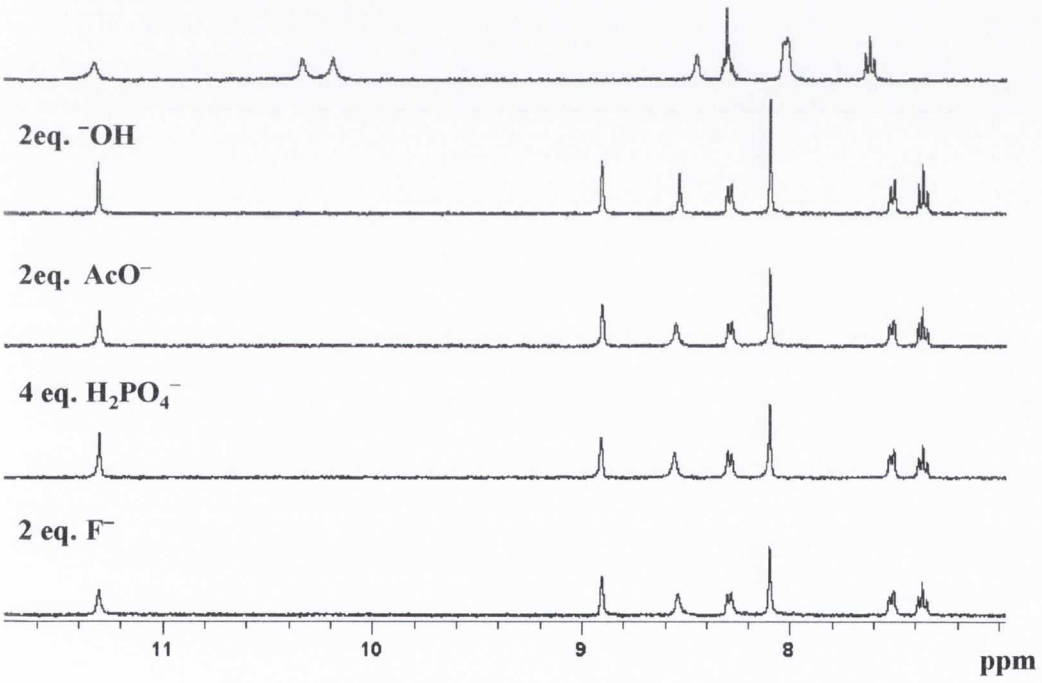


Figure B37: ^{1}H NMR (400 MHz, DMSO-d_6) titration of **61** with various anions.

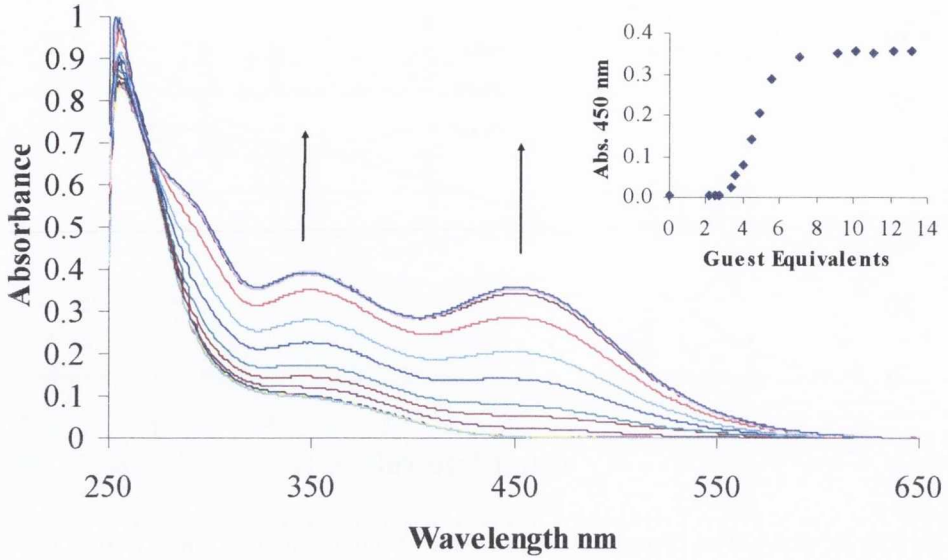


Figure B38: The changes in the absorption spectrum of **62** [2.4×10^{-5} M] upon titration with TBAOH (0 → 19 equivalents) in 4:1 DMSO-H_2O. **Insert**: The changes at 350 nm against (0 → 6 equivalents).

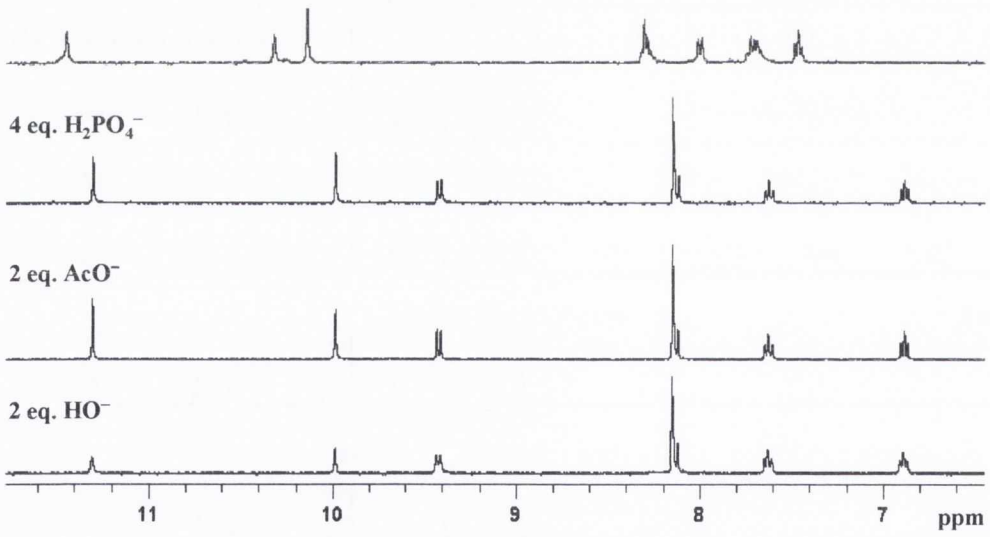


Figure B39: ^{1}H NMR (400 MHz, DMSO-d_6) titration of **62** with various anions.

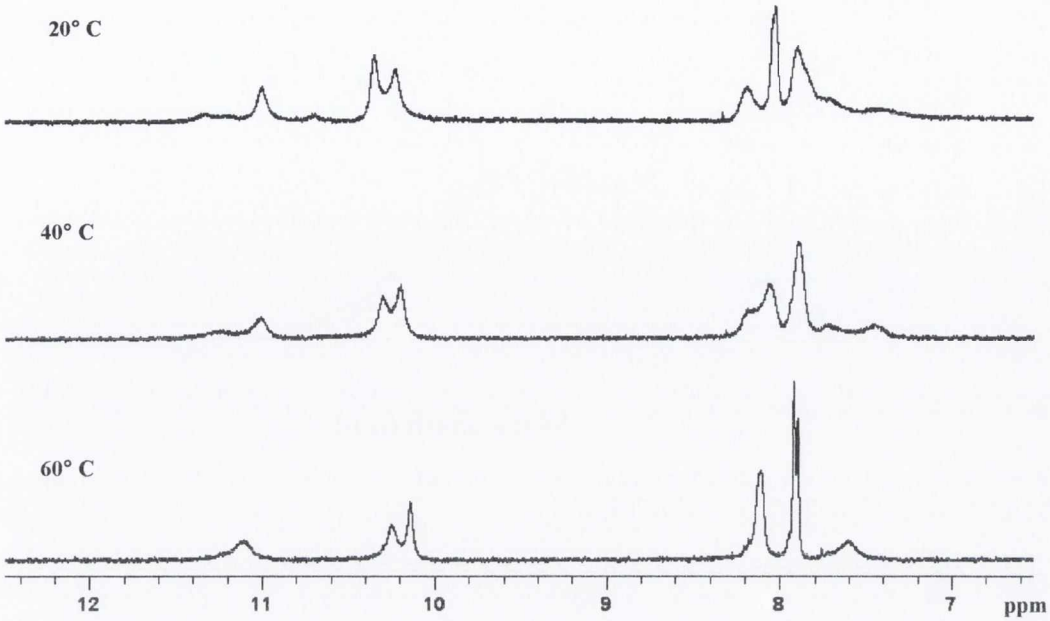


Figure C1: The VT ^{1}H NMR spectra of **75** in DMSO-d_6.

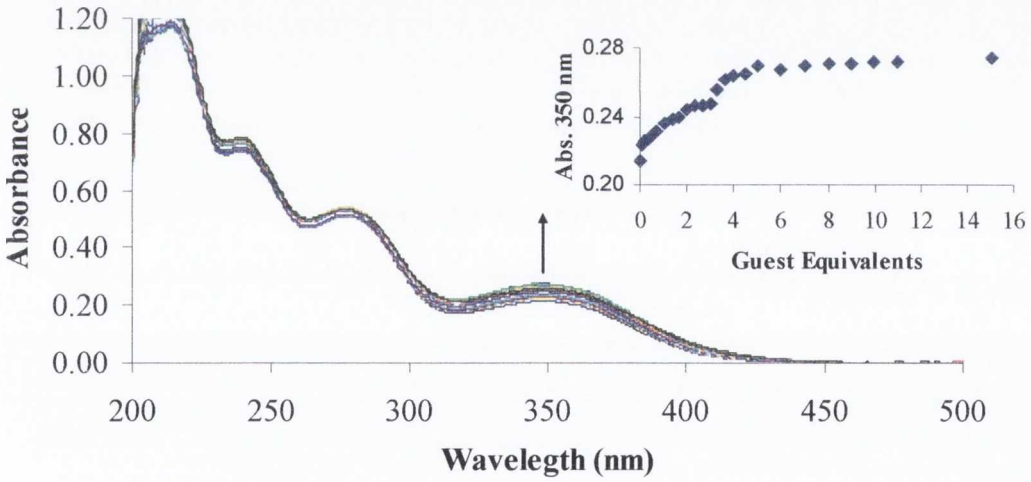


Figure C2: The changes in the absorption spectrum of **70** [2.44×10^{-5} M] upon titration with F^- (0→16 equivalents) in MeOH.

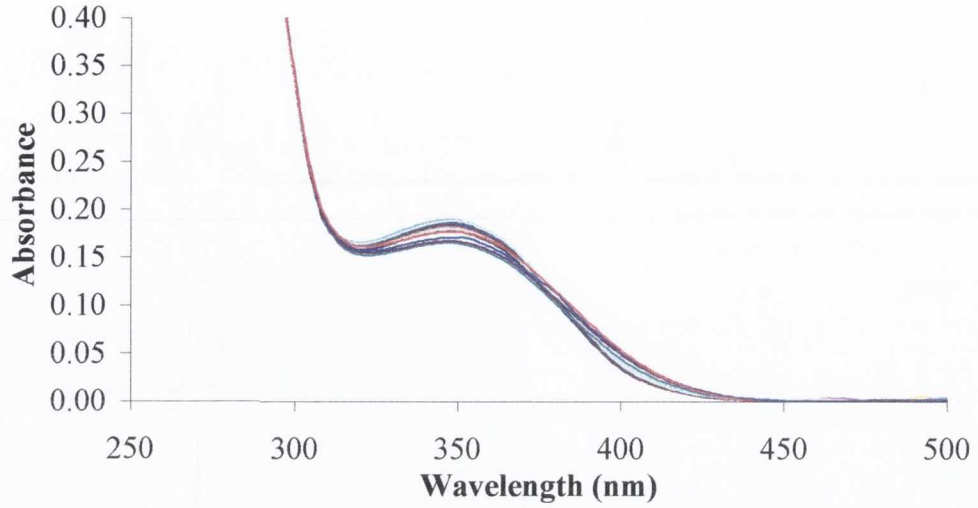


Figure C3: The changes in the ICT transition of the absorption spectrum of **70** [2.44×10^{-5} M] upon titration with $H_2PO_4^-$ (0→148 equivalents) in MeOH.

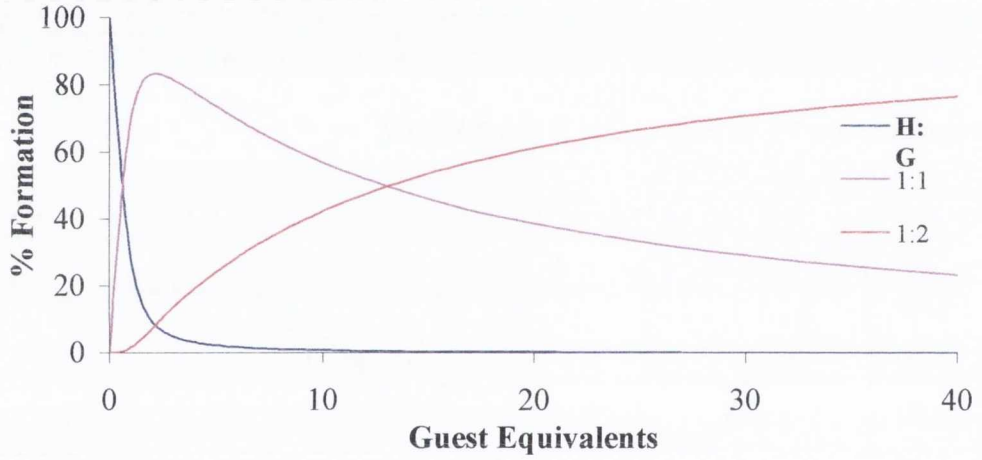


Figure C4: The species distribution diagram of **71** [2.5×10^{-5} M] upon titration with AcO^- (0→40 equivalents) in MeOH

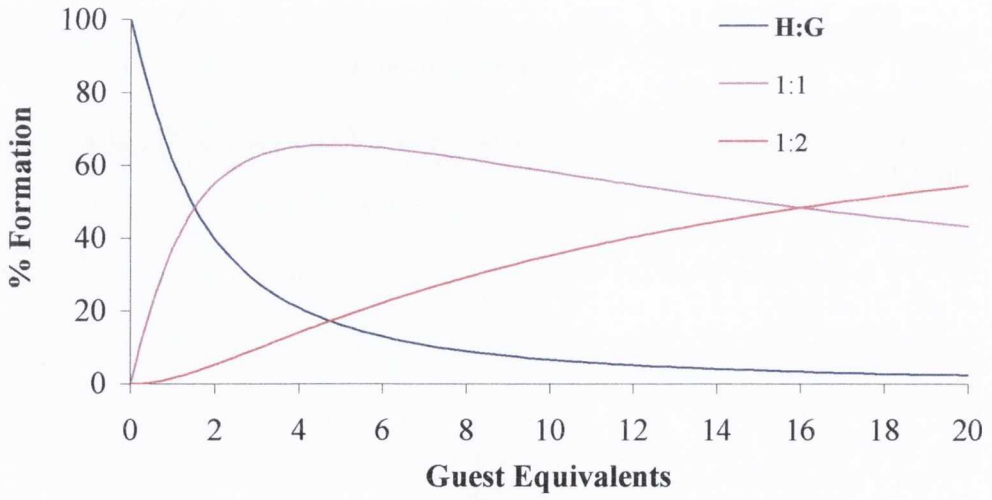


Figure C5: The species distribution diagram of **71** [1.6×10^{-5} M] upon titration with F^- (0→20 equivalents) in MeOH.

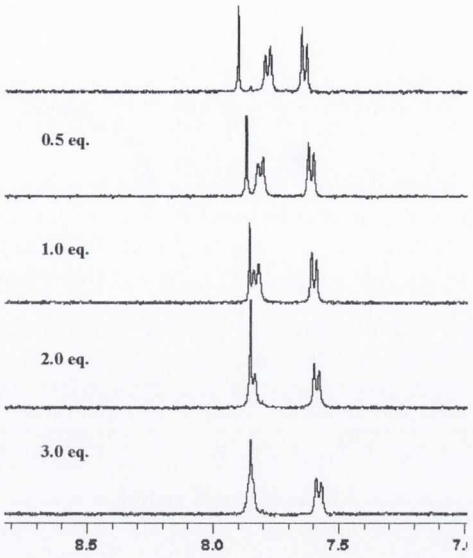


Figure C6: The changes in the ^{1}H NMR spectra of **70** upon titration with AcO^- in MeOH-d_3.

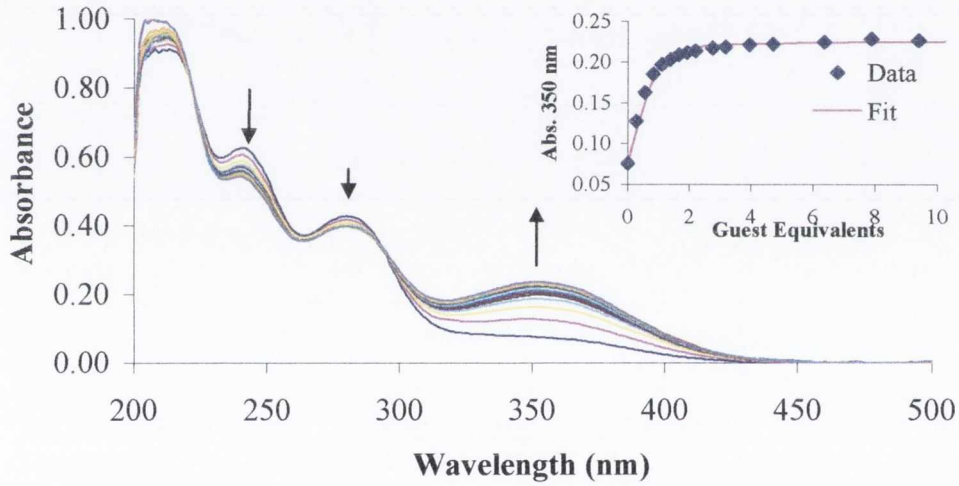


Figure C7: The changes in the absorption spectrum of **70** [2.5×10^{-5} M] upon titration with AcO^- (0→40 equivalents) in EtOH. **Insert**: The changes at 350 nm with 1:2 fit, shown from 0→10 equivalents.

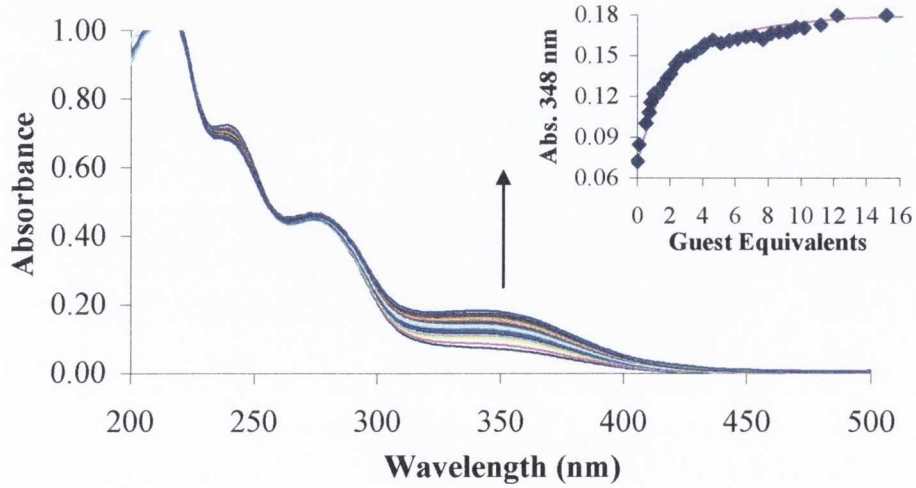


Figure C8: The changes in the absorption spectrum of **70** [1.7×10^{-5} M] upon titration with AcO^- (0→16 equivalents) in 1:1 EtOH-H_2O. **Insert**: The changes at 350 nm with 1:1 fit.

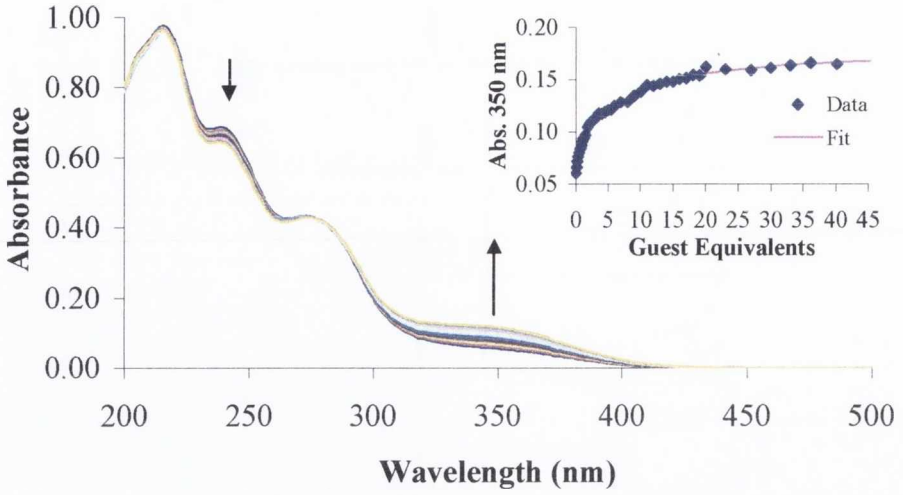


Figure C9: The changes in the absorption spectrum of **70** [1.66×10^{-5} M] upon titration with F^- (0→45 equivalents) in 1:1 EtOH-H_2O. Insert: The changes at 350 nm with 1:1 fit obtained from SPECFIT™.

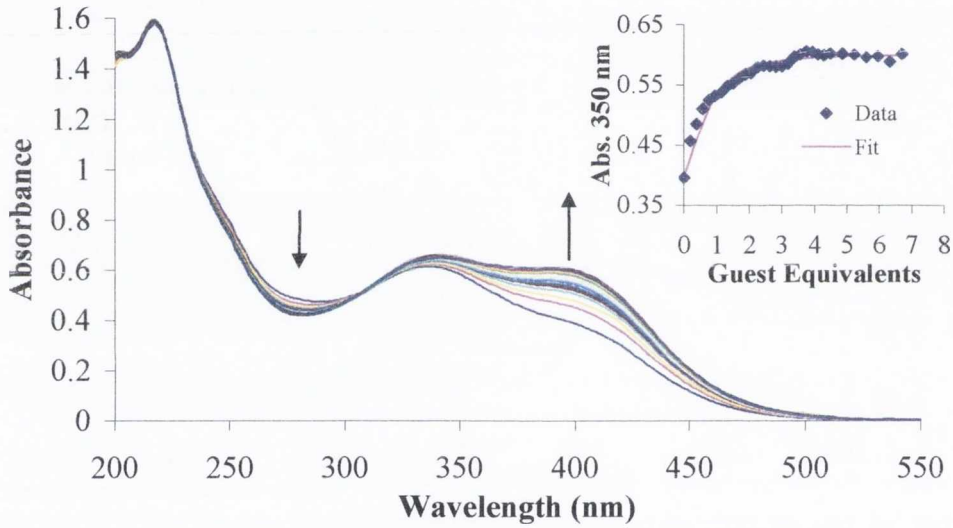


Figure C10: The changes in the absorption spectrum of **71** [1.65×10^{-5} M] upon titration with $H_2PO_4^-$ (0→6 equivalents) in 1:1 MeOH-H_2O. **Insert**: The changes at 350 nm with 1:1 fit obtained from SPECFIT™

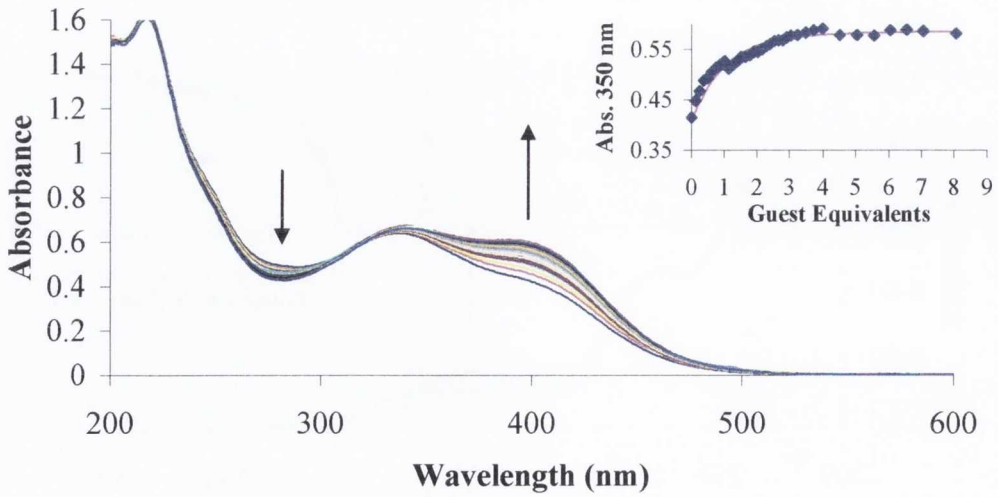


Figure C11: The changes in the absorption spectrum of **71** [1.65×10^{-5} M] upon titration with $H_2PO_4^-$ (0→6 equivalents) in 1:1 MeOH-H_2O. **Insert**: The changes at 350 nm with 1:1 fit obtained from SPECFIT™

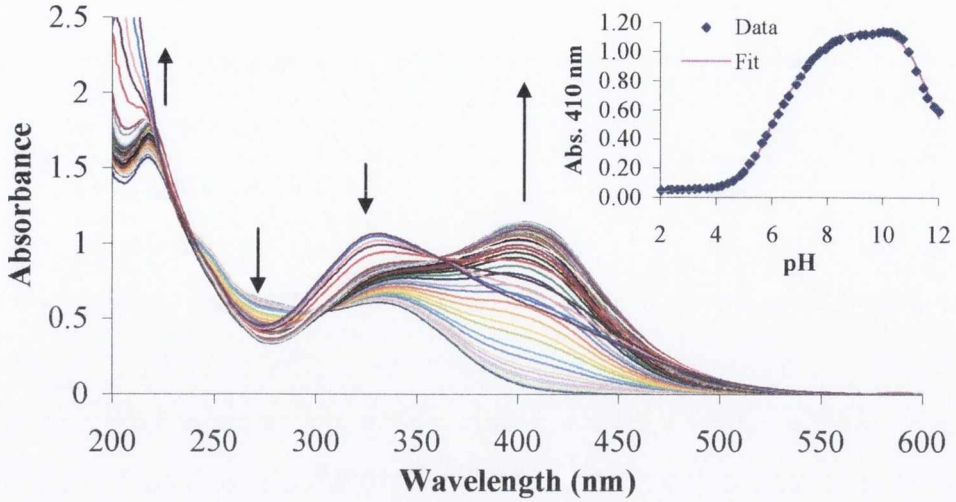


Figure C12: The changes in the absorption spectrum of **71** [1.75×10^{-5} M] as a function of pH. **Insert:** The changes at 410 nm with fit obtained from SPECFIT^{TM}.

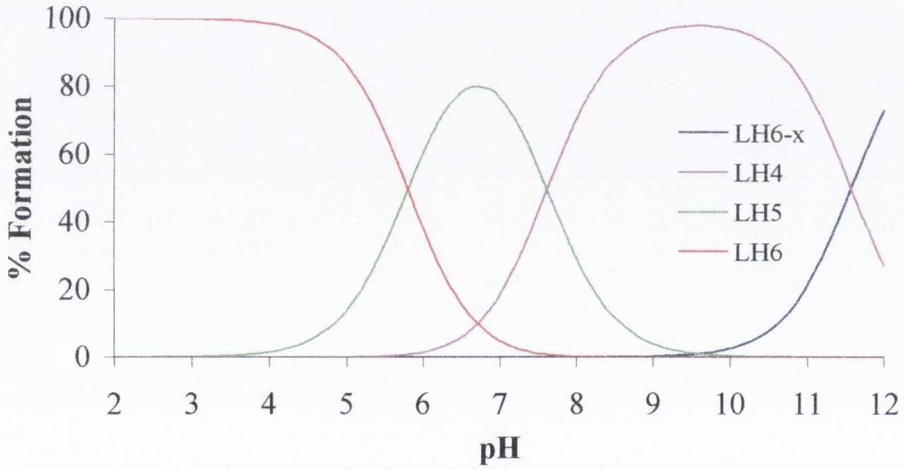


Figure C13: The species distribution diagram of **71** as a function of pH

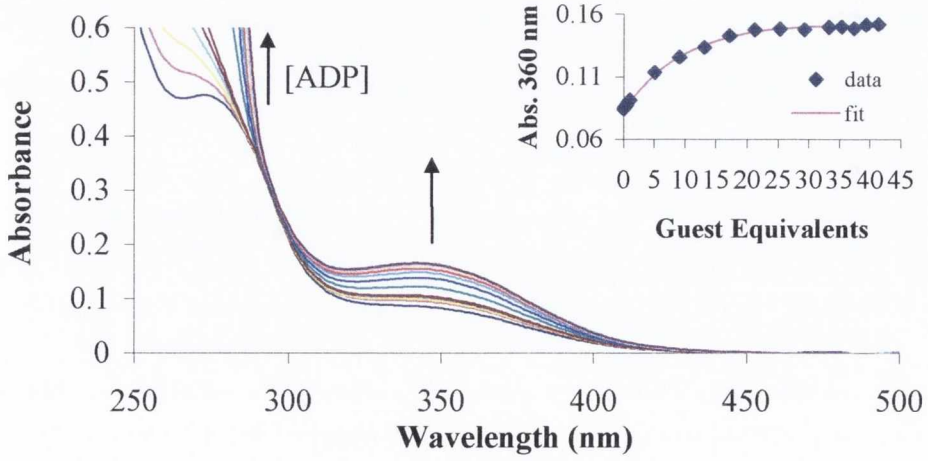


Figure C14: The changes in the absorption spectrum of **70** [1.75×10^{-5} M] upon titration with ADP in 1:1 EtOH-H_2O. **Insert:** The changes at 360 nm with 1:1 fit obtained from SPECFIT^{TM}.

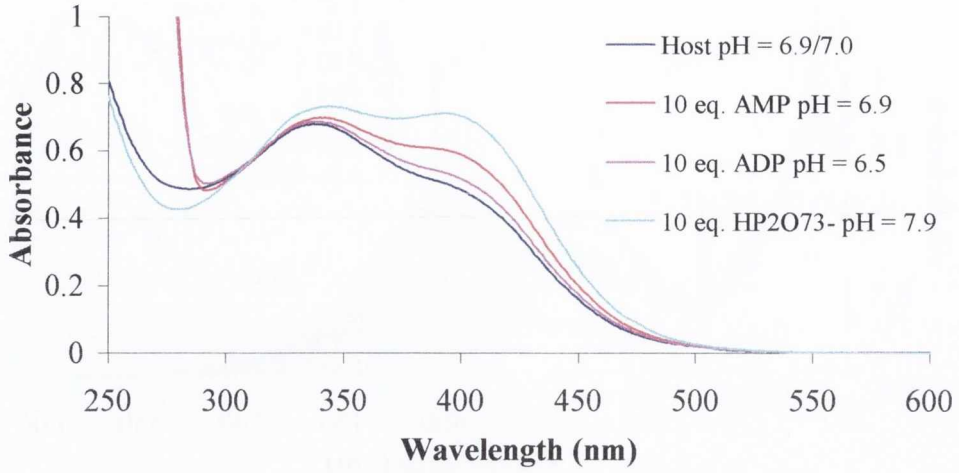


Figure C15: The changes in the ICT transition of the absorption spectra of **71** [1.7×10^{-5} M] upon the addition of 10 equivalents of various anions in 1:1 MeOH-H_2O, and the corresponding pH changes.

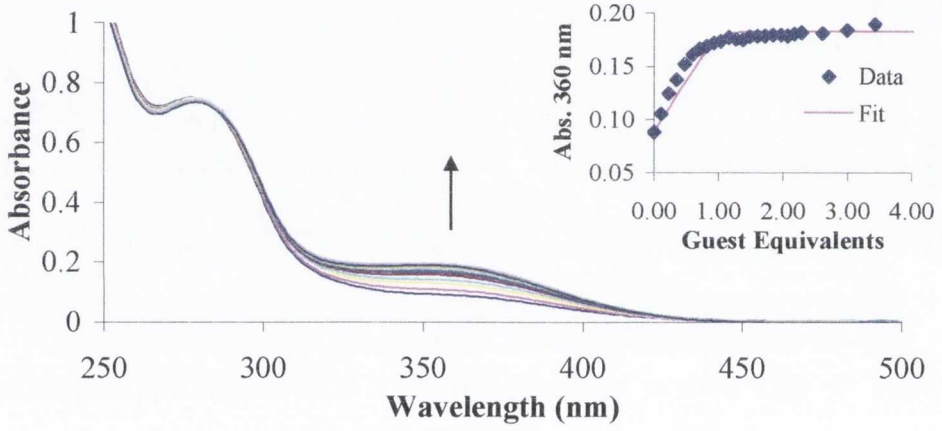


Figure C16: The changes in the ICT transition of the absorption spectra of **74** [1.5×10^{-5} M] upon titration with AcO^- in EtOH. **Insert**: The changes at 360 nm and 1:1 fit obtained fron SPECFIT™.

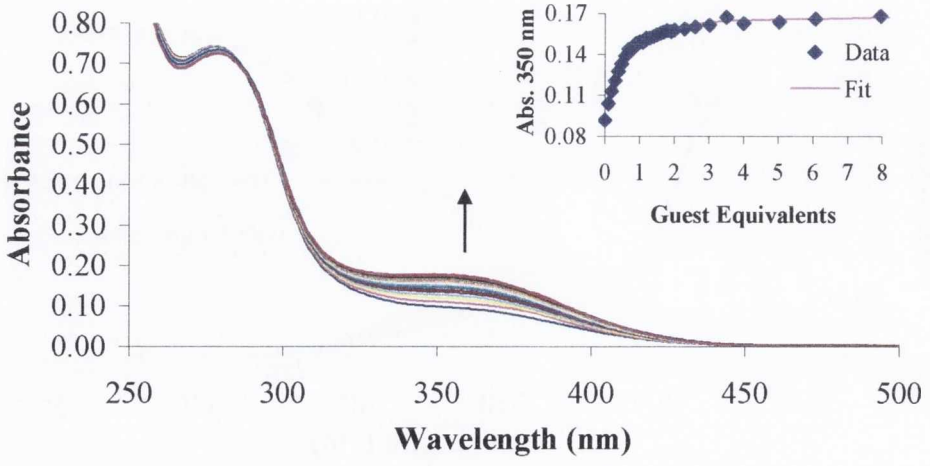


Figure C17: The changes in the ICT transition of the absorption spectra of **74** [1.9×10^{-5} M] upon titration with F^- in EtOH. **Insert**: The changes at 360 nm and 1:1 fit obtained from SPECFIT™.

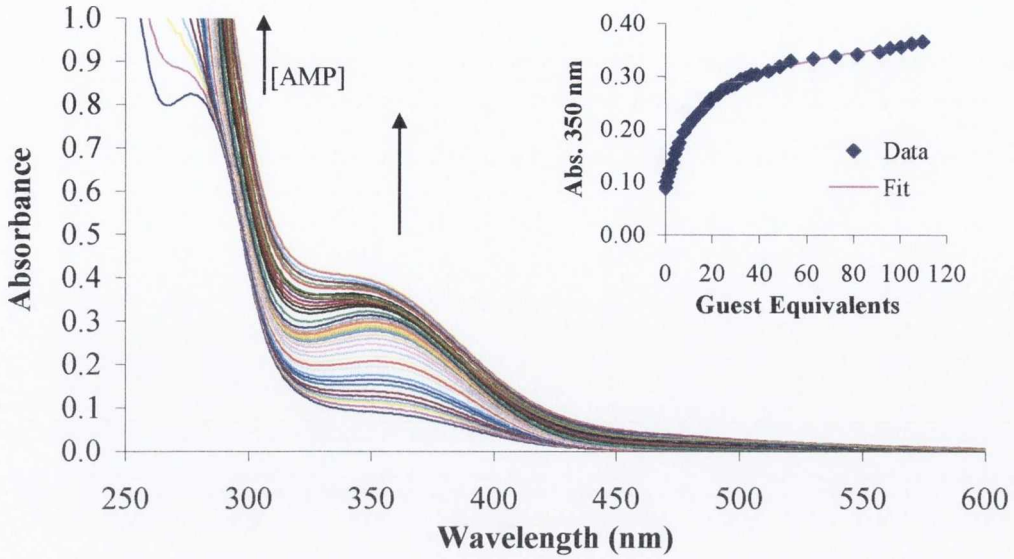


Figure C18: The changes in the ICT transition of the absorption spectra of **74** [1.9×10^{-5} M] upon titration with AcO^- in EtOH. **Insert**: The changes at 360 nm and 1:1 fit obtained from SPECFIT™.

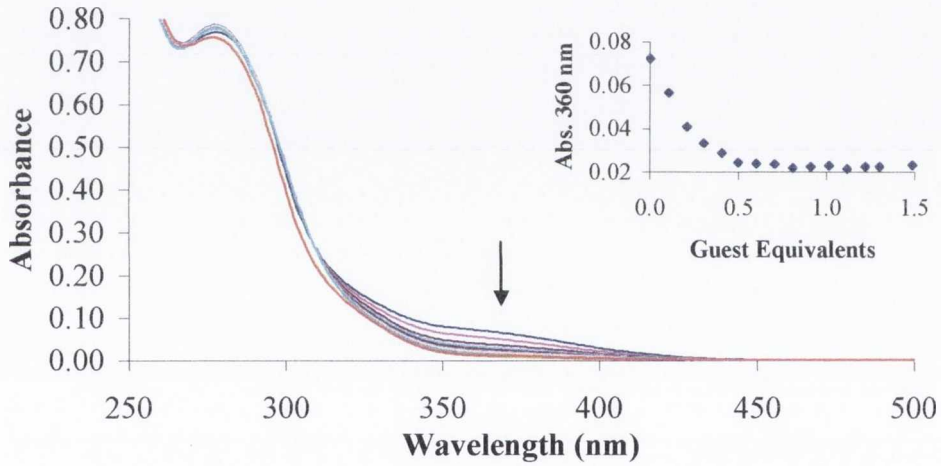


Figure C19: The changes in the ICT transition of the absorption spectra of **74** [1.9×10^{-5} M] upon titration with HSO_4^- in EtOH. **Insert**: The changes at 360 nm.

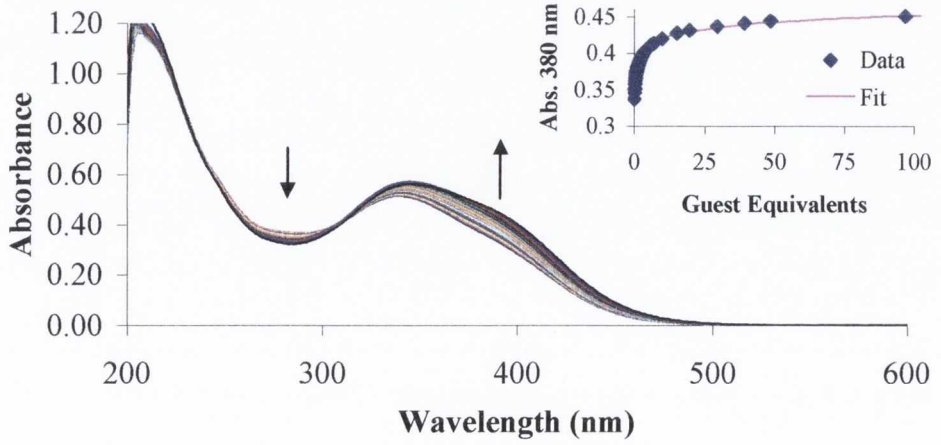


Figure C20: The changes in the absorption spectra of **75** [1.1×10^{-5} M] upon titration with AcO^- in MeOH. **Insert**: The changes at 380 nm with 1:2 H:G fit obtained from SPECFIT™.

Table 1. Crystal data and structure refinement for shelxs.

Identification code	**54**	
Empirical formula	C27 H35 N9 O9 S5	
Formula weight	789.99	
Temperature	150(2) K	
Wavelength	0.71070 Å	
Crystal system	Triclinic	
Space group	P-1	
Unit cell dimensions	a = 14.489(3) Å	α= 87.377(7)°.
	b = 15.929(5) Å	β= 68.142(6)°.
	c = 17.154(5) Å	γ = 81.773(8)°.
Volume	3636.5(17) $Å^3$	
Z	4	
Density (calculated)	1.443 Mg/m^3	
Absorption coefficient	0.381 mm^{-1}	
F(000)	1648	
Crystal size	0.27 x 0.20 x 0.08 mm^3	
Theta range for data collection	1.28 to 25.00°.	
Index ranges	-16<=h<=17, -18<=k<=18, -20<=l<=20	
Reflections collected	36636	
Independent reflections	12589 [R(int) = 0.0430]	
Completeness to theta = 25.00°	98.3 %	
Absorption correction	Semi-empirical from equivalents	
Max. and min. transmission	1.00000 and 0.79000	
Refinement method	Full-matrix least-squares on F^2	
Data / restraints / parameters	12589 / 0 / 914	
Goodness-of-fit on F^2	1.066	
Final R indices [I>2sigma(I)]	R1 = 0.0815, wR2 = 0.2394	
R indices (all data)	R1 = 0.0943, wR2 = 0.2713	
Largest diff. peak and hole	5.173 and -1.678 $e.Å^{-3}$	